

REPORT DOCUMENTATION PAGE

Public reporting burden for this collection of information is estimated to average 1 hour per response, including the time for reviewing existing data sources, gathering the data needed, and completing and reviewing the collection of information. Send comments regarding this burden estimate or any aspect of this collection of information, including suggestions for reducing this burden, to Washington Headquarters Services, Directorate for Information Operations and Reports, Paperwork Reduction Project (0704-0188), Washington, DC 20543-0188.

AFRL-SR-BL-TR-98-

0407

[illegible]

DTIC QUALITY INSPECTED 4

19980504 168

Technical report has been reviewed and is
approved for public release IAW AFR 190-12
Distribution is unlimited.
J. Beggs
AFRL Program Manager

AFRL-SR-BL-TR-98-

A
d

0407

MICROWAVE SCATTERING AND SYNTHETIC APERTURE RADAR IMAGING OF TARGETS BURIED IN RANDOM MEDIA

by

ROBERT G. ATKINS

S.B. Electrical Engineering and Computer Science,
Massachusetts Institute of Technology, Cambridge
June 1987

S.M. Electrical Engineering and Computer Science,
Massachusetts Institute of Technology, Cambridge
February 1988

E.E. Electrical Engineering and Computer Science,
Massachusetts Institute of Technology, Cambridge
June 1989

Submitted to the Department of Electrical
Engineering and Computer Science in Partial
Fulfillment of the Requirements for the
Degree of

DOCTOR OF PHILOSOPHY

at the

MASSACHUSETTS INSTITUTE OF TECHNOLOGY

June 1993

©Robert George Atkins, 1993

The author hereby grants to M.I.T. permission to reproduce and to distribute copies of
this thesis document in whole or in part.

Signature of Author

Robert G. Atkins

Department of Electrical Engineering and Computer Science
March, 1993

Certified by

J. Au Kong

Professor Jin Au Kong
Thesis Supervisor

Accepted by

Campbell L. Searle, Chairman
Committee on Graduate Students

MICROWAVE SCATTERING AND SYNTHETIC APERTURE RADAR IMAGING OF TARGETS BURIED IN RANDOM MEDIA

by

ROBERT G. ATKINS

Submitted to the Department of Electrical Engineering and Computer Science
March 1993, in partial fulfillment of the requirements for the Degree of
Doctor of Philosophy

Abstract

Detection and identification of targets buried within layers of vegetation or geophysical media such as snow, ice, or soil, continues to be an area of substantial interest and active research. Analysis of electromagnetic sensor systems for applications of this type share the common difficulty that the natural environment surrounding the buried target can not easily be characterized in a deterministic manner, and a statistical description of the media and the resulting electromagnetic propagation and scattering must be employed. Coupling between the deterministic target and its random surroundings modifies the signature of the target and lends an incoherent component to the signal measured by the sensing system. Prediction of these physical effects of the random environment is necessary before the performance of individual sensing mechanisms may be analyzed, however, little theoretical modeling has previously been done to support this prediction.

Hence, to provide greater physical insight into the effects of a random environment on the scattering characteristics of a buried target, several entirely new models are developed for the fields scattered from targets beneath or within layered regions of continuous random media. In the simplest case, the deterministic scatterer is taken as a point target, located beneath a slab of isotropic random media, characterized by a spherically symmetric correlation function. Strong fluctuation theory is applied to determine the effective mean permittivity of the random region, and the first order distorted Born approximation is utilized in computing the incoherent field scattered by the random media. The total field is shown to be composed of a target return, characteristic of scattering in the presence of the mean permittivity alone, a clutter return representing direct scattering by the random media, and two interaction terms describing the multi-path scattering between the target and random layer. The statistics of these scattered fields are computed, including the variance and the correlations for varied azimuth angle and frequency, and results are shown to illustrate the dependance of the statistics on several geometrical and physical parameters. An alternate repre-

sentation is introduced in which the total return is expressed as the freespace return modified by a complex phase term, where the real part embodies the random phase fluctuations of the scattered field, and where the imaginary part gives the amplitude fluctuations and mean attenuation. For the case of a small phase error, expressions are derived for the variance and correlation of the phase fluctuations, and the dependance on geometrical and physical parameters is again shown. To treat more complex physical environments, the model is extended to include multiple layers of random media, described by non-isotropic, azimuthally symmetric correlation functions and uniaxial effective permittivities, and the effects of the additional layers, non-spherical scatterers, and uniaxial permittivities on the scattered field statistics are illustrated.

To allow analysis of the interaction of more complex targets with a random environment, two additional models are developed. For electrically small targets, a Method of Moments approach is utilized in calculating the scattered field of the target. An integral equation is derived for the current induced on the perfectly conducting surface, and this current is expanded as a weighted series of basis function terms. The integral equation is tested to produce a linear system in the unknown current weights, allowing solution for the current and integration to determine the scattered field. For electrically large targets, a Physical Optics approach is applied in calculating the target scattered field, and the induced surface current is given by the tangent plane approximation. In both frequency regimes, the scattering from the random media is calculated using the first order distorted Born approximation. Results are shown to illustrate the effects of target size, shape, and orientation on the variance and correlation statistics of the scattered field, and these results are compared to those for the point target.

To illustrate the effect of the random media on the detection and classification capability of an imaging sensor, the models are applied to the analysis of a synthetic aperture radar (SAR) system. A simple SAR processing scheme is adopted, and the random media induced degradation is seen to depend on both the variance and correlation of the incoherent target return. Range-cross range images are formed for a point target beneath a random slab, and these are compared with the ideal freespace response. Effects of the obscuring layer are shown to include a mean attenuation, a range bias, and a blurring of both range and cross range responses. The extent of the blurring is seen to vary with the polarization, bandwidth, and integration angle of the SAR system.

Thesis Supervisor : Prof. J. A. Kong

Readers : Prof. F. R. Morgenthaler
Dr. R. T. Shin

DEPARTMENT OF ELECTRICAL ENGINEERING AND COMPUTER SCIENCE
MASSACHUSETTS INSTITUTE OF TECHNOLOGY
CAMBRIDGE MASSACHUSETTS 02139

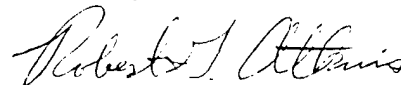
Office 26-317
TEL: (617) 253-5784
FAX: (617) 253-0987
May 12, 1993

Prof. Warren Peele
NDSEGF Fellowship Program
Management Office
Central Florida Facility
11th & Massachusetts Ave.
St. Cloud, FL 34769

Dear Prof. Peele:

Enclosed please find a copy of my Ph.D. thesis entitled "Microwave Scattering and Synthetic Aperture Radar Imaging of Targets Buried in Random Media," which is requested as part of my participation in the NDSEGF Fellowship program under your direction. I have also sent a copy to my mentor in the program, Mr. Edmund Zelnio of the Air Force Avionics Laboratory at Wright Patterson Air Force Base. I hope that you will find this material useful and interesting, and I ask only that you respect the fact this work has not yet been published. If I can assist you further in any way, you may contact me after May 17 at MIT Lincoln Laboratory at (617)-981-1010.

Sincerely,



Robert G. Atkins

Enclosures

JUN 14 1993
JBF

Acknowledgements

This thesis represents the final chapter in what has been nearly a decade of my life at MIT. For the success and happiness I have found in these years, I owe thanks to many - both for their support of my technical efforts, and for their friendship through good and difficult times alike. I am sure I will be unsuccessful in my attempt to name all, but I hope that those omitted will know that they are appreciated just the same.

For my start in both research and electromagnetic wave theory, I owe MIT Lincoln Laboratory, which afforded me the opportunity to work on challenging problems during my summers, first as a VI-A Co-op student, and later as a summer staff member. I wish to thank Dr. David Briggs and Dr. Lewis Thurman for providing me this opportunity, and to also thank all the members of Group 45 (now 101 and 105) for their friendship and their help in many of my technical endeavors. To the softball team (Cruisers, Bad News, ... I've lost track what we're called now) - thanks for letting me play, and to the bridge crew - thanks for letting me learn.

No one at the Laboratory has been more helpful with the technical problems and issues I have faced than Dr. Robert Shin, initially as my VI-A company supervisor, and now as a reader for this thesis. I wish to thank him for the opportunities he has provided me, both at Lincoln Lab, and in my research group at MIT, and also just for being there to answer what was sometimes a myriad of questions.

At MIT, I wish to thank my thesis adviser, Prof. Kong, for allowing me to be part of the EWT research group, and to interact with such a diverse collection of bright students. Prof. Kong provided my formal introduction to electromagnetic wave theory, and enthused me in this area with his energetic teaching. I also wish to thank Prof.

6 ACKNOWLEDGEMENTS

Morgenthaler, for his time and interest, not only as a reader for this thesis, but also as the Chairman of my Area Exam.

Finally, rounding out the technical side of these acknowledgements, I am thankful for the financial support I have received from the National Science Foundation and the United States Air Force, in the form of NSF and NDSEGF fellowships. I also wish to thank Edmund Zelnio, my mentor in the NDSEGF program, for his continuing interest in this work.

Perhaps equally important to the technical support which contributed to this thesis, however, are the many people I have met during the past decade who have lent their friendship and encouragement, when the task of completing this work seemed insurmountable. Others have shared with me in the not-so-academic diversions, which have been a necessary occasional escape from course work and research.

As a freshman, it was the upperclassmen of MacGregor J-Entry - Al, Andy A., Brad, Jack, Joe, Kleo, ... - who taught me so much about MIT, and helped me find confidence in my ability to succeed here. Later, as an upperclassman myself, the freshmen - Pete, Tamal, Cliff, Ajiit, Pat, ... - taught me even more. Thanks guys!

To the IM hockey teams that I've been fortunate enough to play for over the past five years - J-Entry, Chemistry, and the Tigers - thanks for letting me skate. And to the TEM volleyball team - Ike, Check, Lam, Nelson, Ali, Murat, Dave, Chen, Anand, Jake, Victor, Kevin, Matt, Song, Greg, Shane, ... I know I've missed a few others - thanks for letting me set for you. Thanks also to Bob Shin for coaching our rookie season.

In my research group, I've made many friends and had the opportunity to spend time, both technical and not, with the smartest collection of people I have ever known. Thanks to those that braved the cold - Ike, Judy, Ann, Mike, Check, Nelson, Harold, Ali ... - to hit the slopes on our group ski trips. Also thanks to my office mates from over the years - Dr. Ali, David A., and Li-Fang - for braving my bad days, and for your friendship and conversation. To Murat, Ali, Greg, and Jake - thanks for playing v-ball - I guess you're elected the new captain Greg. Please, no more 9 AM football games, though. And thanks for the bidding conventions Jake - I'm ready whenever you want to play duplicate again. To Nelson, I owe you much - not only for your friendship, but also because much of this work grew out of your Master's Thesis, and the technical discussions we've had. The v-ball team misses you, but I suppose it's nicer playing on California sand, huh?

Outside my research group I have been fortunate to find a collection of friends, who always have seemed to be there when I needed them most. First, the current "rink rat", Kevin Y. - thanks for not crushing me in the corners. You should go out for Varsity next year, but you'd probably get less ice time that way. To Claire - thanks for teaching me all about periodic media. Your plants are still alive, but barely, so you'd better rescue them soon. To my roommate, Anand, thanks most, I suppose, for just putting up with me,... and for having such a big TV. Also thanks for letting me scrub for the Tigers. Victor, thanks for all the food your Mom keeps feeding us. And thanks for organizing so many trips to movies, skiing, etc. - they've provided much needed diversions from this thesis.

To Kevin L. and Susan - you two have been the best friends anyone could ask for. Thanks for introducing me to Sci-Fi, and always being there to see me through the "cycle of fire" that grad school often seemed. I hope you know how much I appreciate your support and friendship - well, at least now you will. Also Kevin, thanks for all the technical discussions, both here and summers at Lincoln.

To my brother Steve, thanks I guess for just being my brother. And also for first teaching me to skate, introducing me to J. Crew clothes, and a whole lot of other stuff too. Don't get lost in Australia - I'd miss playing on the same line.

Jane, you've been here for perhaps the hardest part - the end, where the light at the end of the tunnel is visible, but doesn't seem to be getting closer fast enough. But you've given this idiot a reason to graduate, and made finishing-up at least a little bit nicer than it would have been without you. Thanks doesn't seem enough - so share with me this sunrise...

Finally, to my parents, who have always been ready to drop everything to help out, be it in school, sports, or life in general. Without their support and encouragement, I would never have made it to MIT, nor succeeded here as I have. To my Mom, I also owe thanks for her expert \TeX advice and help in formatting this thesis. Mom, Dad, you wanted a Doctor - sorry it took so long.

*Each man has a hope, a vision,
an altruistic dream,
a wish that keeps him going,
a meaning for the scheme.
Don't give up the fire.
Don't sell out for less.
The goal is just the ending,
to a never ending quest.*

*For the family and friends,
who help keep the fire burning...*

Table of Contents

Abstract	3
Acknowledgements	5
Table of Contents	11
List of Figures	17
Chapter 1 Introduction	29
1.1 Previous Work	33
1.1.1 SAR Signal Processing	34
1.1.2 Forest Propagation	38
1.2 Modeling of Propagation and Scattering	42
1.2.1 Stochastic Medium Scattering	43
1.2.1.1 Dielectric Slab Model	43
1.2.1.2 Discrete Scatterer Model	44
1.2.1.3 Continuous Random Media Model	47
1.2.2 Target Scattering	53
1.2.2.1 Low Frequency Target Modeling	54

12 TABLE OF CONTENTS

1.2.2.2 High Frequency Target Modeling . . .	59
1.3 Description of Thesis	61
Chapter 2 Scattering of a Point Target Beneath a Layer of Continuous Random Media	67
2.1 Geometry and Random Media Model	68
2.2 Scattering Terms	72
2.3 Field Calculations	78
2.3.1 Target/Clutter Autocorrelation	78
2.3.2 Clutter - Target/Clutter Correlation . . .	83
2.3.3 Target Autocorrelation	84
2.3.4 Clutter Autocorrelation	85
2.4 Field Variance and Correlation Results	91
2.4.1 Scattered Field Variance	92
2.4.2 Scattered Field Correlation	108
Appendix A Electric Field / Electric Source Greens Function and Incident Field Expressions for an Isotropic Layered Media	123
Appendix B Correlation of Scattered Field Components	131
B.1 Target/Clutter - Target/Clutter Correlation .	132
B.2 Clutter/Target - Clutter/Target Correlation .	133
B.3 Target/Clutter - Clutter/Target Correlation .	134
B.4 Clutter - Target/Clutter Correlation	135
B.5 Clutter - Clutter/Target Correlation	136
B.6 Target - Target Correlation	137

B.7 Clutter – Clutter Correlation	138
Chapter 3 Phase Fluctuations of a Point Target Beneath a Layer of Continuous Random Media	139
3.1 Formulation	140
3.2 Complex Correlation of the Incoherent Fields .	143
3.3 Variance of Phase Fluctuations	146
3.4 Correlation of Phase Fluctuations	150
Appendix C Complex Correlation of Scattered Field Components	157
C.1 Target/Clutter – Target/Clutter Complex Correlation	158
C.2 Clutter/Target – Clutter/Target Complex Correlation	159
C.3 Target/Clutter – Clutter/Target Complex Correlation	160
C.4 Target – Target Complex Correlation	161
Chapter 4 Scattering of a Point Target in a Multi-Layer Uniaxial Con- tinuous Random Media	163
4.1 Geometry and Random Media Model	164
4.2 Scattering Terms and Field Calculations . . .	167
4.2.1 Scattered Field Components	168
4.2.2 Incoherent Field Statistics	170
4.2.3 Coherent Field Power	175
4.3 Variance and Correlation Results	177

14 TABLE OF CONTENTS

4.3.1 Effect of the Random Medium Correlation Length	177
4.3.2 Effect of a Larger Fractional Volume of Scatterers	185
4.3.3 Effect of a Uniaxial Correlation Function	189
4.3.4 Effect of an Additional Stratification Layer	196
Appendix D Strong Fluctuation Theory for the Effective Permittivity	211
Appendix E Electric Field / Electric Source Green's Function and Incident Field Expressions for a Uniaxial Layered Media	231
Appendix F Incoherent Field Correlation for a Point Target and Layered Continuous Uniaxial Random Media with the Target in a Non-Random Layer ($t \neq f$)	241
F.1 Evaluation of the Complex β_z Integration	241
F.2 Correlation of Scattered Field Components	249
F.2.1 Target/Clutter - Target/Clutter Correlation	253
F.2.2 Clutter/Target - Clutter/Target Correlation	254
F.2.3 Target/Clutter - Clutter/Target Correlation	255

Appendix G Incoherent Field Correlation for a Point Target and Layered

Continuous Uniaxial Random Media with the Target in the

Random Layer ($t = f$) 257

G.1 Derivation of the Incoherent Field Correlation

. 258

G.1.1 Evaluation of σ_{TC-TC}^{UU} and σ_{TC-TC}^{NN} . . 262

G.1.2 Evaluation of σ_{TC-TC}^{UN} and σ_{TC-TC}^{NU} . . 264

G.1.3 Evaluation of $\sigma_{TC-TC}^{\bar{U}\bar{U}}$ 268

G.1.4 Evaluation of $\sigma_{TC-TC}^{\bar{U}\bar{N}}$, $\sigma_{TC-TC}^{\bar{N}\bar{U}}$, $\sigma_{TC-TC}^{\bar{U}U}$,
and $\sigma_{TC-TC}^{\bar{N}N}$ 269

G.2 Correlation of Scattered Field Components . . 279

G.2.1 Target/Clutter - Target/Clutter Correlation

. 279

G.2.2 Clutter/Target - Clutter/Target Correlation

. 293

G.2.3 Target/Clutter - Clutter/Target Correlation

. 299

Chapter 5 Scattering of an Electrically Large Plate Target in a Layered

Continuous Random Media 307

5.1 Geometry and Random Media Model 308

5.2 Scattering Terms 312

5.3 Field Calculations 318

5.3.1 Coherent Field 318

5.3.2 Incoherent Fields 328

16 TABLE OF CONTENTS

5.4 Variance and Correlation Results	337
Appendix H Magnetic Field / Electric Source Green's Function and Incident Magnetic Field Expressions for a Uniaxial Layered Media	365
Appendix I Correlation of Scattered Field Components for an Electrically Large Target Buried in a Layered Random Media	369
I.1 Target/Clutter - Target/Clutter Correlation	370
I.2 Clutter/Target - Clutter/Target Correlation	372
I.3 Target/Clutter - Clutter/Target Correlation	374
I.4 Target - Target Correlation	376
Chapter 6 Scattering from an Electrically Small Target in a Layered Continuous Random Media	379
6.1 Method of Moments Formulation	380
6.2 Triangular Patch Modeling	393
Chapter 7 SAR Imaging of a Point Target Beneath a Layered Continuous Random Media	427
7.1 SAR Processing	428
7.2 Approximate Evaluation of the SAR Response	436
7.3 SAR Point Target Imaging Results	448
Chapter 8 Summary and Future Work	477
References	485
Index of Notation	497

List of Figures

1.1	An example of the use of penetrating synthetic aperture radar is in the detection and imaging of structures buried beneath forest foliage.	31
2.1	Geometry of the buried target problem with a point target located beneath a slab of isotropic random media.	69
2.2	Scattering mechanisms for Target-Clutter interaction including the direct clutter return (a), target-clutter multi-path (b), clutter-target multi-path (c), target-clutter-target multi-path (d), and direct target return (e). . . .	76
2.3	Geometry of the SAR antenna patterns for transmit and receive and for two different orientations.	86
2.4	Geometry of the field variance and correlation results.	92
2.5	Dependence of the coherent target scattering cross section, σ_{T-T} , on elevation angle. Results are given at 1.120 GHz for a 10 m slab with $z_T = 10$ m. Shown is the case with $\epsilon_0 = \epsilon_2 = \epsilon_o$ and $\epsilon_{1m} = (1.0505 + .001794i)\epsilon_o$ (solid). For comparison, the free space case (dashed), and the case with a lossy media ($\epsilon_2 = (6.0 + 0.6i)\epsilon_o$) in region 2 (dotted) are also pictured.	96
2.6	Dependence of the target/clutter scattering cross section, σ_{TC-TC} , on elevation angle for $\epsilon_0 = \epsilon_2 = \epsilon_o$ (solid) $\epsilon_0 = \epsilon_2 = (1.0505 + .001794i)\epsilon_o$ (dash). Results are given at 1.120 GHz for a 10 m slab with $z_T = 10$ m and with $\epsilon_{1m} = (1.0505 + .001794i)\epsilon_o$	97
2.7	Dependence of the target/clutter scattering cross section, σ_{TC-TC} , on elevation angle for $z_T = 10$ m (solid) and $z_T = 15$ m (dash). Results are given at 1.120 GHz for a 10 m slab with $\epsilon_0 = \epsilon_2 = \epsilon_o$ and $\epsilon_{1m} = (1.0505 + .001794i)\epsilon_o$	98

18 LIST OF FIGURES

- 2.8 Dependence of the target-clutter scattering cross section, σ_{TC-TC} , on elevation angle for $\epsilon_2 = \epsilon_o$ (solid) and $\epsilon_2 = (6.0 + 0.6i)\epsilon_o$ (dash). Results are given at 1.120 GHz for a 10 m slab with $z_T = 10$ m and with $\epsilon_o = \epsilon_o$ and $\epsilon_{1m} = (1.0505 + .001794i)\epsilon_o$ 99
- 2.9 Dependence of the coherent target scattering cross section, σ_{T-T} , (solid) and the target/clutter scattering cross section, σ_{TC-TC} , (dash) on target depth. Results are shown for normal incidence ($\theta = 0^\circ$) at 1.120 GHz with a 10 m slab and with $\epsilon_o = \epsilon_2 = \epsilon_o$ and $\epsilon_{1m} = (1.0505 + .001794i)\epsilon_o$ 102
- 2.10 Dependence of the coherent target scattering cross section, σ_{T-T} , (solid) and the target/clutter scattering cross section, σ_{TC-TC} , (dash) on slab thickness. Results are shown for normal incidence ($\theta = 0^\circ$) at 1.120 GHz with the target positioned immediately below the lower interface ($z_T = d$), and with $\epsilon_o = \epsilon_2 = \epsilon_o$ and $\epsilon_{1m} = (1.0505 + .001794i)\epsilon_o$ 103
- 2.11 Dependence of the coherent target scattering cross section, σ_{T-T} , (solid) and the target-clutter scattering cross section, σ_{TC-TC} , (dash) on frequency for normal incidence ($\theta = 0^\circ$). Results are given for a 10 m slab with $z_T = 10$ m and with $\epsilon_o = \epsilon_2 = \epsilon_o$ and $\epsilon_{1m} = (1.0505 + .001794i)\epsilon_o$ 104
- 2.12 Dependence of the clutter-target/clutter correlation, σ_{C-TC} , on elevation angle for the HH (solid) and VV (dash) polarizations. Results are given at 1.120 GHz for a 10 m slab with $z_T = 10$ m and with $\epsilon_o = \epsilon_2 = \epsilon_o$ and $\epsilon_{1m} = (1.0505 + .001794i)\epsilon_o$ 105
- 2.13 Dependence of the clutter-target/clutter correlation, σ_{C-TC} , on frequency for normal incidence ($\theta = 0^\circ$). Results are given for a 10 m slab with $z_T = 10$ m and with $\epsilon_o = \epsilon_2 = \epsilon_o$ and $\epsilon_{1m} = (1.0505 + .001794i)\epsilon_o$ 106
- 2.14 Correlation of the target/clutter multi-path return, $\sigma_{TC-TC}(\theta_1, \theta_2)$, over $\theta_d = \theta_2 - \theta_1$ for $\theta_1 = 0^\circ$ and for HH (solid) and VV (dash) polarizations. Results are given at 1.120 GHz for a 10 m slab with $z_T = 10$ m and with $\epsilon_o = \epsilon_2 = \epsilon_o$ and $\epsilon_{1m} = (1.0505 + .001794i)\epsilon_o$ 110
- 2.15 Correlation of the target/clutter multi-path return, $\sigma_{TC-TC}(\theta_1, \theta_2)$, over $\theta_d = \theta_2 - \theta_1$ for the HH polarization and for $\theta_1 = 0^\circ$ (solid) $\theta_1 = 40^\circ$ (dash), and $\theta_1 = 60^\circ$ (dots). Results are given at 1.120 GHz for a 10 m slab with $z_T = 10$ m and with $\epsilon_o = \epsilon_2 = \epsilon_o$ and $\epsilon_{1m} = (1.0505 + .001794i)\epsilon_o$ 111
- 2.16 Correlation of the target/clutter multi-path return, $\sigma_{TC-TC}(\theta_1, \theta_2)$, over $\theta_d = \theta_2 - \theta_1$ for the VV polarization and for $\theta_1 = 0^\circ$ (solid) $\theta_1 = 40^\circ$ (dash), and $\theta_1 = 60^\circ$ (dots). Results are given at 1.120 GHz for a 10 m slab with $z_T = 10$ m and with $\epsilon_o = \epsilon_2 = \epsilon_o$ and $\epsilon_{1m} = (1.0505 + .001794i)\epsilon_o$ 112
- 2.17 Correlation of the target/clutter multi-path return, $\sigma_{TC-TC}(\theta_1, \theta_2)$, over $\theta_d = \theta_2 - \theta_1$ for the HH polarization and for $z_T = 10$ m (solid) and $z_T = 15$ m

- (dash). Results are given at 1.120 GHz for a 10 m slab with $\theta_1 = 0^\circ$ and with $\epsilon_0 = \epsilon_2 = \epsilon_o$ and $\epsilon_{1m} = (1.0505 + .001794i)\epsilon_o$ 115
- 2.18 Correlation of the target/clutter multi-path return, $\sigma_{TC-TC}(\phi_2 - \phi_1)$, over $\phi_d = \phi_2 - \phi_1$ for $\theta = 40^\circ$ and for HH (solid) and VV (dash) polarizations. Results are given at 1.120 GHz for a 10 m slab with $z_T = 10$ m and with $\epsilon_0 = \epsilon_2 = \epsilon_o$ and $\epsilon_{1m} = (1.0505 + .001794i)\epsilon_o$ 116
- 2.19 Correlation of the target/clutter multi-path return, $\sigma_{TC-TC}(\phi_2 - \phi_1)$, over $\phi_d = \phi_2 - \phi_1$ for the HH polarization and for $\theta = 20^\circ$ (solid), $\theta = 40^\circ$ (dash), and $\theta = 60^\circ$ (dots). Results are given at 1.120 GHz for a 10 m slab with $z_T = 10$ m and with $\epsilon_0 = \epsilon_2 = \epsilon_o$ and $\epsilon_{1m} = (1.0505 + .001794i)\epsilon_o$. . . 117
- 2.20 Correlation of the target/clutter multi-path return, $\sigma_{TC-TC}(\phi_2 - \phi_1)$, over $\phi_d = \phi_2 - \phi_1$ for the VV polarization and for $\theta = 20^\circ$ (solid), $\theta = 40^\circ$ (dash), and $\theta = 60^\circ$ (dots). Results are given at 1.120 GHz for a 10 m slab with $z_T = 10$ m and with $\epsilon_0 = \epsilon_2 = \epsilon_o$ and $\epsilon_{1m} = (1.0505 + .001794i)\epsilon_o$. . . 118
- 2.21 Correlation of the target/clutter multi-path return, $\sigma_{TC-TC}(f_1, f_2)$, over $f_d = f_2 - f_1$ for normal incidence ($\theta_1 = \theta_2 = 0^\circ$) and for $f_1 = 1120$ MHz (solid), $f_1 = 1110$ MHz (dash), and $f_1 = 1130$ MHz (dots). Results are given for a 10 m slab with $z_T = 10$ m and with $\epsilon_0 = \epsilon_2 = \epsilon_o$ and $\epsilon_{1m} = (1.0505 + .001794i)\epsilon_o$ 119
- 2.22 Correlation, $\sigma_{C-TC}(\phi_2 - \phi_1)$, of the clutter return at one azimuth, ϕ_1 , with the target/clutter return at a second, ϕ_2 , for $\theta_1 = \theta_2 = 40^\circ$ and for the HH (solid) and VV (dash) polarizations. Results are given at 1.120 GHz for a 10 m slab with $z_T = 10$ m and with $\epsilon_0 = \epsilon_2 = \epsilon_o$ and $\epsilon_{1m} = (1.0505 + .001794i)\epsilon_o$ 120
- 2.23 Correlation, $\sigma_{C-TC}(f_1, f_2)$, of the clutter return at one frequency, f_1 , with the target/clutter return at a second, f_2 , for normal incidence ($\theta_1 = \theta_2 = 0^\circ$) and for $f_1 = 1120$ MHz. Results are given for a 10 m slab with $z_T = 10$ m and with $\epsilon_0 = \epsilon_2 = \epsilon_o$ and $\epsilon_{1m} = (1.0505 + .001794i)\epsilon_o$ 121
- A.1 Geometry of the layered media for which the Greens function and incident field expressions are calculated. For the Greens function, $\overline{G}_{lm}(\vec{r}, \vec{r}')$, the terms contributing to the propagation of the wave from layer m to layer ℓ are shown for the case where $\ell < m$ 124
- 3.1 Dependence of Phase Fluctuation Variance on elevation angle for $\epsilon_2 = \epsilon_o$ (solid) and $\epsilon_2 = (6.0 + 0.6i)\epsilon_o$ (dash). Results are given at 1.120 GHz for a 10 m slab with $z_T = 10$ m and with $\epsilon_0 = \epsilon_o$ and $\epsilon_{1m} = (1.0505 + .001794i)\epsilon_o$ 148
- 3.2 Dependence of Phase Fluctuation Variance on frequency for normal incidence ($\theta = 0^\circ$). Results are given for a 10 m slab with $z_T = 10$ m and with $\epsilon_0 = \epsilon_2 = \epsilon_o$ and $\epsilon_{1m} = (1.0505 + .001794i)\epsilon_o$ 149

- 3.3 Correlation of Phase Fluctuations over $\theta_d = \theta_2 - \theta_1$ for the HH polarization and for $\theta_1 = 0^\circ$ (solid), $\theta_1 = 40^\circ$ (dash), and $\theta_1 = 60^\circ$ (dots). Results are given at 1.120 GHz for a 10 m slab with $z_T = 10$ m and with $\epsilon_0 = \epsilon_2 = \epsilon_o$ and $\epsilon_{1m} = (1.0505 + .001794i)\epsilon_o$ 152
- 3.4 Correlation of Phase Fluctuations over $\theta_d = \theta_2 - \theta_1$ for the VV polarization and for $\theta_1 = 0^\circ$ (solid), $\theta_1 = 40^\circ$ (dash), and $\theta_1 = 60^\circ$ (dots). Results are given at 1.120 GHz for a 10 m slab with $z_T = 10$ m and with $\epsilon_0 = \epsilon_2 = \epsilon_o$ and $\epsilon_{1m} = (1.0505 + .001794i)\epsilon_o$ 153
- 3.5 Correlation of Phase Fluctuations over $\phi_d = \phi_2 - \phi_1$ for the HH polarization and for $\theta = 20^\circ$ (solid), $\theta = 40^\circ$ (dash), and $\theta = 60^\circ$ (dots). Results are given at 1.120 GHz for a 10 m slab with $z_T = 10$ m and with $\epsilon_0 = \epsilon_2 = \epsilon_o$ and $\epsilon_{1m} = (1.0505 + .001794i)\epsilon_o$ 154
- 3.6 Correlation of Phase Fluctuations over $\phi_d = \phi_2 - \phi_1$ for the VV polarization and for $\theta = 20^\circ$ (solid), $\theta = 40^\circ$ (dash), and $\theta = 60^\circ$ (dots). Results are given at 1.120 GHz for a 10 m slab with $z_T = 10$ m and with $\epsilon_0 = \epsilon_2 = \epsilon_o$ and $\epsilon_{1m} = (1.0505 + .001794i)\epsilon_o$ 155
- 3.7 Correlation of Phase Fluctuations over $f_d = f_2 - f_1$ for normal incidence ($\theta_1 = \theta_2 = 0^\circ$) and for $f_1 = 1120$ MHz (solid), $f_1 = 1110$ MHz (dash), and $f_1 = 1130$ MHz (dots). Results are given for a 10 m slab with $z_T = 10$ m and with $\epsilon_0 = \epsilon_2 = \epsilon_o$ and $\epsilon_{1m} = (1.0505 + .001794i)\epsilon_o$ 156
- 4.1 Geometry of the multi-layer scattering problem with N layers, and with the point target located in layer t , and the random media in layer f 166
- 4.2 Dependence of the coherent target scattering cross section, σ_{T-T} , on elevation angle for $\ell = .0072$ m and $\epsilon_{1m} = (1.0516 + .002417i)\epsilon_o$ (solid) and for $\ell = .0052$ m and $\epsilon_{1m} = (1.0505 + .001794i)\epsilon_o$ (dash). Results are given at 1.120 GHz for a 10 m slab with $z_T = 10$ m and with $\epsilon_0 = \epsilon_2 = \epsilon_o$ 179
- 4.3 Dependence of the incoherent target/clutter scattering cross section, σ_{TC-TC} , on elevation angle for $\ell = .0072$ m and $\epsilon_{1m} = (1.0516 + .002417i)\epsilon_o$ (solid) and for $\ell = .0052$ m and $\epsilon_{1m} = (1.0505 + .001794i)\epsilon_o$ (dash). Results are given at 1.120 GHz for a 10 m slab with $z_T = 10$ m and with $\epsilon_0 = \epsilon_2 = \epsilon_o$. For both solid and dashed curves, the VV result is higher at large incident angles. 181
- 4.4 Correlation of the target/clutter multi-path return, σ_{TC-TC} , over $\phi_d = \phi_2 - \phi_1$ for $\ell = .0072$ m and $\epsilon_{1m} = (1.0516 + .002417i)\epsilon_o$ (solid) and for $\ell = .0052$ m and $\epsilon_{1m} = (1.0505 + .001794i)\epsilon_o$ (dash). Results are given at 1.120 GHz for a 10 m slab with $z_T = 10$ m, $\theta = 60^\circ$, and with $\epsilon_0 = \epsilon_2 = \epsilon_o$ 182
- 4.5 Correlation of the target/clutter multi-path return, σ_{TC-TC} , over $f_d = f_2 - f_1$ for $\ell = .0072$ m and $\epsilon_{1m} = (1.0516 + .002417i)\epsilon_o$ (solid) and for $\ell = .0052$ m and $\epsilon_{1m} = (1.0505 + .001794i)\epsilon_o$ (dash). Results are given with a center

- frequency $f_c = 1.120$ GHz for a 10 m slab with $z_T = 10$ m, $\theta = 60^\circ$, and with $\epsilon_0 = \epsilon_2 = \epsilon_o$ 183
- 4.6 Dependence of the coherent target scattering cross section, σ_{T-T} , on elevation angle for $f_V = 4.17\%$ and $\epsilon_{1m} = (1.1360 + .005478i)\epsilon_o$ (solid) and for $f_V = 1.67\%$ and $\epsilon_{1m} = (1.0505 + .001794i)\epsilon_o$ (dash). Results are given at 1.120 GHz for a 10 m slab with $z_T = 10$ m and with $\epsilon_0 = \epsilon_2 = \epsilon_o$. In each case the random medium correlation length is $\ell = 0.0052$ m. 187
- 4.7 Dependence of the target/clutter scattering cross section, σ_{TC-TC} , on elevation angle for $f_V = 4.17\%$, $\epsilon_{1m} = (1.1360 + .005478i)\epsilon_o$, and $\delta = .433835$ (solid) and for $f_V = 1.67\%$, $\epsilon_{1m} = (1.0505 + .001794i)\epsilon_o$, and $\delta = .146822$ (dash). Results are given at 1.120 GHz for a 10 m slab with $z_T = 10$ m and with $\epsilon_0 = \epsilon_2 = \epsilon_o$. In each case the random medium correlation length is $\ell = 0.0052$ m. 188
- 4.8 Dependence of the target/clutter scattering cross section, σ_{TC-TC} , on elevation angle for $f_V = 0.05\%$, $\epsilon_{1m} = (1.0014 + .000047701i)\epsilon_o$, and $\delta = .003972$ (solid) and for $f_V = 1.67\%$, $\epsilon_{1m} = (1.0505 + .001794i)\epsilon_o$, and $\delta = .146822$ (dash). Results are given at 1.120 GHz for a 10 m slab with $z_T = 10$ m and with $\epsilon_0 = \epsilon_2 = \epsilon_o$. In each case the random medium correlation length is $\ell = 0.0052$ m. 190
- 4.9 Correlation of the target/clutter multi-path return, σ_{TC-TC} , over $\phi_d = \phi_2 - \phi_1$ for $f_V = 4.17\%$, $\epsilon_{1m} = (1.1360 + .005478i)\epsilon_o$, and $\delta = .433835$ (solid) and for $f_V = 1.67\%$, $\epsilon_{1m} = (1.0505 + .001794i)\epsilon_o$, and $\delta = .146822$ (dash). Results are given at 1.120 GHz for a 10 m slab with $z_T = 10$ m, $\theta = 60^\circ$, and with $\epsilon_0 = \epsilon_2 = \epsilon_o$. In each case the random medium correlation length is $\ell = 0.0052$ m. 191
- 4.10 Correlation of the target/clutter multi-path return, σ_{TC-TC} , over $f_d = f_2 - f_1$ for $f_V = 4.17\%$, $\epsilon_{1m} = (1.1360 + .005478i)\epsilon_o$, and $\delta = .433835$ (solid) and for $f_V = 1.67\%$, $\epsilon_{1m} = (1.0505 + .001794i)\epsilon_o$, and $\delta = .146822$ (dash). Results are given at 1.120 GHz for a 10 m slab with $z_T = 10$ m, $\theta = 60^\circ$, and with $\epsilon_0 = \epsilon_2 = \epsilon_o$. In each case the random medium correlation length is $\ell = 0.0052$ m. 192
- 4.11 Dependence of the coherent target scattering cross section, σ_{T-T} , on elevation angle for the uniaxial correlation function with $\ell_\perp = .0052$ m and $\ell_z = .0156$ m (solid) and for the isotropic correlation function with $\ell = .0052$ m (dash). Results are given at 1.120 GHz for a 10 m slab with $z_T = 10$ m and with $\epsilon_0 = \epsilon_2 = \epsilon_o$ 195
- 4.12 Dependence of the target/clutter scattering cross section, σ_{TC-TC} , on elevation angle for the uniaxial correlation function with $\ell_\perp = .0052$ m and $\ell_z = .0156$ m (solid) and for the isotropic correlation function with $\ell = .0052$ m (dash). Results are given at 1.120 GHz for a 10 m slab with $z_T = 10$ m and with $\epsilon_0 = \epsilon_2 = \epsilon_o$ 197

22 LIST OF FIGURES

- 4.13 Correlation of the target/clutter multi-path return, σ_{TC-TC} , over $\phi_d = \phi_2 - \phi_1$ for the uniaxial correlation function with $\ell_{\perp} = .0052$ m and $\ell_z = .0156$ m (solid) and for the isotropic correlation function with $\ell = .0052$ m (dash). Results are given at 1.120 GHz for a 10 m slab with $z_T = 10$ m, with $\theta = 60^\circ$, and with $\epsilon_0 = \epsilon_2 = \epsilon_o$ 198
- 4.14 Correlation of the target/clutter multi-path return, σ_{TC-TC} , over $f_d = f_2 - f_1$ for the uniaxial correlation function with $\ell_{\perp} = .0052$ m and $\ell_z = .0156$ m (solid) and for the isotropic correlation function with $\ell = .0052$ m (dash). Results are given at 1.120 GHz for a 10 m slab with $z_T = 10$ m, with $\theta = 60^\circ$, and with $\epsilon_0 = \epsilon_2 = \epsilon_o$ 199
- 4.15 Dependence of the coherent target scattering cross section, σ_{T-T} , on elevation angle for a three layer configuration with a ground plane (solid) and for a two layer configuration without the added layer (dash). Results are given at 1.120 GHz for a 10 m random slab with $z_T = 15$ m and with $\epsilon_0 = \epsilon_2 = \epsilon_o$ 202
- 4.16 Dependence of the target/clutter scattering cross section, σ_{TC-TC} , on elevation angle for a three layer configuration with a ground plane (solid) and for a two layer configuration without the added layer (dash). Results are given at 1.120 GHz for a 10 m random slab with $z_T = 15$ m and with $\epsilon_0 = \epsilon_2 = \epsilon_o$ 203
- 4.17 Dependence of the coherent target scattering cross section, σ_{T-T} , (solid) and the target/clutter scattering cross section, σ_{TC-TC} , (dash) on the thickness, d_2 , of the target region. Results are shown for normal incidence ($\theta = 0^\circ$) at 1.120 GHz with the target positioned 1 m above the interface between regions 2 and 3 ($z_T = d_2 + d_1 - 1.0$). 205
- 4.18 Dependence of the coherent target scattering cross section, σ_{T-T} , (solid) and the target/clutter scattering cross section, σ_{TC-TC} , (dash) on the target depth, z_T . Results are shown for normal incidence ($\theta = 0^\circ$) at 1.120 GHz with a 10 m slab and with a 6 m depth to the target region. 206
- 4.19 Correlation of the target/clutter multi-path return, σ_{TC-TC} , over $\phi_d = \phi_2 - \phi_1$ for three-layer (solid), and two-layer (dash) configurations. In each case the results are given for a 10 m random slab, a frequency of 1.12 GHz, a 40° elevation angle, and a target depth of 15 m. 207
- 4.20 Correlation of the target/clutter multi-path return, σ_{TC-TC} , over $f_d = f_2 - f_1$ for three-layer (solid), and two-layer (dash) configurations. In each case the results are given for a 10 m random slab, a center frequency of 1.12 GHz, a 40° elevation angle, and a target depth of 15 m. 208
- E.1 Geometry of the layered media for which the Greens function and incident field expressions are calculated. For the Greens function, $\overline{\overline{G}}_{pm}(\vec{r}, \vec{r}')$, the terms

- contributing to the propagation of the wave from layer m to layer p are shown for the case where $p < m$ 232
- 5.1 Geometry of the multi-layer scattering problem with N layers, and with the plate target located in layer t , and the random media in layer f . . . 309
- 5.2 Geometry of an individual polygonal facet composing the target. Shown is the i th facet which is arbitrarily chosen to have three vertices. 310
- 5.3 Scattering mechanisms for target/clutter interaction including the target/clutter multi-path (a), clutter/target multi-path (b), and direct target return (c). 317
- 5.4 Dependence of the coherent target scattering cross section, σ_{T-T} , on elevation angle for a 60 cm by 60 cm square plate. Shown are the HH (dash) and VV (dots) returns at a frequency of 1.12 GHz for a 10 m thick, isotropic random slab, with freespace above and below, and with the target positioned 5 m below the lower interface. Also show for comparison is the freespace plate cross section (solid). 339
- 5.5 Dependence of the coherent target scattering cross section, σ_{T-T} , (solid) and the incoherent multi-path terms, σ_{TC-TC} (long-dash), σ_{CT-CT} (dots), and σ_{TC-CT} (short-dash), on elevation angle for a 60 cm by 60 cm square plate. Shown is the HH polarization at a frequency of 1.12 GHz for a 10 m thick, isotropic random slab, with freespace above and below, and with the target positioned 5 m below the lower interface. 340
- 5.6 Dependence of the coherent target scattering cross section, σ_{T-T} , (solid) and the incoherent multi-path terms, σ_{TC-TC} (long-dash), σ_{CT-CT} (dots), and σ_{TC-CT} (short-dash), on elevation angle for a 60 cm by 60 cm square plate. Shown is the VV polarization at a frequency of 1.12 GHz for a 10 m thick, isotropic random slab, with freespace above and below, and with the target positioned 5 m below the lower interface. 341
- 5.7 Dependence of the coherent target scattering cross section, σ_{T-T} , (solid) and the incoherent multi-path return, σ_{TC-TC} (long-dash), on media thickness for a 60 cm by 60 cm square plate. Shown is the HH polarization at a frequency of 1.12 GHz and at normal incidence to the isotropic random slab, with freespace above and below, and with the target positioned 5 m below the lower interface. 345
- 5.8 Dependence of the coherent target scattering cross section, σ_{T-T} , (solid) and the incoherent multi-path term, σ_{TC-TC} , (long-dash) on target depth for a 60 cm by 60 cm square plate. Shown are the results for normal incidence at a frequency of 1.12 GHz for a 10 m thick, isotropic random slab, with freespace above and below. 346

24 LIST OF FIGURES

- 5.9 Dependence of the coherent target scattering cross section, σ_{T-T} , (solid) and the incoherent multi-path terms, σ_{TC-TC} , (long-dash) on frequency for a 60 cm by 60 cm square plate. Shown is the HH polarization at normal incidence to a 10 m thick, isotropic random slab, with freespace above and below, and with the target positioned 5 m below the lower interface. 348
- 5.10 Dependence of the coherent target scattering cross section, σ_{T-T} , (solid) and the incoherent multi-path terms, σ_{TC-TC} (long-dash), σ_{CT-CT} (dots), and σ_{TC-CT} (short-dash), on azimuth angle for a 60 cm by 60 cm square plate. Shown is the HH polarization at a frequency of 1.12 GHz and elevation angle of $\theta = 50^\circ$, for a 10 m thick, isotropic random slab, with freespace above and below, and with the target positioned 5 m below the lower interface. . . 350
- 5.11 Dependence of the coherent target scattering cross section, σ_{T-T} , (solid) and the incoherent multi-path terms, σ_{TC-TC} (long-dash), σ_{CT-CT} (dots), and σ_{TC-CT} (short-dash), on azimuth angle for a 60 cm by 60 cm square plate. Shown is the VV polarization at a frequency of 1.12 GHz and elevation angle of $\theta = 50^\circ$, for a 10 m thick, isotropic random slab, with freespace above and below, and with the target positioned 5 m below the lower interface. . . 351
- 5.12 Correlation of the incoherent multi-path scattering terms, σ_{TC-TC} (long-dash), σ_{CT-CT} (dots), and σ_{TC-CT} (short-dash), over changes in azimuth angle for a 60 cm by 60 cm square plate. Shown is the HH polarization at a frequency of 1.12 GHz for incidence at 50° to a 10 m thick, isotropic random slab, with freespace above and below, and with the target positioned 5 m below the lower interface. 353
- 5.13 Correlation of the incoherent multi-path scattering terms, σ_{TC-TC} (long-dash), σ_{CT-CT} (dots), and σ_{TC-CT} (short-dash), over changes in azimuth angle for a 60 cm by 60 cm square plate. Shown is the VV polarization at a frequency of 1.12 GHz for incidence at 50° to a 10 m thick, isotropic random slab, with freespace above and below, and with the target positioned 5 m below the lower interface. 354
- 5.14 Correlation of the incoherent multi-path scattering terms, σ_{TC-TC} (long-dash), σ_{CT-CT} (dots), and σ_{TC-CT} (short-dash), over changes in frequency for a 60 cm by 60 cm square plate. Shown is the HH polarization for incidence at 50° to a 10 m thick, isotropic random slab, with freespace above and below, and with the target positioned 5 m below the lower interface. 355
- 5.15 Correlation of the incoherent multi-path scattering terms, σ_{TC-TC} (long-dash), σ_{CT-CT} (dots), and σ_{TC-CT} (short-dash), over changes in frequency for a 60 cm by 60 cm square plate. Shown is the VV polarization for incidence at 50° to a 10 m thick, isotropic random slab, with freespace above and below, and with the target positioned 5 m below the lower interface. 356
- 5.16 Correlation of the incoherent multi-path scattering term, σ_{TC-TC} , over changes in azimuth angle for a 60 cm by 60 cm square plate at depths of

- 10m (solid) and 15m (dash) below the upper interface of the random slab. Shown are the results at a frequency of 1.12 GHz for incidence at 50° to a 10 m thick, isotropic random slab, with freespace above and below. . . . 359
- 5.17 Correlation of the incoherent multi-path scattering term, σ_{TC-TC} , over changes in azimuth angle for a 60 cm by 60 cm square plate, and for incidence at 30° (solid) and 50° (dash) to the random slab. Shown are the results at a frequency of 1.12 GHz for a 10 m thick, isotropic random slab, with freespace above and below, and with the target located 5 m below the lower interface of the slab. . . . 360
- 5.18 Correlation of the incoherent multi-path scattering term, σ_{TC-TC} , over changes in azimuth angle for a 60 cm by 60 cm square plate, and for center azimuths of 0° (solid), 10° (dash), and 20° (dots). Shown are the results at a frequency of 1.12 GHz for incidence at an elevation angle of 50° to a 10 m thick, isotropic random slab, with freespace above and below, and with the target located 5 m below the lower interface of the slab. . . . 361
- 5.19 Correlation of the incoherent multi-path scattering term, σ_{TC-TC} , over changes in frequency for a 60 cm by 60 cm square plate, and for center frequencies of 1110 MHz (solid), 1120 MHz (dash), and 1130 MHz (dots). Shown are the results for incidence at an elevation angle of 50° to a 10 m thick, isotropic random slab, with freespace above and below, and with the target located 5 m below the lower interface of the slab. . . . 362
- 5.20 Correlation of the incoherent multi-path scattering term, σ_{TC-TC} , over changes in azimuth angle for a point target (solid), a 60 cm by 60 cm square plate (dash), and for a 270 cm by 270 cm plate (dots). Shown are the results at a frequency of 1.12 GHz for incidence at an elevation angle of 50° to a 10 m thick, isotropic random slab, with freespace above and below, and with the target located 5 m below the lower interface of the slab. . . . 363
- H.1 Geometry of the layered media for which the Greens function and incident field expressions are calculated. For the Greens function, $\bar{\bar{G}}_{pm}(\bar{r}, \bar{r}')$, the terms contributing to the propagation of the wave from layer m to layer p are shown for the case where $p < m$ 366
- 6.1 Geometry of the multi-layer scattering problem with N layers, and with the electrically small target located in layer t , and the random media in layer f 382
- 6.2 Scattering mechanisms for target/clutter interaction including the direct target return (a), clutter/target multi-path (b), target/clutter multi-path (c), and target/clutter/target multi-path (d) returns. . . . 390
- 6.3 Geometry of the bi-triangular subdomain patch, where T^+ and T^- are the two connected triangular regions of the domain, and where r_c^+ and r_c^- are the respective centroids of these regions. . . . 394

26 LIST OF FIGURES

- 6.4 Geometry of the integration over each triangular subdomain region. Shown is the case where $z_{cm}^a > z'$ for the unshaded region, $T_n^a - T_n^a$ 398
- 6.5 Geometry of the subregions for the substitution of variables in the integration of a triangular region. An arbitrary position, \bar{r}' , is expressed as a weighted average of the triangle corners, \bar{r}_1 , \bar{r}_2 , and \bar{r}_3 , where the weights are found from the ratio of the subregion areas, A_1 , A_2 , and A_3 to the overall area of the triangle. 399
- 7.1 Block Diagram of the simple SAR processor used in the analysis of the random medium's effect on the imaging of a point target. 429
- 7.2 Geometry of the SAR flight path defining the incident and scattering directions for the random media multi-path problem. 434
- 7.3 Coordinate transformation geometry for the transformation from the integration variables x'_1 and x'_2 to x_d and x_1 . The integration region is shaded in each case. 442
- 7.4 Azimuth-Frequency Correlation, σ_{TC-TC} , of the HH polarized target/clutter multi-path field for a two-layer geometry with a 10 m slab of isotropic random media, and with the target positioned 5 m below the slab. Results are shown for an elevation angle of $\theta = 70^\circ$, and with a center frequency of 1.12 GHz. 451
- 7.5 Azimuth-Frequency Correlation, σ_{TC-TC} , of the VV polarized target/clutter multi-path field for a two-layer geometry with a 10 m slab of isotropic random media, and with the target positioned 5 m below the slab. Results are shown for an elevation angle of $\theta = 70^\circ$, and with a center frequency of 1.12 GHz. 453
- 7.6 Range - Cross Range SAR response of a Point target in free space using a 40 MHz bandwidth and an integration angle of approximately 2° . Rectangular weightings were used over the integration aperture and frequency bandwidth. 455
- 7.7 Range - Cross Range SAR response of a Point target 5m below a 10m slab of random media for the HH polarization, using a 40 MHz bandwidth and an integration angle of approximately 2° . Rectangular weightings were used over the integration aperture and frequency bandwidth. 457
- 7.8 Range - Cross Range SAR response of a Point target 5m below a 10m slab of random media for the VV polarization, using a 40 MHz bandwidth and an integration angle of approximately 2° . Rectangular weightings were used over the integration aperture and frequency bandwidth. 459

- 7.9 Range SAR response of a point target in free space (solid) and 5m below a 10m slab of random media (dash) for the HH polarization, using a 40 MHz bandwidth and an integration angle of approximately 2° . Rectangular weightings were used over the integration aperture and frequency bandwidth. . . 463
- 7.10 Range SAR response of a point target in free space (solid) and 5m below a 10m slab of random media (dash) for the VV polarization, using a 40 MHz bandwidth and an integration angle of approximately 2° . Rectangular weightings were used over the integration aperture and frequency bandwidth. . . 464
- 7.11 Coherent (solid) and incoherent (dash) SAR response in range of a point target 5m below a 10m slab of random media for the HH polarization, using a 40 MHz bandwidth and an integration angle of approximately 2° . Rectangular weightings were used over the integration aperture and frequency bandwidth. 465
- 7.12 Coherent (solid) and incoherent (dash) SAR response in range of a point target 5m below a 10m slab of random media for the VV polarization, using a 40 MHz bandwidth and an integration angle of approximately 2° . Rectangular weightings were used over the integration aperture and frequency bandwidth. 466
- 7.13 Range SAR response of a point target 5m below a 10m slab of random media, processed with a filter matched to the freespace case (solid) and to the case of a slab of equivalent effective permittivity (dash). Shown is the HH polarization, using a 40 MHz bandwidth and an integration angle of approximately 2° . Rectangular weightings were used over the integration aperture and frequency bandwidth. 468
- 7.14 Cross range SAR response of a point target in free space (solid) and 5m below a 10m slab of random media (dash) for the HH polarization, using a 40 MHz bandwidth and an integration angle of approximately 2° . Rectangular weightings were used over the integration aperture and frequency bandwidth. 470
- 7.15 Cross range SAR response of a point target in free space (solid) and 5m below a 10m slab of random media (dash) for the VV polarization, using a 40 MHz bandwidth and an integration angle of approximately 2° . Rectangular weightings were used over the integration aperture and frequency bandwidth. 471
- 7.16 Coherent (solid) and incoherent (dash) SAR response in cross range of a point target 5m below a 10m slab of random media for the HH polarization, using a 40 MHz bandwidth and an integration angle of approximately 2° . Rectangular weightings were used over the integration aperture and frequency bandwidth. 472

28 LIST OF FIGURES

- 7.17 Coherent (solid) and incoherent (dash) SAR response in cross range of a point target 5m below a 10m slab of random media for the VV polarization, using a 40 MHz bandwidth and an integration angle of approximately 2° . Rectangular weightings were used over the integration aperture and frequency bandwidth. 473
- 7.18 Total (solid) and incoherent (dash) SAR responses in cross range of a point target 5m below a 10m slab of random media for the HH polarization, and for an integration angle of approximately 2° . Shown is the effect of the processing bandwidth on the cross range response. Rectangular weightings were used over the integration aperture and frequency bandwidth. 475
- 7.19 Total (solid) and incoherent (dash) SAR responses in range of a point target 5m below a 10m slab of random media for the HH polarization, and for a bandwidth of 40 MHz. Shown is the effect of the integration aperture on the range response. Rectangular weightings were used over the integration aperture and frequency bandwidth. 476

Chapter 1

Introduction

Detection and identification of targets buried within layers of vegetation or geophysical media such as snow, ice, or soil, continues to be an area of substantial interest and active research [1-3]. Analysis of electromagnetic sensor systems for applications of this type share the common difficulty that the natural environment surrounding the buried target can not be easily characterized in a deterministic manner, and a statistical description of the media and the resulting electromagnetic propagation and scattering must be employed. Coupling between the deterministic target and its random surroundings modifies the signature of the target, and lends an incoherent component to the signal measured by the sensing system. Prediction of these physical effects of the random environment is necessary, therefore, before the performance of individual

sensing mechanisms may be analyzed.

One such sensing mechanism recently considered for these applications is the use of low frequency, synthetic aperture radar (SAR) with the potential of penetrating geophysical layers, and providing high resolution images of the structures beneath [1-6]. Synthetic aperture radar obtains an azimuth or cross-range resolution which is much sharper than that realizable with a conventional antenna and radar processor. The improved performance is achieved by exploiting the presence of a Doppler shift in the field scattered by points located to the side of the track of the airborne or spaceborne radar platform motion. Frequency analysis of the signal received as a function of position along the flight track allows identification of the cross-range positions of the scatterers with resolution which is finer than the real antenna beamwidth of the radar. This processing of the signal is analogous to coherently integrating the received field over a synthetic aperture which is typically much longer than the physical antenna dimension. High resolution in range is also achieved, either by transmitting a chirped pulse and compressing the received signal, or by stepping the radar frequency over a specified bandwidth and coherently integrating the return at each frequency to synthesize the response of a narrow pulse. The high resolution achievable with SAR provides improved performance in identification applications by allowing higher quality imaging of ground structures than with conventional radar, and in detection applications allows greater accuracy through the higher signal-to-clutter ratios obtainable with smaller resolution cells. Consequently, design and analysis of SAR systems has received considerable attention [1-17].

Propagation and scattering in a random geophysical environment introduces two effects, however, which degrade the performance of SAR systems in both detection and

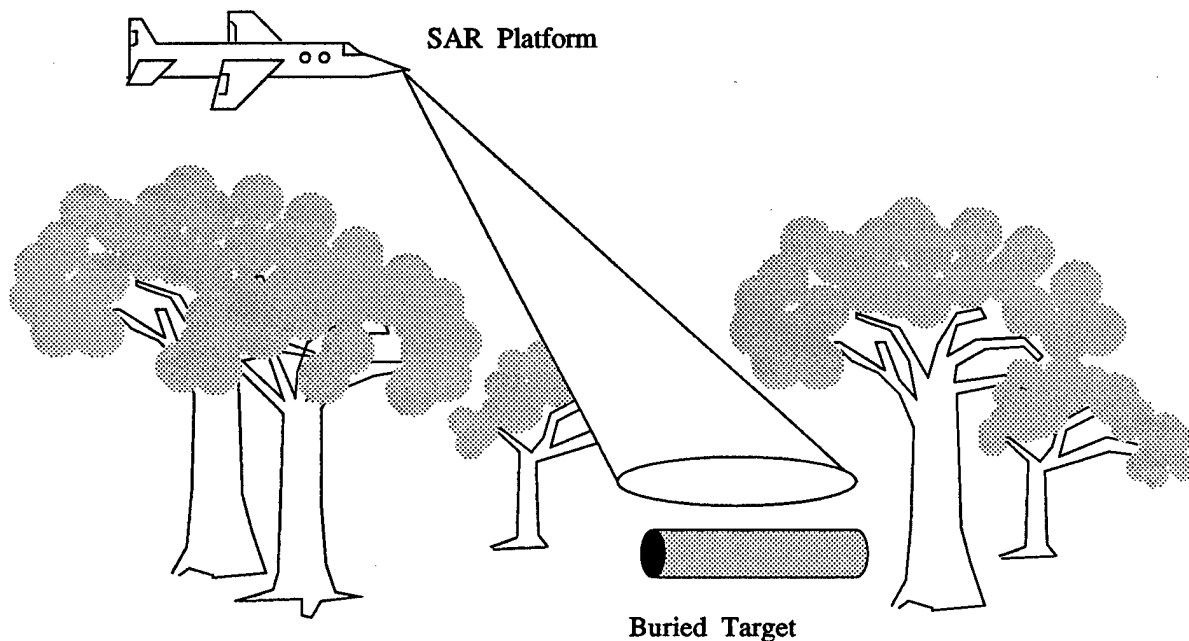


Figure 1.1. An example of the use of penetrating synthetic aperture radar is in the detection and imaging of structures buried beneath forest foliage.

imaging of buried structures. The first effect is the attenuation of the incident and scattered waves, resulting from both absorption and scattering in the random layers. This attenuation reduces the signal-to-clutter ratio, and causes an associated loss of detection accuracy. The second effect is a random phase fluctuation in the scattered field, caused by contributions to the total field, which arise from multi-path scattering in the propagation to and from the target, and which possess random amplitudes and varying phase delays. These multi-path contributions are generated by interactions between the target and random environmental scatterers, and summing these contributions leads to a total return which not only has a random component to its amplitude, but a random phase variation as well. This random phase, which changes with the azimuth of the sensor, limits the ability of the SAR processing to focus over

synthetic apertures which are comparable to or larger than the correlation length of the phase variation, and leads to a reduction in cross-range resolution. Similarly, the fluctuations limit coherency between measurements at distinct frequencies, and reduce the ability to synthesize narrow pulses, and to obtain high resolution in range. To determine the overall performance degradation which arises from the presence of the obscuring foliage, the effects of both attenuation and random phase incoherence on the SAR system must be considered.

While the problems of scattering from deterministic targets and random media have both been treated separately in the past, little theoretical modeling has been considered for the problem of the interaction between a deterministic target and a random surrounding environment. Hence to provide previously unavailable physical insight into this issue, this thesis addresses the problem of scattering from deterministic targets buried in regions of layered random media. Models for the electromagnetic interaction between the target and random media are developed, and these models are used to derive the statistics of the incoherent fields scattered by the target. To facilitate the analysis of SAR and other sensor systems, not only the power scattered by the target and media, but also the correlations of the target signature in aspect angle and frequency are determined. Finally, the results of these physical models are applied with a simple model of a SAR processor, and range-cross range images are formed to illustrate the effect of the random media on the detection and imaging of microwave targets.

1.1. Previous Work

Analysis of these random media effects can be separated into two distinctly different issues, the problem of firstly determining the extent of the attenuation and fluctuations induced by the target environment, and the problem of secondly determining the degradation these levels of signal loss and fluctuation produce in the output of the sensing system signal processor. The first step of this analysis is physical in nature, and requires development of a theoretical model, which describes the electromagnetic interactions between target, and random media, and which allows prediction of the total scattered field of the buried target, and modeling of the signal received by the sensing system. In contrast, the second step is a signal processing issue, requiring analysis of a chosen receiver model to determine the effect of the degradation of the received signal on performance measures, such as resolution or detection accuracy. This later step is not specific to an understanding of the environmental effects, but is common to the prediction of performance under other sources of degradation, and for this reason has received more previous attention. In the following, both facets of this problem are addressed in the context of a specific sensor and specific geophysical environment obscuring the target. Previous analysis of the signal processing issues related to degradation of a synthetic aperture radar system are reviewed first, and a discussion of relevant results relating to propagation and scattering in a forest environment are presented thereafter.

1.1.1. SAR Signal Processing

The primary effect of the attenuation experienced in propagation through geophysical layers is a reduction of the signal-to-clutter and signal-to-noise ratios, for fixed levels of clutter power and receiver noise. Since detection accuracy is primarily determined by the contrast between the signal or target portion of the response, and those portions of the SAR output due to noise sources, the attenuation of the target return will cause a loss in detection accuracy. The receiver operating characteristics, expressing tradeoffs between detection accuracy and false alarm rate, show a dependence on signal-to-noise ratio which has been extensively studied, and is known for a variety of detection algorithms [18-20].

The mean level of received power is also affected by the presence of a multi-path component in the scattered field at the SAR receiver. The interfaces between the stratification layers in the media surrounding the target redirect power in the direction of the receiver, which would otherwise be lost for a target located in free space. Typically, these multi-path returns are composed of a mean coherent part, and a fluctuating or incoherent part, where the later incoherent portion will always increase the total, mean received power, but where the coherent portion will interfere with the direct return, and may either increase or decrease the effective target signature. Hence, these scattering mechanisms will either improve or diminish the signal-to-clutter ratio, and will have a corresponding effect on target detectability. More significantly, however, the incoherent portion of the multi-path return arises from the same random media or rough surface which give rise to the backscattered clutter return, and consequently, this portion of the signal may be correlated with the clutter return. For noise sources

which are correlated with the signal to be detected, a matched filter is no longer the optimal detection processor, and as previously shown, a mis-matched filter will provide improved detection accuracy [21].

Another potential effect of the multi-path portion of the received signal is to introduce either blurring or false targets in the processed SAR image. Multiple reflections between the target and the layered media boundaries will produce return signals with time delays greater than that of the direct return from the target. Consequently these reflections may cause either blurring of the SAR image in the range direction, or if resolved, false target images, spaced in range. A similar effect has been observed previously in the detection of airborne targets with other types of airborne radar [22].

The fluctuations of amplitude and phase present in the incoherent portion of the multi-path return also lead to degradation of the resolution achievable in imaging target structures. If perfectly correlated across the coherent integration angle and frequency bandwidth of the SAR processor, this contribution would lead only to a stronger response in the processed output. However, when this portion becomes decorrelated over the spatial or frequency extents of the processing, the resulting phase errors lead to a response blurred in range and cross-range. Summing this incoherent response with the output due to the coherent portion of the received signal, tends to degrade the overall resolution.

This phase fluctuation effect on SAR performance has been previously investigated in the context of fluctuations arising from atmospheric propagation, uncompensated platform motion, and instabilities of the transmitter/receiver local oscillator [6,10-13]. Greene and Moller [10] examine the effect of Normally distributed random phase errors on synthetic array gain patterns, and employ both analytical and Monte

Carlo approaches to evaluate degradations, which include rms beam canting, beam spread, peak gain reduction, and sidelobe level increase. Under the assumption of small fluctuation variance, the main-lobe to sidelobe power was seen to be the performance measure most sensitive to phase errors. Brown and Palermo [11] consider the effect of phase errors on resolution by examining the spread of the Fourier transform of a function modified by a multiplicative factor of random phase, and obtain simple expressions for the rms tilting and radius of gyration of the pattern. Zelenka and Falk [12] similarly describe the effect on SAR image quality, but for damped, non-stationary phase and amplitude errors characteristic of damped mechanical vibrations of the sensor platform. Both wide-band and narrow-band errors were seen to increase the sidelobe to main-lobe energy ratio, and, consequently, decrease the signal-to-noise ratio of the system. In addition, for the narrow-band case, where the phase error was manifested as a damped sinusoidal function, paired echoes were introduced, leading to high sidelobes which could be misinterpreted as false targets positioned symmetrically about the real target.

For the small bandwidth case, Harger [6] approximates the phase error using the first few terms of its Taylor series. The linear term is seen to produce beam canting, but introduces no loss of resolution or change in sidelobe level. In contrast, quadratic errors are found to cause a loss in resolution, a decrease in the amplitude of the maximum of the response, and an increase in sidelobe level. In each case, the degradation becomes worse as the variance of the phase error is increased. When compared to quadratic errors, cubic errors are seen to cause a more dramatic increase in sidelobe level and a beam canting of the peak, but show less effect on resolution or peak gain. Harger also examines the effect of bandwidth on the above degradations, and shows that,

for fixed variance, all of the performance measures degrade further as the correlation length of the phase error is reduced. For correlation lengths large in comparison to the synthetic aperture, the phase error becomes essentially constant, and a large variance may be tolerated. In contrast, for fluctuations correlated over distances smaller than the synthetic aperture, the variance must be small to avoid catastrophic degradation in performance. Elachi and Evans [13] verify this result numerically, and conclude that the effect on the gain pattern is not appreciable provided that the standard deviation of the phase is less than π , and that the correlation length of the phase is greater than the aperture length.

Considerable attention has also been focused on the problem of optimizing the SAR processing to reduce the effects of the phase fluctuation. Because the noise is multiplicative rather than additive, a linear matched filter processor will no longer be optimal, and in general, better results are possible by employing a nonlinear processing structure. Brown and Palermo [11] consider only a linear processor, but calculate the choice of illumination function or synthetic aperture weighting function which minimizes the mean square resolution. Harger [14] investigates a linear minimum variance estimator for a random signal with complex Gaussian phase error added to random noise, where the correlation length of the phase noise is short in comparison to the aperture length. It is shown that for the purpose of deriving the optimal linear estimator, it is possible to replace the multiplicative error with an equivalent additive error, which results in a processor that is similar to the optimal processor in the absence of the phase noise, but with an optimized gain. Harger also examines the problem of optimal nonlinear processing using the maximum likelihood criterion, and derives a likelihood functional which contains a linear term realizable as a matched filter, and a nonlinear

term in the form of a quadratic functional [15]. In the case where the variance of the multiplicative error approaches zero, the second term of the processor vanishes, and it is shown to reduce to the matched filter which is optimal for additive noise. When the phase error becomes large, however, or the additive noise small, the matched filter component of the processor vanishes, leaving the quadratic functional. This later limiting processor is seen to coherently integrate only over regions in which the phase is well correlated, and then incoherently sum the contributions from each such region. Raney [16] suggests a similar result in the SAR imaging of scenes which are subject to random fade, and concludes that performance is optimized when the partial coherence of the processor is matched to that of the scene.

1.1.2. Forest Propagation

Despite this relatively extensive analysis of SAR processor performance, most of the work presented assumes relatively arbitrary models for the propagation loss and phase noise, and much less effort has been extended to the problem of modeling the physical effects of propagation and scattering in a geophysical environment. Of these effects, only that of mean attenuation has been analyzed extensively, since it is a factor in the performance of other microwave sensors and communications systems. One geophysical medium for which attenuation has received considerable examination is that of forest vegetation. This foliage medium is also of particular interest in the analysis of penetrating synthetic aperture radar systems.

Measurements over a variety of frequency regimes have determined numerous factors which affect foliage attenuation. At frequencies below 800 MHz, Tewari et. al. [23] show an increase in loss with increasing frequency, and a higher attenuation

for vertical polarization than for horizontal, although this latter polarization dependence is seen to diminish at higher frequencies. At microwave and millimeter wave frequencies, Schwering et. al. [24] also observe an increasing loss with frequency, and relatively little polarization dependence. Ulaby et. al. [25] demonstrate this same polarization independence in experiments at L-band. The lack of dependence on orientation at higher frequencies is seen to arise from the random arrangement of the scatterers which compose the canopy layer. In contrast, at lower frequencies, the vertical orientation of the trunk component of the vegetation leads to a higher attenuation for vertical polarization than for horizontal. Measurements by Mougín et. al. [26] of individual, cylindrical-shaped vegetation components such as twigs and needles similarly show that geometrical and orientation parameters are significant for scatterers with radii smaller than a wavelength, but for larger radii, the loss is governed primarily by the biomass and dielectric properties of the scatterers. These results at X-band also show increasing loss with either increasing foliage density or water content. For lower frequency propagation in jungle vegetation, Tewari et. al. [23] observe a similar increase in loss for measurements during the wet season during which both the vegetation and ground contain more moisture. Krevsky [27] compares attenuation through jungle and mid-latitude woods at HF and VHF frequencies, and demonstrates a larger loss for the jungle, resulting from the denser vegetation. The dependence of the mean attenuation on vegetation type and density for propagation through the crown region of individual trees is also shown by Ulaby et. al. [28] at millimeter wavelengths.

The mean power received through a forest transmission path consists of contributions from other propagation mechanisms in addition to the direct wave described above. In particular, at low frequencies, the lateral wave, or "tree-top" mode, which

propagates along the boundary between the vegetation canopy and the air above, may contribute significantly to the received signal. Tewari et. al. [23] show that at frequencies from 50 to 800 MHz, the direct contribution dominates at only extremely short ranges, while the lateral wave is the leading propagation mechanism at longer ranges. For sufficiently low frequencies and long distances, Tamir [29] demonstrates that the sky wave, or single reflection from the ionosphere, may also represent a significant mode. Finally, for an antenna placed near the ground, Dence and Tamir [30] conclude the ground reflection may be important, although this effect is lessened as the antenna is moved to greater heights. These results demonstrate that, in general, boundary effects may impact propagation. In application to the SAR problem, the sky wave will be absent, and it is expected that the importance of the lateral wave will diminish at the higher frequencies of interest where the canopy upper interface becomes less electrically smooth. In contrast, however, the ground reflection may still be significant, and must be considered.

Analysis of these boundary effects becomes further complicated when the problem of scattering from a target placed in the foliage is examined. Coupling between the target and the ground surface or the air-vegetation boundary may alter the scattering characteristics of the target, and modify its effective radar cross section. Scattering from conductors or dielectric inhomogeneities buried in a stratified media has been considered in the analysis of microstrip lines and antennas [115-117], the detection of underground mines, tunnels, or pipes [102], and the reconstruction of soil profiles for geophysical prospecting [118]. Results for the fields scattered by an infinitely long circular cylinder possessing a radial stratified internal structure, and buried in a lossy halfspace, are obtained by Mahmoud et. al. [120]. Multi-pole line current excitations at the cylinder

axis are used to represent the source of the scattered fields, and it is seen that these currents vary significantly when the air-ground interface is removed. Tsalamengas [121] considers scattering from a conducting cylinder buried in a stratified ferrite medium using an integral equation, moment method approach. Similar analysis for cylinders or bodies of revolution at the interface of a layered media is performed by Marx [91] using a method of moments (MoM) approach, and by Chang and Mei [119] using a unimoment approach. Scattering from arbitrarily-shaped buried objects is considered by Hill [123] using the Born approximation for the low contrast case, and by Oates et. al. [102] who give a Finite Difference-Time Domain (FD-TD) solution. General three dimensional formulations for arbitrary objects is presented by Kristensson [122] using the Transition matrix formalism, and by Michalski and Zheng [92-93] using a MoM solution of the mixed potential integral equation (MPIE).

In addition to the boundary interactions, there are also multiple scattering contributions to the received power which arise from the scattering within the inhomogeneous foliage layer. This scattering not only has an effect on the mean level of received power, but causes amplitude and phase fluctuations of the scattered field. Even at low frequencies, Tewari et. al. [23] observe large variations in the received field when moving the antenna by a few wavelengths. Also seen is a substantial depolarization of the received field due to vegetation scattering. At higher frequencies, Schwering et. al. [24] observe both the depolarization effect and a broadening of the antenna beamwidth due to scattering.

Analysis of the phase fluctuation effect is given by Chu [74-76] for the problem of one-way propagation through a foliage layer. Results are presented for both the variance of the fluctuations, and the correlation of the fluctuations with respect to receiver

separation. Ayasli et. al. [1,3,35] and Klein et. al. [2] give results for polarimetric SAR measurements at C, L, and UHF-bands, where tone generators and corner reflectors were placed in forested regions to determine the attenuation and phase fluctuation effects for one and two-way propagation. The dependance of these effects on frequency, polarization, depression angle, vegetation density, and diurnal changes is also examined. The attenuation effect is analyzed by comparing returns from corner reflectors placed in open areas to that from reflectors located under foliage, and the SAR image degradation in cross-range is studied by synthesizing two-way responses from received CW tone generator signals.

1.2. Modeling of Propagation and Scattering

The previous results described above give some insight into both the physical effects of a geophysical environment such as forest vegetation on propagation and scattering, and the corresponding degradations introduced in SAR performance. In particular, polarimetric SAR measurements presented by Ayasli et. al. [1,3] demonstrate both attenuation and phase fluctuation effects. However, too few sites were considered in these measurements to obtain statistical averages for the loss and fluctuations experienced, and to quantitatively determine the effects of the environmental parameters on the results. Consequently, extending these results to forest types, depression angles, or variations of other parameters different from those measured, or to entirely different types of environmental media, is difficult without extensive modeling. Some effort at this modeling is presented by Chu [74-76], but his results are limited to a single layer

of random media with a receiver beneath, and in calculating the correlation function of the phase fluctuations, only the spatial correlation is considered, and only for one-way transmission at normal incidence to the random layer. Hence, to properly treat the problem of scattering from a target in a random environment, more extensive modeling is needed.

This modeling problem consists of two distinct aspects, namely the deterministic problem of treating the interactions of the electromagnetic wave and target, and the stochastic problem of analyzing the scattering of the wave by the random inhomogeneities of the environment surrounding the target. Individually, each of these problems has been considered previously, and a number of models have been developed to treat each. It is the purpose of this thesis to combine these two problems to model scattering from a target in a random environment. Before discussing how these two modeling problems have been merged in this thesis, however, it is useful to review several of the approaches which have been developed to treat the individual problems. In the following, three approaches to modeling an environment with random inhomogeneities are presented first. A number of methods of modeling scattering from deterministic targets are presented thereafter.

1.2.1. Stochastic Medium Scattering

1.2.1.1. Dielectric Slab Model

The simplest model for a forest or other geophysical medium with random inhomogeneities is that of a lossy dielectric slab. This model is utilized by Tamir [29] in the analysis of low frequency, radio propagation through forest and jungle vegetation,

where the forest is represented as a lossy halfspace. Dence and Tamir [30] and Sachs and Wyatt [31] extend the model by including the presence of an imperfectly conducting ground surface, and Cavalcante et. al. [32-33] further refine this representation by utilizing separate layers for the canopy and trunk regions of the vegetation. Tewari et. al. [34] also present a method of determining the relative permittivity and conductivity of the slab from measurements of the attenuation of the lateral wave propagation.

This simple model has found application primarily at low frequencies, where the effect of the inhomogeneous nature of the random region is less significant. Sachs and Wyatt [31] suggest conditions under which the model remains valid, and these restrictions all limit the upper frequencies with which it may be applied. While this model is capable of predicting the mean attenuation through a geophysical layer, it does not predict the incoherent scattering which arises from the inhomogeneities, and consequently can not be used in the SAR problem to determine the phase or amplitude fluctuations of the received signal.

1.2.1.2. Discrete Scatterer Model

To determine the incoherent scattering which arises in the random region, the inhomogeneous character of the environment must be modeled. The most direct method for incorporating this effect is to represent the media as a random ensemble of discrete scatterers in a homogeneous background. These scatterers are described by their shape and scattering characteristics, and by the probability distributions for their size, density, and orientation. The mean field arising for wave propagation through an unbounded region of such scatterers can be determined, and from this field, an effective propagation constant derived. First order incoherent scattering can then be accounted for using the

distorted Born approximation, where the zeroth order field is taken as the mean field derived initially, and where the difference between the scatterer permittivity and that of the effective background media is treated as the source giving rise to the incoherent field.

The discrete scatterer approach was first analyzed using a particle treatment and the Boltzman integro-differential equation for transport processes. This single or independent scattering approach is equivalent to a geometrical optics ray treatment, which neglects the coherence between scatterers, and is only valid for electrically large scatterer separations. Foldy [36] and Tewersky [37] extend this approach to include some multiple scattering, but only for the case of tenuous media. Foldy obtains the propagation constant for the mean field, assuming an ensemble of isotropic point scatterers. Tewersky [37] performs similar analysis, but for a slab of large, tenuous, dielectric spheres, and Brown [38] treats an infinite volume of Rayleigh particles. The multiple scattering treated by the Foldy-Tewersky integral equation is only of the forward scattering type, however, and back-and-forth scattering between particles is neglected. Lax [39] extends the Foldy approximation, by considering anisotropic scattering, and by allowing scatterers which are randomly, partially, or completely ordered, thus, removing the limitation to tenuous media. Tewersky [37] uses this approach to solve for the mean field for non-sparse scattering where the correlation of the scatterers can not be neglected, and applies the Quasi-Crystalline approximation (QCA). Tsang and Kong [40] extend this analysis further, and utilize the Quasi-Crystalline approximation with Coherent Potential (QCA-CP).

This discrete scatterer approach has been applied extensively to model propagation through and scattering from natural environments such as vegetation. Lang

[41] considers a half-space of dielectric discs, and utilizes this model to predict the backscattering coefficients of a leafy canopy. Foldy's approximation is employed to derive an equation for the mean field, allowing determination of the effective propagation constant of the foliage, and the correlation of the scattered field is obtained from the distorted Born approximation. Brown and Curry [42] utilize the Foldy-Tewersky approach along with a Rayleigh scattering assumption to model trunks, branches, and needles as electrically thin cylinders, and to obtain the propagation constant of the coherent field. Lopes et. al. [43] also use an infinite circular cylinder scattering function in determining the polarimetric loss factor for propagation through cylindrically-shaped forest components.

In addition to the above wave theory approach, the effects of propagation and scattering for discrete random media have also been analyzed using the radiative transfer approach. This technique treats the scattering of power in the medium, and yields a simpler method, which neglects coherence effects, but which still allows incorporation of multiple scattering. Tsang et. al. [44] use this method to treat scattering from a layer of randomly oriented, small ellipsoids over a homogeneous dielectric halfspace. For thick layers, it is shown that the results are identical to those obtained with the coherent wave approach utilizing Foldy's method and the distorted Born approximation. A radiative transfer model is utilized by Ulaby et. al. [45] to predict backscattering from a forest canopy at microwave frequencies. Scattering from the canopy, and trunk regions, as well as the ground surface beneath, is considered, and several multiple scattering mechanisms are also included. Ulaby et. al. [28] and Schwering et. al. [24] also use radiative transfer models to analyze propagation through foliage canopies at millimeter wavelengths.

1.2.1.3. Continuous Random Media Model

An alternative to the discrete scatterer approach is to instead model the stochastic medium as a layer of inhomogeneous permittivity, containing a spatially homogeneous mean component, and a randomly fluctuating component which varies continuously as a function of position. In this approach, the physical description of the medium is specified by describing the statistics of the permittivity, including the mean, variance, and spatial correlation of the permittivity fluctuations, and is in contrast to the discrete scatterer approach, where it is the characteristics and statistics of the individual scatterers which is assumed. In this manner, the continuous model, in effect, adds a layer of abstraction in the physical modeling of the medium, since the parameters of the continuous model reflect the underlying discrete nature of the medium, and are chosen to produce the same phenomenological effects, but these parameters are not necessarily directly measurable as any physical feature or quantity of the environment.

As in the discrete scatterer approach, however, to determine the mean attenuation and incoherent scattering produced by the random media, it is necessary to determine first the mean or coherent field, and then the variance or correlation of the field. An integral equation for the mean field may be obtained by treating the fluctuating component of the permittivity as an effective source of radiation, and the solution of this integral equation may be given in the form of an infinite Neumann series. Renormalizing this series, the Dyson equation for the mean field is obtained, where the coherent field is expressed as the zeroth order field in the absence of scattering summed with an integral of the mean field multiplied by a mass operator. This later term accounts, in general, for all coherent scattering effects.

In the limit when the fluctuations of the random media are both of small variance and of small scale (or small correlation length), then scattering has little impact on the effective propagation constant, and the effective permittivity reduces to the mean permittivity. The first order incoherent field can then be found by truncating the original Neumann (Born) series, and utilizing the first order Born approximation, which accounts for single scattering in the media. This approach has been used extensively for media composed of weak scatterers. Tsang and Kong [48] use this method to determine the microwave emissivity of a half-space, and Zuniga and Kong [49] and Zuniga et. al. [50] later applied the Born approximation to determine the backscatter coefficient for the active remote sensing of two-layer and three-layer configurations. In these later configurations, it was shown that unlike the half-space case in which the vertical polarized return is always dominant, the additional interfaces can lead to cases in which the horizontal return is larger. Cross-polarized returns were obtained using the Born approximation, either by assuming anisotropic media [51] or by extending the iteration to second order in albedo [52].

An improved estimate of the effective permittivity is possible if coherent scattering effects are considered. To include these scattering effects, formal solution of the Dyson equation for the mean field is necessary. Since exact solution is intractable, two popular approximations have been considered, the bilocal approximation and the nonlinear approximation. In the bilocal approximation, only the first term of the mass operator is preserved in the Dyson equation, limiting solution to single scattering of the mean wave. Multiple scattering effects are still included in part, but coherence of higher order scattering is omitted, such that back-and-forth scattering is neglected.

Karal and Keller [53-54] apply the bilocal approximation under the assumptions

of weak fluctuations and small scale correlation lengths, and show that the resulting propagation constant for the mean field is complex even for non-dissipative media. This loss arises from scattering in which the power in the coherent wave is transferred to the incoherent portion of the wave, yielding a smaller mean field. Tatarskii and Gertsenshtein [55] remove the restriction of weak fluctuations, and consider strong fluctuation theory in which the bilocal approximation is renormalized. The permittivity of the homogeneous background, or the quasi-static effective permittivity, is no longer taken as the mean permittivity, but is chosen such that the renormalized scattering source has zero mean. Tatarskii [56] extends the above results to the case of large scale fluctuations, removing the restriction to small correlation lengths, and Ryzhov and Tamoikin [57] give conditions for the validity of the bilocal approximation under both large and small scale assumptions.

The initial derivation of the strong fluctuation theory result was done for the case of scalar wave propagation in the random media. For the vector electromagnetic case, the analysis is further complicated by the singular nature of the dyadic Green's function, and straightforward extension of the scalar theory leads to a series expression for the effective permittivity which contains terms in powers of the variance of the fluctuations. This complication adds the further criterion of small variance for validity of the results. Tamoikin [58], however, shows that this restriction, and the presence of the above terms in the series expansion for the permittivity, can be removed by choosing an appropriate exclusion volume for the Green's function, which corresponds in shape to the embedded scatterers which compose the random media. More generally, for a given correlation function describing the permittivity fluctuations, an exclusion volume can be found to eliminate the above secular terms. Tsang and Kong [59] repeat this

analysis, and compare the results of the weak and strong theories for several isotropic and anisotropic correlation functions. Also shown is an equivalence of the results of the random media model with those of the discrete scatterer approach under Foldy's approximation, in the overlapping regions of validity.

An alternative to the bilocal approximation is the nonlinear approximation to the Dyson equation. This approximation has been derived by several, either by resumming the series defining the exact mass operator, or from energy conservation arguments. The approximate integral expression resulting from the nonlinear method differs from that of the bilocal approximation in the replacement of the zeroth order field by the mean field in the approximated mass operator. Consequently, additional scattering terms are included in the nonlinear approximation, and it is generally considered more accurate than the bilocal approximation. Lee and Kong [60] utilize the nonlinear approximation for the problem of a two layer anisotropic random medium, and solve the approximate Dyson equation using a two variable expansion technique.

Most of the above analysis is performed for the case of an unbounded random region. Bassanini et. al. [61] treat the layered case by replacing each random region with the effective permittivity which would result if that region were of infinite extent. In general, however, this approximation is not valid, since for bounded media the integral operators of the Dyson equation are no longer of a convolutional type. The domain of integration will be finite, and the mass operator will no longer depend exclusively on the relative coordinate positions. Rosenbaum [62] considers the problem of a bounded region with permittivity fluctuations in one dimension perpendicular to the boundary. It is seen that the presence of the interface perturbs the mean field to a significant extent over a large distance from the boundary, and results in a graded effective per-

mittivity profile as a function of the distance from the interface. However, in the case of three dimensional fluctuations, it is seen that these interface effects are confined to a transition region at the boundary which is only on the order of a wavelength in thickness. Stogryn [63] applies the bilocal approximation for a bounded region, but explicitly considers the boundary effect, and treats the vertical dependence of the permittivity numerically. The results again show the depth dependence of the permittivity, and indicate an increase in the size of the transition layer for larger correlation lengths, but overall confirm that the transition region is typically small. Fung and Fung [64] utilize the bilocal approximation with a half-space random media, and treat the depth dependence by introducing additional wave modes. Two downward propagation constants are obtained, where the first corresponds to that of the equivalent unbounded case, and where the second is very lossy, creating the transition region of limited extent at the boundary. Tan and Fung [65] also consider the nonlinear approximation to the half-space problem, where the approximated Dyson equation is solved by the two variable expansion technique, yielding a perturbation solution carried out to zeroth order.

Numerous examples exist in which the random medium model has been applied to analyze propagation through or scattering from vegetation, snow and ice, and atmospheric inhomogeneities [66-71]. Fung and Ulaby [69] apply the above half-space model, with strong fluctuation theory and a small scale, cylindrically symmetric correlation function, to analyze the scattering from vegetation. The vegetation is modeled as a combination of water and solid material using the de Loor mixing formula [72], and the solid is modeled as a combination of vegetation material and air using the Pierce mixing formula [73]. Fung [70] later adds the effect of the ground by considering a two layer configuration, and illustrates the dependence of the bistatic scattering coefficients on

vegetation depth, moisture content, and fractional volume. Tan and Fung [71] also consider an azimuthally non-symmetric correlation function to model the depolarization of the bistatically scattered field.

The only attempt to analyze the phase fluctuations induced by propagation through a random layer, is presented by Chu [74-76]. The variance of the phase fluctuations for a receiver below a random layer, and transmitter above is determined for the case of small fluctuations of the phase, where the exponential phase term can be accurately described by the first two terms of its Taylor series. Strong fluctuation theory was employed to determine the effective permittivity, and the distorted Born approximation was carried to first order to obtain the incoherent portion of the transmitted field. The effects of incidence angle, medium depth, fractional volume of scatterers, and correlation length are illustrated. Also considered is the autocorrelation of the phase as a function of receiver separation, for the special case of normal incidence to the layered media.

In addition to the above wave theory approaches, the analysis of continuously random media has also been considered using the radiative transfer method. Tsang and Kong [78] utilize the RT approach and consider thermal emission from a half-space region of laminar structure, possessing one dimensional fluctuations. This half-space problem is later extended to treat media with a nonuniform temperature profile, but with three dimensional random fluctuations [79]. The radiative transfer equations are derived and then solved either with an integral equation approach in the case of small albedo, or with a numerical approach in the more general case. Tsang and Kong [80] also consider the radiative transfer solution for the active remote sensing of a half-space region, and determine the backscatter cross section. The solution is

formulated as a series iteration, where the first term includes single scattering only, and where the second term includes double scattering and leads to depolarization of the field. In addition, it is shown that the radiative transfer equations can be derived from a solution of the Dyson equation using the two variable expansion technique under the nonlinear approximation, and a solution of the Bethe-Salpeter equation under the ladder approximation [81]. Finally, Fisher [82] combines the wave theory and radiative transfer approaches, characterizing the medium on a small scale using the Born approximation, but utilizing transport theory to propagate the average intensity through the media.

1.2.2. Target Scattering

The second aspect of the SAR problem which requires extensive modeling, is the scattering of the incident radiation by the deterministic, but generally complex target, which is to be detected and imaged. When an arbitrary object is illuminated by an electromagnetic wave, part of the incident energy may be absorbed as heat, and the rest is radiated or scattered in many directions. In the radar detection of such an object, what is of interest is the amount of power scattered back towards the transmitter (monostatic case), or the amount scattered to a receiver in some other direction (bistatic case). Radar cross section (RCS) is a measure of this scattered power, and is defined as the area intercepting that amount of power which, when scattered isotropically, produces an echo at the radar equal to that from the object [83].

For most targets of interest, there is no simple relation between the actual physical size of the target, and the effective area seen by the radar. For objects buried in a stratified or inhomogeneous media, the problem is further complicated by the effect

of the boundaries or inhomogeneities. Hence, a variety of methods of estimating the radar cross section have been developed to eliminate the need to rely exclusively on actual measurements (often involving costly facilities and equipment). These prediction techniques have been discussed in a variety of sources [83-124], and are generally grouped into low frequency techniques, applicable to electrically small targets, and high frequency techniques, employing approximate solutions for electrically large, canonical geometries. In the discussion below, both of these classes of prediction methods are considered.

1.2.2.1. Low Frequency Target Modeling

One of the most popular and overall most accurate RCS estimation techniques is the Method of Moments (MoM) [83-93]. MoM predicts the fields scattered by an object by solving numerically the integral form of Maxwell's equations. To determine the currents induced on the target, the surface currents are represented with a set of basis functions of given functional dependence, but of unknown amplitude. This representation reduces the problem from that of determining the surface current as a continuous function defined over the surface, to that of solving for the unknown coefficients of the basis functions. Two types of basis functions, subdomain and entire domain, have been considered, where subdomain basis functions are each defined only on small subsections or patches of the surface, and where entire domain basis functions are often expressed as modes over the entire surface. The resulting integral equation is tested, multiplying the equation by a set of testing or weighting functions and integrating over the surface. In the simplest case the weighting functions are chosen to be Dirac delta functions, and the result is a testing of the integral equation at specific points of the surface.

Alternately, the weighting functions are often chosen identical to the basis functions, and the testing procedure is referred to as Galerkin's method. The effect of testing the integral equation is to convert it to a linear system of equations, which may be solved to determine the unknown coefficients of the basis functions. Once the surface currents are known, it is a simple problem to integrate these currents to determine the scattered fields.

The Method of Moments technique has been extensively applied to a large number of problems [84-93]. Scattering from thin wire structures has been considered both in application to wire antennas [84], and in the use of wire-grid models for more arbitrary conductors [85-86]. A better approximation to scattering from conducting surfaces is given by the triangular grid and bitriangular subdomain method presented by Rao et. al. [87]. This formulation was further extended by Rogers [88] to treat conductors coated with a layer of dielectric. Kiang [89] employed overlapped bitriangular basis functions to treat conductors possessing junctions between target components.

Although the development of the MoM technique was first done for objects in otherwise homogeneous regions, it may be extended to treat targets in stratified media by employing a more complex Green's function which accounts for the presence of the boundaries. Marx [91] considers scattering from cylinders and other bodies of revolution located at the interface of a layered media. More generally, Michalski and Zheng [92-93] formulate the problem of scattering from arbitrary conductors buried in a stratified media using a MoM solution of the mixed potential integral equation.

The advantage of the MoM technique lies in the exact solution it provides, within the limits of the numerical modeling which is necessary. In order to obtain accurate results, however, a relatively dense sampling of the surface current is required, with

approximately ten unknowns per wavelength (or 100 unknowns per square wavelength). This density requirement can result in extremely large systems of equations for large targets or high frequencies, and the necessary matrix inversion can become computationally expensive. Hence, for practical reasons, application of MoM is generally limited to electrically small targets.

A second technique applicable in the case of electrically small targets is the Finite Difference-Time Domain (FD-TD) algorithm [94-102]. In contrast to the MoM approach, where the integral form of Maxwell's equations is solved numerically, the FD-TD technique provides a numerical solution to the differential form of Maxwell's equations. The time-dependant form of these equations is discretized on a spatial and temporal grid, and to truncate the infinite region surrounding the target, a finite computational domain is chosen, and an absorbing boundary condition (ABC) is imposed at the outer surface, preventing reflections of outgoing waves. The fields scattered by the target are found within the computational domain by stepping the discretized equations in time, and alternately computing the electric and magnetic fields at the nodes of the spatial grid. Far field results may be obtained by integrating the near-zone fields over a closed surface about the target.

One of the first formulations of the FD-TD method is that described by Yee [94], where a rectangular grid is chosen, and the center difference approximation is utilized in discretizing Maxwell's equations. Each rectangular box of the lattice is constructed with the electric fields defined at the center points of the edges, and with the magnetic field defined at the center of the faces. This geometry results in approximations to Maxwell's equations which possess second order accuracy in both space and time. Conducting or dielectric scatterers are represented using a staircase approximation to their actual

shape, which accurately models rectangular targets, but is a greater approximation for slanted or curved surfaces. To obtain accurate results, the spacing in the discretization must again be small, and is generally taken as no larger than one tenth of a wavelength. In addition, the maximum temporal step is determined by the smallest grid dimension, and must be set to avoid instabilities in the time stepping procedure.

In two dimensional problems, the above approach can also be applied by considering a two-dimensional rectangular discretization of the scatterer and surrounding region, however, a better approach to model slanted or curved surfaces is to employ a triangular grid [95], which provides a linear interpolation of the scatterer shape. This method also enables a circular or elliptical outer boundary for the computational domain, escaping the problem of treating the absorbing boundary conditions for the corners in the rectangular grid. Maxwell's equations are discretized on the triangular grid using a combination of the finite difference approximation, and the control region approach [96]. In three dimensional problems, a similar approach has been considered using tetrahedral grids, but the complexity of the geometry involved has limited the usefulness of this discretization.

Several choices of absorbing boundary conditions have been considered, but for rectangular grids, the most common is the second-order approximation of Engquist and Majda [97]. For the corners where second-order boundary conditions can not be applied, an average of first-order boundary conditions for the faces forming the corner is often taken. For triangular grids, a second-order boundary condition given by Lee [98] may be employed. Results have shown that for both rectangular and triangular grids, truncation of the lattice with the second-order boundary condition is very effective in eliminating reflections, provided that the wave is incident at an angle near normal to

the surface [99-100].

The Finite Difference-Time Domain algorithm has successfully been applied in the analysis of a great variety of problems. This method has also found application for problems involving layered media or buried structures. Li [101] utilizes FD-TD in the analysis of scattering from surface discontinuities of a conducting plane. For two dimensional discontinuities, both rectangular and triangular grids are applied, the effect of gap size and shape are studied, and the results are compared with those obtained with the MoM approach. A rectangular grid is also employed in the analysis of scattering from three dimensional discontinuities. Oates et. al. [102] apply the FD-TD algorithm to predict scattering from both structural cracks and steel reinforcement buried within a concrete slab. Pulse excitation is utilized to determine the transient response of the concrete structure.

When only sinusoidal steady-state solutions are required, a modification of the FD-TD technique which may be utilized is the Finite Difference-Frequency Domain method. This algorithm again considers the numerical solution of the differential form of Maxwell's equations, but in time-harmonic form. The resulting discretization leads to the formation of a large linear system for the unknown complex field quantities. The number of unknowns in this approach is typically larger than with MoM, since the entire space is discretized, rather than only the target surface, however, the resulting system for FD-FD is sparse, unlike the MoM matrix which is generally full. Solution of the sparse linear system yields the fields within the computational domain, which can again be integrated to obtain the far field results.

1.2.2.2. High Frequency Target Modeling

Practical computational considerations restrict application of the above numerical methods to electrically small structures, where the number of unknowns to be determined remains tractable. To overcome this limitation, several high frequency RCS prediction methods have been utilized. One of the oldest and simplest techniques is that of Geometrical Optics [83,103], which assumes that the incident and scattered fields can be treated as rays, and that all of the scattering is from isolated specular points. Ray tracing is used to follow scattering of the incident field, and a simple relation involving the radii of curvature at the specular point allows calculation of the reflected wave. This method fails, however, for geometries containing caustics, in which an infinite collection of rays converge, as for example in the far field of structures with infinite radius of curvature. Furthermore, Geometrical Optics predicts only surface reflections, and neglects diffraction from edges and surface discontinuities.

This second deficiency was first corrected by Keller [104-105], developing the Geometrical Theory of Diffraction (GTD) [104-106,109] which yields diffraction coefficients to predict the amplitude and phase of the rays diffracted from the edges of a structure. These results were extended by Kouyoumjian and Pathak [107] in the Uniform Theory of Diffraction (UTD) [105,107-108] which eliminated the singularity which Keller's diffraction coefficients suffered at the shadow and reflection boundaries. The singularity experienced for caustics can be eliminated by the Method of Equivalent Currents [83], which defines fictitious non-physical currents on the surface of the object, and then integrates over these to determine the fields. Often, however, this integration must be done numerically.

A better technique to predict the fields scattered from flat or singly curved surfaces is the Method of Physical Optics [83,110-111]. Physical Optics approximates the induced current on the surface by assuming each point locally behaves as if it were part of an infinite planar surface tangent to the surface at that point. The reflected fields are then obtained by integrating over this tangent-plane approximated surface current, and for simple shapes, such as plates and cylinders, this integration can be done analytically to yield closed-form solutions. Although, like Geometrical Optics, Physical Optics neglects the edge-diffraction effect, this diffracted field can be added by Ufimtsev's Physical Theory of Diffraction (PTD) [112-113].

The advantage of these high frequency methods lies in the fact that the results for simple shapes are available in closed form, and, hence, are not computationally expensive to evaluate. More complex targets can be modeled by piecing together the simpler canonical shapes, and adding coherently the contributions from each part. Multiple interactions between target components are more difficult to include, but can be treated in the Geometrical Optics approach at the expense of more complex ray tracing. Some development of multiple scattering methods for Physical Optics has also been performed [114]. Treatment of targets buried in stratified media is similar to that for multiple scattering, and must include explicitly the interactions between the target and boundary interfaces.

1.3. Description of Thesis

The discussion above has detailed several models which have been previously utilized in the analysis of propagation and scattering for media with spatially random inhomogeneities. These models have been applied to the remote sensing of foliage, snow, ice, and a variety of other natural environmental media. Similarly, a number of techniques useful in the prediction of wave interaction with deterministic scatterers have been discussed. These methods have found application in a diversity of problems, including the prediction of target radar cross section, the design of antennas, and the analysis of microstrip line and patch structures. Thus, individually, both the problem of scattering from a deterministic target, and the problem of propagation and scattering in a stochastic medium, have been extensively addressed. The more complex problem, however, in which the deterministic target is surrounded by a random medium, and where the coupling between the target and its stochastic environment is significant, has received little attention.

It is the purpose of this thesis to treat this latter problem of scattering by a deterministic target buried in a layered media. Models are developed for the electromagnetic interaction between the target and random media, and these models are used to characterize statistically the target scattered field, and to determine the effect of the surrounding random environment on the target signature. To facilitate the analysis of SAR and other sensor systems, not only the power scattered by the target, but also the correlations of the target signature in aspect angle and frequency are determined. The results of the physical models are then applied with a simple description of a SAR pro-

cessor to form range-cross range images and illustrate directly the effect of the random media on the detection and imaging of buried targets.

The approach taken here is to begin with a relatively simple configuration, and then to gradually add complexity, both to the media and to the target. Chapter 2 begins the analysis by considering a two region problem, with a bounded slab of continuous random media, characterized by a spherically-symmetric correlation function modeling spherical or statistically isotropic scatterers, and with a point target located in a half-space of isotropic media below the slab. The initial choice of a point target is seen to be useful not only for its simplicity, but also because it is appropriate to an analysis of the impulse response of a synthetic aperture radar or other imaging sensor, and allows analysis of the random media effects on this impulse response. The sensor is assumed to be located at a distant location in the half-space above the random slab, such that the source of illumination is effectively a plane wave, and such that the scattered field of the target is sought in the far-field.

The strong fluctuation theory is applied to derive an effective permittivity for the random layer, and the first order distorted Born approximation is used to determine the incoherent component of the scattered field. The scattered field in this approach is seen to be composed of a coherent term representing the direct return from the target, and two incoherent terms, representing coupling between the target and random media. The variances of the incoherent terms are calculated, and the dependance on incidence angle, target depth, polarization, and slab thickness is examined. The correlations of the incoherent terms over both changes in azimuth angle and changes in frequency are determined, and the dependance of these correlations on elevation angle, target depth, polarization, and center frequency are shown.

Chapter 3 considers an alternate representation of the random media effects examined in the previous chapter. In this new description, the target signature is represented as the coherent return arising in the absence of permittivity fluctuations, multiplied by an exponential of random, complex phase. The real part of this phase is seen to embody the phase fluctuations or phase error of the received signal, while the imaginary part reflects the amplitude fluctuation and mean attenuation of the return. This phase fluctuation representation of the random media effects is useful because it allows comparison with the previous analysis of many other phase error effects of SAR systems, such as platform motion or oscillator instability. For the case where the fluctuations are small, expressions are derived for the variance and correlation of the phase fluctuations, and the dependence of these statistics on several physical and geometrical parameters is illustrated.

Chapter 4 extends the model developed in Chapter 2 by considering additional layers of stratification, and by allowing the permittivity of each region to be uniaxial with a vertically oriented optic axis. The target is a point scatterer as before, but now may be located in an arbitrary region of the layered media. Several independent layers of random media may be considered, where each is characterized by a non-isotropic, but azimuthally symmetric correlation function.

Strong fluctuation theory is again applied to derive the effective permittivity of each random region, and these permittivities are now found to be uniaxial. The distorted Born approximation is again utilized to determine the incoherent component of the scattered field, and the target signature is seen to consist of the same sum of a coherent, direct return and two multi-path interaction terms. Statistics of the incoherent return are calculated, and the effect of elevation angle, polarization, fractional

volume of scatterers, random medium correlation length, a non-isotropic correlation function, and additional layers of stratification on the results for field variance and both azimuthal and frequency correlations is shown.

Chapters 5 and 6 further extend the model of Chapter 4 by considering more realistic targets. Chapter 5 again considers a layered geometry with an arbitrary number of regions, each of uniaxial permittivity, and again allows modeling of multiple, independent, random layers, each characterized by a non-spherical but azimuthally symmetric correlation function. The point target, however, is replaced by a perfectly conducting target of arbitrary shape, composed of flat, polygonal plates. Strong fluctuation theory is again used to calculate the effective permittivities of the random regions, and the first order distorted Born approximation is utilized to treat the scattering from the random media. The scattering from the deterministic target is modeled using a Physical Optics formulation, where the induced surface current is given by the tangent plane approximation. This high frequency approach is useful for electrically large targets and structures possessing electrically slow surface curvature.

Similar to the point target, the plate target is found to possess a signature consisting of a coherent, direct return component, and an incoherent component arising from coupling between the target and random media. Expressions for the variance and correlation statistics of the incoherent scattered fields are derived, and results are illustrated for simple square plate targets. The dependence of these statistics on elevation angle, polarization, target depth, target size, and target orientation is shown, and these results are compared with those of the simpler point target.

In contrast, Chapter 6 treats the same problem of a complex, perfectly conducting target buried in a layered random media, but for the case of an electrically small target.

The numerical Method of Moments approach is used to treat the scattering of the deterministic target. As previously, an effective mean permittivity is derived for each random region using strong fluctuation theory, and the incoherent field scattered by the random media is determined from the first order distorted Born approximation. An integral equation is derived for the current induced on the target, and this current is represented as a weighted series of basis function terms. The integral equation is then tested to produce a linear system of equations which may be solved to determine the unknown basis function weights.

This method is applied to an arbitrary target using bi-triangular subdomain basis functions, and point testing of the integral equation. The target signature is again seen to consist of a coherent or direct scattering return, and an incoherent portion arising from interactions with the random media. Expressions for the statistics, variance and correlation, of the incoherent fields are again derived.

Finally, Chapter 7 utilizes the physical models of the previous chapters, along with a simple SAR processing scheme, to demonstrate the effect of the random media on the imaging capabilities of a SAR system. The scattered field of the target is related to the signal received by the SAR sensor, and a statistical description of the received signal is obtained. The SAR processing algorithm is then employed to produce range-cross range images of a point target beneath a layer of random media, and these are compared with free-space images to determine the extent of the induced blurring and other random media effects. The dependance of the performance degradation on polarization, bandwidth, and integration angle is also shown.

Chapter 8 summarizes the work presented here, comments on some of the more significant results, and suggests future extensions of this modeling and analysis.

Chapter 2

Scattering of a Point Target Beneath a Layer of Continuous Random Media

This chapter begins the analysis of the phenomenological effects of a random scattering environment on the fields received by a synthetic aperture radar. In this initial treatment, the representation of the target environment is limited, with only a single layer of random media characterized by an isotropic correlation function, and with the target taken as a point scatterer, located in a homogeneous half-space below the random layer. The geometry of this model, and the characteristics of the continuous random medium treatment of the target environment are discussed first. Strong Fluctuation theory is employed to determine the effective permittivity of the random layer, and the distorted Born approximation is used to obtain the scattered fields. The total received field is seen to consist of a coherent term representing the direct target

return, an incoherent term due to scattering from the random media alone, and two incoherent multi-path terms, arising from interactions between the target and random media. The statistics of the incoherent fields are calculated, including the variance, and the correlation in both azimuth angle and frequency. Finally, the effect of a variety of geometrical and physical parameters on these statistics is then illustrated.

2.1. Geometry and Random Media Model

The configuration used to investigate the attenuation and phase perturbation effects introduced by the presence of a random layer between the target and radar, is shown in Figure 2.1. A three region, vertically stratified geometry is employed in which region 0 refers to the upper half-space containing the source and observation point, region 1 is the slab containing the random scatterers, and region 2 is the lower half-space containing the target. The upper interface between regions 0 and 1 is taken to be at $z = 0$, and the lower interface at $z = -d$.

The target is taken to be a point target, located at a depth $z = z_T$, and possessing an isotropic cross section for backscatter. This target behaves as a dipole re-radiator of the incident illumination, such that the scattered field can be found as the field arising from a dipole with current density given by (2.1).

$$\bar{J}_T = \alpha \bar{E}_{i_T} \delta(\bar{r} - \bar{r}_T) \quad (2.1)$$

In the above, \bar{E}_{i_T} is the total field incident on the target, \bar{r}_T is the position of the target, and α is a variable parameter which determines the free-space monostatic radar

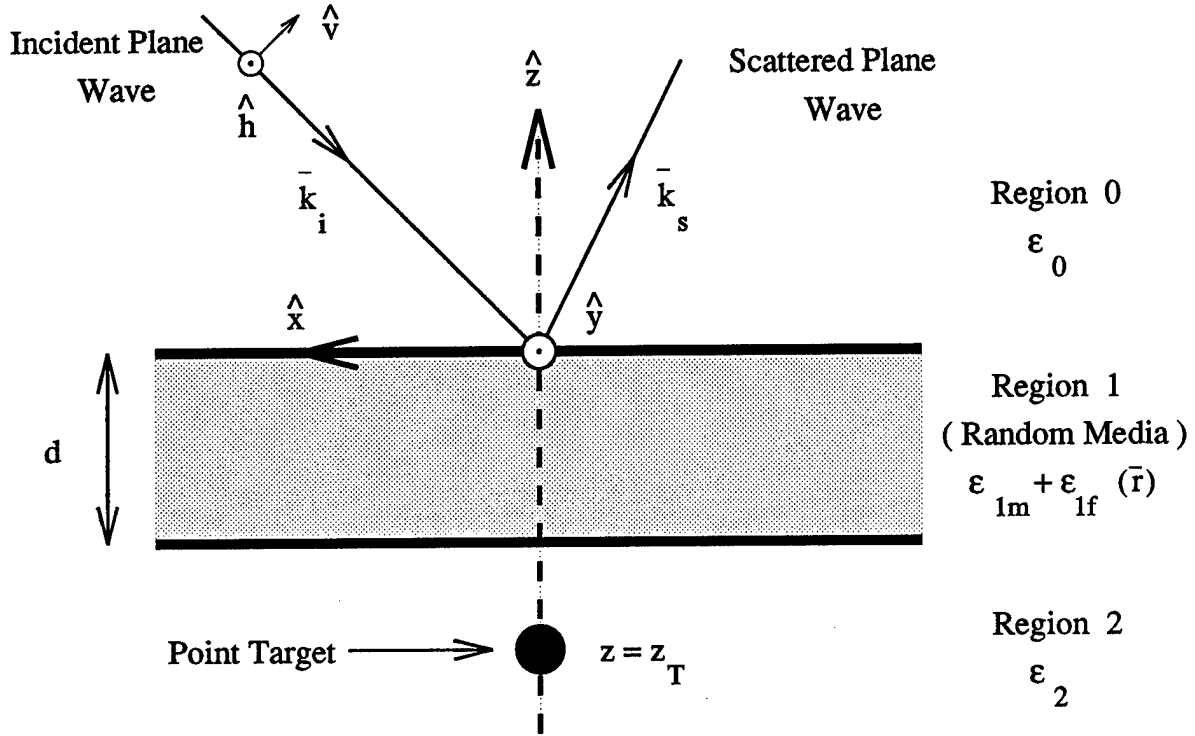


Figure 2.1. Geometry of the buried target problem with a point target located beneath a slab of isotropic random media.

cross section, σ , of the point scatterer. For a chosen value of α , this cross-section can be shown to be given by (2.2),

$$\sigma = \frac{\omega^2 \mu^2 \alpha^2}{2\pi} \quad (2.2)$$

where ω is the angular frequency of the illuminating source, and μ is the free-space permittivity.

For practical SAR systems, the footprint of the real antenna beam main lobe is, in general, sufficiently wide that the quadratic phase delay for ground patches within the footprint can not be neglected. Presently, however, it is of interest to calculate also

the target return and the return due to interaction between the target and surrounding foliage. This later contribution is limited to a region much smaller than the antenna footprint, both by losses in the random layer, and by the near-field effect of a target closely situated to the slab of scatterers. Hence, it is possible to assume the radar is positioned in the far-field of the smaller contributing region, and, thus, that the incident and received fields will have plane wave form. The illuminating field is taken to be given by (2.3),

$$\overline{E}_0 = \left[E_i^{TE} \hat{h}(-k_{0z_i}) + E_i^{TM} \hat{v}(-k_{0z_i}) \right] e^{i\overline{k}_{\perp i} \cdot \overline{r}_{\perp}} e^{-ik_{0z_i} z} \quad (2.3)$$

where $\hat{h}(-k_{0z_i})$ and $\hat{v}(-k_{0z_i})$ are unit vectors in the polarization direction of the incident TE and TM waves respectively, and where

$$\begin{aligned} \overline{k}_{0i} &= k_{x_i} \hat{x} + k_{y_i} \hat{y} - k_{0z_i} \hat{z} \\ &= k(\sin \theta_i \cos \phi_i \hat{x} + \sin \theta_i \sin \phi_i \hat{y} - \cos \theta_i \hat{z}) \end{aligned} \quad (2.4)$$

is the incident propagation vector. A time dependance of $e^{-i\omega t}$ is omitted in the above.

Regions 0 and 2 are assumed to be homogeneous with constant permittivities ϵ_0 and ϵ_2 respectively. Region 1 is assumed to have a spatially random permittivity possessing a spherical correlation function, designed to model the inclusion of spherical scatterers with dimensions which are assumed small in comparison to the illuminating wavelength. To allow high permittivity contrast between the background and embedded materials, Strong Fluctuation theory [55-59] is utilized in determining an effective mean permittivity which accounts for propagation losses in the random layer arising

from both absorption and scattering. Under the above assumptions, the effective permittivity has been shown by Tsang et. al. [143] to be given by (2.5),

$$\epsilon_{eff} = \epsilon_g + \epsilon_o \frac{2}{3} k_o^2 \int_0^\infty dr r C_\xi(\bar{r}) + i \frac{2}{3} k_o^2 k_g \epsilon_o U \quad (2.5)$$

where

$$U = \int_0^\infty dr r^2 C_\xi(\bar{r}) \quad (2.6)$$

and where ϵ_g is the effective permittivity in the extreme low frequency limit where attenuation due to absorption dominates over that due to scattering. Determination of ϵ_g can be made from (2.7), where ϵ_s is the permittivity of the scatterers, and f is their fractional volume.

$$f \left(\frac{\epsilon_s - \epsilon_g}{\epsilon_s + 2\epsilon_g} \right) + (1 - f) \left(\frac{\epsilon_o - \epsilon_g}{\epsilon_o + 2\epsilon_g} \right) = 0 \quad (2.7)$$

In the above, $\xi(\bar{r})$ is the re-normalized scattering source, and its correlation is assumed to take the form of (2.8),

$$C_\xi(|\bar{r}_1 - \bar{r}_2|) = \langle \xi(\bar{r}_1) \xi^*(\bar{r}_2) \rangle = \delta e^{-|\bar{r}_1 - \bar{r}_2|/\ell} \quad (2.8)$$

where δ is the variance of $\xi(\bar{r})$, and where ℓ is the correlation length, determined approximately by the size of the scatterers. The Strong Fluctuation theory derivation of the effective permittivity is described in greater detail in Appendix D. The field arising from scattering by the random media can be determined using the first order distorted Born approximation [66-68,143] given by (2.9),

$$\bar{E}_{0i}^{(1)}(\bar{r}) \simeq k_o^2 \int d\bar{r}' \bar{G}_{01}(\bar{r}, \bar{r}') \cdot \xi(\bar{r}') \cdot \bar{E}_1^{(0)}(\bar{r}') \quad (2.9)$$

where $\overline{\overline{G}}_{01}(\vec{r}, \vec{r}')$ is the dyadic Greens function for the two layer configuration with source in region 1 and observation point in region 0, and which assumes for region 1 the effective permittivity calculated above. $\overline{E}_1^{(0)}(\vec{r})$ is the total zeroth order field in region 1 with the calculated effective permittivity and in the absence of fluctuations.

2.2. Scattering Terms

In the past, the above distorted Born approximation has been used to calculate the backscattering coefficient for a random media [49-50,52,66-68]. For this application, the zeroth order field, $\overline{E}_1^{(0)}(\vec{r})$, is taken to be the incident plane wave, plus the reflections due to the two boundaries. In the present problem, the zeroth order field will also have contributions due to scattering from the target, and the total field in region 1 will take the form of (2.10),

$$\overline{E}_1^{(0)}(\vec{r}) = \overline{E}_{1i}(\vec{r}) + i\omega\mu\alpha \int d\vec{r}' \overline{\overline{G}}_{12}(\vec{r}, \vec{r}') \cdot \overline{E}_{2i}(\vec{r}') \delta(\vec{r}' - \vec{r}_T) \quad (2.10)$$

where the first term is the field due to the incident illumination, and the second term is the field scattered by the target. The above field is scattered by the random media and received at the radar where the scattered field is given by the distorted Born approximation, as in (2.11).

$$\begin{aligned} \overline{E}_{0a}^{(1)} = \int d\vec{r}' \overline{\overline{G}}_{01}(\vec{r}, \vec{r}') \cdot Q(\vec{r}') \cdot [\overline{E}_{1i}(\vec{r}') + i\omega\mu\alpha \int d\vec{r}'' \overline{\overline{G}}_{12}(\vec{r}', \vec{r}'') \cdot \\ \overline{E}_{2i}(\vec{r}'') \delta(\vec{r}'' - \vec{r}_T)] \end{aligned} \quad (2.11)$$

In the above $Q(\bar{r}) = k_0^2 \xi(\bar{r})$, and the outer integral is over the volume of the random slab. In addition to the direct path, however, the field scattered by the random media may also return to the receiver after being scattered by the target. The field scattered by the random media and illuminating the target is given by (2.12),

$$\begin{aligned} \bar{E}_2^{(1)} = \int d\bar{r}' \bar{G}_{21}(\bar{r}, \bar{r}') \cdot Q(\bar{r}') \cdot [\bar{E}_{1i}(\bar{r}') + i\omega\mu\alpha \int d\bar{r}'' \bar{G}_{12}(\bar{r}', \bar{r}'') \cdot \\ \bar{E}_{2i}(\bar{r}'') \delta(\bar{r}'' - \bar{r}_T)] \end{aligned} \quad (2.12)$$

and the scattered field at the receiver is found from (2.13).

$$\begin{aligned} \bar{E}_{0b}^{(1)}(\bar{r}) = i\omega\mu\alpha \int d\bar{r}' \bar{G}_{02}(\bar{r}, \bar{r}') \cdot \delta(\bar{r}' - \bar{r}_T) \cdot \left\{ \int d\bar{r}'' \bar{G}_{21}(\bar{r}', \bar{r}'') \cdot Q(\bar{r}'') \cdot \right. \\ \left. [\bar{E}_{1i}(\bar{r}'') + i\omega\mu\alpha \int d\bar{r}''' \bar{G}_{12}(\bar{r}'', \bar{r}''') \cdot \bar{E}_{2i}(\bar{r}''') \delta(\bar{r}''' - \bar{r}_T)] \right\} \end{aligned} \quad (2.13)$$

The expressions of (2.11) and (2.13) together give all the incoherent scattering terms which arise under the first order distorted Born approximation. It is useful to identify each of these terms individually, and each is shown diagrammatically in Figure 2.2. The first term, shown in Figure 2.2a, is given by (2.14), and represents the scattered field in the absence of the target. This term is the field calculated previously in formulations for the backscattering cross section of the random media [66-68]†, and will be labeled

† The definition of $\bar{E}_C(\bar{r})$ given by (2.14) is inappropriate for the SAR problem, since for this term (unlike the others) the incident field can not be treated as a plane wave, but will exhibit a quadratic phase due to the large real antenna footprint, and an amplitude variation which is a function of the real antenna gain pattern. A corrected definition of $\bar{E}_C(\bar{r})$ is given shortly.

here as the clutter return, $\overline{E}_C(\bar{r})$.

$$\overline{E}_C(\bar{r}) = \int d\bar{r}' \overline{G}_{01}(\bar{r}, \bar{r}') \cdot Q(\bar{r}') \cdot \overline{E}_{1i}(\bar{r}') \quad (2.14)$$

The second term, shown in Figure 2.2b, arises from the wave which scatters first from the target, and then the random media, before returning to the receiver. This term will be denoted the target/clutter multi-path field and is given by (2.15).

$$\overline{E}_{TC}(\bar{r}) = i\omega\mu\alpha \int d\bar{r}' \overline{G}_{01}(\bar{r}, \bar{r}') \cdot Q(\bar{r}') \cdot \int d\bar{r}'' \overline{G}_{12}(\bar{r}', \bar{r}'') \cdot \overline{E}_{2i}(\bar{r}'') \delta(\bar{r}'' - \bar{r}_T) \quad (2.15)$$

The similar term of Figure 2.2c is that given in (2.16), and arises from the wave which is scattered first by the random media, and then by the target, before returning to the receiver. This field represents a second multi-path interaction, and is referred to as the clutter/target term.

$$\overline{E}_{CT}(\bar{r}) = i\omega\mu\alpha \int d\bar{r}' \overline{G}_{01}(\bar{r}, \bar{r}') \cdot \delta(\bar{r}' - \bar{r}_T) \cdot \int d\bar{r}'' \overline{G}_{21}(\bar{r}', \bar{r}'') \cdot Q(\bar{r}'') \cdot \overline{E}_{1i}(\bar{r}'') \quad (2.16)$$

Finally, the last incoherent term shown in Figure 2.2d is given by (2.17), and describes the wave which is scattered first by the target, then by the random media, and finally again by the target. This term is denoted the target/clutter/target return, and is a third multi-path term. However, for reasonable values of α , corresponding to reasonable point scatterer cross sections, this term which represents a higher order multiple

interaction, will be less significant than the first two multi-path mechanisms, and for this reason is neglected in further analysis.

$$\begin{aligned} \overline{E}_{TCT}(\bar{r}) = & -\omega^2 \mu^2 \alpha^2 \int d\bar{r}' \overline{G}_{02}(\bar{r}, \bar{r}') \cdot \delta(\bar{r}' - \bar{r}_T) \cdot \int d\bar{r}'' \overline{G}_{21}(\bar{r}', \bar{r}'') \cdot \\ & Q(\bar{r}'') \cdot \int d\bar{r}''' \overline{G}_{12}(\bar{r}'', \bar{r}''') \cdot \overline{E}_{2i}(\bar{r}''') \cdot \delta(\bar{r}''' - \bar{r}_T) \end{aligned} \quad (2.17)$$

In addition to the incoherent terms, the direct return from the target exists as pictured in Figure 2.2e, and is given by (2.18).

$$\overline{E}_T(\bar{r}) = i\omega\mu\alpha \int d\bar{r}' \overline{G}_{02}(\bar{r}, \bar{r}') \cdot \overline{E}_{2i}(\bar{r}') \cdot \delta(\bar{r}' - \bar{r}_T) \quad (2.18)$$

Neglecting \overline{E}_{TCT} , the total received field is given by the sum of the above terms,

$$\overline{E}_s = \overline{E}_T + \overline{E}_C + \overline{E}_{TC} + \overline{E}_{CT} \quad (2.19)$$

and the corresponding received power is given by (2.20).

$$\begin{aligned} P = & \langle \overline{E}_s \cdot \overline{E}_s^* \rangle \\ = & |\overline{E}_T|^2 + \langle \overline{E}_C \cdot \overline{E}_C^* \rangle + \langle \overline{E}_{TC} \cdot \overline{E}_{TC}^* \rangle + \langle \overline{E}_{CT} \cdot \overline{E}_{CT}^* \rangle + \\ & 2\text{Re} \{ \langle \overline{E}_C \cdot \overline{E}_{TC}^* \rangle + \langle \overline{E}_C \cdot \overline{E}_{CT}^* \rangle + \langle \overline{E}_{TC} \cdot \overline{E}_{CT}^* \rangle \} \end{aligned} \quad (2.20)$$

It is clear from the above that, in general, seven distinct terms contribute to the returned power. However, in the backscatter case of interest for SAR systems, it can be shown that $\overline{E}_{TC}(\bar{r})$ and $\overline{E}_{CT}(\bar{r})$ are reciprocal terms, and, thus, are equal for

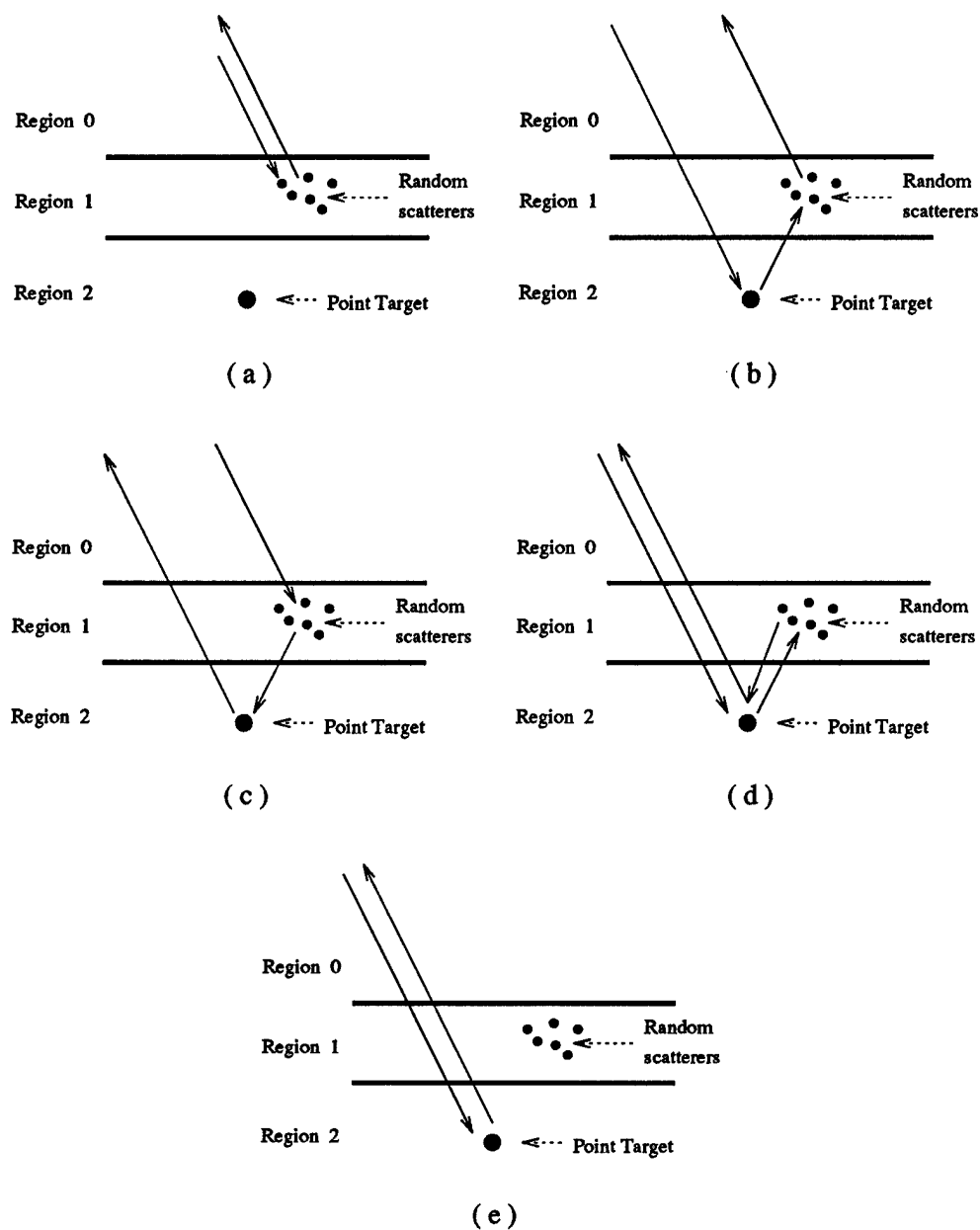


Figure 2.2. Scattering mechanisms for Target-Clutter interaction including the direct clutter return (a), target-clutter multi-path (b), clutter-target multi-path (c), target-clutter-target multi-path (d), and direct target return (e).

horizontal (HH) and vertical (VV) transmit and receive polarization pairs[†]. Hence, the above simplifies to

$$\overline{E}_s = \overline{E}_T + \overline{E}_C + 2\overline{E}_{TC} \quad (2.21)$$

and

$$P = |\overline{E}_T|^2 + \langle \overline{E}_C \cdot \overline{E}_C^* \rangle + 4\langle \overline{E}_{TC} \cdot \overline{E}_{TC}^* \rangle + 4\text{Re} \{ \langle \overline{E}_C \cdot \overline{E}_{TC}^* \rangle \} \quad (2.22)$$

The first term of (2.22) is the expected target return, attenuated by losses in the intervening random media, and represents the coherent return from the target. The second term is the expected return from the clutter, and in the context of SAR will be a function of not only the random media, but also the SAR geometry and antenna pattern. The third term above indicates that the target return is no longer purely deterministic, but now contains a random component, which will lead to both amplitude and phase fluctuations. Finally, the fourth term indicates that the target return, or signal component, and the clutter component are correlated, and this correlation may affect the accuracy of chosen detection algorithms.

[†] For cross polarized returns, $E_{TC}(HV) = E_{CT}(VH)$ and $E_{TC}(VH) = E_{CT}(HV)$.

2.3. Field Calculations

In calculation of the received signal power at a given aspect angle and frequency, only the variances of the above field quantities are required. However, analysis of the effect of the random layer on the coherent SAR processing used to synthesize high resolution in range and cross-range, requires knowledge of the correlation of the field components in angle and frequency. For this reason, the following calculations are generalized to determine $\langle E_1(\bar{k}_{as}, \bar{k}_{ai}) \cdot E_2^*(\bar{k}_{bs}, \bar{k}_{bi}) \rangle$, where \bar{k}_{ai} and \bar{k}_{as} are the incident and scattering propagation vectors for one frequency and one aspect, and where \bar{k}_{bi} and \bar{k}_{bs} are the same for a second frequency-aspect pair. For application to SAR, only the backscatter case with $\bar{k}_{ai} = -\bar{k}_{as}$ and $\bar{k}_{bi} = -\bar{k}_{bs}$, is required, but for completeness the bistatic case is considered.

2.3.1. Target/Clutter Autocorrelation

The first term considered is the autocorrelation of \bar{E}_{TC} , determined from (2.15), and given by (2.23),

$$\begin{aligned}
 \sigma_{TC-TC}^{p_a p_b}(\bar{k}_{as}, \bar{k}_{ai}, \bar{k}_{bs}, \bar{k}_{bi}) &= 4\pi r^2 \langle \hat{p}_a \cdot \bar{E}_{TC}(\bar{k}_{as}, \bar{k}_{ai}) \times \hat{p}_b^* \cdot \bar{E}_{TC}^*(\bar{k}_{bs}, \bar{k}_{bi}) \rangle \\
 &= 4\pi r^2 |\alpha'|^2 \int dV_1 \int dV_2 \int dV_3 \int dV_4 \\
 &\quad \hat{p}_a \cdot \bar{G}_{01}^a(\bar{r}, \bar{r}_1) \cdot \bar{G}_{12}^a(\bar{r}_1, \bar{r}_3) \cdot \bar{E}_{2ai}(\bar{r}_3) \delta(\bar{r}_3 - \bar{r}_T) \times \\
 &\quad \hat{p}_b^* \cdot \bar{G}_{01}^{b*}(\bar{r}, \bar{r}_2) \cdot \bar{G}_{12}^{b*}(\bar{r}_2, \bar{r}_4) \cdot \bar{E}_{2bi}^*(\bar{r}_4) \delta(\bar{r}_4 - \bar{r}_T) \times \\
 &\quad C_Q(\bar{r}_1 - \bar{r}_2)
 \end{aligned} \tag{2.23}$$

where $\alpha' = i\omega\mu\alpha$ and $C_Q(\bar{r}) = k_o^4 C_\xi(\bar{r})$. In the above, \hat{p}_a and \hat{p}_b are the receive

polarizations, which will be taken to be either $\hat{h}(k_{0z})$ or $\hat{v}(k_{0z})$, corresponding to TE and TM polarizations of the scattered waves. It is assumed that the difference in frequencies is sufficiently small that the effective permittivity and renormalized scattering source can be considered the same at the two frequencies. The above is normalized such that for $\bar{k}_{as} = \bar{k}_{bs}$ and $\bar{k}_{ai} = \bar{k}_{bi}$, σ_{TC-TC} is the effective bistatic cross section arising from this multi-path scattering mechanism, and has units of square meters.

The dyadic Greens functions $\bar{G}_{01}(\bar{r}, \bar{r}')$ and $\bar{G}_{12}(\bar{r}, \bar{r}')$ appearing above are given in Appendix A along with the expression for the field $\bar{E}_{2i}(\bar{r})$ incident in region 2. Since the observation point is assumed to be in the far-field of the significant scattering region, the asymptotic, far-field form of $\bar{G}_{01}(\bar{r}, \bar{r}')$ is utilized. Hence, the above can be rewritten as

$$\begin{aligned}
 \sigma_{TC-TC} = & \frac{|\alpha'|^2}{4\pi} \int dV_1 \int dV_2 \int dV_3 \int dV_4 \int d\bar{k}_{\perp a} \int d\bar{k}_{\perp b} \delta(\bar{r}_3 - \bar{r}_T) \delta(\bar{r}_4 - \bar{r}_T) \times \\
 & \left\{ \hat{p}_a \cdot e^{-i\bar{k}_{\perp a} \cdot \bar{r}_{1\perp}} \left[\bar{H}_{01+}^a(\bar{k}_{\perp a}) e^{-ik_{1za}z_1} + \bar{H}_{01-}^a(\bar{k}_{\perp a}) e^{ik_{1za}z_1} \right] \right. \\
 & e^{i\bar{k}_{\perp a} \cdot \bar{r}_{1\perp}} e^{-i\bar{k}_{\perp a} \cdot \bar{r}_{3\perp}} \sum_{q,q'=+,-} \bar{F}_{12_{qq'}}^a(\bar{k}_{\perp a}) e^{iqk_{1za}z_1} e^{-iq'k_{2za}z_3} \\
 & e^{i\bar{k}_{\perp ai} \cdot \bar{r}_{3\perp}} \left[\bar{E}_{2ai}^+ e^{-ik_{2zai}z_3} + \bar{E}_{2ai}^- e^{ik_{2zai}z_3} \right] \Big\} \times \\
 & \left\{ \hat{p}_b \cdot e^{i\bar{k}_{\perp b} \cdot \bar{r}_{2\perp}} \left[\bar{H}_{01+}^{b*}(\bar{k}_{\perp b}) e^{ik_{1zb}^*z_2} + \bar{H}_{01-}^{b*}(\bar{k}_{\perp b}) e^{-ik_{1zb}^*z_2} \right] \right. \\
 & e^{-i\bar{k}_{\perp b} \cdot \bar{r}_{2\perp}} e^{i\bar{k}_{\perp b} \cdot \bar{r}_{4\perp}} \sum_{\ell,\ell'=+,-} \bar{F}_{12_{\ell\ell'}}^{b*}(\bar{k}_{\perp b}) e^{-i\ell k_{1zb}^*z_2} e^{i\ell' k_{2zb}^*z_4} \\
 & e^{-i\bar{k}_{\perp bi} \cdot \bar{r}_{4\perp}} \left[\bar{E}_{2bi}^{+*} e^{ik_{2zbi}^*z_4} + \bar{E}_{2bi}^{-*} e^{-ik_{2zbi}^*z_4} \right] \Big\} \times \\
 & C_Q(\bar{r}_1 - \bar{r}_2)
 \end{aligned} \tag{2.24}$$

where \bar{H}_{01+} , \bar{H}_{01-} , $\bar{F}_{12_{qq'}}$, \bar{E}_{2i}^+ , and \bar{E}_{2i}^- are all defined in Appendix A. Replacing

$C_Q(\bar{r})$ with its spectral representation, keeping only non-zero terms, and using a more compact notation yields (2.25),

$$\begin{aligned} \sigma_{TC-TC} = & \int_{-d}^0 dz_1 \int_{-d}^0 dz_2 \int_{-\infty}^{\infty} d\bar{r}_{1\perp} \int_{-\infty}^{\infty} d\bar{r}_{2\perp} \int dV_3 \int dV_4 \int_{-\infty}^{\infty} d\bar{k}_{\perp a} \int_{-\infty}^{\infty} d\bar{k}_{\perp b} \int_{-\infty}^{\infty} d\beta_z \int_{-\infty}^{\infty} d\bar{\beta}_{\perp} \\ & \delta(\bar{r}_3 - \bar{r}_T) \delta(\bar{r}_4 - \bar{r}_T) \sum_{\substack{s,s',q',\ell'=+ \\ p,p',q,\ell=+,-}} A_{TC-TC}^{pp'ss'qq'\ell'\ell'} \Phi(\bar{\beta}) e^{i(\bar{k}_{\perp a} - \bar{k}_{\perp as} - \bar{\beta}_{\perp}) \cdot \bar{r}_{1\perp}} e^{-i(\bar{k}_{\perp a} - \bar{k}_{\perp ai}) \cdot \bar{r}_{3\perp}} \times \\ & e^{-i(\bar{k}_{\perp b} - \bar{k}_{\perp bs} - \bar{\beta}_{\perp}) \cdot \bar{r}_{2\perp}} e^{i(\bar{k}_{\perp b} - \bar{k}_{\perp bi}) \cdot \bar{r}_{4\perp}} e^{-i(pk_{1za} - qk_{1za} + \beta_z)z_1} e^{-i(q'k_{2za} + sk_{2za})z_3} \times \\ & e^{i(p'k_{1zb} - \ell k_{1zb} + \beta_z)z_2} e^{i(\ell'k_{2zb} + s'k_{2zb})z_4} \end{aligned} \quad (2.25)$$

where

$$\begin{aligned} A_{TC-TC}^{pp'ss'qq'\ell'\ell'} = & \frac{|\alpha'|^2}{4\pi} \left[\hat{p}_a \cdot \bar{H}_{01p}^a(\bar{k}_{\perp as}) \cdot \bar{F}_{12qq'}^a(\bar{k}_{\perp a}) \cdot \bar{E}_{2ai}^s \right] \times \\ & \left[\hat{p}_b \cdot \bar{H}_{01p'}^b(\bar{k}_{\perp bs}) \cdot \bar{F}_{12\ell\ell'}^b(\bar{k}_{\perp b}) \cdot \bar{E}_{2bi}^{s'} \right]^* \end{aligned} \quad (2.26)$$

and the spectral density corresponding to the correlation function, $C_Q(\bar{r})$, of (2.8) is given by

$$\Phi(\bar{\beta}) = \delta k_o^4 \frac{\ell^3}{\pi^2(1 + \beta^2 \ell^2)^2} \quad (2.27)$$

The integrals over \bar{r}_3 and \bar{r}_4 in (2.25) can be done trivially with the use of the two delta functions. In addition, the integral over $\bar{r}_{1\perp}$ can be performed to yield another delta function in $\bar{k}_{\perp a} - \bar{k}_{\perp as} - \bar{\beta}_{\perp}$. This third delta function allows trivial integration over $\bar{\beta}_{\perp}$, with the result given by (2.28).

$$\sigma_{TC-TC} = \int_{-d}^0 dz_1 \int_{-d}^0 dz_2 \int_{-\infty}^{\infty} d\bar{r}_{2\perp} \int_{-\infty}^{\infty} d\bar{k}_{\perp a} \int_{-\infty}^{\infty} d\bar{k}_{\perp b} \int_{-\infty}^{\infty} d\beta_z (2\pi)^2 \sum A_{TC-TC}^{pp'ss'qq'\ell'\ell'} \times$$

$$\begin{aligned}
& \Phi(\bar{k}_{\perp a} - \bar{k}_{\perp as}, \beta_z) e^{-i(\bar{k}_{\perp a} - \bar{k}_{\perp b} - \bar{k}_{\perp ai} + \bar{k}_{\perp bi}) \cdot \bar{r}_{\perp T}} \times \\
& e^{-i(\bar{k}_{\perp b} - \bar{k}_{\perp bs} - \bar{k}_{\perp ai} + \bar{k}_{\perp as}) \cdot \bar{r}_{\perp T}} e^{-i(q'k_{2za} + sk_{2zai} - \ell'k_{2zb}^* - s'k_{2zbi}^*)z_T} \times \\
& e^{-i(pk_{1zas} - qk_{1za} + \beta_z)z_1} e^{i(p'k_{1zbs}^* - \ell k_{1zb}^* + \beta_z)z_2}
\end{aligned} \tag{2.28}$$

Similarly, it is possible to integrate $\bar{r}_{2\perp}$ to obtain a delta function which can be used to perform the $\bar{k}_{\perp a}$ integration. The result is given by (2.29),

$$\begin{aligned}
\sigma_{TC-TC} = & \int_{-d}^0 dz_1 \int_{-d}^0 dz_2 \int_{-\infty}^{\infty} d\bar{k}_{\perp b} \int_{-\infty}^{\infty} d\beta_z (2\pi)^4 \sum A_{TC-TC}^{pp'ss'qq'\ell\ell'} \Phi(\bar{k}_{\perp b} - \bar{k}_{\perp bs}, \beta_z) \times \\
& e^{-i(\bar{k}_{\perp as} - \bar{k}_{\perp bs} - \bar{k}_{\perp ai} + \bar{k}_{\perp bi}) \cdot \bar{r}_{\perp T}} e^{-i(q'k_{2zc} + sk_{2zai} - \ell'k_{2zb}^* - s'k_{2zbi}^*)z_T} \times \\
& e^{-i(pk_{1zas} - qk_{1zc} + \beta_z)z_1} e^{i(p'k_{1zbs}^* - \ell k_{1zb}^* + \beta_z)z_2}
\end{aligned} \tag{2.29}$$

where

$$\bar{k}_{\perp c} = \bar{k}_{\perp b} + \bar{k}_{\perp as} - \bar{k}_{\perp bs} \tag{2.30}$$

and

$$k_{nzc} = \sqrt{k_n^2 - |\bar{k}_{\perp c}|^2} \tag{2.31}$$

$A_{TC-TC}^{pp'ss'qq'\ell\ell'}$ in (2.29) is as in (2.26) but with $\bar{k}_{\perp a}$ replaced by $\bar{k}_{\perp c}$. The two integrations over z_1 and z_2 can be done directly yielding the further simplification of (2.32).

$$\begin{aligned}
\sigma_{TC-TC} = & \int_{-\infty}^{\infty} d\bar{k}_{\perp b} \int_{-\infty}^{\infty} d\beta_z (2\pi)^4 \sum A_{TC-TC}^{pp'ss'qq'\ell\ell'} \Phi(\bar{k}_{\perp b} - \bar{k}_{\perp bs}, \beta_z) \times \\
& e^{-i(\bar{k}_{\perp as} - \bar{k}_{\perp bs} - \bar{k}_{\perp ai} + \bar{k}_{\perp bi}) \cdot \bar{r}_{\perp T}} e^{-i(q'k_{2zc} + sk_{2zai} - \ell'k_{2zb}^* - s'k_{2zbi}^*)z_T} \times \\
& \frac{1 - e^{i(pk_{1zas} - qk_{1zc} + \beta_z)d}}{pk_{1zas} - qk_{1zc} + \beta_z} \cdot \frac{1 - e^{-i(p'k_{1zbs}^* - \ell k_{1zb}^* + \beta_z)d}}{p'k_{1zbs}^* - \ell k_{1zb}^* + \beta_z}
\end{aligned} \tag{2.32}$$

Finally, the integral of (2.32) can be broken into two parts, the first of which is convergent in the upper half-plane of β_z , and the second convergent in the lower half-plane. Poles of the resulting integrands occur at $\beta_z = qk_{1z_c} - pk_{1z_a}$, and $\beta_z = \ell k_{1z_b}^* - p'k_{1z_b}^*$. The spectral function $\Phi(\bar{\beta})$ has poles of its own, but, in the low loss case, the contribution from these will be small in comparison to the dominant poles of the remainder of the integrand, and, therefore, the poles of $\Phi(\bar{\beta})$ are neglected. The result after performing the β_z integral using the appropriate infinite half-circle contours in the upper and lower half-planes, and extracting the residues of the relevant poles, is given by (2.33).

$$\begin{aligned}
 \sigma_{TC-TC} = & (2\pi)^5 i \int_{-\infty}^{\infty} d\bar{k}_{\perp b} \sum_{\substack{s,s',q',\ell'=+ \\ p,p',q,\ell=+,-}} A_{TC-TC}^{pp'ss'qq'\ell\ell'} \times \\
 & e^{-i(\bar{k}_{\perp a} - \bar{k}_{\perp b}, -\bar{k}_{\perp a} + \bar{k}_{\perp b}) \cdot \bar{r}_{\perp T}} e^{-i(qk_{2z_c} + sk_{2z_{ai}} - \ell'k_{2z_b}^* - s'k_{2z_{bi}}^*)z_T} \times \\
 & \left[\frac{\Phi(\bar{k}_{\perp b} - \bar{k}_{\perp b}, \ell k_{1z_b}^* - p'k_{1z_b}^*)}{pk_{1z_a} - qk_{1z_c} + \ell k_{1z_b}^* - p'k_{1z_b}^*} - \frac{\Phi(\bar{k}_{\perp b} - \bar{k}_{\perp b}, qk_{1z_c} - pk_{1z_a})}{pk_{1z_a} - qk_{1z_c} + \ell k_{1z_b}^* - p'k_{1z_b}^*} \times \right. \\
 & \left. e^{i(pk_{1z_a} - qk_{1z_c} + \ell k_{1z_b}^* - p'k_{1z_b}^*)d} \right] \quad (2.33)
 \end{aligned}$$

Elimination of the final integral is not possible without introducing approximations, and in obtaining the results of the next section the above expression was evaluated numerically. The derivations of the clutter/target autocorrelation and the target/clutter - clutter/target correlation are similar to the above and are omitted. The final expressions, however, are given in Appendix B.

2.3.2. Clutter – Target/Clutter Correlation

The second class of correlations to consider are those between the clutter return and the target/clutter or clutter/target multi-path contributions. The original expression for the clutter – target/clutter correlation is obtained by suitably combining (2.14) and (2.15) to yield (2.34).

$$\begin{aligned}
 \sigma_{C-TC}^{p_a p_b}(\bar{k}_{as}, \bar{k}_{ai}, \bar{k}_{bs}, \bar{k}_{bi}) &= 4\pi r^2 \left\langle \hat{p}_a \cdot \bar{E}_C(\bar{k}_{as}, \bar{k}_{ai}) \hat{p}_b^* \cdot \bar{E}_{TC}^*(\bar{k}_{bs}, \bar{k}_{bi}) \right\rangle \\
 &= 4\pi r^2 \alpha'^* \int dV_1 \int dV_2 \int dV_3 \hat{p}_a \cdot \bar{G}_{01}^a(\bar{r}, \bar{r}_1) \cdot \bar{E}_{1ai}^{(0)}(\bar{r}_1) \times \\
 &\quad \hat{p}_b^* \cdot \bar{G}_{01}^{b*}(\bar{r}, \bar{r}_2) \cdot \bar{G}_{12}^{b*}(\bar{r}_2, \bar{r}_3) \cdot \\
 &\quad \bar{E}_{2bi}^{(0)*}(\bar{r}_3 - \bar{r}_T) C_Q(\bar{r}_1 - \bar{r}_2)
 \end{aligned} \tag{2.34}$$

Using the expressions of Appendix A for the Greens functions and incident fields, the above can be rewritten as shown in (2.35),

$$\begin{aligned}
 \sigma_{C-TC} &= \int_{-d}^0 dz_1 \int_{-d}^0 dz_2 \int_{-\infty}^{\infty} d\bar{r}_{1\perp} \int_{-\infty}^{\infty} d\bar{r}_{2\perp} \int dV_3 \int_{-\infty}^{\infty} d\bar{k}_{\perp b} \int d\bar{\beta}_{\perp} \int_{-\infty}^{\infty} d\beta_z \\
 &\quad \delta(\bar{r}_3 - \bar{r}_T) \sum_{\substack{s', q' = + \\ p, p', s, q = +, -}} A_{C-TC}^{pp'ss'qq'} \Phi(\bar{\beta}) \times \\
 &\quad e^{i(\bar{k}_{\perp ai} - \bar{k}_{\perp as} - \bar{\beta}_{\perp}) \cdot \bar{r}_{1\perp}} e^{-i(\bar{k}_{\perp b} - \bar{k}_{\perp bs} - \bar{\beta}_{\perp}) \cdot \bar{r}_{2\perp}} e^{-i(\bar{k}_{\perp bi} - \bar{k}_{\perp b}) \cdot \bar{r}_{3\perp}} \times \\
 &\quad e^{-i(pk_{1zas} + sk_{1zai} + \beta_z)z_1} e^{i(p'k_{1zbs} - qk_{1zb} + \beta_z)z_2} e^{i(q'k_{2zb} + s'k_{2zbi})z_3}
 \end{aligned} \tag{2.35}$$

where

$$\begin{aligned}
 A_{C-TC}^{pp'ss'qq'} &= \frac{\alpha'^*}{4\pi} \left[\hat{p}_a \cdot \bar{H}_{01p}^a(\bar{k}_{\perp as}) \cdot \bar{E}_{1ai}^s \right] \times \\
 &\quad \left[\hat{p}_b^* \cdot \bar{H}_{01p'}^{b*}(\bar{k}_{\perp bs}) \cdot \bar{F}_{12qq'}^b(\bar{k}_{\perp b}) \cdot \bar{E}_{2ai}^{s'} \right]^*
 \end{aligned} \tag{2.36}$$

Performing the integration in a manner analogous to that used previously with the autocorrelation σ_{TC-TC} , yields the final result in closed form given by (2.37),

$$\begin{aligned} \sigma_{C-TC} = & (2\pi)^5 i \sum_{\substack{s', q' = + \\ p, p', s, q = +, -}} A_{C-TC}^{pp'ss'qq'} e^{i(q'k_{2z_b}^* + s'k_{2z_{bi}}^*)z_T} e^{-i(\bar{k}_{\perp bi} - \bar{k}_{\perp ai} - \bar{k}_{\perp bs} + \bar{k}_{\perp as}) \cdot \bar{r}_{\perp T}} \times \\ & \left[\frac{\Phi(\bar{k}_{\perp ai} - \bar{k}_{\perp as}, -p'k_{1z_{bs}}^* + qk_{1z_b}^*)}{pk_{1z_{as}} + sk_{1z_{ai}} - p'k_{1z_{bs}}^* + qk_{1z_b}^*} - \frac{\Phi(\bar{k}_{\perp ai} - \bar{k}_{\perp as}, -pk_{1z_{as}} - sk_{1z_{ai}}^*)}{pk_{1z_{as}} + sk_{1z_{ai}} - p'k_{1z_{bs}}^* + qk_{1z_b}^*} \right] \times \\ & e^{i(pk_{1z_{as}} + sk_{1z_{ai}} - p'k_{1z_{bs}}^* + qk_{1z_b}^*)d} \end{aligned} \quad (2.37)$$

with

$$\bar{k}_{\perp b} = \bar{k}_{\perp ai} + \bar{k}_{\perp bs} - \bar{k}_{\perp as} \quad (2.38)$$

$$k_{nz_b} = \sqrt{k_n^2 - |\bar{k}_{\perp b}|^2} \quad (2.39)$$

The derivation of the clutter-clutter/target return is similar and the final result is given in Appendix B.

2.3.3. Target Autocorrelation

It is necessary to determine the power and correlation of the coherent target return, \bar{E}_T . Beginning with (2.18), and substituting the expressions of Appendix A yields,

$$\begin{aligned} \sigma_{T-T}^{p_a p_b}(\bar{k}_{as}, \bar{k}_{ai}, \bar{k}_{bs}, \bar{k}_{bi}) &= \hat{p}_a \cdot \bar{E}_T(\bar{k}_{as}, \bar{k}_{ai}) \times \hat{p}_b^* \cdot \bar{E}_T^*(\bar{k}_{bs}, \bar{k}_{bi}) \\ &= \sum_{p, p', s, s' = +} A_{T-T}^{pp'ss'} e^{-i(pk_{2z_{as}} + sk_{2z_{ai}} - p'k_{2z_{bs}}^* - s'k_{2z_{bi}}^*)z_T} \times \\ & \quad e^{-i(\bar{k}_{\perp as} - \bar{k}_{\perp bs} - \bar{k}_{\perp ai} + \bar{k}_{\perp bi}) \cdot \bar{r}_{\perp T}} \end{aligned} \quad (2.40)$$

where

$$A_{T-T}^{pp's's'} = \frac{|\alpha'|^2}{(4\pi r)^2} \left[\hat{p}_a \cdot \overline{\overline{H}}_{02_p}^a(\bar{k}_{\perp a,s}) \cdot \overline{E}_{2_{ai}}^s \right] \times \left[\hat{p}_b \cdot \overline{\overline{H}}_{02_{p'}}^b(\bar{k}_{\perp b,s}) \cdot \overline{E}_{2_{bi}}^{s'} \right]^* \quad (2.41)$$

2.3.4. Clutter Autocorrelation

Unlike the calculation of previous terms, formulation of the clutter return power and autocorrelation requires knowledge of the geometry of the SAR system and specification of the antenna pattern. This requirement arises because the region from which scattering contributes to the received field is not limited to a small area about the target, but is instead limited only by the finite beamwidth of the real antenna pattern. This larger effective scattering region is, in general, sufficiently large that the radar is no longer in the far-field, and the linear phase dependence over the scattering region must be augmented by a quadratic term. The geometry considered here is more general than that required in the SAR application, and, as shown in Figure 2.3, allows for four separate antenna patterns, two transmit and two receive, each with its own orientation.

For a radar located at (x_r, y_r, z_r) and a beam center at $(x_c, y_c, 0)$, the distance to a point $(x_c + x, y_c + y, 0)$ is given approximately by (2.42),

$$\begin{aligned} r &= \sqrt{z_r^2 + (y_r - y_c - y)^2 + (x_r - x_c - x)^2} \\ &\approx r_c - x \frac{(x_r - x_c)}{r_c} - y \frac{(y_r - y_c)}{r_c} + \frac{x^2 + y^2}{2r_c} \end{aligned} \quad (2.42)$$

where

$$r_c = \sqrt{z_r^2 + (y_r - y_c)^2 + (x_r - x_c)^2} \quad (2.43)$$

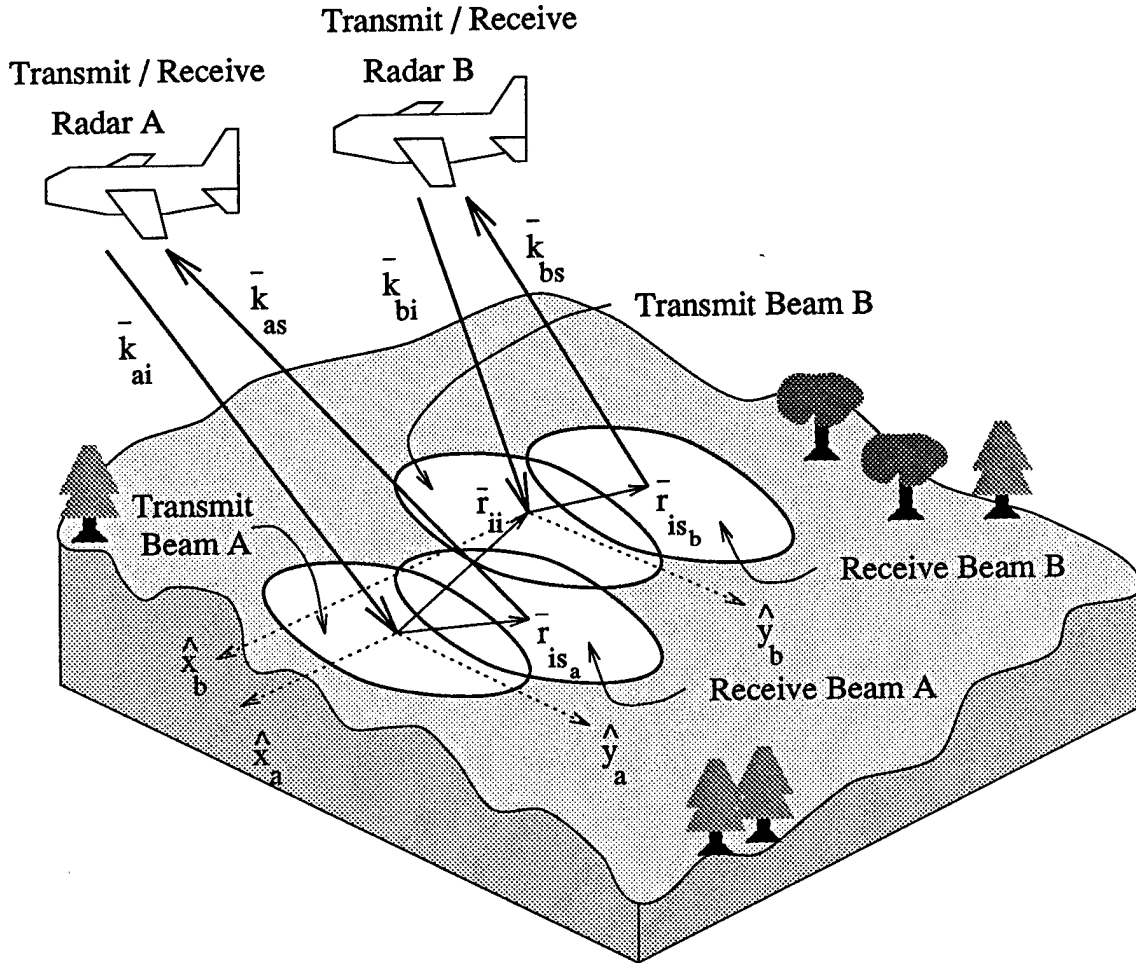


Figure 2.3. Geometry of the SAR antenna patterns for transmit and receive and for two different orientations.

Hence, the phase delay, ikr , can be written as

$$\begin{aligned} ikr &\approx ikr_c \pm i\bar{k}_\perp \cdot \bar{r}_\perp + ik \frac{x^2 + y^2}{2r_c} \\ &= ikr_c \pm i\bar{k}'_\perp \cdot \bar{r}_\perp \end{aligned} \quad (2.44)$$

where

$$\bar{r}_\perp = x\hat{x} + y\hat{y} \quad (2.45)$$

$$\bar{k}'_{\perp} = \bar{k}_{\perp} \pm \frac{1}{2} \frac{k}{r_c} \bar{r}_{\perp} \quad (2.46)$$

and where the positive sign is taken for \bar{k}_{\perp} in the incident direction (radar to ground), and the negative sign is taken for \bar{k}_{\perp} in the scattering direction. If the center of the first incident beam (a) is taken as the origin of a ground coordinate system from which $\bar{r}_{\perp a}$ and $\bar{r}_{\perp b}$ are measured, then the positions measured from each of the beam centers are given by (2.47),

$$\bar{r}_{\perp ai} = \bar{r}_{\perp a} \quad (2.47a)$$

$$\bar{r}_{\perp as} = \bar{r}_{\perp a} - \bar{r}_{is_a} \quad (2.47b)$$

$$\bar{r}_{\perp bi} = \bar{r}_{\perp b} - \bar{r}_{ii} \quad (2.47c)$$

$$\bar{r}_{\perp bs} = \bar{r}_{\perp b} - \bar{r}_{ii} - \bar{r}_{is_b} \quad (2.47d)$$

where \bar{r}_{ii} , \bar{r}_{is_a} , and \bar{r}_{is_b} are as shown in Figure 2.3. Using (2.47), the perpendicular components of each propagation vector at each position on the ground can be written from (2.46) as given in (2.48).

$$\bar{k}'_{\perp ai} = \bar{k}_{\perp ai} + \frac{1}{2} \frac{k_a}{r_{ai}} \bar{r}_{\perp a} \quad (2.48a)$$

$$\bar{k}'_{\perp as} = \bar{k}_{\perp as} - \frac{1}{2} \frac{k_a}{r_{as}} (\bar{r}_{\perp a} - \bar{r}_{is_a}) \quad (2.48b)$$

$$\bar{k}'_{\perp bi} = \bar{k}_{\perp bi} + \frac{1}{2} \frac{k_b}{r_{bi}} (\bar{r}_{\perp b} - \bar{r}_{ii}) \quad (2.48c)$$

$$\bar{k}'_{\perp bs} = \bar{k}_{\perp bs} - \frac{1}{2} \frac{k_b}{r_{bs}} (\bar{r}_{\perp b} - \bar{r}_{ii} - \bar{r}_{is_b}) \quad (2.48d)$$

The above propagation vectors describe the local plane wave nature of the fields at each point on the surface. If it is assumed that locally the fields can be calculated as

if the incident and scattered fields are indeed plane waves, weighted by the antenna gain to that point on the surface, then the ratio of the received to transmitted power is given by (2.49).

$$\begin{aligned}
 P_{C-C}^{p_a p_b} = & \frac{\lambda_a \lambda_b}{(4\pi)^4 r_{ai} r_{as} r_{bi} r_{bs}} e^{i(k_a r_{ai} + k_a r_{as} - k_b r_{bi} - k_b r_{bs})} \int dz_a \int d\bar{r}_{\perp a} \int dz_b \int d\bar{r}_{\perp b} \\
 & \hat{p}_a \cdot e^{-i\bar{k}'_{\perp a} \cdot (\bar{r}_{\perp a} - \bar{r}_{is_a})} \left[\overline{H}_{01+}^a(\bar{k}'_{\perp a}) e^{-ik'_{1z_a} z_a} + \overline{H}_{01-}^a(\bar{k}'_{\perp a}) e^{ik'_{1z_a} z_a} \right] \\
 & e^{i\bar{k}'_{\perp a} \cdot \bar{r}_{\perp a}} \left[\overline{E}_{1ai}^+(\bar{k}'_{\perp a}) e^{-ik'_{1z_{ai}} z_a} + \overline{E}_{1ai}^-(\bar{k}'_{\perp a}) e^{ik'_{1z_{ai}} z_a} \right] \times \\
 & \hat{p}_b^* \cdot e^{i\bar{k}'_{\perp b} \cdot (\bar{r}_{\perp b} - \bar{r}_{ii} - \bar{r}_{is_b})} \left[\overline{H}_{01+}^{b*}(\bar{k}'_{\perp b}) e^{ik'_{1z_b} z_b} + \overline{H}_{01-}^{b*}(\bar{k}'_{\perp b}) e^{-ik'_{1z_b} z_b} \right] \\
 & e^{-i\bar{k}'_{\perp b} \cdot (\bar{r}_{\perp b} - \bar{r}_{ii})} \left[\overline{E}_{1bi}^{+*}(\bar{k}'_{\perp b}) e^{ik'_{1z_{bi}} z_b} + \overline{E}_{1bi}^{-*}(\bar{k}'_{\perp b}) e^{-ik'_{1z_{bi}} z_b} \right] C_Q(\bar{r}_{\perp a} - \bar{r}_{\perp b}) \times \\
 & \sqrt{G_{ai}(\bar{r}_{\perp a}) G_{as}(\bar{r}_{\perp a} - \bar{r}_{is_a}) G_{bi}(\bar{r}_{\perp b} - \bar{r}_{ii}) G_{bs}(\bar{r}_{\perp b} - \bar{r}_{ii} - \bar{r}_{is_b})} \quad (2.49)
 \end{aligned}$$

It is also assumed in the above that the antenna patterns are real (symmetric aperture distributions), such that the antenna pattern does not introduce a direction dependent phase term. The far field Green's function kernel, \overline{H}_{01} , and the expression for the incident field, \overline{E}_{1i} , are given in Appendix A. In order to express the above in a form more similar to previous terms, a near-field radar cross section can be defined as in (2.50),

$$\sigma = P \frac{(4\pi)^3 r_{\text{avg}}^4}{\lambda_a \lambda_b G_a G_b} \quad (2.50)$$

where $r_{\text{avg}} = (r_{ai} + r_{as} + r_{bi} + r_{bs})/4$, $G_a = (G_{ai} + G_{as})/2$, and $G_b = (G_{bi} + G_{bs})/2$, with G_{ai} , G_{as} , G_{bi} , and G_{bs} the peak gains of the four antennas.† Hence, rewriting (2.49)

† The above near-field radar cross section definition is not necessary and is some-

in RCS form, using a more compact notation, and eliminating the absolute phase term yields,

$$\begin{aligned} \sigma_{C-C}^{p_a p_b} = & \int dz_a \int d\bar{r}_{\perp a} \int dz_b \int d\bar{r}_{\perp b} \sum_{p, p', s, s' = +, -} A_{C-C}^{pp'ss'} \times \\ & e^{i(\bar{k}'_{\perp ai} - \bar{k}'_{\perp as}) \cdot \bar{r}_{\perp a}} e^{-i(\bar{k}'_{\perp bi} - \bar{k}'_{\perp bs}) \cdot \bar{r}_{\perp b}} C_Q(\bar{r}_{\perp a} - \bar{r}_{\perp b}) \times \\ & e^{-ipk'_{1za} z_a} e^{-isk'_{1za} z_a} e^{ip'k'_{1zb} z_b} e^{is'k'_{1zb} z_b} \end{aligned} \quad (2.51)$$

where

$$\begin{aligned} A_{C-C}^{pp'ss'} = & \frac{1}{4\pi} \frac{r_{\text{avg}}^4}{r_{ai} r_{as} r_{bi} r_{bs}} \left[\hat{p}_a \cdot \bar{H}_{01p}^a(\bar{k}'_{\perp as}) \cdot \bar{E}_{1ai}^s(\bar{k}'_{\perp ai}) \right] \times \\ & \left[\hat{p}_b \cdot \bar{H}_{01p'}^b(\bar{k}'_{\perp bs}) \cdot \bar{E}_{1bi}^{s'}(\bar{k}'_{\perp bi}) \right]^* \times \\ & \sqrt{\frac{G_{ai}(\bar{r}_{\perp a})}{G_a} \cdot \frac{G_{as}(\bar{r}_{\perp a} - \bar{r}_{is_a})}{G_a} \cdot \frac{G_{bi}(\bar{r}_{\perp b} - \bar{r}_{ii})}{G_b} \cdot \frac{G_{bs}(\bar{r}_{\perp b} - \bar{r}_{ii} - \bar{r}_{is_b})}{G_b}} \times \\ & e^{i\bar{k}'_{\perp as} \cdot \bar{r}_{is_a}} e^{-i\bar{k}'_{\perp bs} \cdot \bar{r}_{is_b}} e^{i(\bar{k}'_{\perp bi} - \bar{k}'_{\perp bs}) \cdot \bar{r}_{ii}} \end{aligned} \quad (2.52)$$

To perform the integration in the above expression, the variable transformation, $\bar{r}_{\perp b} = \bar{r}_{\perp a} - \bar{r}_{\perp d}$, is first introduced. The correlation function limits the contributions to the integral to be from the region where $\bar{r}_{\perp d}$ is small, typically the first few correlation lengths. Since it is also assumed that the correlation length is small compared to a wavelength, the variation of $\bar{k}'_{\perp bi}$ and $\bar{k}'_{\perp bs}$ (and consequently k'_{1zbi} and k'_{1zbs}) with $\bar{r}_{\perp d}$ can be neglected. Physically this approximation corresponds to the assumption that what arbitrary, but makes more sense for the SAR problem where typically $r_{ai} = r_{as} = r_{bi} = r_{bs}$ and $G_{ai} = G_{as} = G_{bi} = G_{bs}$.

the plane wave approximation is valid over a distance of several correlation lengths. Making the substitution of variables, utilizing this approximation, and representing the correlation function by the transform of its spectral density, (2.53) is obtained.

$$\begin{aligned} \sigma_{C-C} = & \int dz_a \int d\bar{r}_{\perp a} \int dz_b \int d\bar{r}_{\perp b} \int d\beta_z \int d\bar{\beta}_{\perp} \sum A_{C-C}^{pp'ss'} \Phi(\bar{\beta}) \times \\ & e^{i(\bar{k}'_{\perp ai} - \bar{k}'_{\perp as} - \bar{k}'_{\perp bi} + \bar{k}'_{\perp bs}) \cdot \bar{r}_{\perp a}} e^{i(\bar{k}'_{\perp bi} - \bar{k}'_{\perp bs} - \bar{\beta}_{\perp}) \cdot \bar{r}_{\perp b}} \times \\ & e^{-i(pk'_{1za} + sk'_{1zai} + \beta_z)z_a} e^{i(p'k'_{1zb} + s'k'_{1zbi} + \beta_z)z_b} \end{aligned} \quad (2.53)$$

In the above, $\bar{k}'_{\perp ai}$ and $\bar{k}'_{\perp as}$ are as in (2.48), and $\bar{k}'_{\perp bi}$ and $\bar{k}'_{\perp bs}$ are as in (2.48) with $\bar{r}_{\perp a}$ replacing $\bar{r}_{\perp b}$. The integration over $\bar{r}_{\perp b}$ may be performed to yield a delta function in $\bar{k}'_{\perp bi} - \bar{k}'_{\perp bs} - \bar{\beta}_{\perp}$, which can then be used to perform the $\bar{\beta}_{\perp}$ integration. The result is given by (2.54).

$$\begin{aligned} \sigma_{C-C} = & \int dz_a \int dz_b \int d\bar{r}_{\perp a} \int d\beta_z (2\pi)^2 \sum A_{C-C}^{pp'ss'} \Phi(\bar{k}'_{\perp bi} - \bar{k}'_{\perp bs}, \beta_z) \times \\ & e^{i(\bar{k}'_{\perp ai} - \bar{k}'_{\perp as} - \bar{k}'_{\perp bi} + \bar{k}'_{\perp bs}) \cdot \bar{r}_{\perp a}} e^{-i(pk'_{1za} + sk'_{1zai} + \beta_z)z_a} \times \\ & e^{i(p'k'_{1zb} + s'k'_{1zbi} + \beta_z)z_b} \end{aligned} \quad (2.54)$$

The two z integrations can then be performed directly to obtain (2.55).

$$\begin{aligned} \sigma_{C-C} = & \int d\bar{r}_{\perp a} \int d\beta_z (2\pi)^2 \sum A_{C-C}^{pp'ss'} \Phi(\bar{k}'_{\perp bi} - \bar{k}'_{\perp bs}, \beta_z) e^{i(\bar{k}'_{\perp ai} - \bar{k}'_{\perp as} - \bar{k}'_{\perp bi} + \bar{k}'_{\perp bs}) \cdot \bar{r}_{\perp a}} \times \\ & \frac{1 - e^{i(pk'_{1za} + sk'_{1zai} + \beta_z)d}}{pk'_{1za} + sk'_{1zai} + \beta_z} \cdot \frac{1 - e^{-i(p'k'_{1zb} + s'k'_{1zbi} + \beta_z)d}}{p'k'_{1zb} + s'k'_{1zbi} + \beta_z} \end{aligned} \quad (2.55)$$

Finally, the β_z integration can be evaluated using contour integration methods as discussed previously for σ_{TC-TC} . The final result below gives the correlation as an

integral over the illuminated surface.

$$\begin{aligned} \sigma_{C-C} = & 8\pi^3 i \int d\bar{\tau}_{\perp a} \sum_{p,p',s,s'=+,-} A_{C-C}^{pp'ss'} e^{i(\bar{k}'_{\perp ai} - \bar{k}'_{\perp as} - \bar{k}'_{\perp bi} + \bar{k}'_{\perp bs}) \cdot \bar{\tau}_{\perp a}} \times \\ & \left[\frac{\Phi(\bar{k}'_{\perp bi} - \bar{k}'_{\perp bs}, -p'k'_{1zbs} - s'k'_{1zbi})}{pk'_{1zas} + sk'_{1zai} - p'k'_{1zbs} - s'k'_{1zbi}} - \frac{\Phi(\bar{k}'_{\perp bi} - \bar{k}'_{\perp bs}, -pk'_{1zas} - sk'_{1zai})}{pk'_{1zas} + sk'_{1zai} - p'k'_{1zbs} - s'k'_{1zbi}} \right] \times \\ & e^{i(pk'_{1zas} + sk'_{1zai} - p'k'_{1zbs} - s'k'_{1zbi})d} \end{aligned} \quad (2.56)$$

2.4. Field Variance and Correlation Results

In this section, many of the results derived in the previous section are illustrated by evaluating the variance and correlation of the scattering components as a function of aspect angle and frequency, as well as several other parameters of the random medium and target geometry. The geometry for which the results are calculated is shown in Figure 2.4. The direction of incidence is described by azimuth angle, ϕ , and elevation angle, θ , measured from vertical. The random slab is of depth d , and is characterized by an effective permittivity $\epsilon_{\text{eff}} = (1.0505 + 0.001794i)\epsilon_0$, a renormalized scattering source variance $\delta = .146822$, and correlation length $\ell = 0.0052$ m. These parameters are chosen to model forest vegetation at a frequency of 1.12 GHz, and with an assumed fractional volume of scatterers equal 1.67%. The procedure used to determine these parameters is that described by Chu [74-76], and is repeated in Appendix D. Finally, the target is located at a depth $z = -z_T$, and is chosen to have a free space radar cross section of 0 dBsm. The results for the variance of scattering contributions at single

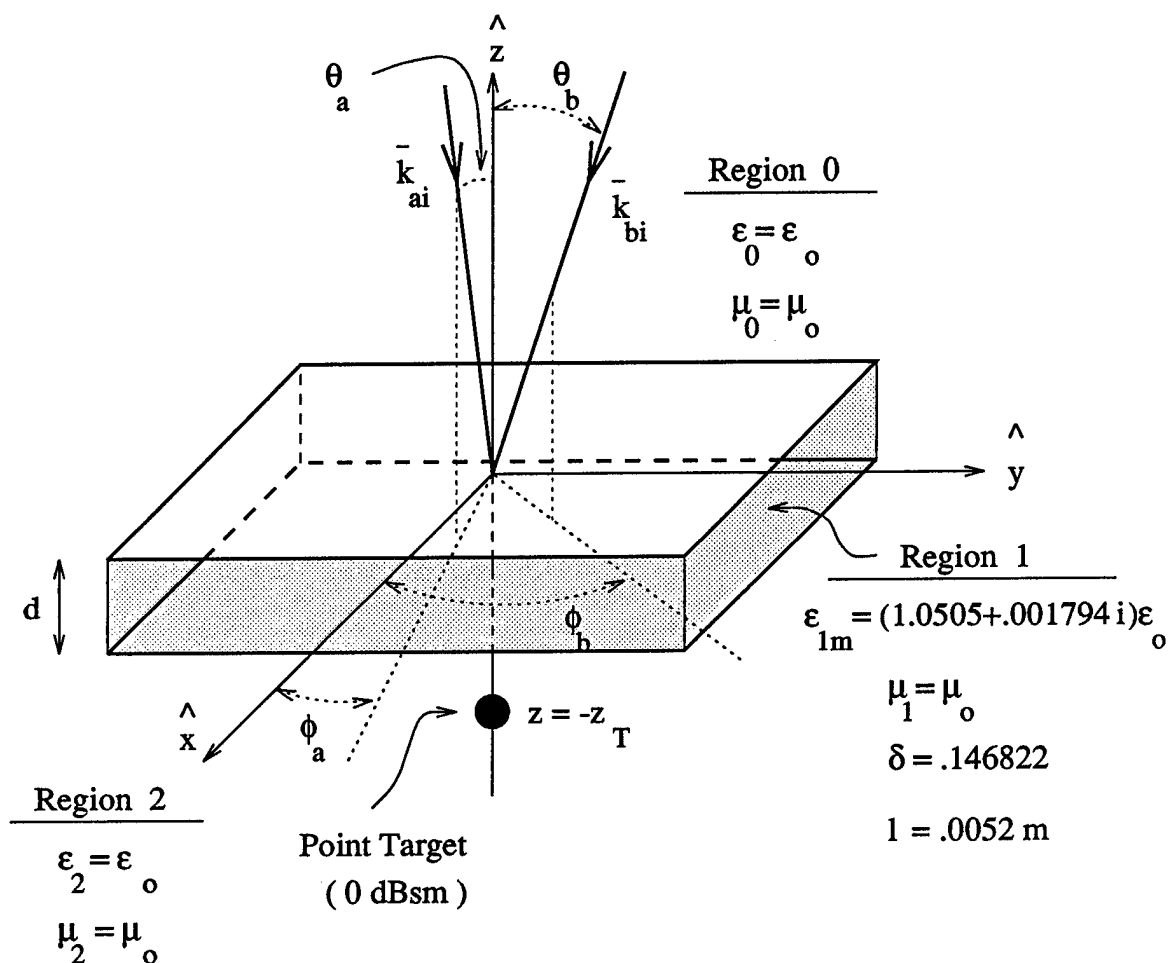


Figure 2.4. Geometry of the field variance and correlation results.

aspects and frequencies are shown first, and the correlations between two aspects or frequencies is shown thereafter.

2.4.1. Scattered Field Variance

The first results of Figure 2.5 show the coherent target cross section, σ_{T-T} , as a function of incidence angle. The three sets of curves show results for different choices

of medium parameters in the three regions. For all three results, the frequency is 1.12 GHz, the slab depth is taken as $d = 10$ m, and the upper region is assumed to be free space. In addition, the target is located at $z = -10$ m, just beneath the lower interface. In the first set of curves (solid), the slab region is assumed to have the parameters described above, and the bottom region is assumed to be free space. For comparison, the second curve (long-dash) shows the free space result, where the random slab is removed and replaced by free space, such that the cross section is independent of angle. At normal incidence, the propagation through the foliage is seen to attenuate the return by approximately 3.5 dB, as compared to the free space case, and this attenuation increases at higher incidence angles as the propagation path through the lossy slab lengthens and more power is lost to reflections at the boundaries. Both HH and VV polarizations are shown, although there is little difference between the two since the effective permittivity of the slab is very close to free space, and the Brewster angle effect is small. In contrast, the third result (short-dash) shows the effect of replacing the free space below the random slab by a lossy media with $\epsilon_2 = (6.0 + 0.6i)\epsilon_0$. The overall magnitude of the return for all aspect angles is decreased since the reflection coefficient at the lower boundary is now much larger. In addition, for large incidence angles, the VV return is stronger than HH because the Brewster angle effect at the lower interface allows more VV power to penetrate and reach the target.

In Figure 2.6 is shown the scattering cross section, σ_{TC-TC} , arising from the target/clutter multi-path mechanism, where the frequency, random medium, and target positioning are as in the previous figure. The first set of curves (solid) shows the result for free space above and below the random slab. The overall magnitude at normal incidence is approximately 12.5 dB below the coherent return, and, as with the coherent

return, the magnitude declines for increased angles of incidence, but at a slower rate. In addition, the two polarizations are not identical as is true for the coherent return, but instead the VV return is up to 2 dB larger. This effect is not due to the difference in boundary reflections, since the TE and TM reflection coefficients are nearly identical as discussed above.

The second set of curves (dashed) makes this point even clearer by replacing the free space above and below the slab by a media having permittivity equal to the effective permittivity of the slab, and, thus, eliminating the influence of the boundaries all together. One effect removing the boundaries has is the change in the behavior for larger incidence angles. Unlike previously where the return decreases for angles approaching grazing, the scattering now increases at larger angles. It is clear that the overall dependance with angle is a combination of several effects which individually tend to increase or decrease the return. Both the higher reflection coefficients at angles closer to grazing, and the increased attenuation due to the longer path, tend to decrease the return. In contrast, the longer path in the slab also allows a greater opportunity for scattering which tends to increase the return. Hence, without the effect of the boundaries, this later effect dominates. When the boundaries are added, the net effect is a decrease with angle, but at a rate slower than that seen in the coherent return.

The other effect seen in this second set of curves is the maintained difference between the VV and HH polarized returns. This result indicates that the difference is due to the geometry of the scattering between the target and random media, and not due to differences in the boundary interactions. Since the target is placed very close to the random media, most of the contributing scattering will arise from a small circular region about the target. The phase across this region will vary fastest in

the plane of incidence because of the added linear phase delay in this direction. In contrast, perpendicular to the plane of incidence, the phase differences are due only to the distance between the target and the scatterer, and will vary more slowly. The horizontal polarization will lead to a target which behaves as a dipole perpendicular to the plane of incidence, and which reradiates more of the power in the plane of incidence, over which the phase is varying more rapidly. For this reason there is more cancellation leading to a smaller return. In contrast, the vertical polarization leads to a target which behaves as a dipole lying in the plane of incidence, and radiating more power perpendicular to this plane where there is a slower phase change. For this reason, less phase cancellation occurs, and a stronger return is obtained. This geometrical effect is believed to explain the higher VV return in the absence of boundaries.

The above effect should become less pronounced as the target is moved out of the near-field of the random media, such that the region (Fresnel zone) from which significant scattering arises becomes more broadside to the dipole target for both HH and VV polarizations. Figure 2.7 compares the result obtained previously for the target immediately beneath the slab (solid) with the result of moving the target 5 meters below the lower boundary (dash). As expected, the distinction between the polarizations becomes lost for the later case.

Next is shown the effect of replacing the free space region below the slab with the same lossy media ($\epsilon_2 = (6.0 + 0.6i)\epsilon_0$) used above. Figure 2.8 compares the previous result for free space in region 2 (solid) with this new result (dashed). Overall the return is smaller for the later result, since the higher reflection coefficient at the lower interface limits the power reaching the target, and reduces the multi-path return as it did the coherent return. Now, however, the VV polarization is no longer larger than HH for

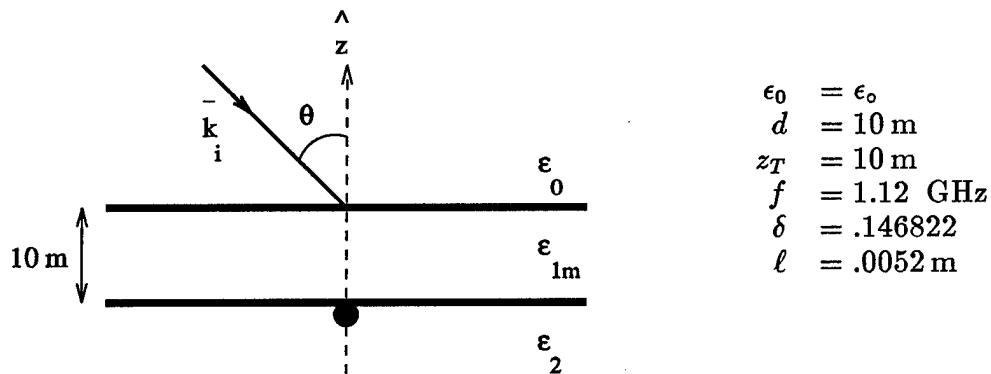
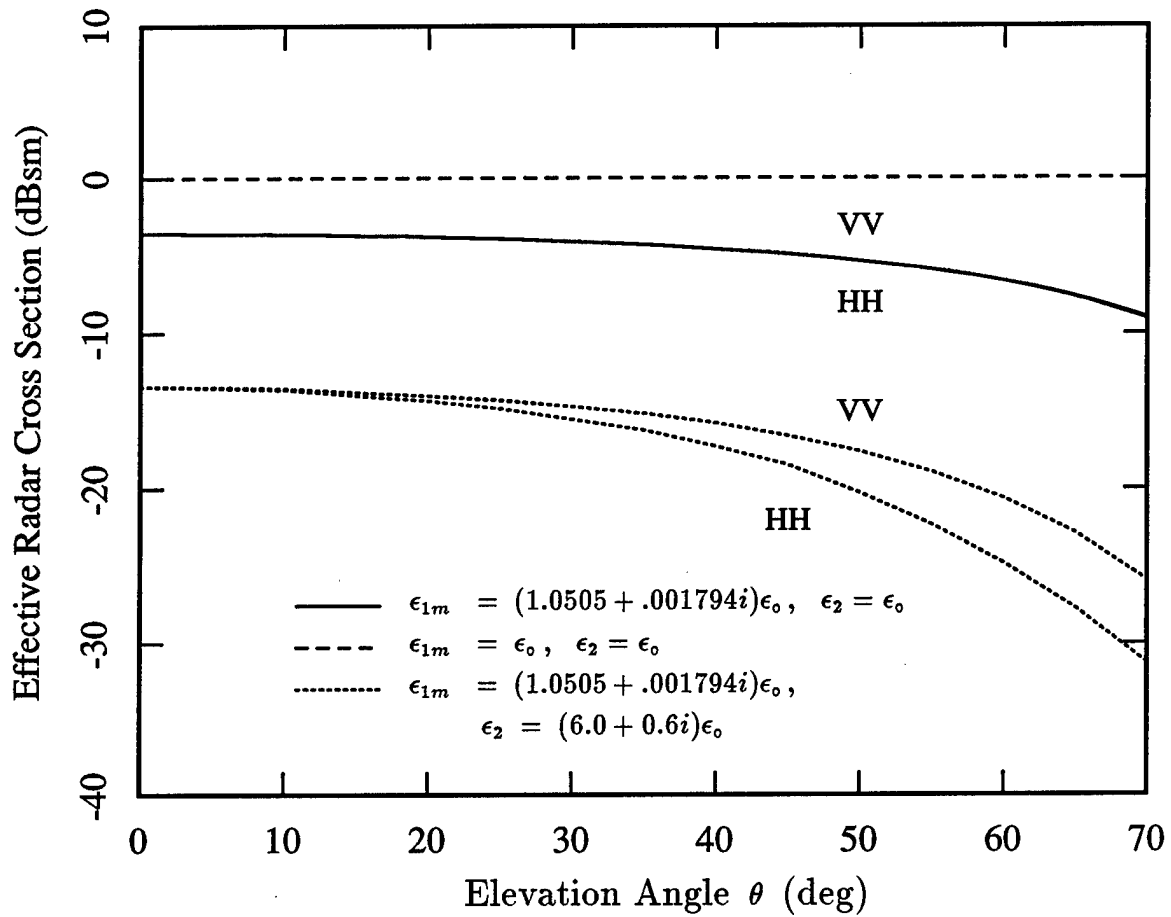


Figure 2.5. Dependence of the coherent target scattering cross-section, σ_{T-T} , on elevation angle. Results are given at 1.120 GHz for a 10 m slab with $z_T = 10 \text{ m}$. Shown is the case with $\epsilon_0 = \epsilon_2 = \epsilon_0$ and $\epsilon_{1m} = (1.0505 + .001794i)\epsilon_0$ (solid). For comparison, the free space case (dashed), and the case with a lossy media ($\epsilon_2 = (6.0 + 0.6i)\epsilon_0$) in region 2 (dotted) are also pictured.

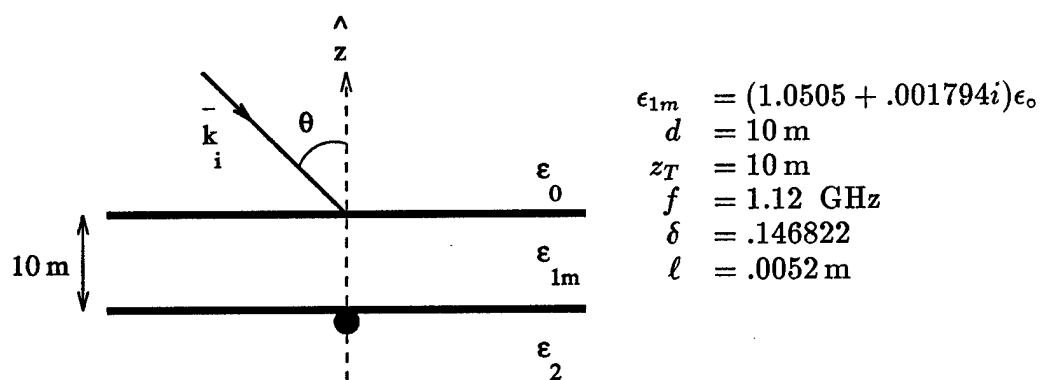
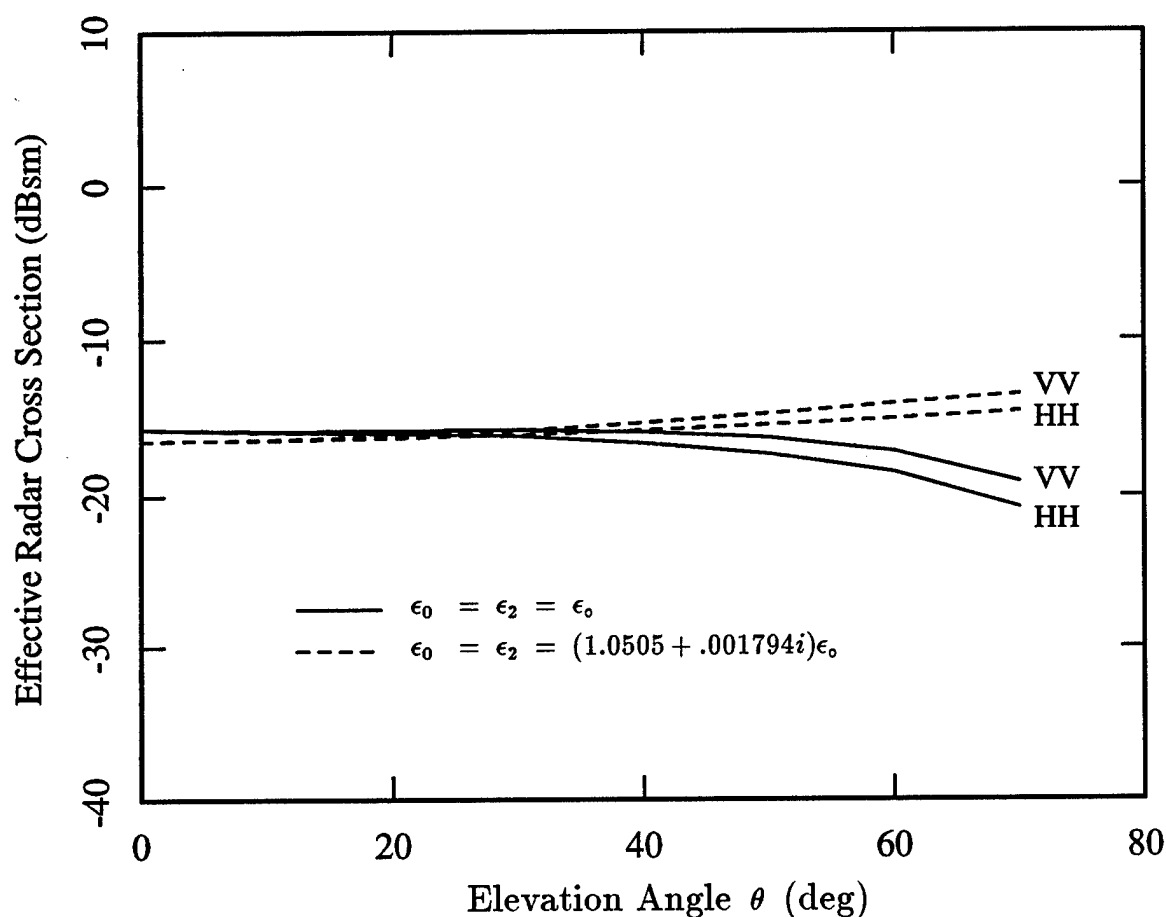


Figure 2.6. Dependence of the target/clutter scattering cross section, σ_{TC-TC} , on elevation angle for $\epsilon_0 = \epsilon_2 = \epsilon_0$ (solid) and $\epsilon_0 = \epsilon_2 = (1.0505 + .001794i)\epsilon_0$ (dash). Results are given at 1.120 GHz for a 10 m slab with $z_T = 10 \text{ m}$ and with $\epsilon_{1m} = (1.0505 + .001794i)\epsilon_0$.

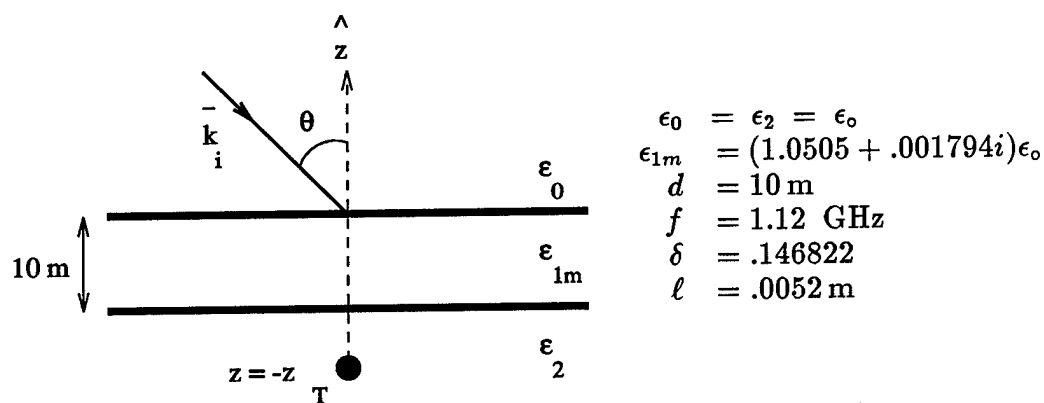
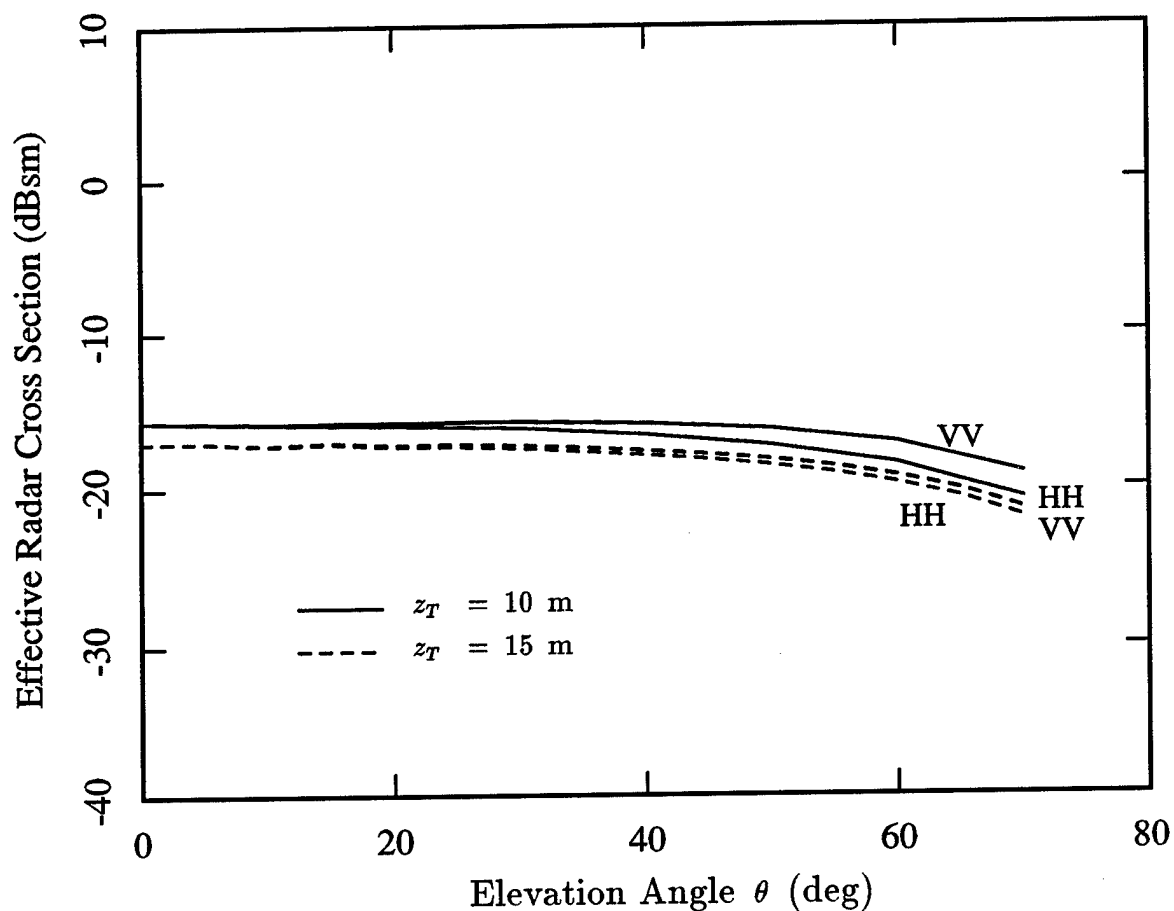


Figure 2.7. Dependence of the target/clutter scattering cross section, σ_{TC-TC} , on elevation angle for $z_T = 10$ m (solid) and $z_T = 15$ m (dash). Results are given at 1.120 GHz for a 10 m slab with $\epsilon_0 = \epsilon_2 = \epsilon_0$ and $\epsilon_{1m} = (1.0505 + .001794i)\epsilon_0$.

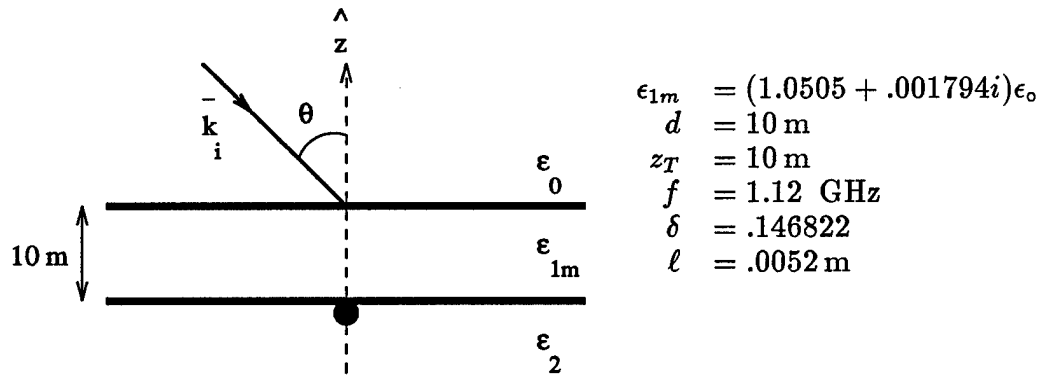
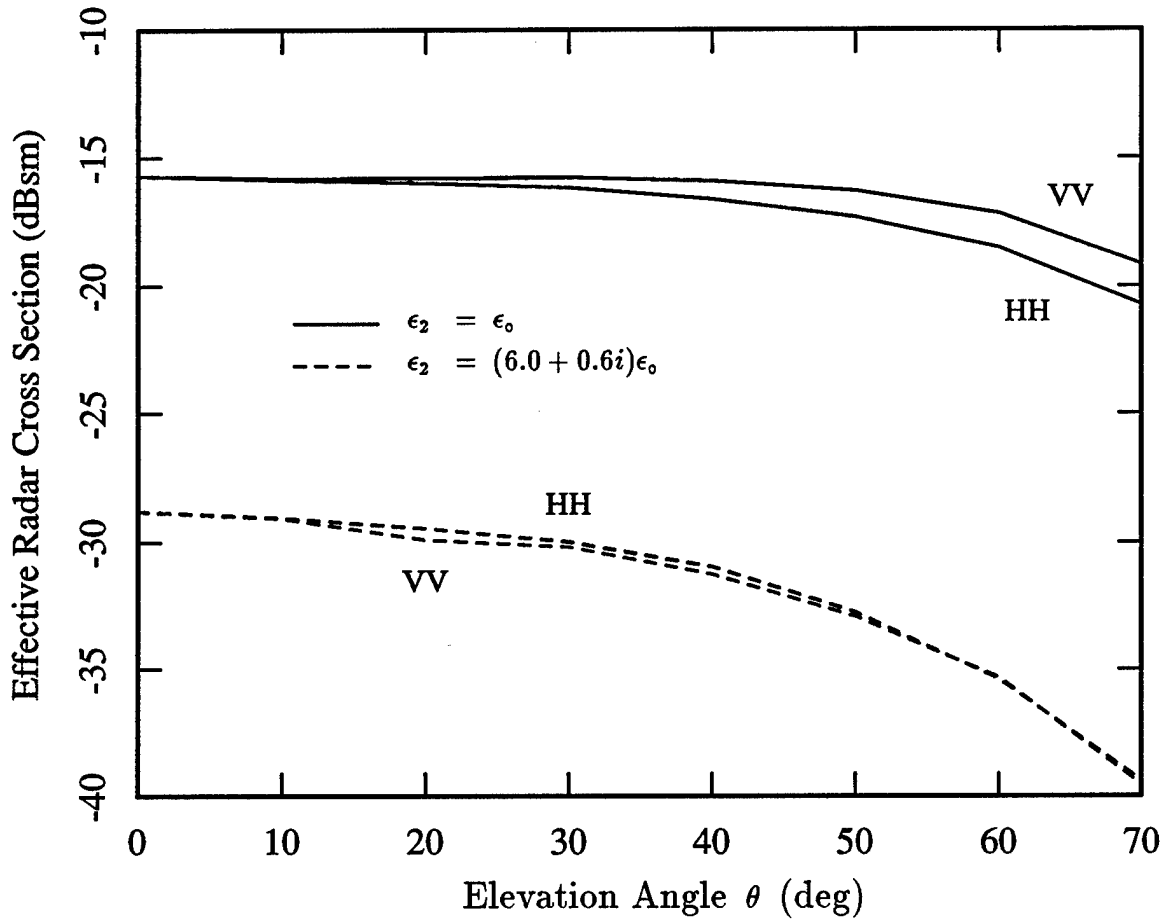


Figure 2.8. Dependence of the target-clutter scattering cross section, σ_{TC-TC} , on elevation angle for $\epsilon_2 = \epsilon_0$ (solid) and $\epsilon_2 = (6.0 + 0.6i)\epsilon_0$ (dash). Results are given at 1.120 GHz for a 10 m slab with $z_T = 10 \text{ m}$ and with $\epsilon_0 = \epsilon_0$ and $\epsilon_{1m} = (1.0505 + .001794i)\epsilon_0$.

large incidence angles, but the two polarizations give approximately the same return. This effect is believed to be due to the increased reflection from the lower interface, which increases the HH return reaching the radar after first being scattered by the target and random media. This increase is sufficient to overcome the Brewster angle effect which allows more power to reach the target in the VV case and which would otherwise cause a larger VV return. This effect is similar to the result observed by Zuniga [49] who demonstrated that for thin random layers, the reflection from the lower interface makes it possible to obtain a backscatter return larger for the HH polarization than for the VV case.

Figure 2.9 shows the dependance of σ_{T-T} (solid) and σ_{TC-TC} (dash) on the depth of the target below the upper interface. Results are given for the case of normal incidence with the frequency and other parameters the same as previous figures. As expected, the magnitude of the coherent return is seen to be independent of depth since there is no loss in region 2. Similarly, the target/clutter multi-path return is found to be independent of depth, since the $1/r^2$ loss for the interaction between the target and random scatterers increases with increased target depth, but the area of the Fresnel zone within the slab from which scattering contributions arise also increases as r^2 for increasing target depths. Hence, the net effect is an independence with depth. A small exception to this is seen for target positions very close to the random media, where the near-field effect causes a slight increase in the scattered return.

Figure 2.10 shows the effect of the thickness, d , of the random slab on σ_{T-T} and σ_{TC-TC} , for a target positioned in free space immediately below the lower interface. The coherent return decreases with a linear exponential rate for increasing thickness, since the slab is lossy and this change increases the path length in the slab region.

The effect on σ_{TC-TC} is different for two different ranges of d . For small values of d , increasing the thickness adds more random media by which the target scattered field may be rescattered, and leads to a larger multi-path return. This increase is the expected result, since in the limit as the slab thickness approaches zero, the multi-path contribution must disappear. In contrast, however, for larger values of thickness, the effect of adding more scatterers saturates, and the added attenuation from the increased path length through the random slab leads to a decrease in the returned field. The saturation arises in part because the added scatterers are further from the target and suffer a greater $1/r^2$ loss in propagation from the target, and also in part because the path delay for the added scatterers may be such as to cause destructive interference with the contributions from existing scatterers.

Figure 2.11 shows the dependance of σ_{T-T} and σ_{TC-TC} with frequency over a small 20 MHz band about 1.12 GHz. The bandwidth shown is picked to be typical of that used in a SAR application. Both σ_{T-T} and σ_{TC-TC} are seen to be only weakly dependent on frequency, with higher frequencies leading to a slight increase in the target/clutter return, and a slight decrease in the coherent target return. This result demonstrates that the target/clutter multi-path field is not strictly stationary over frequency, and the correlation between returns at two frequencies, which will be shown shortly, will be seen to be a function of both frequencies rather than only the difference.

Figure 2.12 shows the correlation, σ_{C-TC} , between the clutter return and the target/clutter multi-path return as a function of incidence angle. Only the magnitude of the correlation is plotted. The most significant feature of this result is the overall magnitude, which at normal incidence is approximately 27 dB lower than the σ_{TC-TC} cross section, and 40 dB lower than the coherent cross section, σ_{T-T} . The oscillations

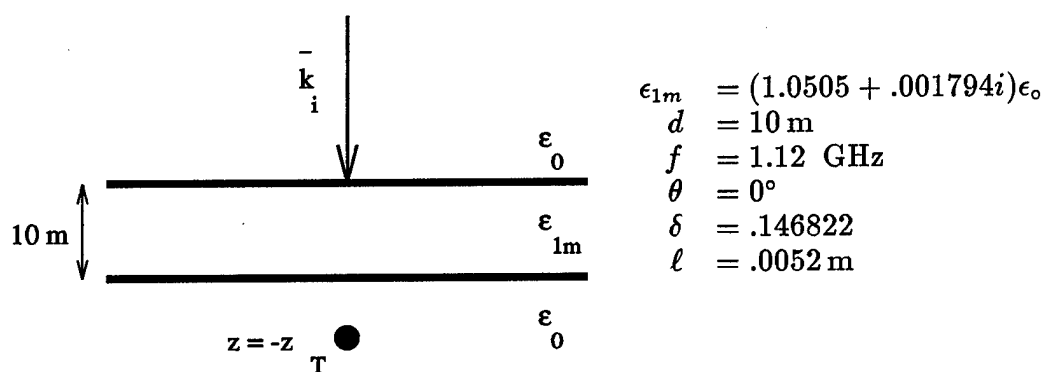
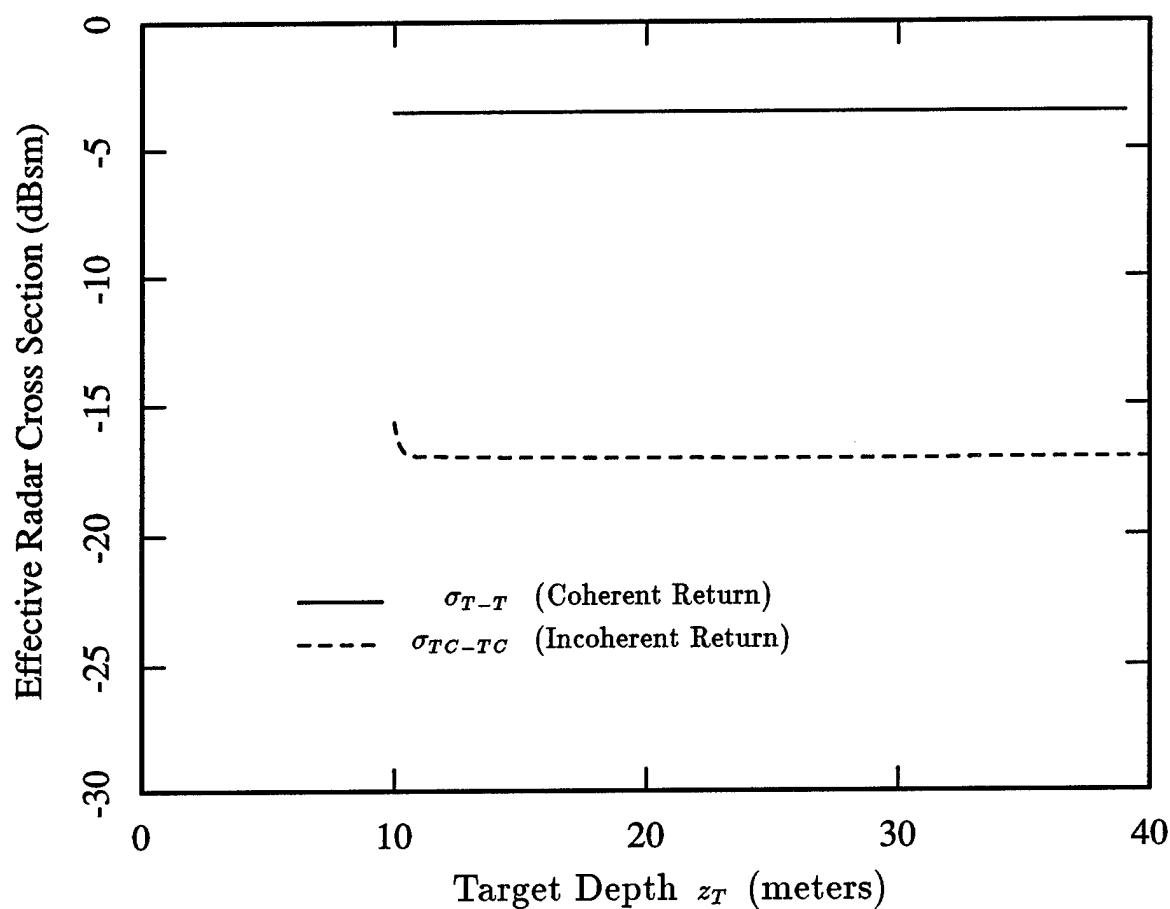


Figure 2.9. Dependence of the coherent target scattering cross section, σ_{T-T} , (solid) and the target/clutter scattering cross section, σ_{TC-TC} , (dash) on target depth. Results are shown for normal incidence ($\theta = 0^\circ$) at 1.120 GHz with a 10 m slab and with $\epsilon_0 = \epsilon_2 = \epsilon_0$ and $\epsilon_{1m} = (1.0505 + .001794i)\epsilon_0$.

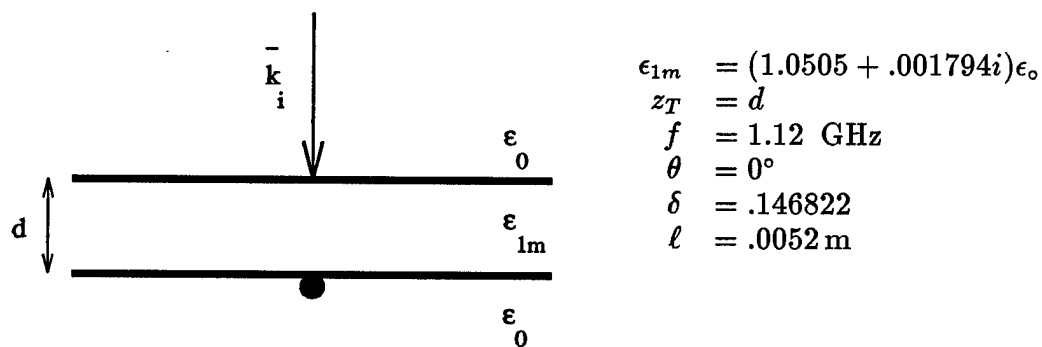
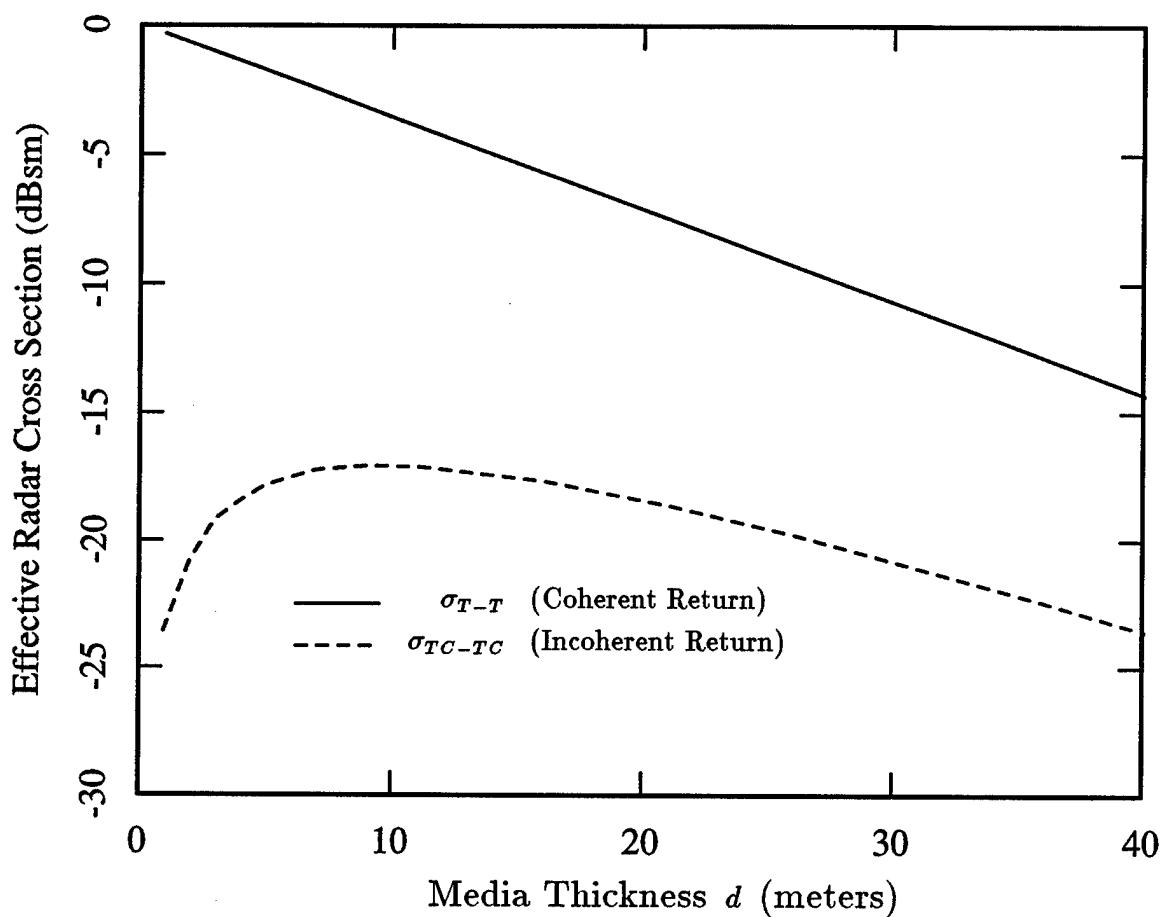


Figure 2.10. Dependence of the coherent target scattering cross section, σ_{T-T} , (solid) and target/clutter scattering cross section, σ_{TC-TC} , (dash) on slab thickness. Results are shown for normal incidence ($\theta = 0^\circ$) at 1.120 GHz with the target positioned immediately below the lower interface ($z_T = d$), and with $\epsilon_0 = \epsilon_2 = \epsilon_0$ and $\epsilon_{1m} = (1.0505 + .001794i)\epsilon_0$.

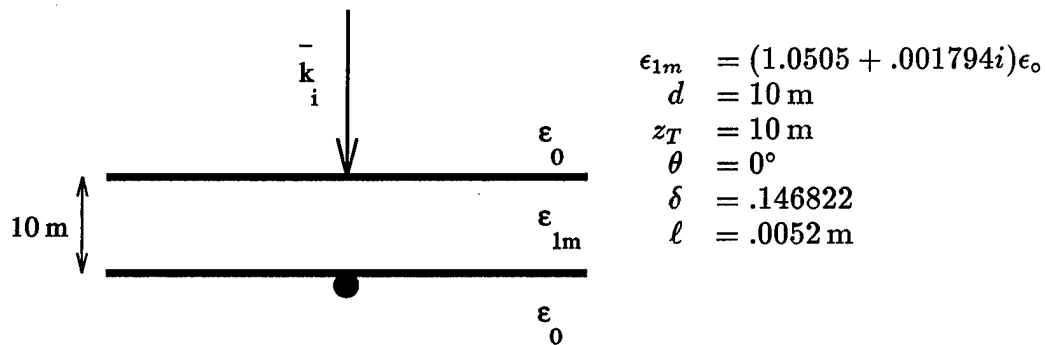
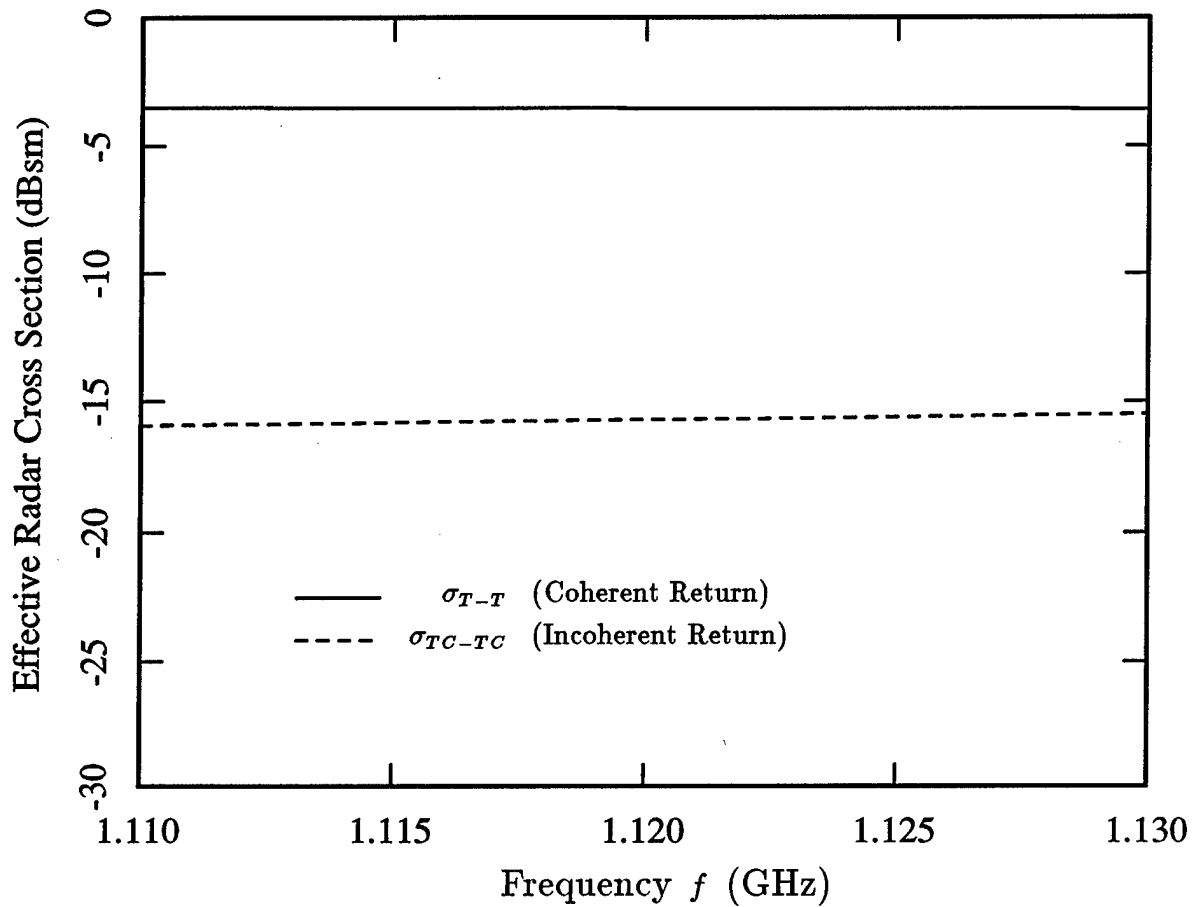


Figure 2.11. Dependence of the coherent target scattering cross section, σ_{T-T} , (solid) and the target-clutter scattering cross section, σ_{TC-TC} , (dash) on frequency for normal incidence ($\theta = 0^\circ$). Results are given for a 10 m slab with $z_T = 10 \text{ m}$ and with $\epsilon_0 = \epsilon_2 = \epsilon_0$ and $\epsilon_{1m} = (1.0505 + .001794i)\epsilon_0$.

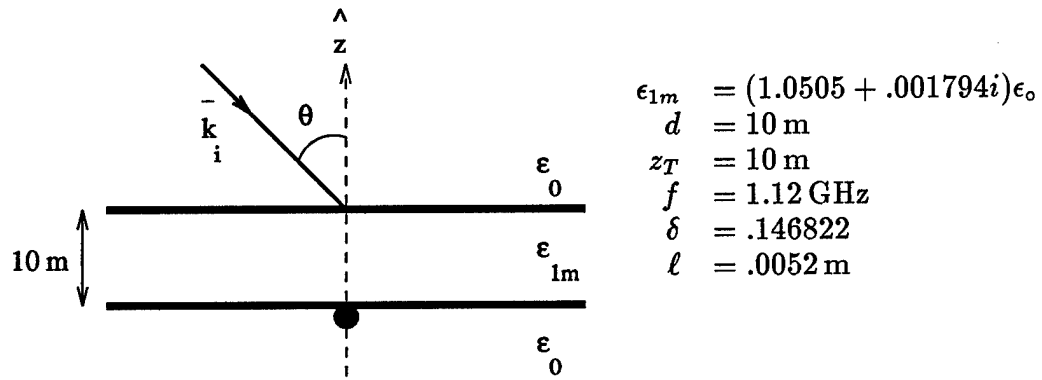
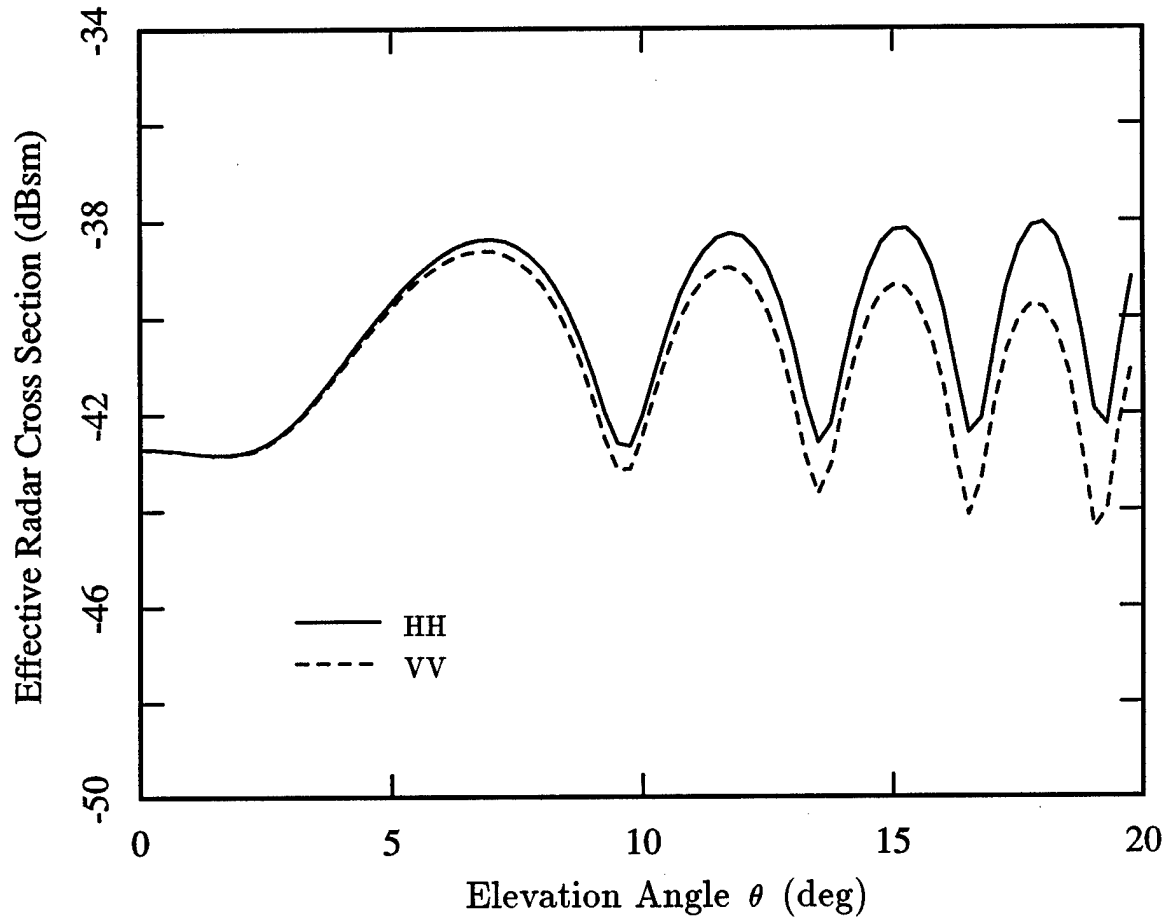


Figure 2.12. Dependence of the clutter-target/clutter correlation, σ_{C-TC} , on elevation angle for the HH (solid) and VV (dash) polarizations. Results are given at 1.120 GHz for a 10 m slab with $z_T = 10$ m and with $\epsilon_0 = \epsilon_2 = \epsilon_0$ and $\epsilon_{1m} = (1.0505 + .001794i)\epsilon_0$.

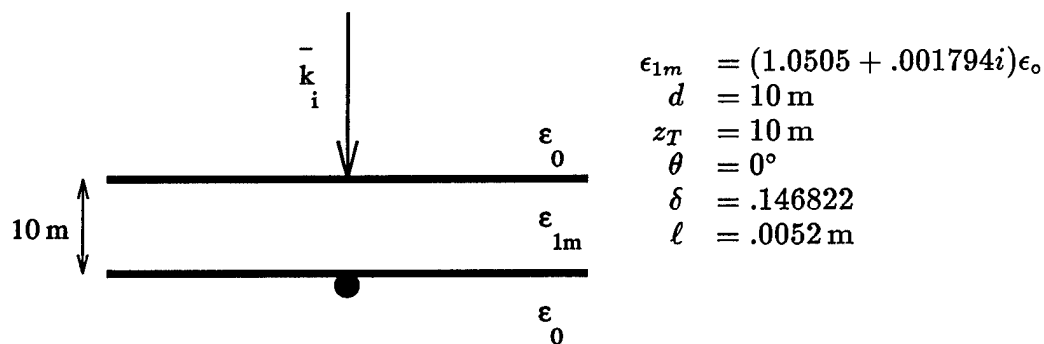
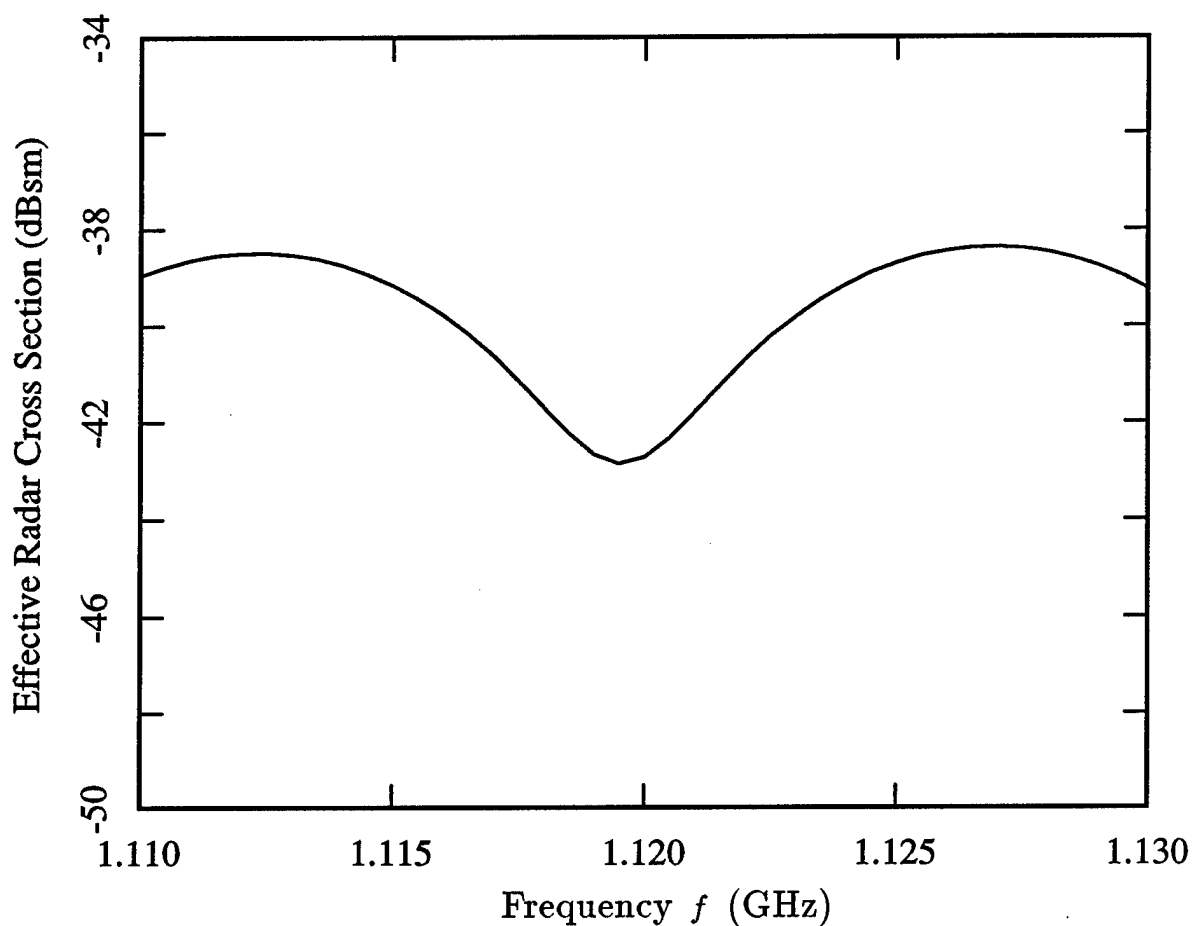


Figure 2.13. Dependence of the clutter-target/clutter correlation, σ_{C-TC} , on frequency for normal incidence ($\theta = 0^\circ$). Results are given for a 10 m slab with $z_T = 10$ m and with $\epsilon_0 = \epsilon_2 = \epsilon_0$ and $\epsilon_{1m} = (1.0505 + .001794i)\epsilon_0$.

with increasing incidence angle are due to the phase difference between the clutter and target/clutter returns which changes with angle, leading to aspects where the two are on average more in phase (peaks) or more in quadrature (troughs). The higher correlation for the HH polarization can be explained by the fact that for this polarization the target acts like a dipole perpendicular to the plane of incidence, radiating more of its power into this plane. Furthermore, in this plane the phase delay for the radar-target-clutter-radar path is most like that of the radar-clutter-radar path, assuming in each case the same random scatterer. In contrast, for the VV polarization the target acts like a dipole lying in the plane of incidence and radiating more power perpendicular to the plane of incidence. Points off of the plane of incidence have greater differences in phase delay between the paths through that point for the two scattering mechanisms. For this reason, the coherency between the HH return from the clutter and the HH return from the target/clutter multi-path is higher than the coherency for the VV polarization, and, consequently, the correlation is higher for HH.

Finally, Figure 2.13 shows the magnitude of the correlation σ_{C-TC} as a function of frequency over a 20 MHz band centered at 1.12 GHz. The result is shown for the case of normal incidence on the random media. The result is seen to oscillate with a range of approximately 5 dB, again arising from the changes in coherency between the two scattered fields which results when the change in frequency affects the phase delay for individual scatterers in the random layers.

2.4.2. Scattered Field Correlation

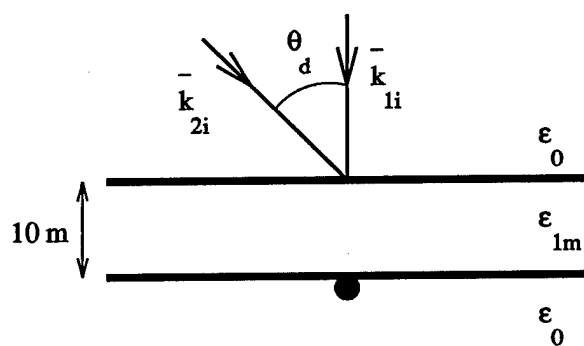
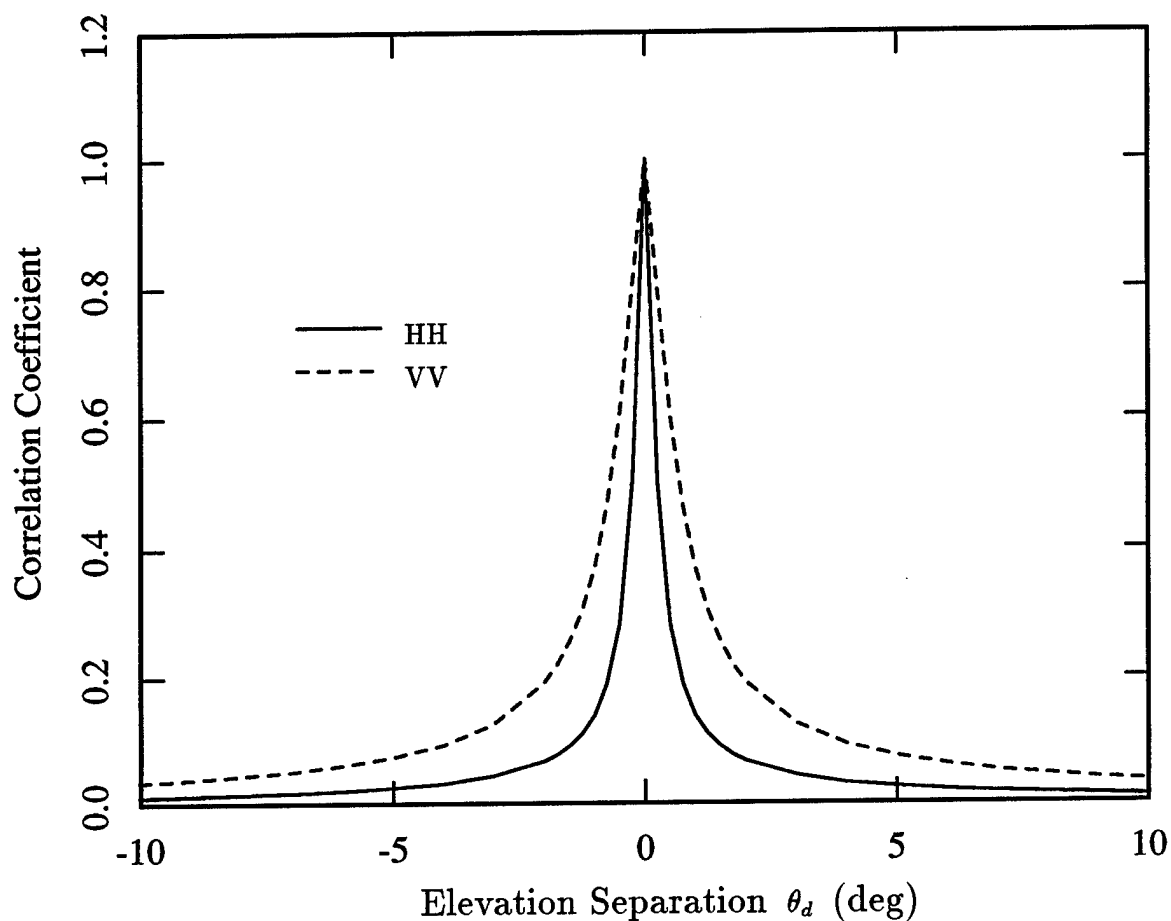
Figures 2.14-2.16 show the correlation, $\sigma_{TC-TC}(\theta_1, \theta_2)$, of the target/clutter return for a fixed angle, θ_1 , with the target/clutter return at a varied angle, θ_2 . The results are calculated at a frequency of 1.12 GHz, with a medium thickness $d = 10$ m, and with the target in free space immediately below the lower interface. In each case, the correlation is normalized by the result for $\theta_1 = \theta_2$.

Figure 2.14 compares the result for the HH polarization (solid) with that for VV (dash) where in both cases $\theta_1 = 0^\circ$ (normal incidence). In each case the correlation drops sharply for the first 1° or 2° , then decays more gradually for larger values of $\theta_2 - \theta_1$. However, the decorrelation for the HH polarization is faster than that seen for VV. This difference is again probably due to the behavior of the point target which acts as a dipole lying in the plane of incidence for the VV case, and as a dipole perpendicular to this plane for the HH case. Hence, in the HH case, less power is scattered from the target in directions perpendicular to the incidence plane as compared to the VV case. Since the phase change for changing $\theta_2 - \theta_1$ occurs only between scatterers separated in the plane of incidence, the VV dipole radiates more power to scatterers located so as to experience less phase shift relative to one another. For this reason the VV return remains correlated longer than the HH return.

The effect of polarization on the decorrelation rate shows that the correlation is affected in general by the shape of the region of random scatterers from which significant multi-path scattering arises. Since this region represents an aperture (or volume) with randomly varying excitation amplitude, it is expected that the return which results will remain correlated over angular changes which cause no significant phase shift across

the aperture. In the present problem with the target immediately below the random layer, the shape of the contributing region is expected to be roughly hemi-spherical (ignoring for the moment the above polarization effect), centered about and directly above the target. Because this volume has a greater horizontal extent than vertical height, it is expected that a given separation $\theta_2 - \theta_1$ will lead to the greatest phase shift across the region for $\theta_1 = 0^\circ$ and, thus, the correlation will be sharper for θ_1 near normal incidence. Figure 2.15 shows a comparison of the correlation of the HH return over $\theta_2 - \theta_1$ for several values of θ_1 , and it is clear that the correlation is in fact sharpest for $\theta_1 = 0^\circ$, and drops more gradually for larger values of θ_1 . Hence, the correlation is not a function of only $\theta_2 - \theta_1$, but depends on θ_1 as well. Consequently, the correlation is not symmetric for any choice of $\theta_1 \neq 0^\circ$.

Figure 2.16 gives a similar comparison of correlations for several values of θ_1 , but is shown for the VV polarization. Unlike the previous case the correlation is now sharper for larger incidence angles, θ_1 , although the difference between results for varied θ_1 is less significant than for the HH polarization. The reason for the different behavior in the VV case is the combination of the two previously discussed effects of scattering region shape. The overall hemi-spherical nature of the scattering region should lead to a slower decorrelation as with the above HH case. However, the effect of the dipole target, which was seen to lead to a sharper correlation at normal incidence for the HH case than for the VV case, becomes less dominant as the center angle is increased. The reduction of this target polarization effect is expected to lead to sharper correlations for larger incidence angles. The net effect of these two mechanisms is a change which produces a slight increase in the sharpness of the correlation for angles closer to grazing.



$$\begin{aligned} \epsilon_{1m} &= (1.0505 + .001794i)\epsilon_0 \\ d &= 10 \text{ m} \\ z_T &= 10 \text{ m} \\ \theta_1 &= 0^\circ \\ f &= 1.12 \text{ GHz} \\ \delta &= .146822 \\ \ell &= .0052 \text{ m} \end{aligned}$$

Figure 2.14. Correlation of the target/clutter multi-path return, $\sigma_{TC-TC}(\theta_1, \theta_2)$, over $\theta_d = \theta_2 - \theta_1$ for $\theta_1 = 0^\circ$ and for HH (solid) and VV (dash) polarizations. Results are given at 1.120 GHz for a 10 m slab with $z_T = 10$ m and with $\epsilon_0 = \epsilon_2 = \epsilon_0$ and $\epsilon_{1m} = (1.0505 + .001794i)\epsilon_0$.

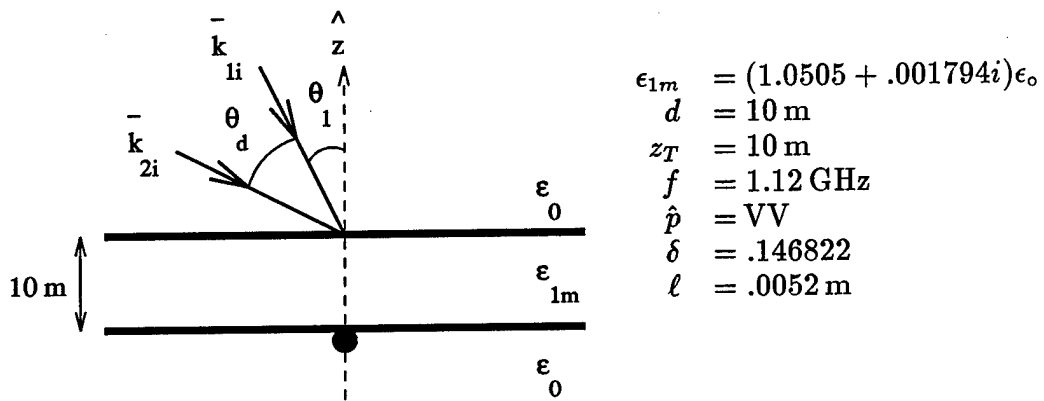
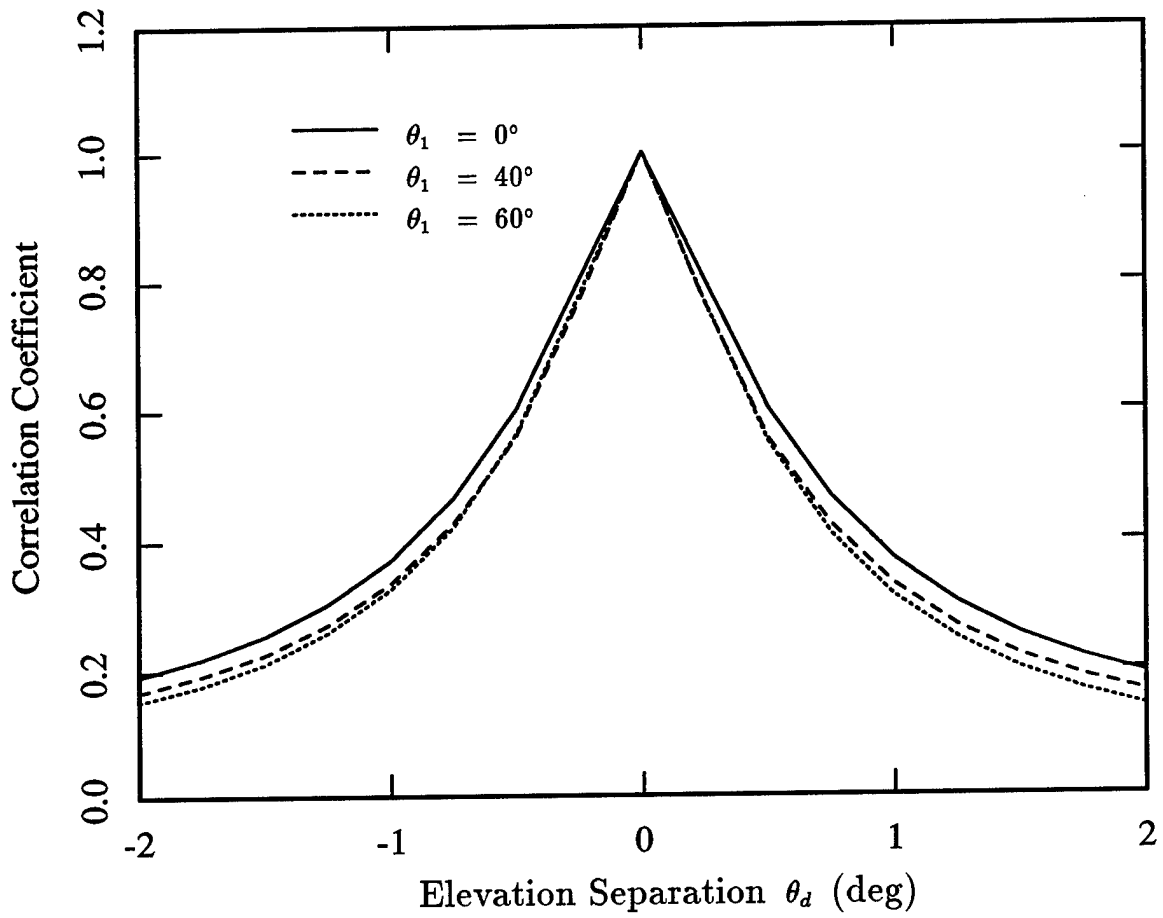


Figure 2.16. Correlation of the target/clutter multi-path return, $\sigma_{TC-TC}(\theta_1, \theta_2)$, over $\theta_d = \theta_2 - \theta_1$ for the VV polarization and for $\theta_1 = 0^\circ$ (solid), $\theta_1 = 40^\circ$ (dash), and $\theta_1 = 60^\circ$ (dots). Results are given at 1.120 GHz for a 10 m slab with $z_T = 10 \text{ m}$ and with $\epsilon_0 = \epsilon_2 = \epsilon_o$ and $\epsilon_{1m} = (1.0505 + .001794i)\epsilon_o$.

In addition to the shape of the region of random scatterers, the extent of the correlation in angle is also affected by the overall size of this region. As the region becomes larger the phase change across the region will be larger for a given change of incidence angle, and the return is expected to become decorrelated faster. To illustrate this effect, Figure 2.17 shows a comparison of the correlation, $\sigma_{TC-TC}(\theta_1, \theta_2)$, for a target located at $z_T = 10$ m (solid) and a target at $z_T = 15$ m (dash). In both cases, the polarization is horizontal and $\theta_1 = 0^\circ$. Increasing the depth of the target leads to an increase in the size of the Fresnel zone from which multi-path scattering arises and is expected to cause a sharper decline in the correlation function. The results of Figure 2.17 display this effect with the correlation for the case $z_T = 15$ m decreasing more rapidly. Hence, unlike the variance of the target/clutter return, which was shown to be independent of target depth (with $\epsilon_2 = \epsilon_o$), the correlation of the field is clearly affected by target position.

While all the above results give the correlation function for changes in elevation angle, for application to the SAR problem, it is of greater interest to determine the correlation over changing azimuth angle. Figure 2.18 shows the correlation, $\sigma_{TC-TC}(\phi_2 - \phi_1)$ for HH (solid) and VV (dash) polarizations. Both cases are shown for an elevation angle of $\theta_1 = \theta_2 = 40^\circ$ with the target positioned at $z_T = 10$ m. Because of the azimuthal symmetry, the correlation is now a function of only the difference of azimuth angles, $\phi_2 - \phi_1$.

Unlike the correlation in elevation angle, the correlation in azimuth shows that the HH fields decorrelate more slowly than the VV fields. Again, the reason for this difference arises from the dipole nature of the target, and the effect on the shape of the scattering region in the random layer. The VV dipole radiates more power in the

horizontal plane than does the HH dipole. Since the phase change for changing azimuth is experienced for scatterers separated in the horizontal direction, the HH case radiates less power to scatterers which experience phase shifts for changing azimuth angle, and, thus, the HH fields remain correlated over a wider range of azimuth angles.

Figures 2.19 and 2.20 show the effect of changing the elevation angle, $\theta_1 = \theta_2$, on the correlation, $\sigma_{TC-TC}(\phi_2 - \phi_1)$, for HH and VV polarizations, respectively. Geometrically it can be shown that at larger elevation angles, the phase delay across the scattering region will change more rapidly with changing ϕ . Consequently, it is seen that the correlation function in azimuth drops more rapidly for larger elevation angles.

Figure 2.21 shows the correlation, $\sigma_{TC-TC}(f_1, f_2)$, of the multi-path target/clutter return over frequency for a typical SAR bandwidth of 20 MHz. The correlation is calculated at normal incidence with $z_T = 10$ m for several center frequencies near 1.12 GHz. The small differences between the results at different center frequencies show once again that this field component is weakly stationary in frequency over a small bandwidth. The overall correlation is very similar to that seen over a small angular extent ϕ which would be typical of the integration angle of a SAR system. As will be shown in Chapter 7, this result suggests that there will be a degradation of resolution in both range and cross-range.

Finally, Figures 2.22 and 2.23 show the correlation, $\sigma_{C-TC}(\phi_2 - \phi_1)$, of the clutter return at one angle ϕ_1 with the target/clutter return at a second angle ϕ_2 , and the correlation, $\sigma_{C-TC}(f_1, f_2)$, of the clutter return at one frequency with the target/clutter return at a second. Both of these correlations are seen to have magnitudes which rise above one. This result arises because the correlations are normalized to a value of one where the angular or frequency separation is zero. Since both correlations are cross

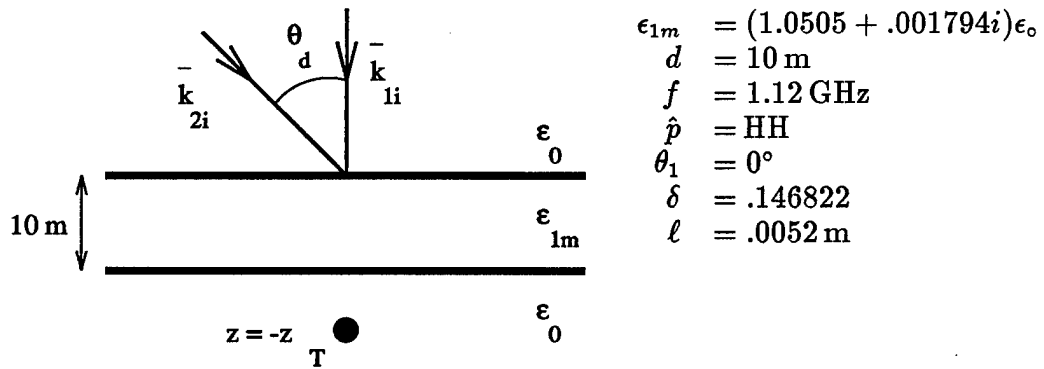
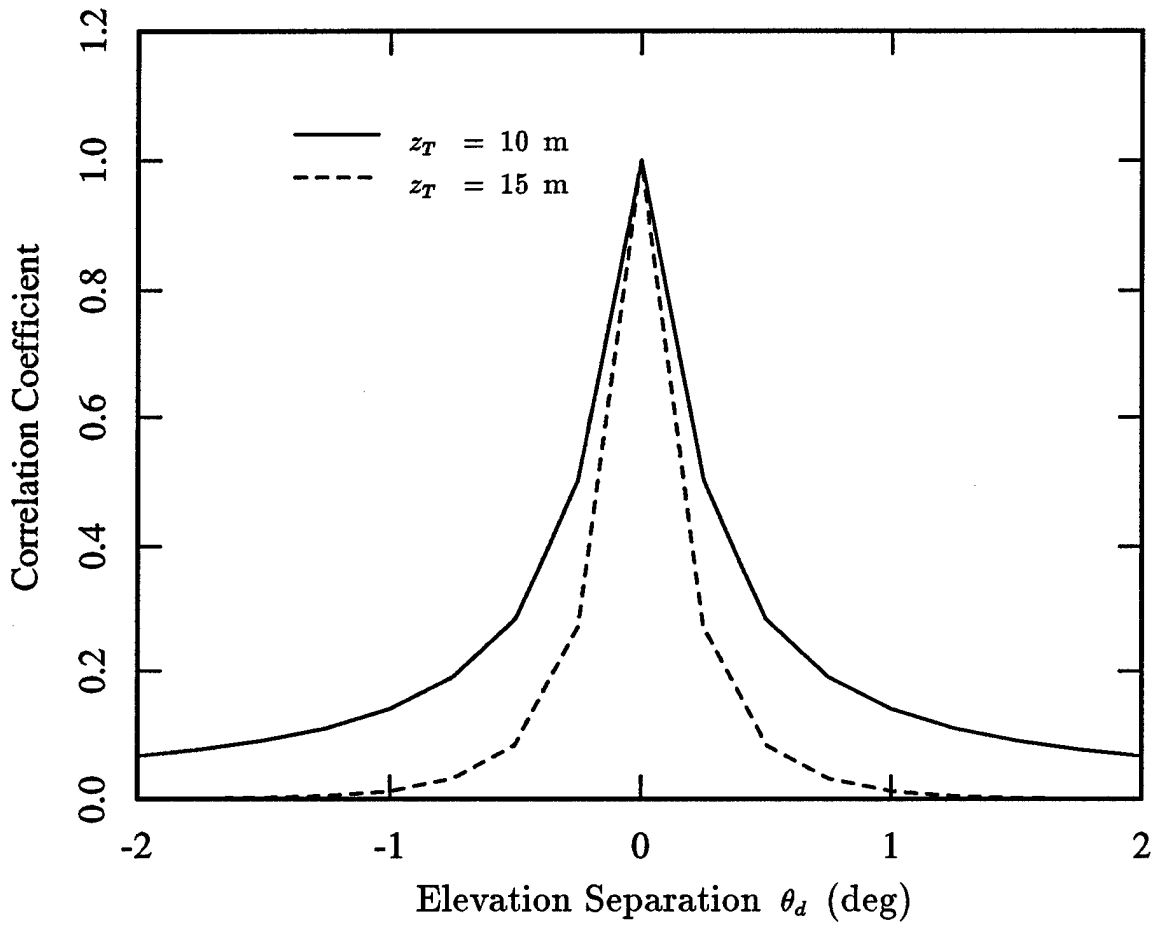
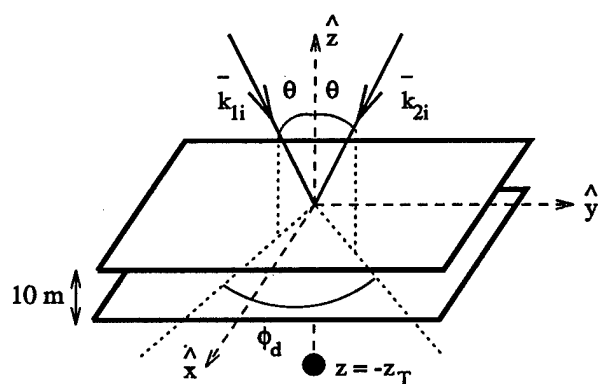
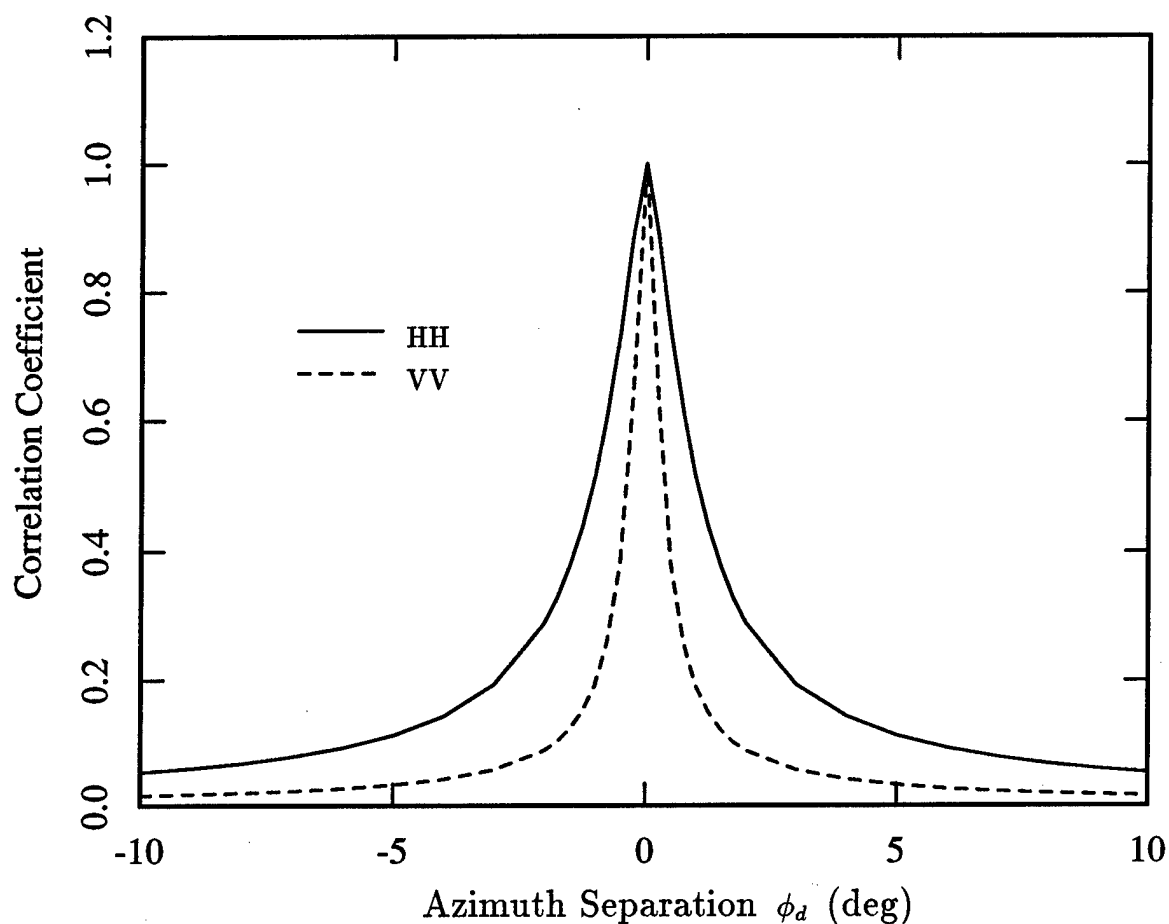
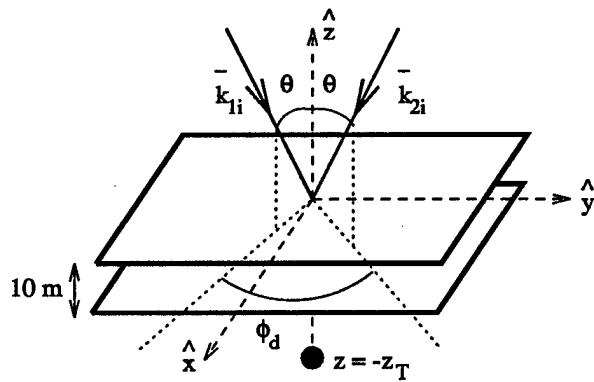
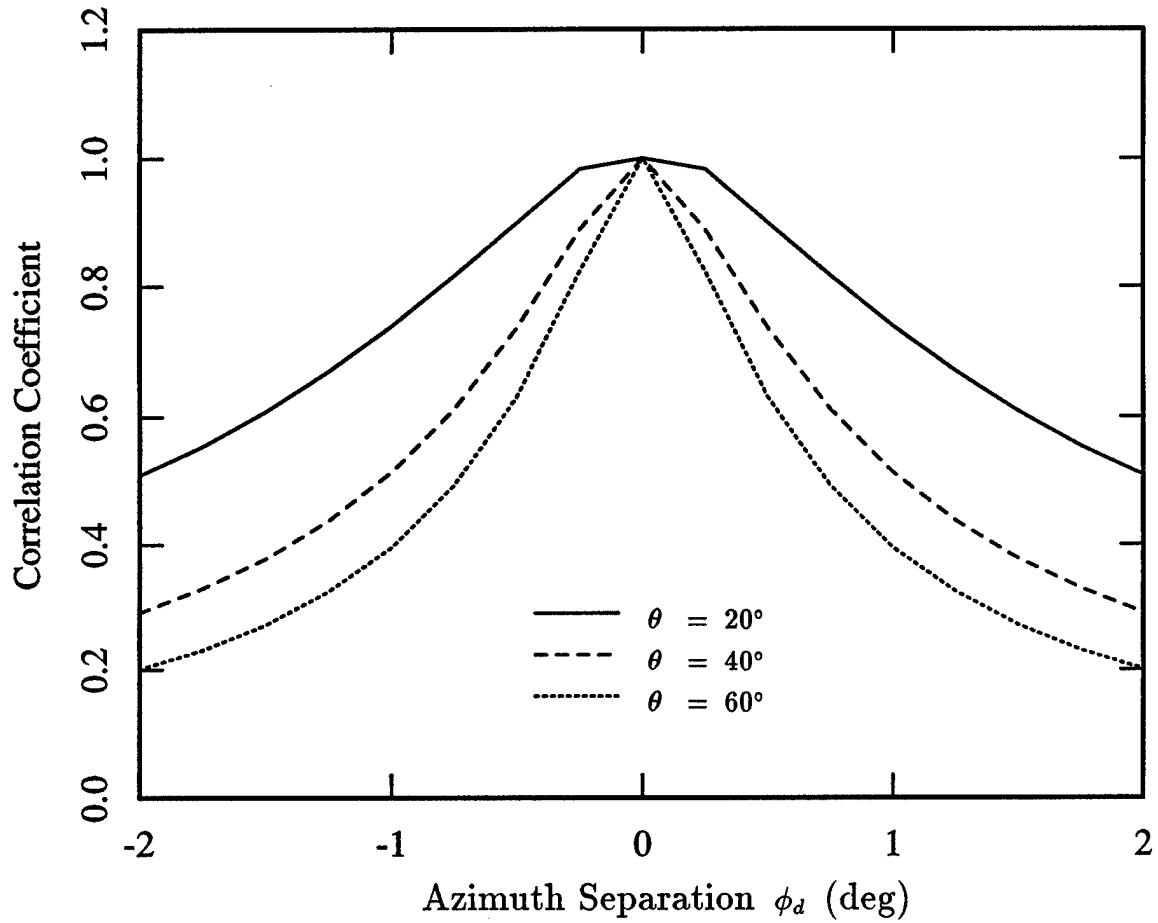


Figure 2.17. Correlation of the target/clutter multi-path return, $\sigma_{TC-TC}(\theta_1, \theta_2)$, over $\theta_d = \theta_2 - \theta_1$ for the HH polarization and for $z_T = 10$ m (solid) and $z_T = 15$ m (dash). Results are given at 1.120 GHz for a 10 m slab with $\theta_1 = 0^\circ$ and with $\epsilon_0 = \epsilon_2 = \epsilon_0$ and $\epsilon_{1m} = (1.0505 + .001794i)\epsilon_0$.



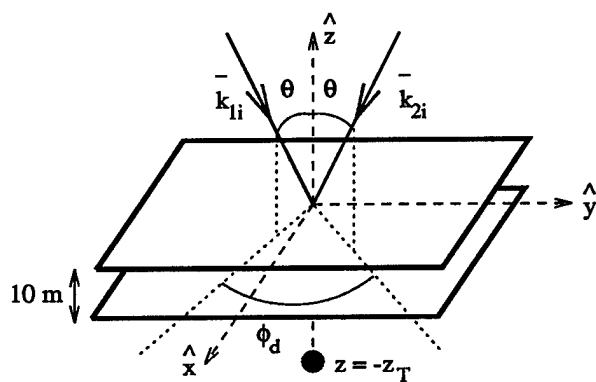
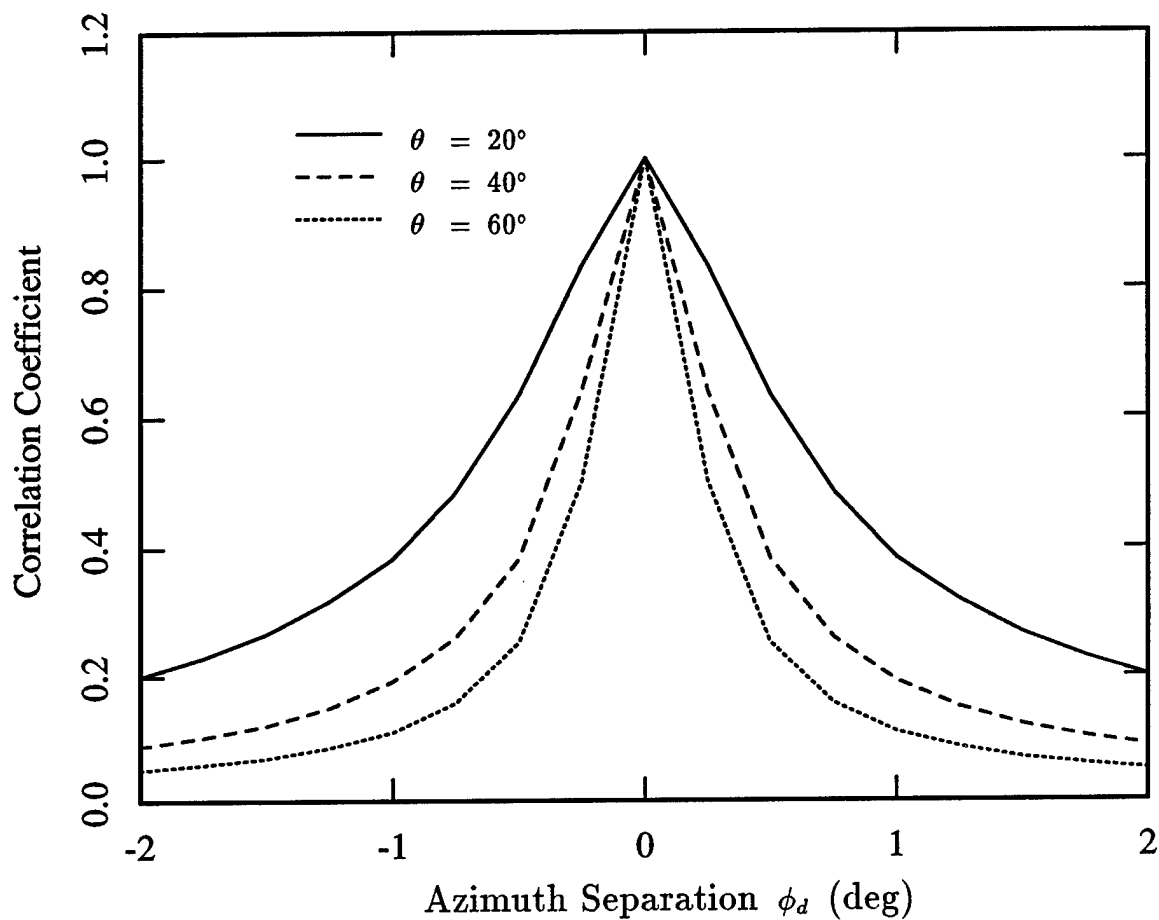
$$\begin{aligned}
 \epsilon_0 &= \epsilon_2 = \epsilon_o \\
 \epsilon_{1m} &= (1.0505 + .001794i)\epsilon_o \\
 d &= 10 \text{ m} \\
 z_T &= 10 \text{ m} \\
 f &= 1.12 \text{ GHz} \\
 \theta_1 &= 40^\circ \\
 \delta &= .146822 \\
 \ell &= .0052 \text{ m}
 \end{aligned}$$

Figure 2.18. Correlation of the target/clutter multi-path return, $\sigma_{TC-TC}(\phi_2 - \phi_1)$, over $\phi_d = \phi_2 - \phi_1$ for $\theta = 40^\circ$ and for HH (solid) and VV (dash) polarizations. Results are given at 1.120 GHz for a 10 m slab with $z_T = 10$ m and with $\epsilon_0 = \epsilon_2 = \epsilon_o$ and $\epsilon_{1m} = (1.0505 + .001794i)\epsilon_o$.



$$\begin{aligned}
 \epsilon_0 &= \epsilon_2 = \epsilon_o \\
 \epsilon_{1m} &= (1.0505 + .001794i)\epsilon_o \\
 d &= 10 \text{ m} \\
 z_T &= 10 \text{ m} \\
 f &= 1.12 \text{ GHz} \\
 \hat{p} &= \text{HH} \\
 \delta &= .146822 \\
 \ell &= .0052 \text{ m}
 \end{aligned}$$

Figure 2.19. Correlation of the target/clutter multi-path return, $\sigma_{TC-TC}(\phi_2 - \phi_1)$, over $\phi_d = \phi_2 - \phi_1$ for the HH polarization and for $\theta = 20^\circ$ (solid), $\theta = 40^\circ$ (dash), and $\theta = 60^\circ$ (dots). Results are given at 1.120 GHz for a 10 m slab with $z_T = 10$ m and with $\epsilon_0 = \epsilon_2 = \epsilon_o$ and $\epsilon_{1m} = (1.0505 + .001794i)\epsilon_o$.



$$\begin{aligned}
 \epsilon_0 &= \epsilon_2 = \epsilon_o \\
 \epsilon_{1m} &= (1.0505 + .001794i)\epsilon_o \\
 d &= 10 \text{ m} \\
 z_T &= 10 \text{ m} \\
 f &= 1.12 \text{ GHz} \\
 \hat{p} &= \text{VV} \\
 \delta &= .146822 \\
 \ell &= .0052 \text{ m}
 \end{aligned}$$

Figure 2.20. Correlation of the target/clutter multi-path return, $\sigma_{TC-TC}(\phi_2 - \phi_1)$, over $\phi_d = \phi_2 - \phi_1$ for the VV polarization and for $\theta = 20^\circ$ (solid), $\theta = 40^\circ$ (dash), and $\theta = 60^\circ$ (dots). Results are given at 1.120 GHz for a 10 m slab with $z_T = 10$ m and with $\epsilon_0 = \epsilon_2 = \epsilon_o$ and $\epsilon_{1m} = (1.0505 + .001794i)\epsilon_o$.

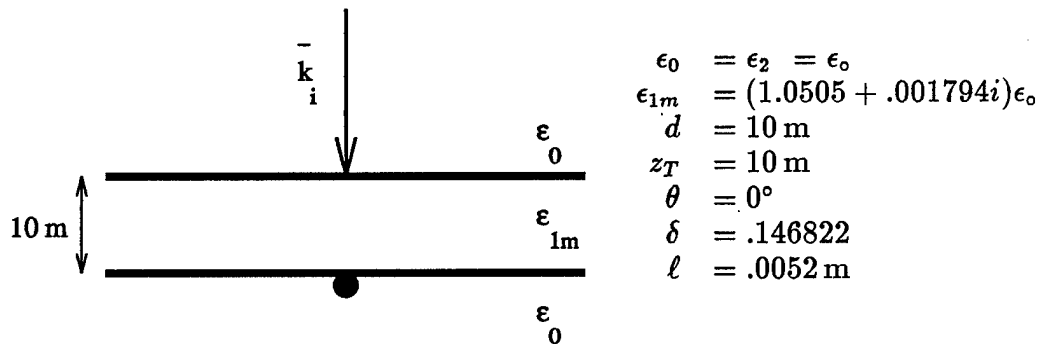
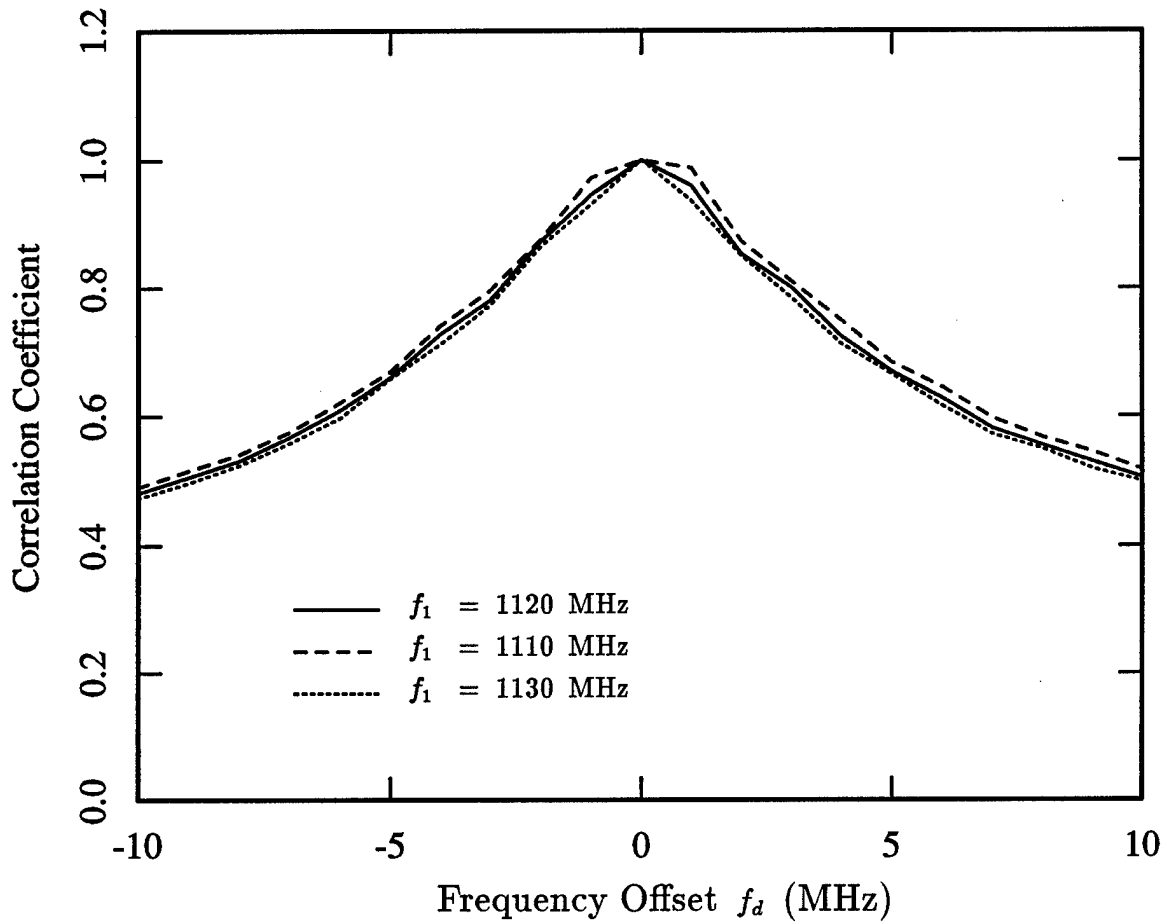
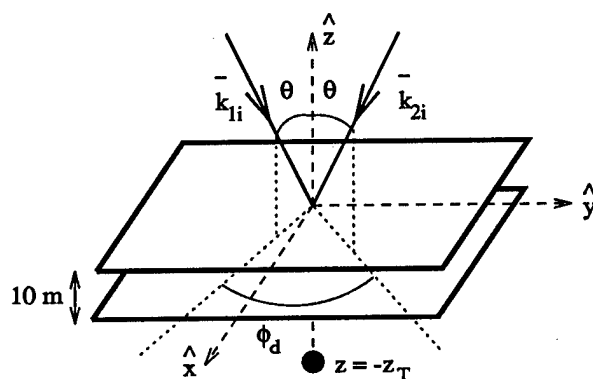
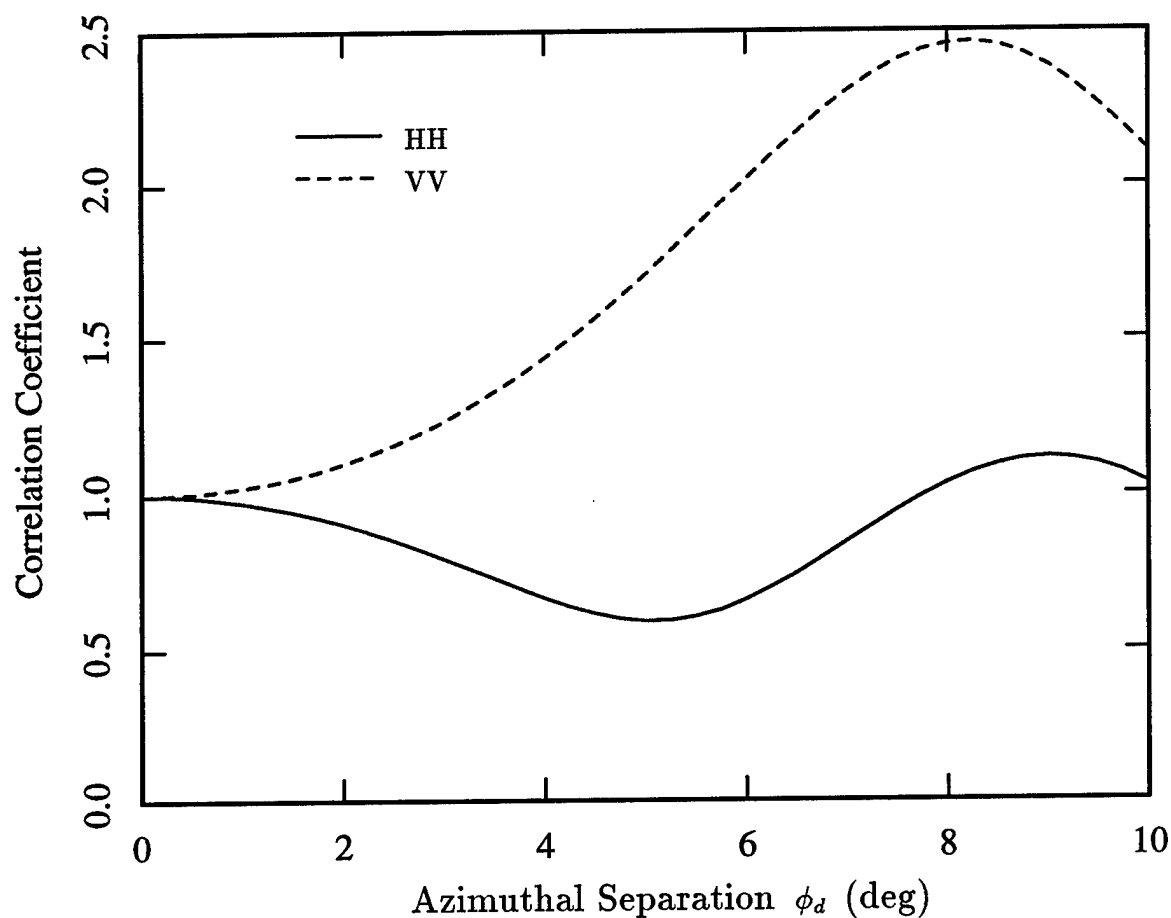


Figure 2.21. Correlation of the target/clutter multi-path return, $\sigma_{TC-TC}(f_1, f_2)$, over $f_d = f_2 - f_1$ for normal incidence ($\theta_1 = \theta_2 = 0^\circ$) and for $f_1 = 1120$ MHz (solid), $f_1 = 1110$ MHz (dash), and $f_1 = 1130$ MHz (dots). Results are given for a 10 m slab with $z_T = 10$ m and with $\epsilon_0 = \epsilon_2 = \epsilon_0$ and $\epsilon_{1m} = (1.0505 + .001794i)\epsilon_0$.



$$\begin{aligned}
 \epsilon_0 &= \epsilon_2 = \epsilon_o \\
 \epsilon_{1m} &= (1.0505 + .001794i)\epsilon_o \\
 d &= 10 \text{ m} \\
 z_T &= 10 \text{ m} \\
 \theta &= 40^\circ \\
 f &= 1.12 \text{ GHz} \\
 \delta &= .146822 \\
 \ell &= .0052 \text{ m}
 \end{aligned}$$

Figure 2.22. Correlation, $\sigma_{C-TC}(\phi_2 - \phi_1)$, of the clutter return at one azimuth, ϕ_1 , with the target/clutter return at a second, ϕ_2 , for $\theta_1 = \theta_2 = 40^\circ$ and for HH (solid) and VV (dash) polarizations. Results are given at 1.120 GHz for a 10 m slab with $z_T = 10$ m and with $\epsilon_0 = \epsilon_2 = \epsilon_o$ and $\epsilon_{1m} = (1.0505 + .001794i)\epsilon_o$.

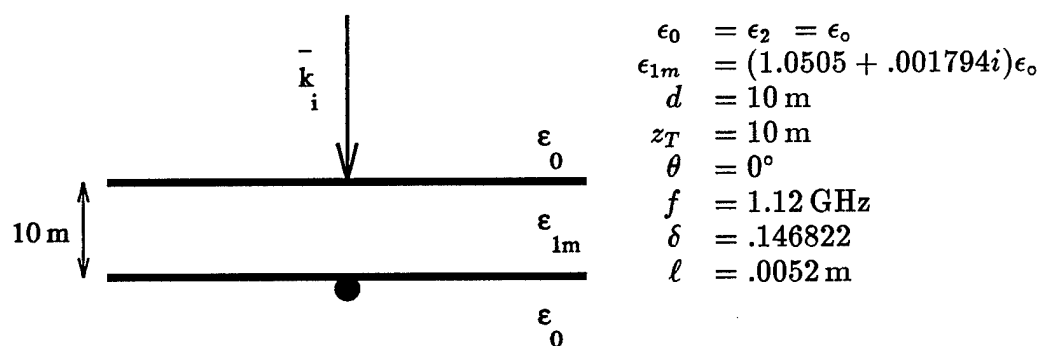
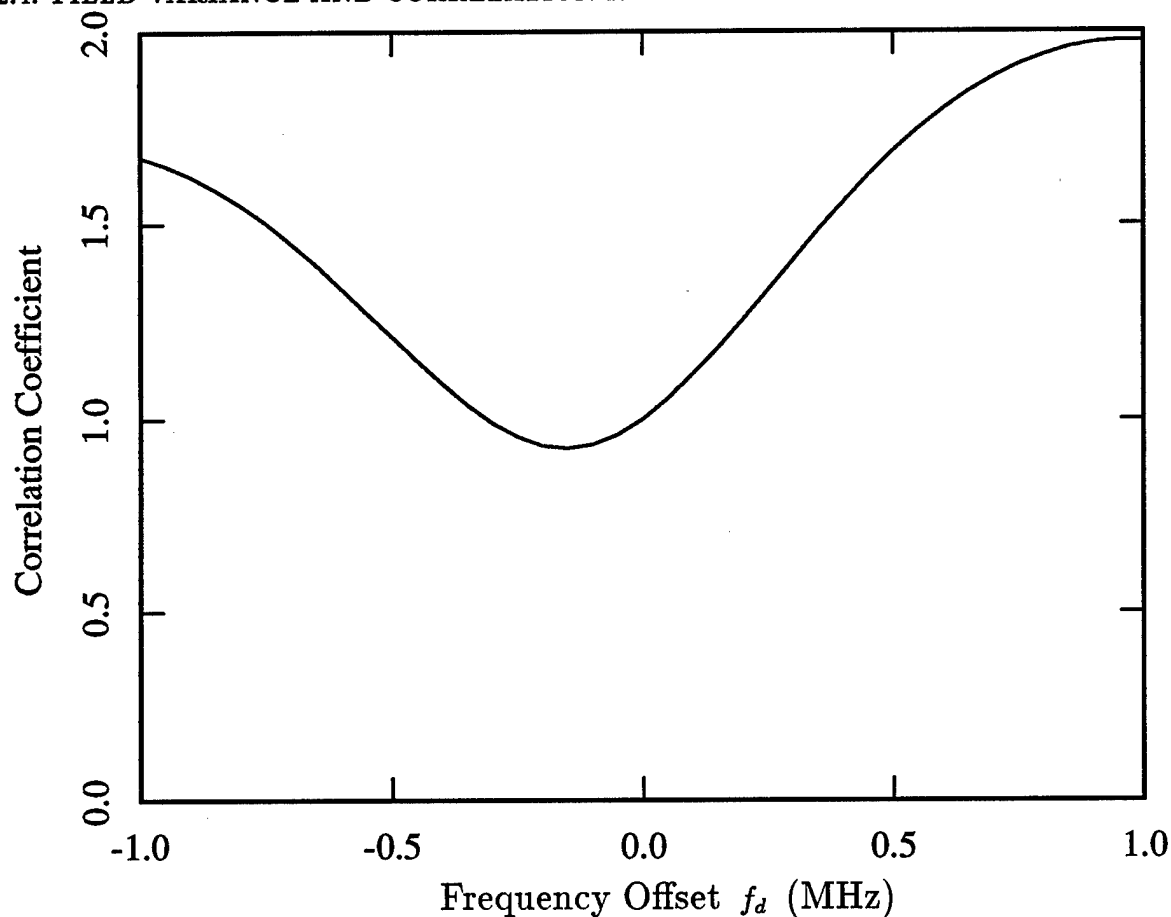


Figure 2.23. Correlation, $\sigma_{C-TC}(f_1, f_2)$, of the clutter return at one frequency, f_1 , with the target/clutter return at a second, f_2 , for normal incidence ($\theta_1 = \theta_2 = 0^\circ$) and for $f_1 = 1120$ MHz. Results are given for a 10 m slab with $z_T = 10$ m and with $\epsilon_0 = \epsilon_2 = \epsilon_o$ and $\epsilon_{1m} = (1.0505 + .001794i)\epsilon_o$.

correlations between the clutter field and the target-clutter field, it is possible that the two fields will correlate better for non-zero separations than for zero separation, leading to correlations above one. Physically, this result is probably arising because the relative phases of individual scatterers in the random media are more the same for the clutter and target-clutter returns when compared at two different angles or two different frequencies than when compared at the same angle and frequency.

Appendix A

Electric Field / Electric Source Green's Function and Incident Field Expressions for an Isotropic Layered Media

The form of the Greens function used here is that given by Ali [144]. For an arbitrary vertically stratified media with source point in layer m , and observation point in layer ℓ , and where $\ell > m$ (i.e., the source above the observation point), the spectral form of the Dyadic Greens function is given by (A.1),

$$\begin{aligned} \overline{\overline{G}}_{\ell m}(\bar{r}, \bar{r}') = & \frac{i}{8\pi^2} \int \int_{-\infty}^{\infty} d\bar{k}_{\perp} \frac{1}{k_{mz}} \sum_{s=\text{TE, TM}} \frac{X_{\cap m \rightarrow \ell}^s}{1 - R_{\cup m}^s R_{\cap m}^s e^{2ik_{mz}h_m}} \times \\ & \sum_{p=+,-} \sum_{p'=+,-} \hat{u}^s(pk_{\ell z}) e^{i\bar{k}_{\perp} \cdot \bar{r}_{\perp}} e^{ipk_{\ell z}z_{\ell}} C_{\cap}^s(p) \times \\ & \hat{u}^s(p'k_{mz}) e^{-i\bar{k}_{\perp} \cdot \bar{r}'_{\perp}} e^{-ip'k_{mz}z'_m} C_{\cap}^{ts}(p') \end{aligned} \quad (\text{A.1})$$

where z_{ℓ} and z_m are given in terms of z measured from the uppermost interface as

$$z_{\ell} = z + d_{\ell-1} \quad (\text{A.2})$$

$$z'_m = z' + d_m \quad (\text{A.3})$$

Similarly, for $\ell < m$, the Greens function is written as in (A.4),

$$\overline{\overline{G}}_{\ell m}(\bar{r}, \bar{r}') = \frac{i}{8\pi^2} \int \int_{-\infty}^{\infty} d\bar{k}_{\perp} \frac{1}{k_{mz}} \sum_{s=\text{TE, TM}} \frac{X_{\cup m \rightarrow \ell}^s}{1 - R_{\cup m}^s R_{\cap m}^s e^{2ik_{mz}h_m}} \times$$

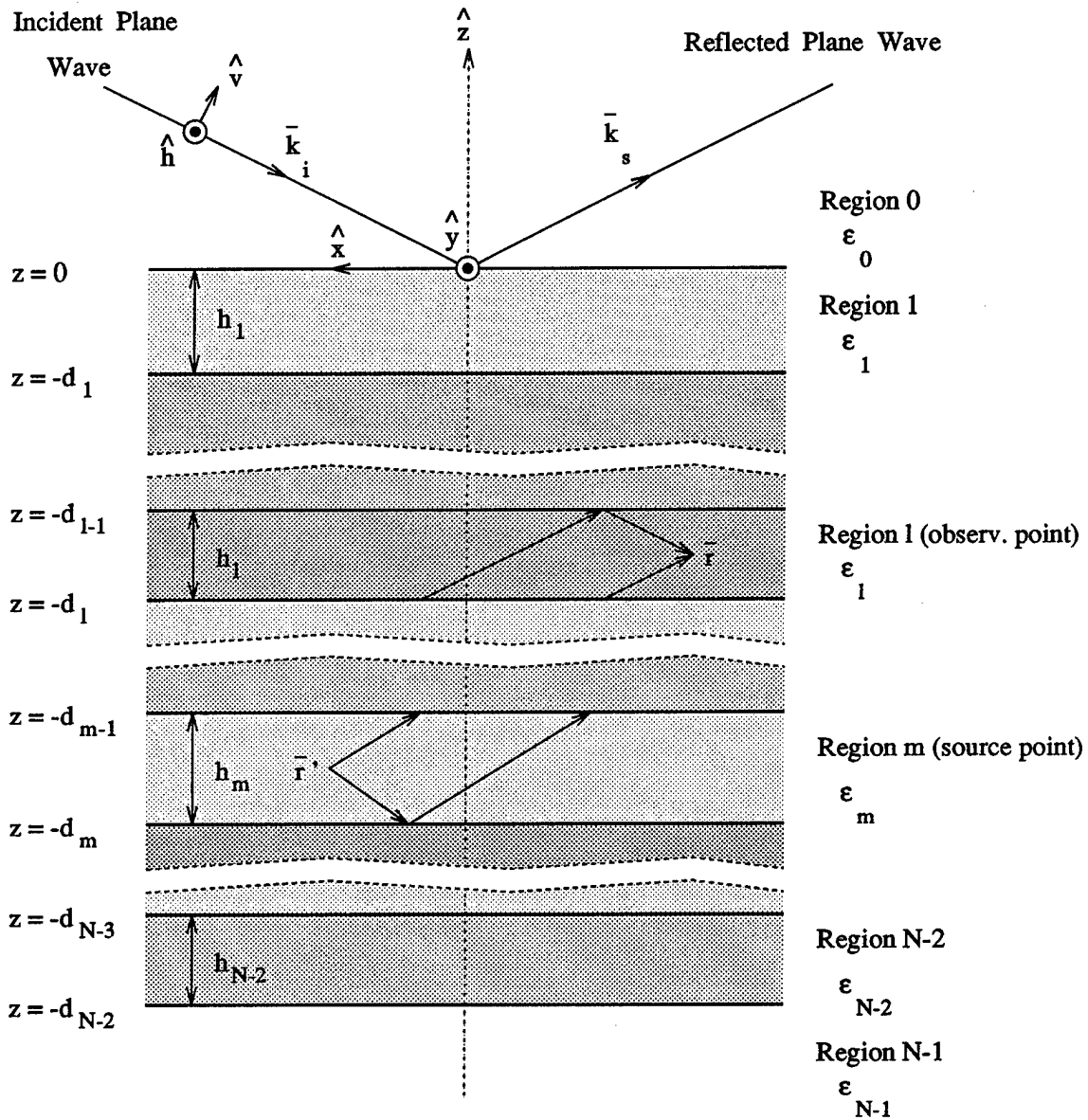


Figure A.1. Geometry of the layered media for which the Greens function and incident field expressions are calculated. For the Greens function, $\overline{G}_{lm}(\vec{r}, \vec{r}')$, the terms contributing to the propagation of the wave from layer m to layer l are shown for the case where $l < m$.

$$\sum_{p=+,-} \sum_{p'=+,-} \hat{u}^s(pk_{tz}) e^{i\vec{k}_\perp \cdot \vec{r}_\perp} e^{ipk_{tz}z_\ell} C_\cup^s(p) \times \\ \hat{u}^s(p'k_{mz}) e^{-i\vec{k}_\perp \cdot \vec{r}'_\perp} e^{-ip'k_{mz}z'_m} C'^s_\cup(p') \quad (A.4)$$

where

$$z_\ell = z + d_\ell \quad (A.5)$$

$$z'_m = z' + d_{m-1} \quad (A.6)$$

In the above, h_m is the thickness of the layer m , and the boundary below layer m occurs at $z = -d_m$. The unit vectors $\hat{u}^s(\pm k_z)$ are defined as shown below.

$$\hat{u}^{\text{TE}}(k_z) = \hat{h}(k_z) = \hat{x} \frac{k_y}{k_\perp} - \hat{y} \frac{k_x}{k_\perp} \quad (A.7)$$

$$\hat{u}^{\text{TE}}(-k_z) = \hat{h}(-k_z) = \hat{x} \frac{k_y}{k_\perp} - \hat{y} \frac{k_x}{k_\perp} \quad (A.8)$$

$$\hat{u}^{\text{TM}}(k_z) = \hat{v}(k_z) = -\frac{k_z}{k} \left(\hat{x} \frac{k_x}{k_\perp} + \hat{y} \frac{k_y}{k_\perp} \right) + \hat{z} \frac{k_\perp}{k} \quad (A.9)$$

$$\hat{u}^{\text{TM}}(-k_z) = \hat{v}(-k_z) = \frac{k_z}{k} \left(\hat{x} \frac{k_x}{k_\perp} + \hat{y} \frac{k_y}{k_\perp} \right) + \hat{z} \frac{k_\perp}{k} \quad (A.10)$$

In addition, the functions $C_\cap^s(p)$, $C_\cup^s(p)$, $C'^s_\cap(p')$, and $C'^s_\cup(p')$ are as given below.

$$C_\cap^s(+)=R_\cap^s(k_{tz})e^{2ik_{tz}h_\ell} \quad (A.11)$$

$$C_\cap^s(-)=1 \quad (A.12)$$

$$C_\cup^s(+)=1 \quad (A.13)$$

$$C_\cup^s(-)=R_\cup^s(k_{tz})e^{2ik_{tz}h_\ell} \quad (A.14)$$

$$C''_{\cap}(+) = R_{\cup m}^s(k_{mz})e^{2ik_{mz}h_m} \quad (A.15)$$

$$C''_{\cap}(-) = 1 \quad (A.16)$$

$$C''_{\cup}(+) = 1 \quad (A.17)$$

$$C''_{\cup}(-) = R_{\cap m}^s(k_{mz})e^{2ik_{mz}h_m} \quad (A.18)$$

The multi-layer reflection coefficients for downward and upward propagation through the layered media are given recursively by

$$R_{\cap \ell}^s = \frac{R_{\ell(\ell+1)}^s + R_{\cap(\ell+1)}^s e^{2ik_{\ell(\ell+1)z}h_{\ell(\ell+1)}}}{1 + R_{\cap(\ell+1)}^s R_{\ell(\ell+1)}^s e^{2ik_{\ell(\ell+1)z}h_{\ell(\ell+1)}}} \quad (A.19)$$

where $R_{\cap(n-1)}^s = R_{(n-1)n}^s$ for Region n below the bottom boundary, and by

$$R_{\cup \ell}^s = \frac{R_{\ell(\ell-1)}^s + R_{\cup(\ell-1)}^s e^{2ik_{\ell(\ell-1)z}h_{\ell(\ell-1)}}}{1 + R_{\cup(\ell-1)}^s R_{\ell(\ell-1)}^s e^{2ik_{\ell(\ell-1)z}h_{\ell(\ell-1)}}} \quad (A.20)$$

where $R_{\cup 1}^s = R_{10}^s$ for Region 0 above the top boundary. In the above, the individual layer reflection coefficients for TE and TM cases are given by (A.21) and (A.22).

$$R_{ij}^{TE} = \frac{\mu_j k_{iz} - \mu_i k_{jz}}{\mu_j k_{iz} + \mu_i k_{jz}} \quad (A.21)$$

$$R_{ij}^{TM} = \frac{\epsilon_j k_{iz} - \epsilon_i k_{jz}}{\epsilon_j k_{iz} + \epsilon_i k_{jz}} \quad (A.22)$$

Finally, the downward and upward transmission coefficients are given by

$$X_{\cap m \rightarrow \ell}^{TE} = X_{\cap m \rightarrow \ell-1}^{TE} e^{ik_{\ell(\ell-1)z}h_{\ell(\ell-1)}} \frac{(1 + R_{\cap(\ell-1)}^{TE})}{(1 + R_{\cap \ell}^{TE} e^{2ik_{\ell z}h_{\ell}})} \quad (A.23)$$

$$X_{\cap m \rightarrow \ell}^{TM} = \frac{k_{\ell}}{k_{\ell z}} \frac{k_{(\ell-1)z}}{k_{(\ell-1)}} X_{\cap m \rightarrow \ell-1}^{TM} e^{ik_{\ell(\ell-1)z}h_{\ell(\ell-1)}} \frac{(1 - R_{\cap(\ell-1)}^{TM})}{(1 - R_{\cap \ell}^{TM} e^{2ik_{\ell z}h_{\ell}})} \quad (A.24)$$

where for $\ell = m + 1$

$$X_{\cap m \rightarrow m+1}^{TE} = \frac{1 + R_{\cap m}^{TE}}{1 + R_{\cap(m+1)}^{TE} e^{2ik_{(m+1)z}h_{(m+1)}}} \quad (A.25)$$

$$X_{\cap m \rightarrow m+1}^{TM} = \frac{k_{(m+1)}}{k_{(m+1)z}} \frac{k_{mz}}{k_m} \frac{1 - R_{\cap m}^{TM}}{1 - R_{\cap(m+1)}^{TM} e^{2ik_{(m+1)z}h_{(m+1)}}} \quad (A.26)$$

and

$$X_{\cup m \rightarrow \ell}^{TE} = X_{\cup m \rightarrow \ell+1}^{TE} e^{ik_{(\ell+1)z}h_{(\ell+1)}} \frac{(1 + R_{\cup(\ell+1)}^{TE})}{(1 + R_{\cup \ell}^{TE} e^{2ik_{\ell z}h_{\ell}})} \quad (A.27)$$

$$X_{\cup m \rightarrow \ell}^{TM} = \frac{k_{\ell}}{k_{\ell z}} \frac{k_{(\ell+1)z}}{k_{(\ell+1)}} X_{\cup m \rightarrow \ell+1}^{TM} e^{ik_{(\ell+1)z}h_{(\ell+1)}} \frac{(1 - R_{\cup(\ell+1)}^{TM})}{(1 - R_{\cup \ell}^{TM} e^{2ik_{\ell z}h_{\ell}})} \quad (A.28)$$

where for $\ell = m - 1$

$$X_{\cup m \rightarrow m-1}^{TE} = \frac{1 + R_{\cup m}^{TE}}{1 + R_{\cup(m-1)}^{TE} e^{2ik_{(m-1)z}h_{(m-1)}}} \quad (A.29)$$

$$X_{\cup m \rightarrow m-1}^{TM} = \frac{k_{(m-1)}}{k_{(m-1)z}} \frac{k_{mz}}{k_m} \frac{1 - R_{\cup m}^{TM}}{1 - R_{\cup(m-1)}^{TM} e^{2ik_{(m-1)z}h_{(m-1)}}} \quad (A.30)$$

The two dyadic Greens functions above can be combined and written in the simpler form of (A.31) below,

$$\overline{\overline{G}}_{\ell m}^{\cup \cap}(\vec{r}, \vec{r}') = \int \int_{-\infty}^{\infty} d\vec{k}_{\perp} \sum_{p, p' = +, -} e^{i\vec{k}_{\perp} \cdot (\vec{r} - \vec{r}')} e^{ipk_{\ell z}z} e^{-ip'k_{mz}z'} \overline{\overline{F}}_{pp'}^{\cup \cap}(\vec{k}_{\perp}) \quad (A.31)$$

where

$$\begin{aligned} \overline{\overline{F}}_{pp'}^{\cup \cap}(\vec{k}_{\perp}) &= \frac{i}{8\pi^2} \frac{1}{k_{mz}} \sum_{s=\text{TE, TM}} \frac{X_{\cup \cap m \rightarrow \ell}^s}{1 - R_{\cup m}^s R_{\cap m}^s e^{2ik_{mz}h_m}} \times \\ &\hat{u}^s(pk_{\ell z}) \hat{u}^s(p'k_{mz}) C_{\cup \cap}^s(p) C_{\cup \cap}^{s'}(p') e^{ipk_{\ell z}(z_{\ell} - z)} e^{-ip'k_{mz}(z'_m - z')} \end{aligned} \quad (A.32)$$

From the above, $\overline{\overline{F}}_{12_{pp'}}$ and $\overline{\overline{F}}_{21_{pp'}}$ can easily be evaluated.

It is also necessary to evaluate the far field form of the above Greens function for a source in layer 1 or 2 and the observation point at a distance in region 0. The above can be simplified for this case by evaluating the integral with a stationary phase approximation [145]. The derivation is omitted, but the result is given by (A.33),

$$\overline{\overline{G}}_{0m}^{\text{ff}}(\bar{r}, \bar{r}') = \frac{e^{ikr}}{4\pi r} \sum_{p=+,-} \overline{\overline{H}}_{0m_p}(\bar{k}_{\perp}) e^{-i\bar{k}_{\perp} \cdot \bar{r}'_{\perp}} e^{-ipk_{mz} z'} \quad (\text{A.33})$$

where

$$\begin{aligned} \overline{\overline{H}}_{0m_p}(\bar{k}_{\perp}) = \frac{k_{0z}}{k_{mz}} \sum_{s=\text{TE, TM}} \frac{X_{\cup m \rightarrow 0}^s}{1 - R_{\cup m}^s R_{\cap m}^s e^{2ik_{mz} h_m}} \times \\ \hat{u}^s(k_{0z}) \hat{u}^s(pk_{mz}) C_{\cup}^s(+) C_{\cup}^{\prime s}(p) e^{-ipk_{mz} d_{m-1}} \end{aligned} \quad (\text{A.34})$$

In the above, \bar{k}_{\perp} is the perpendicular component of the wave vector in the direction of scattering to the far field observation point. The two equations above allow evaluation of $\overline{\overline{H}}_{01_p}$ and $\overline{\overline{H}}_{02_p}$.

Finally, it is necessary to evaluate the incident fields in each region arising from a far field plane wave source. The field incident on the upper boundary is assumed to take the form of (A.35),

$$\overline{E}_i = [E_i^{\text{TE}} \hat{h}(-k_{0zi}) + E_i^{\text{TM}} \hat{v}(-k_{0zi})] e^{i\bar{k}_{\perp i} \cdot \bar{r}_{\perp}} e^{-ik_{0zi} z} \quad (\text{A.35})$$

where E_i^{TE} and E_i^{TM} are the magnitudes of the TE and TM components of the field, and where $\bar{k}_{\perp i}$ is the perpendicular component of the wave vector of the incident plane wave. The general form of the total field in each layer is then given by (A.36),

$$\overline{E}_{li}(\bar{r}) = e^{i\bar{k}_{\perp i} \cdot \bar{r}_{\perp}} \sum_{p=+,-} \overline{E}_{li}^p(\bar{k}_{\perp i}) e^{-ipk_{li} z} \quad (\text{A.36})$$

where for $\ell > 0$

$$\overline{E}_{\ell i}^p(\overline{k}_{\perp}) = \sum_{s=\text{TE, TM}} E_i^s X_{\ell 0 \rightarrow \ell}^s \hat{u}^s(-pk_{\ell z}) C_{\ell}^s(-p) e^{-ipk_{\ell z} d_{\ell-1}} \quad (A.37)$$

From the above the total fields incident in regions 1 and 2 can easily be determined.

Appendix B

Correlation of Scattered Field Components

The following gives the expressions for the correlations of all scattered field components, including the target scattered field, the clutter scattered field, and the multi-path interaction contributions. In all the expressions, Φ is the spectral density associated with the correlation of the renormalized scattering source which was given by (2.27).

B.1. Target/Clutter – Target/Clutter Correlation

$$\begin{aligned}
& \sigma_{TC-TC}^{p_a p_b}(\bar{k}_{as}, \bar{k}_{ai}, \bar{k}_{bs}, \bar{k}_{bi}) \\
&= 4\pi r^2 \left\langle \hat{p}_a \cdot \bar{E}_{TC}(\bar{k}_{as}, \bar{k}_{ai}) \hat{p}_b^* \cdot \bar{E}_{TC}^*(\bar{k}_{bs}, \bar{k}_{bi}) \right\rangle \\
&= (2\pi)^5 i \int_{-\infty}^{\infty} d\bar{k}_{\perp b} \sum_{\substack{s, s', q', \ell' = + \\ p, p', q, \ell = +, -}} A_{TC-TC}^{pp'ss'qq'\ell\ell'} \times \\
& \quad e^{-i(\bar{k}_{\perp as} - \bar{k}_{\perp bs} - \bar{k}_{\perp ai} + \bar{k}_{\perp bi}) \cdot \bar{r}_{\perp T}} e^{-i(q'k_{2za} + sk_{2zai} - \ell'k_{2zb} - s'k_{2zbi})z_T} \times \\
& \quad \left[\frac{\Phi(\bar{k}_{\perp b} - \bar{k}_{\perp bs}, \ell k_{1zb}^* - p'k_{1zb}^*)}{pk_{1zas} - qk_{1za} + \ell k_{1zb}^* - p'k_{1zb}^*} - \frac{\Phi(\bar{k}_{\perp b} - \bar{k}_{\perp bs}, qk_{1za} - pk_{1zas})}{pk_{1zas} - qk_{1za} + \ell k_{1zb}^* - p'k_{1zb}^*} \right] \times \\
& \quad e^{i(pk_{1zas} - qk_{1za} + \ell k_{1zb}^* - p'k_{1zb}^*)d} \quad (B.1)
\end{aligned}$$

where

$$\begin{aligned}
A_{TC-TC}^{pp'ss'qq'\ell\ell'} &= \frac{|\alpha'|^2}{4\pi} \left[\hat{p}_a \cdot \bar{H}_{01p}^a(\bar{k}_{\perp as}) \cdot \bar{F}_{12qq'}^a(\bar{k}_{\perp as}) \cdot \bar{E}_{2ai}^s \right] \times \\
& \quad \left[\hat{p}_b \cdot \bar{H}_{01p'}^b(\bar{k}_{\perp bs}) \cdot \bar{F}_{12\ell\ell'}^b(\bar{k}_{\perp bs}) \cdot \bar{E}_{2bi}^{s'} \right]^* \quad (B.2)
\end{aligned}$$

and

$$\bar{k}_{\perp a} = \bar{k}_{\perp b} + \bar{k}_{\perp as} - \bar{k}_{\perp bs} \quad (B.3)$$

B.2. Clutter/Target – Clutter/Target Correlation

$$\begin{aligned}
& \sigma_{CT-CT}^{p_a p_b}(\bar{k}_{as}, \bar{k}_{ai}, \bar{k}_{bs}, \bar{k}_{bi}) \\
&= 4\pi r^2 \left\langle \hat{p}_a \cdot \bar{E}_{CT}(\bar{k}_{as}, \bar{k}_{ai}) \hat{p}_b^* \cdot \bar{E}_{CT}^*(\bar{k}_{bs}, \bar{k}_{bi}) \right\rangle \\
&= (2\pi)^5 i \int_{-\infty}^{\infty} d\bar{k}_{\perp b} \sum_{\substack{p, p', -q, -\ell = + \\ s, s', q', \ell' = +, -}} A_{CT-CT}^{pp'ss'qq'\ell\ell'} \times \\
& \quad e^{-i(\bar{k}_{\perp as} - \bar{k}_{\perp bs} - \bar{k}_{\perp ai} + \bar{k}_{\perp bi}) \cdot \bar{r}_{\perp T}} e^{-i(p k_{2za} - q k_{2zb} + \ell k_{2z_b}^* - p' k_{2z_b}^*) z_T} \times \\
& \quad \left[\frac{\Phi(\bar{k}_{\perp bi} - \bar{k}_{\perp b}, -\ell' k_{1zb}^* - s' k_{1zbi}^*)}{q' k_{1za} + s k_{1zai} - \ell' k_{1zb}^* - s' k_{1zbi}^*} - \frac{\Phi(\bar{k}_{\perp bi} - \bar{k}_{\perp b}, -q' k_{1za} - s k_{1zai})}{q' k_{1za} + s k_{1zai} - \ell' k_{1zb}^* - s' k_{1zbi}^*} \right] \times \\
& \quad e^{i(q' k_{1za} + s k_{1zai} - \ell' k_{1zb}^* - s' k_{1zbi}^*) d} \quad (B.4)
\end{aligned}$$

where

$$\begin{aligned}
A_{CT-CT}^{pp'ss'qq'\ell\ell'} &= \frac{|\alpha'|^2}{4\pi} \left[\hat{p}_a \cdot \bar{H}_{02p}^a(\bar{k}_{\perp as}) \cdot \bar{F}_{21_{qq'}}^a(\bar{k}_{\perp a}) \cdot \bar{E}_{1ai}^s \right] \times \\
& \quad \left[\hat{p}_b \cdot \bar{H}_{02p'}^b(\bar{k}_{\perp bs}) \cdot \bar{F}_{21_{\ell\ell'}}^b(\bar{k}_{\perp b}) \cdot \bar{E}_{1bi}^{s'} \right]^* \quad (B.5)
\end{aligned}$$

and

$$\bar{k}_{\perp a} = \bar{k}_{\perp b} + \bar{k}_{\perp ai} - \bar{k}_{\perp bi} \quad (B.6)$$

B.3. Target/Clutter – Clutter/Target Correlation

$$\begin{aligned}
& \sigma_{TC-CT}^{p_a p_b}(\bar{k}_{as}, \bar{k}_{ai}, \bar{k}_{bs}, \bar{k}_{bi}) \\
&= 4\pi r^2 \langle \hat{p}_a \cdot \bar{E}_{TC}(\bar{k}_{as}, \bar{k}_{ai}) \hat{p}_b^* \cdot \bar{E}_{CT}^*(\bar{k}_{bs}, \bar{k}_{bi}) \rangle \\
&= (2\pi)^5 i \int_{-\infty}^{\infty} d\bar{k}_{\perp b} \sum_{\substack{p', s, q', -\ell = + \\ p, s', q, \ell' = +, -}} A_{TC-CT}^{pp'ss'qq'\ell\ell'} \times \\
& \quad e^{-i(\bar{k}_{\perp as} - \bar{k}_{\perp bs} - \bar{k}_{\perp ai} + \bar{k}_{\perp bi}) \cdot \bar{r}_{\perp T}} e^{-i(q'k_{2za} + sk_{2zi} + \ell k_{2zb} - p'k_{2zs})z_T} \times \\
& \quad \left[\frac{\Phi(\bar{k}_{\perp bi} - \bar{k}_{\perp b}, -\ell'k_{1zb}^* - s'k_{1zbi}^*)}{pk_{1zas} - qk_{1za} - \ell'k_{1zb}^* - s'k_{1zbi}^*} - \frac{\Phi(\bar{k}_{\perp bi} - \bar{k}_{\perp b}, qk_{1za} - pk_{1zas})}{pk_{1zas} - qk_{1za} - \ell'k_{1zb}^* - s'k_{1zbi}^*} \times \right. \\
& \quad \left. e^{i(pk_{1zas} - qk_{1za} - \ell'k_{1zb}^* - s'k_{1zbi}^*)d} \right] \tag{B.7}
\end{aligned}$$

where

$$\begin{aligned}
A_{TC-CT}^{pp'ss'qq'\ell\ell'} &= \frac{|\alpha'|^2}{4\pi} \left[\hat{p}_a \cdot \bar{H}_{01p}^a(\bar{k}_{\perp as}) \cdot \bar{F}_{12qq'}^a(\bar{k}_{\perp a}) \cdot \bar{E}_{2ai}^s \right] \times \\
& \quad \left[\hat{p}_b \cdot \bar{H}_{02p'}^b(\bar{k}_{\perp bs}) \cdot \bar{F}_{21\ell\ell'}^b(\bar{k}_{\perp b}) \cdot \bar{E}_{1bi}^{s'} \right]^* \tag{B.8}
\end{aligned}$$

and

$$\bar{k}_{\perp a} = -\bar{k}_{\perp b} + \bar{k}_{\perp as} + \bar{k}_{\perp bi} \tag{B.9}$$

B.4. Clutter – Target/Clutter Correlation

$$\begin{aligned}
& \sigma_{C-TC}^{p_a p_b}(\bar{k}_{as}, \bar{k}_{ai}, \bar{k}_{bs}, \bar{k}_{bi}) \\
&= 4\pi r^2 \left\langle \hat{p}_a \cdot \bar{E}_C(\bar{k}_{as}, \bar{k}_{ai}) \hat{p}_b^* \cdot \bar{E}_{TC}^*(\bar{k}_{bs}, \bar{k}_{bi}) \right\rangle \\
&= (2\pi)^5 i \sum_{\substack{s', q' = + \\ p, p', s, q = +, -}} A_{C-TC}^{pp'ss'qq'} e^{i(q'k_{2z_b}^* + s'k_{2z_{bi}}^*)z_T} e^{-i(\bar{k}_{\perp bi} - \bar{k}_{\perp ai} - \bar{k}_{\perp bs} + \bar{k}_{\perp as}) \cdot \bar{r}_{\perp T}} \times \\
& \quad \left[\frac{\Phi(\bar{k}_{\perp ai} - \bar{k}_{\perp as}, -p'k_{1z_{bs}}^* + qk_{1z_b}^*)}{pk_{1z_{as}} + sk_{1z_{ai}} - p'k_{1z_{bs}}^* + qk_{1z_b}^*} - \frac{\Phi(\bar{k}_{\perp ai} - \bar{k}_{\perp as}, -pk_{1z_{as}} - sk_{1z_{ai}}^*)}{pk_{1z_{as}} + sk_{1z_{ai}} - p'k_{1z_{bs}}^* + qk_{1z_b}^*} \right] \times \\
& \quad e^{i(pk_{1z_{as}} + sk_{1z_{ai}} - p'k_{1z_{bs}}^* + qk_{1z_b}^*)d} \quad (B.10)
\end{aligned}$$

where

$$\begin{aligned}
A_{C-TC}^{pp'ss'qq'} &= \frac{\alpha'^*}{4\pi} \left[\hat{p}_a \cdot \bar{H}_{01_p}^a(\bar{k}_{\perp as}) \cdot \bar{E}_{1ai}^s \right] \times \\
& \quad \left[\hat{p}_b^* \cdot \bar{H}_{01_{p'}}^b(\bar{k}_{\perp bs}) \cdot \bar{F}_{12_{qq'}}^b(\bar{k}_{\perp b}) \cdot \bar{E}_{2ai}^{s'} \right]^* \quad (B.11)
\end{aligned}$$

and

$$\bar{k}_{\perp b} = \bar{k}_{\perp ai} + \bar{k}_{\perp bs} - \bar{k}_{\perp as} \quad (B.12)$$

B.5. Clutter – Clutter/Target Correlation

$$\begin{aligned}
& \sigma_{C-CT}^{p_a p_b}(\bar{k}_{as}, \bar{k}_{ai}, \bar{k}_{bs}, \bar{k}_{bi}) \\
&= 4\pi r^2 \langle \hat{p}_a \cdot \bar{E}_C(\bar{k}_{as}, \bar{k}_{ai}) \hat{p}_b^* \cdot \bar{E}_{CT}^*(\bar{k}_{bs}, \bar{k}_{bi}) \rangle \\
&= (2\pi)^5 i \sum_{\substack{p', s', q' = +, - \\ p, s, s', q' = +, -}} A_{C-CT}^{pp'ss'qq'} e^{i(-qk_{2z_b}^* + p'k_{2z_b}^*)z_T} e^{-i(\bar{k}_{\perp bi} - \bar{k}_{\perp ai} - \bar{k}_{\perp bs} + \bar{k}_{\perp as}) \cdot \bar{r}_{\perp T}} \times \\
& \quad \left[\frac{\Phi(\bar{k}_{\perp ai} - \bar{k}_{\perp as}, -s'k_{1z_{bi}}^* - q'k_{1z_b}^*)}{pk_{1z_{as}} + sk_{1z_{ai}} - s'k_{1z_{bi}}^* - q'k_{1z_b}^*} - \frac{\Phi(\bar{k}_{\perp ai} - \bar{k}_{\perp as}, -pk_{1z_{as}} - sk_{1z_{ai}}^*)}{pk_{1z_{as}} + sk_{1z_{ai}} - s'k_{1z_{bi}}^* - q'k_{1z_b}^*} \right] \times \\
& \quad e^{i(pk_{1z_{as}} + sk_{1z_{ai}} - s'k_{1z_{bi}}^* - q'k_{1z_b}^*)d} \quad (B.13)
\end{aligned}$$

where

$$\begin{aligned}
A_{C-CT}^{pp'ss'qq'} &= \frac{\alpha'^*}{4\pi} \left[\hat{p}_a \cdot \bar{H}_{01p}^a(\bar{k}_{\perp as}) \cdot \bar{E}_{1ai}^s \right] \times \\
& \quad \left[\hat{p}_b^* \cdot \bar{H}_{02p'}^b(\bar{k}_{\perp bs}) \cdot \bar{F}_{21qq'}^b(\bar{k}_{\perp bi}) \cdot \bar{E}_{1ai}^{s'} \right]^* \quad (B.14)
\end{aligned}$$

and

$$\bar{k}_{\perp b} = \bar{k}_{\perp ai} - \bar{k}_{\perp as} + \bar{k}_{\perp bi} \quad (B.15)$$

B.6. Target – Target Correlation

$$\begin{aligned}
 \sigma_{T-T}^{p_a p_b}(\bar{k}_{as}, \bar{k}_{ai}, \bar{k}_{bs}, \bar{k}_{bi}) &= \hat{p}_a \cdot \bar{E}_T(\bar{k}_{as}, \bar{k}_{ai}) \times \hat{p}_b^* \cdot \bar{E}_T^*(\bar{k}_{bs}, \bar{k}_{bi}) \\
 &= \sum_{p, p', s, s' = +} A_{T-T}^{pp's's'} e^{-i(p k_{2z_{as}} + s k_{2z_{ai}} - p' k_{2z_{bs}} - s' k_{2z_{bi}})z_T} \times \\
 &\quad e^{-i(\bar{k}_{\perp as} - \bar{k}_{\perp bs} - \bar{k}_{\perp ai} + \bar{k}_{\perp bi}) \cdot \bar{r}_{\perp T}} \quad (B.16)
 \end{aligned}$$

where

$$A_{T-T}^{pp's's'} = \frac{|\alpha'|^2}{(4\pi r)^2} \left[\hat{p}_a \cdot \bar{H}_{02_p}^a(\bar{k}_{\perp as}) \cdot \bar{E}_{2_{ai}}^s \right] \times \left[\hat{p}_b \cdot \bar{H}_{02_{p'}}^b(\bar{k}_{\perp bs}) \cdot \bar{E}_{2_{bi}}^{s'} \right]^* \quad (B.17)$$

B.7. Clutter – Clutter Correlation

$$\begin{aligned}
\sigma_{C-C}^{p_a p_b} = & 8\pi^3 i \int d\bar{r}_{\perp a} \sum_{p, p', s, s' = +, -} A_{C-C}^{pp'ss'} e^{i(\bar{k}'_{\perp ai} - \bar{k}'_{\perp as} - \bar{k}'_{\perp bi} + \bar{k}'_{\perp bs}) \cdot \bar{r}_{\perp a}} \times \\
& \left[\frac{\Phi(\bar{k}'_{\perp bi} - \bar{k}'_{\perp bs}, -p'k'_{1zbs} - s'k'_{1zbi})}{pk'_{1zas} + sk'_{1zai} - p'k'_{1zbs} - s'k'_{1zbi}} - \frac{\Phi(\bar{k}'_{\perp bi} - \bar{k}'_{\perp bs}, -pk'_{1zas} - sk'_{1zai})}{pk'_{1zas} + sk'_{1zai} - p'k'_{1zbs} - s'k'_{1zbi}} \right] \times \\
& e^{i(pk'_{1zas} + sk'_{1zai} - p'k'_{1zbs} - s'k'_{1zbi})d} \quad (B.18)
\end{aligned}$$

where

$$\begin{aligned}
A_{C-C}^{pp'ss'} = & \frac{1}{4\pi} \frac{r_{\text{avg}}^4}{r_{ai} r_{as} r_{bi} r_{bs}} \left[\hat{p}_a \cdot \bar{H}_{01p}^a(\bar{k}'_{\perp as}) \cdot \bar{E}_{1ai}^s(\bar{k}'_{\perp ai}) \right] \times \\
& \left[\hat{p}_b \cdot \bar{H}_{01p'}^b(\bar{k}'_{\perp bs}) \cdot \bar{E}_{1bi}^{s'}(\bar{k}'_{\perp bi}) \right]^* \times \\
& \sqrt{\frac{G_{ai}(\bar{r}_{\perp a})}{G_a} \cdot \frac{G_{as}(\bar{r}_{\perp a} - \bar{r}_{isa})}{G_a} \cdot \frac{G_{bi}(\bar{r}_{\perp b} - \bar{r}_{ii})}{G_b} \cdot \frac{G_{bs}(\bar{r}_{\perp b} - \bar{r}_{ii} - \bar{r}_{isb})}{G_b}} \times \\
& e^{i\bar{k}'_{\perp as} \cdot \bar{r}_{isa}} e^{-i\bar{k}'_{\perp bs} \cdot \bar{r}_{isb}} e^{i(\bar{k}'_{\perp bi} - \bar{k}'_{\perp bs}) \cdot \bar{r}_{ii}} \quad (B.19)
\end{aligned}$$

Chapter 3

Phase Fluctuations of a Point Target Beneath a Layer of Continuous Random Media

The previous chapter presented an analysis of the coherent and incoherent fields scattered by a point target beneath a layer of random media. In the representation which was used, the signal component of the return is viewed as a sum of a coherent mean component and a randomly varying incoherent component of zero mean. The effect of the random media was seen to be an attenuation of the coherent return when compared to the free space case, and the corruption of this mean signal by an additive random noise source.

While the analysis of the previous chapter is sufficient to evaluate the performance degradations of a typical SAR processing scheme, an alternate representation has often been employed in the analysis of similar sources of degradation for SAR sys-

tems. When examining the effects of SAR platform motion, atmospheric effects, or oscillator instability, these sources of degradation are generally considered to cause a phase or multiplicative noise in the received signal. Hence, to allow comparison with this previous analysis, it is of interest to re-formulate the representation of Chapter 2, and to treat the effect of the random media as introducing a phase fluctuation in the received field.

This chapter considers this alternative representation of the random media effects, where the target signature is represented as the coherent return arising in the absence of permittivity fluctuations, multiplied by an exponential of random, complex phase. The real part of this phase is seen to embody the phase fluctuations or error of the received signal, while the imaginary part reflects the amplitude fluctuation and mean attenuation of the return. In the case where the fluctuations are small, expressions are derived for the variance and correlation of the fluctuations, both over angular and frequency offsets, and the dependance of these statistics on several physical and geometrical parameters is illustrated.

3.1. Formulation

As will be shown in Chapter 7, the variance and correlation expressions of Chapter 2 provide the results necessary to analyze the performance of a typical SAR processing scheme. In the representation used previously, the signal component of the return is viewed as a sum of a coherent mean component and a randomly varying incoherent component of zero mean. An alternate representation of the signal return is suggested

by (3.1), where the effect of the random layer is introduced as an exponential of random complex phase multiplying the coherent return.

$$E_s = E_T e^{i\Phi} \quad (3.1)$$

The complex phase, Φ , has real part, ψ , corresponding to the phase fluctuation in the returned signal, and has imaginary part, γ , referring to the amplitude or attenuation fluctuation.

$$\Phi = \psi + i\gamma \quad (3.2)$$

The representation given by (3.1) and (3.2) is of interest since the variance of the phase fluctuations, $\langle \psi\psi \rangle$, will determine in part the phase error introduced while focusing the synthetic aperture for cross-range resolution, or in compressing a chirped pulse for range resolution. The effect of random phase errors on SAR performance has been previously studied in the context of other phase noise sources such as platform motion and atmospheric interference [6,10-13]. Past results have shown that for non-catastrophic degradation in performance, the phase fluctuations must remain relatively small. For this case of small fluctuations, it is possible to relate the two representations using the approximation shown in (3.3).

$$\begin{aligned} E_s &= E_T + E_{TC} + E_{CT} \\ &= E_T e^{i\Phi} \approx E_T (1 + i\Phi) \end{aligned} \quad (3.3)$$

From the above it is clear that Φ can be found from E_T , E_{TC} , and E_{CT} as shown in (3.4),

$$\Phi = -i \frac{E_{TC} + E_{CT}}{E_T} \quad (3.4)$$

Furthermore, the variance of the phase fluctuation can be found from the complex phase as shown in (3.5).

$$\begin{aligned}\sigma_{\psi\psi} = \langle \psi\psi \rangle &= \frac{\langle \Phi\Phi^* \rangle + \text{Re} \langle \Phi\Phi \rangle}{2} \\ &= \frac{\langle \bar{E}_{TC} \cdot \bar{E}_{TC}^* \rangle + \langle \bar{E}_{CT} \cdot \bar{E}_{CT}^* \rangle + 2\text{Re} \langle \bar{E}_{TC} \cdot \bar{E}_{CT}^* \rangle}{2|\bar{E}_T|^2} \\ &\quad \text{Re} \left[\frac{\langle \bar{E}_{TC} \cdot \bar{E}_{TC} \rangle + \langle \bar{E}_{CT} \cdot \bar{E}_{CT} \rangle + 2\langle \bar{E}_{TC} \cdot \bar{E}_{CT} \rangle}{2(\bar{E}_T \cdot \bar{E}_T)} \right] \quad (3.5)\end{aligned}$$

Similarly, (3.5) can be generalized to determine the correlation of the phase fluctuation as given by (3.6).

$$\begin{aligned}\sigma_{\psi\psi}^{p_a p_b}(\bar{k}_{as}, \bar{k}_{ai}, \bar{k}_{bs}, \bar{k}_{bi}) &= \frac{\sigma_{TC-TC}^{p_a p_b} + \sigma_{CT-CT}^{p_a p_b} + 2\text{Re} \sigma_{TC-CT}^{p_a p_b}}{2\sigma_{T-T}^{p_a p_b}} \\ &\quad \text{Re} \left[\frac{\hat{\sigma}_{TC-TC}^{p_a p_b} + \hat{\sigma}_{CT-CT}^{p_a p_b} + 2\text{Re} \hat{\sigma}_{TC-CT}^{p_a p_b}}{2\hat{\sigma}_{T-T}^{p_a p_b}} \right] \quad (3.6)\end{aligned}$$

where

$$\hat{\sigma}_{TC-TC}^{p_a p_b}(\bar{k}_{as}, \bar{k}_{ai}, \bar{k}_{bs}, \bar{k}_{bi}) = \langle \hat{p}_a \cdot \bar{E}_{TC}(\bar{k}_{as}, \bar{k}_{ai}) \times \hat{p}_b \cdot \bar{E}_{TC}(\bar{k}_{bs}, \bar{k}_{bi}) \rangle \quad (3.7)$$

and similar definitions exist for $\hat{\sigma}_{CT-CT}$, $\hat{\sigma}_{TC-CT}$, and $\hat{\sigma}_{T-T}$. The last of these terms, $\hat{\sigma}_{T-T}$, can be determined by a trivial change of (2.40) and (2.41), and the result is given in Appendix C. The other three terms can be derived in a manner analogous to that presented for σ_{TC-TC} . The derivation of $\hat{\sigma}_{TC-TC}$ is presented below, and the final results for all three incoherent terms are given in Appendix C.

3.2. Complex Correlation of the Incoherent Fields

The complex correlation of (3.7) can be rewritten from (2.23) by removing the conjugation operators, and the result is given by (3.8),

$$\begin{aligned} \hat{\sigma}_{TC-TC}^{p_a p_b} &= 4\pi r^2 \alpha'^2 \int dV_1 \int dV_2 \int dV_3 \int dV_4 \\ &\quad \hat{p}_a \cdot \overline{\overline{G}}_{01}^a(\bar{r}, \bar{r}_1) \cdot \overline{\overline{G}}_{12}^a(\bar{r}_1, \bar{r}_3) \cdot \overline{E}_{2ai}(\bar{r}_3) \delta(\bar{r}_3 - \bar{r}_T) \times \\ &\quad \hat{p}_b \cdot \overline{\overline{G}}_{01}^b(\bar{r}, \bar{r}_2) \cdot \overline{\overline{G}}_{12}^b(\bar{r}_2, \bar{r}_4) \cdot \overline{E}_{2ai}(\bar{r}_4) \delta(\bar{r}_4 - \bar{r}_T) \times \\ &\quad \hat{C}_Q(\bar{r}_1 - \bar{r}_2) \end{aligned} \quad (3.8)$$

where $\alpha' = i\omega\mu\alpha$ and where $\hat{C}_Q(\bar{r})$ is given by (3.9).

$$\hat{C}_Q(|\bar{r}_1 - \bar{r}_2|) = k_o^4 \langle \xi(\bar{r}_1) \xi(\bar{r}_2) \rangle = \hat{\delta} k_o^4 e^{-|\bar{r}_1 - \bar{r}_2|/\ell} \quad (3.9)$$

In the above, $\hat{\delta}$ is the complex variance of $\xi(\bar{r})$. The dyadic Green's functions $\overline{\overline{G}}_{01}(\bar{r}, \bar{r}')$ and $\overline{\overline{G}}_{12}(\bar{r}, \bar{r}')$ appearing in the above are given in Appendix A, along with the expression for the field $\overline{E}_{2i}(\bar{r})$ incident in region 2. Since the observation point is in the far-field, the asymptotic form of $\overline{\overline{G}}_{01}(\bar{r}, \bar{r}')$ is utilized. Hence, the above can be rewritten as (3.10),

$$\begin{aligned} \hat{\sigma}_{TC-TC}^{p_a p_b} &= \frac{\alpha'^2}{4\pi} e^{2ikr} \int dV_1 \int dV_2 \int dV_3 \int dV_4 \int d\bar{k}_{\perp a} \int d\bar{k}_{\perp b} \hat{C}_Q(\bar{r}_1 - \bar{r}_2) \times \\ &\quad \hat{p}_a \cdot e^{-i\bar{k}_{\perp a} \cdot \bar{r}_{1\perp}} \left[\overline{\overline{H}}_{01+}^a(\bar{k}_{\perp a}) e^{-ik_{1za} z_1} + \overline{\overline{H}}_{01-}^a(\bar{k}_{\perp a}) e^{ik_{1za} z_1} \right] \cdot \\ &\quad e^{i\bar{k}_{\perp a} \cdot \bar{r}_{1\perp}} e^{-i\bar{k}_{\perp a} \cdot \bar{r}_{3\perp}} \sum_{q, \ell=+, -} \overline{\overline{F}}_{12\ell q}^a(\bar{k}_{\perp a}) e^{i\ell k_{1za} z_1} e^{-iqk_{2za} z_3}. \end{aligned}$$

$$\begin{aligned}
& e^{i\bar{k}_{\perp ai} \cdot \bar{r}_{3\perp}} \left[\bar{E}_{2ai}^+ e^{-ik_{2zai} z_3} + \bar{E}_{2ai}^- e^{ik_{2zai} z_3} \right] \times \\
& \hat{p}_b \cdot e^{-i\bar{k}_{\perp bs} \cdot \bar{r}_{2\perp}} \left[\bar{H}_{01+}^b(\bar{k}_{\perp bs}) e^{-ik_{1zbs} z_2} + \bar{H}_{01-}^b(\bar{k}_{\perp bs}) e^{ik_{1zbs} z_2} \right] \cdot \\
& e^{i\bar{k}_{\perp b} \cdot \bar{r}_{2\perp}} e^{-i\bar{k}_{\perp b} \cdot \bar{r}_{4\perp}} \sum_{q', \ell' = +, -} \bar{F}_{12\ell'q'}^b(\bar{k}_{\perp b}) e^{i\ell' k_{1zbs} z_2} e^{-iq' k_{2zbs} z_4} \cdot \\
& e^{i\bar{k}_{\perp bi} \cdot \bar{r}_{4\perp}} \left[\bar{E}_{2bi}^+ e^{-ik_{2zbi} z_4} + \bar{E}_{2bi}^- e^{ik_{2zbi} z_4} \right] \times \delta(\bar{r}_3 - \bar{r}_T) \delta(\bar{r}_4 - \bar{r}_T) \quad (3.10)
\end{aligned}$$

where \bar{H}_{01+} , \bar{H}_{01-} , $\bar{F}_{12\ell q}$, \bar{E}_{2i}^+ , and \bar{E}_{2i}^- are all defined in Appendix A. Replacing $\hat{C}_Q(\bar{r})$ with its spectral representation, keeping only non-zero terms, and using a more compact notation yields (3.11),

$$\begin{aligned}
\hat{\sigma}_{TC-TC}^{p_a p_b} = & \int_{-d}^0 dz_1 \int_{-d}^0 dz_2 \int_{-\infty}^{\infty} d\bar{r}_{1\perp} \int_{-\infty}^{\infty} d\bar{r}_{2\perp} \int dV_3 \int dV_4 \int_{-\infty}^{\infty} d\bar{k}_{\perp a} \int_{-\infty}^{\infty} d\bar{k}_{\perp b} \int_{-\infty}^{\infty} d\bar{\beta}_{\perp} \int_{-\infty}^{\infty} d\beta_z \\
& \delta(\bar{r}_3 - \bar{r}_T) \delta(\bar{r}_4 - \bar{r}_T) \sum_{\substack{s, s', q, q' = + \\ p, p', \ell, \ell' = +, -}} \hat{A}_{TC-TC}^{pp'ss'qq'\ell\ell'} \hat{\Phi}(\bar{\beta}) e^{i(\bar{k}_{\perp a} - \bar{k}_{\perp as} - \bar{\beta}_{\perp}) \cdot \bar{r}_{1\perp}} \times \\
& e^{-i(\bar{k}_{\perp a} - \bar{k}_{\perp ai}) \cdot \bar{r}_{3\perp}} e^{i(\bar{k}_{\perp b} - \bar{k}_{\perp bs} + \bar{\beta}_{\perp}) \cdot \bar{r}_{2\perp}} e^{-i(\bar{k}_{\perp b} - \bar{k}_{\perp bi}) \cdot \bar{r}_{4\perp}} e^{-i(p k_{1zas} - \ell k_{1za} + \beta_z) z_1} \times \\
& e^{-i(q k_{2za} + s k_{2zai}) z_3} e^{-i(p' k_{1zbs} - \ell' k_{1zb} - \beta_z) z_2} e^{-i(q' k_{2zb} + s' k_{2zbi}) z_4} \quad (3.11)
\end{aligned}$$

where

$$\begin{aligned}
\hat{A}_{TC-TC}^{pp'ss'qq'\ell\ell'} = & \frac{\alpha'^2}{4\pi} e^{2ikr} \left[\hat{p}_a \cdot \bar{H}_{01p}^a(\bar{k}_{\perp as}) \cdot \bar{F}_{12\ell q}^a(\bar{k}_{\perp a}) \cdot \bar{E}_{2ai}^s \right] \times \\
& \left[\hat{p}_b \cdot \bar{H}_{01p'}^b(\bar{k}_{\perp bs}) \cdot \bar{F}_{12\ell'q'}^b(\bar{k}_{\perp b}) \cdot \bar{E}_{2bi}^{s'} \right] \quad (3.12)
\end{aligned}$$

The integrals over \bar{r}_3 and \bar{r}_4 can be done trivially using the two delta functions. In addition, the $\bar{r}_{1\perp}$ integral can be done directly to obtain another delta function, and this third delta function can be used to perform the $\bar{\beta}_{\perp}$ integration. The result is given

by (3.13).

$$\begin{aligned}
\hat{\sigma}_{TC-TC}^{p_a p_b} = & \int_{-d}^0 dz_1 \int_{-d}^0 dz_2 \int_{-\infty}^{\infty} d\bar{\tau}_{2\perp} \int_{-\infty}^{\infty} d\bar{k}_{\perp a} \int_{-\infty}^{\infty} d\bar{k}_{\perp b} \int_{-\infty}^{\infty} d\beta_z \sum_{\substack{s, s', q, q' = + \\ p, p', \ell, \ell' = +, -}} (2\pi)^2 \times \\
& \hat{A}_{TC-TC}^{pp'ss'qq'\ell\ell'} \hat{\Phi}(\bar{k}_{\perp a} - \bar{k}_{\perp as}, \beta_z) e^{-i(\bar{k}_{\perp a} + \bar{k}_{\perp b} - \bar{k}_{\perp ai} - \bar{k}_{\perp bi}) \cdot \bar{\tau}_{\perp T}} \times \\
& e^{-i(qk_{2za} + sk_{2zai} + q'k_{2zb} + s'k_{2zbi})z_T} e^{i(\bar{k}_{\perp b} - \bar{k}_{\perp bs} + \bar{k}_{\perp a} - \bar{k}_{\perp as}) \cdot \bar{\tau}_{2\perp}} \times \\
& e^{-i(pk_{1zas} - \ell k_{1za} + \beta_z)z_1} e^{-i(p'k_{1zbs} - \ell'k_{1zb} - \beta_z)z_2}
\end{aligned} \tag{3.13}$$

Similarly, it is possible to integrate $\bar{\tau}_{2\perp}$ and obtain a delta function which can be used to integrate $\bar{k}_{\perp a}$. The result is shown in (3.14),

$$\begin{aligned}
\hat{\sigma}_{TC-TC}^{p_a p_b} = & \int_{-d}^0 dz_1 \int_{-d}^0 dz_2 \int_{-\infty}^{\infty} d\bar{k}_{\perp b} \int_{-\infty}^{\infty} d\beta_z \sum_{\substack{s, s', q, q' = + \\ p, p', \ell, \ell' = +, -}} (2\pi)^4 \hat{A}_{TC-TC}^{pp'ss'qq'\ell\ell'} \times \\
& \hat{\Phi}(\bar{k}_{\perp bs} - \bar{k}_{\perp b}, \beta_z) e^{-i(\bar{k}_{\perp as} + \bar{k}_{\perp bs} - \bar{k}_{\perp ai} - \bar{k}_{\perp bi}) \cdot \bar{\tau}_{\perp T}} \times \\
& e^{-i(qk_{2zc} + sk_{2zai} + q'k_{2zb} + s'k_{2zbi})z_T} \times \\
& e^{-i(pk_{1zas} - \ell k_{1zc} + \beta_z)z_1} e^{-i(p'k_{1zbs} - \ell'k_{1zb} - \beta_z)z_2}
\end{aligned} \tag{3.14}$$

where $\bar{k}_{\perp c} = \bar{k}_{\perp as} + \bar{k}_{\perp bs} - \bar{k}_{\perp b}$. The two integrations over z_1 and z_2 can be done directly to yield (3.15).

$$\begin{aligned}
\hat{\sigma}_{TC-TC}^{p_a p_b} = & \int_{-\infty}^{\infty} d\bar{k}_{\perp b} \int_{-\infty}^{\infty} d\beta_z \sum_{\substack{s, s', q, q' = + \\ p, p', \ell, \ell' = +, -}} (2\pi)^4 \hat{A}_{TC-TC}^{pp'ss'qq'\ell\ell'} \times \\
& \hat{\Phi}(\bar{k}_{\perp bs} - \bar{k}_{\perp b}, \beta_z) e^{-i(\bar{k}_{\perp as} + \bar{k}_{\perp bs} - \bar{k}_{\perp ai} - \bar{k}_{\perp bi}) \cdot \bar{\tau}_{\perp T}} \times \\
& e^{-i(qk_{2zc} + sk_{2zai} + q'k_{2zb} + s'k_{2zbi})z_T} \times \\
& \frac{1 - e^{i(pk_{1zas} - \ell k_{1zc} + \beta_z)d}}{pk_{1zas} - \ell k_{1zc} + \beta_z} \cdot \frac{1 - e^{-i(-p'k_{1zbs} + \ell'k_{1zb} + \beta_z)d}}{-p'k_{1zbs} + \ell'k_{1zb} + \beta_z}
\end{aligned} \tag{3.15}$$

Finally, the β_z integration can be done by breaking the integrand into portions convergent in the upper and lower half-spaces of the complex β_z plane, and closing the complex integration contour upward and downward, respectively, at infinite radius. The integral can then be evaluated from the residue contributions of the enclosed poles. The final result is given by (3.16).

$$\begin{aligned} \hat{\sigma}_{TC-TC}^{p_a p_b} = (2\pi)^5 i \int_{-\infty}^{\infty} d\bar{k}_{\perp b} \sum_{\substack{s, s', q, q' = + \\ p, p', \ell, \ell' = +, -}} \hat{A}_{TC-TC}^{pp'ss'qq'\ell\ell'} \times \\ e^{-i(\bar{k}_{\perp a s} + \bar{k}_{\perp b s} - \bar{k}_{\perp a i} - \bar{k}_{\perp b i}) \cdot \bar{r}_{\perp T}} e^{-i(qk_{2z c} + sk_{2z a i} + q'k_{2z b} + s'k_{2z b i})z_T} \times \\ \left[\frac{\hat{\Phi}(\bar{k}_{\perp b s} - \bar{k}_{\perp b}, -\ell'k_{1z b} + p'k_{1z b s})}{pk_{1z a s} - \ell k_{1z c} - \ell'k_{1z b} + p'k_{1z b s}} - \frac{\hat{\Phi}(\bar{k}_{\perp b s} - \bar{k}_{\perp b}, \ell k_{1z c} - pk_{1z a s})}{pk_{1z a s} - \ell k_{1z c} - \ell'k_{1z b} + p'k_{1z b s}} \times \right. \\ \left. e^{i(pk_{1z a s} - \ell k_{1z c} - \ell'k_{1z b} + p'k_{1z b s})d} \right] \quad (3.16) \end{aligned}$$

The other two complex correlation terms can be derived in a similar manner, and the final expressions are given in Appendix C.

3.3. Variance of Phase Fluctuations

Figure 3.1 shows the variance of the phase fluctuations of the target return as a function of the incidence angle, θ . The parameters of the random medium are those assumed previously in Chapter 2, and the target is again located immediately below the lower interface. The slab thickness is assumed to be 10 m, and the frequency used is 1.12 GHz.

In the calculation of the results, it was found that the second term of (3.6) contributed little, since the integrands of the expressions for $\hat{\sigma}_{TC-TC}$, $\hat{\sigma}_{CT-CT}$, and

δ_{TC-CT} oscillate rapidly. For this reason, the behavior of the phase fluctuations is determined primarily by the first term, which consists of the ratio of the incoherent return to the coherent return. Hence, the effect of many parameters can be determined by examining the results of Section 2.4.

The first result (solid) of Figure 3.1 is shown for the case of free space in region 2. The standard deviation of the phase at normal incidence is approximately 20° , and this level increases slightly with angle. The small increase can be expected from the results of Figures 2.5 and 2.6 where it can be seen that both σ_{TC-TC} and σ_{T-T} decrease with angle, but the coherent component decreases at a faster rate. Similarly, the VV and HH polarizations for σ_{T-T} are almost identical, while for σ_{TC-TC} , VV is larger. Hence, it is expected that the phase fluctuations should be larger for the VV polarization, and the figure agrees with this result.

The second result of Figure 3.1 (dashed) shows the effect of replacing the free space below the slab with a lossy media of permittivity $\epsilon_2 = (6.0 + 0.6i)\epsilon_0$. The earlier results of Section 2.4 showed that both the coherent and incoherent target returns were decreased by this change, and the net result here is for the phase fluctuations to remain relatively unaffected. Since, however, the incoherent term is relatively polarization independent, while the Brewster angle effect yields a higher coherent return for the VV polarization, it is expected as discovered that the phase fluctuations are now larger for the HH polarization.

Figure 3.2 shows the standard deviation of the phase fluctuation versus frequency, for a 20 MHz band centered at 1.12 GHz. The parameters used are the same as the free space case above, with the incidence angle now fixed normal to the surface. As expected from previous results, the phase fluctuation shows little change across the

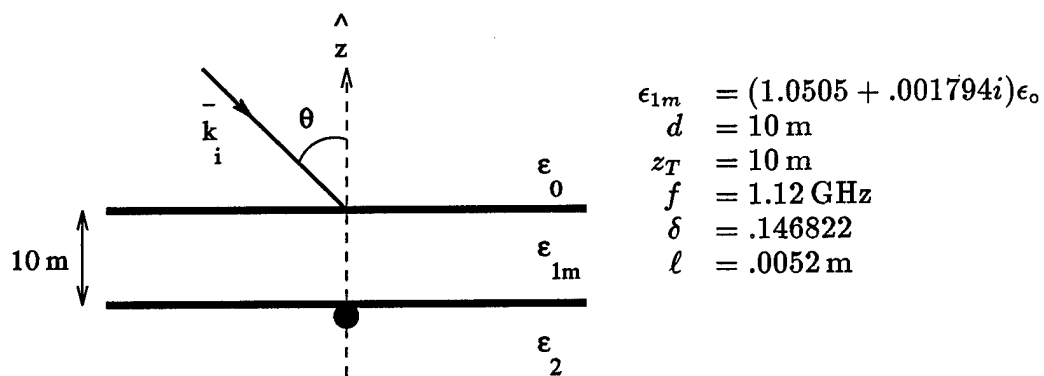
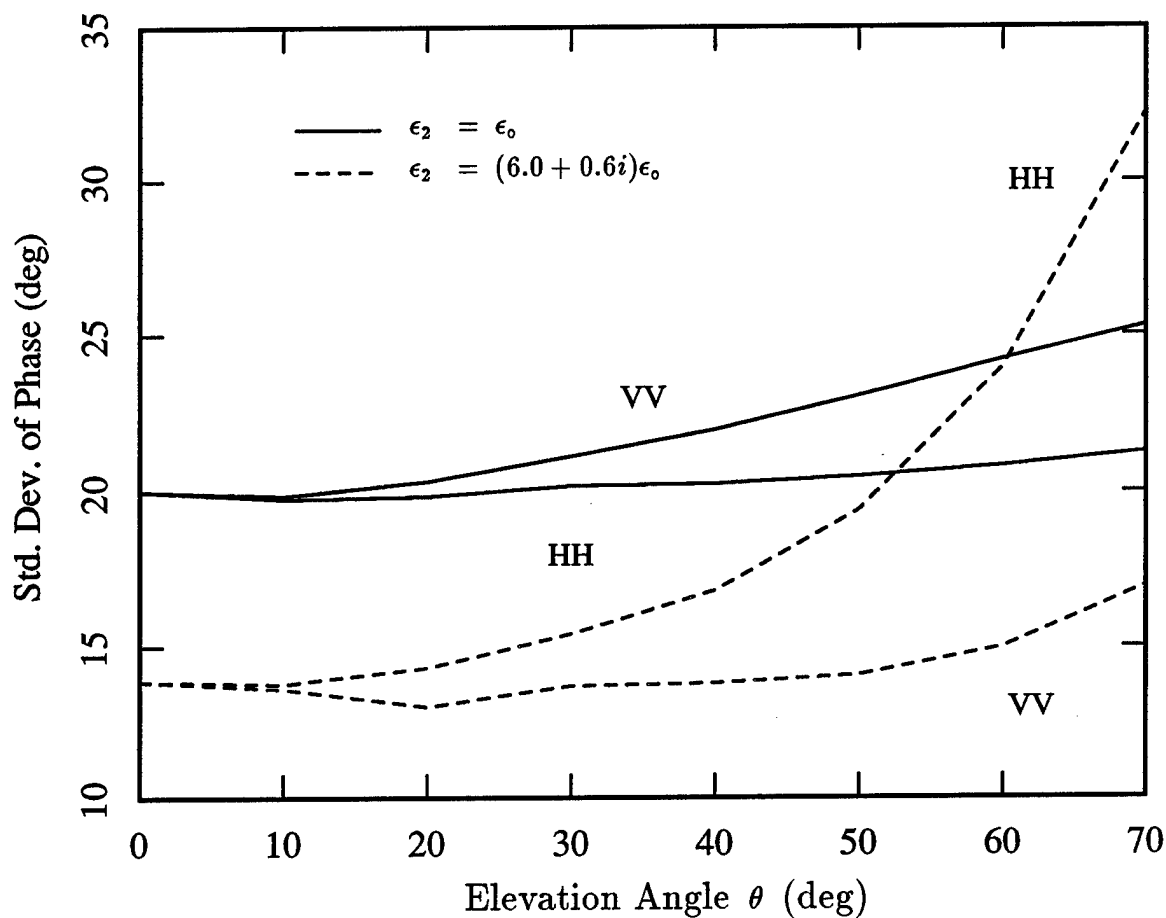


Figure 3.1. Dependence of Phase Fluctuation Variance on elevation angle for $\epsilon_2 = \epsilon_0$ (solid) and $\epsilon_2 = (6.0 + 0.6i)\epsilon_0$ (dash). Results are given at 1.120 GHz for a 10 m slab with $z_T = 10 \text{ m}$ and with $\epsilon_0 = \epsilon_0$ and $\epsilon_{1m} = (1.0505 + .001794i)\epsilon_0$.

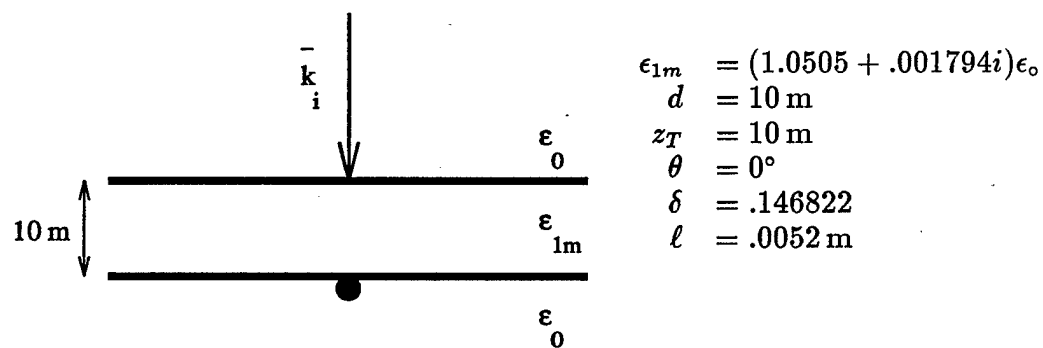
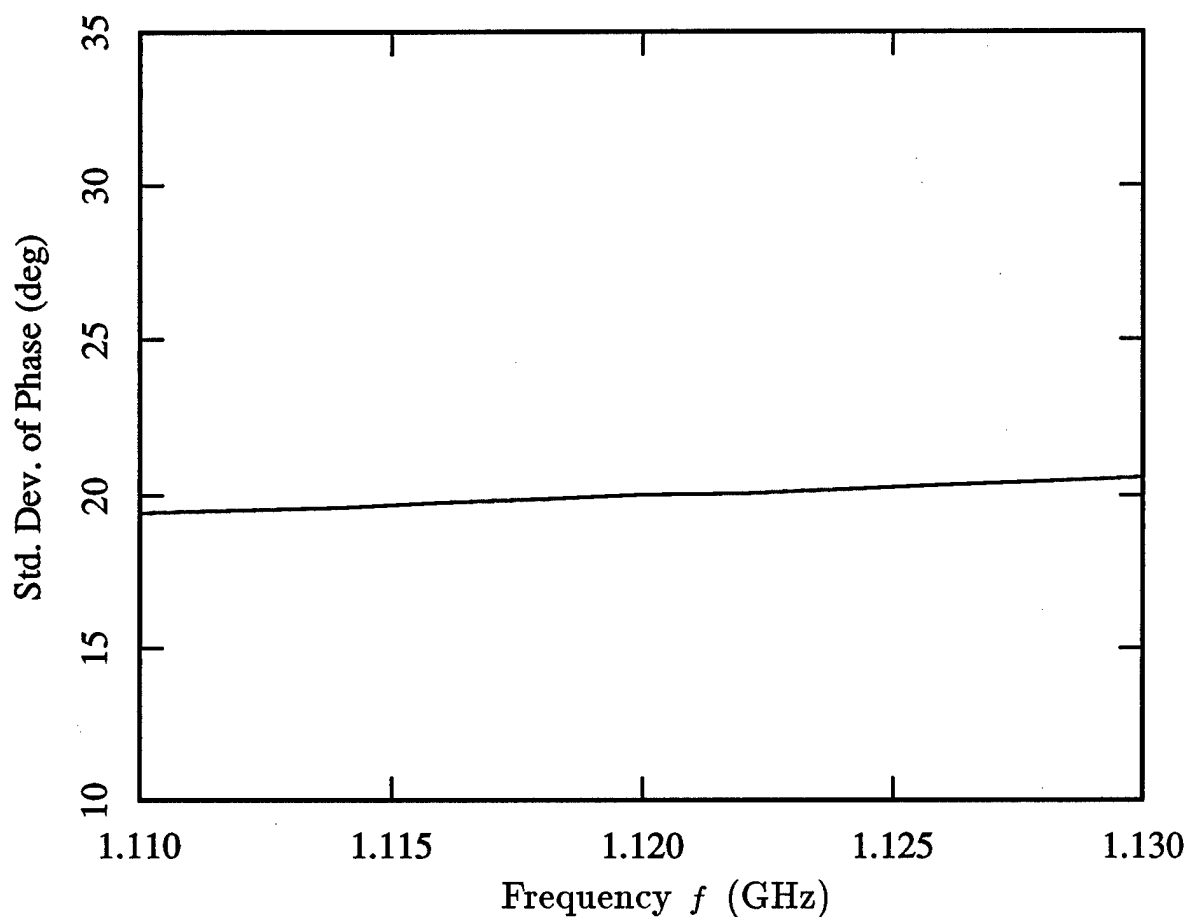


Figure 3.2. Dependence of Phase Fluctuation Variance on frequency for normal incidence ($\theta = 0^\circ$). Results are given for a 10 m slab with $z_T = 10 \text{ m}$ and with $\epsilon_0 = \epsilon_2 = \epsilon_0$ and $\epsilon_{1m} = (1.0505 + .001794i)\epsilon_0$.

narrow band, and there is only a slight upward trend with increasing frequency.

3.4. Correlation of Phase Fluctuations

Figures 3.3 and 3.4 show the correlation of the phase fluctuation at one fixed elevation angle, θ_1 , with the phase fluctuation at a varied angle, θ_2 , for the HH and VV polarizations, respectively. Again the result is not stationary and depends on the value of θ_1 , with results shown for several values. The parameters are as above, with a frequency of 1.12 GHz, a slab thickness of 10 m, and the target located in free space immediately below the lower boundary. It is expected that the behavior of the correlation will be very much like that of the incoherent term alone, and indeed this appears to be true. Overall, the HH return decorrelates faster than the VV polarization, and the correlations for both polarizations again show opposite dependence with respect to center angle, with the HH return decorrelating at a slower rate for increased θ_1 , and the VV return decorrelating at a faster rate. The reasons for these effects are identical to those described earlier for the correlation of the target/clutter multi-path return.

A similar comparison between the correlation of phase fluctuations and that of the target/clutter multi-path field is exhibited in the azimuthal correlations. Figures 3.5 and 3.6 show the correlation of the phase fluctuation over azimuthal separation angle, $\phi_2 - \phi_1$, for HH and VV polarizations, respectively. The results for each polarization are shown for several elevation angles, $\theta_1 = \theta_2$. Overall, the VV polarization decorrelates faster than the HH polarization, and in both cases the decorrelation occurs faster for angles further from normal incidence.

Finally, Figure 3.7 shows the correlation of the phase fluctuation at a center frequency, f_1 , with that at frequencies, f_2 , varying in a bandwidth of 20 MHz about f_1 . Several values of center frequency near 1.12 GHz are shown, since again the phase is not strictly stationary with frequency. It is clear from the results, however, that for the narrow bandwidth shown, the differences between correlations for varied center frequencies are small, and the correlation is approximately dependant on the frequency difference alone.

The angular extent shown in Figures 3.5 and 3.6 represents a typical integration angle for coherent integration by a SAR processor. Similarly, the bandwidth of Figure 3.7 is chosen to represent a typical SAR bandwidth for range processing. In each case, the phase is clearly not perfectly correlated across the aperture or frequency band, and it is expected that the system resolution will be lowered as a result. In addition, since the shape and extent of the correlation function in angle and frequency are comparable, it is expected that the degree of degradation to range and cross-range resolutions will be roughly similar.

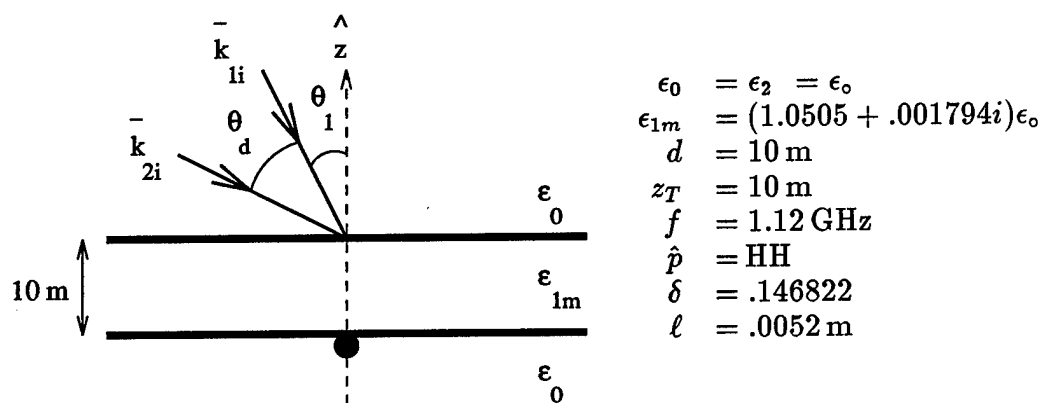
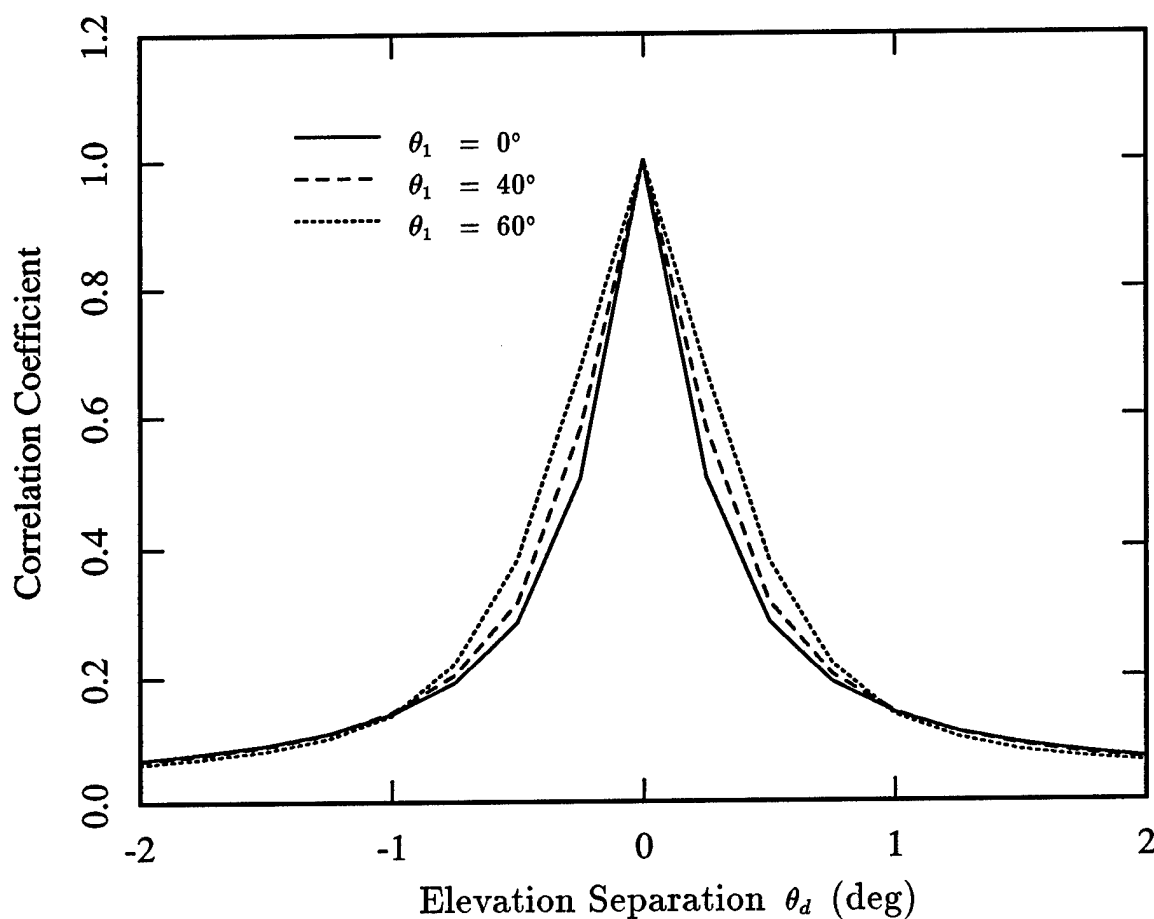


Figure 3.3. Correlation of Phase Fluctuations over $\theta_d = \theta_2 - \theta_1$ for the HH polarization and for $\theta_1 = 0^\circ$ (solid), $\theta_1 = 40^\circ$ (dash), and $\theta_1 = 60^\circ$ (dots). Results are given at 1.120 GHz for a 10 m slab with $z_T = 10 \text{ m}$ and with $\epsilon_0 = \epsilon_2 = \epsilon_0$ and $\epsilon_{1m} = (1.0505 + .001794i)\epsilon_0$.

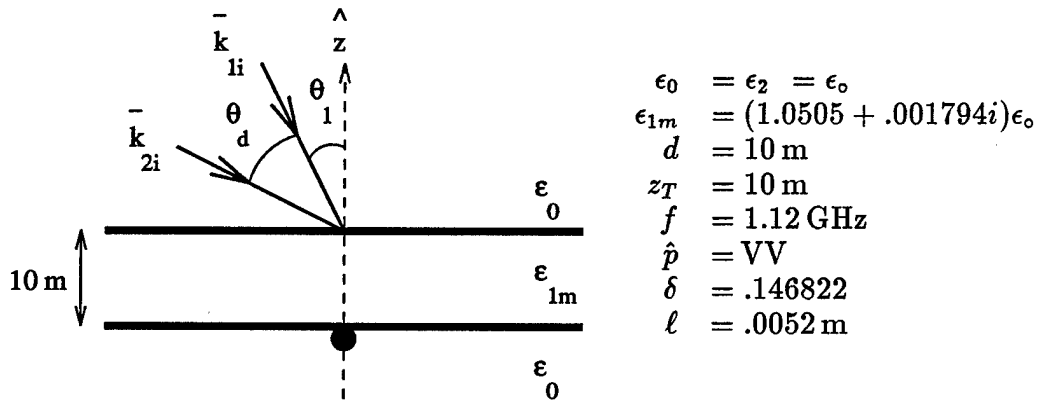
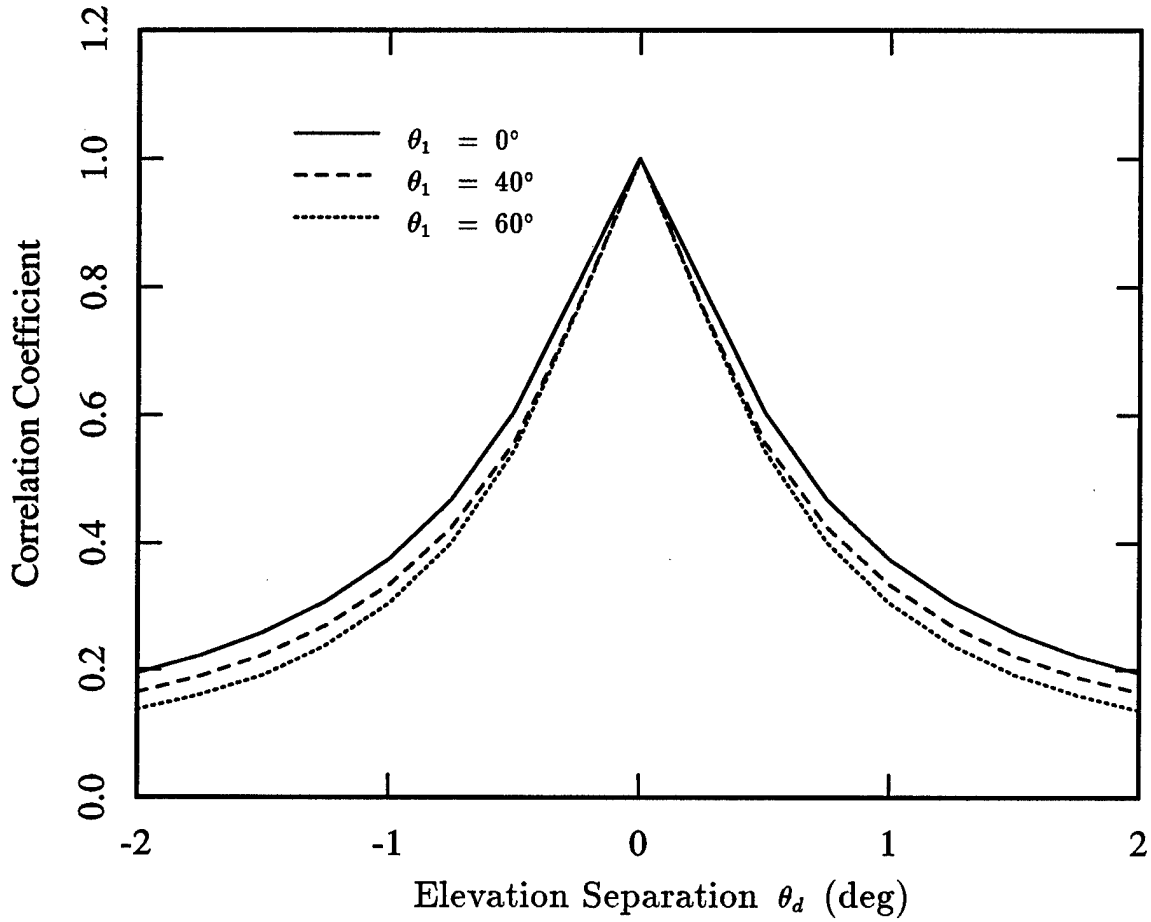
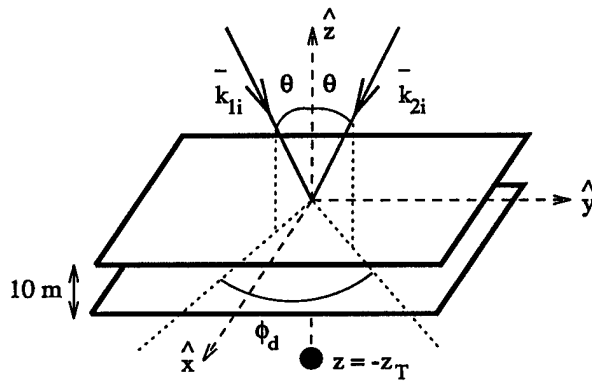
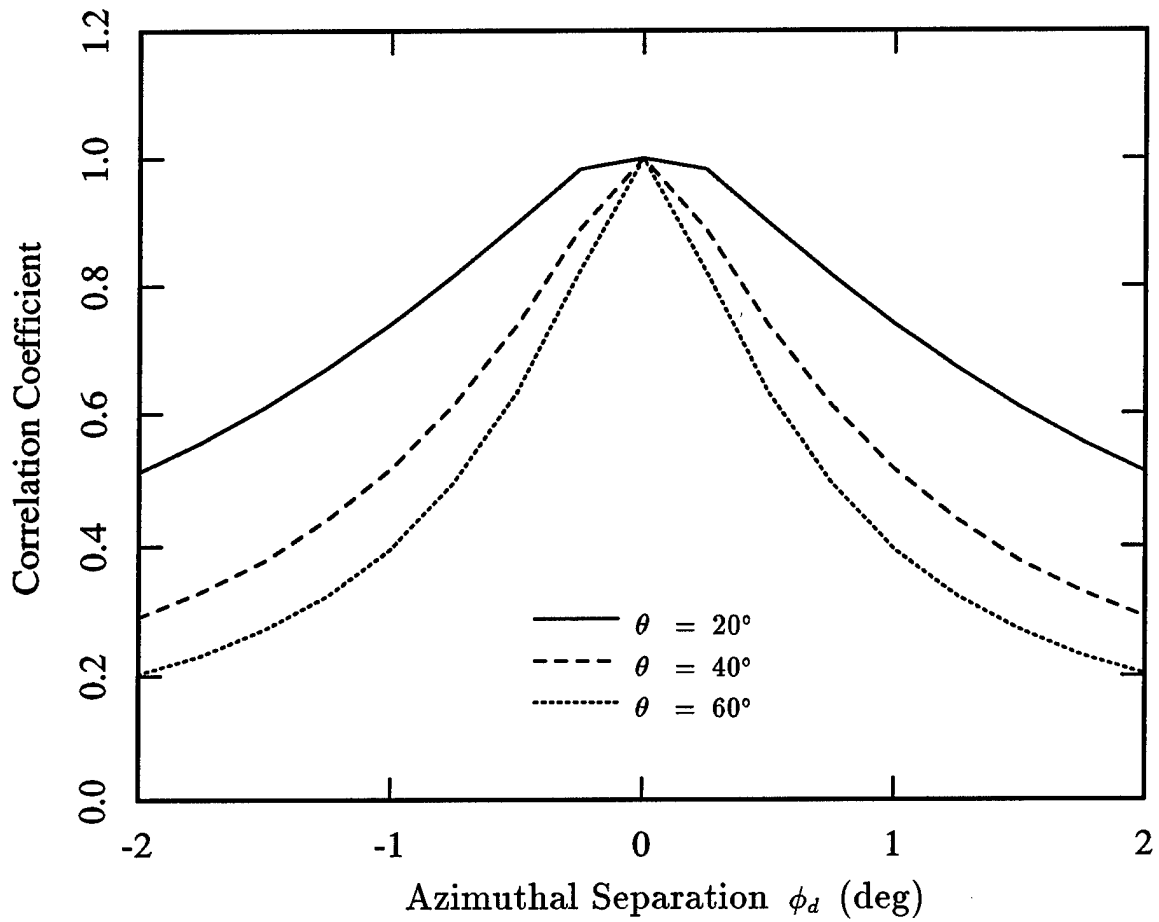
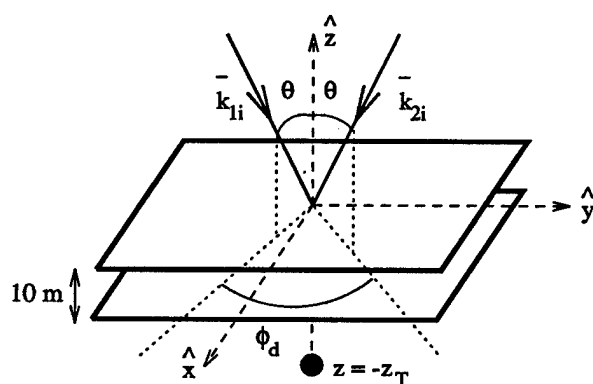
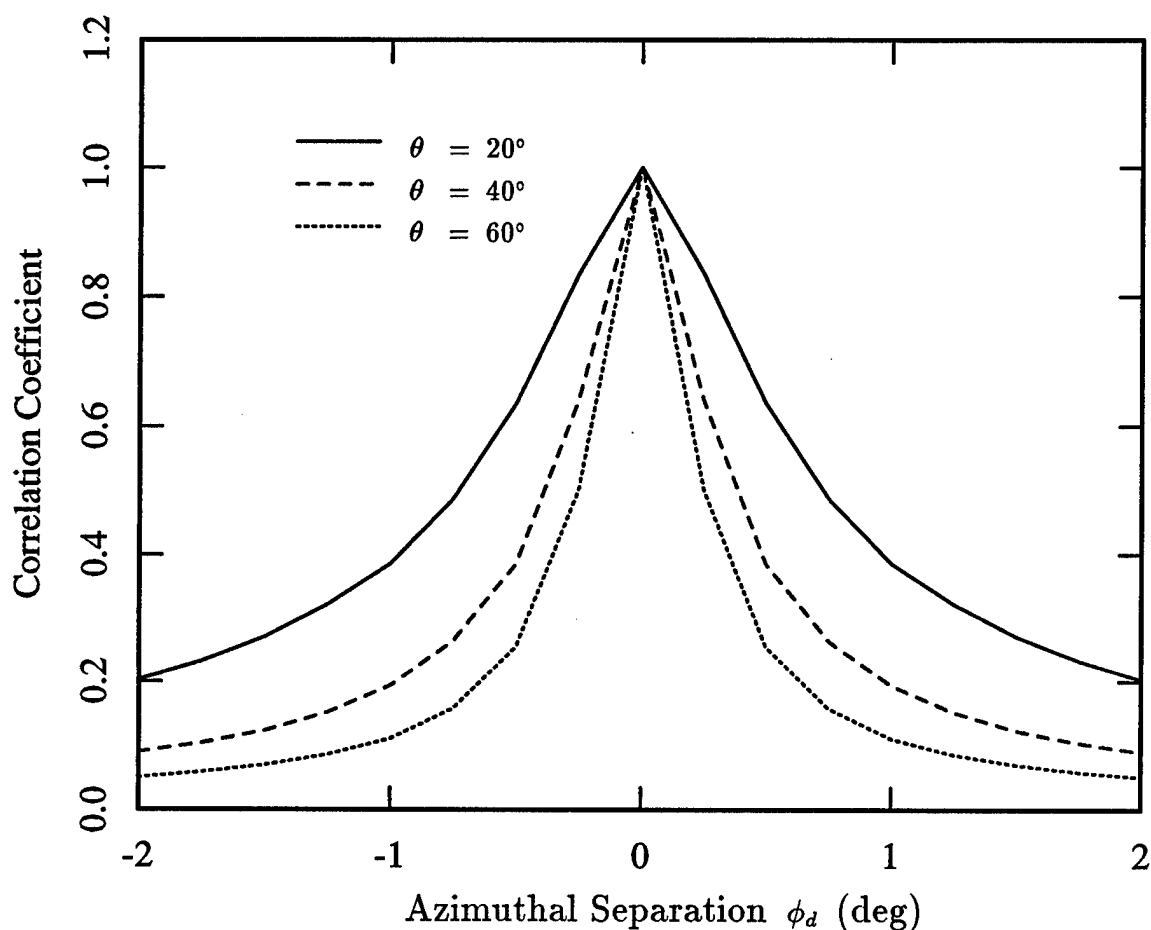


Figure 3.4. Correlation of Phase Fluctuations over $\theta_d = \theta_2 - \theta_1$ for the VV polarization and for $\theta_1 = 0^\circ$ (solid), $\theta_1 = 40^\circ$ (dash), and $\theta_1 = 60^\circ$ (dots). Results are given at 1.120 GHz for a 10 m slab with $z_T = 10 \text{ m}$ and with $\epsilon_0 = \epsilon_2 = \epsilon_0$ and $\epsilon_{1m} = (1.0505 + .001794i)\epsilon_0$.



$$\begin{aligned} \epsilon_0 &= \epsilon_2 = \epsilon_o \\ \epsilon_{1m} &= (1.0505 + .001794i)\epsilon_o \\ d &= 10 \text{ m} \\ z_T &= 10 \text{ m} \\ f &= 1.12 \text{ GHz} \\ \hat{p} &= \text{HH} \\ \delta &= .146822 \\ \ell &= .0052 \text{ m} \end{aligned}$$

Figure 3.5. Correlation of Phase Fluctuations over $\phi_d = \phi_2 - \phi_1$ for the HH polarization and for $\theta = 20^\circ$ (solid), $\theta = 40^\circ$ (dash), and $\theta = 60^\circ$ (dots). Results are given at 1.120 GHz for a 10 m slab with $z_T = 10$ m and with $\epsilon_0 = \epsilon_2 = \epsilon_o$ and $\epsilon_{1m} = (1.0505 + .001794i)\epsilon_o$.



$$\begin{aligned}
 \epsilon_0 &= \epsilon_2 = \epsilon_o \\
 \epsilon_{1m} &= (1.0505 + .001794i)\epsilon_o \\
 d &= 10 \text{ m} \\
 z_T &= 10 \text{ m} \\
 f &= 1.12 \text{ GHz} \\
 \hat{p} &= VV \\
 \delta &= .146822 \\
 \ell &= .0052 \text{ m}
 \end{aligned}$$

Figure 3.6. Correlation of Phase Fluctuations over $\phi_d = \phi_2 - \phi_1$ for the VV polarization and for $\theta = 20^\circ$ (solid), $\theta = 40^\circ$ (dash), and $\theta = 60^\circ$ (dots). Results are given at 1.120 GHz for a 10 m slab with $z_T = 10$ m and with $\epsilon_0 = \epsilon_2 = \epsilon_o$ and $\epsilon_{1m} = (1.0505 + .001794i)\epsilon_o$.

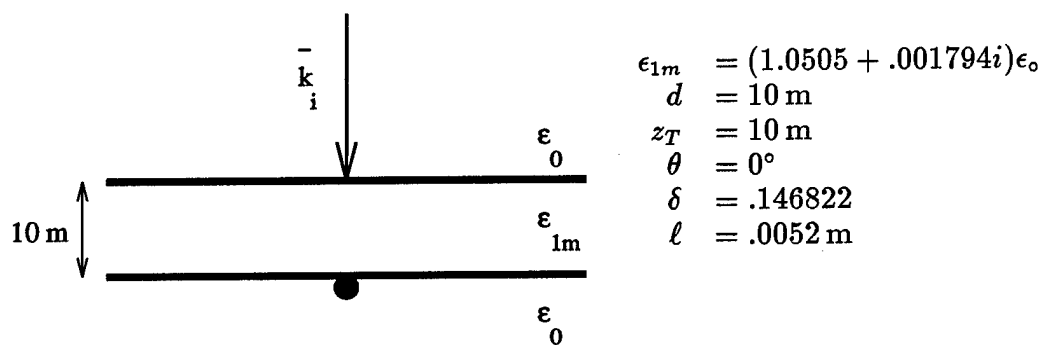
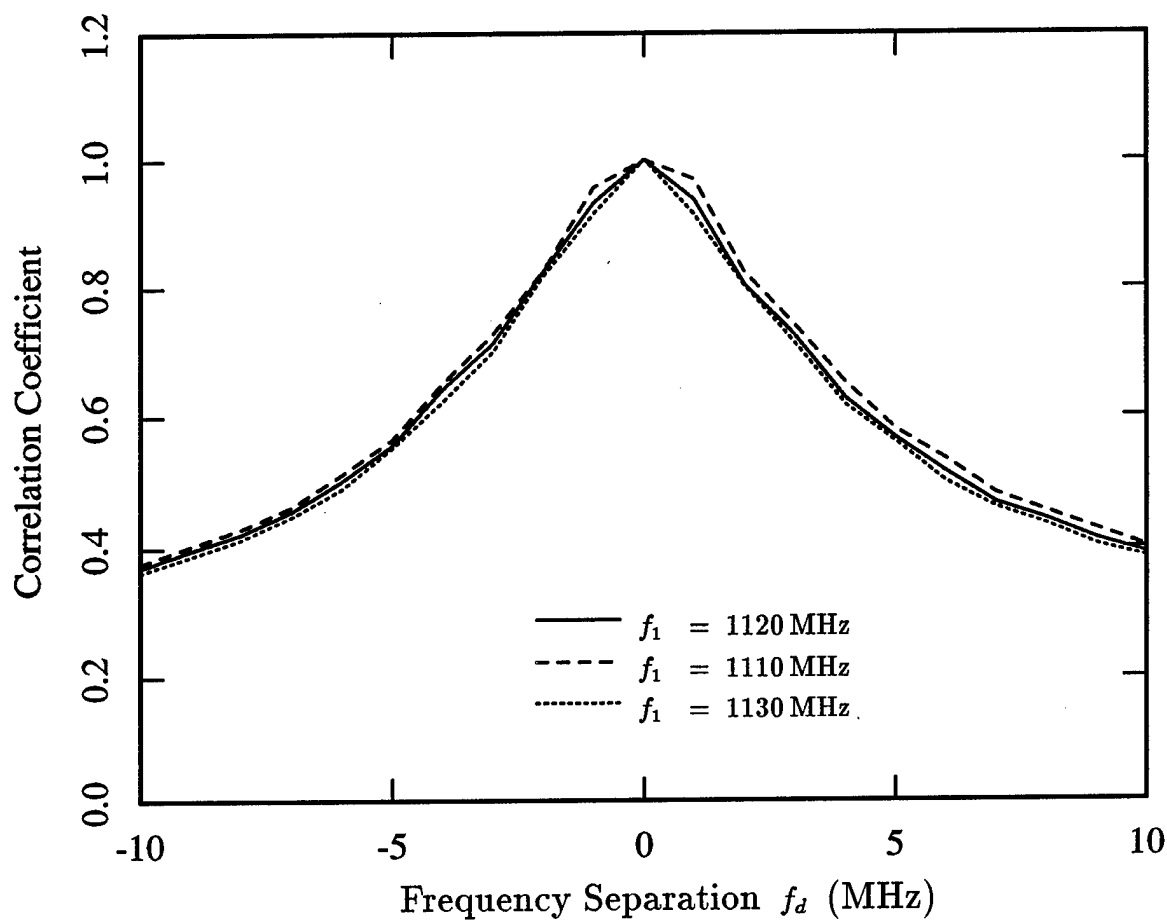


Figure 3.7. Correlation of Phase Fluctuations over $f_d = f_2 - f_1$ for normal incidence ($\theta_1 = \theta_2 = 0^\circ$) and for $f_1 = 1120$ MHz (solid), $f_1 = 1110$ MHz (dash), and $f_1 = 1130$ MHz (dots). Results are given for a 10 m slab with $z_T = 10$ m and with $\epsilon_0 = \epsilon_2 = \epsilon_0$ and $\epsilon_{1m} = (1.0505 + .001794i)\epsilon_0$.

Appendix C

Complex Correlation of Scattered Field Components

The following gives the complex correlation (unconjugated) of the target and target-clutter multi-path scattering terms. In all of the expressions below $\hat{\Phi}$ is the spectral density associated with the complex correlation of the renormalized scattering source, $\xi(\bar{r})$, and is given by (C.1),

$$\hat{\Phi}(\bar{\beta}) = \hat{\delta} k_o^4 \frac{\ell^3}{\pi^2 (1 + \beta^2 \ell^2)^2} \quad (C.1)$$

where $\hat{\delta}$ is the complex variance of $\xi(\bar{r})$.

C.1. Target/Clutter – Target/Clutter Complex Correlation

$$\begin{aligned}
& \hat{\sigma}_{TC-TC}^{p_a p_b}(\bar{k}_{as}, \bar{k}_{ai}, \bar{k}_{bs}, \bar{k}_{bi}) \\
&= 4\pi r^2 \left\langle \hat{p}_a \cdot \bar{E}_{TC}(\bar{k}_{as}, \bar{k}_{ai}) \hat{p}_b \cdot \bar{E}_{TC}(\bar{k}_{bs}, \bar{k}_{bi}) \right\rangle \\
&= (2\pi)^5 i \int_{-\infty}^{\infty} d\bar{k}_{\perp b} \sum_{\substack{s, s', q', \ell' = + \\ p, p', q, \ell = +, -}} \hat{A}_{TC-TC}^{pp'ss'qq'\ell\ell'} \times \\
& \quad e^{-i(\bar{k}_{\perp as} + \bar{k}_{\perp bs} - \bar{k}_{\perp ai} - \bar{k}_{\perp bi}) \cdot \bar{r}_{\perp T}} e^{-i(q'k_{2za} + sk_{2zai} + \ell'k_{2zb} + s'k_{2zbi})z_T} \times \\
& \quad \left[\frac{\hat{\Phi}(\bar{k}_{\perp bs} - \bar{k}_{\perp b}, -\ell k_{1zb} + p'k_{1zbs})}{pk_{1zas} - qk_{1za} - \ell k_{1zb} + p'k_{1zbs}} - \frac{\hat{\Phi}(-\bar{k}_{\perp b} + \bar{k}_{\perp bs}, qk_{1za} - pk_{1zas})}{pk_{1zas} - qk_{1za} - \ell k_{1zb} + p'k_{1zbs}} \right] \times \\
& \quad e^{i(pk_{1zas} - qk_{1za} - \ell k_{1zb} + p'k_{1zbs})d} \quad (C.2)
\end{aligned}$$

where

$$\begin{aligned}
\hat{A}_{TC-TC}^{pp'ss'qq'\ell\ell'} &= \frac{\alpha'^2}{4\pi} e^{2ikr} \left[\hat{p}_a \cdot \bar{H}_{01p}^a(\bar{k}_{\perp as}) \cdot \bar{F}_{12qq'}^a(\bar{k}_{\perp a}) \cdot \bar{E}_{2ai}^s \right] \times \\
& \quad \left[\hat{p}_b \cdot \bar{H}_{01p'}^b(\bar{k}_{\perp bs}) \cdot \bar{F}_{12\ell\ell'}^b(\bar{k}_{\perp b}) \cdot \bar{E}_{2bi}^{s'} \right] \quad (C.3)
\end{aligned}$$

and

$$\bar{k}_{\perp a} = -\bar{k}_{\perp b} + \bar{k}_{\perp as} + \bar{k}_{\perp bs} \quad (C.4)$$

C.2. Clutter/Target – Clutter/Target Complex Correlation

$$\begin{aligned}
& \hat{\sigma}_{CT-CT}^{p_a p_b}(\bar{k}_{as}, \bar{k}_{ai}, \bar{k}_{bs}, \bar{k}_{bi}) \\
&= 4\pi r^2 \left\langle \hat{p}_a \cdot \bar{E}_{CT}(\bar{k}_{as}, \bar{k}_{ai}) \hat{p}_b \cdot \bar{E}_{CT}(\bar{k}_{bs}, \bar{k}_{bi}) \right\rangle \\
&= (2\pi)^5 i \int_{-\infty}^{\infty} d\bar{k}_{\perp b} \sum_{\substack{p, p', q, \ell = + \\ s, s', q', \ell' = +, -}} \hat{A}_{CT-CT}^{pp'ss'qq'\ell\ell'} \times \\
& \quad e^{-i(\bar{k}_{\perp as} + \bar{k}_{\perp bs} - \bar{k}_{\perp ai} - \bar{k}_{\perp bi}) \cdot \bar{r}_{\perp T}} e^{-i(pk_{2za} - qk_{2zb} - \ell k_{2zi} + p'k_{2zbi})z_T} \times \\
& \quad \left[\frac{\hat{\Phi}(\bar{k}_{\perp b} - \bar{k}_{\perp bi}, \ell'k_{1zb} + s'k_{1zbi})}{q'k_{1za} + sk_{1zai} + \ell'k_{1zb} + s'k_{1zbi}} - \frac{\hat{\Phi}(\bar{k}_{\perp b} - \bar{k}_{\perp bi}, -q'k_{1za} - sk_{1zai})}{q'k_{1za} + sk_{1zai} + \ell'k_{1zb} + s'k_{1zbi}} \times \right. \\
& \quad \left. e^{i(q'k_{1za} + sk_{1zai} + \ell'k_{1zb} + s'k_{1zbi})d} \right] \tag{C.5}
\end{aligned}$$

where

$$\begin{aligned}
\hat{A}_{CT-CT}^{pp'ss'qq'\ell\ell'} &= \frac{\alpha'^2}{4\pi} e^{2ikr} \left[\hat{p}_a \cdot \bar{H}_{02p}^a(\bar{k}_{\perp as}) \cdot \bar{F}_{21qq'}^a(\bar{k}_{\perp a}) \cdot \bar{E}_{1ai}^s \right] \times \\
& \quad \left[\hat{p}_b \cdot \bar{H}_{02p'}^b(\bar{k}_{\perp bs}) \cdot \bar{F}_{21\ell\ell'}^b(\bar{k}_{\perp b}) \cdot \bar{E}_{1bi}^{s'} \right] \tag{C.6}
\end{aligned}$$

and

$$\bar{k}_{\perp a} = -\bar{k}_{\perp b} + \bar{k}_{\perp ai} + \bar{k}_{\perp bi} \tag{C.7}$$

C.3. Target/Clutter – Clutter/Target Complex Correlation

$$\begin{aligned}
& \hat{\sigma}_{TC-CT}^{p_a p_b}(\bar{k}_{as}, \bar{k}_{ai}, \bar{k}_{bs}, \bar{k}_{bi}) \\
&= 4\pi r^2 \langle \hat{p}_a \cdot \bar{E}_{TC}(\bar{k}_{as}, \bar{k}_{ai}) \hat{p}_b \cdot \bar{E}_{CT}(\bar{k}_{bs}, \bar{k}_{bi}) \rangle \\
&= (2\pi)^5 i \int_{-\infty}^{\infty} d\bar{k}_{\perp b} \sum_{\substack{p', s, q', -\ell = + \\ p, s', q, \ell' = +, -}} \hat{A}_{TC-CT}^{pp'ss'qq'\ell\ell'} \times \\
& \quad e^{-i(\bar{k}_{\perp as} + \bar{k}_{\perp bs} - \bar{k}_{\perp ai} - \bar{k}_{\perp bi}) \cdot \bar{r}_{\perp T}} e^{-i(q'k_{2za} + sk_{2zi} - \ell k_{2zb} + p'k_{2zs})z_T} \times \\
& \quad \left[\frac{\hat{\Phi}(\bar{k}_{\perp b} - \bar{k}_{\perp bi}, \ell'k_{1zb} + s'k_{1zbi})}{pk_{1zas} - qk_{1za} + \ell'k_{1zb} + s'k_{1zbi}} - \frac{\hat{\Phi}(\bar{k}_{\perp b} - \bar{k}_{\perp bi}, qk_{1za} - pk_{1zas})}{pk_{1zas} - qk_{1za} + \ell'k_{1zb} + s'k_{1zbi}} \times \right. \\
& \quad \left. e^{i(pk_{1zas} - qk_{1za} + \ell'k_{1zb} + s'k_{1zbi})d} \right] \quad (C.8)
\end{aligned}$$

where

$$\begin{aligned}
\hat{A}_{TC-CT}^{pp'ss'qq'\ell\ell'} &= \frac{\alpha'^2}{4\pi} e^{2ikr} \left[\hat{p}_a \cdot \bar{H}_{01p}^a(\bar{k}_{\perp as}) \cdot \bar{F}_{12qq'}^a(\bar{k}_{\perp a}) \cdot \bar{E}_{2ai}^s \right] \times \\
& \quad \left[\hat{p}_b \cdot \bar{H}_{02p'}^b(\bar{k}_{\perp bs}) \cdot \bar{F}_{21\ell\ell'}^b(\bar{k}_{\perp b}) \cdot \bar{E}_{1bi}^{s'} \right] \quad (C.9)
\end{aligned}$$

and

$$\bar{k}_{\perp a} = \bar{k}_{\perp b} + \bar{k}_{\perp as} - \bar{k}_{\perp bi} \quad (C.10)$$

C.4. Target – Target Complex Correlation

$$\begin{aligned}
 \hat{\sigma}_{T-T}^{p_a p_b}(\bar{k}_{as}, \bar{k}_{ai}, \bar{k}_{bs}, \bar{k}_{bi}) &= \hat{p}_a \cdot \bar{E}_T(\bar{k}_{as}, \bar{k}_{ai}) \times \hat{p}_b \cdot \bar{E}_T(\bar{k}_{bs}, \bar{k}_{bi}) \\
 &= \sum_{p, p', s, s' = +} \hat{A}_{T-T}^{pp' ss'} e^{-i(p k_{2z_{as}} + s k_{2z_{ai}} + p' k_{2z_{bs}} + s' k_{2z_{bi}}) z_T} \times \\
 &\quad e^{-i(\bar{k}_{\perp as} + \bar{k}_{\perp bs} - \bar{k}_{\perp ai} - \bar{k}_{\perp bi}) \cdot \bar{r}_{\perp T}} \quad (C.11)
 \end{aligned}$$

where

$$\hat{A}_{T-T}^{pp' ss'} = \frac{\alpha'^2}{(4\pi r)^2} e^{2ikr} \left[\hat{p}_a \cdot \overline{\vec{H}}_{02_p}^a(\bar{k}_{\perp as}) \cdot \bar{E}_{2_{ai}}^s \right] \times \left[\hat{p}_b \cdot \overline{\vec{H}}_{02_{p'}}^b(\bar{k}_{\perp bs}) \cdot \bar{E}_{2_{bi}}^{s'} \right] \quad (C.12)$$

Chapter 4

Scattering of a Point Target in a Multi-Layer Uniaxial Continuous Random Media

The results presented in Chapters 2 and 3 are limited to the consideration of a single random layer with half-spaces above and below. In modeling many physical situations of interest, it is necessary to consider a media which is stratified into a greater number of regions, and which includes more than one layer with random spatial variations in permittivity. In particular, a more accurate representation of a forested area requires two foliage regions, modeling the canopy and trunk layers individually, with free space above, and with a half-space of more dense permittivity modeling the earth below. In addition, the trunk region of the foliage will exhibit a difference in scattering characteristics between horizontal and vertical polarizations, because of the predominantly vertical orientation of the trunks, and, hence, must be modeled

by non-isotropic scatterers, leading to a vertically uniaxial effective permittivity and non-isotropic correlation function for this region.

In this chapter, the results of the previous two chapters will be extended to allow a more accurate modeling of a greater variety of physical situations. The geometry considered will now consist of an arbitrary number of layers with half-spaces above and below, and with the point target located in any of these layers. The permittivity of each layer will be allowed to be uniaxial with a vertically oriented optic axis. Any number of layers may be assumed random, each with a non-isotropic, but azimuthally symmetric correlation function.[†] Expressions for the coherent and incoherent multipath fields will be derived again using the first order distorted Born approximation, and these will be used to determine the statistics of the incoherent fields. The effect of various physical and geometrical parameters on both the variance and correlation of the field will be illustrated, and the effect of a uniaxial correlation function and of additional layers of stratification will be determined by comparison with the previous results for the two-layer case.

4.1. Geometry and Random Media Model

The multi-layer configuration which will be considered here is that shown in Figure 4.1. The space is separated into N regions with $N - 2$ bounded layers and with half-spaces above and below. The top interface between regions 0 and 1 is assumed

[†] Each random layer will be assumed to be independent of the others so that the effects of each can be superposed incoherently.

to occur at $z = 0$, and the other interfaces occur at depths $z = -d_i$, where i is the number of the region directly above the boundary. The target is assumed to be located in an arbitrary layer, t , at a total depth $z = z_T$, and the target again behaves as a dipole re-radiator of the field incident upon it, with an induced current density given by (2.1) and (2.2). In general, an arbitrary number of layers might contain random permittivity fluctuations, but since each such layer will be assumed independent of all others, the result for the general case can be synthesized by summing incoherently the effects of each layer individually. Hence, for simplicity, the random fluctuations of permittivity will be limited to a single arbitrary layer, f .

It will again be assumed that the source of illumination and the observation point are in the far-field of both the target and that region of random media which contributes significantly to the multi-path return. Hence, the illumination will be of plane wave form, as given by (2.3) and (2.4), where for simplicity, it is assumed that region 0 is isotropic. All other regions are allowed to be uniaxial, each with a vertical (untilted) optic axis, such that the permittivity of the i th layer is given by (4.1).

$$\bar{\epsilon}_i = \begin{bmatrix} \epsilon_i & 0 & 0 \\ 0 & \epsilon_i & 0 \\ 0 & 0 & \epsilon_{zi} \end{bmatrix} \quad (4.1)$$

The correlation function associated with the continuous random media is designed to model the inclusion of scatterers which are small in comparison to the illuminating wavelength, and which exhibit azimuthal symmetry. To allow a high permittivity contrast between the background and embedded materials, Strong Fluctuation theory is again utilized in determining the effective mean permittivity. Because of the non-isotropic, but azimuthally symmetric correlation function, this permittivity will be

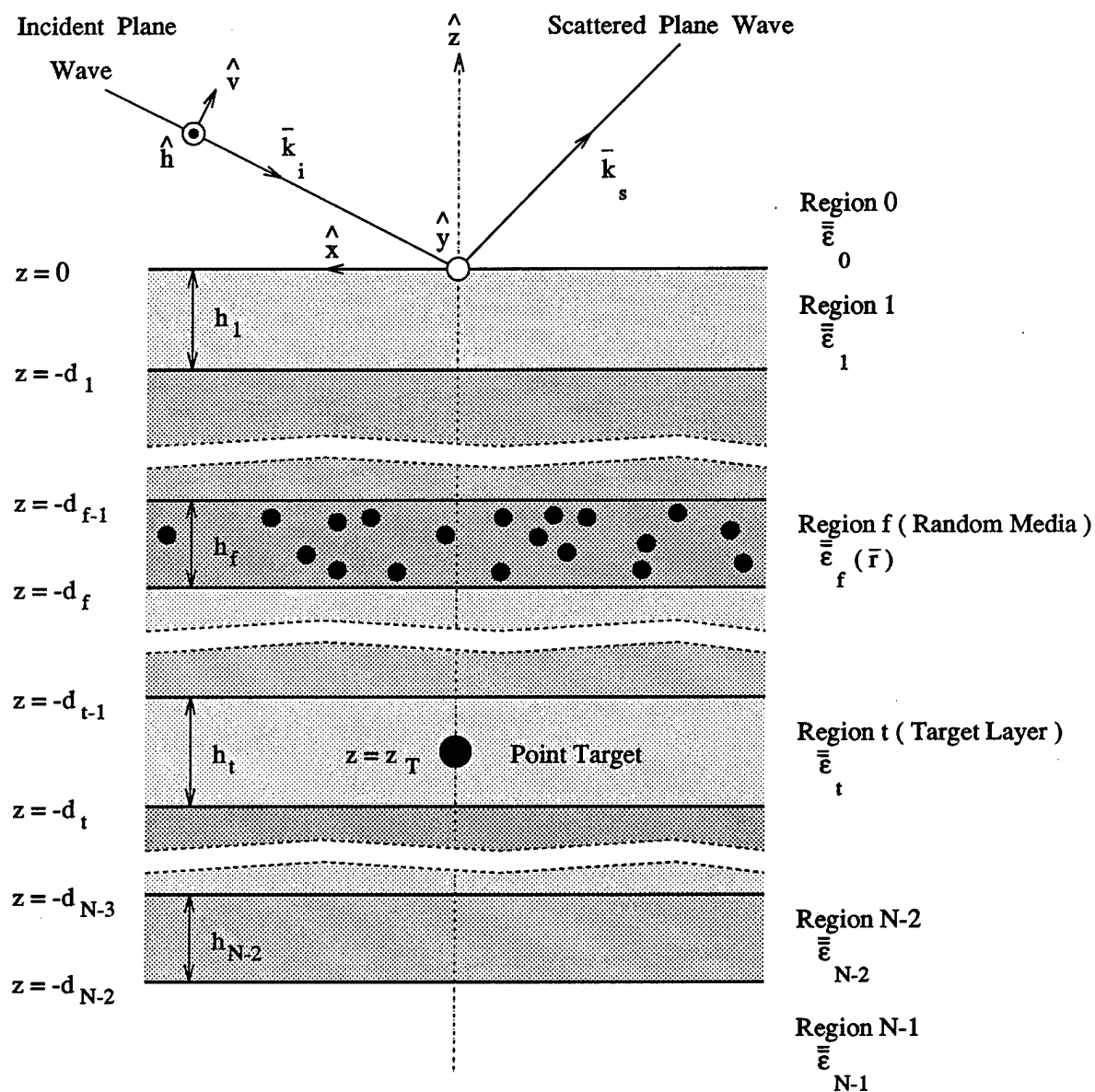


Figure 4.1. Geometry of the multi-layer scattering problem with N layers, and with the point target located in layer t , and the random media in layer f .

uniaxial (untilted) similar to the other non-random layers. A description of the process used to derive the effective permittivity is given in Appendix D.

The field resulting from the scattering which occurs in the random layer can be determined by the first order distorted Born approximation of (4.2),

$$\overline{E}_{0,}^{(1)} \simeq k_o^2 \int d\overline{r}' \overline{G}_{0f}(\overline{r}, \overline{r}') \cdot \overline{\xi}(\overline{r}') \cdot \overline{E}_f^{(0)}(\overline{r}') \quad (4.2)$$

where $\overline{E}_f^{(0)}$ is the mean field in the random media, or equivalently, the field present when the random media is replaced by a homogeneous layer with permittivity equal to that of the calculated effective permittivity. $\overline{G}_{0f}(\overline{r}, \overline{r}')$ is the dyadic Green's function for the stratified configuration with the observation point in region 0, and the source in the random layer, where again the random fluctuations are replaced by the homogeneous layer of effective permittivity. Finally, $\overline{\xi}(\overline{r})$ is the renormalized scattering source which represents the embedded scatterers after the coherent effects of their scattering have been removed. Hence, the randomness of the media is described by its effective permittivity, $\overline{\epsilon}_f$, and by the renormalized scattering source, the correlation of which is given by (4.3).

$$C_{\alpha\beta\gamma\rho}(\overline{r}_1 - \overline{r}_2) = k_o^4 \left\langle [\overline{\xi}(\overline{r}_1)]_{\alpha\beta} [\overline{\xi}(\overline{r}_2)]_{\gamma\rho} \right\rangle \quad (4.3)$$

4.2. Scattering Terms and Field Calculations

As with the simpler case treated in the previous chapters, the overall scattered

field will again consist of a direct coherent return from the point target, an incoherent return produced by direct backscatter by the random media, and a series of multi-path returns, describing the interaction between the target and random scatterers. Again, the direct backscatter properties of the random media have been investigated previously, and this analysis will not be repeated here. Instead, the coherent and incoherent components of the target signature will be determined, and the variance and correlation statistics of the latter multi-path component will be calculated. The expressions for each of the scattered field components are first determined below. The variance and correlation of the incoherent fields are calculated thereafter.

4.2.1. Scattered Field Components

The field scattered by the continuous random media is given by the distorted Born approximation of (4.2), where the zeroth order field in the random media consists not only of the incident field, but also the field produced by scattering of the incident field from the target. In addition, the field scattered by the random media not only scatters in the observation direction, but also is scattered to the target, where it is then scattered again to return to the receiver. Hence, within the limit of the first-order distorted Born approximation, there exist four fields created by scattering from the random media, and these fields parallel those of (2.14)-(2.17) for the simpler two-layer, isotropic case. The first represents the direct return from the random media, as given by (4.6), where $\overline{Q}(\vec{r}) = k_o^2 \overline{\xi}(\vec{r})$, and where this field is again denoted the clutter return, $\overline{E}_C(\vec{r})$.

$$\overline{E}_C(\bar{r}) = \int_{V_f} d\bar{r}' \overline{G}_{of}(\bar{r}, \bar{r}') \cdot \overline{Q}(\bar{r}') \cdot \overline{E}_{fi}(\bar{r}') \quad (4.6)$$

As noted above, this term has been examined previously, and since it is independent of the target, it will not be considered part of the signature of interest, and will consequently be ignored here. The second incoherent term of (4.7) is the field scattered first from the target, and then the random media, and this multi-path term is again denoted the target/clutter field.

$$\overline{E}_{TC}(\bar{r}) = i\omega\mu\alpha \int_{V_f} d\bar{r}' \overline{G}_{of}(\bar{r}, \bar{r}') \cdot \overline{Q}(\bar{r}') \cdot \int d\bar{r}'' \overline{G}_{ft}(\bar{r}', \bar{r}'') \cdot \overline{E}_{ti}(\bar{r}'') \delta(\bar{r}'' - \bar{r}_T) \quad (4.7)$$

The third term is the similar multi-path term expressing scattering in the opposite direction,

$$\overline{E}_{CT}(\bar{r}) = i\omega\mu\alpha \int d\bar{r}' \overline{G}_{ot}(\bar{r}, \bar{r}') \cdot \delta(\bar{r}' - \bar{r}_T) \cdot \int_{V_f} d\bar{r}'' \overline{G}_{tf}(\bar{r}', \bar{r}'') \cdot \overline{Q}(\bar{r}'') \cdot \overline{E}_{fi}(\bar{r}'') \quad (4.8)$$

and is denoted the clutter/target field. The final term which arises under the first order distorted Born approximation is the target/clutter/target multi-path term given by (4.9).

$$\begin{aligned} \overline{E}_{TCT}(\bar{r}) = & -\omega^2\mu^2\alpha^2 \int d\bar{r}' \overline{G}_{ot}(\bar{r}, \bar{r}') \cdot \delta(\bar{r}' - \bar{r}_T) \cdot \int_{V_f} d\bar{r}'' \overline{G}_{tf}(\bar{r}', \bar{r}'') \cdot \\ & \overline{Q}(\bar{r}'') \cdot \int d\bar{r}''' \overline{G}_{ft}(\bar{r}'', \bar{r}''') \cdot \overline{E}_{ti}(\bar{r}''') \cdot \delta(\bar{r}''' - \bar{r}_T) \end{aligned} \quad (4.9)$$

For reasonable values of α corresponding to reasonable point scatterer cross sections, this last multi-path term will again be small in comparison to the first two, and for this reason it is again neglected in further analysis.

In addition to the incoherent terms, there exists again the coherent or direct target return, \bar{E}_T , which is given by (4.10).

$$\bar{E}_T(\bar{r}) = i\omega\mu\alpha \int d\bar{r}' \bar{G}_{ot}(\bar{r}, \bar{r}') \cdot \bar{E}_{ti}(\bar{r}') \cdot \delta(\bar{r}' - \bar{r}_T) \quad (4.10)$$

The above terms compose the return from the point target and the continuous random media. In the analysis which now follows, the power returned by the coherent mechanism, and the variance and correlation of the incoherent multi-path mechanisms are calculated.

4.2.2. Incoherent Field Statistics

As with the simpler case of a two-layer media presented in Chapter 2, what is of interest is to determine those statistics of the multi-path fields which are needed in analyzing the effect of the random media on the operation of synthetic aperture radar. Again what is required is not only the incoherent power at any angle or frequency, but also the correlation of the field over azimuth and frequency changes within the integration angle and bandwidth which is processed. Although bistatic results are not necessary, the derivation here is again generalized to include this freedom for the sake of completeness. The case considered here is restricted to the case where the target and random media are in different layers, however, the special case where the target is in the random layer is treated in Appendix G.

The correlation which is considered here first is the autocorrelation of the target/clutter scattering mechanism. The other two correlations, namely the autocorrelation of the clutter/target return, and the cross correlation between the two, have similar derivations, which are omitted. The final results for all terms, however, are given in Appendix F.

The correlation is formed from (4.7), and is given by (4.11),

$$\begin{aligned}
 \sigma_{TC-TC}^{\hat{p}_a \hat{p}_b}(\bar{k}_{as}, \bar{k}_{ai}, \bar{k}_{bs}, \bar{k}_{bi}) &= 4\pi r^2 \langle \hat{p}_a \cdot \bar{E}_{TC}(\bar{k}_{as}, \bar{k}_{ai}) \times \hat{p}_b^* \cdot \bar{E}_{TC}^*(\bar{k}_{bs}, \bar{k}_{bi}) \rangle \\
 &= 4\pi r^2 |\alpha|^2 \int d\bar{r}_1 \int_{V_f} d\bar{r}_2 \int d\bar{r}_3 \int_{V_f} d\bar{r}_4 \langle \hat{p}_a \cdot \bar{G}_{0f}^a(\bar{r}, \bar{r}_2) \cdot \bar{Q}(\bar{r}_2) \cdot \\
 &\quad \bar{G}_{ft}^a(\bar{r}_2, \bar{r}_1) \cdot \bar{E}_{tai}(\bar{r}_1) \delta(\bar{r}_1 - \bar{r}_T) \times \hat{p}_b^* \cdot \bar{G}_{0f}^{b*}(\bar{r}, \bar{r}_4) \cdot \bar{Q}^*(\bar{r}_4) \cdot \\
 &\quad \bar{G}_{ft}^{b*}(\bar{r}_4, \bar{r}_3) \cdot \bar{E}_{tbi}^*(\bar{r}_3) \delta(\bar{r}_3 - \bar{r}_T) \rangle
 \end{aligned} \tag{4.11}$$

where $\alpha' = i\omega\mu\alpha$ and where \hat{p}_a and \hat{p}_b are unit vectors in the direction of the polarization of the received field. It is assumed that the difference in frequencies is sufficiently small that the effective permittivity and renormalized scattering source can be considered the same at the two frequencies. The dyadic Green's function and incident electric fields which appear in the above are given in Appendix E. Since the observation point is in the far-field, the far-field form of $\bar{G}_{0f}(\bar{r}, \bar{r}')$ can be utilized. Substituting these expressions, the result of (4.12) is obtained.

$$\sigma_{TC-TC}^{\hat{p}_a \hat{p}_b} = \frac{|\alpha'|^2}{4\pi} \sum_{\substack{p,s,q,\ell, \\ p',s',q',\ell'=+,-}} \sum_{\substack{u,v,w, \\ u',v',w'=TE,TM}} \sum_{\alpha,\beta,\gamma,\rho=x,y,z} \iiint d\bar{r}_1 \iiint d\bar{r}_3$$

$$\begin{aligned}
& \iiint_{V_f} d\bar{r}_1 \iiint_{V_f} d\bar{r}_4 \iint d\bar{k}_{\perp a} \iint d\bar{k}_{\perp b} C_{\alpha\beta\gamma\rho}(\bar{r}_2 - \bar{r}_4) \delta(\bar{r}_1 - \bar{r}_T) \delta(\bar{r}_3 - \bar{r}_T) \times \\
& \left[\hat{p}_a \cdot \overline{\overline{H}}_{0f_p}^{(u)}(\bar{k}_{\perp a}) \right]_{\alpha} \left[\overline{\overline{F}}_{ft_{\ell q}}^{(v)}(\bar{k}_{\perp a}) \cdot \overline{E}_{t_{ai}}^{s,(w)} \right]_{\beta} \times \\
& \left[\hat{p}_b \cdot \overline{\overline{H}}_{0f_p}^{(u')}(\bar{k}_{\perp b}) \right]_{\gamma}^* \left[\overline{\overline{F}}_{ft_{\ell' q'}}^{(v')}(\bar{k}_{\perp b}) \cdot \overline{E}_{t_{bi}}^{s',(w')} \right]_{\rho}^* \times \\
& e^{i(\bar{k}_{\perp ai} - \bar{k}_{\perp a}) \cdot \bar{r}_{1\perp}} e^{-i(s k_{iz_{ai}}^{(w)} + q k_{iz_{a}}^{(v)}) z_1} e^{i(\bar{k}_{\perp a} - \bar{k}_{\perp as}) \cdot \bar{r}_{2\perp}} e^{i(\ell k_{fz_a}^{(v)} - p k_{fz_{as}}^{(u)}) z_2} \times \\
& e^{-i(\bar{k}_{\perp bi} - \bar{k}_{\perp b}) \cdot \bar{r}_{3\perp}} e^{i(s' k_{iz_{bi}}^{(w')} + q' k_{iz_b}^{(v')}) z_3} e^{-i(\bar{k}_{\perp b} - \bar{k}_{\perp bs}) \cdot \bar{r}_{4\perp}} e^{-i(\ell' k_{fz_b}^{(v')} - p' k_{fz_{bs}}^{(u')}) z_4} \quad (4.12)
\end{aligned}$$

The above integrals over z_2 and z_4 have limits from $z = -d_f$ to $z = -d_{f-1}$. A change of variables is made such that the new limits will be from $z = -h_f$ to $z = 0$. Since the correlation is dependant only on the difference between z_2 and z_4 , only the phase terms will be affected by this change of variables. In addition, the correlation function will be represented as the Fourier transform of its spectral function, $\Phi_{\alpha\beta\gamma\rho}(\bar{\beta})$. The result of rewriting (4.12) with these changes is given by (4.13),

$$\begin{aligned}
\sigma_{TC-TC}^{\hat{p}_a \hat{p}_b} = & \sum_{\substack{p', s', q', \ell', \ell' = +, - \\ p, s, q, \ell, \ell = +, -}} \sum_{\substack{u', v', w', w' = TE, TM \\ u, v, w, w' = TE, TM}} \sum_{\alpha, \beta, \gamma, \rho = x, y, z} \\
& \iiint d\bar{r}_1 \iiint d\bar{r}_3 \iint d\bar{r}_{2\perp} \iint d\bar{r}_{4\perp} \int_{-h_f}^0 dz_2 \int_{-h_f}^0 dz_4 \\
& \iint d\bar{k}_{\perp a} \iint d\bar{k}_{\perp b} \iint d\bar{\beta}_{\perp} \int d\beta_z \Phi_{\alpha\beta\gamma\rho}(\bar{\beta}) A_{TC-TC}^{\alpha\beta\gamma\rho} \delta(\bar{r}_1 - \bar{r}_T) \delta(\bar{r}_3 - \bar{r}_T) \times \\
& e^{i(\bar{k}_{\perp ai} - \bar{k}_{\perp a}) \cdot \bar{r}_{1\perp}} e^{i(\bar{k}_{\perp a} - \bar{k}_{\perp as} - \bar{\beta}_{\perp}) \cdot \bar{r}_{2\perp}} e^{-i(\bar{k}_{\perp bi} - \bar{k}_{\perp b}) \cdot \bar{r}_{3\perp}} e^{-i(\bar{k}_{\perp b} - \bar{k}_{\perp bs} - \bar{\beta}_{\perp}) \cdot \bar{r}_{4\perp}} \times \\
& e^{-i(s k_{iz_{ai}}^{(w)} + q k_{iz_a}^{(v)}) z_1} e^{i(\ell k_{fz_a}^{(v)} - p k_{fz_{as}}^{(u)} - \beta_z) z_2} e^{i(s' k_{iz_{bi}}^{(w')} + q' k_{iz_b}^{(v')}) z_3} \times \\
& e^{-i(\ell' k_{fz_b}^{(v')} - p' k_{fz_{bs}}^{(u')} - \beta_z) z_4} e^{-i(\ell k_{fz_a}^{(v)} - p k_{fz_{as}}^{(u)} - \ell' k_{fz_b}^{(v')} + p' k_{fz_{bs}}^{(u')}) d_{f-1}} \quad (4.13)
\end{aligned}$$

where

$$A_{TC-TC}^{\alpha\beta\gamma\rho}_{pp'ss'qq'\ell\ell'} = \frac{|\alpha'|}{4\pi} \left[\hat{p}_a \cdot \overline{H}_{0f_p}^{(u)}(\bar{k}_{\perp a}) \right]_{\alpha} \left[\overline{F}_{ft_{\ell q}}^{(v)}(\bar{k}_{\perp a}) \cdot \overline{E}_{t_{ai}}^{s,(w)} \right]_{\beta} \times \\ \left[\hat{p}_b \cdot \overline{H}_{0f_p'}^{(u')}(\bar{k}_{\perp b}) \right]_{\gamma}^* \left[\overline{F}_{ft_{\ell' q'}}^{(v')}(\bar{k}_{\perp b}) \cdot \overline{E}_{t_{bi}}^{s',(w')} \right]_{\rho}^* \quad (4.14)$$

In the above, the two integrals, $\bar{\tau}_1$ and $\bar{\tau}_3$, over the target can be done trivially using the two delta functions. The integration over $\bar{\tau}_{2\perp}$ can be done to obtain another delta function, with the result shown by (4.15).

$$\sigma_{TC-TC}^{\hat{p}_a \hat{p}_b} = \sum_{\substack{p',s',q',\ell' = +,- \\ p,s,q,\ell}} \sum_{u',v',w' = TE,TM} \sum_{\alpha,\beta,\gamma,\rho = x,y,z} \iint d\bar{\tau}_{4\perp} \int_{-h_f}^0 dz_2 \int_{-h_f}^0 dz_4 \iint d\bar{k}_{\perp a} \\ \iint d\bar{k}_{\perp b} \iint d\bar{\beta}_{\perp} \int d\beta_z (2\pi)^2 \Phi_{\alpha\beta\gamma\rho}(\bar{\beta}) A_{TC-TC}^{\alpha\beta\gamma\rho}_{pp'ss'qq'\ell\ell'} \delta(\bar{k}_{\perp a} - \bar{k}_{\perp a_s} - \bar{\beta}_{\perp}) \times \\ e^{i(\bar{k}_{\perp a_i} - \bar{k}_{\perp a} - \bar{k}_{\perp b_i} + \bar{k}_{\perp b}) \cdot \bar{\tau}_{T\perp}} e^{-i(s k_{iz_{ai}}^{(w)} + q k_{iz_a}^{(v)} - s' k_{iz_{bi}}^{(w')*} - q' k_{iz_b}^{(v')*}) z_T} \times \\ e^{-i(\ell k_{fz_a}^{(v)} - p k_{fz_{as}}^{(u)} - \ell' k_{fz_b}^{(v')*} + p' k_{fz_{bs}}^{(u')*}) d_{f-1}} e^{-i(\bar{k}_{\perp b} - \bar{k}_{\perp b_s} - \bar{\beta}_{\perp}) \cdot \bar{\tau}_{4\perp}} \times \\ e^{i(\ell k_{fz_a}^{(v)} - p k_{fz_{as}}^{(u)} - \beta_z) z_2} e^{-i(\ell' k_{fz_b}^{(v')*} - p' k_{fz_{bs}}^{(u')*} - \beta_z) z_4} \quad (4.15)$$

The delta function generated above allows the $\bar{\beta}_{\perp}$ integral to be performed trivially. The $\bar{\tau}_{4\perp}$ integral can then be done to generate another delta function, as shown in (4.16).

$$\sigma_{TC-TC}^{\hat{p}_a \hat{p}_b} = \sum_{\substack{p',s',q',\ell' = +,- \\ p,s,q,\ell}} \sum_{u',v',w' = TE,TM} \sum_{\alpha,\beta,\gamma,\rho = x,y,z} \int_{-h_f}^0 dz_2 \int_{-h_f}^0 dz_4 \iint d\bar{k}_{\perp a} \iint d\bar{k}_{\perp b} \int d\beta_z$$

$$\begin{aligned}
& (2\pi)^4 \Phi_{\alpha\beta\gamma\rho}(\bar{k}_{\perp a} - \bar{k}_{\perp a s}, \beta_z) A_{TC-TC}^{\alpha\beta\gamma\rho}{}_{pp's's'qq'\ell\ell'}{}^{uu'vv'ww'} \delta(\bar{k}_{\perp a} + \bar{k}_{\perp b s} - \bar{k}_{\perp a s} - \bar{k}_{\perp b}) \times \\
& e^{i(\bar{k}_{\perp a i} - \bar{k}_{\perp a} - \bar{k}_{\perp b i} + \bar{k}_{\perp b}) \cdot \bar{r}_{T\perp}} e^{-i(sk_{iz a i}^{(w)} + qk_{iz a}^{(v)} - s'k_{iz b i}^{(w')*} - q'k_{iz b}^{(v')*})z_T} \times \\
& e^{-i(\ell k_{fz a}^{(v)} - pk_{fz a s}^{(u)} - \ell'k_{fz b}^{(v')*} + p'k_{fz b s}^{(u')*})d_{f-1}} e^{-i(pk_{fz a s}^{(u)} - \ell k_{fz a}^{(v)} + \beta_z)z_2} \times \\
& e^{i(p'k_{fz b s}^{(u')*} - \ell'k_{fz b}^{(v')*} + \beta_z)z_4} \tag{4.16}
\end{aligned}$$

The delta function can be used to perform the $\bar{k}_{\perp b}$ integral, and the z_2 and z_4 integrals can then be done directly to yield (4.17),

$$\begin{aligned}
\sigma_{TC-TC}^{\hat{p}_a \hat{p}_b} = & \sum_{\substack{p', s', q', \ell' = +, - \\ p, s, q, \ell}} \sum_{\substack{u, v, w, \\ u', v', w' = TE, TM}} \sum_{\alpha, \beta, \gamma, \rho = x, y, z} \iint d\bar{k}_{\perp a} \int d\beta_z (2\pi)^4 \times \\
& \Phi_{\alpha\beta\gamma\rho}(\bar{k}_{\perp a} - \bar{k}_{\perp a s}, \beta_z) A_{TC-TC}^{\alpha\beta\gamma\rho}{}_{pp's's'qq'\ell\ell'}{}^{uu'vv'ww'} e^{i(\bar{k}_{\perp a i} - \bar{k}_{\perp a s} - \bar{k}_{\perp b i} + \bar{k}_{\perp b s}) \cdot \bar{r}_{T\perp}} \times \\
& e^{-i(sk_{iz a i}^{(w)} + qk_{iz a}^{(v)} - s'k_{iz b i}^{(w')*} - q'k_{iz b}^{(v')*})z_T} e^{-i(\ell k_{fz a}^{(v)} - pk_{fz a s}^{(u)} - \ell'k_{fz b}^{(v')*} + p'k_{fz b s}^{(u')*})d_{f-1}} \times \\
& \frac{1 - e^{i(pk_{fz a s}^{(u)} - \ell k_{fz a}^{(v)} + \beta_z)h_f}}{pk_{fz a s}^{(u)} - \ell k_{fz a}^{(v)} + \beta_z} \cdot \frac{1 - e^{-i(p'k_{fz b s}^{(u')*} - \ell'k_{fz b}^{(v')*} + \beta_z)h_f}}{p'k_{fz b s}^{(u')*} - \ell'k_{fz b}^{(v')*} + \beta_z} \tag{4.17}
\end{aligned}$$

where $\bar{k}_{\perp c}$ is given by (4.18),

$$\bar{k}_{\perp c} = \bar{k}_{\perp a} + \bar{k}_{\perp b s} - \bar{k}_{\perp a s} \tag{4.18}$$

and where A_{TC-TC} is as in (4.14) but with $\bar{k}_{\perp b}$ replaced by $\bar{k}_{\perp c}$. Finally, the β_z integral can be done using complex residue theory, splitting the integrand into portions convergent in the upper and lower half-planes of the complex β_z plane, and including

the residue contributions from the appropriate poles. Again $\Phi_{\alpha\beta\gamma\rho}$ may have poles of its own, but in the low-loss case these will be less significant than those of the remainder of the integrand, and, therefore, are neglected here. Appendix F gives a more detailed result where these poles have been included for a specific class of correlation functions. The final desired result after this integration is given by (4.19).

$$\begin{aligned}
 \sigma_{TC-TC}^{\hat{p}_a\hat{p}_b} = & (2\pi)^5 i \sum_{\substack{p,s,q,\ell, \\ p',s',q',\ell'=+,-}} \sum_{\substack{u,v,w, \\ u',v',w'=TE,TM}} \sum_{\alpha,\beta,\gamma,\rho=x,y,z} \iint d\bar{k}_{\perp a} A_{TC-TC}^{\alpha\beta\gamma\rho \substack{pp'ss'qq'\ell\ell' \\ uu'vv'ww'}} \times \\
 & e^{i(\bar{k}_{\perp ai} - \bar{k}_{\perp as} - \bar{k}_{\perp bi} + \bar{k}_{\perp bs}) \cdot \bar{r}_{T\perp}} e^{-i(sk_{izai}^{(u)} + qk_{iza}^{(v)} - s'k_{izbi}^{(w')*} - q'k_{izc}^{(v')*})z_T} \times \\
 & e^{-i(\ell k_{fza}^{(v)} - pk_{fza}^{(u)} - \ell'k_{fzc}^{(v')*} + p'k_{fzb}^{(u')*})d_f - 1} \times \\
 & \left[\frac{\Phi_{\alpha\beta\gamma\rho}(\bar{k}_{\perp a} - \bar{k}_{\perp as}, \ell'k_{fzc}^{(v')*} - p'k_{fzb}^{(u')*})}{pk_{fza}^{(u)} - \ell k_{fza}^{(v)} + \ell'k_{fzc}^{(v')*} - p'k_{fzb}^{(u')*}} - \right. \\
 & \frac{\Phi_{\alpha\beta\gamma\rho}(\bar{k}_{\perp a} - \bar{k}_{\perp as}, \ell k_{fza}^{(v)} - pk_{fza}^{(u)})}{pk_{fza}^{(u)} - \ell k_{fza}^{(v)} + \ell'k_{fzc}^{(v')*} - p'k_{fzb}^{(u')*}} \times \\
 & \left. e^{i(pk_{fza}^{(u)} - \ell k_{fza}^{(v)} + \ell'k_{fzc}^{(v')*} - p'k_{fzb}^{(u')*})h_f} \right] \quad (4.19)
 \end{aligned}$$

The derivations of $\sigma_{CT-CT}^{\hat{p}_a\hat{p}_b}$ and $\sigma_{TC-CT}^{\hat{p}_a\hat{p}_b}$ are similar and are not given here. The final expressions for all terms, however, are given in Appendix F.

4.2.3. Coherent Field Power

The power of the direct or coherent target return can be found directly as the squared magnitude of (4.10). However, to be consistent with the incoherent results and to provide for the SAR processing to be considered shortly, a correlation is defined

as the product of the coherent field received for one angle and frequency with the conjugate of that received at a second angle/frequency pair. The result is $\sigma_{T-T}^{\hat{p}_a \hat{p}_b}$, which is defined below, and which for the case where the two angle/frequency pairs are identical, represents the effective radar cross section of the target arising from the coherent return.

$$\begin{aligned}
 \sigma_{T-T}^{\hat{p}_a \hat{p}_b}(\bar{k}_{as}, \bar{k}_{ai}, \bar{k}_{bs}, \bar{k}_{bi}) &= 4\pi r^2 \langle \hat{p}_a \cdot \bar{E}_T(\bar{k}_{as}, \bar{k}_{ai}) \times \hat{p}_b^* \cdot \bar{E}_T^*(\bar{k}_{bs}, \bar{k}_{bi}) \rangle \\
 &= \frac{|\alpha'|}{4\pi} \sum_{p,s,p',s'=+,-} \sum_{u,w,u',w'=TE,TM} \left[\hat{p}_a \cdot \bar{H}_{0t_p}^{(u)}(\bar{k}_{\perp as}) \cdot \bar{E}_{tai}^{s,(w)} \right] \times \\
 &\quad \left[\hat{p}_b \cdot \bar{H}_{0t_{p'}}^{(u')}(\bar{k}_{\perp bs}) \cdot \bar{E}_{tbi}^{s',(w')} \right]^* e^{-i\bar{k}_{\perp as} \cdot \bar{r}_{T\perp}} e^{-ipk_{izas}^{(u)} z_T} \times \\
 &\quad e^{i\bar{k}_{\perp ai} \cdot \bar{r}_{T\perp}} e^{-isk_{izai}^{(w)} z_T} e^{i\bar{k}_{\perp bs} \cdot \bar{r}_{T\perp}} e^{ip'k_{izbs}^{(u')} z_T} e^{-i\bar{k}_{\perp bi} \cdot \bar{r}_{T\perp}} e^{is'k_{izbi}^{(w')} z_T} \quad (4.20)
 \end{aligned}$$

The above can be written in a form more consistent with the previous expressions for the incoherent fields, and this final result is given by (4.21),

$$\begin{aligned}
 \sigma_{T-T}^{\hat{p}_a \hat{p}_b} &= \sum_{p,s,p',s'=+,-} \sum_{u,w,u',w'=TE,TM} A_{T-T}^{\overline{pp' ss'}} e^{i(\bar{k}_{\perp ai} - \bar{k}_{\perp bi} + \bar{k}_{\perp bs} - \bar{k}_{\perp as}) \cdot \bar{r}_{T\perp}} \times \\
 &\quad e^{-i(pk_{izas}^{(u)} + sk_{izai}^{(w)} - p'k_{izbs}^{(u')} - s'k_{izbi}^{(w')}) z_T} \quad (4.21)
 \end{aligned}$$

where A_{T-T} is given by (4.22).

$$A_{T-T}^{\overline{pp' ss'}} = \frac{|\alpha'|}{4\pi} \left[\hat{p}_a \cdot \bar{H}_{0t_p}^{(u)}(\bar{k}_{\perp as}) \cdot \bar{E}_{tai}^{s,(w)} \right] \cdot \left[\hat{p}_b \cdot \bar{H}_{0t_{p'}}^{(u')}(\bar{k}_{\perp bs}) \cdot \bar{E}_{tbi}^{s',(w')} \right]^* \quad (4.22)$$

4.3. Variance and Correlation Results

In this section, the new extended results derived above are used to show the effect of a variety of physical and geometrical parameters on the resultant coherent and incoherent returns. The effects of changes in the correlation length and fractional volume of scatterers for the random media are first examined. For the incoherent terms, both the variance and correlation effects are demonstrated. The correlation function is then changed to a uniaxial type, and the effects of non-isotropic scatterers are shown. Finally, an additional layer is added to the geometry, in the form of an extra boundary below the target, and the effects of this dense reflecting boundary are seen.

4.3.1. Effect of the Random Medium Correlation Length

To examine the effects of the correlation length of the random media, the same two-layer geometry of Chapter 2 is employed. The random media is located in a slab of 10 m thickness, with a free-space above and below, and with the target located immediately below the lower boundary of the the random region. The frequency employed is again 1.12 GHz, and the scatterers in the random media are assumed to be isotropic, leading to an isotropic correlation function and effective permittivity. In the previous results of Chapter 2, this effective permittivity was derived assuming a fractional volume of scatterers equal to 1.67%, and a correlation length of 0.0052 m, which yields an relative effective permittivity of $1.0505 + 0.001794i$. In contrast, a longer correlation length of 0.0072 m is now considered, yielding a slightly more dense and lossy effective permittivity of $1.0516 + 0.002417i$.

Figure 4.2 shows the effect of this increase in correlation length on the coherent return from the point target. Since this is the coherent return, the only effect is through the change in effective permittivity which results. The new result for the longer correlation length is shown by the solid curve, and the previous result from Chapter 2 is shown dashed. As expected, the longer correlation length result is attenuated more, since the effective permittivity is now more lossy, showing the greater amount of coherent scattering loss in traveling down and back through the random region. Both polarizations are again shown, however, as before the HH and VV returns are nearly identical because the contrast between the effective permittivity of the random media and the free space above and below is small, yielding little in the way of boundary reflection effects which might serve to distinguish the two polarizations.

Figure 4.3 shows a similar comparison between the incoherent target/clutter multi-path returns for the two correlation lengths. The solid curve is the result for $\ell = 0.0072$ m, and the dash curve is that for $\ell = 0.0052$ m. Unlike the coherent case above, the effect of the increased correlation length is to increase the incoherent return. Again the added loss in the effective permittivity for the longer correlation length will tend to decrease the incoherent return as with the coherent return. However, for the incoherent term, this effect is countered by the increased scattered power which arises because individual scatterers will now contribute coherently with their neighbors over a larger distance. Hence, the total return, expressed as a sum of contributions from all the scatterers in the random layer, will now be more of a coherent sum than previously. The overall effect leads to a increase in the incoherent return for longer random medium correlation lengths.

The combined effect of an attenuated coherent return, and enhanced incoherent

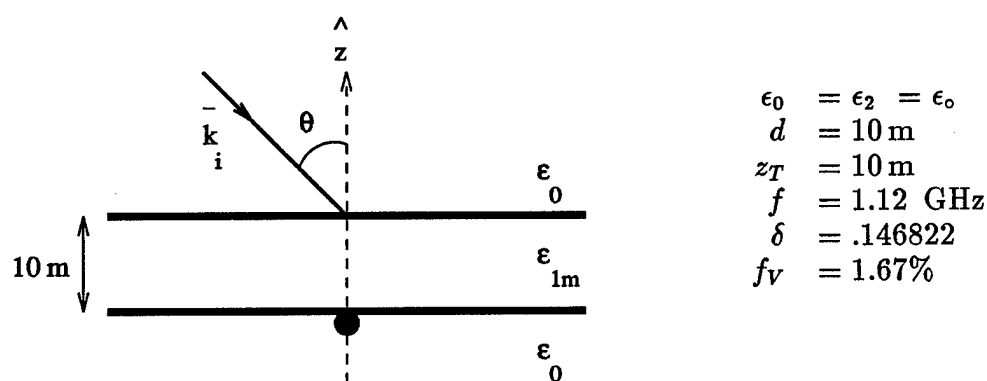
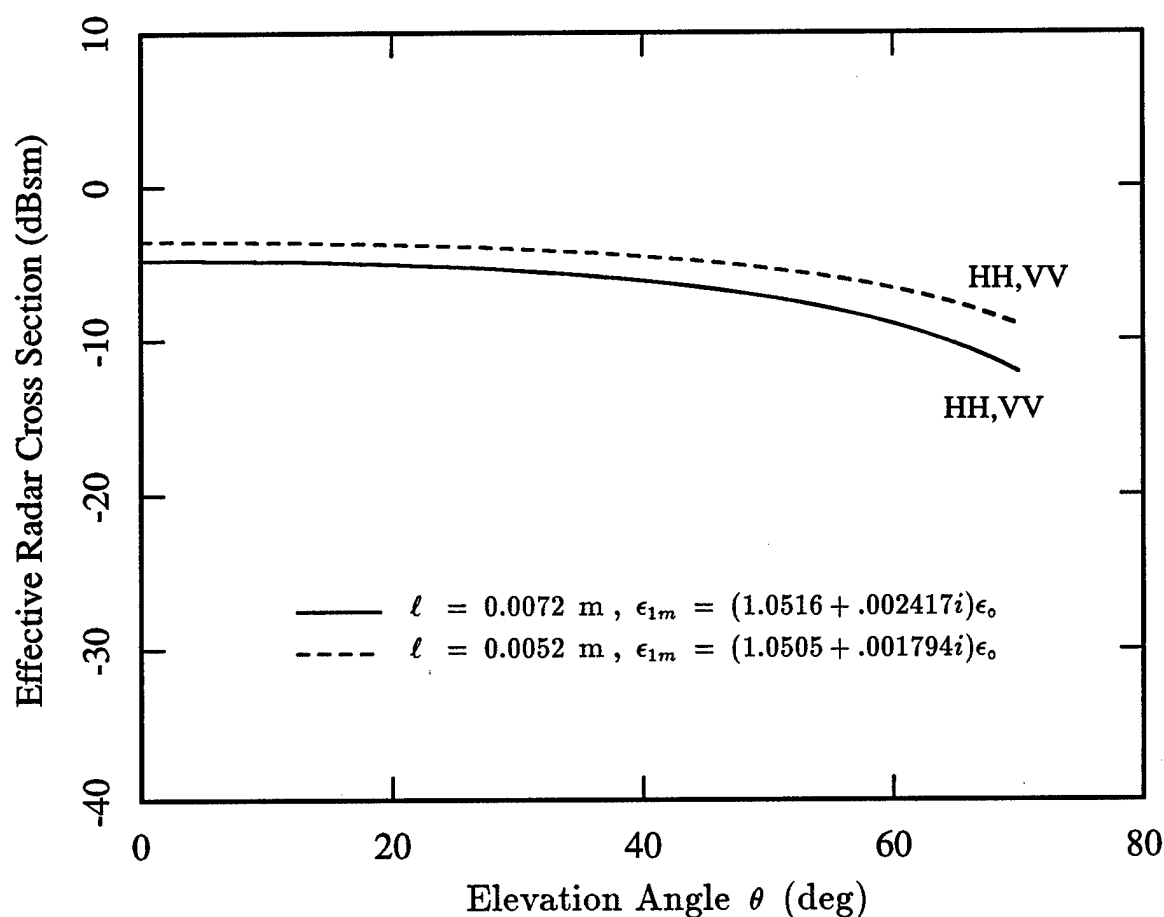


Figure 4.2. Dependence of the coherent target scattering cross section, σ_{T-T} , on elevation angle for $\ell = .0072$ m and $\epsilon_{1m} = (1.0516 + .002417i)\epsilon_0$ (solid) and for $\ell = .0052$ m and $\epsilon_{1m} = (1.0505 + .001794i)\epsilon_0$ (dash). Results are given at 1.120 GHz for a 10 m slab with $z_T = 10$ m and with $\epsilon_0 = \epsilon_2 = \epsilon_0$.

return will lead to a degradation in SAR performance for longer correlation lengths. This effect results because the variance of the phase fluctuations is approximately proportional to the ratio of the incoherent to coherent returns, as was shown in Chapter 3. Hence, although not shown explicitly here, longer random medium correlation lengths will lead to larger phase fluctuations in the target signature.

The effect of the random medium correlation length on the correlation of the incoherent return over azimuth and frequency is shown in Figures 4.4 and 4.5. The correlations are done with an elevation angle of $\theta = 60^\circ$ and a center frequency $f_c = 1.12$ GHz. Again the result with $\ell = 0.0072$ m is shown by the solid curves, and the result with the shorter correlation length of $\ell = 0.0052$ m is given by the dash curves. In both correlations, the effect of the increased random medium correlation length is seen to be small, in particular in comparison to the much greater polarization effect in the azimuthal correlation of Figure 4.4. As discussed previously in Chapter 2, the primary factors in determining the rate at which the incoherent return will decorrelate are the size and shape of the region within the random slab which is contributing significantly to the multi-path field. A vertical polarization to the illuminating field, and the resulting vertical orientation of the dipole-like point target, leads to a scattering region within the random slab which is wider perpendicular to the direction of incidence than that for the corresponding horizontally polarized case, and which therefore experiences a more rapid phase change with changing azimuth. This more rapid phase change leads in turn to a more rapid decorrelation of the return for the VV case as shown in Figure 4.4. The effect of the polarization on the frequency correlation, although not discussed in Chapter 2, can be understood with similar reasoning. Both horizontal and vertical orientations to the dipole point target lead to scattering regions within the random media which

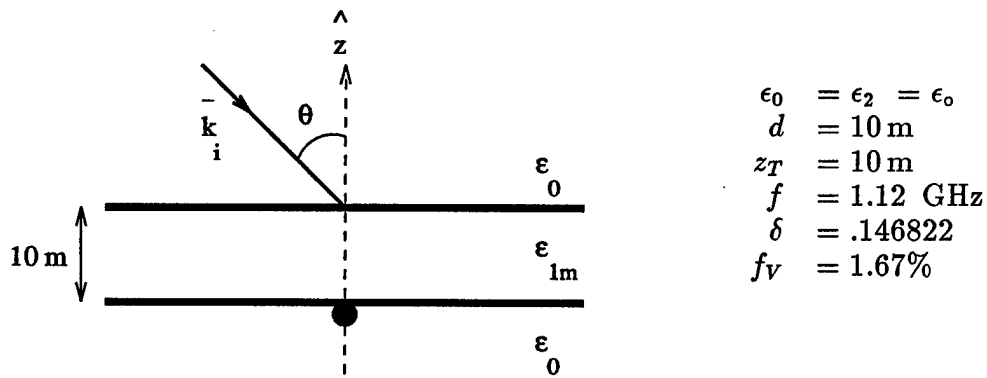
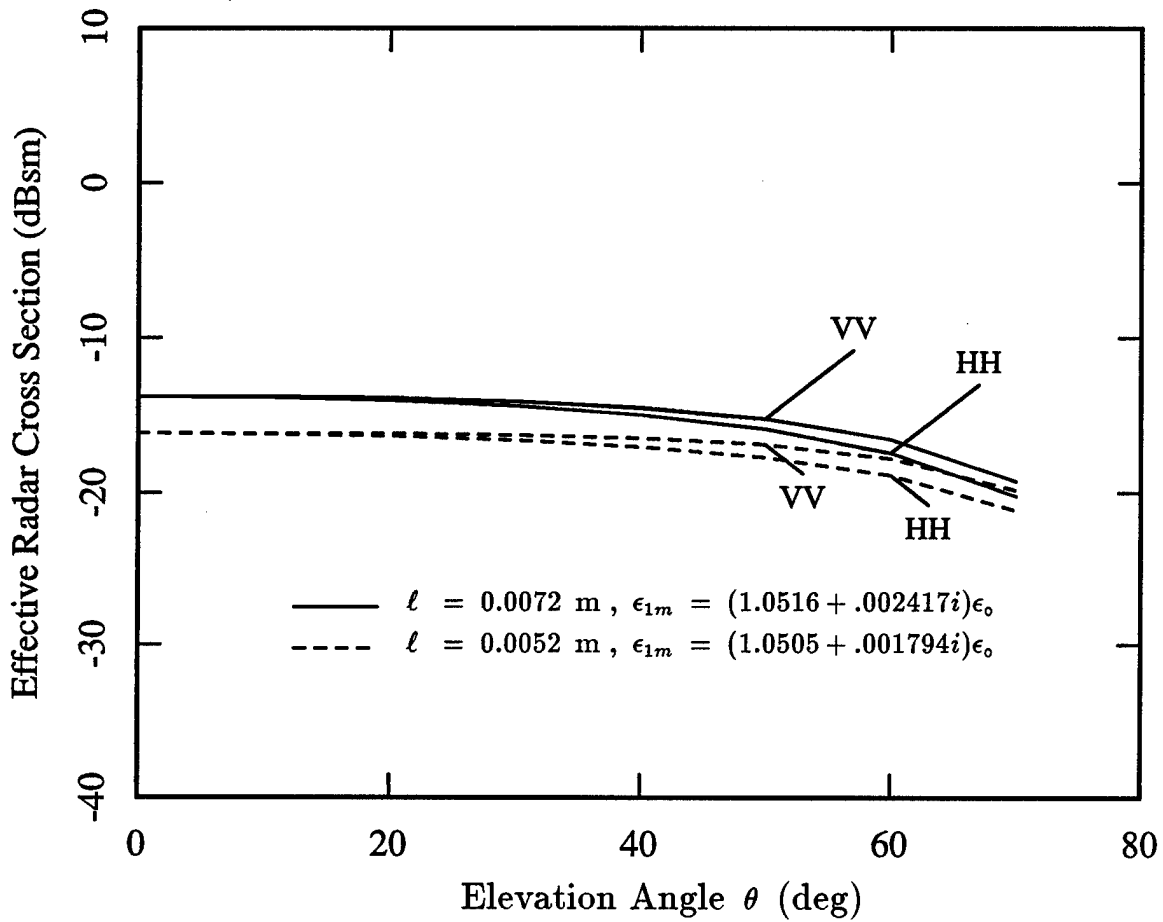
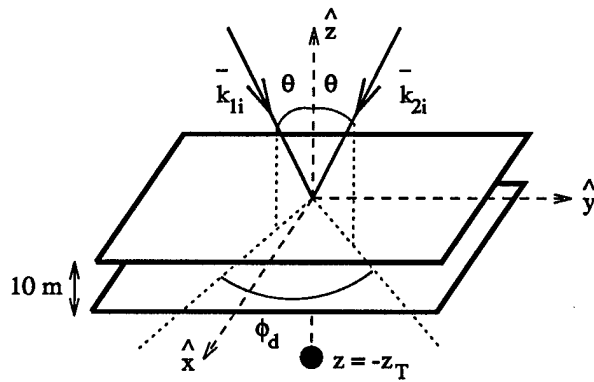
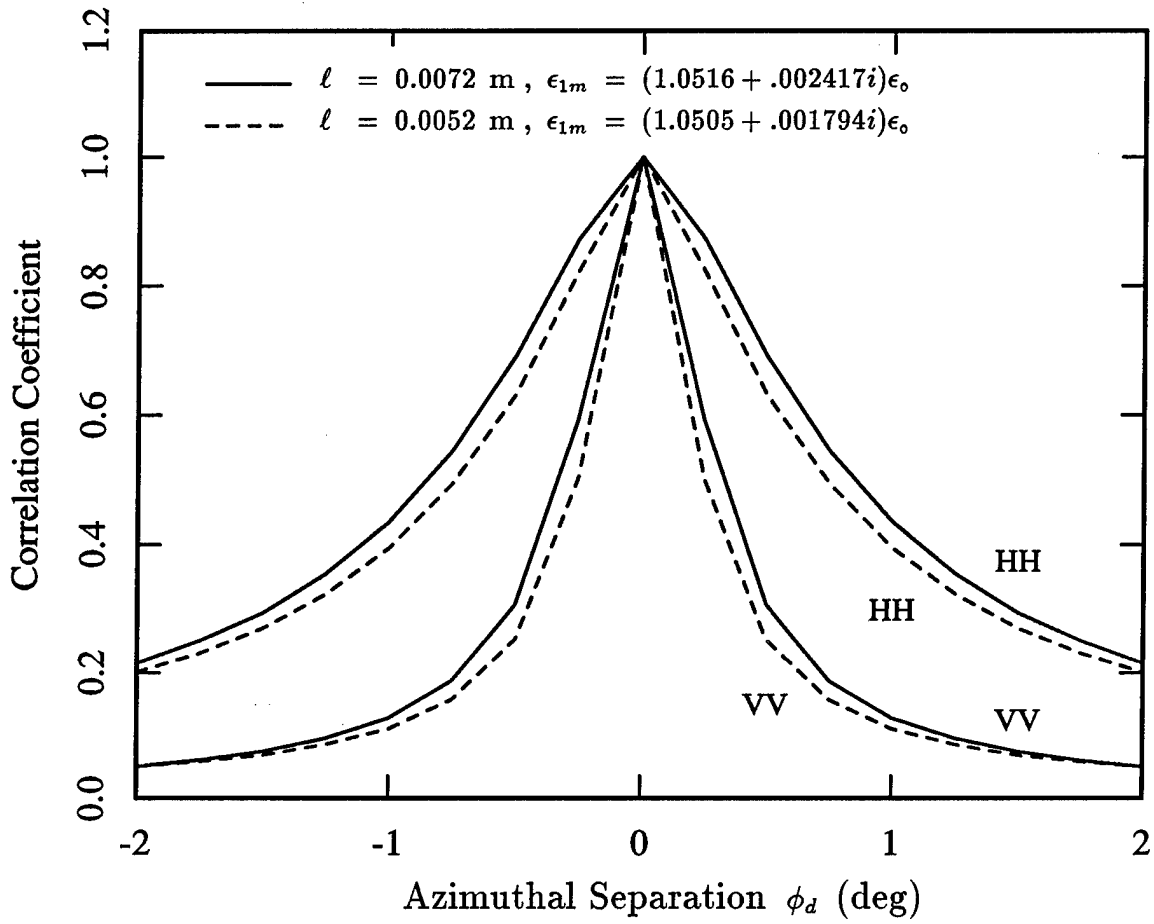


Figure 4.3. Dependence of the incoherent target/clutter scattering cross section, σ_{TC-TC} , on elevation angle for $l = .0072$ m and $\epsilon_{1m} = (1.0516 + .002417i)\epsilon_0$ (solid) and for $l = .0052$ m and $\epsilon_{1m} = (1.0505 + .001794i)\epsilon_0$ (dash). Results are given at 1.120 GHz for a 10 m slab with $z_T = 10$ m and with $\epsilon_0 = \epsilon_2 = \epsilon_0$. For both solid and dashed curves, the VV result is higher at large incident angles.



$$\begin{aligned}
 \epsilon_0 &= \epsilon_2 = \epsilon_o \\
 d &= 10 \text{ m} \\
 z_T &= 10 \text{ m} \\
 \theta &= 60^\circ \\
 f &= 1.12 \text{ GHz} \\
 \delta &= .146822 \\
 f_V &= 1.67\%
 \end{aligned}$$

Figure 4.4. Correlation of the target/clutter multi-path return, σ_{TC-TC} , over $\phi_d = \phi_2 - \phi_1$ for $\ell = .0072$ m and $\epsilon_{1m} = (1.0516 + .002417i)\epsilon_o$ (solid) and for $\ell = .0052$ m and $\epsilon_{1m} = (1.0505 + .001794i)\epsilon_o$ (dash). Results are given at 1.120 GHz for a 10 m slab with $z_T = 10$ m, $\theta = 60^\circ$, and with $\epsilon_0 = \epsilon_2 = \epsilon_o$.

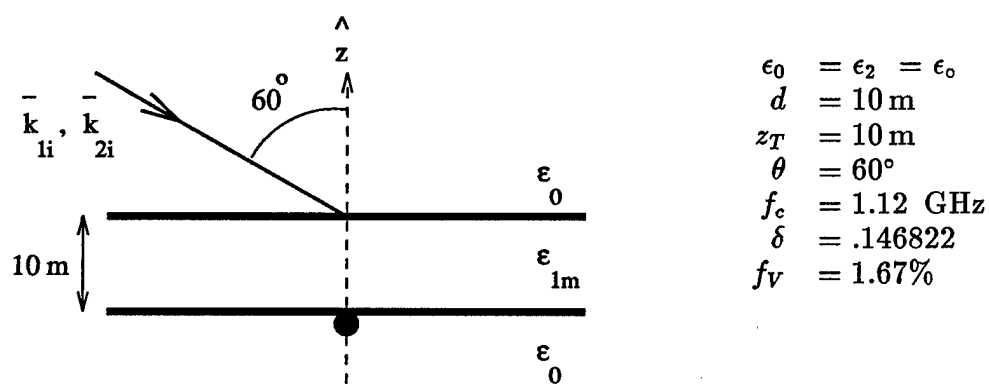
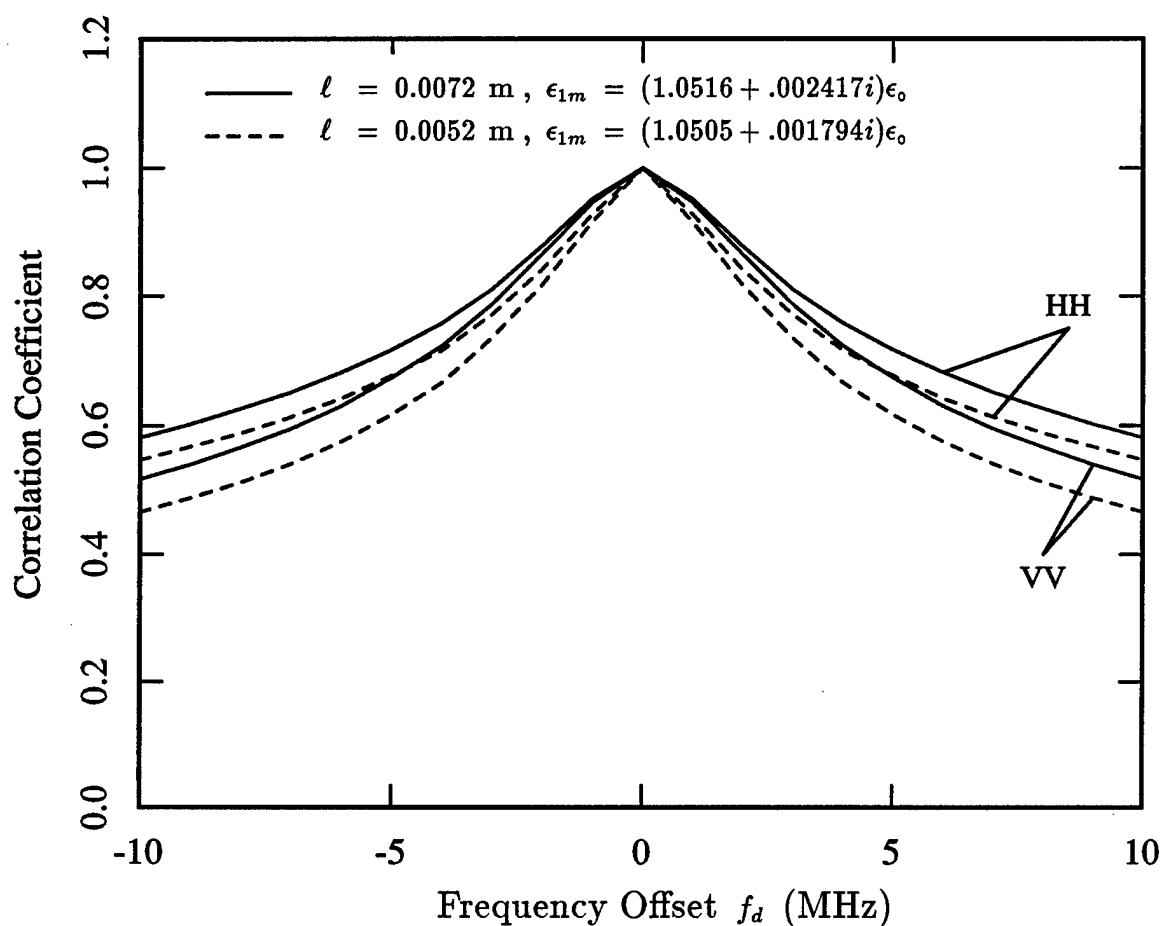


Figure 4.5. Correlation of the target/clutter multi-path return, σ_{TC-TC} , over $f_d = f_2 - f_1$ for $l = .0072 \text{ m}$ and $\epsilon_{1m} = (1.0516 + .002417i)\epsilon_0$ (solid) and for $l = .0052 \text{ m}$ and $\epsilon_{1m} = (1.0505 + .001794i)\epsilon_0$ (dash). Results are given with a center frequency $f_c = 1.120 \text{ GHz}$ for a 10 m slab with $z_T = 10 \text{ m}$, $\theta = 60^\circ$, and with $\epsilon_0 = \epsilon_2 = \epsilon_0$.

are similarly spread in range, along the direction of incidence and scattering. For this reason, the phase change across the region with changing frequency is similar for both polarizations, and the correlation in frequency is much less sensitive to polarization, as shown by Figure 4.5.

If the random medium correlation length were comparable in size to the dimensions of the contributing scattering region within the random medium, then increasing the correlation length would reduce the rate of decorrelation, because even though the phase changed across this region, the return would still be coherent, with all the scatterers on the region correlated. In the present situation, however, the random medium correlation length is much smaller than the size of the scattering region within the random medium, and a small change in this correlation length will do little to affect the lack of correlation between scatterers on one side of the contributing region, and scatterers on the other. Consequently, the scattered field arising from the region as a whole will still become decorrelated when the azimuth or frequency is changed significantly enough to cause a significant phase change across the region. On the scale of the correlation length, the corresponding phase change for this change of azimuth or frequency will be much smaller, and therefore, the field from individual regions of correlation length size will decorrelate very little. Hence, increasing the correlation length will do little to reduce the overall decorrelation, since over the region size it would effect (on the scale of the correlation length) the scatterer are already well correlated. It is for this reason that increasing the random medium correlation length has very little effect on either the azimuthal or frequency correlation, and only causes a slightly slower rate of decorrelation as seen in both Figures 4.4 and 4.5.

4.3.2. Effect of a Larger Fractional Volume of Scatterers

To examine the effects of the fractional volume of scatterers on the coherent and incoherent point target signatures, the two layer geometry considered above is again used. The random slab is 10 m in thickness with free space above and below, and with the target located directly below the lower boundary of the slab. The same isotropic correlation function with exponential dependence is assumed, and the correlation length is taken to be 0.0052 m, as in Chapter 2. The fractional volume of scatterers of 1.67%, which was used in Chapter 2, leads to an effective relative permittivity at 1.12 GHz of $1.0505 + 0.001794i$, and a renormalized scattering source variance of $\delta = .146822$. In contrast, a fractional volume of 4.17%, considered here, leads to an effective permittivity of $1.1360 + 0.005478i$, and a scattering source variance of $\delta = .433835$.

Figure 4.6 shows the effect of the increased fractional volume on the coherent return from the point target. The horizontally and vertically polarized returns for the larger fractional volume of 4.17% are shown by the solid curves, and the previous results for $f_v = 1.67\%$ by the dashed curves. For increased fractional volume, there is an accompanying increase in the effective loss of the random slab, since there are a greater density of scatterers to interfere with propagation through the random layer. Hence, as expected, the higher fractional volume case displays a greater attenuation, consistent with the more lossy effective permittivity. Again both polarizations remain very comparable since the increase in fractional volume is not sufficient to change the electrical density of the random slab significantly from that of free space, and to introduce noticeable boundary reflection effects.

Figure 4.7 shows a similar effect in the incoherent target/clutter multi-path return

when the fractional volume is increased. Again the results for higher fractional volume are attenuated more than the results at the lower fractional volume. Comparing Figures 4.6 and 4.7, however, it can be seen that the increase in attenuation in the coherent return is larger than that for the incoherent field. This smaller increase in attenuation for the incoherent term is the result of two opposing consequences of increasing the density of scatterers in the random layer. Like the coherent return, the incoherent field experiences a greater loss in traveling through the random layer, resulting from the more lossy effective permittivity at higher fractional volumes. In contrast, however, the higher density of scatterers provides more opportunity to scatter energy back in the direction of the receiver. In the present situation, the former of these two effects is the more dominant, and the increased effective loss leads to a decreased incoherent return.

Note, however, that at very low fractional volumes, the effect will be quite the opposite. Figure 4.8 compares the result at the former fractional volume of 1.67% (dash curve) with a smaller fractional volume of .05% (solid curve). Now it can be seen that increasing the fractional volume from the smaller value leads to an increase in the incoherent return. Hence, the dependance on fractional volume is such that the incoherent cross section increases with increasing fractional volume initially, then saturates and begins to decrease for larger fractional volumes. This dependance is the same as that seen in Chapter 2 for media thickness, where the incoherent return increased initially with increasing media thicknesses, but eventually the enhancement from added scatterers was countered by the increased loss from the longer path through the slab, and, thus, the return decreased for large media thicknesses. Figure 4.8 also shows in the low fractional volume case, an increase in the return for the VV polarization with increas-

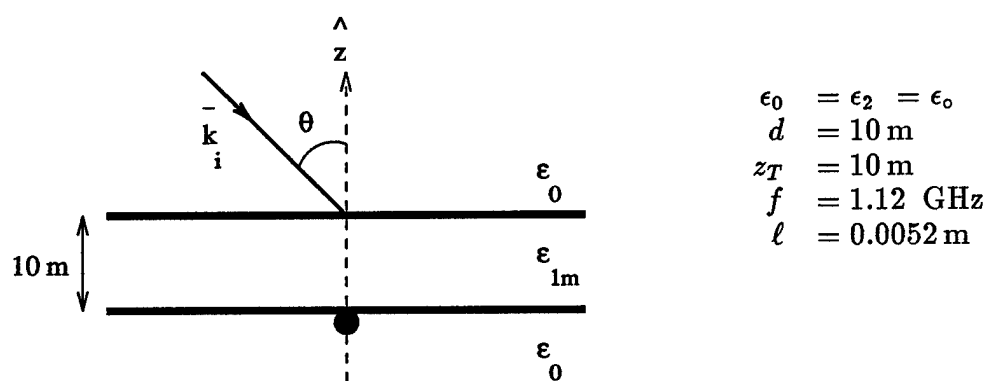
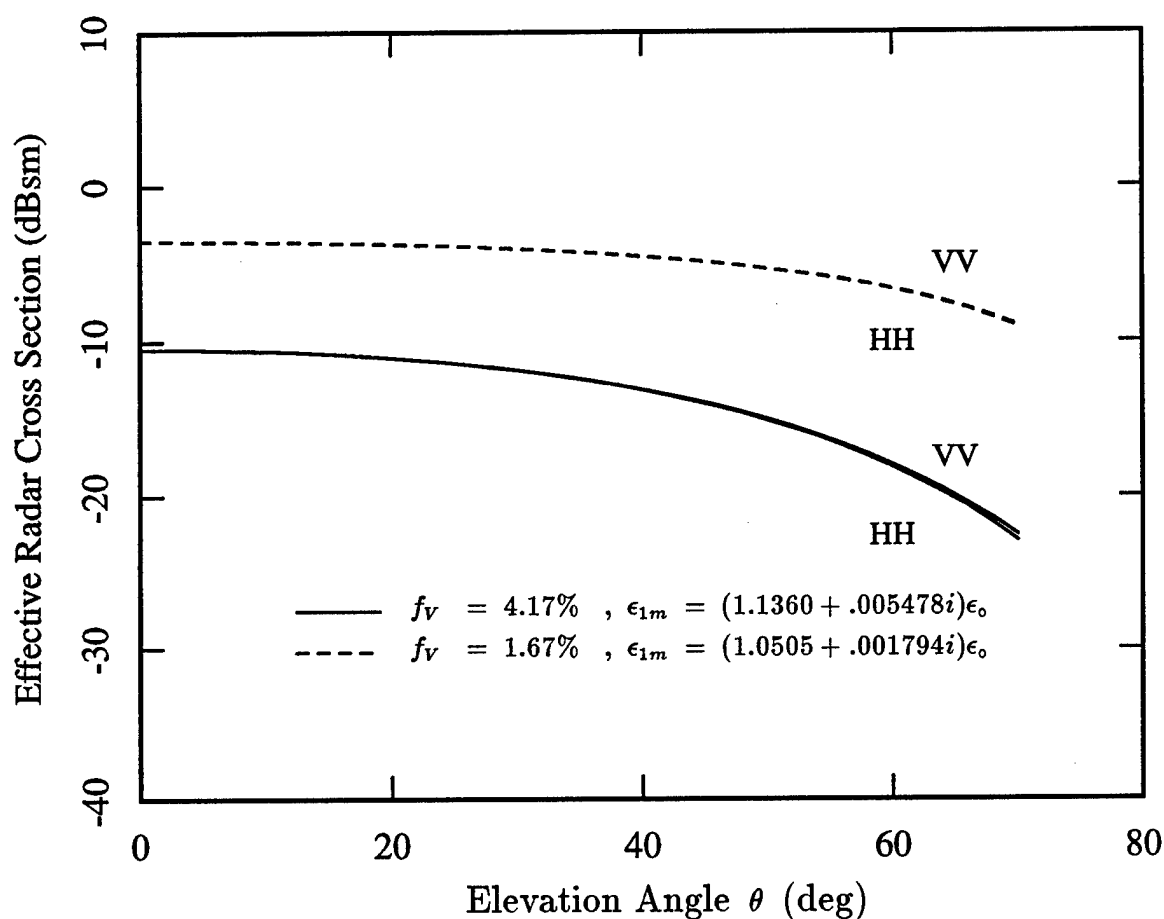


Figure 4.6. Dependence of the coherent target scattering cross section, σ_{T-T} , on elevation angle for $f_V = 4.17\%$ and $\epsilon_{1m} = (1.1360 + .005478i)\epsilon_0$ (solid) and for $f_V = 1.67\%$ and $\epsilon_{1m} = (1.0505 + .001794i)\epsilon_0$ (dash). Results are given at 1.120 GHz for a 10 m slab with $z_T = 10 \text{ m}$ and with $\epsilon_0 = \epsilon_2 = \epsilon_0$. In each case the random medium correlation length is $\ell = 0.0052 \text{ m}$.

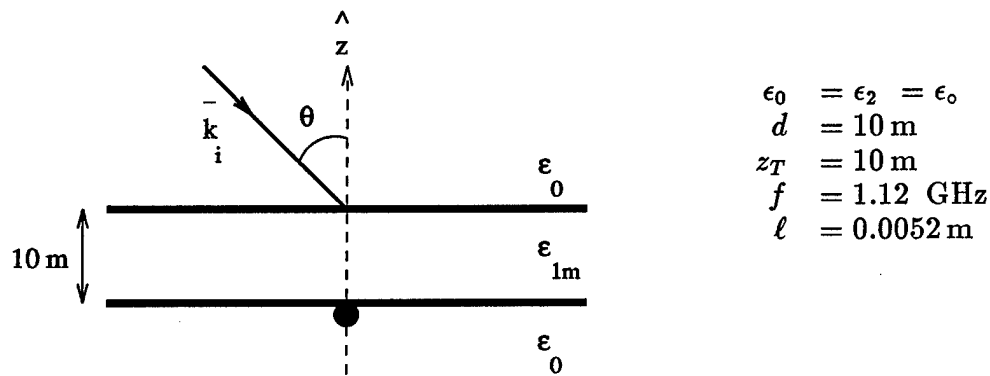
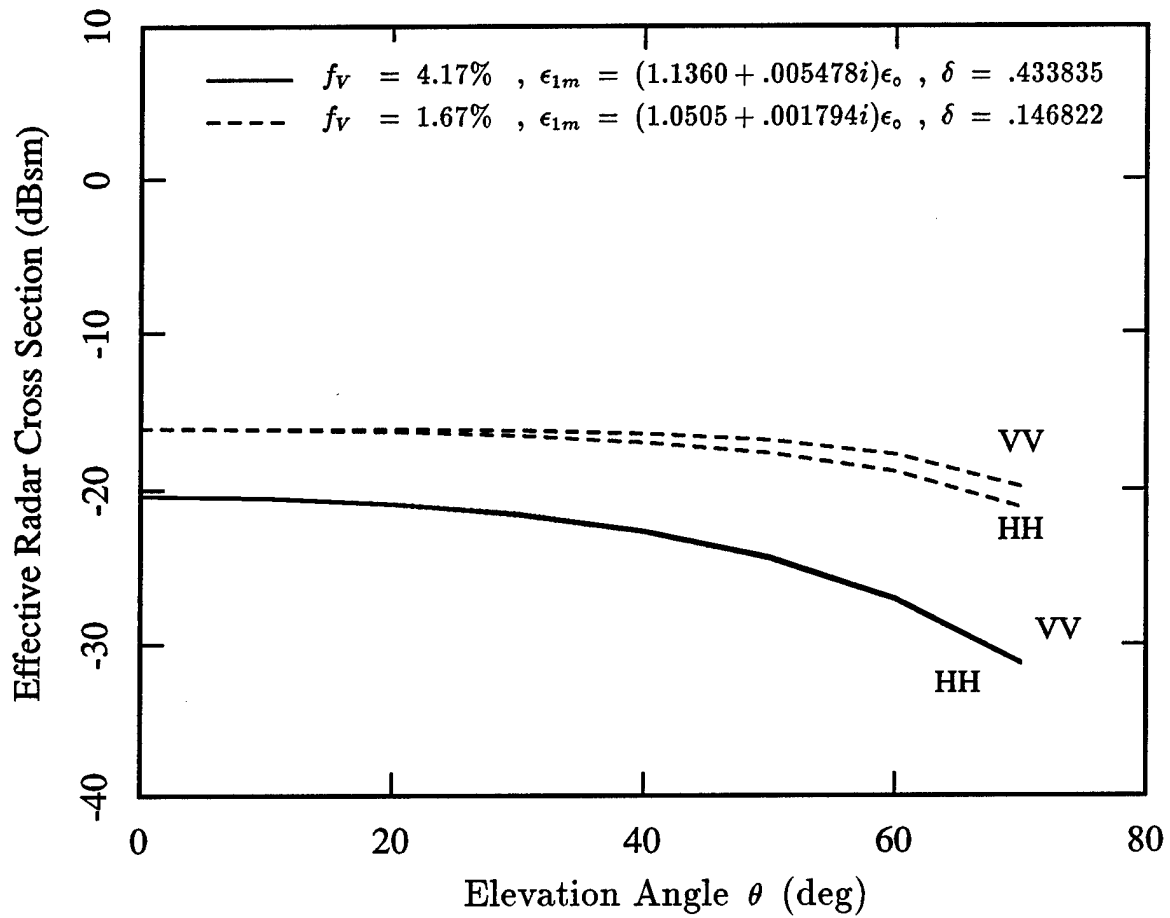


Figure 4.7. Dependence of the target/clutter scattering cross section, σ_{TC-TC} , on elevation angle for $f_V = 4.17\%$, $\epsilon_{1m} = (1.1360 + .005478i)\epsilon_0$, and $\delta = .433835$ (solid) and for $f_V = 1.67\%$, $\epsilon_{1m} = (1.0505 + .001794i)\epsilon_0$, and $\delta = .146822$ (dash). Results are given at 1.120 GHz for a 10 m slab with $z_T = 10$ m and with $\epsilon_0 = \epsilon_2 = \epsilon_0$. In each case the random medium correlation length is $\ell = 0.0052$ m.

ing angle. Again this result arises from the larger number of scatterers encountered for longer path lengths through the media, an effect which is sufficient to overcome the additional path loss when the fractional volume is small.

Figures 4.9 and 4.10 show the effect of increasing the fractional volume of scatterers on the azimuthal and frequency correlations of the incoherent target/clutter multi-path. An elevation angle of $\theta = 60^\circ$, and a center frequency of 1.12 GHz, are again assumed, and the correlations over a $\pm 2^\circ$ azimuthal separation, and ± 10 MHz frequency separation are shown. In both cases, the results for the higher fractional volume of scatterers (solid curve), display a slower rate of decorrelation. Again, the rate of decorrelation is primarily determined by the size of the region of contributing scatterers within the random slab, and the greater loss in the slab for the higher fractional volume case, tends to decrease the effective size of the contributing region, since scatterers further from the point target will now experience a greater path loss in the propagation from the target. With the effective region of scatterers smaller, a fixed change in angle produces less phase change across the region, and correspondingly less decorrelation in the scattered field.

4.3.3. Effect of a Uniaxial Correlation Function

In this section, the effects of non-isotropic scatterers and the resulting uniaxial correlation function are considered. The correlation function utilized here is that of (D.81) of Appendix D, which exhibits an azimuthally symmetric gaussian behavior in the horizontal plane, and an exponential decay in the vertical direction. Hence, the correlation function depends on two correlation lengths, ℓ_ρ and ℓ_z , defining the rate of decorrelation in the horizontal and vertical directions respectively. The radial

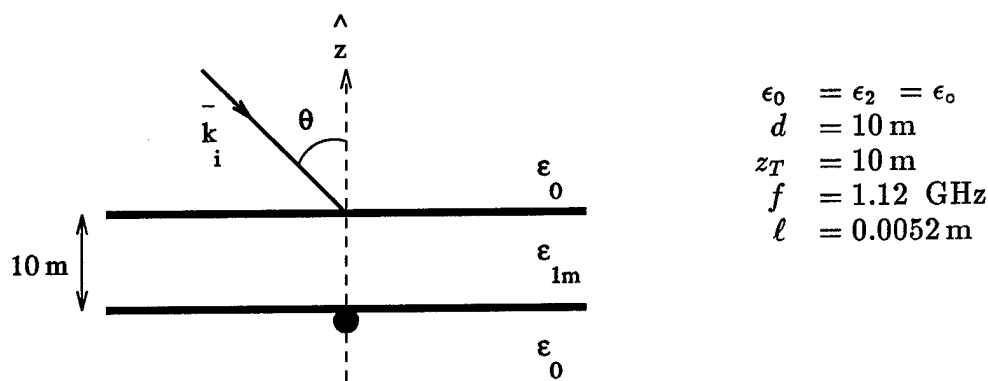
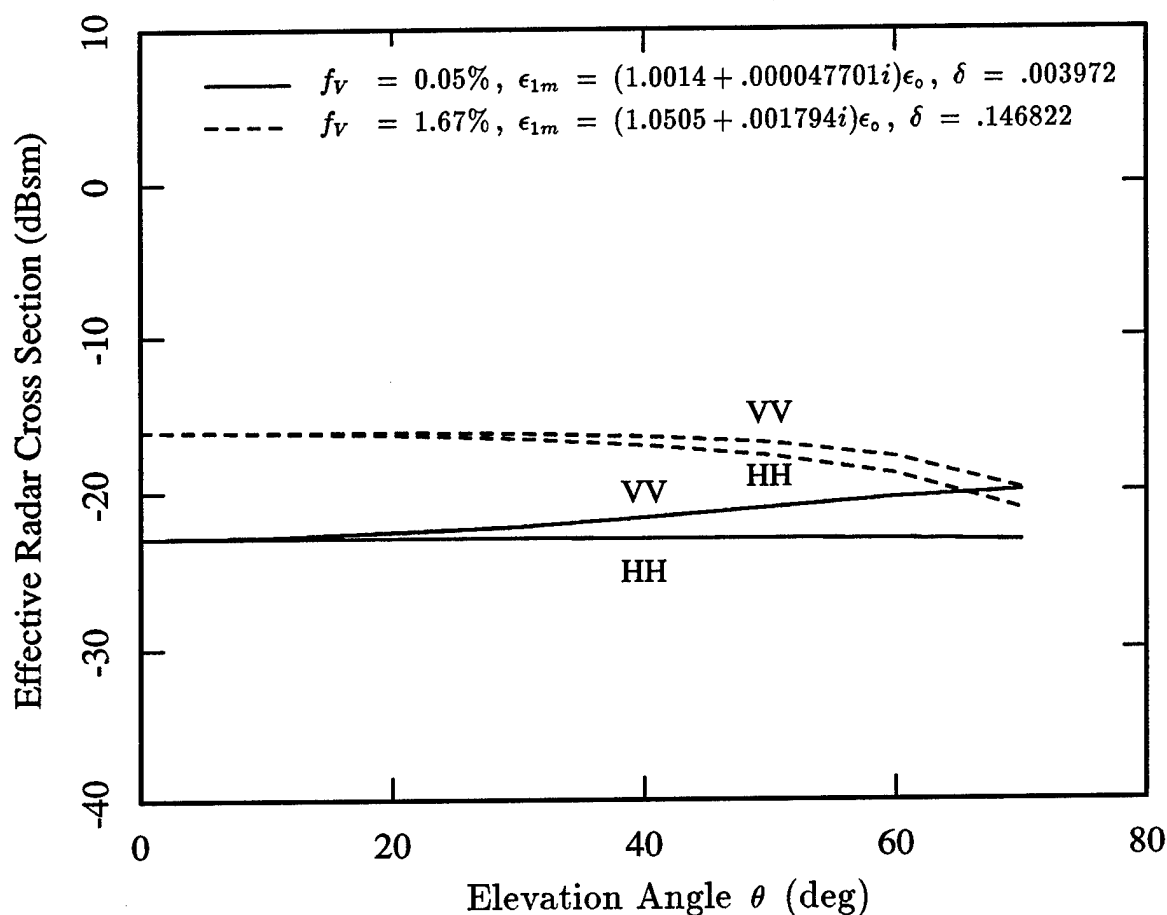


Figure 4.8. Dependence of the target/clutter scattering cross section, σ_{TC-TC} , on elevation angle for $f_V = 0.05\%$, $\delta = .003972$, and $\epsilon_{1m} = (1.0014 + .000047701i)\epsilon_0$ (solid) and for $f_V = 1.67\%$, $\delta = .146822$, and $\epsilon_{1m} = (1.0505 + .001794i)\epsilon_0$ (dash). Results are given at 1.120 GHz for a 10 m slab with $z_T = 10 \text{ m}$ and with $\epsilon_0 = \epsilon_2 = \epsilon_0$. In each case the random medium correlation length is $\ell = 0.0052 \text{ m}$.

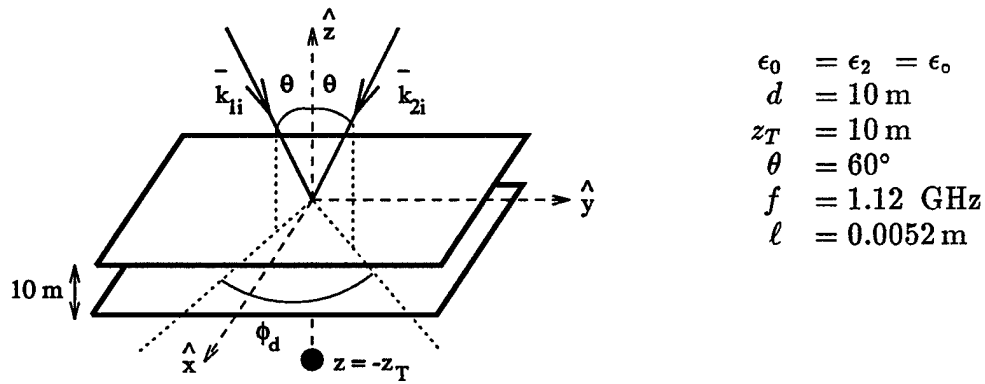
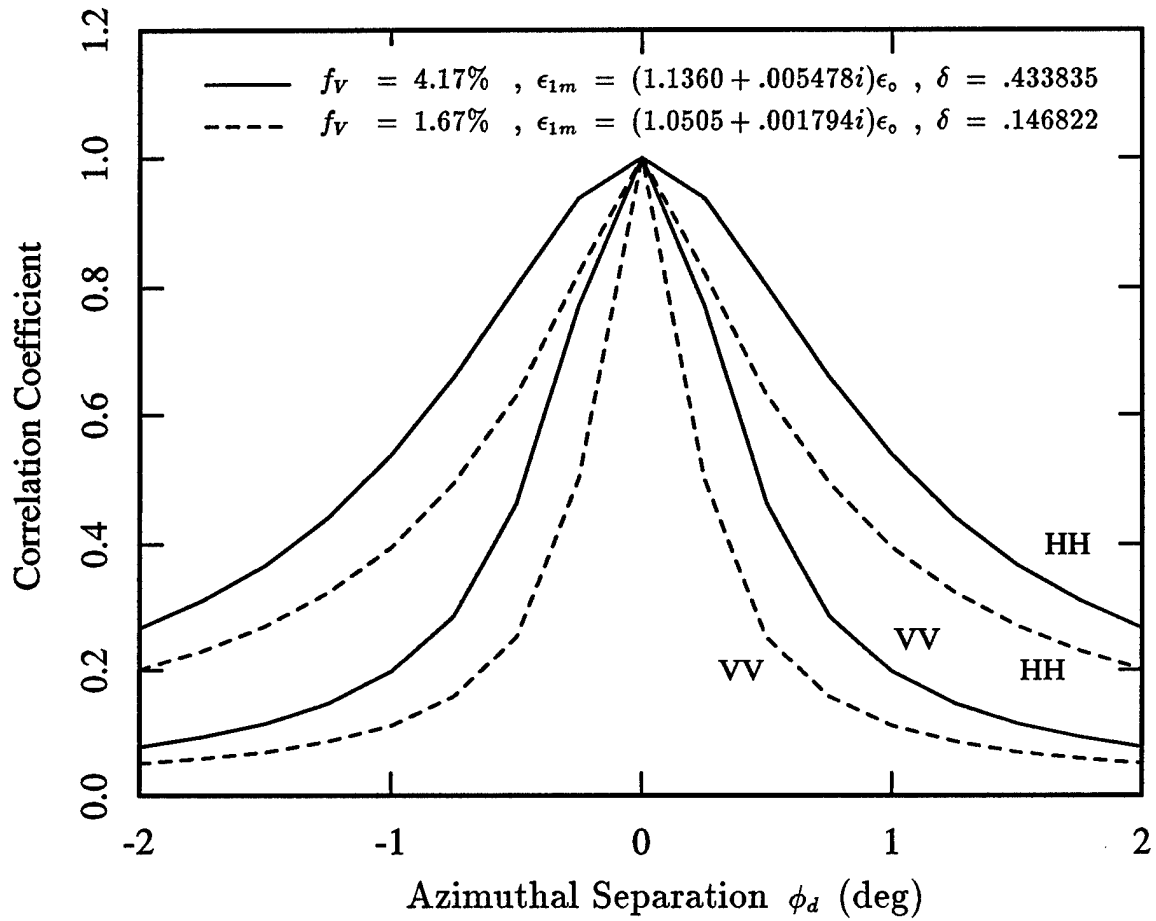


Figure 4.9. Correlation of the target/clutter multi-path return, σ_{TC-TC} , over $\phi_d = \phi_2 - \phi_1$ for $f_V = 4.17\%$, $\epsilon_{1m} = (1.1360 + .005478i)\epsilon_0$, and $\delta = .433835$ (solid) and for $f_V = 1.67\%$, $\epsilon_{1m} = (1.0505 + .001794i)\epsilon_0$, and $\delta = .146822$ (dash). Results are given at 1.120 GHz for a 10 m slab with $z_T = 10$ m, $\theta = 60^\circ$, and with $\epsilon_0 = \epsilon_2 = \epsilon_0$. In each case the random medium correlation length is $\ell = 0.0052$ m.

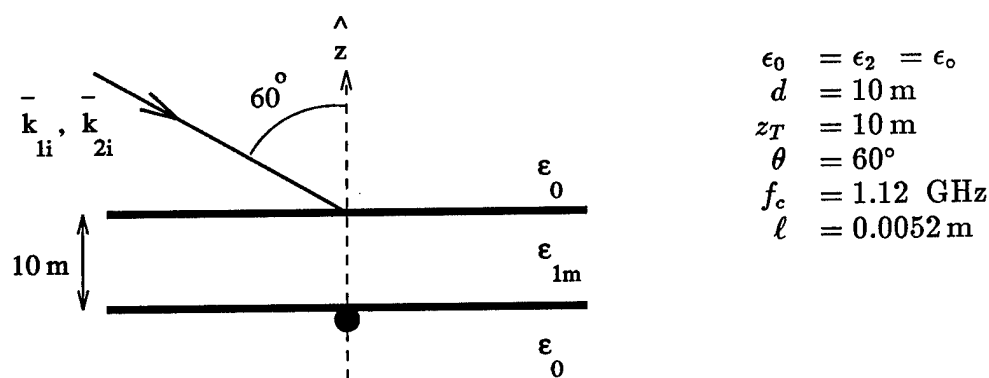
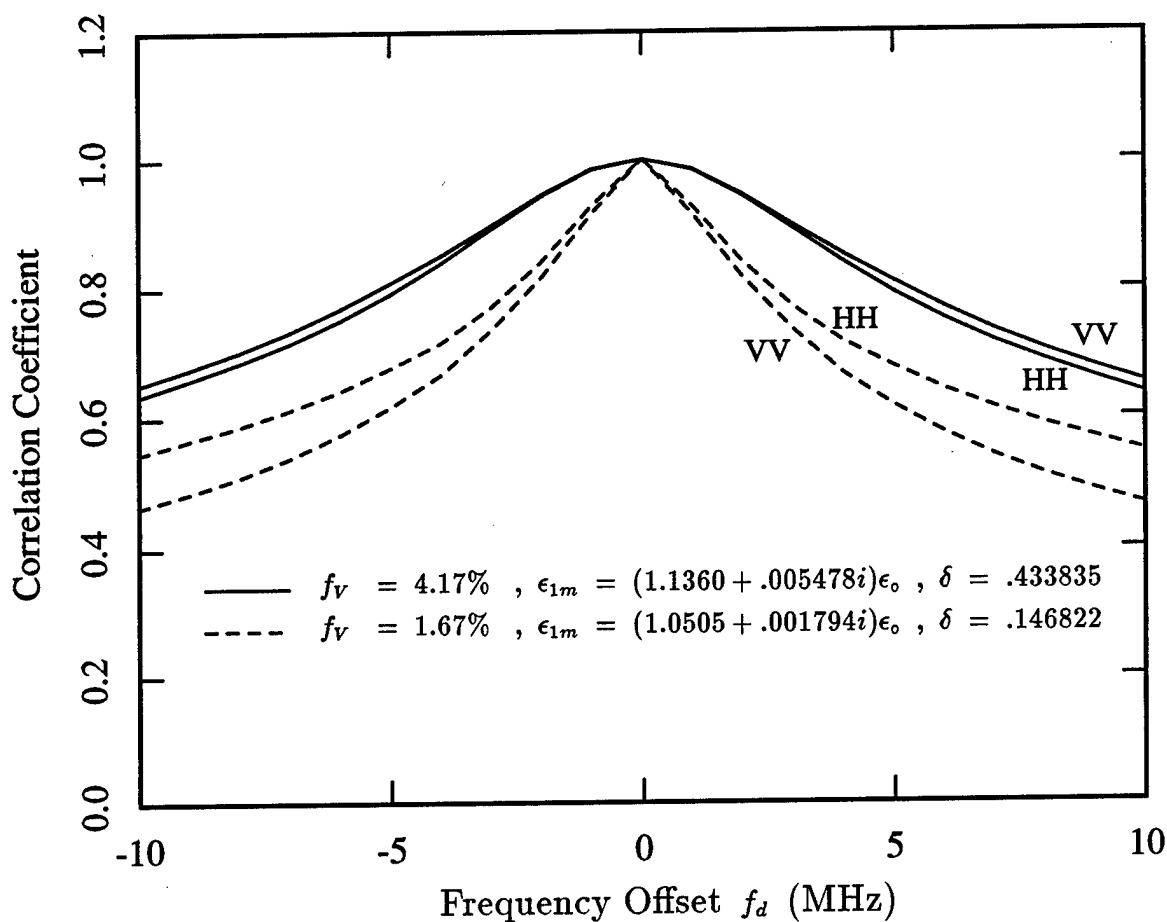


Figure 4.10. Correlation of the target/clutter multi-path return, σ_{TC-TC} , over $f_d = f_2 - f_1$ for $f_V = 4.17\%$, $\epsilon_{1m} = (1.1360 + .005478i)\epsilon_0$, and $\delta = .433835$ (solid) and for $f_V = 1.67\%$, $\epsilon_{1m} = (1.0505 + .001794i)\epsilon_0$, and $\delta = .146822$ (dash). Results are given at 1.120 GHz for a 10 m slab with $z_T = 10 \text{ m}$, $\theta = 60^\circ$, and with $\epsilon_0 = \epsilon_2 = \epsilon_0$. In each case the random medium correlation length is $\ell = 0.0052 \text{ m}$.

correlation length ℓ_p is taken to be .0052 m, and the vertical correlation length, ℓ_z is taken to be three times as large, or .0156 m. Hence, this correlation function models scatterers which are elongated in the vertical direction, and which are individually or on average symmetric in azimuth.

The effective permittivity which results from this assumed correlation function is uniaxial (untilted) as stated previously. At a frequency of 1.12 GHz and with a fractional volume of scatterers of 1.67%, the x and y components of the diagonal permittivity tensor are $\epsilon_{1m\perp} = (1.0442 + 0.001327i)\epsilon_0$, and the z component of the permittivity is given by $\epsilon_{1mz} = (1.0839 + 0.004739i)\epsilon_0$. In comparison to the permittivity of $\epsilon_{1m} = (1.0505 + 0.001794i)\epsilon_0$ obtained with the isotropic correlation function, it can be seen that the perpendicular component of permittivity for the uniaxial case shows smaller loss, while the vertical component shows a greater loss. The larger loss in the vertical component of the permittivity results from the fact the scatterers are elongated in that direction, and thus have a larger scattering cross section for vertically polarized waves. Similarly, since the overall fractional volume is the same, with the scatterers elongated vertically, they must be thinner in the horizontal direction, and have a smaller scattering cross section for a horizontally polarized wave.

In addition, the variance of the re-normalized scattering source is not isotropic, and instead the three distinct variances are given by $\delta_{\perp\perp} = .115700$, $\delta_{zz} = .390404$, and $\delta_{\perp z} = .212485$. When compared to $\delta = 0.146822$ for the isotropic case, the individual components for the uniaxial case again indicate the scattering will be strongest for a vertically polarized wave.

Figure 4.11 shows the effect of the new uniaxial media on the coherent return from the point target. Again the geometry is two-layer with free space above and below the

random slab, and with the target directly below the lower interface of the 10 m thick random layer. At normal incidence, the new results for the uniaxial media show slightly less loss. This is again because for the coherent wave the attenuation is determined almost entirely by the mean loss of the random layer, and for the horizontal wave, this loss is smaller in the uniaxial case. Unlike the isotropic result, however, where the loss for HH and VV waves remained identical as the elevation angle was moved away from normal incidence, in the uniaxial case, there is a much greater loss at large angles for VV. For the vertical polarization not only, does the path length through the media increase at larger angles, but the propagation constant becomes more lossy as the wave becomes oriented more vertically.

Figure 4.12 shows a similar comparison for the incoherent target/clutter multipath return. Unlike the coherent case, however, at elevation angles close to normal incidence, the return in the presence of the uniaxial random media is now weaker than that for the isotropic random media, although the difference is again small. Despite the reduced propagation loss through the uniaxial media for the TE wave, the scattering is also weaker as exhibited by the difference between $\delta_{\perp\perp}$ in the uniaxial case, and δ in the isotropic case. For this reason, the overall effect is the small decrease in the power of the incoherent return. At larger elevation angles there exists a small difference between HH and VV returns for the isotropic case. As discussed previously in Chapter 2, this difference arises from the dipole-like scattering geometry of the point target. This geometric effect, however, is not sufficient to overcome the added propagation loss experienced by the TM wave in the uniaxial case, which leads to a significantly lower return for the vertical polarization than for the horizontal polarization. The difference between HH and VV incoherent returns is smaller, however, than that seen in Fig-

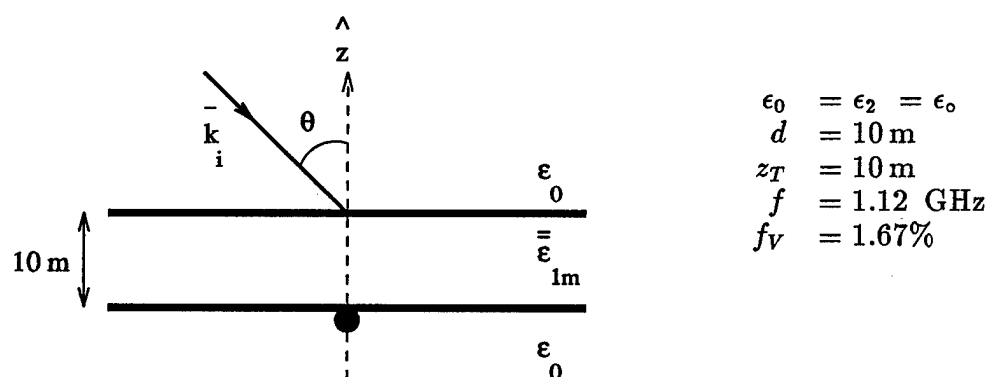
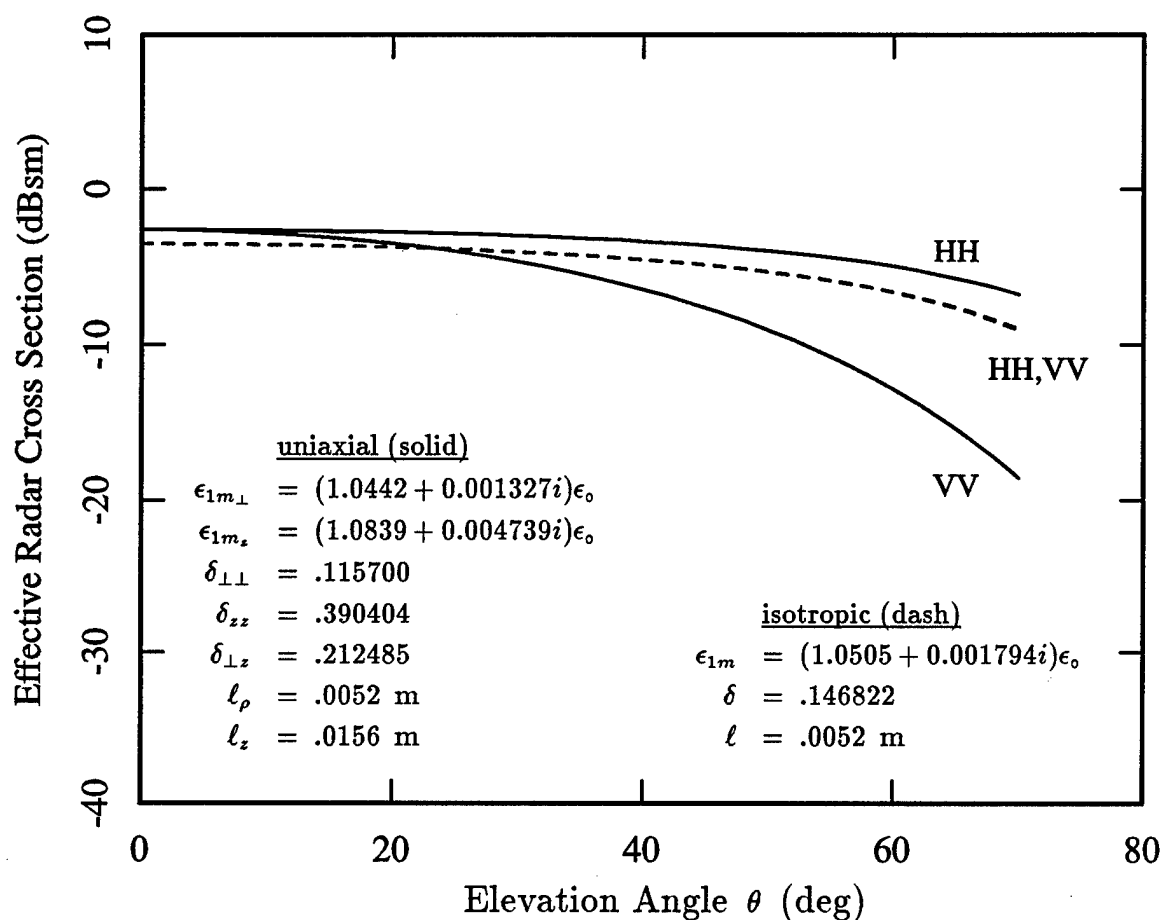


Figure 4.11. Dependence of the coherent target scattering cross section, σ_{T-T} , on elevation angle for the uniaxial correlation function with $\ell_\perp = .0052$ m and $\ell_z = .0156$ m (solid) and for the isotropic correlation function with $\ell = .0052$ m (dash). Results are given at 1.120 GHz for a 10 m slab with $z_T = 10$ m and with $\epsilon_0 = \epsilon_2 = \epsilon_0$.

ure 4.11 for the coherent returns, in part, because the scattering is stronger for the TM wave than for the TE wave, and this effect overcomes part of the effect of the added coherent loss.

Figures 4.13 and 4.14 compare the azimuthal and frequency correlations of the target/clutter multi-path field for the uniaxial (solid) and isotropic (dash) cases. In both correlations, the rate of decorrelation for the horizontally polarized returns is very similar for both the uniaxial and isotropic random media. In contrast, in both correlations, the decorrelation of the VV return is significantly slower for the uniaxial random media than in the isotropic case. This result once again demonstrates the principle discussed above when examining changes of the media correlation length or fractional volume, where it was seen that the rate of decorrelation is affected by the size of the region of random media contributing to the multi-path field. The coherent loss in the random slab for TM waves is significantly greater for the uniaxial case than for the isotropic case, leading to a smaller effective scattering region, and a slower decorrelation rate. In contrast, the loss for the TE wave is comparable for both uniaxial and isotropic cases, and hence, the correlations of the HH returns are much more comparable between these two cases.

4.3.4. Effect of an Additional Stratification Layer

In this section, the effects of an additional layer of electrically dense material placed beneath the target, are considered. This additional region allows modeling, for instance, of the presence of an air-ground boundary below the target and random foliage region. The geometry utilized here consists of two bounded layers where the upper of these regions contains the random media, and the lower, free-space region

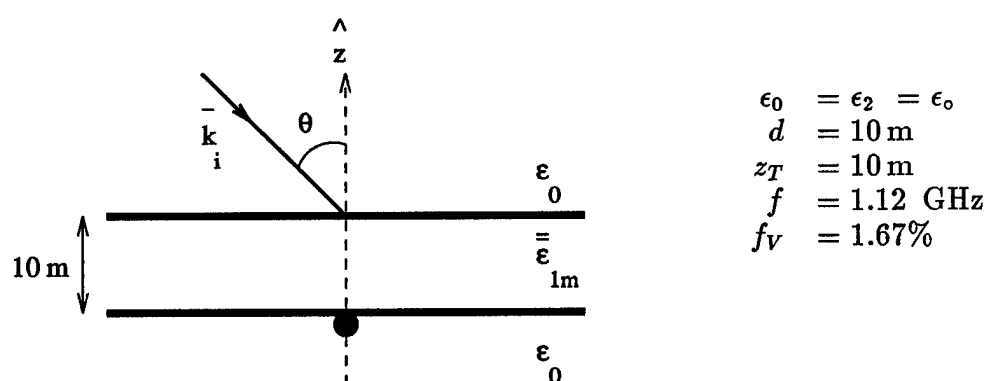
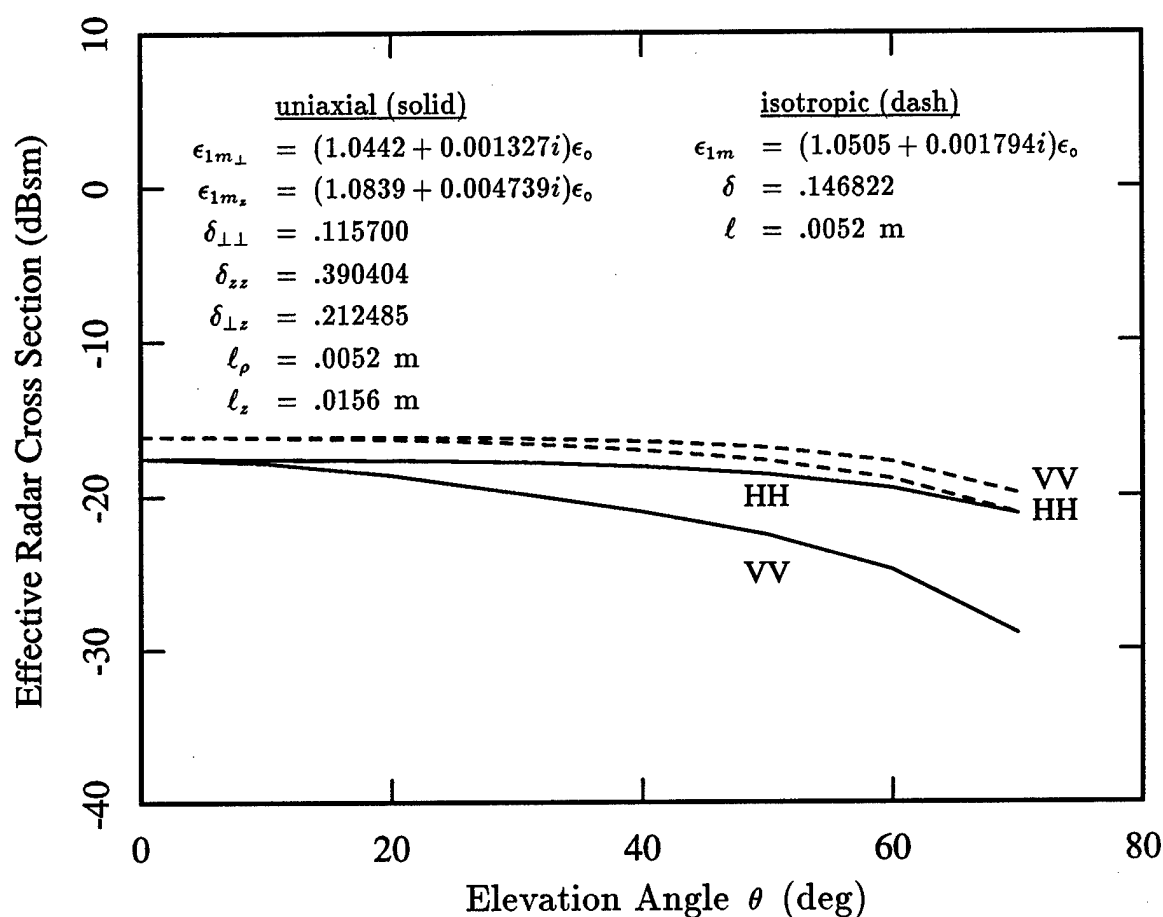
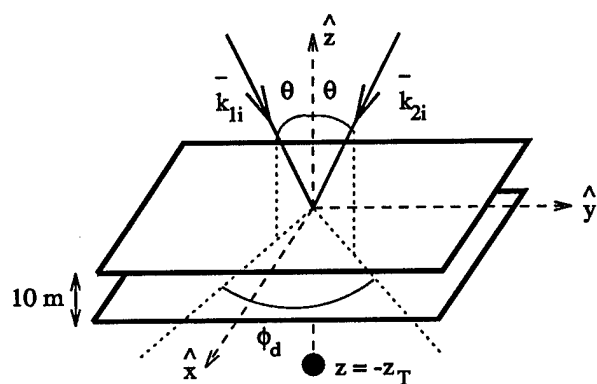
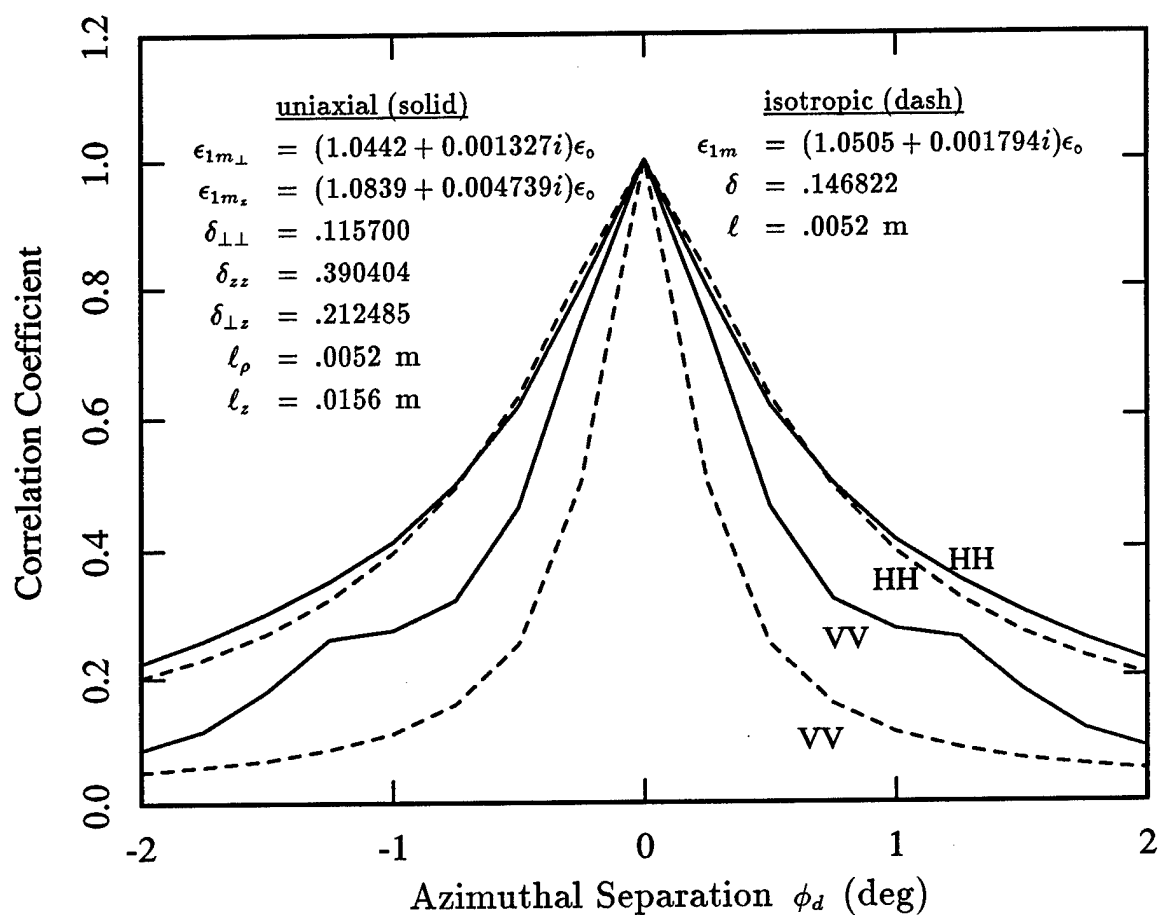


Figure 4.12. Dependence of the target/clutter scattering cross section, σ_{TC-TC} , on elevation angle for the uniaxial correlation function with $\ell_\perp = .0052 \text{ m}$ and $\ell_z = .0156 \text{ m}$ (solid) and for the isotropic correlation function with $\ell = .0052 \text{ m}$ (dash). Results are given at 1.120 GHz for a 10 m slab with $z_T = 10 \text{ m}$ and with $\epsilon_0 = \epsilon_2 = \epsilon_0$.



$$\epsilon_0 = \epsilon_2 = \epsilon_0$$

$$d = 10 \text{ m}$$

$$z_T = 10 \text{ m}$$

$$\theta = 60^\circ$$

$$f = 1.12 \text{ GHz}$$

$$f_V = 1.67\%$$

Figure 4.13. Correlation of the target/clutter multi-path return, σ_{TC-TC} , over $\phi_d = \phi_2 - \phi_1$ for the uniaxial correlation function with $\ell_{\perp} = .0052 \text{ m}$ and $\ell_z = .0156 \text{ m}$ (solid) and for the isotropic correlation function with $\ell = .0052 \text{ m}$ (dash). Results are given at 1.120 GHz for a 10 m slab with $z_T = 10 \text{ m}$, with $\theta = 60^\circ$, and with $\epsilon_0 = \epsilon_2 = \epsilon_0$.

contains the target. Above these two regions is a half-space of free-space permittivity, and below is a half-space with permittivity $\epsilon_3 = (2.908 + 0.410i)\epsilon_0$, which is chosen to represent a typical dry soil[127]. For simplicity, the random media is once again taken as isotropic, with fractional volume $f_V = 1.67\%$ and correlation length $\ell = 0.0052$ m, which leads to the effective permittivity of $\epsilon_{1m} = (1.0505 + 0.001794i)\epsilon_0$.

Figure 4.15 compares the coherent return from the point target for this new three layer geometry (solid) with that shown previously for the two-layer case (dash). In both cases, the target is at a total depth of 15 m, which corresponds for the three-layer case to a position 1 m above the interface between regions 2 and 3. Unlike the two-layer result which is relatively flat over the elevation angles shown, this new result oscillates about the former return. At normal incidence, the three-layer result is higher, and in fact exceeds the 0 dBsm free-space cross-section of the target. This stronger return is the result of the reflections from the new interface beneath the target, which interfere constructively with the target return in the absence of this boundary, to increase the overall return. Similarly, the oscillation occurs because the relative phase of the reflection contribution changes as the path length is increased at larger elevation angles, and consequently the interference with the directly scattered target field is sometimes constructive and sometimes destructive. In addition, there exists a significant difference between the HH and VV returns in the new three-layer result, unlike the two-layer case where the two polarizations appear identical. This result arises because the contrast in permittivities between regions 2 and 3 is large, the reflection significant as noted above, and the reflection coefficient different for TE and TM waves. In particular, at larger elevation angles, the TM wave experiences a Brewster angle effect where the reflection becomes small, and consequently, the three-layer VV result

approaches that of the two-layer case.

Figure 4.16 shows a similar comparison between three-layer and two-layer cases for the incoherent target/clutter multi-path return. The three-layer result shows the same effects seen in the coherent result, namely an oscillation in the return with elevation angle, and a significant difference between polarizations at larger angles. Unlike the coherent results, however, the oscillations of the three-layer case are not centered about the two-layer result, and the VV returns for large angles are different for two and three-layer cases. This difference arises because the scattering from the target to the random media is independent of incidence angle, and the effect of the additional boundary will be the same for all incidence angles. Because the HH and VV returns for the three-layer case are biased above the two-layer results, it is clear that for the target position and geometry considered here, the additional layer enhances the scattering between the target and random media. In contrast, the incidence on the target is still subject to interference between the direct and reflected paths, and this interference will change with incidence angle, leading to the oscillations (smaller in amplitude than the coherent case) and the Brewster angle effects observed.

Figure 4.17 shows the effect of the thickness of the target layer on the coherent (solid) and target/clutter multi-path (dash) returns. These results are shown for normal incidence with the target always positioned 1 m above the lower interface of region 2. Because the distance between the target and this boundary is fixed, the interference effects between the direct and reflected paths to the target (and from the target in the coherent case) will not vary. Hence, the coherent result is expected to be relatively independent of the region thickness as shown. The small ripple in the coherent result is believed to be due to the interference effect of a small secondary reflection involving

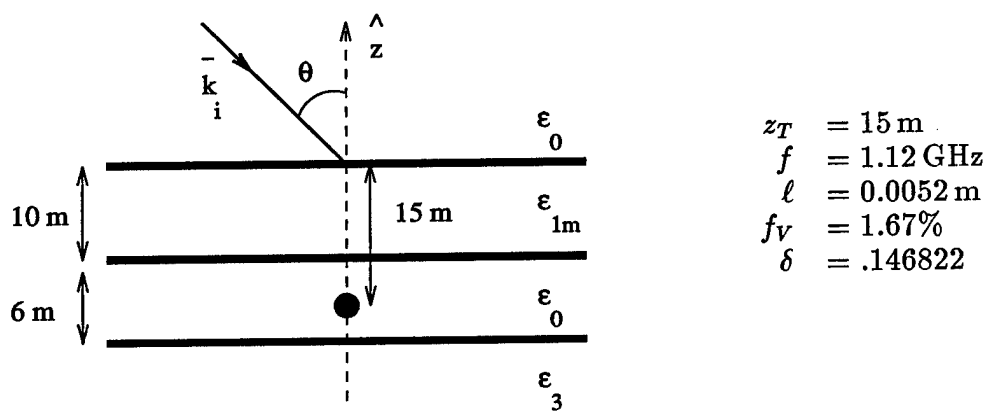
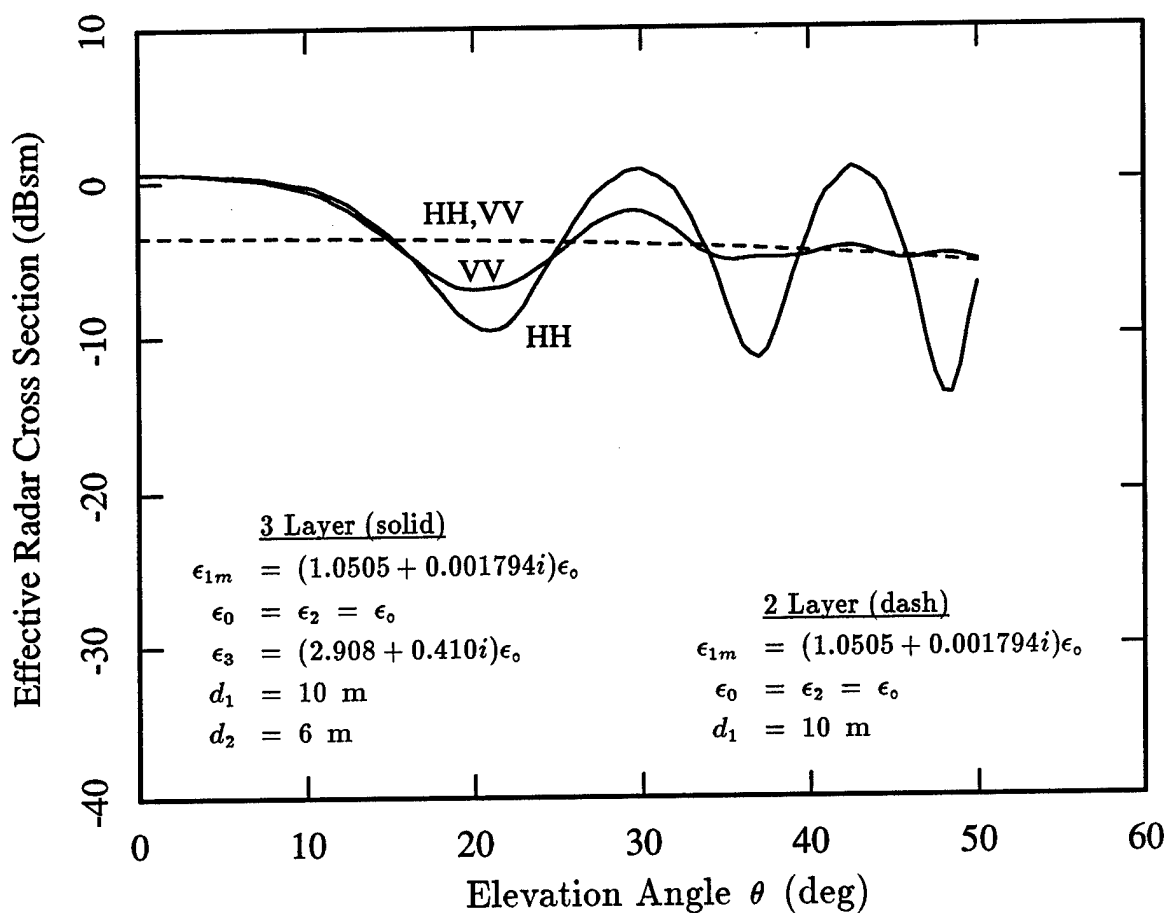


Figure 4.15. Dependence of the coherent target scattering cross section, σ_{T-T} , on elevation angle for a three layer configuration with a ground plane (solid) and for a two layer configuration without the added layer (dash). Results are given at 1.120 GHz for a 10 m random slab with $z_T = 15 \text{ m}$ and with $\epsilon_0 = \epsilon_2 = \epsilon_0$.

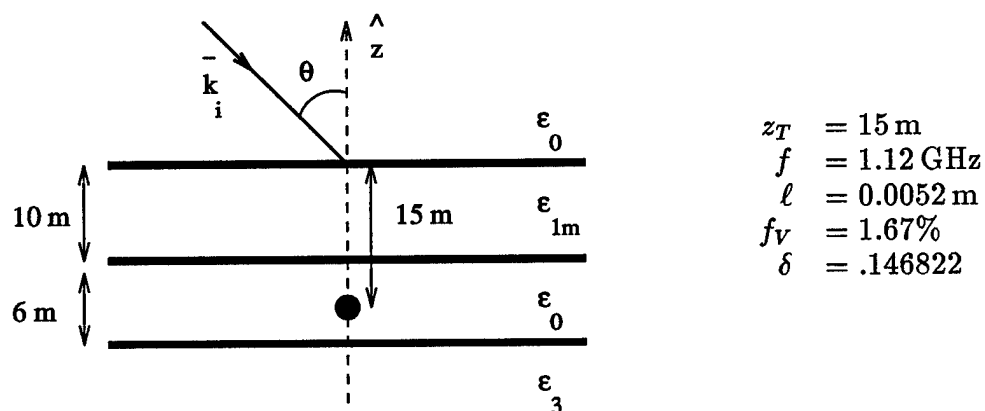
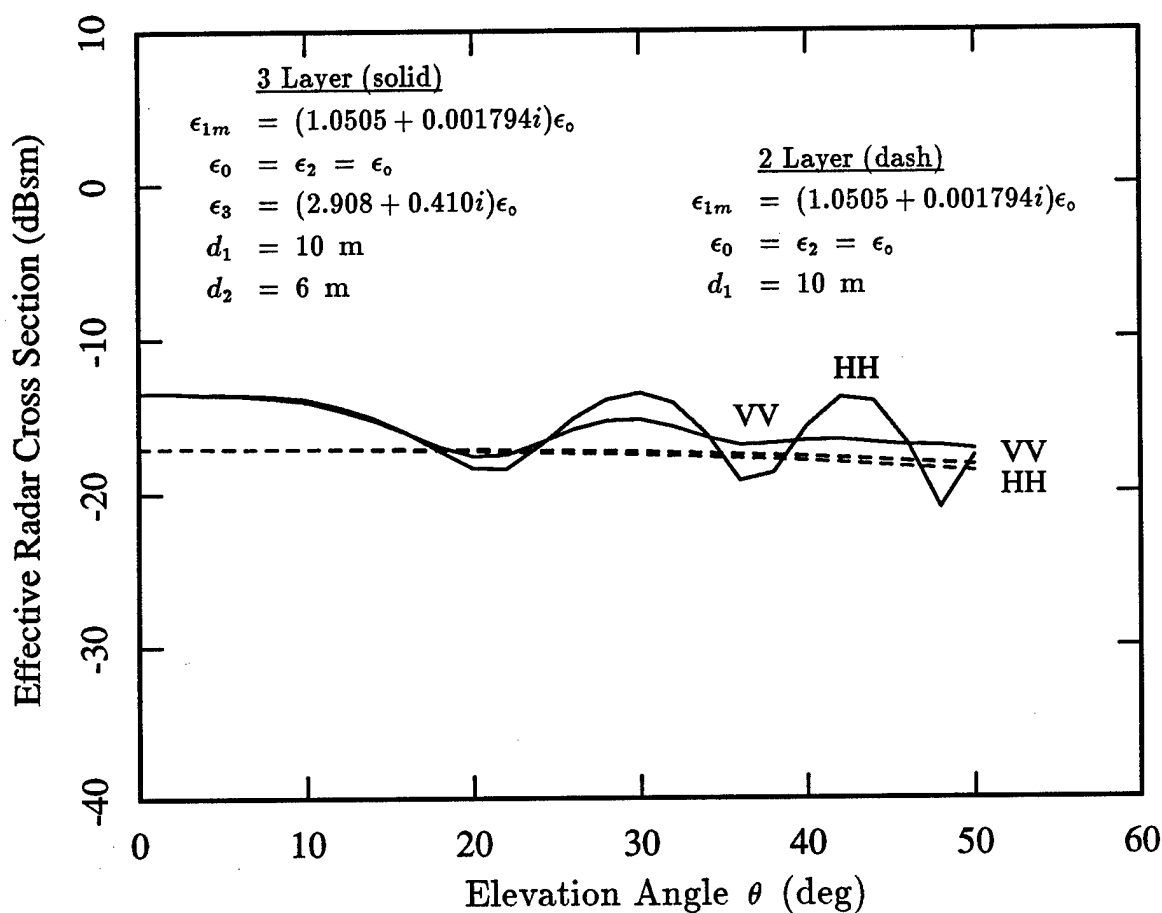


Figure 4.16. Dependence of the target/clutter scattering cross section, σ_{TC-TC} , on elevation angle for a three layer configuration with a ground plane (solid) and for a two layer configuration without the added layer (dash). Results are given at 1.120 GHz for a 10 m random slab with $z_T = 15$ m and with $\epsilon_0 = \epsilon_2 = \epsilon_0$.

the boundaries above and below the target. The path length of this doubly reflected return would vary with the thickness of the target region, and would lead to the small interference effect seen. In addition, as shown in Chapter 2, the incoherent return is independent of the depth of the target beneath the random media, and that effect is seen again in the result here.

In contrast, Figure 4.18 shows the effect of changing the target depth within a region of fixed thickness. In this case, the distance between the target and the reflective boundary below is varied from 1 m at a target depth of 15 m, to effectively zero at a target depth of 16 m. Both the coherent return (solid), and incoherent return (dash) are shown, and both exhibit the same oscillating behavior, which occurs when the direct and reflected paths to the point target interfere with each other. Note that again the oscillations for the incoherent return are smaller in amplitude, since the interference for scattering from the target to the random media, or random media back to the receiver is a function of the position of the scatterer within the random media, and consequently the interference effect is averaged over all the scatterers, tending to smooth the effect when compared to the coherent scattering mechanism.

Figures 4.19 and 4.20 show the correlation of the target/clutter multi-path field in azimuth angle and frequency respectively. The result for the three-layer case considered here (solid) is compared with the result for the two-layer geometry of Chapter 2. It is apparent for both correlations, the new three-layer result decorrelates faster than the two-layer case. A new effect which impacts the correlation behavior of the multi-path field is demonstrated by this result. Previously it was shown that the rate of decorrelation was linked to the size and shape of the region of the random layer which significantly contributed to the multi-path scattering mechanism. A larger region ex-

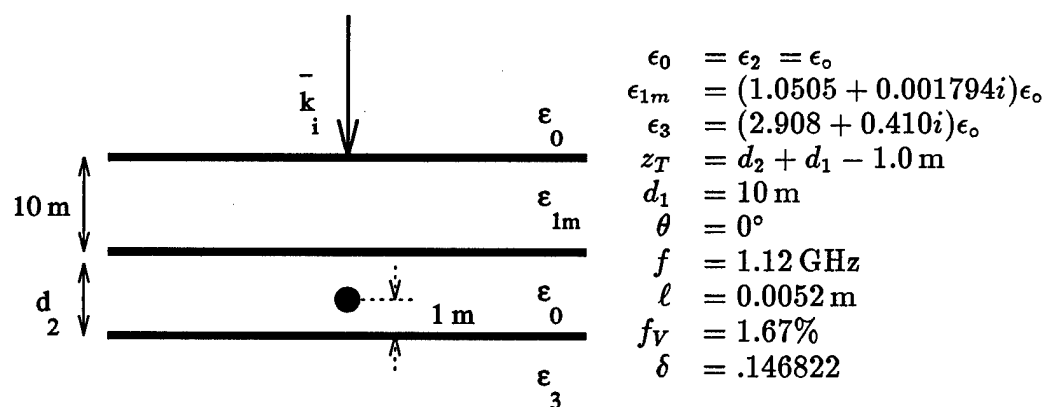
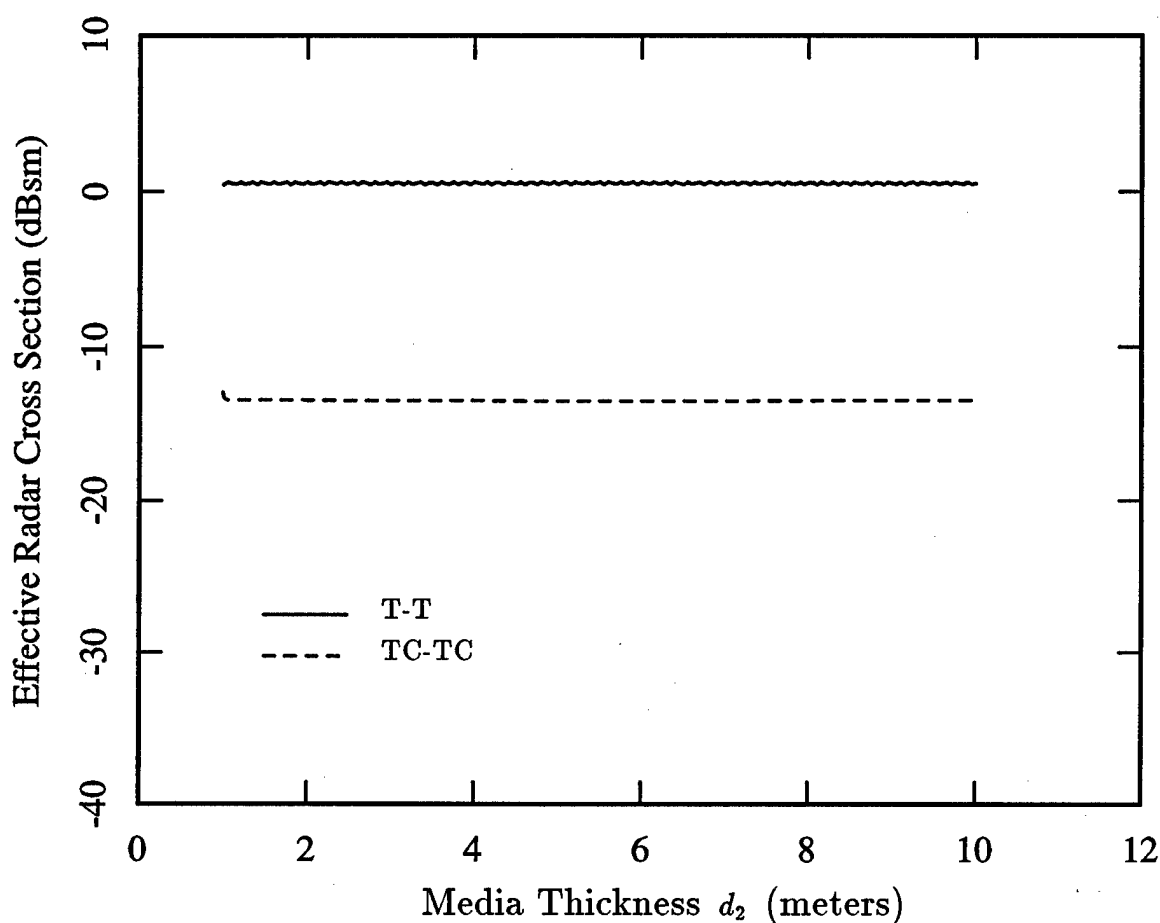


Figure 4.17. Dependence of the coherent target scattering cross section, σ_{T-T} , (solid) and the target/clutter scattering cross section, σ_{TC-TC} , (dash) on the thickness, d_2 , of the target region. Results are shown for normal incidence ($\theta = 0^\circ$) at 1.120 GHz with the target positioned 1 m above the interface between regions 2 and 3 ($z_T = d_2 + d_1 - 1.0$).

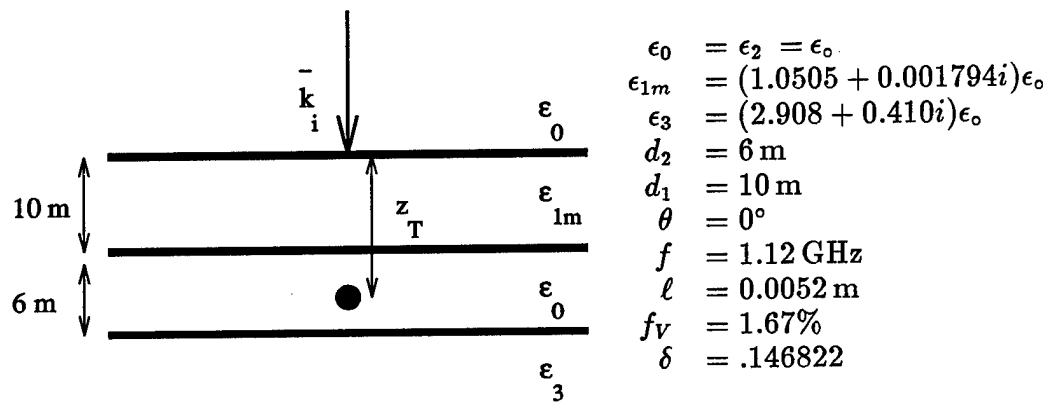
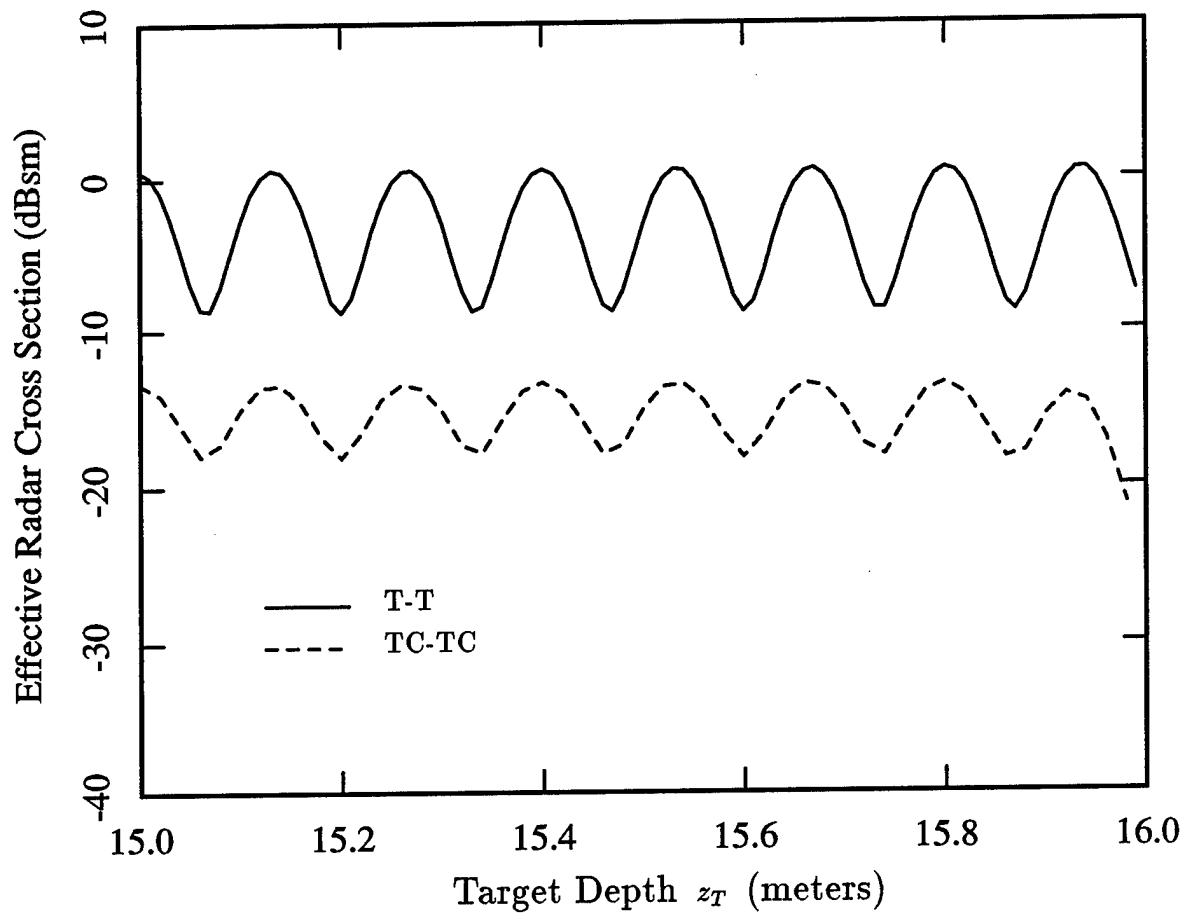
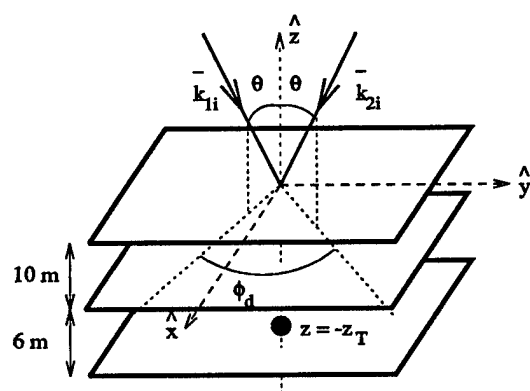
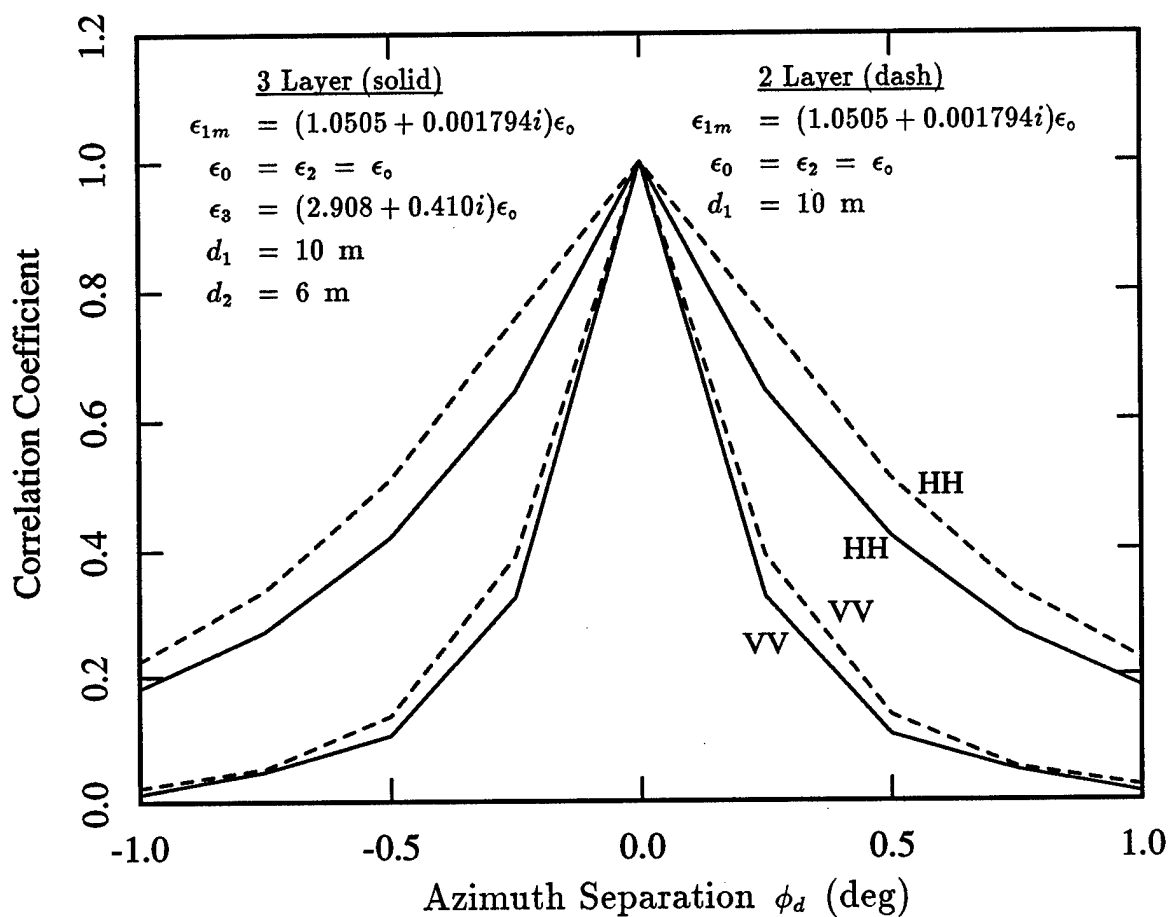


Figure 4.18. Dependence of the coherent target scattering cross section, σ_{T-T} , (solid) and the target/clutter scattering cross section, σ_{TC-TC} , (dash) on the target depth, z_T . Results are shown for normal incidence ($\theta = 0^\circ$) at 1.120 GHz with a 10 m slab and with a 6 m depth to the target region.



$$\begin{aligned} z_T &= 15 \text{ m} \\ \theta &= 40^\circ \\ f &= 1.12 \text{ GHz} \\ \ell &= 0.0052 \text{ m} \\ f_V &= 1.67\% \\ \delta &= .146822 \end{aligned}$$

Figure 4.19. Correlation of the target/clutter multi-path return, σ_{TC-TC} , over $\phi_d = \phi_2 - \phi_1$ for three-layer (solid), and two-layer (dash) configurations. In each case the results are given for a 10 m random slab, a frequency of 1.12 GHz, a 40° elevation angle, and a target depth of 15 m.

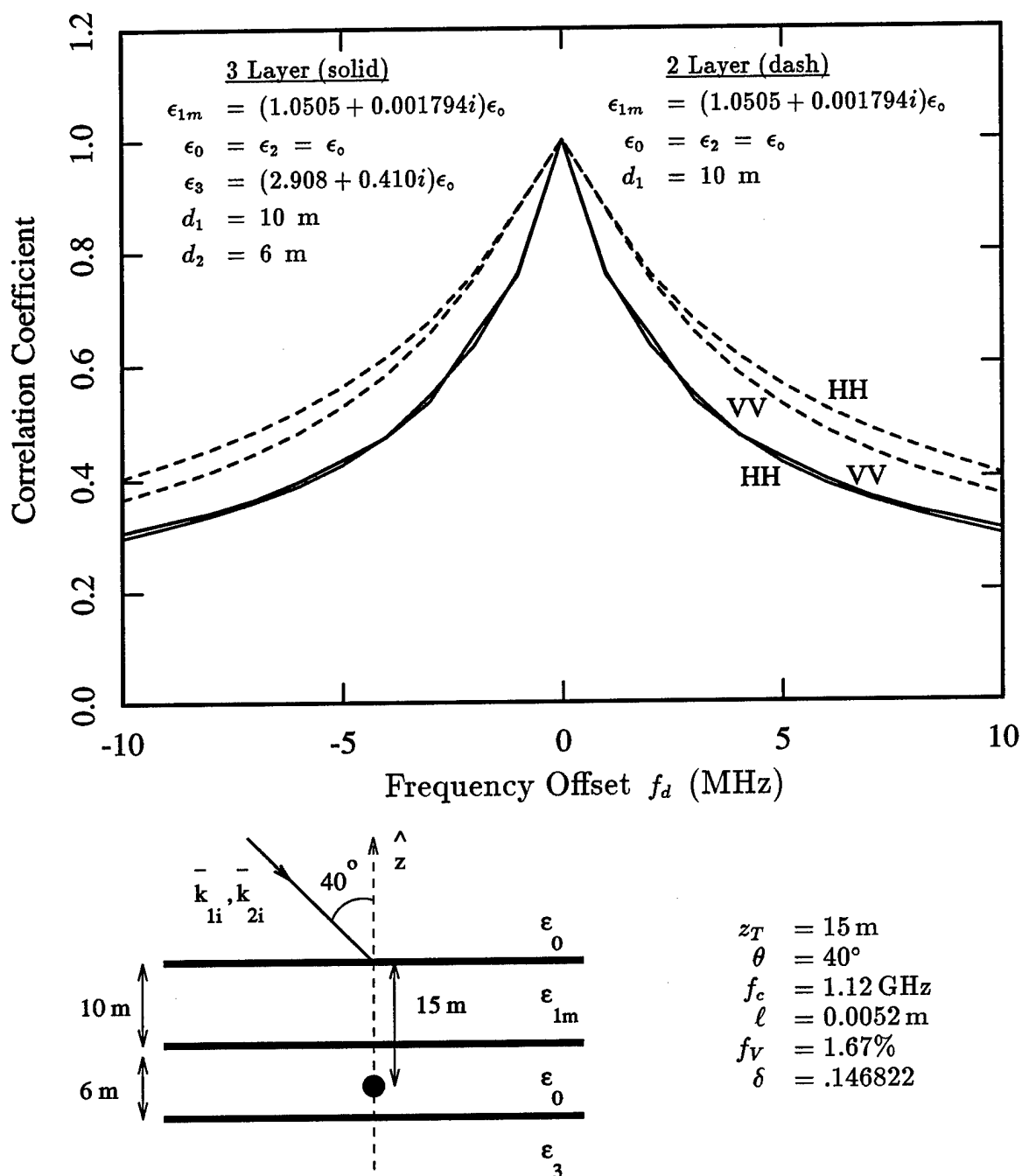


Figure 4.20. Correlation of the target/clutter multi-path return, σ_{TC-TC} , over $f_d = f_2 - f_1$ for three-layer (solid), and two-layer (dash) configurations. In each case the results are given for a 10 m random slab, a center frequency of 1.12 GHz, a 40° elevation angle, and a target depth of 15 m.

periences a more rapid phase change between points on opposite sides of the region as either the azimuth angle or frequency is changed. This size factor was dominant in determining the rate of decorrelation because the shape of the region itself did not change or move over the angular differences or frequency offsets considered, but only the phase across the region changed. With the reflective boundary now added below the target, the scattering from the target to the random media can be viewed as arising from the combination of the target and an image of the target located below the reflective boundary. Since these are spaced by a distance larger than a wavelength, the target and image together produce an interference pattern in the random media, producing scattering only from regions in which the two interfere constructively. A change in the incident propagation vector may change the relative phase of the target and image, and shift the interference pattern in the random media. Consequently, not only does a phase change occur across the contributing region of random scatterers, but the shape of this region or its placement within the random media may also change. Hence, the multi-path field will decorrelate more rapidly, producing the results seen in the two figures.

Appendix D

Strong Fluctuation Theory for the Effective Permittivity

In this Appendix, Strong Fluctuation Theory is applied to derive the effective permittivity of a random media with an anisotropic but azimuthally symmetric correlation function. This correlation function models the inclusion of azimuthally symmetric elliptical scatterers embedded in a background media, where the permittivity contrast between background and scatterers may be large, provided that the scatterers are electrically small. Appropriate correlation functions may be derived from this discrete scatterer model as shown elsewhere [67], however, it is assumed here that the derivation of effective permittivity begins with a continuous random model with a known correlation function. A general expression for the effective permittivity is derived as in [59], and then evaluated for several specific choices of the correlation function.

From symmetry arguments it is clear that the azimuthal symmetry of the scatterers and resulting correlation function will lead to an effective permittivity which is uniaxial. Hence, the homogeneous vector wave equation for the electric field will be written as in (D.1),

$$\nabla \times \nabla \times \bar{E} - k_o^2 \frac{\bar{\epsilon}_g}{\epsilon_o} \cdot \bar{E} = \frac{k_o^2}{\epsilon_o} (\bar{I}\epsilon(\bar{r}) - \bar{\epsilon}_g) \cdot \bar{E} \quad (D.1)$$

where $\bar{\epsilon}_g$ is a deterministic effective background permittivity which is uniaxial and

takes the form of (D.2)

$$\bar{\epsilon}_g = \begin{bmatrix} \epsilon_g & 0 & 0 \\ 0 & \epsilon_g & 0 \\ 0 & 0 & \epsilon_{gz} \end{bmatrix} \quad (D.2)$$

This permittivity will be determined later in such a manner that the resulting expression for the effective permittivity will remain valid even for strong fluctuations of permittivity. The solution for the total electric field of (D.1) can be expressed in integral form, as in (D.3),

$$\bar{E}(\bar{r}) = \bar{E}_i(\bar{r}) + k_o^2 \int d\bar{r}' \bar{G}_g(\bar{r}, \bar{r}') \cdot \left(\frac{\bar{I} \epsilon(\bar{r}') - \bar{\epsilon}_g}{\epsilon_o} \right) \cdot \bar{E}(\bar{r}') \quad (D.3)$$

where $\bar{E}_i(\bar{r})$ is the incident wave, and where $\bar{G}_g(\bar{r}, \bar{r}')$ is the dyadic Greens function for a homogeneous media of permittivity $\bar{\epsilon}_g$. Since the observation point in the above is within the source region, the singularity term of the Greens function must be considered, and $\bar{G}(\bar{r}, \bar{r}')$ will be composed of a principal value part and a singularity part.

$$\bar{G}_g(\bar{r}, \bar{r}') = PS \bar{G}_g(\bar{r}, \bar{r}') - \frac{\bar{S}}{k_o^2} \delta(\bar{r} - \bar{r}') \quad (D.4)$$

The dyadic coefficient \bar{S} of the singularity portion will be uniaxial, and together with the shape of the exclusion volume will be determined later to again prevent secular terms in the scattering contribution to the effective permittivity which have no frequency dependence and which would restrict the solution to weak fluctuations.

The source portion of the integral of (D.3) can be expressed as the product of two functions as given by (D.5),

$$\bar{\xi}(\bar{r}) \cdot \bar{F}(\bar{r}) = \left(\frac{\bar{I} \epsilon(\bar{r}) - \bar{\epsilon}_g}{\epsilon_o} \right) \cdot \bar{E}(\bar{r}) \quad (D.5)$$

and after substituting the above and (D.4) into (D.3), the result of (D.6) is obtained,

$$\begin{aligned}
 \overline{E}(\overline{r}) &= \overline{E}_i(\overline{r}) + k_o^2 \int d\overline{r}' PS \overline{G}_g(\overline{r}, \overline{r}') \cdot \overline{\xi}(\overline{r}') \cdot \overline{F}(\overline{r}') \\
 &\quad - \overline{S} \cdot \overline{\xi}(\overline{r}) \cdot \overline{F}(\overline{r}) \cdot \left[\overline{I} + \overline{S} \cdot \left(\frac{\overline{I} \epsilon(\overline{r}) - \overline{\epsilon}_g}{\epsilon_o} \right) \right] \cdot \overline{E}(\overline{r}) \\
 &= \overline{E}_i(\overline{r}) + k_o^2 \int d\overline{r}' PS \overline{G}_g(\overline{r}, \overline{r}') \cdot \overline{\xi}(\overline{r}') \cdot \overline{F}(\overline{r}') \cdot \overline{F}(\overline{r}) \\
 &= \overline{E}_i(\overline{r}) + k_o^2 \int d\overline{r}' PS \overline{G}_g(\overline{r}, \overline{r}') \cdot \overline{\xi}(\overline{r}') \cdot \overline{F}(\overline{r}') \quad (D.6)
 \end{aligned}$$

and where $\overline{F}(\overline{r})$ is given by (D.7).

$$\overline{F}(\overline{r}) = \left[\overline{I} + \overline{S} \frac{(\overline{I} \epsilon(\overline{r}) - \overline{\epsilon}_g)}{\epsilon_o} \right] \cdot \overline{E}(\overline{r}) \quad (D.7)$$

From (D.5) and (D.7), $\overline{\xi}(\overline{r})$ can be shown to be uniaxial, and given by (D.8),

$$\begin{aligned}
 \overline{\xi}(\overline{r}) &= \left(\frac{\overline{I} \epsilon(\overline{r}) - \overline{\epsilon}_g}{\epsilon_o} \right) \left[\overline{I} + \frac{\overline{S} (\overline{I} \epsilon(\overline{r}) - \overline{\epsilon}_g)}{\epsilon_o} \right]^{-1} \\
 &= \begin{bmatrix} \xi(\overline{r}) & 0 & 0 \\ 0 & \xi(\overline{r}) & 0 \\ 0 & 0 & \xi_z(\overline{r}) \end{bmatrix} \quad (D.8)
 \end{aligned}$$

where $\xi(\overline{r})$ and $\xi_z(\overline{r})$ are as in (D.9) and (D.10).

$$\xi(\overline{r}) = \frac{\epsilon(\overline{r}) - \epsilon_g}{\epsilon_o + S[\epsilon(\overline{r}) - \epsilon_g]} \quad (D.9)$$

$$\xi_z(\overline{r}) = \frac{\epsilon(\overline{r}) - \epsilon_{gz}}{\epsilon_o + S_z[\epsilon(\overline{r}) - \epsilon_{gz}]} \quad (D.10)$$

Equation (D.6) has a formal iterative solution in the form of the Neumann series of (D.11).

$$\begin{aligned}
 \bar{F}(\bar{r}) = & \bar{F}^{(0)}(\bar{r}) + \int d\bar{r}_1 PS \bar{G}_g(\bar{r}, \bar{r}_1) \cdot k_o^2 \bar{\xi}(\bar{r}_1) \cdot \bar{F}^{(0)}(\bar{r}_1) \\
 & + \int d\bar{r}_1 \int d\bar{r}_2 PS \bar{G}_g(\bar{r}, \bar{r}_1) \cdot k_o^2 \bar{\xi}(\bar{r}_1) \cdot PS \bar{G}_g(\bar{r}_1, \bar{r}_2) \cdot k_o^2 \bar{\xi}(\bar{r}_2) \cdot \bar{F}^{(0)}(\bar{r}_2) \\
 & + \dots
 \end{aligned} \tag{D.11}$$

It is assumed at this point that the permittivity fluctuations have Gaussian statistics. Taking the ensemble average of (D.11), all odd terms will be zero since we require $\langle \xi(\bar{r}) \rangle = \langle \xi_z(\bar{r}) \rangle = 0$ to eliminate secular terms. Furthermore, all even terms can be expressed as combinations of the two point statistics because of the assumed Gaussianity. Hence, the ensemble average of (D.11) takes the form of (D.12).

$$\begin{aligned}
 \langle F(\bar{r}) \rangle = & \bar{F}^{(0)}(\bar{r}) + \sum_{\alpha, \beta, \gamma, \rho} \int d\bar{r}_1 \int d\bar{r}_2 [PS \bar{G}_g(\bar{r}, \bar{r}_1)]_{\alpha} [PS \bar{G}_g(\bar{r}_1, \bar{r}_2)]_{\beta\gamma} \\
 & \left[\bar{F}^{(0)}(\bar{r}_2) \right]_{\rho} k_o^4 \left\langle [\bar{\xi}(\bar{r}_1)]_{\alpha\beta} [\bar{\xi}(\bar{r}_2)]_{\gamma\rho} \right\rangle \\
 & + \sum_{\substack{\alpha, \beta, \gamma, \rho, \\ \alpha', \beta', \gamma', \rho'}} \int d\bar{r}_1 \int d\bar{r}_2 \int d\bar{r}_3 \int d\bar{r}_4 [PS \bar{G}_g(\bar{r}, \bar{r}_1)]_{\alpha} [PS \bar{G}_g(\bar{r}_1, \bar{r}_2)]_{\beta\gamma} \\
 & [PS \bar{G}_g(\bar{r}_2, \bar{r}_3)]_{\rho\alpha'} [PS \bar{G}_g(\bar{r}_3, \bar{r}_4)]_{\beta'\gamma'} [\bar{F}^{(0)}(\bar{r}_4)]_{\rho'} \\
 & k_o^8 \left\{ \left\langle [\bar{\xi}(\bar{r}_1)]_{\alpha\beta} [\bar{\xi}(\bar{r}_2)]_{\gamma\rho} \right\rangle \left\langle [\bar{\xi}(\bar{r}_3)]_{\alpha'\beta'} [\bar{\xi}(\bar{r}_4)]_{\gamma'\rho'} \right\rangle \right. \\
 & + \left\langle [\bar{\xi}(\bar{r}_1)]_{\alpha\beta} [\bar{\xi}(\bar{r}_4)]_{\gamma'\rho'} \right\rangle \left\langle [\bar{\xi}(\bar{r}_2)]_{\gamma\rho} [\bar{\xi}(\bar{r}_3)]_{\alpha'\beta'} \right\rangle \\
 & \left. + \left\langle [\bar{\xi}(\bar{r}_1)]_{\alpha\beta} [\bar{\xi}(\bar{r}_3)]_{\alpha'\beta'} \right\rangle \left\langle [\bar{\xi}(\bar{r}_2)]_{\gamma\rho} [\bar{\xi}(\bar{r}_4)]_{\gamma'\rho'} \right\rangle \right\} \\
 & + \dots
 \end{aligned} \tag{D.12}$$

The above may be expressed in graphical form by the use of Feynman diagrams [125], where a node represents a vertex over which spatial integration is performed, a single line indicates the propagation of the field from node to node, a double line represents here the ensemble average $\langle \bar{F}(\bar{r}) \rangle$, and the arcs represent ensemble averaging between two node points. Hence, the above can be rewritten in Feynman diagram form as given by (D.13),

$$\begin{aligned}
 \text{==} &= \text{—} + \text{—} \text{---} \text{—} \\
 &+ \left[\text{—} \text{---} \text{—} \text{---} \text{—} + \text{—} \text{---} \text{---} \text{---} \text{—} + \right. \\
 &\quad \left. \text{—} \text{---} \text{---} \text{---} \text{---} \text{—} \right] \\
 &+ \dots
 \end{aligned} \tag{D.13}$$

where

$$\text{==} = \langle \bar{F}(\bar{r}) \rangle \tag{D.14}$$

$$\text{—} = \bar{F}^{(0)}(\bar{r}) \tag{D.15}$$

$$\begin{aligned}
 \text{—} \text{---} \text{—} &= \sum_{\alpha, \beta, \gamma, \rho} \int d\bar{r}_1 \int d\bar{r}_2 [PS \bar{G}_g(\bar{r}, \bar{r}_1)]_{\alpha} [PS \bar{G}_g(\bar{r}_1, \bar{r}_2)]_{\beta\gamma} \\
 &\quad [\bar{F}^{(0)}(\bar{r}_2)]_{\rho} k_{\circ}^A \left\langle [\bar{\xi}(\bar{r}_1)]_{\alpha\beta} [\bar{\xi}(\bar{r}_2)]_{\gamma\rho} \right\rangle
 \end{aligned} \tag{D.16}$$

and where the higher order terms follow in a similar manner.

A strongly connected Feynman diagram is one which cannot be split at any point without breaking a correlation connection. The mass operator is defined as the sum of

all of the strongly connected diagrams as shown by (D.17).

$$\begin{aligned}
 \otimes &= \text{---}\overset{\curvearrowright}{\bullet}\text{---}\bullet + \text{---}\overset{\curvearrowright}{\bullet}\overset{\curvearrowright}{\bullet}\text{---}\bullet + \text{---}\overset{\curvearrowright}{\bullet}\overset{\curvearrowright}{\bullet}\overset{\curvearrowright}{\bullet}\text{---}\bullet \\
 &+ \text{---}\overset{\curvearrowright}{\bullet}\overset{\curvearrowright}{\bullet}\overset{\curvearrowright}{\bullet}\overset{\curvearrowright}{\bullet}\text{---}\bullet + \dots
 \end{aligned}
 \tag{D.17}$$

Using the mass operator, the strongly connected parts of the right hand side of (D.13) can be represented as in (D.18).

$$\begin{aligned}
 \text{---}\otimes\text{---} &= \text{---}\overset{\curvearrowright}{\bullet}\text{---}\bullet + \text{---}\overset{\curvearrowright}{\bullet}\overset{\curvearrowright}{\bullet}\text{---}\bullet \\
 &+ \text{---}\overset{\curvearrowright}{\bullet}\overset{\curvearrowright}{\bullet}\overset{\curvearrowright}{\bullet}\text{---}\bullet + \dots
 \end{aligned}
 \tag{D.18}$$

Similarly the weakly connected portion of (D.13) which are constructed of two strongly connected components can be represented as two connected mass operators.

$$\begin{aligned}
 \text{---}\otimes\otimes\text{---} &= \text{---}\overset{\curvearrowright}{\bullet}\overset{\curvearrowright}{\bullet}\text{---}\bullet \\
 &+ \text{---}\overset{\curvearrowright}{\bullet}\overset{\curvearrowright}{\bullet}\overset{\curvearrowright}{\bullet}\text{---}\bullet + \dots
 \end{aligned}
 \tag{D.19}$$

Hence, the entire expression of (D.13) may be expressed in the series of (D.20),

$$\begin{aligned}
 \equiv &= \text{---} + \text{---}\otimes\text{---} + \text{---}\otimes\otimes\text{---} \\
 &+ \text{---}\otimes\otimes\otimes\text{---} + \dots
 \end{aligned}
 \tag{D.20}$$

which can be rewritten in the form of (D.21)

$$\begin{aligned}
= & \text{---} + \text{---} \otimes \left[\text{---} + \text{---} \otimes \text{---} \right. \\
& \left. + \text{---} \otimes \otimes \text{---} + \dots \right] \\
= & \text{---} + \text{---} \otimes \text{---}
\end{aligned} \tag{D.21}$$

Equation (D.21) is Dyson's equation, which in analytical form is given by (D.22),

$$\langle \bar{F}(\bar{r}) \rangle = \bar{E}_i(\bar{r}) + \int d\bar{r}_1 \int d\bar{r}_2 PS \bar{G}_g(\bar{r}, \bar{r}_1) \cdot \bar{\xi}(\bar{r}_1, \bar{r}_2) \cdot \langle \bar{F}(\bar{r}_2) \rangle \tag{D.22}$$

where $\bar{\xi}(\bar{r}_1, \bar{r}_2)$ is the dyadic mass operator. To simplify the above, the bilocal approximation is introduced in which only the first term of the mass operator is preserved. Hence, (D.21) becomes (D.23),

$$= \text{---} + \text{---} \text{---} \tag{D.23}$$

which includes all weakly connected terms which are constructed from bilocal diagrams, as shown by (D.24).

$$= \text{---} + \text{---} \text{---} + \text{---} \text{---} \text{---} + \dots \tag{D.24}$$

In analytic form, the bilocal approximation to (D.22) produces (D.25) below,

$$\langle \bar{F}(\bar{r}) \rangle = \bar{E}_i(\bar{r}) + k_o^2 \int d\bar{r}_1 \int d\bar{r}_2 PS \bar{G}_g(\bar{r}, \bar{r}_1) \cdot \bar{\xi}_{eff}(\bar{r}_1 - \bar{r}_2) \langle \bar{F}(\bar{r}_2) \rangle \tag{D.25}$$

where $\bar{\xi}_{eff}(\bar{r}_1 - \bar{r}_2)$ is given by (D.26).

$$\bar{\xi}_{eff}(\bar{r}_1 - \bar{r}_2) = k_o^2 \langle \bar{\xi}(\bar{r}_1) \cdot PS \bar{G}_g(\bar{r}_1, \bar{r}_2) \cdot \bar{\xi}(\bar{r}_2) \rangle \tag{D.26}$$

From the bilocally approximated Dyson's equation, it is now of interest to derive an expression for the effective permittivity. Taking the ensemble average of (D.6) yields (D.27),

$$\langle \bar{F}(\bar{r}) \rangle = \bar{E}_i(\bar{r}) + k_o^2 \int d\bar{r}' PS \bar{G}_g(\bar{r}, \bar{r}') \cdot \langle \bar{\xi}(\bar{r}') \cdot \bar{F}(\bar{r}') \rangle \quad (D.27)$$

and comparing with (D.25) above, yields (D.28).

$$\langle \bar{\xi}(\bar{r}) \cdot \bar{F}(\bar{r}) \rangle = \int d\bar{r}' \bar{\xi}_{eff}(\bar{r} - \bar{r}') \langle \bar{F}(\bar{r}') \rangle \quad (D.28)$$

Furthermore, $\langle \bar{F}(\bar{r}) \rangle$ is from (D.7), given by (D.29),

$$\langle \bar{F}(\bar{r}) \rangle = \left(\bar{I} - \bar{S} \frac{\bar{\epsilon}_g}{\epsilon_0} \right) \cdot \langle \bar{E}(\bar{r}) \rangle + \frac{\bar{S} \langle \bar{D}(\bar{r}) \rangle}{\epsilon_0} \quad (D.29)$$

and $\langle \bar{\xi}(\bar{r}) \cdot \bar{F}(\bar{r}) \rangle$ is from (D.5), given by (D.30),

$$\langle \bar{\xi}(\bar{r}) \cdot \bar{F}(\bar{r}) \rangle = \frac{\langle \bar{D}(\bar{r}) \rangle}{\epsilon_0} - \frac{\bar{\epsilon}_g}{\epsilon_0} \cdot \langle \bar{E}(\bar{r}) \rangle \quad (D.30)$$

where $\langle \bar{D}(\bar{r}) \rangle = \langle \epsilon(\bar{r}) \bar{E}(\bar{r}) \rangle$. If the above three equations are Fourier transformed using the relation of (D.31),

$$A(\bar{k}) = \int d\bar{r} A(\bar{r}) e^{-i\bar{k} \cdot \bar{r}} \quad (D.31)$$

and if the second two equations are substituted into the first, then the result is given by (D.32).

$$\begin{aligned} \frac{\langle \bar{D}(\bar{k}) \rangle}{\epsilon_0} &= \frac{\bar{\epsilon}_g}{\epsilon_0} \cdot \langle \bar{E}(\bar{k}) \rangle + \bar{\xi}_{eff}(\bar{k}) \left(\bar{I} - \bar{S} \frac{\bar{\epsilon}_g}{\epsilon_0} \right) \cdot \langle \bar{E}(\bar{k}) \rangle \\ &\quad + \bar{\xi}_{eff}(\bar{k}) \bar{S} \frac{\langle \bar{D}(\bar{k}) \rangle}{\epsilon_0} \end{aligned} \quad (D.32)$$

Rearranging the above yields (D.33).

$$\langle \overline{D}(\vec{k}) \rangle = (\overline{I} - \overline{\xi}_{eff}(\vec{k}) \overline{S})^{-1} [\overline{\epsilon}_g + \overline{\xi}_{eff}(\vec{k}) (\epsilon_0 \overline{I} - \overline{S} \overline{\epsilon}_g)] \langle \overline{E}(\vec{k}) \rangle \quad (D.33)$$

The definition of the effective permittivity $\overline{\epsilon}_{eff}(\vec{k})$, is that it satisfies $\langle \overline{D}(\vec{k}) \rangle = \overline{\epsilon}_{eff}(\vec{k}) \langle \overline{E}(\vec{k}) \rangle$, such that from the above the effective permittivity can be identified as in (D.34).

$$\begin{aligned} \overline{\epsilon}_{eff}(\vec{k}) &= (\overline{I} - \overline{\xi}_{eff}(\vec{k}) \overline{S})^{-1} [\overline{\epsilon}_g + \overline{\xi}_{eff}(\vec{k}) (\epsilon_0 \overline{I} - \overline{S} \overline{\epsilon}_g)] \\ &= \overline{\epsilon}_g + \epsilon_0 (\overline{I} - \overline{\xi}_{eff}(\vec{k}) \overline{S})^{-1} \overline{\xi}_{eff}(\vec{k}) \end{aligned} \quad (D.34)$$

For the bilocal approximation to be valid, $|\overline{\xi}_{eff}(\vec{k})| \ll 1$, such that the above can be approximated by (D.35).

$$\overline{\epsilon}_{eff}(\vec{k}) \simeq \overline{\epsilon}_g + \epsilon_0 \overline{\xi}_{eff}(\vec{k}) \quad (D.35)$$

Furthermore, for low frequencies, the dispersion effect in the effective permittivity is negligible, and $\overline{\xi}_{eff}(\vec{k})$ may be approximated by its value $\overline{\xi}_{eff}^0$ at $\vec{k} = 0$. Thus, the final expression for the effective permittivity is given by (D.36).

$$\overline{\epsilon}_{eff} = \overline{\epsilon}_g + \epsilon_0 \overline{\xi}_{eff}^0 \quad (D.36)$$

The bilocally approximated mass operator of (D.26) can be rewritten as in (D.37),

$$[\xi_{eff}(\vec{r})]_{\alpha\beta} = \sum_{\gamma,\rho} k_o^2 \Lambda_{\alpha\gamma\rho\beta} R_\xi(\vec{r}) [PS \overline{G}_g(\vec{r})]_{\gamma\rho} \quad (D.37)$$

where $R_\xi(\bar{r})$ is the normalized correlation function with $R_\xi(0) = 1$, and where $\Lambda_{\alpha\gamma\rho\beta}$ gives the variance and cross variances of elements of $\bar{\xi}$. Since $\bar{\xi}$ is diagonal, the only non-zero portions of $\Lambda_{\alpha\gamma\rho\beta}$ will be for $\alpha = \gamma$ and $\beta = \rho$ where,

$$\Lambda_{xxxx} = \Lambda_{xyxy} = \Lambda_{yyxx} = \Lambda_{yyyy} = \langle \xi(\bar{r}) \xi(\bar{r}) \rangle = \hat{\delta}_\xi \quad (D.38)$$

$$\Lambda_{zzzz} = \langle \xi_z(\bar{r}) \xi_z(\bar{r}) \rangle = \hat{\delta}_{\xi_z} \quad (D.39)$$

$$\Lambda_{xxzz} = \Lambda_{yyzz} = \Lambda_{zzxx} = \Lambda_{zzyy} = \langle \xi(\bar{r}) \xi_z(\bar{r}) \rangle = \hat{\delta}_{\xi\xi_z} \quad (D.40)$$

Hence, the Fourier transform of (D.37) at $\bar{k} = 0$ is given by (D.41).

$$\left[\bar{\xi}_{eff}^0 \right]_{\alpha\beta} = \Lambda_{\alpha\alpha\beta\beta} k_o^2 \int_{-\infty}^{\infty} d\bar{r} \left[PS \bar{G}_g(\bar{r}) \right]_{\alpha\beta} R_\xi(\bar{r}) \quad (D.41)$$

Substituting from (D.4) yields (D.42),

$$\left[\bar{\xi}_{eff}^0 \right]_{\alpha\beta} = \Lambda_{\alpha\alpha\beta\beta} \left\{ k_o^2 \int_{-\infty}^{\infty} d\bar{r} \left[\bar{G}_g(\bar{r}) \right]_{\alpha\beta} R_\xi(\bar{r}) + \left[\bar{S} \right]_{\alpha\beta} \right\} \quad (D.42)$$

and with the Fourier relations of (D.43) and (D.44),

$$R_\xi(\bar{r}) = \int_{-\infty}^{\infty} d\bar{k} \Phi_\xi(\bar{k}) e^{-i\bar{k} \cdot \bar{r}} \quad (D.43)$$

$$\bar{G}_g(\bar{r}) = \frac{1}{8\pi^3} \int_{-\infty}^{\infty} d\bar{k} \bar{G}_g(\bar{k}) e^{i\bar{k} \cdot \bar{r}} \quad (D.44)$$

Equation (D.42) can be rewritten as in (D.45).

$$\left[\bar{\xi}_{eff}^0 \right]_{\alpha\beta} = \Lambda_{\alpha\alpha\beta\beta} \left\{ \frac{k_o^2}{8\pi^3} \int_{-\infty}^{\infty} d\bar{r} \int_{-\infty}^{\infty} d\bar{k} \int_{-\infty}^{\infty} d\bar{k}' \left[\bar{G}_g(\bar{k}) \right]_{\alpha\beta} \Phi_\xi(\bar{k}') e^{i(\bar{k}-\bar{k}') \cdot \bar{r}} + \left[\bar{S} \right]_{\alpha\beta} \right\} \quad (D.45)$$

Performing the \bar{r} integral yields a delta function, which can be used to perform the \bar{k}' integral. The result is given by (D.46).

$$\left[\bar{\xi}_{eff}^0 \right]_{\alpha\beta} = \Lambda_{\alpha\alpha\beta\beta} \left\{ k_o^2 \int_{-\infty}^{\infty} d\bar{k} \left[\bar{G}_g(\bar{k}) \right]_{\alpha\beta} \Phi_{\xi}(\bar{k}) + \left[\bar{S} \right]_{\alpha\beta} \right\} \quad (D.46)$$

In the above, $\Phi_{\xi}(\bar{k})$ is the spectral function associated with the correlation function, and $\bar{G}_g(\bar{k})$ is the Fourier transform of the Green's function, and is given by (D.47),

$$\begin{aligned} \bar{G}_g(\bar{k}) = & \frac{1}{k_{\rho}^2 D^{TE}(\bar{k})} \begin{bmatrix} k_y^2 & -k_x k_y & 0 \\ -k_x k_y & k_x^2 & 0 \\ 0 & 0 & 0 \end{bmatrix} \\ & - \frac{\epsilon_o / \epsilon_{gz}}{k_o^2 D^{TM}(\bar{k})} \begin{bmatrix} \frac{k_{\rho}^2 - k_o^2 \frac{\epsilon_{gz}}{\epsilon_o}}{k_{\rho}^2} k_x^2 & \frac{k_{\rho}^2 - k_o^2 \frac{\epsilon_{gz}}{\epsilon_o}}{k_{\rho}^2} k_x k_y & k_x k_z \\ \frac{k_{\rho}^2 - k_o^2 \frac{\epsilon_{gz}}{\epsilon_o}}{k_{\rho}^2} k_y k_x & \frac{k_{\rho}^2 - k_o^2 \frac{\epsilon_{gz}}{\epsilon_o}}{k_{\rho}^2} k_y^2 & k_y k_z \\ k_z k_x & k_z k_y & k_z^2 - k_o^2 \frac{\epsilon_g}{\epsilon_o} \end{bmatrix} \end{aligned} \quad (D.47)$$

where

$$D^{TE}(\bar{k}) = k_{\rho}^2 + k_z^2 - k_o^2 \frac{\epsilon_g}{\epsilon_o} \quad (D.48)$$

$$D^{TM}(\bar{k}) = k_z^2 + \frac{\epsilon_g}{\epsilon_{gz}} \left(k_{\rho}^2 - k_o^2 \frac{\epsilon_{gz}}{\epsilon_o} \right) \quad (D.49)$$

and where $k_{\rho}^2 = k_x^2 + k_y^2$.

For an azimuthally symmetric correlation function, the integral of (D.46) will be odd if $\alpha \neq \rho$. Therefore, the $\bar{\xi}_{eff}^0$ will be uniaxial, and take the form of (D.50),

$$\bar{\xi}_{eff}^0 = \begin{bmatrix} \xi_{\perp} & 0 & 0 \\ 0 & \xi_{\perp} & 0 \\ 0 & 0 & \xi_z \end{bmatrix} \quad (D.50)$$

where ξ_{\perp} and ξ_z are given by (D.51) and (D.52),

$$\xi_{\perp} = \hat{\delta}_{\xi} (I_{\perp} + S) \quad (D.51)$$

$$\xi_z = \hat{\delta}_{\xi_z} (I_z + S_z) \quad (D.52)$$

and where I_{\perp} and I_z are the result of (D.46) evaluated for $\alpha = \rho = x$ (or y) and $\alpha = \beta = z$, respectively. For the bilocal approximation to be valid $|\bar{\xi}_{eff}^0| \ll 1$ and for this to not require $\delta_{\xi}, \delta_{\xi_z} \ll 1$, then S and S_z must be chosen to cancel the frequency independent portion of I_{\perp} and I_z such that (D.51) and (D.52) will become small for low frequencies. Hence it is from the above that the form of \bar{S} is chosen.

Thus, to review, the method of determining the effective permittivity of a region with scatterers of fractional volume f with permittivity ϵ_s in a background of permittivity ϵ_b is as follows: The correlation function $R_{\xi}(\bar{r})$ of the random media is first determined from the discrete scatterer problem, and I_{\perp} and I_z are determined from (D.46) using this correlation function, and are expressed in terms of an unknown permittivity $\bar{\epsilon}_g$. S and S_z are then chosen to cancel the frequency independent portions of I_{\perp} and I_z . Using the expressions for S and S_z , ϵ_g and ϵ_{gz} are found by requiring that the effective scattering source $\bar{\xi}(\bar{r})$ be zero mean. This results in the two non-linear coupled equations of (D.53) and (D.54), which can be solved for ϵ_g and ϵ_{gz} .

$$\left\langle \frac{\epsilon(\bar{r}) - \epsilon_g}{\epsilon_o + S[\epsilon(\bar{r}) - \epsilon_g]} \right\rangle = \frac{\epsilon_b - \epsilon_g}{\epsilon_o + S(\epsilon_b - \epsilon_g)} (1 - f) + \frac{\epsilon_s - \epsilon_g}{\epsilon_o + S(\epsilon_s - \epsilon_g)} f = 0 \quad (D.53)$$

$$\left\langle \frac{\epsilon(\bar{r}) - \epsilon_{gz}}{\epsilon_o + S_z[\epsilon(\bar{r}) - \epsilon_{gz}]} \right\rangle = \frac{\epsilon_b - \epsilon_{gz}}{\epsilon_o + S_z(\epsilon_b - \epsilon_{gz})} (1 - f) + \frac{\epsilon_s - \epsilon_{gz}}{\epsilon_o + S_z(\epsilon_s - \epsilon_{gz})} f = 0 \quad (D.54)$$

Once ϵ_g and ϵ_{gz} are known, the variances $\hat{\delta}_\xi$ and $\hat{\delta}_{\xi_z}$ can be found from (D.55) and (D.56).

$$\hat{\delta}_\xi = \left(\frac{\epsilon_b - \epsilon_g}{\epsilon_o + S(\epsilon_b - \epsilon_g)} \right)^2 (1 - f) + \left(\frac{\epsilon_S - \epsilon_g}{\epsilon_o + S(\epsilon_S - \epsilon_g)} \right)^2 f \quad (D.55)$$

$$\hat{\delta}_{\xi_z} = \left(\frac{\epsilon_b - \epsilon_{gz}}{\epsilon_o + S_z(\epsilon_b - \epsilon_{gz})} \right)^2 (1 - f) + \left(\frac{\epsilon_S - \epsilon_{gz}}{\epsilon_o + S_z(\epsilon_S - \epsilon_{gz})} \right)^2 f \quad (D.56)$$

Finally, the desired effective permittivity is given by (D.57),

$$\epsilon_{eff} = \begin{bmatrix} \epsilon_\perp & 0 & 0 \\ 0 & \epsilon_\perp & 0 \\ 0 & 0 & \epsilon_z \end{bmatrix} \quad (D.57)$$

where ϵ_\perp and ϵ_z are given by (D.58) and (D.59)

$$\epsilon_\perp = \epsilon_g + \epsilon_o \hat{\delta}_\xi (I_\perp + S) \quad (D.58)$$

$$\epsilon_z = \epsilon_{gz} + \epsilon_o \hat{\delta}_{\xi_z} (I_z + S) \quad (D.59)$$

The above method for determining the effective permittivity can be used with any correlation function, provided that S , S_z , I_\perp , and I_z are calculated from (D.46). Below several correlation functions and the corresponding expressions for S , S_z , I_\perp , and I_z are given. The first two correlation functions represent special cases which are not only azimuthally symmetric, but entirely isotropic with spherical symmetry. For these cases $S = S_z$ and $I = I_\perp = I_z$. The first is a step type correlation, which is unity inside a radius R , and which is zero outside.

$$R_\xi^a(\bar{r}) = \begin{cases} 1, & r < \ell \\ 0, & \text{else} \end{cases} \quad (D.60)$$

The corresponding expressions for S and I are given by (D.61) and (D.62), where I has been approximated in the low frequency limit.

$$I^a = -S^a + \frac{1}{3} k_o^2 \ell^2 + i \frac{2}{9} k_o^2 \ell^2 k_g \ell \quad (D.61)$$

$$S^a = \frac{1}{3} \frac{\epsilon_0}{\epsilon_g} \quad (D.62)$$

The second isotropic correlation is the exponential type given by (D.63).

$$R_\xi^b(\bar{r}) = \exp(-r/\ell) \quad (D.63)$$

The corresponding spectral density function is given by (D.64),

$$\Phi_\xi^b(\bar{k}) = \frac{\ell^3}{\pi^2 (1 + k^2 \ell^2)^2} \quad (D.64)$$

and I and S are given by (D.65) and (D.66).

$$I^b = -S^b + \frac{2}{3} k_o^2 \ell^2 \frac{(1 - k_g^2 \ell^2)}{(1 + k_g^2 \ell^2)^2} + i \frac{4}{3} k_o^2 \ell^2 k_g \ell \frac{1}{(1 + k_g^2 \ell^2)^2} \quad (D.65)$$

$$S^b = \frac{1}{3} \frac{\epsilon_0}{\epsilon_g} \quad (D.66)$$

The remaining correlation functions are anisotropic with azimuthal symmetry. The results for I_\perp , I_z , S , and S_z are taken from [59]. The first is again a step-type correlation, which is unity inside an elliptical bounds, and which is zero outside.

$$R_\xi^c(\bar{r}) = \begin{cases} 1, & \frac{x^2+y^2}{\ell_p^2} + \frac{z^2}{\ell_z^2} \leq 1 \\ 0, & \text{else} \end{cases} \quad (D.67)$$

The corresponding spectral function is given by (D.68),

$$\Phi_{\xi}^c(\bar{k}) = \frac{\ell_{\rho}^2 \ell_z}{2\pi^2} \frac{j_1\left(\sqrt{k_{\rho}^2 \ell_{\rho}^2 + k_z^2 \ell_z^2}\right)}{\sqrt{k_{\rho}^2 \ell_{\rho}^2 + k_z^2 \ell_z^2}} \quad (D.68)$$

where $j_1(x)$ is the spherical Bessel function of order 1, and where S , S_z , I_{\perp} , and I_z are given by (D.69) – (D.72),

$$\begin{aligned} I_{\perp}^c = & -S^c + \frac{k_o^2 \ell_{\rho} \ell_z}{8} A_1 + \frac{k_o^2 \ell_{\rho} \ell_z}{8} \frac{1}{\sqrt{b}} \left[\frac{\sqrt{bh^2}}{m} - \frac{A_2}{2} \right] \\ & + \frac{i}{6} \sqrt{\frac{\epsilon_g}{\epsilon_0}} k_o^3 \ell_{\rho}^2 \ell_z + \frac{ik_o^3 \ell_{\rho}^2 \ell_z}{18} \frac{\epsilon_{gz}}{\sqrt{\epsilon_0 \epsilon_g}} \end{aligned} \quad (D.69)$$

$$\begin{aligned} I_z^c = & -S_z^c + \frac{k_o^2 \ell_{\rho} \ell_z \sqrt{b}}{4} \left[-\frac{\sqrt{bh^2}}{m} + \left(m + \frac{1}{2}\right) A_2 \right] \\ & + i \frac{2}{g} \sqrt{\frac{\epsilon_g}{\epsilon_0}} k_o^3 \ell_{\rho}^2 \ell_z \end{aligned} \quad (D.70)$$

$$S^c = \frac{h \epsilon_0}{4\sqrt{\epsilon_g \epsilon_{gz}}} \left[\frac{2}{\sqrt{bh^2}} \left(1 + \frac{1}{m}\right) - A_2 \right] \quad (D.71)$$

$$S_z^c = \frac{h(b)^{\frac{3}{2}}}{2} \frac{\epsilon_0}{\epsilon_g} \left[-\frac{2}{m\sqrt{bh^2}} + A_2 \right] \quad (D.72)$$

where in the above $b = \epsilon_g/\epsilon_{gz}$, $h = \ell_z/\ell_{\rho}$, $m = bh^2 - 1$, and A_1 and A_2 are given by (D.73) and (D.74).

$$A_1 = \begin{cases} \frac{1}{\sqrt{h^2-1}} \ln \left(\frac{h+\sqrt{h^2-1}}{h-\sqrt{h^2-1}} \right), & h > 1 \\ \frac{2}{\sqrt{1-h^2}} \sin^{-1} \left(\sqrt{1-h^2} \right), & h < 1 \end{cases} \quad (D.73)$$

$$A_2 = \begin{cases} \frac{1}{(m)^{\frac{3}{2}}} \ln \left(\frac{\sqrt{bh^2}+\sqrt{m}}{\sqrt{bh^2}-\sqrt{m}} \right), & m > 0 \\ \frac{2}{m\sqrt{-m}} \sin^{-1} \left(\sqrt{-m} \right), & m < 0 \end{cases} \quad (D.74)$$

The second anisotropic correlation function displays Gaussian dependence as given by (D.75).

$$R_{\xi}^d(\bar{r}) = \exp \left(-\frac{x^2 + y^2}{\ell_{\rho}^2} - \frac{z^2}{\ell_z^2} \right) \quad (D.75)$$

The corresponding spectral density function is given by (D.76),

$$\Phi_{\xi}^d(\bar{k}) = \frac{\ell_{\rho}^2 \ell_z}{8\pi^{\frac{3}{2}}} \exp \left(-\frac{k_{\rho}^2 \ell_{\rho}^2}{4} - \frac{k_z^2 \ell_z^2}{4} \right) \quad (D.76)$$

and I_{\perp} , I_z , S , and S_z are given by (D.77) – (D.80) with h , b , m , A_1 , and A_2 as above.

$$\begin{aligned} I_{\perp}^d = & -S^d + \frac{k_0^2 \ell_{\rho} \ell_z A_1}{8} + \frac{1}{8} \sqrt{\frac{\epsilon_{gz}}{\epsilon_g}} k_0^2 \ell_{\rho} \ell_z \left[\frac{\sqrt{h^2 b}}{m} - \frac{1}{2} A_2 \right] \\ & + i \frac{\sqrt{\pi}}{8} k_0^3 \ell_{\rho}^2 \ell_z \sqrt{\frac{\epsilon_g}{\epsilon_0}} + i \frac{\sqrt{\pi}}{24} k_0^3 \ell_{\rho}^2 \ell_z \frac{\epsilon_{gz}}{\sqrt{\epsilon_g \epsilon_0}} \end{aligned} \quad (D.77)$$

$$\begin{aligned} I_z^d = & -S_z^d + \frac{\sqrt{b} k_0^2 \ell_{\rho} \ell_z}{4} \left[-\frac{\sqrt{b h^2}}{m} + \left(m + \frac{1}{2} \right) A_2 \right] \\ & + i k_0^3 \ell_{\rho}^2 \ell_z \frac{\sqrt{\pi}}{6} \sqrt{\frac{\epsilon_g}{\epsilon_0}} \end{aligned} \quad (D.78)$$

$$S^d = \frac{h \epsilon_0}{4 \sqrt{\epsilon_g \epsilon_{gz}}} \left[\frac{2}{\sqrt{h^2 b}} \left(1 + \frac{1}{m} \right) - A_2 \right] \quad (D.79)$$

$$S_z^d = \frac{h \epsilon_0}{2 \epsilon_g} (b)^{\frac{3}{2}} \left[-\frac{2}{m \sqrt{b h^2}} + A_2 \right] \quad (D.80)$$

The last anisotropic correlation function has gaussian dependence horizontally, and exponential dependence vertically.

$$R_{\xi}^e = \exp \left(-\frac{x^2 + y^2}{\ell_{\rho}^2} - \frac{|z|}{\ell_z} \right) \quad (D.81)$$

The corresponding spectral function is given by (D.82),

$$\Phi_{\xi}^e(k) = \frac{\ell_{\rho}^2 \ell_z}{4\pi^2} \exp\left(-\frac{k_{\rho}^2 \ell_{\rho}^2}{4}\right) \frac{1}{1 + k_z^2 \ell_z^2} \quad (D.82)$$

and I_{\perp} , I_z , S , and S_z are given by (D.83) – (D.86), where again h and b are as above.

$$\begin{aligned} I_{\perp}^e = & -S^e + \frac{k_o^2 \ell_{\rho}^2}{4} \frac{\epsilon_{gz}}{\epsilon_g} \int_0^{\frac{\pi}{2}} d\theta \sin \theta \cos \theta \times \\ & \exp\left(\frac{\tan^2 \theta}{4h^2 b}\right) \operatorname{erfc}\left(\frac{\tan \theta}{2h\sqrt{b}}\right) \\ & + \frac{k_o^2 \ell_{\rho}^2}{8} \int_0^{\frac{\pi}{2}} d\theta \tan \theta \exp\left(\frac{\tan^2 \theta}{4h^2}\right) \operatorname{erfc}\left(\frac{\tan \theta}{2h}\right) \\ & + \frac{i k_o^3 \ell_{\rho}^2 \ell_z}{12} \frac{\epsilon_{gz}}{\sqrt{\epsilon_g \epsilon_0}} + \frac{i k_o^3 \ell_{\rho}^2 \ell_z}{4} \sqrt{\frac{\epsilon_g}{\epsilon_0}} \end{aligned} \quad (D.83)$$

$$\begin{aligned} I_z^e = & -S_z^e + \frac{k_o^2 \ell_{\rho}^2}{2} \int_0^{\frac{\pi}{2}} d\theta \sin^2 \theta \tan \theta \times \\ & \exp\left(\frac{\tan^2 \theta}{4h^2 b}\right) \operatorname{erfc}\left(\frac{\tan \theta}{2h\sqrt{b}}\right) \\ & + \frac{i k_o^3}{3} \ell_{\rho}^2 \ell_z \sqrt{\frac{\epsilon_g}{\epsilon_0}} \end{aligned} \quad (D.84)$$

$$\begin{aligned} S^e = & \frac{1}{2\pi h} \frac{\sqrt{\epsilon_{gz}} \epsilon_0}{(\epsilon_g)^{\frac{3}{2}}} \int_0^{\frac{\pi}{2}} d\theta \sin \theta \tan^2 \theta \times \\ & \left\{ \sqrt{\pi} - \pi \frac{\tan \theta}{2h\sqrt{b}} \exp\left(\frac{\tan^2 \theta}{4h^2 b}\right) \operatorname{erfc}\left(\frac{\tan \theta}{2h\sqrt{b}}\right) \right\} \end{aligned} \quad (D.85)$$

$$S_z^e = \frac{\epsilon_0}{\sqrt{\epsilon_g \epsilon_{gz}}} \frac{1}{h\pi} \int_0^{\frac{\pi}{2}} d\theta \left\{ \sqrt{\pi} - \pi \frac{\tan \theta}{2h\sqrt{b}} \exp\left(\frac{\tan^2 \theta}{4h^2 b}\right) \operatorname{erfc}\left(\frac{\tan \theta}{2h\sqrt{b}}\right) \right\} \quad (D.86)$$

In this thesis, two of the above correlation functions are used in studying the effect of random media on the scattering of buried targets. Initially, the spherical exponential

correlation function (b) is utilized to model statistically isotropic scatterers. Later, in examining the effects of non-isotropic scatterers, the gaussian-exponential correlation function (e) is applied.

In each case, the scattering material is chosen to roughly model the characteristics of vegetation, which is composed of a mixture of bulk vegetation material and water. The de Looz mixing formula [72,128] is utilized to determine an overall scatterer permittivity. The host material is assumed to have a permittivity of $3\epsilon_0$, and the water inclusions at a frequency of 1.12 GHz and with a salinity of 10 parts per thousand, have a complex permittivity of $(76.0 + 32.5i)\epsilon_0$. With an assumed volume of inclusions of 0.6 (60%), the resulting scatterer permittivity is $(39.86 + 16.257i)\epsilon_0$.

Strong Fluctuation theory can now be applied with this scatterer permittivity and with a background of freespace. For the two correlation functions, and for an assortment of fractional volumes and correlation lengths, the resulting effective permittivities are shown below. Also shown are the variances and complex variances of the associated renormalized scattering sources.

Correlation	f_v	ℓ	ϵ_{eff}
b	1.67%	.0052m	1.0505+.001794i
b	1.67%	.0072m	1.0516+.002417i
b	4.17%	.0052m	1.1360+.005478i
b	0.05%	.0052m	1.0014+4.77E-5i
e	1.67%	.0052m (ℓ_ρ)	1.0442+.001327i ($\epsilon_{\text{eff}\perp}$)
		.0156m (ℓ_z)	1.0839+.004739i ($\epsilon_{\text{eff}z}$)

Table D.1. Effective permittivities calculated using Strong Fluctuation theory, for the two correlation types, and for several choices of fractional volume and correlation length.

Correlation	f_v	ℓ	δ
b	1.67%	.0052m	.146822
b	1.67%	.0072m	.146822
b	4.17%	.0052m	.433835
b	0.05%	.0052m	.003972
e	1.67%	.0052m (ℓ_ρ)	.115700 ($\delta_{\perp\perp}$)
		.0156m (ℓ_z)	.390404 (δ_{zz})
			.212485-.004497i ($\delta_{\perp z}$)

Table D.2. Renormalized scattering source variances calculated using Strong Fluctuation theory, for the two correlation types, and for several choices of fractional volume and correlation length.

Correlation	f_v	ℓ	$\hat{\delta}$
b	1.67%	.0052m	.1466+.008268i
b	1.67%	.0072m	.1466+.008268i
b	4.17%	.0052m	.4329+.028121i
b	0.05%	.0052m	.00397+.000205i
e	1.67%	.0052m (ℓ_ρ)	.1156+.005828i ($\hat{\delta}_{\perp\perp}$)
		.0156m (ℓ_z)	.3887+.03614i ($\hat{\delta}_{zz}$)
			.2120+.01519i ($\hat{\delta}_{\perp z}$)

Table D.3. Renormalized scattering source complex variances calculated using Strong Fluctuation theory, for the two correlation types, and for several choices of fractional volume and correlation length.

Appendix E

Electric Field / Electric Source Green's Function and Incident Field Expressions for a Uniaxial Layered Media

This Appendix gives the expressions for the Green's function for the electric field arising from an electric current in a uniaxial layered media. Forms are given for both the case where the source and receiver are in different layers, as well as the case where they are in the same region. Also given is the far-field form of the Green's function for a distant observation point in region 0. Finally, the expression is given for the incident field in each layer arising from a plane wave originating in region 0 and propagating downwards.

The media is described in each layer, m , by an isotropic permeability, μ_m , and a uniaxial permittivity, $\bar{\epsilon}_m$, with a vertically oriented optic axis, such that the permittivity tensor will be diagonal in the form of (E.1).

$$\bar{\epsilon}_m = \begin{bmatrix} \epsilon_m & 0 & 0 \\ 0 & \epsilon_m & 0 \\ 0 & 0 & \epsilon_{zm} \end{bmatrix} \quad (E.1)$$

The form of the Green's function used here is that given by Ali [144]. For an electric current source, $\bar{J}_m(\bar{r})$, located in layer m , the electric field resulting at an observation point, \bar{r} , in region p is given by (E.2),

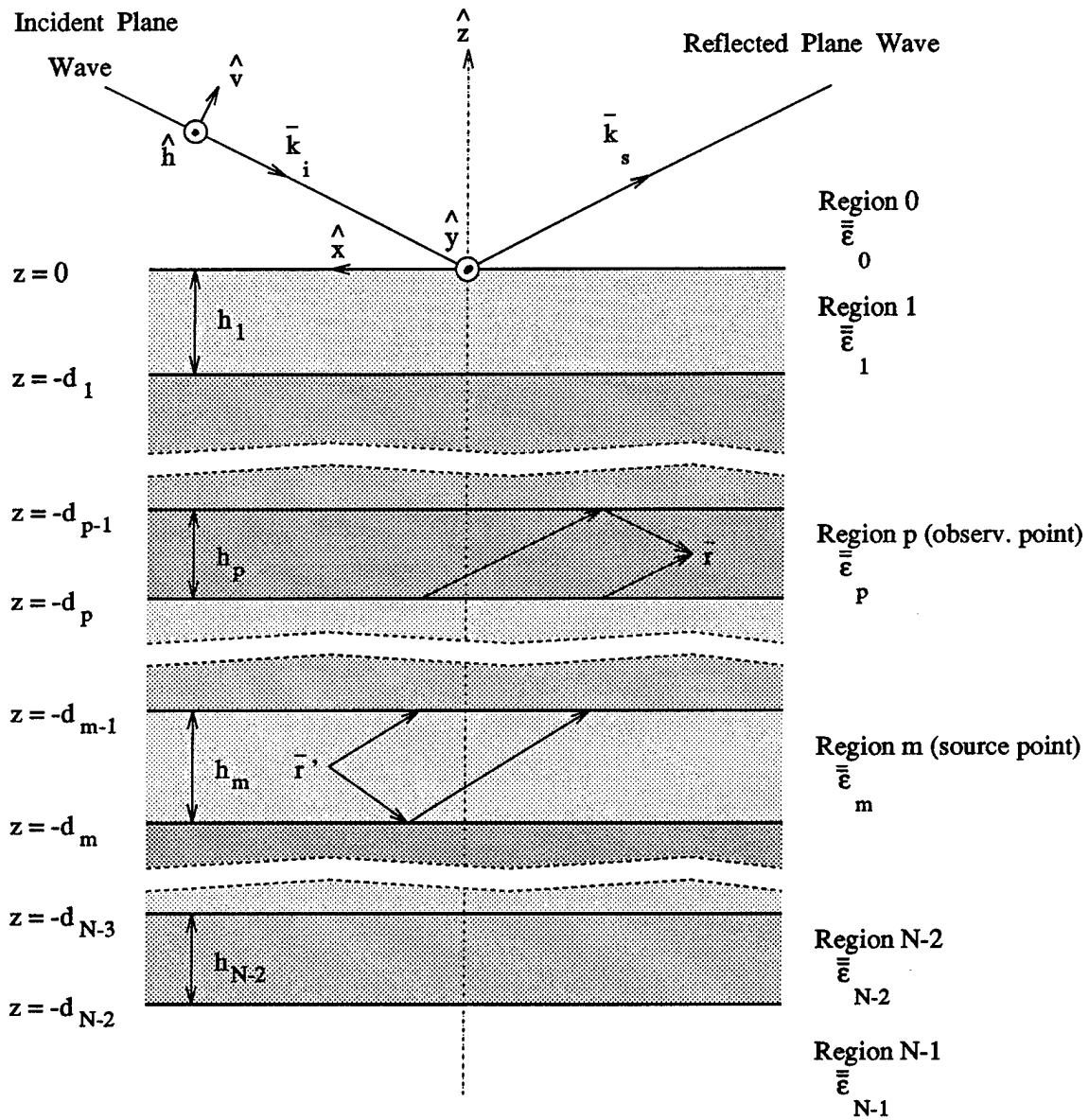


Figure E.1. Geometry of the layered media for which the Greens function and incident field expressions are calculated. For the Greens function, $\bar{G}_{pm}(\vec{r}, \vec{r}')$, the terms contributing to the propagation of the wave from layer m to layer p are shown for the case where $p < m$.

$$\bar{E}_p(\bar{r}) = i\omega\mu_m \iint_{V_j} d\bar{r}' \bar{G}_{pm}(\bar{r}, \bar{r}') \cdot \bar{J}_m(\bar{r}') \quad (E.2)$$

where $\bar{G}_{pm}(\bar{r}, \bar{r}')$ is the Green's function, which for the case where $p \neq m$ can be written as (E.3),

$$\begin{aligned} \bar{G}_{pm}^{un}(\bar{r}, \bar{r}') = \sum_{q, \ell=+, -} \sum_{v=TE, TM} \iint d\bar{k}_\perp \bar{F}_{pm\ell q}^{(v)un}(\bar{k}_\perp) \times \\ e^{i\bar{k}_\perp \cdot (\bar{r}_\perp - \bar{r}'_\perp)} e^{i\ell k_{pz}^{(v)} z} e^{-iqk_{mz}^{(v)} z'} \end{aligned} \quad (E.3)$$

where $\bar{F}_{pm\ell q}^{(v)un}(\bar{k}_\perp)$ is given by (E.4).

$$\begin{aligned} \bar{F}_{pm\ell q}^{(v)un}(\bar{k}_\perp) = \frac{i}{8\pi^2} \cdot \frac{1}{k_{mz}^{(v)}} \frac{X_{\cup \cap m \rightarrow p}^{(v)}}{1 - R_{\cup m}^{(v)} R_{\cap m}^{(v)} e^{2ik_{mz}^{(v)} h_m}} \bar{u}^{(v)}(\ell k_{pz}^{(v)}) \bar{u}^{(v)}(q k_{mz}^{(v)}) \times \\ C_{\cup \cap}^{(v)}(\ell) C_{\cup \cap}^{(v)}(q) e^{i\ell k_{pz}^{(v)}(z_p - z)} e^{-iqk_{mz}^{(v)}(z'_m - z')} \end{aligned} \quad (E.4)$$

If $z \geq z'$, then in the above the following definitions apply

$$C_{\cup}^{(v)}(+) = 1 \quad (E.5)$$

$$C_{\cup}^{(v)}(-) = R_{\cup p}^{(v)} e^{2ik_{pz}^{(v)} h_p} \quad (E.6)$$

$$C_U^{(v)}(+) = 1 \quad (E.7)$$

$$C_U^{(v)}(-) = R_{\cap m}^{(v)} e^{2ik_m^{(v)} h_m} \quad (E.8)$$

$$z_p - z = d_p \quad (E.9)$$

$$z'_m - z' = d_{m-1} \quad (E.10)$$

while if $z < z'$, then the following alternate definitions apply.

$$C_{\cap}^{(v)}(+) = R_{\cap p}^{(v)} e^{2ik_p^{(v)} h_p} \quad (E.11)$$

$$C_{\cap}^{(v)}(-) = 1 \quad (E.12)$$

$$C'_{\cap}^{(v)}(+) = R_{\cup m}^{(v)} e^{2ik_m^{(v)} h_m} \quad (E.13)$$

$$C'_{\cap}^{(v)}(-) = 1 \quad (E.14)$$

$$z_p - z = d_{p-1} \quad (E.15)$$

$$z'_m - z' = d_m \quad (E.16)$$

For the case where $p = m$ (source and observation point in the same layer), then the Green's function is given by (E.17),

$$\begin{aligned} \overline{G}_{mm}^{un}(\bar{r}, \bar{r}') = \overline{D} \delta(\bar{r} - \bar{r}') + \sum_{q, \ell = +, -} \sum_{v = TE, TM} \iint d\bar{k}_{\perp a} \overline{F}_{m \cup n_{\ell q}}^{(v)}(\bar{k}_{\perp}) \times \\ e^{i\bar{k}_{\perp} \cdot (\bar{r}_{\perp} - \bar{r}'_{\perp})} e^{i\ell k_{mz}^{(v)} z} e^{-iqk_{mz}^{(v)} z'} \end{aligned} \quad (E.17)$$

where

$$\begin{aligned} \overline{F}_{m \cup n_{\ell q}}^{(v)}(\bar{k}_{\perp}) = \frac{i}{8\pi} \frac{1}{k_{mz}^{(v)}} \frac{1}{1 - R_{\cap m}^{(v)} R_{\cup m}^{(v)} e^{2i\ell k_{mz}^{(v)} h_m}} \overline{u}^{(v)}(\ell k_{mz}^{(v)}) \overline{u}^{(v)}(qk_{mz}^{(v)}) \times \\ C_{\cap n}^{(v)}(\ell) C'_{\cup n}{}^{(v)}(q) e^{i\ell k_{mz}^{(v)}(z_m - z)} e^{-iqk_{mz}^{(v)}(z'_m - z')} \end{aligned} \quad (E.18)$$

and where

$$\overline{D} = -\frac{\hat{z}\hat{z}}{\omega^2 \mu \epsilon_{z_m}} \quad (E.19)$$

For the case where $z \geq z'$, $C_{\cap \cup}^{(v)}$ and $C'_{\cap \cup}{}^{(v)}$ are given by (E.20)-(E.23),

$$C_{\cap \cup}^{(v)}(+)=1 \quad (E.20)$$

$$C_{\cap \cup}^{(v)}(-)=R_{\cup m}^{(v)} \quad (E.21)$$

$$C'_{=U}{}^{(v)}(+)=1 \quad (E.22)$$

$$C'_{=U}{}^{(v)}(-)=R_{\cap m}^{(v)} e^{2ik_m^{(v)}h_m} \quad (E.23)$$

and for the case $z < z'$, $C_{=\cap}^{(v)}$ and $C'_{=\cap}{}^{(v)}$ are given by (E.24)-(E.27).

$$C_{=\cap}^{(v)}(+)=R_{\cap m}^{(v)} e^{2ik_m^{(v)}h_m} \quad (E.24)$$

$$C_{=\cap}^{(v)}(-)=1 \quad (E.25)$$

$$C'_{=\cap}{}^{(v)}(+)=R_{\cup m}^{(v)} \quad (E.26)$$

$$C'_{=\cap}{}^{(v)}(-)=1 \quad (E.27)$$

For both cases ($z \geq z'$ and $z < z'$), z_m and z'_m are given by (E.28).

$$z_m - z = z'_m - z' = d_{m-1} \quad (E.28)$$

For the case where the source is in layer m , and the observation point is at a distant location in region 0, a far-field form of the above Green's function may be derived. This far-field Green's function is given by (E.29),

$$\overline{\overline{G}}_{0m}^{\text{f.f.}}(\bar{r}, \bar{r}') = \frac{e^{ikr}}{4\pi r} \sum_{p=+,-} \sum_{u=TE, TM} \overline{\overline{H}}_{0m_p}^{(u)}(\bar{k}_{\perp s}) e^{-i\bar{k}_{\perp s} \cdot \bar{r}'_{\perp}} e^{-ipk_{mz}^{(u)} z'} \quad (E.29)$$

where

$$\begin{aligned} \overline{\overline{H}}_{0m_p}^{(u)}(\bar{k}_{\perp s}) &= \frac{k_{0z}^{(u)}}{k_{mz}^{(u)}} \cdot \frac{X_{\cup m \rightarrow 0}^{(u)}}{1 - R_{\cup m}^{(u)} R_{\cap m}^{(u)} e^{2ik_{mz}^{(u)} h_m}} \times \\ &\quad \overline{u}^{(u)}(k_{0z}^{(u)}) \overline{u}^{(u)}(pk_{mz}^{(u)}) C_{\cup}^{(u)}(+) C_{\cup}^{\prime (u)}(p) e^{-ipk_{mz}^{(u)} d_{m-1}} \end{aligned} \quad (E.30)$$

and where the propagation vector in the scattering direction (towards the observation point) is given by (E.31).

$$\bar{k}_{ms}^{(u)} = \bar{k}_{\perp s} + k_{mz}^{(u)} \hat{z} \quad (E.31)$$

Finally, for a plane wave of the form of (E.32) incident on the layered media from region 0,

$$\overline{E}_i(\bar{r}) = [E_i^{TE} \hat{h}(-k_{0zi}^{(w)}) + E_i^{TM} \hat{v}(-k_{0zi}^{(w)})] e^{i\bar{k}_{\perp i} \cdot \bar{r}_{\perp}} e^{-ik_{0zi}^{(w)} z} \quad (E.32)$$

the resulting total field in each region will be given by (E.33),

$$\overline{E}_{\ell_i}(\bar{r}) = \sum_{s=+,-} \sum_{w=TE, TM} \overline{E}_{\ell_i}^{s,(w)}(\bar{k}_{\perp i}) e^{i\bar{k}_{\perp i} \cdot \bar{r}_{\perp}} e^{-isk_{\ell zi}^{(w)} z} \quad (E.33)$$

where

$$\overline{E}_{\ell_i}^{s,(w)}(\overline{k}_\perp) = E_i^{(w)} X_{\cap_0 \rightarrow \ell}^{(w)} \overline{u}^{(w)}(-s k_{\ell_z}^{(w)}) C_{\cap}^{(w)}(-s) e^{-is k_{\ell_z}^{(w)} d_{\ell-1}} \quad (E.34)$$

In all of the above, the \hat{z} component of the propagation vector in a particular layer can be found from (E.35) for the TE case, and from (E.36) for the TM case,

$$k_{mz}^{(TE)} = \sqrt{k_m^2 - k_\perp^2} \quad (E.35)$$

$$k_{mz}^{(TM)} = \sqrt{k_m^2 - \frac{\epsilon_m}{\epsilon_{zm}} k_\perp^2} \quad (E.36)$$

where $k_\perp^2 = k_x^2 + k_y^2$ and $k_m^2 = \omega^2 \mu_m \epsilon_m$. The polarization vectors are given by (E.37) for the TE case, and by (E.38) for the TM case.

$$\overline{u}^{(TE)}(\pm k_{mz}^{(TE)}) = \hat{h}(\pm k_{mz}^{(TE)}) = \frac{k_y}{k_\perp} \hat{x} - \frac{k_x}{k_\perp} \hat{y} \quad (E.37)$$

$$\overline{u}^{(TM)}(\pm k_{mz}^{(TM)}) = \overline{v}(\pm k_{mz}^{(TM)}) = \mp \frac{k_{mz}^{(TM)}}{k_m} \left(\frac{k_x}{k_\perp} \hat{x} + \frac{k_y}{k_\perp} \hat{y} \right) - \frac{k_\perp}{k_m} \cdot \frac{\epsilon_m}{\epsilon_{zm}} \hat{z} \quad (E.38)$$

The multi-layer reflection coefficients for downward and upward propagation through the layered media are given recursively by

$$R_{\cap_m}^{(u)} = \frac{R_{m(m+1)}^{(u)} + R_{\cap(m+1)}^{(u)} e^{2ik_{(m+1)z}^{(u)} h_{m+1}}}{1 + R_{\cap(m+1)}^{(u)} R_{m(m+1)}^{(u)} e^{2ik_{(m+1)z}^{(u)} h_{m+1}}} \quad (E.39)$$

where $R_{\cap(N-1)}^{(u)} = R_{(N-1)N}^{(u)}$ for region N below the bottom boundary, and by

$$R_{\cup_m}^{(u)} = \frac{R_{m(m-1)}^{(u)} + R_{\cup(m-1)}^{(u)} e^{2ik_{(m-1)z}^{(u)} h_{m-1}}}{1 + R_{\cup(m-1)}^{(u)} R_{m(m-1)}^{(u)} e^{2ik_{(m-1)z}^{(u)} h_{m-1}}} \quad (E.40)$$

where $R_{\cup_1}^{(u)} = R_{10}^{(u)}$ for region 0 above the top boundary. In the above, the individual layer reflection coefficients for the TE and TM cases are given by (E.41) and (E.42).

$$R_{ij}^{(TE)} = \frac{\mu_j k_{iz}^{(TE)} - \mu_i k_{jz}^{(TE)}}{\mu_j k_{iz}^{(TE)} + \mu_i k_{jz}^{(TE)}} \quad (E.41)$$

$$R_{ij}^{(TM)} = \frac{\epsilon_j k_{iz}^{(TM)} - \epsilon_i k_{jz}^{(TM)}}{\epsilon_j k_{iz}^{(TM)} + \epsilon_i k_{jz}^{(TM)}} \quad (E.42)$$

Finally, the downward and upward transmission coefficients are given by

$$X_{\cap m \rightarrow \ell}^{(TE)} = X_{\cap m \rightarrow (\ell-1)}^{(TE)} e^{ik_{(\ell-1)z}^{(TE)} h_{\ell-1}} \frac{(1 + R_{\cap(\ell-1)}^{(TE)})}{(1 + R_{\cap \ell}^{(TE)} e^{2ik_{\ell z}^{(TE)} h_{\ell}})} \quad (E.43)$$

$$X_{\cap m \rightarrow \ell}^{(TM)} = \frac{k_{\ell}}{k_{\ell z}^{(TM)}} \cdot \frac{k_{(\ell-1)}^{(TM)}}{k_{\ell-1}} X_{\cap m \rightarrow (\ell-1)}^{(TE)} e^{ik_{(\ell-1)z}^{(TE)} h_{\ell-1}} \frac{(1 - R_{\cap(\ell-1)}^{(TM)})}{(1 - R_{\cap \ell}^{(TM)} e^{2ik_{\ell z}^{(TM)} h_{\ell}})} \quad (E.44)$$

where for $\ell = m + 1$

$$X_{\cap m \rightarrow (m+1)}^{(TE)} = \frac{1 + R_{\cap m}^{(TE)}}{1 + R_{\cap(m+1)}^{(TE)} e^{2ik_{(m+1)z}^{(TE)} h_{m+1}}} \quad (E.45)$$

$$X_{\cap m \rightarrow (m+1)}^{(TM)} = \frac{k_{m+1}}{k_{(m+1)z}^{(TM)}} \cdot \frac{k_{mz}^{(TM)}}{k_m} \cdot \frac{1 - R_{\cap m}^{(TM)}}{1 - R_{\cap(m+1)}^{(TM)} e^{2ik_{(m+1)z}^{(TM)} h_{m+1}}} \quad (E.46)$$

and

$$X_{\cup_{m \rightarrow \ell}}^{(TE)} = X_{\cup_{m \rightarrow (\ell+1)}}^{(TE)} e^{ik_{(\ell+1)z}^{(TE)} h_{\ell+1}} \frac{(1 + R_{\cup_{(\ell+1)}}^{(TE)})}{(1 + R_{\cup_{\ell}}^{(TE)} e^{2ik_{\ell z}^{(TE)} h_{\ell}})} \quad (E.47)$$

$$X_{\cup_{m \rightarrow \ell}}^{(TM)} = \frac{k_{\ell}}{k_{\ell z}^{(TM)}} \cdot \frac{k_{(\ell+1)z}^{(TM)}}{k_{\ell+1}} X_{\cup_{m \rightarrow (\ell+1)}}^{(TE)} e^{ik_{(\ell+1)z}^{(TE)} h_{\ell+1}} \frac{(1 - R_{\cup_{(\ell+1)}}^{(TM)})}{(1 - R_{\cup_{\ell}}^{(TM)} e^{2ik_{\ell z}^{(TM)} h_{\ell}})} \quad (E.48)$$

where for $\ell = m - 1$

$$X_{\cup_{m \rightarrow (m-1)}}^{(TE)} = \frac{1 + R_{\cup_m}^{(TE)}}{1 + R_{\cup_{(m-1)}}^{(TE)} e^{2ik_{(m-1)z}^{(TE)} h_{m-1}}} \quad (E.49)$$

$$X_{\cup_{m \rightarrow (m-1)}}^{(TM)} = \frac{k_{m-1}}{k_{(m-1)z}^{(TM)}} \cdot \frac{k_{mz}^{(TM)}}{k_m} \cdot \frac{1 - R_{\cup_m}^{(TM)}}{1 - R_{\cup_{(m-1)}}^{(TM)} e^{2ik_{(m-1)z}^{(TM)} h_{m-1}}} \quad (E.50)$$

Appendix F

Incoherent Field Correlation for a Point Target and Layered Continuous Uniaxial Random Media with the Target in a Non-Random Layer ($t \neq f$)

This Appendix gives the expressions for the correlation of the multi-path incoherent target return for a stratified multi-layer uniaxial random media with a single layer of continuous random media, and with a point scatterer target located in a different layer. The result given here is more correct than that of the proceeding chapter because the contributions of the poles of the spectral function, $\Phi_{\alpha\beta\gamma\rho}(\bar{\beta})$, are now included in the evaluation of the final β_z integration. This Appendix shows the revised derivation of this final step for a class of spectral functions possessing only first and second order poles. The derivation is again done only for $\sigma_{TC-TC}^{\hat{p}_a\hat{p}_b}$, however, the other two correlations are similar, and the final results for all three are given at the end of the Appendix.

F.1. Evaluation of the Complex β_z Integration

From Equation (4.17), the expression for the autocorrelation of the target/clutter multi-path return is shown below

$$\begin{aligned}
\sigma_{TC-TC}^{\hat{p}_a \hat{p}_b} = & \sum_{s', p', q', \ell' = +, -} \sum_{u', v', w' = TE, TM} \sum_{\alpha, \beta, \gamma, \rho = x, y, z} \iint d\bar{k}_{\perp a} \int d\beta_z (2\pi)^4 A_{TC-TC}^{\alpha\beta\gamma\rho}{}_{pp'ss'qq'\ell\ell'}{}_{uu'vv'ww'} \times \\
& \Phi_{\alpha\beta\gamma\rho}(\bar{k}_{\perp a} - \bar{k}_{\perp a s}, \beta_z) e^{i(\bar{k}_{\perp a s} - \bar{k}_{\perp b s} + \bar{k}_{\perp b s} - \bar{k}_{\perp a s}) \cdot \bar{r}_{T\perp}} e^{-i(s k_{z a i}^{(w)} + q k_{z a}^{(v)} - s' k_{z b i}^{(w')} - q' k_{z c}^{(v')}) z_T} \times \\
& e^{-i(\ell k_{f z a}^{(v)} - p k_{f z a s}^{(u)} - \ell' k_{f z c}^{(v')*} + p' k_{f z b s}^{(u')*}) d_{f-1}} \times \left[1 - e^{i(p k_{f z a s}^{(u)} - \ell k_{f z a}^{(v)} + \beta_z) h_f} - \right. \\
& \left. e^{-i(p' k_{f z b s}^{(u')*} - \ell' k_{f z c}^{(v')*} + \beta_z) h_f} + e^{i(p k_{f z a s}^{(u)} - p' k_{f z b s}^{(u')*} - \ell k_{f z a}^{(v)} + \ell' k_{f z c}^{(v')*}) h_f} \right] \times \\
& \frac{1}{[\beta_z - (\ell k_{f z a}^{(v)} - p k_{f z a s}^{(u)})] [\beta_z - (\ell' k_{f z c}^{(v')*} - p' k_{f z b s}^{(u')*})]}
\end{aligned} \tag{F.1}$$

where the two final terms of (4.17) have been multiplied through. There are two obvious poles of the above integrand, which occur at $\beta_z = \ell k_{f z a}^{(v)} - p k_{f z a s}^{(u)}$ and $\beta_z = \ell' k_{f z c}^{(v')*} - p' k_{f z b s}^{(u')*}$. In addition, however, the spectral function $\Phi_{\alpha\beta\gamma\rho}(\bar{\beta}_{\perp}, \beta_z)$ may have poles of its own. For the purpose of calculating only the variance of the field from the above expression, and when the media is only of low loss, the residues from the above poles will generally dominate over the contributions from the spectral function poles, and these later poles may be ignored. Even in the low-loss case, however, when the correlation of the field is evaluated and the angular or frequency separation becomes large, the contribution from the two primary poles becomes reduced, and the spectral function poles may begin to contribute to a greater extent. For this reason, the β_z complex integral is re-evaluated here, now including all pole contributions.

To allow examination of the spectral function poles, the form of the spectral function must be specified in greater detail. Two common choices for the form of the correlation function and associated spectral functions are given by (F.2) and (F.3).

$$C_1(\bar{r}_1 - \bar{r}_2) = e^{-\frac{|\bar{r}_1 - \bar{r}_2|}{\ell}}$$

$$\Phi_1(\bar{\beta}) = \frac{\ell^3}{\pi^2(1 + \beta^2 \ell^2)^2} \quad (F.2)$$

$$C_2(\bar{r}_1 - \bar{r}_2) = \exp \left(-\frac{x^2 + y^2}{\ell_\rho^2} - \frac{|z|}{\ell_z} \right)$$

$$\Phi_2(\bar{\beta}) = \frac{\ell_\rho^2 \ell_z}{4\pi^2} \exp \left(-\frac{k_\rho^2 \ell_\rho^2}{4} \right) \frac{1}{1 + k_z^2 \ell_z^2} \quad (F.3)$$

Both of the above examples are characterized by first or second order poles in β_z . Hence, it is useful to consider a slightly more general form of the spectral function as given by (F.4).

$$\Phi_{\alpha\beta\gamma\rho}(\bar{\beta}_\perp, \beta_z) = \frac{\Phi_N}{\prod_{m=1}^{N_1} (\beta_z - \beta_{zm}) (\beta_z - \beta_{zm}^*) \prod_{n=1}^{N_2} (\beta_z - \beta_{zn})^2 (\beta_z - \beta_{zn}^*)^2} \quad (F.4)$$

In the above, it is assumed that the correlation function is real, such that the associated spectral function will have poles in conjugate pairs.

To evaluate the integral of (F.1), the integrand is split into a portion convergent in the upper half-plane of complex β_z , and a second portion convergent in the lower half-plane. The two resulting integrals are given by (F.5) and (F.6).

$$I_+ = \int d\beta_z \frac{\Phi_N}{\left[\beta_z - \left(\ell k_{fz_a}^{(v)} - p k_{fz_{a*}}^{(u)}\right)\right] \left[\beta_z - \left(\ell' k_{fz_c}^{(v')*} - p' k_{fz_{b*}}^{(u')*}\right)\right]} \times \frac{1 - e^{i(p k_{fz_{a*}}^{(u)} - \ell k_{fz_a}^{(v)} + bz)h_f} + e^{i(p k_{fz_{a*}}^{(u)} - \ell k_{fz_a}^{(v)} + \ell' k_{fz_c}^{(v')*} - p' k_{fz_{b*}}^{(u')*})h_f}}{\prod_{m=1}^{N_1} (\beta_z - \beta_{z_m}) (\beta_z - \beta_{z_m}^*) \prod_{n=1}^{N_2} (\beta_z - \beta_{z_n})^2 (\beta_z - \beta_{z_n}^*)^2} \quad (F.5)$$

$$I_- = \int d\beta_z \frac{-\Phi_N}{\left[\beta_z - \left(\ell k_{fz_a}^{(v)} - p k_{fz_{a*}}^{(u)}\right)\right] \left[\beta_z - \left(\ell' k_{fz_c}^{(v')*} - p' k_{fz_{b*}}^{(u')*}\right)\right]} \times \frac{e^{-i(p' k_{fz_{b*}}^{(u')*} - \ell' k_{fz_c}^{(v')*} + \beta_z)h_f}}{\prod_{m=1}^{N_1} (\beta_z - \beta_{z_m}) (\beta_z - \beta_{z_m}^*) \prod_{n=1}^{N_2} (\beta_z - \beta_{z_n})^2 (\beta_z - \beta_{z_n}^*)^2} \quad (F.6)$$

Each of the first two primary poles of the above integrands may be located in either the upper or lower half-planes. For the spectral function poles, it will be assumed without loss of generality, the β_{z_m} and β_{z_n} are always in the upper half-plane, and their complex conjugates will, therefore, be in the lower half-plane.

The two integrals I_+ and I_- will be performed by closing the contour in a loop fashion at infinite radius, where the loop will be upwards for the I_+ integral, and downwards for I_- . The portions of the contour at infinity will not contribute in either case, and, therefore, the integral can be found from the residues of the enclosed poles. The two primary poles will be considered before considering the spectral function poles. If the first of these poles is in the upper half-plane, it will contribute to I_+ , and the residue will be given by (F.7).

$$R_{P1}^+ = 2\pi i \Phi_{\alpha\beta\gamma\rho} \left(\bar{k}_{\perp_a} - \bar{k}_{\perp_{a*}}, \ell k_{fz_a}^{(v)} - p k_{fz_{a*}}^{(u)} \right) \frac{e^{i(p k_{fz_{a*}}^{(u)} - \ell k_{fz_a}^{(v)} + \ell' k_{fz_c}^{(v')*} - p' k_{fz_{b*}}^{(u')*})h_f}}{\ell k_{fz_a}^{(v)} - p k_{fz_{a*}}^{(u)} + p' k_{fz_{b*}}^{(u')*} - \ell' k_{fz_c}^{(v')*}} \quad (F.7)$$

In contrast, if the pole is in the lower half-plane, it will instead contribute to I_- with the residue given by (F.8).

$$R_{P1}^- = 2\pi i \Phi_{\alpha\beta\gamma\rho} \left(\bar{k}_{\perp a} - \bar{k}_{\perp a s}, \ell k_{fz_a}^{(v)} - p k_{fz_{as}}^{(u)} \right) \frac{e^{i(p k_{fz_{as}}^{(u)} - \ell k_{fz_a}^{(v)} + \ell' k_{fz_c}^{(v')*} - p' k_{fz_{bs}}^{(u')*})h_f}}{\ell k_{fz_a}^{(v)} - p k_{fz_{as}}^{(u)} + p' k_{fz_{bs}}^{(u')*} - \ell' k_{fz_c}^{(v')*}} \quad (F.8)$$

Comparing R_{P1}^+ with R_{P1}^- it can be seen that the expressions are identical, and the contribution to the overall integral, $I_+ + I_-$, is the same regardless of the location of the pole.

Similarly, for the second primary pole, the residue contribution to I_+ for an upper half-plane location is identical to the contribution to I_- when the pole is in the lower half-plane, and in both cases the result is given by (F.9).

$$R_{P2} = 2\pi i \Phi_{\alpha\beta\gamma\rho} \left(\bar{k}_{\perp a} - \bar{k}_{\perp a s}, \ell' k_{fz_c}^{(v')*} - p' k_{fz_{bs}}^{(u')*} \right) \frac{1}{\ell k_{fz_a}^{(v)} - p k_{fz_{as}}^{(u)} + p' k_{fz_{bs}}^{(u')*} - \ell' k_{fz_c}^{(v')*}} \quad (F.9)$$

The contribution of the first order spectral function poles can be found as a sum of the residues, where for each conjugate pole pair, β_{z_m} contributes to I_+ , and $\beta_{z_m}^*$ contributes to I_- . The overall sum is given by (F.10).

$$R_{S1} = 2\pi i \sum_{m=1}^{N_1} \frac{1 - \frac{e^{i(p k_{fz_{as}}^{(u)} - \ell k_{fz_a}^{(v)} + \beta_{z_m})h_f} + e^{i(p k_{fz_{as}}^{(u)} - \ell k_{fz_a}^{(v)} + \ell' k_{fz_c}^{(v')*} - p' k_{fz_{bs}}^{(u')*})h_f}}{(p k_{fz_{as}}^{(u)} - \ell k_{fz_a}^{(v)} + \beta_{z_m}) (p' k_{fz_{bs}}^{(u')*} - \ell' k_{fz_c}^{(v')*} + \beta_{z_m})}} \times$$

$$\frac{\Phi_N(\bar{k}_{\perp a} - \bar{k}_{\perp a s}, \beta_{z_m})}{\prod_{\substack{m'=1 \\ m' \neq m}}^{N_1} (\beta_{z_m} - \beta_{z_{m'}}) \prod_{m'=1}^{N_1} (\beta_{z_m} - \beta_{z_{m'}}^*) \prod_{n'=1}^{N_2} (\beta_{z_m} - \beta_{z_{n'}})^2 (\beta_{z_m} - \beta_{z_{n'}}^*)^2} +$$

$$\begin{aligned}
& \frac{e^{-i(p'k_{fz_b}^{(u')*} - \ell'k_{fz_c}^{(v')*} + \beta_{z_m}^*)h_f}}{(pk_{fz_a}^{(u)} - \ell k_{fz_a}^{(v)} + \beta_{z_m}^*)(p'k_{fz_b}^{(u')*} - \ell'k_{fz_c}^{(v')*} + \beta_{z_m}^*)} \times \\
& \frac{\Phi_N(\bar{k}_{\perp a} - \bar{k}_{\perp a s}, \beta_{z_m}^*)}{\prod_{m'=1}^{N_1} (\beta_{z_m}^* - \beta_{z_{m'}}) \prod_{\substack{m'=1 \\ m' \neq m}}^{N_1} (\beta_{z_m}^* - \beta_{z_{m'}}^*) \prod_{n'=1}^{N_2} (\beta_{z_m}^* - \beta_{z_{n'}})^2 (\beta_{z_m}^* - \beta_{z_{n'}}^*)^2} \\
& \quad (F.10)
\end{aligned}$$

For the second order poles, the residues for I_+ and I_- are given by (F.11) and (F.12),

$$\begin{aligned}
R_{S2}^+ &= 2\pi i \sum_{n=1}^{N_2} \frac{1}{D_{+n}^2} \left\{ D_{+n} [\Phi'_N(\bar{k}_{\perp a} - \bar{k}_{\perp a s}, \beta_{z_n}) N_{+n} + \Phi_N(\bar{k}_{\perp a} - \bar{k}_{\perp a s}, \beta_{z_n}) N'_{+n}] \right. \\
& \quad \left. - N_{+n} \Phi_N(\bar{k}_{\perp a} - \bar{k}_{\perp a s}, \beta_{z_n}) D'_{+n} \right\} \\
& \quad (F.11)
\end{aligned}$$

$$\begin{aligned}
R_{S2}^- &= 2\pi i \sum_{n=1}^{N_2} \frac{1}{D_{-n}^2} \left\{ D_{-n} [\Phi'_N(\bar{k}_{\perp a} - \bar{k}_{\perp a s}, \beta_{z_n}^*) N_{-n} + \Phi_N(\bar{k}_{\perp a} - \bar{k}_{\perp a s}, \beta_{z_n}^*) N'_{-n}] \right. \\
& \quad \left. - N_{-n} \Phi_N(\bar{k}_{\perp a} - \bar{k}_{\perp a s}, \beta_{z_n}^*) D'_{-n} \right\} \\
& \quad (F.12)
\end{aligned}$$

where D_{+n} , D_{-n} , D'_{+n} , and D'_{-n} are given by (F.13)-(F.16),

$$\begin{aligned}
D_{+n} &= (pk_{fz_a}^{(u)} - \ell k_{fz_a}^{(v)} + \beta_{z_n}) (p'k_{fz_b}^{(u')*} - \ell'k_{fz_c}^{(v')*} + \beta_{z_n}) \prod_{m'=1}^{N_1} (\beta_{z_n} - \beta_{z_{m'}}) (\beta_{z_n} - \beta_{z_{m'}}^*) \times \\
& \quad \prod_{\substack{n'=1 \\ n' \neq n}}^{N_2} (\beta_{z_n} - \beta_{z_{n'}})^2 \prod_{n'=1}^{N_2} (\beta_{z_n} - \beta_{z_{n'}}^*)^2 \\
& \quad (F.13)
\end{aligned}$$

$$D_{-n} = (pk_{fz_a}^{(u)} - \ell k_{fz_a}^{(v)} + \beta_{z_n}^*) (p'k_{fz_b}^{(u')*} - \ell'k_{fz_c}^{(v')*} + \beta_{z_n}^*) \prod_{m'=1}^{N_1} (\beta_{z_n}^* - \beta_{z_{m'}}) (\beta_{z_n}^* - \beta_{z_{m'}}^*) \times$$

$$\prod_{n'=1}^{N_2} (\beta_{z_n}^* - \beta_{z_{n'}})^2 \prod_{\substack{n'=1 \\ n' \neq n}}^{N_2} (\beta_{z_n}^* - \beta_{z_{n'}}^*)^2 \quad (F.14)$$

$$\begin{aligned} D'_{+n} = & \left(pk_{fz_a}^{(u)} - \ell k_{fz_a}^{(v)} + p' k_{fz_b}^{(u')*} - \ell' k_{fz_c}^{(v')*} \right) \prod_{m'=1}^{N_1} (\beta_{z_n} - \beta_{z_{m'}}) (\beta_{z_n} - \beta_{z_{m'}}^*) \times \\ & \prod_{\substack{n'=1 \\ n' \neq n}}^{N_2} (\beta_{z_n} - \beta_{z_{n'}})^2 \prod_{n'=1}^{N_2} (\beta_{z_n} - \beta_{z_{n'}}^*)^2 \\ & + \left(pk_{fz_a}^{(u)} - \ell k_{fz_a}^{(v)} + p' k_{fz_b}^{(u')*} - \ell' k_{fz_c}^{(v')*} + 2\beta_{z_n} \right) \times \\ & \left\{ \prod_{\substack{n'=1 \\ n' \neq n}}^{N_2} (\beta_{z_n} - \beta_{z_{n'}})^2 \prod_{n'=1}^{N_2} (\beta_{z_n} - \beta_{z_{n'}}^*)^2 \sum_{m'=1}^{N_1} \left[\prod_{\substack{m''=1 \\ m'' \neq m'}}^{N_1} (\beta_{z_n} - \beta_{z_{m''}}) \prod_{m''=1}^{N_1} (\beta_{z_n} - \beta_{z_{m''}}^*) + \right. \right. \\ & \left. \left. \prod_{m''=1}^{N_1} (\beta_{z_n} - \beta_{z_{m''}}) \prod_{\substack{m''=1 \\ m'' \neq m'}}^{N_1} (\beta_{z_n} - \beta_{z_{m''}}^*) \right] \right\} \\ & + 2 \prod_{m'=1}^{N_1} (\beta_{z_n} - \beta_{z_{m'}}) (\beta_{z_n} - \beta_{z_{m'}}^*) \times \\ & \left[\sum_{\substack{n'=1 \\ n' \neq n}}^{N_2} (\beta_{z_n} - \beta_{z_{n'}}) \prod_{\substack{n''=1 \\ n'' \neq n' \\ n'' \neq n}}^{N_2} (\beta_{z_n} - \beta_{z_{n''}})^2 \prod_{n''=1}^{N_2} (\beta_{z_n} - \beta_{z_{n''}}^*)^2 + \right. \\ & \left. \sum_{n'=1}^{N_2} (\beta_{z_n} - \beta_{z_{n'}}^*) \prod_{\substack{n''=1 \\ n'' \neq n}}^{N_2} (\beta_{z_n} - \beta_{z_{n''}})^2 \prod_{\substack{n''=1 \\ n'' \neq n'}}^{N_2} (\beta_{z_n} - \beta_{z_{n''}}^*)^2 \right] \quad (F.15) \end{aligned}$$

$$\begin{aligned} D'_{-n} = & \left(pk_{fz_a}^{(u)} - \ell k_{fz_a}^{(v)} + p' k_{fz_b}^{(u')*} - \ell' k_{fz_c}^{(v')*} \right) \prod_{m'=1}^{N_1} (\beta_{z_n}^* - \beta_{z_{m'}}) (\beta_{z_n}^* - \beta_{z_{m'}}^*) \times \\ & \prod_{n'=1}^{N_2} (\beta_{z_n}^* - \beta_{z_{n'}})^2 \prod_{\substack{n'=1 \\ n' \neq n}}^{N_2} (\beta_{z_n}^* - \beta_{z_{n'}}^*)^2 \\ & + \left(pk_{fz_a}^{(u)} - \ell k_{fz_a}^{(v)} + p' k_{fz_b}^{(u')*} - \ell' k_{fz_c}^{(v')*} + 2\beta_{z_n}^* \right) \times \\ & \left\{ \prod_{n'=1}^{N_2} (\beta_{z_n}^* - \beta_{z_{n'}})^2 \prod_{\substack{n'=1 \\ n' \neq n}}^{N_2} (\beta_{z_n}^* - \beta_{z_{n'}}^*)^2 \sum_{m'=1}^{N_1} \left[\prod_{\substack{m''=1 \\ m'' \neq m'}}^{N_1} (\beta_{z_n}^* - \beta_{z_{m''}}) \prod_{m''=1}^{N_1} (\beta_{z_n}^* - \beta_{z_{m''}}^*) + \right. \right. \end{aligned}$$

$$\begin{aligned}
& \prod_{m''=1}^{N_1} (\beta_{z_n}^* - \beta_{z_{m''}}) \prod_{\substack{m''=1 \\ m'' \neq m'}}^{N_1} (\beta_{z_n}^* - \beta_{z_{m''}}^*) \Big] \\
& + 2 \prod_{m'=1}^{N_1} (\beta_{z_n}^* - \beta_{z_{m'}}) (\beta_{z_n}^* - \beta_{z_{m'}}^*) \times \\
& \left[\sum_{n'=1}^{N_2} (\beta_{z_n}^* - \beta_{z_{n'}}) \prod_{\substack{n''=1 \\ n'' \neq n'}}^{N_2} (\beta_{z_n}^* - \beta_{z_{n''}})^2 \prod_{\substack{n''=1 \\ n'' \neq n}}^{N_2} (\beta_{z_n}^* - \beta_{z_{n''}}^*)^2 + \right. \\
& \left. \sum_{\substack{n'=1 \\ n' \neq n}}^{N_2} (\beta_{z_n}^* - \beta_{z_{n'}}) \prod_{n''=1}^{N_2} (\beta_{z_n}^* - \beta_{z_{n''}})^2 \prod_{\substack{n''=1 \\ n'' \neq n'}}^{N_2} (\beta_{z_n}^* - \beta_{z_{n''}}^*)^2 \right] \Big\} \quad (F.16)
\end{aligned}$$

and where N_{+n} , N_{-n} , N'_{+n} , and N'_{-n} are given by (F.17)-(F.20).

$$N_{+n} = 1 - e^{i(p k_{fz_{as}}^{(u)} - \ell k_{fz_a}^{(v)} + \beta_{z_n})h_f} + e^{i(p k_{fz_{as}}^{(u)} - \ell k_{fz_a}^{(v)} + \ell' k_{fz_c}^{(v')*} - p' k_{fz_{bs}}^{(u')*})h_f} \quad (F.17)$$

$$N_{-n} = e^{-i(p' k_{fz_{bs}}^{(u')*} - \ell' k_{fz_c}^{(v')*} + \beta_{z_n}^*)h_f} \quad (F.18)$$

$$N'_{+n} = -i h_f e^{i(p k_{fz_{as}}^{(u)} - \ell k_{fz_a}^{(v)} + \beta_{z_n})h_f} \quad (F.19)$$

$$N'_{-n} = -i h_f e^{-i(p' k_{fz_{bs}}^{(u')*} - \ell' k_{fz_c}^{(v')*} + \beta_{z_n}^*)h_f} \quad (F.20)$$

Hence, the desired expression for the correlation is found by summing all of the above residue contributions.

$$\sigma_{TC-TC}^{\hat{p}_a \hat{p}_b} = \sum_{\substack{s, p, q, \ell, \\ s', p', q', \ell' = +, -}} \sum_{\substack{u, v, w, \\ u', v', w' = TE, TM}} \sum_{\alpha, \beta, \gamma, \rho = x, y, z} \iint d\bar{k}_{\perp a} (2\pi)^4 A_{TC-TC}^{\substack{\alpha\beta\gamma\rho \\ pp'ss'qq'\ell\ell' \\ uu'vv'ww'}} \times$$

$$\begin{aligned}
& e^{i(\bar{k}_{\perp ai} - \bar{k}_{\perp bi} + \bar{k}_{\perp bs} - \bar{k}_{\perp as}) \cdot \bar{r}_{T\perp}} e^{-i(sk_{iz ai}^{(w)} + qk_{iz a}^{(v)} - s'k_{iz bi}^{(w')} - q'k_{iz c}^{(v')})z_T} \times \\
& e^{-i(\ell k_{fz a}^{(v)} - pk_{fz a}^{(u)} + p'k_{fz b}^{(u')} - \ell'k_{fz c}^{(v')})d_{f-1}} \times \\
& [R_{P1} + R_{P2} + R_{S1} + R_{S2}^+ + R_{S2}^-] \quad (F.21)
\end{aligned}$$

The derivation of the complex β_z integration for the other two correlations is similar, and is not presented here. The final results for all three statistics are given in the next section.

F.2. Correlation of Scattered Field Components

The following section gives the final expressions for all of the correlations of the two multi-path scattering components. The function $R_{S1}(\bar{\beta}_{\perp}, \beta_{P1}, \beta_{P2}, h)$ used in the results which follow is defined by (F.22),

$$\begin{aligned}
R_{S1}(\bar{\beta}_{\perp}, \beta_{P1}, \beta_{P2}, h) = & \sum_{m=1}^{N_1} \left\{ \frac{(1 - e^{i(\beta_{zm} - \beta_{P1})h} + e^{i(\beta_{P2} - \bar{\beta}_{\perp 1})h})}{(\beta_{zm} - \beta_{P1})(\beta_{zm} - \beta_{P2}) \prod_{\substack{m'=1 \\ m' \neq m}}^{N_1} (\beta_{zm} - \beta_{zm'})} \times \right. \\
& \frac{\Phi_N(\bar{\beta}_{\perp}, \beta_{zm})}{\prod_{m'=1}^{N_1} (\beta_{zm} - \beta_{zm'}^*) \prod_{n'=1}^{N_2} (\beta_{zm} - \beta_{zn'})^2 (\beta_{zm} - \beta_{zn'}^*)^2} + \\
& \frac{e^{-i(\beta_{zm}^* - \beta_{P2})h}}{(\beta_{zm}^* - \beta_{P1})(\beta_{zm}^* - \beta_{P2}) \prod_{m'=1}^{N_1} (\beta_{zm}^* - \beta_{zm'})} \times \\
& \left. \frac{\Phi_N(\bar{\beta}_{\perp}, \beta_{zm}^*)}{\prod_{\substack{m'=1 \\ m' \neq m}}^{N_1} (\beta_{zm}^* - \beta_{zm'}^*) \prod_{n'=1}^{N_2} (\beta_{zm}^* - \beta_{zn'})^2 (\beta_{zm}^* - \beta_{zn'}^*)^2} \right\} \quad (F.22)
\end{aligned}$$

where N_1 and N_2 are respectively the number of first and second order pole pairs of the spectral function $\Phi_{\alpha\beta\gamma\rho}(\bar{\beta})$, and where these poles are given by β_{z_n} and $\beta_{z_n}^*$ for the first order poles, and by β_{z_n} and $\beta_{z_n}^*$ for the second order poles. Similarly, the function $R_{S2}(\bar{\beta}_\perp, \beta_{P1}, \beta_{P2}, h)$ is given by (F.23),

$$\begin{aligned}
 R_{S2}(\bar{\beta}_\perp, \beta_{P1}, \beta_{P2}, h) = & \sum_{n=1}^{N_2} \frac{1}{D_{+n}^2} \left\{ D_{+n} \left[\Phi'_N(\bar{\beta}_\perp, \beta_{z_n}) N_{+n} + \Phi_N(\bar{\beta}_\perp, \beta_{z_n}) N'_{+n} \right] - \right. \\
 & \left. D'_{+n} \Phi_N(\bar{\beta}_\perp, \beta_{z_n}) N_{+n} \right\} + \\
 & \frac{1}{D_{-n}^2} \left\{ D_{-n} \left[\Phi'_N(\bar{\beta}_\perp, \beta_{z_n}^*) N_{-n} + \Phi_N(\bar{\beta}_\perp, \beta_{z_n}^*) N'_{-n} \right] - \right. \\
 & \left. D'_{-n} \Phi_N(\bar{\beta}_\perp, \beta_{z_n}^*) N_{-n} \right\} \quad (F.23)
 \end{aligned}$$

where N_{+n} , N_{-n} , N'_{+n} , and N'_{-n} are given by (F.24)-(F.27),

$$N_{+n} = 1 - e^{i(\beta_{z_n} - \beta_{P1})h} + e^{i(\beta_{P2} - \beta_{P1})h} \quad (F.24)$$

$$N_{-n} = e^{-i(\beta_{z_n}^* - \beta_{P2})h} \quad (F.25)$$

$$N'_{+n} = -ih e^{i(\beta_{z_n} - \beta_{P1})h} \quad (F.26)$$

$$N'_{-n} = -ih e^{-i(\beta_{z_n}^* - \beta_{P2})h} \quad (F.27)$$

and where D_{+n} , D_{-n} , D'_{+n} , and D'_{-n} are given by (F.28)-(F.31).

$$D_{+n} = (\beta_{z_n} - \beta_{P1})(\beta_{z_n} - \beta_{P2}) \prod_{m'=1}^{N_1} (\beta_{z_n} - \beta_{z_{m'}}) (\beta_{z_n} - \beta_{z_{m'}}^*) \times$$

$$\prod_{\substack{n'=1 \\ n' \neq n}}^{N_2} (\beta_{z_n} - \beta_{z_{n'}})^2 \prod_{n'=1}^{N_2} (\beta_{z_n} - \beta_{z_{n'}}^*)^2 \quad (F.28)$$

$$D_{-n} = (\beta_{z_n}^* - \beta_{P1})(\beta_{z_n}^* - \beta_{P2}) \prod_{m'=1}^{N_1} (\beta_{z_n}^* - \beta_{z_{m'}}) (\beta_{z_n}^* - \beta_{z_{m'}}^*) \times$$

$$\prod_{n'=1}^{N_2} (\beta_{z_n}^* - \beta_{z_{n'}})^2 \prod_{\substack{n'=1 \\ n' \neq n}}^{N_2} (\beta_{z_n}^* - \beta_{z_{n'}}^*)^2 \quad (F.29)$$

$$D'_{+n} = -(\beta_{P1} + \beta_{P2}) \prod_{m'=1}^{N_1} (\beta_{z_n} - \beta_{z_{m'}}) (\beta_{z_n} - \beta_{z_{m'}}^*) \prod_{\substack{n'=1 \\ n' \neq n}}^{N_2} (\beta_{z_n} - \beta_{z_{n'}})^2 \prod_{n'=1}^{N_2} (\beta_{z_n} - \beta_{z_{n'}}^*)^2 +$$

$$(2\beta_{z_n} - \beta_{P1} - \beta_{P2}) \left\{ \prod_{\substack{n'=1 \\ n' \neq n}}^{N_2} (\beta_{z_n} - \beta_{z_{n'}})^2 \prod_{n'=1}^{N_2} (\beta_{z_n} - \beta_{z_{n'}}^*)^2 \times \right.$$

$$\sum_{m'=1}^{N_1} \left[\prod_{\substack{m''=1 \\ m'' \neq m'}}^{N_1} (\beta_{z_n} - \beta_{z_{m''}}) \prod_{m''=1}^{N_2} (\beta_{z_n} - \beta_{z_{m''}}^*) + \right.$$

$$\left. \prod_{m''=1}^{N_2} (\beta_{z_n} - \beta_{z_{m''}}) \prod_{\substack{m''=1 \\ m'' \neq m'}}^{N_1} (\beta_{z_n} - \beta_{z_{m''}}^*) \right] +$$

$$2 \prod_{m'=1}^{N_1} (\beta_{z_n} - \beta_{z_{m'}}) (\beta_{z_n} - \beta_{z_{m'}}^*) \times$$

$$\left[\sum_{\substack{n'=1 \\ n' \neq n}}^{N_2} (\beta_{z_n} - \beta_{z_{n'}}) \prod_{\substack{n''=1 \\ n'' \neq n' \\ n'' \neq n}}^{N_2} (\beta_{z_n} - \beta_{z_{n''}})^2 \prod_{n''=1}^{N_2} (\beta_{z_n} - \beta_{z_{n''}}^*)^2 + \right.$$

$$\left. \sum_{n'=1}^{N_2} (\beta_{z_n} - \beta_{z_{n'}}^*) \prod_{\substack{n''=1 \\ n'' \neq n'}}^{N_2} (\beta_{z_n} - \beta_{z_{n''}})^2 \prod_{\substack{n''=1 \\ n'' \neq n'}}^{N_2} (\beta_{z_n} - \beta_{z_{n''}}^*)^2 \right] \Big\} \quad (F.30)$$

$$D'_{-n} = -(\beta_{P1} + \beta_{P2}) \prod_{m'=1}^{N_1} (\beta_{z_n}^* - \beta_{z_{m'}}) (\beta_{z_n}^* - \beta_{z_{m'}}^*) \times$$

$$\begin{aligned}
& \prod_{n'=1}^{N_2} (\beta_{z_n}^* - \beta_{z_{n'}})^2 \prod_{\substack{n'=1 \\ n' \neq n}}^{N_2} (\beta_{z_n}^* - \beta_{z_{n'}}^*)^2 + \\
& (2\beta_{z_n}^* - \beta_{P1} - \beta_{P2}) \left\{ \prod_{n'=1}^{N_2} (\beta_{z_n}^* - \beta_{z_{n'}})^2 \prod_{\substack{n'=1 \\ n' \neq n}}^{N_2} (\beta_{z_n}^* - \beta_{z_{n'}}^*)^2 \times \right. \\
& \sum_{m'=1}^{N_1} \left[\prod_{\substack{m''=1 \\ m'' \neq m'}}^{N_1} (\beta_{z_n}^* - \beta_{z_{m''}}) \prod_{m''=1}^{N_2} (\beta_{z_n}^* - \beta_{z_{m''}}^*) + \right. \\
& \left. \prod_{m''=1}^{N_2} (\beta_{z_n}^* - \beta_{z_{m''}}) \prod_{\substack{m''=1 \\ m'' \neq m'}}^{N_1} (\beta_{z_n}^* - \beta_{z_{m''}}^*) \right] + \\
& 2 \prod_{m'=1}^{N_1} (\beta_{z_n}^* - \beta_{z_{m'}}) (\beta_{z_n}^* - \beta_{z_{m'}}^*) \times \\
& \left[\sum_{n'=1}^{N_2} (\beta_{z_n}^* - \beta_{z_{n'}}) \prod_{\substack{n''=1 \\ n'' \neq n'}}^{N_2} (\beta_{z_n}^* - \beta_{z_{n''}})^2 \prod_{\substack{n''=1 \\ n'' \neq n}}^{N_2} (\beta_{z_n}^* - \beta_{z_{n''}}^*)^2 + \right. \\
& \left. \sum_{\substack{n'=1 \\ n' \neq n}}^{N_2} (\beta_{z_n}^* - \beta_{z_{n'}}^*) \prod_{n''=1}^{N_2} (\beta_{z_n}^* - \beta_{z_{n''}})^2 \prod_{\substack{n''=1 \\ n'' \neq n'}}^{N_2} (\beta_{z_n}^* - \beta_{z_{n''}}^*)^2 \right] \Big\} \quad (F.31)
\end{aligned}$$

Finally, the function $R_P(\bar{\beta}_\perp, \beta_{P1}, \beta_{P2}, h)$ is given by (F.32).

$$R_P(\bar{\beta}_\perp, \beta_{P1}, \beta_{P2}, h) = \frac{\Phi_{\alpha\beta\gamma\rho}(\bar{\beta}_\perp, \beta_{P2})}{\beta_{P2} - \beta_{P1}} - \frac{\Phi_{\alpha\beta\gamma\rho}(\bar{\beta}_\perp, \beta_{P1})}{\beta_{P2} - \beta_{P1}} e^{i(\beta_{P2} - \beta_{P1})h} \quad (F.32)$$

The correlations are now defined in terms of the above functions.

F.2.1. Target/Clutter - Target/Clutter Correlation

$$\begin{aligned}
\sigma_{TC-TC}^{\hat{p}_a \hat{p}_b}(\bar{k}_{as}, \bar{k}_{ai}, \bar{k}_{bs}, \bar{k}_{bi}) &= 4\pi r^2 \langle \hat{p}_a \cdot \bar{E}_{TC}(\bar{k}_{as}, \bar{k}_{ai}) \times \hat{p}_b^* \cdot \bar{E}_{TC}^*(\bar{k}_{bs}, \bar{k}_{bi}) \rangle \\
&= (2\pi)^5 i \sum_{\substack{p', s', q', \ell' = +, - \\ p', s', q', \ell' = +, -}} \sum_{\substack{u, v, w, \\ u', v', w' = TE, TM}} \sum_{\alpha, \beta, \gamma, \rho = x, y, z} \iint d\bar{k}_{\perp a} A_{TC-TC}^{\alpha\beta\gamma\rho}{}_{pp'ss'qq'\ell\ell'}{}_{uu'vv'ww'} \times \\
&\quad e^{i(\bar{k}_{\perp ai} - \bar{k}_{\perp bi} + \bar{k}_{\perp bs} - \bar{k}_{\perp as}) \cdot \bar{r}_{T\perp}} e^{-i(sk_{\perp ai}^{(w)} + qk_{\perp ai}^{(v)} - s'k_{\perp bi}^{(w')*} - q'k_{\perp bi}^{(v')*})z_T} \times \\
&\quad e^{-i(\ell k_{\perp as}^{(v)} - pk_{\perp as}^{(u)} - \ell'k_{\perp as}^{(v')*} + p'k_{\perp as}^{(u')*})d_{f-1}} \times \\
&\quad \left[R_P(\bar{k}_{\perp a} - \bar{k}_{\perp as}, \ell k_{\perp as}^{(v)} - pk_{\perp as}^{(u)}, \ell'k_{\perp as}^{(v')*} - p'k_{\perp as}^{(u')*}, h_f) + \right. \\
&\quad R_{S1}(\bar{k}_{\perp a} - \bar{k}_{\perp as}, \ell k_{\perp as}^{(v)} - pk_{\perp as}^{(u)}, \ell'k_{\perp as}^{(v')*} - p'k_{\perp as}^{(u')*}, h_f) + \\
&\quad \left. R_{S2}(\bar{k}_{\perp a} - \bar{k}_{\perp as}, \ell k_{\perp as}^{(v)} - pk_{\perp as}^{(u)}, \ell'k_{\perp as}^{(v')*} - p'k_{\perp as}^{(u')*}, h_f) \right] \quad (F.33)
\end{aligned}$$

where

$$\bar{k}_{\perp c} = \bar{k}_{\perp a} + \bar{k}_{\perp bs} - \bar{k}_{\perp as} \quad (F.34)$$

and

$$\begin{aligned}
A_{TC-TC}^{\alpha\beta\gamma\rho}{}_{pp'ss'qq'\ell\ell'}{}_{uu'vv'ww'} &= \frac{|\alpha'|^2}{4\pi} \left[\hat{p}_a \cdot \bar{H}_{0fp}^{(u)}(\bar{k}_{\perp as}) \right]_{\alpha} \cdot \left[\bar{F}_{ft\ell q}^{(v)}(\bar{k}_{\perp a}) \cdot \bar{E}_{tai}^{s,(w)} \right]_{\beta} \times \\
&\quad \left[\hat{p}_b \cdot \bar{H}_{0fp'}^{(u')}(\bar{k}_{\perp bs}) \right]_{\gamma}^* \cdot \left[\bar{F}_{ft\ell' q'}^{(v')}(\bar{k}_{\perp c}) \cdot \bar{E}_{tbi}^{s',(w')} \right]_{\rho}^* \quad (F.35)
\end{aligned}$$

F.2.2. Clutter/Target - Clutter/Target Correlation

$$\begin{aligned}
\sigma_{CT-CT}^{\hat{p}_a \hat{p}_b}(\bar{k}_{as}, \bar{k}_{ai}, \bar{k}_{bs}, \bar{k}_{bi}) &= 4\pi r^2 \langle \hat{p}_a \cdot \bar{E}_{CT}(\bar{k}_{as}, \bar{k}_{ai}) \times \hat{p}_b^* \cdot \bar{E}_{CT}^*(\bar{k}_{bs}, \bar{k}_{bi}) \rangle \\
&= (2\pi)^5 i \sum_{\substack{p,s,q,\ell, \\ p',s',q',\ell'=+,-}} \sum_{\substack{u,v,w, \\ u',v',w'=TE, TM}} \sum_{\alpha,\beta,\gamma,\rho=x,y,z} \iint d\bar{k}_{\perp a} A_{CT-CT}^{\alpha\beta\gamma\rho}{}_{\substack{pp'ss'qq'\ell\ell' \\ uu'vv'ww'}} \times \\
&\quad e^{i(\bar{k}_{\perp ai} - \bar{k}_{\perp bi} + \bar{k}_{\perp bs} - \bar{k}_{\perp as}) \cdot \bar{r}_{T\perp}} e^{i(\ell k_{\perp a}^{(v)} - p k_{\perp as}^{(u)} - \ell' k_{\perp c}^{(v')*} + p' k_{\perp bs}^{(u')*}) z_T} \times \\
&\quad e^{i(s k_{fz ai}^{(w)} + q k_{fz a}^{(v)} - s' k_{fz bi}^{(w')*} - q' k_{fz c}^{(v')*}) d_f - 1} \times \\
&\quad \left[R_P(\bar{k}_{\perp ai} - \bar{k}_{\perp a}, -q k_{fz a}^{(v)} - s k_{fz ai}^{(w)}, -q' k_{fz c}^{(v')*} - s' k_{fz bi}^{(w')*}, h_f) + \right. \\
&\quad R_{S1}(\bar{k}_{\perp ai} - \bar{k}_{\perp a}, -q k_{fz a}^{(v)} - s k_{fz ai}^{(w)}, -q' k_{fz c}^{(v')*} - s' k_{fz bi}^{(w')*}, h_f) + \\
&\quad \left. R_{S2}(\bar{k}_{\perp ai} - \bar{k}_{\perp a}, -q k_{fz a}^{(v)} - s k_{fz ai}^{(w)}, -q' k_{fz c}^{(v')*} - s' k_{fz bi}^{(w')*}, h_f) \right] \quad (F.36)
\end{aligned}$$

where

$$\bar{k}_{\perp c} = \bar{k}_{\perp a} + \bar{k}_{\perp bi} - \bar{k}_{\perp ai} \quad (F.37)$$

and

$$\begin{aligned}
A_{CT-CT}^{\alpha\beta\gamma\rho}{}_{\substack{pp'ss'qq'\ell\ell' \\ uu'vv'ww'}} &= \frac{|\alpha'|^2}{4\pi} \left[\hat{p}_a \cdot \bar{H}_{0t_p}^{(u)}(\bar{k}_{\perp as}) \cdot \bar{F}_{tf_{\ell q}}^{(v)}(\bar{k}_{\perp a}) \right]_{\alpha} \cdot \left[\bar{E}_{fai}^{s,(w)} \right]_{\beta} \times \\
&\quad \left[\hat{p}_b \cdot \bar{H}_{0t_{p'}}^{(u')}(\bar{k}_{\perp bs}) \cdot \bar{F}_{tf_{\ell' q'}}^{(v')}(\bar{k}_{\perp c}) \right]_{\gamma}^* \cdot \left[\bar{E}_{fbi}^{s',(w')} \right]_{\rho}^* \quad (F.38)
\end{aligned}$$

F.2.3. Target/Clutter - Clutter/Target Correlation

$$\begin{aligned}
\sigma_{TC-CT}^{\hat{p}_a \hat{p}_b}(\bar{k}_{as}, \bar{k}_{ai}, \bar{k}_{bs}, \bar{k}_{bi}) &= 4\pi r^2 \langle \hat{p}_a \cdot \bar{E}_{TC}(\bar{k}_{as}, \bar{k}_{ai}) \times \hat{p}_b^* \cdot \bar{E}_{CT}^*(\bar{k}_{bs}, \bar{k}_{bi}) \rangle \\
&= (2\pi)^5 i \sum_{\substack{p', s', q', \ell', \\ p', s', q', \ell' = +, -}} \sum_{\substack{u', v', w', \\ u', v', w' = TE, TM}} \sum_{\alpha, \beta, \gamma, \rho = x, y, z} \iint d\bar{k}_{\perp a} A_{TC-CT}^{\alpha\beta\gamma\rho, pp's's'qq'\ell\ell'} \times \\
&\quad e^{i(\bar{k}_{\perp ai} - \bar{k}_{\perp bi} + \bar{k}_{\perp bs} - \bar{k}_{\perp as}) \cdot \bar{r}_{T\perp}} e^{-i(s k_{iz_{ai}}^{(w)} + q k_{iz_a}^{(v)} + \ell' k_{iz_c}^{(v')*} - p' k_{iz_{bs}}^{(u')*}) z_T} \times \\
&\quad e^{-i(\ell k_{fz_a}^{(v)} - p k_{fz_{as}}^{(u)} + s' k_{fz_{bi}}^{(w')*} + q' k_{fz_c}^{(v')*}) d_{f-1}} \times \\
&\quad \left[R_P(\bar{k}_{\perp a} - \bar{k}_{\perp as}, \ell k_{fz_a}^{(v)} - p k_{fz_{as}}^{(u)}, -q' k_{fz_c}^{(v')*} - s' k_{fz_{bi}}^{(w')*}, h_f) + \right. \\
&\quad R_{S1}(\bar{k}_{\perp a} - \bar{k}_{\perp as}, \ell k_{fz_a}^{(v)} - p k_{fz_{as}}^{(u)}, -q' k_{fz_c}^{(v')*} - s' k_{fz_{bi}}^{(w')*}, h_f) + \\
&\quad \left. R_{S2}(\bar{k}_{\perp a} - \bar{k}_{\perp as}, \ell k_{fz_a}^{(v)} - p k_{fz_{as}}^{(u)}, -q' k_{fz_c}^{(v')*} - s' k_{fz_{bi}}^{(w')*}, h_f) \right] \quad (F.39)
\end{aligned}$$

where

$$\bar{k}_{\perp c} = \bar{k}_{\perp as} + \bar{k}_{\perp bi} - \bar{k}_{\perp a} \quad (F.40)$$

and

$$\begin{aligned}
A_{TC-CT}^{\alpha\beta\gamma\rho, pp's's'qq'\ell\ell'} &= \frac{|\alpha'|^2}{4\pi} \left[\hat{p}_a \cdot \bar{H}_{0f_p}^{(u)}(\bar{k}_{\perp as}) \right]_{\alpha} \cdot \left[\bar{F}_{ft_{\ell q}}^{(v)}(\bar{k}_{\perp a}) \cdot \bar{E}_{tai}^{s, (w)} \right]_{\beta} \times \\
&\quad \left[\hat{p}_b \cdot \bar{H}_{0t_{p'}}^{(u')}(\bar{k}_{\perp bs}) \cdot \bar{F}_{tf_{\ell' q'}}^{(v')}(\bar{k}_{\perp c}) \right]_{\gamma}^* \cdot \left[\bar{E}_{fbi}^{s', (w')} \right]_{\rho}^* \quad (F.41)
\end{aligned}$$

Appendix G

Incoherent Field Correlation for a Point Target and Layered Continuous Random Media with the Target in the Uniaxial Random Layer ($t = f$)

This Appendix gives the expressions for the correlation of the multi-path incoherent target return for a stratified multi-layer uniaxial random media with a single layer of continuous random media, and with the point scatterer target located in this layer. The derivation given here assumes that an effective permittivity for the random media is calculated in the absence of the target, and then the target is placed in the effective media without changing the mean permittivity in its vicinity. For any realistic target, a more rigorous approach would yield an effective permittivity which changes over an electrically small distance surrounding the target. This effect is similar to the fluctuation of effective permittivity experienced near the boundaries of a bounded random layer, which is neglected throughout this work. The boundary region which is affected by this effect is small in comparison to the overall random region, and, therefore, this small permittivity gradient can safely be neglected for the layer boundaries. In contrast, however, despite the small size of this region surrounding the target, because it is close to the target, it may affect the target scattered field, which for the point target here is dependant on the incident field in its vicinity. To avoid this possibility, it is assumed that the target is a true point target in that it occupies no volume which would

displace random media, and that it is a single scatterer in that the field scattered by the target will not scatter off the nearby random inhomogeneities to be re-incident on the target and subsequently scatter again. Under these approximations, the effective permittivity of the region surrounding the target will be unaffected by the presence of the target, and can be assumed to be spatially homogeneous.

The first section derives the expression for the scattered field correlation for the target/clutter multi-path return. The derivations of the other two correlations are similar, and are not presented here. The final results for all three correlations, however, are given in the last section.

G.1. Derivation of the Incoherent Field Correlation

In this section, the autocorrelation of the target/clutter scattered field is derived for the case where the target is located in the same region as the random media. As noted above, the derivations of the other two correlation terms are similar and are not presented here. The correlation σ_{TC-TC} is given by (4.11), and is repeated here for the case $t = f$.

$$\begin{aligned}\sigma_{TC-TC}^{\hat{p}_a \hat{p}_b}(\bar{k}_{as}, \bar{k}_{ai}, \bar{k}_{bs}, \bar{k}_{bi}) &= 4\pi r^2 \langle \hat{p}_a \cdot \bar{E}_{TC}(\bar{k}_{as}, \bar{k}_{ai}) \times \hat{p}_b^* \cdot \bar{E}_{TC}^*(\bar{k}_{bs}, \bar{k}_{bi}) \rangle \\ &= 4\pi r^2 |\alpha'|^2 \int d\bar{r}_1 \int_{V_f} d\bar{r}_2 \int d\bar{r}_3 \int_{V_f} d\bar{r}_4 \left\langle \hat{p}_a \cdot \bar{G}_{0t}^a(\bar{r}, \bar{r}_2) \cdot \bar{Q}(\bar{r}_2) \cdot \right. \\ &\quad \left. \bar{G}_{tt}^a(\bar{r}_2, \bar{r}_1) \cdot \bar{E}_{tai}(\bar{r}_1) \delta(\bar{r}_1 - \bar{r}_T) \times \hat{p}_b^* \cdot \bar{G}_{0t}^{b*}(\bar{r}, \bar{r}_4) \cdot \bar{Q}^*(\bar{r}_4) \cdot \right.\end{aligned}$$

$$\left\langle \overline{G}_{tt}^{b*}(\bar{r}_4, \bar{r}_3) \cdot \overline{E}_{t_{bi}}^*(\bar{r}_3) \delta(\bar{r}_3 - \bar{r}_T) \right\rangle \quad (G.1)$$

The complication in evaluating the above arises because $\overline{G}_{tt}(\bar{r}, \bar{r}')$ has different forms for the observation point above the source and for the observation point below the source. Hence, the integration over the random media must be split into a region above the target, and a region beneath the target. In addition, the Green's function contains a singularity term which treats the co-situation of source and observation point at the target. Thus, where the above correlation contained only one term for a target and random media in different regions, it will now contain nine separate terms. The nine terms are given individually below.

$$\begin{aligned} \sigma_{TC-TC}^{UU} = \lim_{\delta_z \rightarrow 0} 4\pi r^2 |\alpha'|^2 \int_{z_T + \delta_z}^{-d_f - 1} dz_2 \int_{z_T + \delta_z}^{-d_f - 1} dz_4 \iint d\bar{r}_{2\perp} \iint d\bar{r}_{4\perp} \\ \left\langle \hat{p}_a \cdot \overline{G}_{0t}^a(\bar{r}, \bar{r}_2) \cdot \overline{Q}(\bar{r}_2) \cdot \overline{G}_{tU}^a(\bar{r}_2, \bar{r}_T) \cdot \overline{E}_{t_{ai}}(\bar{r}_T) \times \right. \\ \left. \hat{p}_b^* \cdot \overline{G}_{0t}^{b*}(\bar{r}, \bar{r}_4) \cdot \overline{Q}^*(\bar{r}_4) \cdot \overline{G}_{tU}^{b*}(\bar{r}_4, \bar{r}_T) \cdot \overline{E}_{t_{bi}}^*(\bar{r}_T) \right\rangle \quad (G.2) \end{aligned}$$

$$\begin{aligned} \sigma_{TC-TC}^{nn} = \lim_{\delta_z \rightarrow 0} 4\pi r^2 |\alpha'|^2 \int_{-d_f}^{z_T - \delta_z} dz_2 \int_{-d_f}^{z_T - \delta_z} dz_4 \iint d\bar{r}_{2\perp} \iint d\bar{r}_{4\perp} \\ \left\langle \hat{p}_a \cdot \overline{G}_{0t}^a(\bar{r}, \bar{r}_2) \cdot \overline{Q}(\bar{r}_2) \cdot \overline{G}_{t\cap}^a(\bar{r}_2, \bar{r}_T) \cdot \overline{E}_{t_{ai}}(\bar{r}_T) \times \right. \\ \left. \hat{p}_b^* \cdot \overline{G}_{0t}^{b*}(\bar{r}, \bar{r}_4) \cdot \overline{Q}^*(\bar{r}_4) \cdot \overline{G}_{t\cap}^{b*}(\bar{r}_4, \bar{r}_T) \cdot \overline{E}_{t_{bi}}^*(\bar{r}_T) \right\rangle \quad (G.3) \end{aligned}$$

$$\sigma_{TC-TC}^{un} = \lim_{\delta_z \rightarrow 0} 4\pi r^2 |\alpha'|^2 \int_{z_T + \delta_z}^{-d_f - 1} dz_2 \int_{-d_f}^{z_T - \delta_z} dz_4 \iint d\bar{r}_{2\perp} \iint d\bar{r}_{4\perp}$$

$$\begin{aligned}
& \left\langle \hat{p}_a \cdot \overline{G}_{0t}^a(\bar{r}, \bar{r}_2) \cdot \overline{Q}(\bar{r}_2) \cdot \overline{G}_{t\cup}^a(\bar{r}_2, \bar{r}_T) \cdot \overline{E}_{tai}(\bar{r}_T) \times \right. \\
& \left. \hat{p}_b^* \cdot \overline{G}_{0t}^{b*}(\bar{r}, \bar{r}_4) \cdot \overline{Q}^*(\bar{r}_4) \cdot \overline{G}_{t\cap}^{b*}(\bar{r}_4, \bar{r}_T) \cdot \overline{E}_{tbi}^*(\bar{r}_T) \right\rangle \quad (G.4)
\end{aligned}$$

$$\begin{aligned}
\sigma_{TC-TC}^{\cap\cup} &= \lim_{\delta_z \rightarrow 0} 4\pi r^2 |\alpha'|^2 \int_{-d_f}^{z_T - \delta_z} dz_2 \int_{z_T + \delta_z}^{-d_f - 1} dz_4 \iint d\bar{r}_{2\perp} \iint d\bar{r}_{4\perp} \\
& \left\langle \hat{p}_a \cdot \overline{G}_{0t}^a(\bar{r}, \bar{r}_2) \cdot \overline{Q}(\bar{r}_2) \cdot \overline{G}_{t\cap}^a(\bar{r}_2, \bar{r}_T) \cdot \overline{E}_{tai}(\bar{r}_T) \times \right. \\
& \left. \hat{p}_b^* \cdot \overline{G}_{0t}^{b*}(\bar{r}, \bar{r}_4) \cdot \overline{Q}^*(\bar{r}_4) \cdot \overline{G}_{t\cup}^{b*}(\bar{r}_4, \bar{r}_T) \cdot \overline{E}_{tbi}^*(\bar{r}_T) \right\rangle \quad (G.5)
\end{aligned}$$

$$\begin{aligned}
\sigma_{TC-TC}^{\bar{\cap}\bar{\cup}} &= 4\pi r^2 |\alpha'|^2 \iiint d\bar{r}_2 \iiint d\bar{r}_4 \delta(\bar{r}_2 - \bar{r}_T) \delta(\bar{r}_4 - \bar{r}_T) \times \\
& \left\langle \hat{p}_a \cdot \overline{G}_{0t}^a(\bar{r}, \bar{r}_2) \cdot \overline{Q}(\bar{r}_2) \cdot \overline{D}_t^a \cdot \overline{E}_{tai}(\bar{r}_T) \times \right. \\
& \left. \hat{p}_b^* \cdot \overline{G}_{0t}^{b*}(\bar{r}, \bar{r}_4) \cdot \overline{Q}^*(\bar{r}_4) \cdot \overline{D}_t^{b*} \cdot \overline{E}_{tbi}^*(\bar{r}_T) \right\rangle \quad (G.6)
\end{aligned}$$

$$\begin{aligned}
\sigma_{TC-TC}^{\cup\bar{\cap}} &= \lim_{\delta_z \rightarrow 0} 4\pi r^2 |\alpha'|^2 \int_{z_T + \delta_z}^{-d_f - 1} dz_2 \iint d\bar{r}_{2\perp} \iiint d\bar{r}_4 \delta(\bar{r}_4 - \bar{r}_T) \times \\
& \left\langle \hat{p}_a \cdot \overline{G}_{0t}^a(\bar{r}, \bar{r}_2) \cdot \overline{Q}(\bar{r}_2) \cdot \overline{G}_{t\cup}^a(\bar{r}_2, \bar{r}_T) \cdot \overline{E}_{tai}(\bar{r}_T) \times \right. \\
& \left. \hat{p}_b^* \cdot \overline{G}_{0t}^{b*}(\bar{r}, \bar{r}_4) \cdot \overline{Q}^*(\bar{r}_4) \cdot \overline{D}_t^{b*} \cdot \overline{E}_{tbi}^*(\bar{r}_T) \right\rangle \quad (G.7)
\end{aligned}$$

$$\begin{aligned}
\sigma_{TC-TC}^{\cap\bar{\cap}} &= \lim_{\delta_z \rightarrow 0} 4\pi r^2 |\alpha'|^2 \int_{-d_f}^{z_T - \delta_z} dz_2 \iint d\bar{r}_{2\perp} \iiint d\bar{r}_4 \delta(\bar{r}_4 - \bar{r}_T) \times \\
& \left\langle \hat{p}_a \cdot \overline{G}_{0t}^a(\bar{r}, \bar{r}_2) \cdot \overline{Q}(\bar{r}_2) \cdot \overline{G}_{t\cap}^a(\bar{r}_2, \bar{r}_T) \cdot \overline{E}_{tai}(\bar{r}_T) \times \right. \\
& \left. \hat{p}_b^* \cdot \overline{G}_{0t}^{b*}(\bar{r}, \bar{r}_4) \cdot \overline{Q}^*(\bar{r}_4) \cdot \overline{D}_t^{b*} \cdot \overline{E}_{tbi}^*(\bar{r}_T) \right\rangle \quad (G.8)
\end{aligned}$$

$$\begin{aligned}
\sigma_{TC-TC}^{\bar{=}\cup} = \lim_{\delta_z \rightarrow 0} 4\pi r^2 |\alpha'|^2 \iiint d\bar{r}_2 \int_{z_T+\delta_z}^{-d_f-1} dz_4 \iint d\bar{r}_{4\perp} \delta(\bar{r}_2 - \bar{r}_T) \times \\
\left\langle \hat{p}_a \cdot \bar{G}_{0t}^a(\bar{r}, \bar{r}_2) \cdot \bar{Q}(\bar{r}_2) \cdot \bar{D}_t^a \cdot \bar{E}_{tai}(\bar{r}_T) \times \right. \\
\left. \hat{p}_b^* \cdot \bar{G}_{0t}^{b*}(\bar{r}, \bar{r}_4) \cdot \bar{Q}^*(\bar{r}_4) \cdot \bar{G}_{t\cup}^{b*}(\bar{r}_4, \bar{r}_T) \cdot \bar{E}_{tbi}^*(\bar{r}_T) \right\rangle \quad (G.9)
\end{aligned}$$

$$\begin{aligned}
\sigma_{TC-TC}^{\bar{=}\cap} = \lim_{\delta_z \rightarrow 0} 4\pi r^2 |\alpha'|^2 \iiint d\bar{r}_2 \int_{-d_f}^{z_T-\delta_z} dz_4 \iint d\bar{r}_{4\perp} \delta(\bar{r}_2 - \bar{r}_T) \times \\
\left\langle \hat{p}_a \cdot \bar{G}_{0t}^a(\bar{r}, \bar{r}_2) \cdot \bar{Q}(\bar{r}_2) \cdot \bar{D}_t^a \cdot \bar{E}_{tai}(\bar{r}_T) \times \right. \\
\left. \hat{p}_b^* \cdot \bar{G}_{0t}^{b*}(\bar{r}, \bar{r}_4) \cdot \bar{Q}^*(\bar{r}_4) \cdot \bar{G}_{t\cap}^{b*}(\bar{r}_4, \bar{r}_T) \cdot \bar{E}_{tbi}^*(\bar{r}_T) \right\rangle \quad (G.10)
\end{aligned}$$

The first two terms are very similar to the previous expression for the case with the target and media in two different regions, and may be evaluated in the same manner as shown below shortly. The next two terms are related by (G.11),

$$\sigma_{TC-TC}^{\hat{p}_a \hat{p}_b \cap \cup}(\bar{k}_{as}, \bar{k}_{ai}, \bar{k}_{bs}, \bar{k}_{bi}) = [\sigma_{TC-TC}^{\hat{p}_b \hat{p}_a \cup \cap}(\bar{k}_{bs}, \bar{k}_{bi}, \bar{k}_{as}, \bar{k}_{ai})]^* \quad (G.11)$$

and, hence, only one term need be evaluated. Similarly, the last four terms are related by (G.12) and (G.13).

$$\sigma_{TC-TC}^{\hat{p}_a \hat{p}_b \bar{=}\cup}(\bar{k}_{as}, \bar{k}_{ai}, \bar{k}_{bs}, \bar{k}_{bi}) = [\sigma_{TC-TC}^{\hat{p}_b \hat{p}_a \bar{=}\cup}(\bar{k}_{bs}, \bar{k}_{bi}, \bar{k}_{as}, \bar{k}_{ai})]^* \quad (G.12)$$

$$\sigma_{TC-TC}^{\hat{p}_a \hat{p}_b \bar{=}\cap}(\bar{k}_{as}, \bar{k}_{ai}, \bar{k}_{bs}, \bar{k}_{bi}) = [\sigma_{TC-TC}^{\hat{p}_b \hat{p}_a \bar{=}\cap}(\bar{k}_{bs}, \bar{k}_{bi}, \bar{k}_{as}, \bar{k}_{ai})]^* \quad (G.13)$$

In the analysis that follows each of the above terms is evaluated in turn.

G.1.1. Evaluation of σ_{TC-TC}^{UU} and σ_{TC-TC}^{NN}

Both of these terms can be calculated in the same manner as was used for the case where $t \neq f$, since the target is outside of the region of random media under consideration. Hence, the result for σ_{TC-TC}^{UU} will be similar to (F.33)-(F.35) with h_f replaced by h_t^+ in (F.33), and with an appropriate change to the Green's function of (F.35). Hence, σ_{TC-TC}^{UU} is given by (G.14),

$$\begin{aligned}
 \sigma_{TC-TC}^{UU} = & \lim_{\delta_z \rightarrow 0} (2\pi)^5 i \sum_{\substack{p,s,q,\ell, \\ p',s',q',\ell' = +, -}} \sum_{\substack{u,v,w, \\ u',v',w' = TE, TM}} \sum_{\alpha, \beta, \gamma, \rho = x, y, z} \iint d\bar{k}_{\perp a} A_{TC-TC}^{UU} \overset{\alpha\beta\gamma\rho}{pp'ss'qq'\ell\ell'} \times \\
 & e^{i(\bar{k}_{\perp ai} - \bar{k}_{\perp bi} + \bar{k}_{\perp bs} - \bar{k}_{\perp as}) \cdot \bar{r}_{T\perp}} e^{-i(sk_{tzai}^{(w)} + qk_{tza}^{(v)} - s'k_{tzb_i}^{(w')} - q'k_{tzc}^{(v')})z_T} \times \\
 & e^{-i(\ell k_{tza}^{(v)} - pk_{tza}^{(u)} - \ell'k_{tzc}^{(v')*} + p'k_{tzb_s}^{(u')*})d_t} \times \\
 & \left[R_P (\bar{k}_{\perp a} - \bar{k}_{\perp as}, \ell k_{tza}^{(v)} - pk_{tza}^{(u)}, \ell'k_{tzc}^{(v')*} - p'k_{tzb_s}^{(u')}, h_t^+) + \right. \\
 & R_{S1} (\bar{k}_{\perp a} - \bar{k}_{\perp as}, \ell k_{tza}^{(v)} - pk_{tza}^{(u)}, \ell'k_{tzc}^{(v')*} - p'k_{tzb_s}^{(u')}, h_t^+) + \\
 & \left. R_{S2} (\bar{k}_{\perp a} - \bar{k}_{\perp as}, \ell k_{tza}^{(v)} - pk_{tza}^{(u)}, \ell'k_{tzc}^{(v')*} - p'k_{tzb_s}^{(u')}, h_t^+) \right] \quad (G.14)
 \end{aligned}$$

where

$$h_t^+ = -d_{t-1} - z_T - \delta_z \quad (G.15)$$

and

$$\bar{k}_{\perp c} = \bar{k}_{\perp a} + \bar{k}_{\perp bs} - \bar{k}_{\perp as} \quad (G.16)$$

and

$$A_{TC-TC}^{\alpha\beta\gamma\rho}_{\substack{pp'ss'qq'\ell\ell' \\ uu'vv'ww' \\ uu}} = \frac{|\alpha'|^2}{4\pi} \left[\hat{p}_a \cdot \bar{H}_{0t_p}^{(u)}(\bar{k}_{\perp as}) \right]_{\alpha} \left[\bar{F}_{t\cup\ell_q}^{(v)}(\bar{k}_{\perp a}) \cdot \bar{E}_{tai}^{s,(w)} \right]_{\beta} \times \\ \left[\hat{p}_b \cdot \bar{H}_{0t_{p'}}^{(u')}(\bar{k}_{\perp bs}) \right]_{\gamma}^* \left[\bar{F}_{t\cup\ell'q'}^{(v')}(\bar{k}_{\perp c}) \cdot \bar{E}_{tbi}^{s',(w')} \right]_{\rho}^* \quad (G.17)$$

Similarly, $\sigma_{TC-TC}^{\cap\cap}$ can be found by replacing $-d_{f-1}$ with $z_T - \delta_z$ and h_f by h_t^- , and by making the appropriate change in the Green's function.

$$\sigma_{TC-TC}^{\cap\cap} = \lim_{\delta_z \rightarrow 0} (2\pi)^5 i \sum_{\substack{p',s',q',\ell', \\ p',s',q',\ell'=+,-}} \sum_{\substack{u',v',w, \\ u',v',w'=TE,TM}} \sum_{\alpha,\beta,\gamma,\rho=x,y,z} \iint d\bar{k}_{\perp a} A_{TC-TC}^{\alpha\beta\gamma\rho}_{\cap\cap} \times \\ e^{i(\bar{k}_{\perp ai} - \bar{k}_{\perp bi} + \bar{k}_{\perp bs} - \bar{k}_{\perp as}) \cdot \bar{\tau}_{T\perp}} e^{-i(s k_{tza}^{(w)} + q k_{tza}^{(v)} - s' k_{tzb}^{(w')*} - q' k_{tzc}^{(v')*}) z_T} \times \\ e^{-i(\ell k_{tza}^{(v)} - p k_{tza}^{(u)} - \ell' k_{tzc}^{(v')*} + p' k_{tzb}^{(u')*}) (z_T - \delta_z)} \times \\ \left[R_P (\bar{k}_{\perp a} - \bar{k}_{\perp as}, \ell k_{tza}^{(v)} - p k_{tza}^{(u)}, \ell' k_{tzc}^{(v')*} - p' k_{tzb}^{(u')*}, h_t^-) + \right. \\ R_{S1} (\bar{k}_{\perp a} - \bar{k}_{\perp as}, \ell k_{tza}^{(v)} - p k_{tza}^{(u)}, \ell' k_{tzc}^{(v')*} - p' k_{tzb}^{(u')*}, h_t^-) + \\ \left. R_{S2} (\bar{k}_{\perp a} - \bar{k}_{\perp as}, \ell k_{tza}^{(v)} - p k_{tza}^{(u)}, \ell' k_{tzc}^{(v')*} - p' k_{tzb}^{(u')*}, h_t^-) \right] \quad (G.18)$$

where

$$h_t^- = z_T - \delta_z + d_t \quad (G.19)$$

and

$$\bar{k}_{\perp c} = \bar{k}_{\perp a} + \bar{k}_{\perp b s} - \bar{k}_{\perp a s} \quad (G.20)$$

and

$$A_{TC-TC}^{\alpha\beta\gamma\rho, pp'ss'qq'\ell\ell', uu'vv'ww'} = \frac{|\alpha'|^2}{4\pi} \left[\hat{p}_a \cdot \bar{H}_{0t_p}^{(u)}(\bar{k}_{\perp a s}) \right]_{\alpha} \cdot \left[\bar{F}_{t\cap t_q}^{(v)}(\bar{k}_{\perp a}) \cdot \bar{E}_{tai}^{s,(w)} \right]_{\beta} \times \\ \left[\hat{p}_b \cdot \bar{H}_{0t_{p'}}^{(u')}(\bar{k}_{\perp b s}) \right]_{\gamma}^* \cdot \left[\bar{F}_{t\cap t_{q'}}^{(v')}(\bar{k}_{\perp c}) \cdot \bar{E}_{tbi}^{s',(w')} \right]_{\rho}^* \quad (G.21)$$

The functions $R_P(\bar{\beta}_{\perp}, \beta_{P1}, \beta_{P2}, h)$, $R_{S1}(\bar{\beta}_{\perp}, \beta_{P1}, \beta_{P2}, h)$, and $R_{S2}(\bar{\beta}_{\perp}, \beta_{P1}, \beta_{P2}, h)$ are all defined in (F.22)-(F.32).

G.1.2. Evaluation of $\sigma_{TC-TC}^{\cup\cap}$ and $\sigma_{TC-TC}^{\cap\cup}$

Equation (G.4) can be rewritten using the Green's function expressions of Appendix E. The $\bar{\tau}_{2\perp}$ integral can be done to yield a delta function which can then be used to eliminate the $\bar{\beta}_{\perp}$ integral. Similarly, the $\bar{\tau}_{4\perp}$ integral can be done to yield another delta function, and that can be used to trivially perform the $\bar{k}_{\perp b}$ integral. The procedure is, thus, identical to that used previously in (4.12)-(4.18) up to this stage, and the result before performing the z_2 and z_4 integrals is given below in (G.22).

$$\sigma_{TC-TC}^{\cup\cap} = \lim_{\delta_z \rightarrow 0} \sum_{\substack{p,s,q,\ell, \\ p',s',q',\ell'=+,-}} \sum_{\substack{u,v,w, \\ u',v',w'=TE,TM}} \sum_{\alpha,\beta,\gamma,\rho=x,y,z} \int_{\delta_z}^{h_i^+ + \delta_z} dz_2 \int_{-\delta_z - h_i^-}^{-\delta_z} dz_4 \iint d\bar{k}_{\perp a} \int d\beta_z$$

$$\begin{aligned}
(2\pi)^4 \Phi_{\alpha\beta\gamma\rho} (\bar{k}_{\perp a} - \bar{k}_{\perp as}, \beta_z) A_{TC-TC}^{\alpha\beta\gamma\rho}{}_{un}^{pp'ss'qq'\ell\ell'} e^{i(\bar{k}_{\perp ai} - \bar{k}_{\perp bi} + \bar{k}_{\perp bs} - \bar{k}_{\perp as}) \cdot \vec{r}_{T\perp}} \times \\
e^{-i(s k_{iz ai}^{(w)} + q k_{iz a}^{(v)} - s' k_{iz bi}^{(w')*} - q' k_{iz c}^{(v')*}) z_T} e^{i(\ell k_{iz a}^{(v)} - p k_{iz as}^{(u)} - \ell' k_{iz c}^{(v')*} + p' k_{iz bs}^{(u')*}) z_T} \times \\
e^{-i(p k_{iz as}^{(u)} - \ell k_{iz a}^{(v)} + \beta_z) z_2} e^{i(p' k_{iz bs}^{(u')*} - \ell' k_{iz c}^{(v')*} + \beta_z) z_4} \quad (G.22)
\end{aligned}$$

After performing the z_2 and z_4 integrals, the result is given by (G.23).

$$\begin{aligned}
\sigma_{TC-TC}^{un} = \lim_{\delta_z \rightarrow 0} \sum_{\substack{p', s', q', \ell', \\ p', s', q', \ell' = +, -}} \sum_{\substack{u', v', w', \\ u', v', w' = TE, TM}} \sum_{\alpha, \beta, \gamma, \rho = x, y, z} \iint d\bar{k}_{\perp a} \int d\beta_z (2\pi)^4 A_{TC-TC}^{\alpha\beta\gamma\rho}{}_{un}^{pp'ss'qq'\ell\ell'} \\
\Phi_{\alpha\beta\gamma\rho} (\bar{k}_{\perp a} - \bar{k}_{\perp as}, \beta_z) e^{i(\bar{k}_{\perp ai} - \bar{k}_{\perp bi} + \bar{k}_{\perp bs} - \bar{k}_{\perp as}) \cdot \vec{r}_{T\perp}} e^{-i(s k_{iz ai}^{(w)} + q k_{iz a}^{(v)} - s' k_{iz bi}^{(w')*} - q' k_{iz c}^{(v')*}) z_T} \times \\
e^{i(\ell k_{iz a}^{(v)} - p k_{iz as}^{(u)} - \ell' k_{iz c}^{(v')*} + p' k_{iz bs}^{(u')*}) z_T} e^{-i(p k_{iz as}^{(u)} - \ell k_{iz a}^{(v)} + p' k_{iz bs}^{(u')*} - \ell' k_{iz c}^{(v')*} + 2\beta_z) \delta_z} \times \\
\frac{\left(e^{-i(p k_{iz as}^{(u)} - \ell k_{iz a}^{(v)} + \beta_z) h_i^+} - 1 \right)}{p k_{iz as}^{(u)} - \ell k_{iz a}^{(v)} + \beta_z} \cdot \frac{\left(1 - e^{-i(p' k_{iz bs}^{(u')*} - \ell' k_{iz c}^{(v')*} + \beta_z) h_i^-} \right)}{p' k_{iz bs}^{(u')*} - \ell' k_{iz c}^{(v')*} + \beta_z} \quad (G.23)
\end{aligned}$$

The β_z integral which now must be evaluated is that given by (G.24) below.

$$\begin{aligned}
I^{un} = - \int d\beta_z \Phi_{\alpha\beta\gamma\rho} (\bar{k}_{\perp a} - \bar{k}_{\perp as}, \beta_z) e^{-i(p k_{iz as}^{(u)} - \ell k_{iz a}^{(v)} + p' k_{iz bs}^{(u')*} - \ell' k_{iz c}^{(v')*} + 2\beta_z) \delta_z} \times \\
\left[e^{-i(p k_{fz as}^{(u)} - \ell k_{fz a}^{(v)} + \beta_z) h_i^+} e^{-i(p' k_{fz bs}^{(u')*} - \ell' k_{fz c}^{(v')*} + \beta_z) h_i^-} + 1 - \right. \\
\left. e^{-i(p k_{fz as}^{(u)} - \ell k_{fz a}^{(v)} + \beta_z) h_i^+} - e^{-i(p' k_{fz bs}^{(u')*} - \ell' k_{fz c}^{(v')*} + \beta_z) h_i^-} \right] \\
\frac{1}{(p k_{fz as}^{(u)} - \ell k_{fz a}^{(v)} + \beta_z) (p' k_{fz bs}^{(u')*} - \ell' k_{fz c}^{(v')*} + \beta_z)} \quad (G.24)
\end{aligned}$$

The entire integral is convergent in the lower half-plane of complex β_z . Hence, the contour is closed at infinite radius in the lower half-plane, and the integral is given as the sum of residues for poles which lay in the lower half-plane. It appears that the integrand has two poles at $\beta_z = \ell k_{fz_a}^{(v)} - pk_{fz_a}^{(u)}$ and $\beta_z = \ell' k_{fz_c}^{(v')*} - p' k_{fz_b}^{(u')*}$. If these poles are in the upper half-plane, they will not contribute. Similarly, however, if the residues are computed for the case where these poles are in the lower half-plane, it can be seen that the contribution is zero. Hence, these two singularities are removable singularities and not poles. The only pole contributions come from the poles of $\Phi_{\alpha\beta\gamma\rho}(\bar{\beta})$, which again will be assumed to take the form of (F.4). The contribution from the first order poles is given by R_{S1}^{\cup} of (G.25).

$$R_{S1}^{\cup} = 2\pi i \sum_{m=1}^{N_1} \frac{\left(1 - e^{-i(pk_{fz_a}^{(u)} - \ell k_{fz_a}^{(v)} + \beta_{zm}^*)h_t^+}\right) \left(1 - e^{-i(p'k_{fz_b}^{(u')*} - \ell' k_{fz_c}^{(v')*} + \beta_{zm}^*)h_t^-}\right)}{(pk_{fz_a}^{(u)} - \ell k_{fz_a}^{(v)} + \beta_{zm}^*)(p'k_{fz_b}^{(u')*} - \ell' k_{fz_c}^{(v')*} + \beta_{zm}^*)} \times$$

$$\frac{\Phi_N(\bar{k}_{\perp a} - \bar{k}_{\perp a s}, \beta_{zm}^*) e^{-i(pk_{fz_a}^{(u)} - \ell k_{fz_a}^{(v)} + p'k_{fz_b}^{(u')*} - \ell' k_{fz_c}^{(v')*} + 2\beta_{zm}^*)\delta_z}}{\prod_{m'=1}^{N_1} (\beta_{zm}^* - \beta_{zm'}) \prod_{\substack{m'=1 \\ m' \neq m}}^{N_1} (\beta_{zm}^* - \beta_{zm'}) \prod_{n'=1}^{N_2} (\beta_{zm}^* - \beta_{zn'})^2 (\beta_{zm}^* - \beta_{zn'})^2}$$

(G.25)

Similarly, the contribution of the second order poles is given by (G.26),

$$R_{S2}^{\cup} = 2\pi i \sum_{n=1}^{N_2} \frac{1}{D_{-n}^2} \left\{ D_{-n} \left[\Phi'_N(\bar{k}_{\perp a} - \bar{k}_{\perp a s}, \beta_{zn}^*) N_{-n}^{\cup} + \Phi_N(\bar{k}_{\perp a} - \bar{k}_{\perp a s}, \beta_{zn}^*) N_{-n}^{\cup n'} \right] \right.$$

$$\left. - D'_{-n} \Phi_N(\bar{k}_{\perp a} - \bar{k}_{\perp a s}, \beta_{zn}^*) N_{-n}^{\cup} \right\} \quad (G.26)$$

where D_{-n} and D'_{-n} are given by (F.14) and (F.16), and where $N_{-n}^{\cup\cap}$ and $N_{-n}^{\cup\cap'}$ are given by (G.27) and (G.28).

$$N_{-n}^{\cup\cap} = \left[e^{-i(p k_{fz_{as}}^{(u)} - \ell k_{fz_a}^{(v)} + \beta_{zn}^*) \delta_z} - e^{-i(p k_{fz_{as}}^{(u)} - \ell k_{fz_a}^{(v)} + \beta_{zn}^*)(h_t^+ + \delta_z)} \right] \times \\ \left[e^{-i(p' k_{fz_{bs}}^{(u')} - \ell' k_{fz_c}^{(v')} + \beta_{zn}^*) \delta_z} - e^{-i(p' k_{fz_{bs}}^{(u')} - \ell' k_{fz_c}^{(v')} + \beta_{zn}^*)(h_t^- + \delta_z)} \right] \quad (G.27)$$

$$N_{-n}^{\cup\cap'} = i \left(h_t^- + 2\delta_z \right) e^{-i(p k_{fz_{as}}^{(u)} - \ell k_{fz_a}^{(v)} + \beta_{zn}^*) \delta_z} e^{-i(p' k_{fz_{bs}}^{(u')} - \ell' k_{fz_c}^{(v')} + \beta_{zn}^*)(h_t^- + \delta_z)} - \\ 2i\delta_z e^{-i(p k_{fz_{as}}^{(u)} - \ell k_{fz_a}^{(v)} + \beta_{zn}^*) \delta_z} e^{-i(p' k_{fz_{bs}}^{(u')} - \ell' k_{fz_c}^{(v')} + \beta_{zn}^*) \delta_z} + \\ i \left(h_t^+ + 2\delta_z \right) e^{-i(p k_{fz_{as}}^{(u)} - \ell k_{fz_a}^{(v)} + \beta_{zn}^*)(h_t^+ + \delta_z)} e^{-i(p' k_{fz_{bs}}^{(u')} - \ell' k_{fz_c}^{(v')} + \beta_{zn}^*) \delta_z} - \\ i \left(h_t^+ + h_t^- + 2\delta_z \right) e^{-i(p k_{fz_{as}}^{(u)} - \ell k_{fz_a}^{(v)} + \beta_{zn}^*)(h_t^+ + \delta_z)} e^{-i(p' k_{fz_{bs}}^{(u')} - \ell' k_{fz_c}^{(v')} + \beta_{zn}^*)(h_t^- + \delta_z)} \quad (G.28)$$

Hence, the final expression for $\sigma_{TC-TC}^{\cup\cap}$ is given by (G.29),

$$\sigma_{TC-TC}^{\cup\cap} = \lim_{\delta_z \rightarrow 0} (2\pi)^4 \sum_{\substack{p, s, q, \ell, \\ p', s', q', \ell' = +, -}} \sum_{\substack{u, v, w, \\ u', v', w' = TE, TM}} \sum_{\alpha, \beta, \gamma, \rho = x, y, z} \iint d\bar{k}_{\perp a} A_{TC-TC}^{\alpha\beta\gamma\rho}{}_{\cup\cap}^{pp'ss'qq'\ell\ell'} \times \\ e^{i(\bar{k}_{\perp ai} - \bar{k}_{\perp bi} + \bar{k}_{\perp bs} - \bar{k}_{\perp as}) \cdot \vec{r}_{T\perp}} \times \\ e^{-i(s k_{iz_{ai}}^{(w)} + q k_{iz_a}^{(v)} - s' k_{iz_{bi}}^{(w')} - q' k_{iz_c}^{(v')} + p k_{fz_{as}}^{(u)} - \ell k_{fz_a}^{(v)} + \ell' k_{fz_c}^{(v')} - p' k_{fz_{bs}}^{(u')}) z_T} \times \\ [R_{S1}^{\cup\cap} + R_{S2}^{\cup\cap}] \quad (G.29)$$

where

where

$$A_{TC-TC}^{\alpha\beta\gamma\rho, pp'ss', uu'ww'} = \frac{|\alpha'|^2}{4\pi} \left[\hat{p}_a \cdot \overline{H}_{0t_p}^{(u)}(\bar{k}_{\perp as}) \right]_{\alpha} \cdot \left[\overline{D}_t^a \cdot \overline{E}_{tai}^{s,(w)} \right]_{\beta} \times \\ \left[\hat{p}_b \cdot \overline{H}_{0t_p'}^{(u')}(\bar{k}_{\perp bs}) \right]_{\gamma}^* \cdot \left[\overline{D}_t^b \cdot \overline{E}_{tbi}^{s',(w')} \right]_{\rho}^* \quad (G.33)$$

The integration can be done straightforwardly using the two delta functions, and the desired final result is given by (G.34).

$$\sigma_{TC-TC}^{\overline{\overline{=}}} = \sum_{p,s,p',s'=+,-} \sum_{u,w,u',w'=TE,TM} \sum_{\alpha,\beta,\gamma,\rho=x,y,z} A_{TC-TC}^{\alpha\beta\gamma\rho, pp'ss', uu'ww'} C_{\alpha\beta\gamma\rho}(0) \times \\ e^{i(\bar{k}_{\perp ai} - \bar{k}_{\perp bi} + \bar{k}_{\perp bs} - \bar{k}_{\perp as}) \cdot \bar{r}_{T\perp}} e^{-i(sk_{izai}^{(w)} - s'k_{izbi}^{(w')*} + pk_{izas}^{(u)} - p'k_{izbs}^{(u')*})z_T} \quad (G.34)$$

G.1.4. Evaluation of $\sigma_{TC-TC}^{\overline{\overline{=}}}$, $\sigma_{TC-TC}^{\overline{\cap}}$, $\sigma_{TC-TC}^{\overline{\cup}}$, and $\sigma_{TC-TC}^{\overline{\cap\cup}}$

The first term to be considered is that of $\sigma_{TC-TC}^{\overline{\overline{=}}}$, which is defined by (G.7). Substituting the Green's function and incident field expressions of Appendix E yields the result of (G.35).

$$\sigma_{TC-TC}^{\overline{\overline{=}}} = \lim_{\delta_z \rightarrow 0} \sum_{\substack{p,s,q,\ell, \\ p',s'=+,-}} \sum_{\substack{u,v,w, \\ u',w'=TE,TM}} \sum_{\alpha,\beta,\gamma,\rho=x,y,z} \int_{z_T+\delta_z}^{-d_t-1} dz_2 \iint d\bar{r}_{2\perp} \iiint d\bar{r}_4 \\ \iint d\bar{k}_{\perp a} C_{\alpha\beta\gamma\rho}(\bar{r}_2 - \bar{r}_4) A_{TC-TC}^{\alpha\beta\gamma\rho, pp'ss'q\ell, uu'vw'ww'} \delta(\bar{r}_4 - \bar{r}_T) \times \\ e^{i(\bar{k}_{\perp ai} - \bar{k}_{\perp a} - \bar{k}_{\perp bi}) \cdot \bar{r}_{T\perp}} e^{-i(sk_{izai}^{(w)} + qk_{iza}^{(v)} - s'k_{izbi}^{(w')*})z_T} \times \\ e^{i(\bar{k}_{\perp a} - \bar{k}_{\perp as}) \cdot \bar{r}_{2\perp}} e^{i\bar{k}_{\perp bs} \cdot \bar{r}_{4\perp}} e^{i(\ell k_{iza}^{(v)} - pk_{iza}^{(u)})z_2} e^{ip'k_{izbs}^{(u')*}z_4} \quad (G.35)$$

where

$$A_{TC-TC}^{\alpha\beta\gamma\rho, pp'ss'qt, uu'vw w'} = \frac{|\alpha'|^2}{4\pi} \left[\hat{p}_a \cdot \overline{H}_{0t_p}^{(u)}(\bar{k}_{\perp a s}) \right]_{\alpha} \cdot \left[\overline{F}_{t \cup t_q}^{(v)}(\bar{k}_{\perp a}) \cdot \overline{E}_{t_{ai}}^{s, (w)} \right]_{\beta} \times \\ \left[\hat{p}_b \cdot \overline{H}_{0t_p'}^{(u')}(\bar{k}_{\perp b s'}) \right]_{\gamma}^* \cdot \left[\overline{D}_t^b \cdot \overline{E}_{t_{bi}}^{s', (w')} \right]_{\rho}^* \quad (G.36)$$

A transformation is first applied to the above z_2 and z_4 integrations, such that the limits of the z_2 integral in the new coordinate frame will extend from $-h_t^+$ to 0. In addition, the correlation function is represented as the Fourier transformation of its associated spectral function. The result is given by (G.37).

$$\sigma_{TC-TC}^{\cup=} = \lim_{\delta z \rightarrow 0} \sum_{\substack{p, s, q, \ell, \\ p', s' = +, -}} \sum_{\substack{u, v, w, \\ u', w' = TE, TM}} \sum_{\alpha, \beta, \gamma, \rho = x, y, z} \int_{-h_t^+}^0 dz_2 \iint d\bar{\tau}_{2\perp} \iiint d\bar{\tau}_4 \\ \iint d\bar{k}_{\perp a} \iint d\bar{\beta}_{\perp} \int d\beta_z \Phi_{\alpha\beta\gamma\rho}(\bar{\beta}) A_{TC-TC}^{\alpha\beta\gamma\rho, pp'ss'qt, uu'vw w'} \delta(\bar{\tau}_4 - \bar{\tau}_T - d_{t-1}\hat{z}) \times \\ e^{i(\bar{k}_{\perp ai} - \bar{k}_{\perp a} - \bar{k}_{\perp bi}) \cdot \bar{\tau}_{T\perp}} e^{-i(s k_{iz_{ai}}^{(w)} + q k_{iz_{a}}^{(v)} - s' k_{iz_{bi}}^{(w')})z_T} e^{-i(\ell k_{iz_{a}}^{(v)} - p k_{iz_{a s}}^{(u)} + p' k_{iz_{b s}}^{(u')})d_{t-1}} \times \\ e^{i(\bar{k}_{\perp a} - \bar{k}_{\perp a s} - \bar{\beta}_{\perp}) \cdot \bar{\tau}_{2\perp}} e^{i(\bar{k}_{\perp b s} + \bar{\beta}_{\perp}) \cdot \bar{\tau}_{4\perp}} e^{i(\ell k_{iz_{a}}^{(v)} - p k_{iz_{a s}}^{(u)} - \beta_z)z_2} e^{i(p' k_{iz_{b s}}^{(u')} + \beta_z)z_4} \quad (G.37)$$

The $\bar{\tau}_4$ integration in the above can be performed using the delta function from the singularity term of the Green's function. The integration over $\bar{\tau}_{2\perp}$ can then be done to obtain another delta function, and the result is given below.

$$\sigma_{TC-TC}^{\cup=} = \lim_{\delta z \rightarrow 0} (2\pi)^2 \sum_{\substack{p, s, q, \ell, \\ p', s' = +, -}} \sum_{\substack{u, v, w, \\ u', w' = TE, TM}} \sum_{\alpha, \beta, \gamma, \rho = x, y, z} \int_{-h_t^+}^0 dz_2 \iint d\bar{k}_{\perp a} \iint d\bar{\beta}_{\perp} \int d\beta_z \times$$

$$A_{TC-TC}^{\alpha\beta\gamma\rho, pp'ss'q\ell, uu'vwuw'} \Phi_{\alpha\beta\gamma\rho}(\bar{\beta}) \delta(\bar{k}_{\perp a} - \bar{k}_{\perp as} - \bar{\beta}_{\perp}) e^{i(\bar{k}_{\perp ai} - \bar{k}_{\perp a} - \bar{k}_{\perp bi} + \bar{k}_{\perp bs} + \bar{\beta}_{\perp}) \cdot \bar{r}_{T\perp}} \times \\ e^{-i(sk_{iz ai}^{(w)} + qk_{iz a}^{(v)} - s'k_{iz bi}^{(w')*} - p'k_{iz bs}^{(u')*} - \beta_z)z_T} e^{i(\ell k_{iz a}^{(v)} - pk_{iz as}^{(u)} - \beta_z)(z_2 - d_{t-1})} \quad (G.38)$$

The delta function can then be used to perform the $\bar{\beta}_{\perp}$ integration to yield (G.39).

$$\sigma_{TC-TC}^{\text{U=}} = \lim_{\delta z \rightarrow 0} (2\pi)^2 \sum_{\substack{p,s,q,\ell, \\ p',s'=+,-}} \sum_{\substack{u,v,w, \\ u',w'=TE,TM}} \sum_{\alpha,\beta,\gamma,\rho=x,y,z} \int_{-h_t^+}^0 dz_2 \iint d\bar{k}_{\perp a} \int d\beta_z \times \\ A_{TC-TC}^{\alpha\beta\gamma\rho, pp'ss'q\ell, uu'vwuw'} \Phi_{\alpha\beta\gamma\rho}(\bar{k}_{\perp a} - \bar{k}_{\perp as}, \beta_z) e^{i(\bar{k}_{\perp ai} - \bar{k}_{\perp bi} + \bar{k}_{\perp bs} - \bar{k}_{\perp as}) \cdot \bar{r}_{T\perp}} \times \\ e^{-i(sk_{iz ai}^{(w)} + qk_{iz a}^{(v)} - s'k_{iz bi}^{(w')*} - p'k_{iz bs}^{(u')*} - \beta_z)z_T} e^{i(\ell k_{iz a}^{(v)} - pk_{iz as}^{(u)} - \beta_z)(z_2 - d_{t-1})} \quad (G.39)$$

The z_2 integration can then be done directly to yield (G.40).

$$\sigma_{TC-TC}^{\text{U=}} = \lim_{\delta z \rightarrow 0} (2\pi)^2 \sum_{\substack{p,s,q,\ell, \\ p',s'=+,-}} \sum_{\substack{u,v,w, \\ u',w'=TE,TM}} \sum_{\alpha,\beta,\gamma,\rho=x,y,z} \iint d\bar{k}_{\perp a} \int d\beta_z A_{TC-TC}^{\alpha\beta\gamma\rho, pp'ss'q\ell, uu'vwuw'} \times \\ \Phi_{\alpha\beta\gamma\rho}(\bar{k}_{\perp a} - \bar{k}_{\perp as}, \beta_z) e^{i(\bar{k}_{\perp ai} - \bar{k}_{\perp bi} + \bar{k}_{\perp bs} - \bar{k}_{\perp as}) \cdot \bar{r}_{T\perp}} \times \\ e^{-i(sk_{iz ai}^{(w)} + qk_{iz a}^{(v)} - s'k_{iz bi}^{(w')*} - p'k_{iz bs}^{(u')*} - \beta_z)z_T} e^{-i(\ell k_{iz a}^{(v)} - pk_{iz as}^{(u)} - \beta_z)d_{t-1}} \times \\ \frac{1 - e^{-i(\ell k_{iz a}^{(v)} - pk_{iz as}^{(u)} - \beta_z)h_t^+}}{pk_{iz as}^{(u)} - \ell k_{iz a}^{(v)} + \beta_z} \quad (G.40)$$

The β_z integral of the above expression takes the form of (G.41).

$$I^{\text{U=}} = \int d\beta_z \Phi_{\alpha\beta\gamma\rho}(\bar{k}_{\perp a} - \bar{k}_{\perp as}, \beta_z) e^{-i(sk_{iz ai}^{(w)} + qk_{iz a}^{(v)} - s'k_{iz bi}^{(w')*} - p'k_{iz bs}^{(u')*} - \beta_z)z_T} \times \\ e^{-i(\ell k_{iz a}^{(v)} - pk_{iz as}^{(u)} - \beta_z)d_{t-1}} \frac{1 - e^{-i(\ell k_{iz a}^{(v)} - pk_{iz as}^{(u)} - \beta_z)h_t^+}}{pk_{iz as}^{(u)} - \ell k_{iz a}^{(v)} + \beta_z} \quad (G.41)$$

The entire integrand converges in the lower half-plane of complex β_z , hence, the integration path will be closed in a semi-circular fashion at infinite radius in the lower half-plane. The final term can be written as an exponential multiplied by a sinc function, and the denominator, therefore, is not a pole. The only poles again arise from the spectral function, $\Phi_{\alpha\beta\gamma\rho}(\bar{\beta})$, which will be assumed to have the form of (F.4).

The simple pole contribution to the above integral is then given by (G.42),

$$R_{S1}^{U=} = -2\pi i \sum_{m=1}^{N_1} \frac{\left(1 - e^{i(pk_{fza}^{(u)} - \ell k_{fza}^{(v)} + \beta_{zm}^*)h_t^+)}\right) \left(e^{i(pk_{fza}^{(u)} - \ell k_{fza}^{(v)} + \beta_{zm}^*)d_{t-1}}\right)}{pk_{fza}^{(u)} - \ell k_{fza}^{(v)} + \beta_{zm}^*} \times$$

$$\frac{\Phi_N(\bar{k}_{\perp a} - \bar{k}_{\perp as}, \beta_{zm}^*) e^{-i(sk_{tza}^{(w)} + qk_{tza}^{(v)} - s'k_{tzb}^{(w')*} - p'k_{tzb}^{(u')*} - \beta_{zm}^*)z_T}}{\prod_{m'=1}^{N_1} (\beta_{zm}^* - \beta_{zm'}^*) \prod_{\substack{m'=1 \\ m' \neq m}}^{N_1} (\beta_{zm}^* - \beta_{zm'}^*) \prod_{n'=1}^{N_2} (\beta_{zm}^* - \beta_{zn'}^*)^2 (\beta_{zm}^* - \beta_{zn'}^*)^2}$$

(G.42)

and the double pole contribution is given by (G.43),

$$R_{S2}^{U=} = -2\pi i \sum_{n=1}^{N_2} \frac{1}{D_{-n}^{U=2}} \left\{ D_{-n}^{U=} \left[\Phi'_N(\bar{k}_{\perp a} - \bar{k}_{\perp as}, \beta_{zn}^*) N_{-n}^{U=} + \Phi_N(\bar{k}_{\perp a} - \bar{k}_{\perp as}, \beta_{zn}^*) N_{-n}^{U='} \right] - \right.$$

$$\left. D_{-n}^{U='} \Phi_N(\bar{k}_{\perp a} - \bar{k}_{\perp as}, \beta_{zn}^*) N_{-n}^{U=} \right\}$$

(G.43)

where $N_{-n}^{U=}$ and $N_{-n}^{U='}$ are given by (G.44) and (G.45),

$$N_{-n}^{U=} = e^{-i(sk_{tza}^{(w)} + qk_{tza}^{(v)} - s'k_{tzb}^{(w')*} - p'k_{tzb}^{(u')*} - \beta_{zn}^*)z_T} e^{i(pk_{fza}^{(u)} - \ell k_{fza}^{(v)} + \beta_{zn}^*)d_{t-1}} \times$$

$$\left(1 - e^{i(pk_{fz_{as}}^{(u)} - \ell k_{fz_a}^{(v)} + \beta_{z_n}^*)h_t^+}\right) \quad (G.44)$$

$$N_{-n}^{\cup=} = e^{-i(sk_{iz_{ai}}^{(w)} + qk_{iz_a}^{(v)} - s'k_{iz_{bi}}^{(w')*} - p'k_{iz_{bs}}^{(u')*} - \beta_{z_n}^*)z_T} e^{i(pk_{fz_{as}}^{(u)} - \ell k_{fz_a}^{(v)} + \beta_{z_n}^*)d_{t-1}} \times \\ i \left[(z_T + d_{t-1}) + \delta_z e^{i(pk_{fz_{as}}^{(u)} - \ell k_{fz_a}^{(v)} + \beta_{z_n}^*)h_t^+} \right] \quad (G.45)$$

and where $D_{-n}^{\cup=}$ and $D_{-n}^{\cup=}$ are given by (G.46) and (G.47).

$$D_{-n}^{\cup=} = (pk_{fz_{as}}^{(u)} - \ell k_{fz_a}^{(v)} + \beta_{z_n}^*) \prod_{m'=1}^{N_1} (\beta_{z_n}^* - \beta_{z_{m'}}) (\beta_{z_n}^* - \beta_{z_{m'}}) \times \\ \prod_{n'=1}^{N_2} (\beta_{z_n}^* - \beta_{z_{n'}})^2 \prod_{\substack{n'=1 \\ n' \neq n}}^{N_2} (\beta_{z_n}^* - \beta_{z_{n'}})^2 \quad (G.46)$$

$$D_{-n}^{\cup=} = \prod_{m'=1}^{N_1} (\beta_{z_n}^* - \beta_{z_{m'}}) (\beta_{z_n}^* - \beta_{z_{m'}}) \prod_{n'=1}^{N_2} (\beta_{z_n}^* - \beta_{z_{n'}})^2 \prod_{\substack{n'=1 \\ n' \neq n}}^{N_2} (\beta_{z_n}^* - \beta_{z_{n'}})^2 \\ + (pk_{fz_{as}}^{(u)} - \ell k_{fz_a}^{(v)} + \beta_{z_n}^*) \times \\ \left\{ \prod_{n'=1}^{N_2} (\beta_{z_n}^* - \beta_{z_{n'}})^2 \prod_{\substack{n'=1 \\ n' \neq n}}^{N_2} (\beta_{z_n}^* - \beta_{z_{n'}})^2 \times \right. \\ \sum_{m'=1}^{N_1} \left[\prod_{\substack{m''=1 \\ m'' \neq m'}}^{N_1} (\beta_{z_n}^* - \beta_{z_{m''}}) \prod_{m''=1}^{N_1} (\beta_{z_n}^* - \beta_{z_{m''}}) + \right. \\ \left. \prod_{m''=1}^{N_1} (\beta_{z_n}^* - \beta_{z_{m''}}) \prod_{\substack{m''=1 \\ m'' \neq m'}}^{N_1} (\beta_{z_n}^* - \beta_{z_{m''}}) \right] \\ \left. + 2 \prod_{m'=1}^{N_1} (\beta_{z_n}^* - \beta_{z_{m'}}) (\beta_{z_n}^* - \beta_{z_{m'}}) \times \right. \\ \left. \left[\sum_{n'=1}^{N_2} (\beta_{z_n}^* - \beta_{z_{n'}}) \prod_{\substack{n''=1 \\ n'' \neq n'}}^{N_2} (\beta_{z_n}^* - \beta_{z_{n''}})^2 \prod_{\substack{n''=1 \\ n'' \neq n}}^{N_2} (\beta_{z_n}^* - \beta_{z_{n''}})^2 + \right. \right.$$

$$\sum_{\substack{n'=1 \\ n' \neq n}}^{N_2} (\beta_{z_n}^* - \beta_{z_{n'}}^*) \prod_{n''=1}^{N_2} (\beta_{z_n}^* - \beta_{z_{n''}})^2 \prod_{\substack{n''=1 \\ n'' \neq n'}}^{N_2} (\beta_{z_n}^* - \beta_{z_{n''}}^*)^2 \Big] \Big\} \quad (G.47)$$

Hence, the final desired expression for $\sigma_{TC-TC}^{\cup=}$ can be found from the sum of the above pole contributions.

$$\sigma_{TC-TC}^{\cup=} = \lim_{\delta_z \rightarrow 0} i(2\pi)^2 \sum_{\substack{p,s,q,\ell, \\ p',s'=+,-}} \sum_{\substack{u,v,w, \\ u',w'=TE,TM}} \sum_{\alpha,\beta,\gamma,\rho=x,y,z} \iint d\bar{k}_{\perp a} A_{TC-TC}^{\alpha\beta\gamma\rho, pp'ss'q\ell, uu'vw w'} \times \\ e^{i(\bar{k}_{\perp ai} - \bar{k}_{\perp bi} + \bar{k}_{\perp bs} - \bar{k}_{\perp as}) \cdot \bar{r}_{T\perp}} [R_{S1}^{\cup=} + R_{S2}^{\cup=}] \quad (G.48)$$

The second term to be considered is $\sigma_{TC-TC}^{\cap=}$, which is given by (G.8), and which can be written using the expression of Appendix E to yield the result of (G.49),

$$\sigma_{TC-TC}^{\cap=} = \lim_{\delta_z \rightarrow 0} \sum_{\substack{p,s,q,\ell, \\ p',s'=+,-}} \sum_{\substack{u,v,w, \\ u',w'=TE,TM}} \sum_{\alpha,\beta,\gamma,\rho=x,y,z} \int_{-d_i}^{z_T - \delta_z} dz_2 \iint d\bar{r}_{2\perp} \iiint d\bar{r}_4 \\ \iint d\bar{k}_{\perp a} C_{\alpha\beta\gamma\rho}(\bar{r}_2 - \bar{r}_4) A_{TC-TC}^{\alpha\beta\gamma\rho, pp'ss'q\ell, uu'vw w'} \delta(\bar{r}_4 - \bar{r}_T) \times \\ e^{i(\bar{k}_{\perp ai} - \bar{k}_{\perp as} - \bar{k}_{\perp bi}) \cdot \bar{r}_{T\perp}} e^{-i(sk_{iz ai}^{(w)} + qk_{iz a}^{(v)} - s'k_{iz bi}^{(w')})z_T} \times \\ e^{i(\bar{k}_{\perp a} - \bar{k}_{\perp as}) \cdot \bar{r}_{2\perp}} e^{i\bar{k}_{\perp bs} \cdot \bar{r}_{4\perp}} e^{i(\ell k_{iz a}^{(v)} - p k_{iz as}^{(u)})z_2} e^{ip'k_{iz bs}^{(u')}z_4} \quad (G.49)$$

where

$$A_{TC-TC}^{\alpha\beta\gamma\rho, pp'ss'q\ell, uu'vw w'} = \frac{|\alpha'|^2}{4\pi} \left[\hat{p}_a \cdot \overline{H}_{0t_p}^{(u)}(\bar{k}_{\perp a}) \right]_{\alpha} \cdot \left[\overline{F}_{t \cap \ell_q}^{(v)}(\bar{k}_{\perp a}) \cdot \overline{E}_{t_{ai}}^{s,(w)} \right]_{\beta} \times \\ \left[\hat{p}_b \cdot \overline{H}_{0t_{p'}}^{(u')}(\bar{k}_{\perp b}) \right]_{\gamma}^* \cdot \left[\overline{D}_t^b \cdot \overline{E}_{t_{bi}}^{s',(w')} \right]_{\rho}^* \quad (G.50)$$

A transformation is again applied to the z_2 and z_4 integrals such that the limits of the new z_2 integral will extend from $-h_t^-$ to 0. In addition, the correlation function is again represented as the Fourier transform of its spectral function.

$$\sigma_{TC-TC}^{U=} = \lim_{\delta_z \rightarrow 0} \sum_{\substack{p,s,q,\ell, \\ p',s'=+,-}} \sum_{\substack{u,v,w, \\ u',w'=TE,TM}} \sum_{\alpha,\beta,\gamma,\rho=x,y,z} \int_{-h_t^-}^0 dz_2 \iint d\bar{\tau}_{2\perp} \iiint d\bar{\tau}_4 \\ \iint d\bar{k}_{\perp a} \iint d\bar{\beta}_{\perp} \int d\beta_z \Phi_{\alpha\beta\gamma\rho}(\bar{\beta}) A_{TC-TC}^{\alpha\beta\gamma\rho, pp'ss'q\ell, uu'vw w'} \delta(\bar{\tau}_4 - \bar{\tau}_T + (z_T + \delta_z)\hat{z}) \times \\ e^{i(\bar{k}_{\perp ai} - \bar{k}_{\perp a} - \bar{k}_{\perp bi}) \cdot \bar{\tau}_{T\perp}} e^{-i(s k_{iz_{ai}}^{(w)} + q k_{iz_a}^{(v)} - s' k_{iz_{bi}}^{(w')})z_T} e^{i(\ell k_{iz_a}^{(v)} - p k_{iz_{as}}^{(u)} + p' k_{iz_{bs}}^{(u')})^*(z_T - \delta_z)} \times \\ e^{i(\bar{k}_{\perp a} - \bar{k}_{\perp as} - \bar{\beta}_{\perp}) \cdot \bar{\tau}_{2\perp}} e^{i(\bar{k}_{\perp bs} + \bar{\beta}_{\perp}) \cdot \bar{\tau}_{4\perp}} e^{i(\ell k_{iz_a}^{(v)} - p k_{iz_{as}}^{(u)} - \beta_z)z_2} e^{i(p' k_{iz_{bs}}^{(u')} + \beta_z)z_4} \quad (G.51)$$

The $\bar{\tau}_4$ integral can be performed trivially, and the $\bar{\tau}_{2\perp}$ integral can be done to produce another delta function which then allows trivial evaluation of the $\bar{\beta}_{\perp}$ integral. The result is given by (G.52) below.

$$\sigma_{TC-TC}^{U=} = \lim_{\delta_z \rightarrow 0} (2\pi)^2 \sum_{\substack{p,s,q,\ell, \\ p',s'=+,-}} \sum_{\substack{u,v,w, \\ u',w'=TE,TM}} \sum_{\alpha,\beta,\gamma,\rho=x,y,z} \int_{-h_t^-}^0 dz_2 \iint d\bar{k}_{\perp a} \int d\beta_z \times$$

$$\begin{aligned}
& A_{TC-TC}^{\alpha\beta\gamma\rho, pp'ss'q\ell, uu'vw w'} \Phi_{\alpha\beta\gamma\rho} (\bar{k}_{\perp a} - \bar{k}_{\perp as}, \beta_z) \times \\
& e^{i(\bar{k}_{\perp ai} - \bar{k}_{\perp bi} + \bar{k}_{\perp bs} - \bar{k}_{\perp as}) \cdot \bar{r}_{T\perp}} e^{-i(sk_{iz ai}^{(w)} + qk_{iz a}^{(v)} - s'k_{iz bi}^{(w')})z_T} \times \\
& e^{i(\ell k_{iz a}^{(v)} - pk_{iz as}^{(u)} + p'k_{iz bs}^{(u')})^*(z_T - \delta_z)} e^{i(p'k_{iz bs}^{(u')})^* + \beta_z} \delta_z e^{i(\ell k_{iz a}^{(v)} - pk_{iz as}^{(u)} - \beta_z)z_2} \quad (G.52)
\end{aligned}$$

The z_2 integral can then be done directly to yield (G.53).

$$\begin{aligned}
\sigma_{TC-TC}^{\cup=} &= \lim_{\delta_z \rightarrow 0} (2\pi)^2 \sum_{\substack{p,s,q,\ell, \\ p',s'=+,-}} \sum_{\substack{u,v,w, \\ u',w'=TE,TM}} \sum_{\alpha,\beta,\gamma,\rho=x,y,z} \iint d\bar{k}_{\perp a} \int d\beta_z \times \\
& A_{TC-TC}^{\alpha\beta\gamma\rho, pp'ss'q\ell, uu'vw w'} \Phi_{\alpha\beta\gamma\rho} (\bar{k}_{\perp a} - \bar{k}_{\perp as}, \beta_z) \times \\
& e^{i(\bar{k}_{\perp ai} - \bar{k}_{\perp bi} + \bar{k}_{\perp bs} - \bar{k}_{\perp as}) \cdot \bar{r}_{T\perp}} e^{-i(sk_{iz ai}^{(w)} + qk_{iz a}^{(v)} - s'k_{iz bi}^{(w')})z_T} \times \\
& e^{i(\ell k_{iz a}^{(v)} - pk_{iz as}^{(u)} + p'k_{iz bs}^{(u')})^*(z_T - \delta_z)} e^{i(p'k_{iz bs}^{(u')})^* + \beta_z} \delta_z \frac{1 - e^{i(pk_{iz as}^{(u)} - \ell k_{iz a}^{(v)} + \beta_z)h_i^-}}{pk_{fz as}^{(u)} - \ell k_{fz a}^{(v)} + \beta_z} \quad (G.53)
\end{aligned}$$

Hence, the β_z integral takes the form of (G.54).

$$I^{\cap=} = \int d\beta_z \Phi_{\alpha\beta\gamma\rho} (\bar{k}_{\perp a} - \bar{k}_{\perp as}, \beta_z) e^{i(p'k_{iz bs}^{(u')})^* + \beta_z} \delta_z \frac{1 - e^{i(pk_{iz as}^{(u)} - \ell k_{iz a}^{(v)} + \beta_z)h_i^-}}{pk_{fz as}^{(u)} - \ell k_{fz a}^{(v)} + \beta_z} \quad (G.54)$$

The integrand is now convergent in the upper half-plane of complex β_z so the integration path will be closed with an upward oriented semi-circle. The only poles are again those of the spectral function, and the residue contribution of the simple poles will be given by (G.55),

$$R_{S_1}^{\cap=} = 2\pi i \sum_{m=1}^{N_1} \frac{1 - e^{i(pk_{fz_{as}}^{(u)} - \ell k_{fz_a}^{(v)} + \beta_{zm})h_t^-}}{pk_{fz_{as}}^{(u)} - \ell k_{fz_a}^{(v)} + \beta_{zm}} \times$$

$$\frac{\Phi_N(\bar{k}_{\perp a} - \bar{k}_{\perp as}, \beta_{zm}) e^{i(p'k_{fz_{bs}}^{(u')})^* + \beta_{zm})\delta_z}}{\prod_{\substack{m'=1 \\ m' \neq m}}^{N_1} (\beta_{zm} - \beta_{zm'}) \prod_{m'=1}^{N_1} (\beta_{zm} - \beta_{zm'}^*) \prod_{n'=1}^{N_2} (\beta_{zm} - \beta_{zn'})^2 (\beta_{zm} - \beta_{zn'}^*)^2}$$
(G.55)

and the double pole contribution by (G.56),

$$R_{S_2}^{\cap=} = 2\pi i \sum_{n=1}^{N_2} \frac{1}{D_{+n}^{\cap=2}} \left\{ D_{+n}^{\cap=} \left[\Phi'_N(\bar{k}_{\perp a} - \bar{k}_{\perp as}, \beta_{zn}) N_{+n}^{\cap=} + \Phi_N(\bar{k}_{\perp a} - \bar{k}_{\perp as}, \beta_{zn}) N_{+n}^{\cap='} \right] - \right.$$

$$\left. D_{+n}^{\cap='} \Phi_N(\bar{k}_{\perp a} - \bar{k}_{\perp as}, \beta_{zn}) N_{+n}^{\cap=} \right\}$$
(G.56)

where $N_{+n}^{\cap=}$ and $N_{+n}^{\cap='}$ are given by (G.57) and (G.58),

$$N_{+n}^{\cap=} = e^{i(p'k_{fz_{bs}}^{(u')})^* + \beta_{zn})\delta_z} \left(1 - e^{i(pk_{fz_{as}}^{(u)} - \ell k_{fz_a}^{(v)} + \beta_{zn})h_t^-} \right)$$
(G.57)

$$N_{+n}^{\cap='} = i e^{i(p'k_{fz_{bs}}^{(u')})^* + \beta_{zn})\delta_z} \left[\delta_z - (\delta_z + h_t^-) e^{i(pk_{fz_{as}}^{(u)} - \ell k_{fz_a}^{(v)} + \beta_{zn})h_t^-} \right]$$
(G.58)

and where $D_{+n}^{\cap=}$ and $D_{+n}^{\cap='}$ are given by (G.59) and (G.60).

$$D_{+n}^{\cap=} = (pk_{fz_{as}}^{(u)} - \ell k_{fz_a}^{(v)} + \beta_{zn}) \prod_{m'=1}^{N_1} (\beta_{zn} - \beta_{zm'}) (\beta_{zn} - \beta_{zm'}^*) \times$$

$$\prod_{\substack{n'=1 \\ n' \neq n}}^{N_2} (\beta_{z_n} - \beta_{z_{n'}})^2 \prod_{n'=1}^{N_2} (\beta_{z_n} - \beta_{z_{n'}}^*)^2 \quad (G.59)$$

$$\begin{aligned} D_{+n}^{\cap'} &= \prod_{m'=1}^{N_1} (\beta_{z_n} - \beta_{z_{m'}}) (\beta_{z_n} - \beta_{z_{m'}}^*) \prod_{\substack{n'=1 \\ n' \neq n}}^{N_2} (\beta_{z_n} - \beta_{z_{n'}})^2 \prod_{n'=1}^{N_2} (\beta_{z_n} - \beta_{z_{n'}}^*)^2 \\ &+ \left(pk_{fz_{as}}^{(u)} - \ell k_{fz_a}^{(v)} + \beta_{z_n} \right) \times \\ &\quad \left\{ \prod_{\substack{n'=1 \\ n' \neq n}}^{N_2} (\beta_{z_n} - \beta_{z_{n'}})^2 \prod_{n'=1}^{N_2} (\beta_{z_n} - \beta_{z_{n'}}^*)^2 \times \right. \\ &\quad \sum_{m'=1}^{N_1} \left[\prod_{\substack{m''=1 \\ m'' \neq m'}}^{N_1} (\beta_{z_n} - \beta_{z_{m''}}) \prod_{m''=1}^{N_1} (\beta_{z_n} - \beta_{z_{m''}}^*) + \right. \\ &\quad \left. \prod_{m''=1}^{N_1} (\beta_{z_n} - \beta_{z_{m''}}) \prod_{\substack{m''=1 \\ m'' \neq m'}}^{N_1} (\beta_{z_n} - \beta_{z_{m''}}^*) \right] \\ &+ 2 \prod_{m'=1}^{N_1} (\beta_{z_n} - \beta_{z_{m'}}) (\beta_{z_n} - \beta_{z_{m'}}^*) \times \\ &\quad \left[\sum_{\substack{n'=1 \\ n' \neq n}}^{N_2} (\beta_{z_n} - \beta_{z_{n'}}) \prod_{\substack{n''=1 \\ n'' \neq n'}}^{N_2} (\beta_{z_n} - \beta_{z_{n''}})^2 \prod_{n''=1}^{N_2} (\beta_{z_n} - \beta_{z_{n''}}^*)^2 + \right. \\ &\quad \left. \sum_{n'=1}^{N_2} (\beta_{z_n} - \beta_{z_{n'}}^*) \prod_{\substack{n''=1 \\ n'' \neq n}}^{N_2} (\beta_{z_n} - \beta_{z_{n''}})^2 \prod_{\substack{n''=1 \\ n'' \neq n'}}^{N_2} (\beta_{z_n} - \beta_{z_{n''}}^*)^2 \right] \} \quad (G.60) \end{aligned}$$

Hence, the final desired result is given by (G.61).

$$\begin{aligned} \sigma_{TC-TC}^{\cap} &= \lim_{\delta_z \rightarrow 0} i(2\pi)^2 \sum_{\substack{p, s, q, \ell, \\ p', s' = +, -}} \sum_{\substack{u, v, w, \\ u', w' = TE, TM}} \sum_{\alpha, \beta, \gamma, \rho = x, y, z} \iint d\bar{k}_{\perp a} A_{TC-TC}^{\substack{\alpha\beta\gamma\rho \\ pp'ss'q\ell \\ uu'vw w' \\ \cap}} \times \\ &\quad e^{i(\bar{k}_{\perp a i} - \bar{k}_{\perp b i} + \bar{k}_{\perp b s} - \bar{k}_{\perp a s}) \cdot \vec{r}_{T\perp}} e^{-i(sk_{iz_{ai}}^{(w)} + qk_{iz_a}^{(v)} - s'k_{iz_{bi}}^{(w')})z_T} \times \\ &\quad e^{i(\ell k_{iz_a}^{(v)} - pk_{iz_{as}}^{(u)} + p'k_{iz_{bs}}^{(u')})z_T - \delta_z} [R_{S1}^{\cap} + R_{S2}^{\cap}] \quad (G.61) \end{aligned}$$

The other two terms, $\sigma_{TC-TC}^{\bar{u}}$ and $\sigma_{TC-TC}^{\bar{n}}$, can be derived in a similar manner, or determined using the relations of (G.12) and (G.13).

G.2. Correlation of Scattered Field Components

This section gives the final expressions the correlations between the incoherent multi-path components of the target return. The correlation function is assumed to take the form of (F.4), with N_1 conjugate pairs of simple poles at β_{zm} and β_{zm}^* , and N_2 conjugate pairs of double poles at β_{zn} and β_{zn}^* .

G.2.1. Target/Clutter - Target/Clutter Correlation

The overall expression for this correlation is expressed as the sum of nine terms, as shown by (G.62).

$$\begin{aligned}
 \sigma_{TC-TC}^{\hat{p}_a \hat{p}_b}(\bar{k}_{as}, \bar{k}_{ai}, \bar{k}_{bs}, \bar{k}_{bi}) &= 4\pi r^2 \langle \hat{p}_a \cdot \bar{E}_{TC}(\bar{k}_{as}, \bar{k}_{ai}) \times \hat{p}_b^* \cdot \bar{E}_{TC}^*(\bar{k}_{bs}, \bar{k}_{bi}) \rangle \\
 &= \sigma_{TC-TC}^{\bar{u}\bar{u}} + \sigma_{TC-TC}^{\bar{n}\bar{n}} + \sigma_{TC-TC}^{\bar{u}\bar{n}} + \\
 &\quad \sigma_{TC-TC}^{\bar{n}\bar{u}} + \sigma_{TC-TC}^{\bar{u}\bar{u}} + \sigma_{TC-TC}^{\bar{u}\bar{u}} + \\
 &\quad \sigma_{TC-TC}^{\bar{n}\bar{n}} + \sigma_{TC-TC}^{\bar{u}\bar{u}} + \sigma_{TC-TC}^{\bar{n}\bar{n}}
 \end{aligned} \tag{G.62}$$

The first two terms are given by (G.63) and (G.64),

$$\sigma_{TC-TC}^{\bar{u}\bar{u}} = \lim_{\delta_z \rightarrow 0} (2\pi)^5 i \sum_{\substack{p', s', q', \ell', \\ p', s', q', \ell' = +, -}} \sum_{\substack{u', v', w', \\ u', v', w' = TE, TM}} \sum_{\alpha, \beta, \gamma, \rho = x, y, z} \iint d\bar{k}_{\perp a} A_{TC-TC}^{\alpha\beta\gamma\rho}_{\bar{u}\bar{u}} \times$$

$$\begin{aligned}
& e^{i(\bar{k}_{\perp ai} - \bar{k}_{\perp bi} + \bar{k}_{\perp bs} - \bar{k}_{\perp as}) \cdot \bar{\tau} T_{\perp}} e^{-i(s k_{tz ai}^{(w)} + q k_{tz a}^{(v)} - s' k_{tz bi}^{(w')*} - q' k_{tz c}^{(v')*}) z_T} \times \\
& e^{-i(\ell k_{tz a}^{(v)} - p k_{tz as}^{(u)} - \ell' k_{tz c}^{(v')*} + p' k_{tz bs}^{(u')*}) d_{t-1}} \times \\
& \left[R_P^{\text{UU}}(\bar{k}_{\perp a} - \bar{k}_{\perp as}, \ell k_{tz a}^{(v)} - p k_{tz as}^{(u)}, \ell' k_{tz c}^{(v')*} - p' k_{tz bs}^{(u')*}, h_t^+) + \right. \\
& R_{S1}^{\text{UU}}(\bar{k}_{\perp a} - \bar{k}_{\perp as}, \ell k_{tz a}^{(v)} - p k_{tz as}^{(u)}, \ell' k_{tz c}^{(v')*} - p' k_{tz bs}^{(u')*}, h_t^+) + \\
& \left. R_{S2}^{\text{UU}}(\bar{k}_{\perp a} - \bar{k}_{\perp as}, \ell k_{tz a}^{(v)} - p k_{tz as}^{(u)}, \ell' k_{tz c}^{(v')*} - p' k_{tz bs}^{(u')*}, h_t^+) \right] \quad (G.63)
\end{aligned}$$

$$\begin{aligned}
\sigma_{TC-TC}^{\text{UU}} &= \lim_{\delta_z \rightarrow 0} (2\pi)^5 i \sum_{\substack{p,s,q,\ell, \\ p',s',q',\ell' = +,-}} \sum_{\substack{u,v,w, \\ u',v',w' = TE, TM}} \sum_{\alpha, \beta, \gamma, \rho = x, y, z} \iint d\bar{k}_{\perp a} A_{TC-TC}^{\substack{\alpha\beta\gamma\rho \\ pp'ss'qq'\ell\ell' \\ uu'vv'ww' \\ \text{nn}}} \times \\
& e^{i(\bar{k}_{\perp ai} - \bar{k}_{\perp bi} + \bar{k}_{\perp bs} - \bar{k}_{\perp as}) \cdot \bar{\tau} T_{\perp}} e^{-i(s k_{tz ai}^{(w)} + q k_{tz a}^{(v)} - s' k_{tz bi}^{(w')*} - q' k_{tz c}^{(v')*}) z_T} \times \\
& e^{i(\ell k_{tz a}^{(v)} - p k_{tz as}^{(u)} - \ell' k_{tz c}^{(v')*} + p' k_{tz bs}^{(u')*}) (z_T - \delta_z)} \times \\
& \left[R_P^{\text{nn}}(\bar{k}_{\perp a} - \bar{k}_{\perp as}, \ell k_{tz a}^{(v)} - p k_{tz as}^{(u)}, \ell' k_{tz c}^{(v')*} - p' k_{tz bs}^{(u')*}, h_t^-) + \right. \\
& R_{S1}^{\text{nn}}(\bar{k}_{\perp a} - \bar{k}_{\perp as}, \ell k_{tz a}^{(v)} - p k_{tz as}^{(u)}, \ell' k_{tz c}^{(v')*} - p' k_{tz bs}^{(u')*}, h_t^-) + \\
& \left. R_{S2}^{\text{nn}}(\bar{k}_{\perp a} - \bar{k}_{\perp as}, \ell k_{tz a}^{(v)} - p k_{tz as}^{(u)}, \ell' k_{tz c}^{(v')*} - p' k_{tz bs}^{(u')*}, h_t^-) \right] \quad (G.64)
\end{aligned}$$

where

$$\bar{k}_{\perp c} = \bar{k}_{\perp a} + \bar{k}_{\perp bs} - \bar{k}_{\perp as} \quad (G.65)$$

$$h_t^+ = -d_{t-1} - z_T - \delta_z \quad (G.66)$$

$$h_t^- = z_T + d_t - \delta_z \quad (G.67)$$

and

$$A_{TC-TC}^{\alpha\beta\gamma\rho} = \frac{|\alpha'|^2}{4\pi} \left[\hat{p}_a \cdot \overline{H}_{0t_p}^{(u)}(\bar{k}_{\perp a}) \right]_{\alpha} \cdot \left[\overline{F}_{t \cup \ell_q}^{(v)}(\bar{k}_{\perp a}) \cdot \overline{E}_{t_{ai}}^{s,(w)} \right]_{\beta} \times \\ \left[\hat{p}_b \cdot \overline{H}_{0t_{p'}}^{(u')}(\bar{k}_{\perp b}) \right]_{\gamma}^* \cdot \left[\overline{F}_{t \cup \ell'_q}^{(v')}(\bar{k}_{\perp c}) \cdot \overline{E}_{t_{bi}}^{s',(w')} \right]_{\rho}^* \quad (G.68)$$

$$A_{TC-TC}^{\alpha\beta\gamma\rho} = \frac{|\alpha'|^2}{4\pi} \left[\hat{p}_a \cdot \overline{H}_{0t_p}^{(u)}(\bar{k}_{\perp a}) \right]_{\alpha} \cdot \left[\overline{F}_{t \cap \ell_q}^{(v)}(\bar{k}_{\perp a}) \cdot \overline{E}_{t_{ai}}^{s,(w)} \right]_{\beta} \times \\ \left[\hat{p}_b \cdot \overline{H}_{0t_{p'}}^{(u')}(\bar{k}_{\perp b}) \right]_{\gamma}^* \cdot \left[\overline{F}_{t \cap \ell'_q}^{(v')}(\bar{k}_{\perp c}) \cdot \overline{E}_{t_{bi}}^{s',(w')} \right]_{\rho}^* \quad (G.69)$$

The functions $R_P^{\cup\cup}$, $R_{S1}^{\cup\cup}$, and $R_{S2}^{\cup\cup}$ are defined by (G.70)-(G.72),

$$R_P^{\cup\cup}(\bar{\beta}_{\perp}, \beta_{P1}, \beta_{P2}, h) = \frac{\Phi_{\alpha\beta\gamma\rho}(\bar{\beta}_{\perp}, \beta_{P2})}{\beta_{P2} - \beta_{P1}} - \frac{\Phi_{\alpha\beta\gamma\rho}(\bar{\beta}_{\perp}, \beta_{P1})}{\beta_{P2} - \beta_{P1}} e^{i(\beta_{P2} - \beta_{P1})h} \quad (G.70)$$

$$R_{S1}^{\cup\cup}(\bar{\beta}_{\perp}, \beta_{P1}, \beta_{P2}, h) = \sum_{m=1}^{N_1} \left\{ \frac{(1 - e^{i(\beta_{zm} - \beta_{P1})h} + e^{i(\beta_{P2} - \beta_{P1})h})}{(\beta_{zm} - \beta_{P1})(\beta_{zm} - \beta_{P2}) \prod_{\substack{m'=1 \\ m' \neq m}}^{N_1} (\beta_{zm} - \beta_{zm'})} \times \right. \\ \frac{\Phi_N(\bar{\beta}_{\perp}, \beta_{zm})}{\prod_{m'=1}^{N_1} (\beta_{zm} - \beta_{zm'}^*) \prod_{n'=1}^{N_2} (\beta_{zm} - \beta_{zn'})^2 (\beta_{zm} - \beta_{zn'}^*)^2} + \\ \frac{e^{-i(\beta_{zm}^* - \beta_{P2})h}}{(\beta_{zm}^* - \beta_{P1})(\beta_{zm}^* - \beta_{P2}) \prod_{m'=1}^{N_1} (\beta_{zm}^* - \beta_{zm'})} \times \\ \left. \frac{\Phi_N(\bar{\beta}_{\perp}, \beta_{zm}^*)}{\prod_{\substack{m'=1 \\ m' \neq m}}^{N_1} (\beta_{zm}^* - \beta_{zm'}^*) \prod_{n'=1}^{N_2} (\beta_{zm}^* - \beta_{zn'})^2 (\beta_{zm}^* - \beta_{zn'}^*)^2} \right\} \quad (G.71)$$

$$\begin{aligned}
R_{S2}^{\text{UU}}(\bar{\beta}_{\perp}, \beta_{P1}, \beta_{P2}, h) = & \sum_{n=1}^{N_2} \frac{1}{D_{+n}^{\text{UU}2}} \left\{ D_{+n}^{\text{UU}} [\Phi'_N(\bar{\beta}_{\perp}, \beta_{z_n}) N_{+n}^{\text{UU}} + \Phi_N(\bar{\beta}_{\perp}, \beta_{z_n}) N_{+n}^{\text{UU}'}] - \right. \\
& \left. D_{+n}^{\text{UU}'} \Phi_N(\bar{\beta}_{\perp}, \beta_{z_n}) N_{+n}^{\text{UU}} \right\} \\
& \frac{1}{D_{-n}^{\text{UU}2}} \left\{ D_{-n}^{\text{UU}} [\Phi'_N(\bar{\beta}_{\perp}, \beta_{z_n}^*) N_{-n}^{\text{UU}} + \Phi_N(\bar{\beta}_{\perp}, \beta_{z_n}^*) N_{-n}^{\text{UU}'}] - \right. \\
& \left. D_{-n}^{\text{UU}'} \Phi_N(\bar{\beta}_{\perp}, \beta_{z_n}^*) N_{-n}^{\text{UU}} \right\} \\
& (G.72)
\end{aligned}$$

where N_{+n}^{UU} , N_{-n}^{UU} , $N_{+n}^{\text{UU}'}$, and $N_{-n}^{\text{UU}'}$ are given by (G.73)-(G.76),

$$N_{+n}^{\text{UU}} = 1 - e^{i(\beta_{z_n} - \beta_{P1})h} + e^{i(\beta_{P2} - \beta_{P1})h} \quad (G.73)$$

$$N_{-n}^{\text{UU}} = e^{-i(\beta_{z_n}^* - \beta_{P2})h} \quad (G.74)$$

$$N_{+n}^{\text{UU}'} = -ih e^{i(\beta_{z_n} - \beta_{P1})h} \quad (G.75)$$

$$N_{-n}^{\text{UU}'} = -ih e^{-i(\beta_{z_n}^* - \beta_{P2})h} \quad (G.76)$$

and where D_{+n}^{UU} , D_{-n}^{UU} , $D_{+n}^{\text{UU}'}$, and $D_{-n}^{\text{UU}'}$ are given by (G.77)-(G.80).

$$D_{+n}^{\text{UU}} = (\beta_{z_n} - \beta_{P1})(\beta_{z_n} - \beta_{P2}) \prod_{m'=1}^{N_1} (\beta_{z_n} - \beta_{z_{m'}}) (\beta_{z_n} - \beta_{z_{m'}}^*) \times$$

$$\prod_{\substack{n'=1 \\ n' \neq n}}^{N_2} (\beta_{z_n} - \beta_{z_{n'}})^2 \prod_{n'=1}^{N_2} (\beta_{z_n} - \beta_{z_{n'}}^*)^2 \quad (G.77)$$

$$D_{-n}^{UU} = (\beta_{z_n}^* - \beta_{P1}) (\beta_{z_n}^* - \beta_{P2}) \prod_{m'=1}^{N_1} (\beta_{z_n}^* - \beta_{z_{m'}}) (\beta_{z_n}^* - \beta_{z_{m'}}^*) \times$$

$$\prod_{n'=1}^{N_2} (\beta_{z_n}^* - \beta_{z_{n'}})^2 \prod_{\substack{n'=1 \\ n' \neq n}}^{N_2} (\beta_{z_n}^* - \beta_{z_{n'}}^*)^2 \quad (G.78)$$

$$D_{+n}^{UU'} = -(\beta_{P1} + \beta_{P2}) \prod_{m'=1}^{N_1} (\beta_{z_n} - \beta_{z_{m'}}) (\beta_{z_n} - \beta_{z_{m'}}^*) \prod_{\substack{n'=1 \\ n' \neq n}}^{N_2} (\beta_{z_n} - \beta_{z_{n'}})^2 \prod_{n'=1}^{N_2} (\beta_{z_n} - \beta_{z_{n'}}^*)^2 +$$

$$(2\beta_{z_n} - \beta_{P1} - \beta_{P2}) \times$$

$$\left\{ \prod_{\substack{n'=1 \\ n' \neq n}}^{N_2} (\beta_{z_n} - \beta_{z_{n'}})^2 \prod_{n'=1}^{N_2} (\beta_{z_n} - \beta_{z_{n'}}^*)^2 \sum_{m'=1}^{N_1} \left[\prod_{\substack{m''=1 \\ m'' \neq m'}}^{N_1} (\beta_{z_n} - \beta_{z_{m''}}) \prod_{m''=1}^{N_1} (\beta_{z_n} - \beta_{z_{m''}}^*) + \right. \right.$$

$$\left. \prod_{m''=1}^{N_1} (\beta_{z_n} - \beta_{z_{m''}}) \prod_{\substack{m''=1 \\ m'' \neq m'}}^{N_1} (\beta_{z_n} - \beta_{z_{m''}}^*) \right] +$$

$$2 \prod_{m'=1}^{N_1} (\beta_{z_n} - \beta_{z_{m'}}) (\beta_{z_n} - \beta_{z_{m'}}^*) \times$$

$$\left[\sum_{\substack{n'=1 \\ n' \neq n}}^{N_2} (\beta_{z_n} - \beta_{z_{n'}}) \prod_{\substack{n''=1 \\ n'' \neq n' \\ n'' \neq n}}^{N_2} (\beta_{z_n} - \beta_{z_{n''}})^2 \prod_{n''=1}^{N_2} (\beta_{z_n} - \beta_{z_{n''}}^*)^2 + \right.$$

$$\left. \sum_{n'=1}^{N_2} (\beta_{z_n} - \beta_{z_{n'}}^*) \prod_{\substack{n''=1 \\ n'' \neq n}}^{N_2} (\beta_{z_n} - \beta_{z_{n''}})^2 \prod_{\substack{n''=1 \\ n'' \neq n'}}^{N_2} (\beta_{z_n} - \beta_{z_{n''}}^*)^2 \right] \} \quad (G.79)$$

$$D_{-n}^{UU'} = -(\beta_{P1} + \beta_{P2}) \prod_{m'=1}^{N_1} (\beta_{z_n}^* - \beta_{z_{m'}}) (\beta_{z_n}^* - \beta_{z_{m'}}^*) \times$$

$$\prod_{n'=1}^{N_2} (\beta_{z_n}^* - \beta_{z_{n'}})^2 \prod_{\substack{n'=1 \\ n' \neq n}}^{N_2} (\beta_{z_n}^* - \beta_{z_{n'}}^*)^2 +$$

$$(2\beta_{z_n}^* - \beta_{P1} - \beta_{P2}) \times$$

$$\begin{aligned}
& \left\{ \prod_{n'=1}^{N_2} (\beta_{z_n}^* - \beta_{z_{n'}})^2 \prod_{\substack{n'=1 \\ n' \neq n}}^{N_2} (\beta_{z_n}^* - \beta_{z_{n'}}^*)^2 \sum_{m'=1}^{N_1} \left[\prod_{\substack{m''=1 \\ m'' \neq m'}}^{N_1} (\beta_{z_n}^* - \beta_{z_{m''}}) \prod_{m''=1}^{N_1} (\beta_{z_n}^* - \beta_{z_{m''}}^*) + \right. \right. \\
& \quad \left. \prod_{m''=1}^{N_1} (\beta_{z_n}^* - \beta_{z_{m''}}) \prod_{\substack{m''=1 \\ m'' \neq m'}}^{N_1} (\beta_{z_n}^* - \beta_{z_{m''}}^*) \right] + \\
& \quad 2 \prod_{m'=1}^{N_1} (\beta_{z_n}^* - \beta_{z_{m'}}) (\beta_{z_n}^* - \beta_{z_{m'}}^*) \times \\
& \quad \left[\sum_{n'=1}^{N_2} (\beta_{z_n}^* - \beta_{z_{n'}}) \prod_{\substack{n''=1 \\ n'' \neq n'}}^{N_2} (\beta_{z_n}^* - \beta_{z_{n''}})^2 \prod_{\substack{n''=1 \\ n'' \neq n}}^{N_2} (\beta_{z_n}^* - \beta_{z_{n''}}^*)^2 + \right. \\
& \quad \left. \sum_{\substack{n'=1 \\ n' \neq n}}^{N_2} (\beta_{z_n}^* - \beta_{z_{n'}}) \prod_{n''=1}^{N_2} (\beta_{z_n}^* - \beta_{z_{n''}})^2 \prod_{\substack{n''=1 \\ n'' \neq n'}}^{N_2} (\beta_{z_n}^* - \beta_{z_{n''}}^*)^2 \right] \} \quad (G.80)
\end{aligned}$$

The functions $R_P^{\cap\cap}$, $R_{S1}^{\cap\cap}$, and $R_{S2}^{\cap\cap}$ are identical to $R_P^{\cup\cup}$, $R_{S1}^{\cup\cup}$, and $R_{S2}^{\cup\cup}$ respectively.

$$R_P^{\cap\cap}(\bar{\beta}_\perp, \beta_{P1}, \beta_{P2}, h) = R_P^{\cup\cup}(\bar{\beta}_\perp, \beta_{P1}, \beta_{P2}, h) \quad (G.81)$$

$$R_{S1}^{\cap\cap}(\bar{\beta}_\perp, \beta_{P1}, \beta_{P2}, h) = R_{S1}^{\cup\cup}(\bar{\beta}_\perp, \beta_{P1}, \beta_{P2}, h) \quad (G.82)$$

$$R_{S2}^{\cap\cap}(\bar{\beta}_\perp, \beta_{P1}, \beta_{P2}, h) = R_{S2}^{\cup\cup}(\bar{\beta}_\perp, \beta_{P1}, \beta_{P2}, h) \quad (G.83)$$

The second two terms, $\sigma_{TC-TC}^{\cap\cap}$ and $\sigma_{TC-TC}^{\cup\cup}$, are given by (G.84) and (G.85),

$$\sigma_{TC-TC}^{\cap\cap} = \lim_{\delta_z \rightarrow 0} (2\pi)^5 i \sum_{\substack{p, s, q, \ell, \\ p', s', q', \ell' = +, -}} \sum_{\substack{u, v, w, \\ u', v', w' = TE, TM}} \sum_{\alpha, \beta, \gamma, \rho = x, y, z} \iint d\bar{k}_\perp A_{TC-TC}^{\substack{\alpha\beta\gamma\rho \\ pp'ss'qq'\ell\ell' \\ uu'vv'ww' \\ \cap\cap}} \times$$

$$\begin{aligned}
& e^{i(\bar{k}_{\perp ai} - \bar{k}_{\perp bi} + \bar{k}_{\perp bs} - \bar{k}_{\perp as}) \cdot \bar{r}_{T\perp}} \times \\
& e^{-i(s k_{tza}^{(w)} + q k_{tza}^{(v)} - s' k_{tzb}^{(w')*} - q' k_{tzc}^{(v')*} - \ell k_{tza}^{(v)} + p k_{tza}^{(u)} + \ell' k_{tzc}^{(v')*} - p' k_{tzb}^{(u')*}) z_T} \times \\
& \left[R_{S1}^{\cup} (\bar{k}_{\perp a} - \bar{k}_{\perp as}, \ell k_{tza}^{(v)} - p k_{tza}^{(u)}, \ell' k_{tzc}^{(v')*} - p' k_{tzb}^{(u')*}) + \right. \\
& \left. R_{S2}^{\cup} (\bar{k}_{\perp a} - \bar{k}_{\perp as}, \ell k_{tza}^{(v)} - p k_{tza}^{(u)}, \ell' k_{tzc}^{(v')*} - p' k_{tzb}^{(u')*}) \right] \quad (G.84)
\end{aligned}$$

$$\begin{aligned}
\sigma_{TC-TC}^{\cup} &= \lim_{\delta z \rightarrow 0} (2\pi)^5 i \sum_{\substack{p,s,q,\ell, \\ p',s',q',\ell'=+,-}} \sum_{\substack{u,v,w, \\ u',v',w'=TE,TM}} \sum_{\alpha,\beta,\gamma,\rho=x,y,z} \iint d\bar{k}_{\perp} A_{TC-TC}^{\alpha\beta\gamma\rho} \times \\
& e^{i(\bar{k}_{\perp ai} - \bar{k}_{\perp bi} + \bar{k}_{\perp bs} - \bar{k}_{\perp as}) \cdot \bar{r}_{T\perp}} \times \\
& e^{-i(s k_{tza}^{(w)} + q k_{tza}^{(v)} - s' k_{tzb}^{(w')*} - q' k_{tzc}^{(v')*} - \ell k_{tza}^{(v)} + p k_{tza}^{(u)} + \ell' k_{tzc}^{(v')*} - p' k_{tzb}^{(u')*}) z_T} \times \\
& \left[R_{S1}^{\cup} (\bar{k}_{\perp a} - \bar{k}_{\perp as}, \ell k_{tza}^{(v)} - p k_{tza}^{(u)}, \ell' k_{tzc}^{(v')*} - p' k_{tzb}^{(u')*}) + \right. \\
& \left. R_{S2}^{\cup} (\bar{k}_{\perp a} - \bar{k}_{\perp as}, \ell k_{tza}^{(v)} - p k_{tza}^{(u)}, \ell' k_{tzc}^{(v')*} - p' k_{tzb}^{(u')*}) \right] \quad (G.85)
\end{aligned}$$

where $\bar{k}_{\perp c}$, h_t^+ , and h_t^- are given by (G.65)-(G.67), and where

$$\begin{aligned}
A_{TC-TC}^{\alpha\beta\gamma\rho} &= \frac{|\alpha'|^2}{4\pi} \left[\hat{p}_a \cdot \bar{H}_{0tp}^{(u)}(\bar{k}_{\perp as}) \right]_{\alpha} \cdot \left[\bar{F}_{t\cup_{tq}}^{(v)}(\bar{k}_{\perp a}) \cdot \bar{E}_{tai}^{s,(w)} \right]_{\beta} \times \\
& \left[\hat{p}_b \cdot \bar{H}_{0tp'}^{(u')}(\bar{k}_{\perp bs}) \right]_{\gamma}^* \cdot \left[\bar{F}_{t\cap_{t'q'}}^{(v')}(\bar{k}_{\perp c}) \cdot \bar{E}_{tbi}^{s',(w')} \right]_{\rho}^* \quad (G.86)
\end{aligned}$$

$$\begin{aligned}
A_{TC-TC}^{\alpha\beta\gamma\rho} &= \frac{|\alpha'|^2}{4\pi} \left[\hat{p}_a \cdot \bar{H}_{0tp}^{(u)}(\bar{k}_{\perp as}) \right]_{\alpha} \cdot \left[\bar{F}_{t\cap_{tq}}^{(v)}(\bar{k}_{\perp a}) \cdot \bar{E}_{tai}^{s,(w)} \right]_{\beta} \times \\
& \left[\hat{p}_b \cdot \bar{H}_{0tp'}^{(u')}(\bar{k}_{\perp bs}) \right]_{\gamma}^* \cdot \left[\bar{F}_{t\cup_{t'q'}}^{(v')}(\bar{k}_{\perp c}) \cdot \bar{E}_{tbi}^{s',(w')} \right]_{\rho}^* \quad (G.87)
\end{aligned}$$

The functions R_{S1}^{\cup} and R_{S2}^{\cup} are defined by (G.88) and (G.89),

$$\begin{aligned}
R_{S1}^{\text{un}}(\bar{\beta}_\perp, \beta_{P1}, \beta_{P2}) &= \sum_{m=1}^{N_1} \frac{(1 - e^{-i(\beta_{zm}^* - \beta_{P1})h_t^+})(1 - e^{-i(\beta_{zm}^* - \beta_{P2})h_t^-})}{(\beta_{zm}^* - \beta_{P1})(\beta_{zm}^* - \beta_{P2})} \times \\
&\quad \frac{\Phi_N(\bar{\beta}_\perp, \beta_{zm}^*)}{\prod_{m'=1}^{N_1} (\beta_{zm}^* - \beta_{zm'}) \prod_{\substack{m'=1 \\ m' \neq m}}^{N_1} (\beta_{zm}^* - \beta_{zm'})} \times \\
&\quad \frac{e^{-i(2\beta_{zm}^* - \beta_{P1} - \beta_{P2})\delta_z}}{\prod_{n'=1}^{N_2} (\beta_{zm}^* - \beta_{zn'})^2 (\beta_{zm}^* - \beta_{zn'})^2} \quad (G.88)
\end{aligned}$$

$$\begin{aligned}
R_{S2}^{\text{un}}(\bar{\beta}_\perp, \beta_{P1}, \beta_{P2}) &= \sum_{n=1}^{N_2} \frac{1}{D_{-n}^{\text{un}2}} \left\{ D_{-n}^{\text{un}} [\Phi'_N(\bar{\beta}_\perp, \beta_{zn}^*) N_{-n}^{\text{un}} + \Phi_N(\bar{\beta}_\perp, \beta_{zn}^*) N_{-n}^{\text{un}'}] \right. \\
&\quad \left. - D_{-n}^{\text{un}'} \Phi_N(\bar{\beta}_\perp, \beta_{zn}^*) N_{-n}^{\text{un}} \right\} \quad (G.89)
\end{aligned}$$

where N_{-n}^{un} and $N_{-n}^{\text{un}'}$ are given by (G.90) and (G.91),

$$\begin{aligned}
N_{-n}^{\text{un}} &= \left(e^{-i(\beta_{zn}^* - \beta_{P1})\delta_z} - e^{-i(\beta_{zn}^* - \beta_{P1})(h_t^+ + \delta_z)} \right) \times \\
&\quad \left(e^{-i(\beta_{zn}^* - \beta_{P2})\delta_z} - e^{-i(\beta_{zn}^* - \beta_{P2})(h_t^- + \delta_z)} \right) \quad (G.90)
\end{aligned}$$

$$\begin{aligned}
N_{-n}^{\text{un}'} &= i \left(h_t^- + 2\delta_z \right) e^{-i(\beta_{zn}^* - \beta_{P1})\delta_z} e^{-i(\beta_{zn}^* - \beta_{P2})(h_t^- + \delta_z)} - \\
&\quad 2i\delta_z e^{-i(\beta_{zn}^* - \beta_{P1})\delta_z} e^{-i(\beta_{zn}^* - \beta_{P2})\delta_z} + \\
&\quad i \left(h_t^+ + 2\delta_z \right) e^{-i(\beta_{zn}^* - \beta_{P1})(h_t^+ + \delta_z)} e^{-i(\beta_{zn}^* - \beta_{P2})\delta_z} - \\
&\quad i \left(h_t^+ + h_t^- + 2\delta_z \right) e^{-i(\beta_{zn}^* - \beta_{P1})(h_t^+ + \delta_z)} e^{-i(\beta_{zn}^* - \beta_{P2})(h_t^- + \delta_z)} \quad (G.91)
\end{aligned}$$

and where D_{-n}^{un} and $D_{-n}^{\text{un}'}$ are identical to D_{-n}^{uu} and $D_{-n}^{\text{uu}'}$, respectively.

$$D_{-n}^{\cup\cap}(\beta_{P1}, \beta_{P2}) = D_{-n}^{\cup\cup}(\beta_{P1}, \beta_{P2}) \quad (G.92)$$

$$D_{-n}^{\cup\cap'}(\beta_{P1}, \beta_{P2}) = D_{-n}^{\cup\cup'}(\beta_{P1}, \beta_{P2}) \quad (G.93)$$

Similarly, $R_{S1}^{\cup\cup}$ and $R_{S2}^{\cup\cup}$ are defined by (G.94) and (G.95),

$$\begin{aligned} R_{S1}^{\cup\cup}(\bar{\beta}_{\perp}, \beta_{P1}, \beta_{P2}) = & - \sum_{m=1}^{N_1} \frac{(1 - e^{i(\beta_{zm} - \beta_{P1})h_i^-})(1 - e^{-i(\beta_{zm} - \beta_{P2})h_i^+})}{(\beta_{zm} - \beta_{P1})(\beta_{zm} - \beta_{P2})} \times \\ & \frac{\Phi_N(\bar{\beta}_{\perp}, \beta_{zm})}{\prod_{\substack{m'=1 \\ m' \neq m}}^{N_1} (\beta_{zm} - \beta_{zm'}) \prod_{m'=1}^{N_1} (\beta_{zm} - \beta_{zm'}^*)} \times \\ & \frac{e^{i(2\beta_{zm} - \beta_{P1} - \beta_{P2})\delta_z}}{\prod_{n'=1}^{N_2} (\beta_{zm} - \beta_{zn'})^2 (\beta_{zm} - \beta_{zn'}^*)^2} \end{aligned} \quad (G.94)$$

$$\begin{aligned} R_{S2}^{\cup\cup}(\bar{\beta}_{\perp}, \beta_{P1}, \beta_{P2}) = & - \sum_{n=1}^{N_2} \frac{1}{D_{+n}^{\cup\cup 2}} \left\{ D_{+n}^{\cup\cup} [\Phi'_N(\bar{\beta}_{\perp}, \beta_{zn}) N_{+n}^{\cup\cup} + \Phi_N(\bar{\beta}_{\perp}, \beta_{zn}) N_{+n}^{\cup\cup'}] \right. \\ & \left. - D_{+n}^{\cup\cup'} \Phi_N(\bar{\beta}_{\perp}, \beta_{zn}) N_{+n}^{\cup\cup} \right\} \end{aligned} \quad (G.95)$$

where $N_{+n}^{\cup\cup}$ and $N_{+n}^{\cup\cup'}$ are given by (G.96) and (G.97),

$$\begin{aligned} N_{+n}^{\cup\cup} = & \left(e^{i(\beta_{zn} - \beta_{P1})\delta_z} - e^{i(\beta_{zn} - \beta_{P1})(h_i^- + \delta_z)} \right) \times \\ & \left(e^{i(\beta_{zn} - \beta_{P2})\delta_z} - e^{i(\beta_{zn} - \beta_{P2})(h_i^+ + \delta_z)} \right) \end{aligned} \quad (G.96)$$

$$\begin{aligned}
N_{+n}^{\cap\cup'} = & -i \left(h_t^+ + 2\delta_z \right) e^{i(\beta_{zn}-\beta_{P1})\delta_z} e^{i(\beta_{zn}-\beta_{P2})(h_t^++\delta_z)} + \\
& 2i\delta_z e^{i(\beta_{zn}-\beta_{P1})\delta_z} e^{i(\beta_{zn}-\beta_{P2})\delta_z} - \\
& i \left(h_t^- + 2\delta_z \right) e^{i(\beta_{zn}-\beta_{P1})(h_t^-+\delta_z)} e^{i(\beta_{zn}-\beta_{P2})\delta_z} + \\
& i \left(h_t^+ + h_t^- + 2\delta_z \right) e^{i(\beta_{zn}-\beta_{P1})(h_t^-+\delta_z)} e^{i(\beta_{zn}-\beta_{P2})(h_t^++\delta_z)} \quad (G.97)
\end{aligned}$$

and where $D_{+n}^{\cap\cup}$ and $D_{+n}^{\cap\cup'}$ are identical to $D_{+n}^{\cap\cap}$ and $D_{+n}^{\cap\cap'}$, respectively.

$$D_{+n}^{\cap\cup}(\beta_{P1}, \beta_{P2}) = D_{+n}^{\cap\cap}(\beta_{P1}, \beta_{P2}) \quad (G.98)$$

$$D_{+n}^{\cap\cup'}(\beta_{P1}, \beta_{P2}) = D_{+n}^{\cap\cap'}(\beta_{P1}, \beta_{P2}) \quad (G.99)$$

The fifth term, $\sigma_{\overline{TC}-TC}^{\overline{TC}}$, is given by (G.100),

$$\begin{aligned}
\sigma_{\overline{TC}-TC}^{\overline{TC}} = & \sum_{p,s,p',s'=+,-} \sum_{u,w,u',w'=TE, TM} \sum_{\alpha,\beta,\gamma,\rho=x,y,z} A_{\overline{TC}-TC}^{\alpha\beta\gamma\rho}_{pp'ss'} C_{\alpha\beta\gamma\rho}(0) \times \\
& e^{i(\bar{k}_{\perp ai} - \bar{k}_{\perp bi} + \bar{k}_{\perp bs} - \bar{k}_{\perp as}) \cdot \bar{r}_{T\perp}} e^{-i(s k_{iz ai}^{(w)} - s' k_{iz bi}^{(w')*} + p k_{iz as}^{(u)} - p' k_{iz bs}^{(u')*}) z_T} \quad (G.100)
\end{aligned}$$

where

$$\begin{aligned}
A_{\overline{TC}-TC}^{\alpha\beta\gamma\rho}_{pp'ss'} = & \frac{|\alpha'|^2}{4\pi} \left[\hat{p}_a \cdot \overline{H}_{0t_p}^{(u)}(\bar{k}_{\perp as}) \right]_{\alpha} \cdot \left[\overline{D}_t^a \cdot \overline{E}_{tai}^{s,(w)} \right]_{\beta} \times \\
& \left[\hat{p}_b \cdot \overline{H}_{0t_{p'}}^{(u')}(\bar{k}_{\perp bs}) \right]_{\gamma}^* \cdot \left[\overline{D}_t^b \cdot \overline{E}_{tbi}^{s',(w')} \right]_{\rho}^* \quad (G.101)
\end{aligned}$$

The sixth and seventh terms, $\sigma_{TC-TC}^{\cup=}$ and $\sigma_{TC-TC}^{\cap=}$, are given by (G.102) and (G.103),

$$\begin{aligned} \sigma_{TC-TC}^{\cup=} = & -\lim_{\delta z \rightarrow 0} (2\pi)^3 \sum_{\substack{p,s,q,\ell, \\ p',s'=+,-}} \sum_{\substack{u,v,w, \\ u',w'=TE,TM}} \sum_{\alpha,\beta,\gamma,\rho=x,y,z} \iint d\bar{k}_{\perp a} A_{TC-TC}^{\substack{\alpha\beta\gamma\rho \\ pp'ss'q\ell \\ uu'vw w' \\ \cup=}} \times \\ & e^{i(\bar{k}_{\perp ai} - \bar{k}_{\perp bi} + \bar{k}_{\perp bs} - \bar{k}_{\perp as}) \cdot \vec{r}_{T\perp}} e^{-i(sk_{tz ai}^{(w)} + qk_{tz a}^{(v)} - s'k_{tz bi}^{(w')*} - p'k_{tz bs}^{(u')*})z_T} \times \\ & [R_{S1}^{\cup=} (\bar{k}_{\perp a} - \bar{k}_{\perp as}, \ell k_{tz a}^{(v)} - pk_{tz as}^{(u)}) + R_{S2}^{\cup=} (\bar{k}_{\perp a} - \bar{k}_{\perp as}, \ell k_{tz a}^{(v)} - pk_{tz as}^{(u)})] \end{aligned} \quad (G.102)$$

$$\begin{aligned} \sigma_{TC-TC}^{\cap=} = & -\lim_{\delta z \rightarrow 0} (2\pi)^3 \sum_{\substack{p,s,q,\ell, \\ p',s'=+,-}} \sum_{\substack{u,v,w, \\ u',w'=TE,TM}} \sum_{\alpha,\beta,\gamma,\rho=x,y,z} \iint d\bar{k}_{\perp a} A_{TC-TC}^{\substack{\alpha\beta\gamma\rho \\ pp'ss'q\ell \\ uu'vw w' \\ \cap=}} \times \\ & e^{i(\bar{k}_{\perp ai} - \bar{k}_{\perp bi} + \bar{k}_{\perp bs} - \bar{k}_{\perp as}) \cdot \vec{r}_{T\perp}} e^{-i(sk_{tz ai}^{(w)} + qk_{tz a}^{(v)} - s'k_{tz bi}^{(w')*} - p'k_{tz bs}^{(u')*})z_T} \times \\ & [R_{S1}^{\cap=} (\bar{k}_{\perp a} - \bar{k}_{\perp as}, \ell k_{tz a}^{(v)} - pk_{tz as}^{(u)}) + R_{S2}^{\cap=} (\bar{k}_{\perp a} - \bar{k}_{\perp as}, \ell k_{tz a}^{(v)} - pk_{tz as}^{(u)})] \end{aligned} \quad (G.103)$$

where

$$\begin{aligned} A_{TC-TC}^{\substack{\alpha\beta\gamma\rho \\ pp'ss'q\ell \\ uu'vw w' \\ \cup=}} = & \frac{|\alpha'|^2}{4\pi} \left[\hat{p}_a \cdot \overline{H}_{0t_p}^{(u)}(\bar{k}_{\perp as}) \right]_{\alpha} \cdot \left[\overline{F}_{t \cup t_q}^{(v)}(\bar{k}_{\perp a}) \cdot \overline{E}_{tai}^{s,(w)} \right]_{\beta} \times \\ & \left[\hat{p}_b \cdot \overline{H}_{0t_{p'}}^{(u')}(\bar{k}_{\perp bs}) \right]_{\gamma}^* \cdot \left[\overline{D}_t^b \cdot \overline{E}_{tbi}^{s',(w')} \right]_{\rho}^* \end{aligned} \quad (G.104)$$

$$\begin{aligned} A_{TC-TC}^{\substack{\alpha\beta\gamma\rho \\ pp'ss'q\ell \\ uu'vw w' \\ \cap=}} = & \frac{|\alpha'|^2}{4\pi} \left[\hat{p}_a \cdot \overline{H}_{0t_p}^{(u)}(\bar{k}_{\perp as}) \right]_{\alpha} \cdot \left[\overline{F}_{t \cap t_q}^{(v)}(\bar{k}_{\perp a}) \cdot \overline{E}_{tai}^{s,(w)} \right]_{\beta} \times \\ & \left[\hat{p}_b \cdot \overline{H}_{0t_{p'}}^{(u')}(\bar{k}_{\perp bs}) \right]_{\gamma}^* \cdot \left[\overline{D}_t^b \cdot \overline{E}_{tbi}^{s',(w')} \right]_{\rho}^* \end{aligned} \quad (G.105)$$

and where $R_{S1}^{U=}$, $R_{S2}^{U=}$, $R_{S1}^{\cap=}$, and $R_{S2}^{\cap=}$ are given by (G.106)-(G.109).

$$R_{S1}^{U=} = - \sum_{m=1}^{N_1} \frac{\left(1 - e^{i(\beta_{zm}^* - \beta_{P1})h_t^+}\right) \left(e^{i(\beta_{zm}^* - \beta_{P1})d_{t-1}}\right)}{\beta_{zm}^* - \beta_{P1}} \times$$

$$\frac{\Phi_N(\bar{\beta}_\perp, \beta_{zm}^*) e^{i\beta_{zm}^* z_T}}{\prod_{m'=1}^{N_1} (\beta_{zm}^* - \beta_{zm'}) \prod_{\substack{m'=1 \\ m' \neq m}}^{N_1} (\beta_{zm}^* - \beta_{zm'}) \prod_{n'=1}^{N_2} (\beta_{zm}^* - \beta_{zn'})^2 (\beta_{zm}^* - \beta_{zn'})^2}$$
(G.106)

$$R_{S2}^{U=} = - \sum_{n=1}^{N_2} \frac{1}{D_{-n}^{U=2}} \left\{ D_{-n}^{U=} \left[\Phi'_N(\bar{\beta}_\perp, \beta_{zn}^*) N_{-n}^{U=} + \Phi_N(\bar{\beta}_\perp, \beta_{zn}^*) N_{-n}^{U='} \right] \right.$$

$$\left. - D_{-n}^{U='} \Phi_N(\bar{\beta}_\perp, \beta_{zn}^*) N_{-n}^{U=} \right\}$$
(G.107)

$$R_{S1}^{\cap=} = \sum_{m=1}^{N_1} \frac{1 - e^{i(\beta_{zm} - \beta_{P1})h_t^-}}{\beta_{zm} - \beta_{P1}} \times$$

$$\frac{\Phi_N(\bar{\beta}_\perp, \beta_{zm}) e^{i(\beta_{zm} - \beta_{P1})\delta_z}}{\prod_{\substack{m'=1 \\ m' \neq m}}^{N_1} (\beta_{zm} - \beta_{zm'}) \prod_{m'=1}^{N_1} (\beta_{zm} - \beta_{zm'}) \prod_{n'=1}^{N_2} (\beta_{zm} - \beta_{zn'})^2 (\beta_{zm} - \beta_{zn'})^2}$$
(G.108)

$$R_{S2}^{\cap=} = \sum_{n=1}^{N_2} \frac{1}{D_{+n}^{\cap=2}} \left\{ D_{+n}^{\cap=} \left[\Phi'_N(\bar{\beta}_\perp, \beta_{zn}) N_{+n}^{\cap=} + \Phi_N(\bar{\beta}_\perp, \beta_{zn}) N_{+n}^{\cap='} \right] \right.$$

$$\left. - D_{+n}^{\cap='} \Phi_N(\bar{\beta}_\perp, \beta_{zn}) N_{+n}^{\cap=} \right\}$$
(G.109)

The expressions for $N_{-n}^{U=}$, $N_{-n}^{U='}$, $N_{+n}^{\cap=}$, and $N_{+n}^{\cap='}$ are given by (G.110)-(G.113).

$$N_{-n}^{U=} = e^{i\beta_{zn}^* z_T} e^{i(\beta_{zn}^* - \beta_{P1})d_{t-1}} \left(1 - e^{i(\beta_{zn}^* - \beta_{P1})h_t^+}\right)$$
(G.110)

$$N_{-n}^{\cup=} = i \left[(z_T + d_{t-1}) + \delta_z e^{i(\beta_{z_n}^* - \beta_{P1})h_t^+} \right] e^{i\beta_{z_n}^* z_T} e^{i(\beta_{z_n}^* - \beta_{P1})d_{t-1}} \quad (G.111)$$

$$N_{+n}^{\cap=} = e^{i(\beta_{z_n} - \beta_{P1})\delta_z} \left(1 - e^{i(\beta_{z_n} - \beta_{P1})h_t^-} \right) \quad (G.112)$$

$$N_{+n}^{\cap=} = i \left[\delta_z - (\delta_z + h_t^-) e^{i(\beta_{z_n} - \beta_{P1})h_t^-} \right] e^{i(\beta_{z_n} - \beta_{P1})\delta_z} \quad (G.113)$$

The expressions for $D_{-n}^{\cup=}$ and $D_{-n}^{\cup=}$ are given by (G.114) and (G.115),

$$D_{-n}^{\cup=} = (\beta_{z_n}^* - \beta_{P1}) \prod_{m'=1}^{N_1} (\beta_{z_n}^* - \beta_{z_{m'}}) (\beta_{z_n}^* - \beta_{z_{m'}}^*) \times \prod_{n'=1}^{N_2} (\beta_{z_n}^* - \beta_{z_{n'}})^2 \prod_{\substack{n'=1 \\ n' \neq n}}^{N_2} (\beta_{z_n}^* - \beta_{z_{n'}}^*)^2 \quad (G.114)$$

$$D_{-n}^{\cup=} = \prod_{m'=1}^{N_1} (\beta_{z_n}^* - \beta_{z_{m'}}) (\beta_{z_n}^* - \beta_{z_{m'}}^*) \prod_{n'=1}^{N_2} (\beta_{z_n}^* - \beta_{z_{n'}})^2 \prod_{\substack{n'=1 \\ n' \neq n}}^{N_2} (\beta_{z_n}^* - \beta_{z_{n'}}^*)^2 (\beta_{z_n}^* - \beta_{P1}) \times \left\{ \prod_{n'=1}^{N_2} (\beta_{z_n}^* - \beta_{z_{n'}})^2 \prod_{\substack{n'=1 \\ n' \neq n}}^{N_2} (\beta_{z_n}^* - \beta_{z_{n'}}^*)^2 \sum_{m'=1}^{N_1} \left[\prod_{\substack{m''=1 \\ m'' \neq m'}}^{N_1} (\beta_{z_n}^* - \beta_{z_{m''}}) \prod_{m''=1}^{N_1} (\beta_{z_n}^* - \beta_{z_{m''}}^*) + \prod_{m''=1}^{N_1} (\beta_{z_n}^* - \beta_{z_{m''}}) \prod_{\substack{m''=1 \\ m'' \neq m'}}^{N_1} (\beta_{z_n}^* - \beta_{z_{m''}}^*) \right] + 2 \prod_{m'=1}^{N_1} (\beta_{z_n}^* - \beta_{z_{m'}}) (\beta_{z_n}^* - \beta_{z_{m'}}^*) \times \right.$$

$$\begin{aligned}
& \left[\sum_{n'=1}^{N_2} (\beta_{z_n}^* - \beta_{z_{n'}}) \prod_{\substack{n''=1 \\ n'' \neq n'}}^{N_2} (\beta_{z_n}^* - \beta_{z_{n''}})^2 \prod_{\substack{n''=1 \\ n'' \neq n}}^{N_2} (\beta_{z_n}^* - \beta_{z_{n''}}^*)^2 + \right. \\
& \left. \sum_{\substack{n'=1 \\ n' \neq n}}^{N_2} (\beta_{z_n}^* - \beta_{z_{n'}}^*) \prod_{n''=1}^{N_2} (\beta_{z_n}^* - \beta_{z_{n''}})^2 \prod_{\substack{n''=1 \\ n'' \neq n' \\ n'' \neq n}}^{N_2} (\beta_{z_n}^* - \beta_{z_{n''}}^*)^2 \right] \Big\} \\
& \hspace{15em} (G.115)
\end{aligned}$$

and $D_{+n}^{\cap=}$ and $D_{+n}^{\cap=}$ are related to the above by (G.116) and (G.117).

$$D_{+n}^{\cap=}(\beta_{P1}) = [D_{-n}^{\cup=}(\beta_{P1}^*)]^* \quad (G.116)$$

$$D_{+n}^{\cap=}(\beta_{P1}) = [D_{-n}^{\cup=}(\beta_{P1}^*)]^* \quad (G.117)$$

The final two terms, σ_{TC-TC}^{\cup} and σ_{TC-TC}^{\cap} , are given by (G.118) and (G.119),

$$\begin{aligned}
\sigma_{TC-TC}^{\cup} = & - \lim_{\delta_z \rightarrow 0} (2\pi)^3 \sum_{\substack{p,s,p',s', \\ q,\ell=+,-}} \sum_{\substack{u,w,u', \\ v',w'=TE,TM}} \sum_{\alpha,\beta,\gamma,\rho=x,y,z} \iint d\bar{k}_{\perp b} A_{TC-TC}^{\substack{\alpha\beta\gamma\rho \\ pp'ss'q'\ell' \\ uu'v'ww' \\ =\cup}} \times \\
& e^{i(\bar{k}_{\perp ai} - \bar{k}_{\perp bi} + \bar{k}_{\perp bs} - \bar{k}_{\perp as}) \cdot \bar{r}_{T\perp}} e^{-i(s k_{tz ai}^{(w)} + p k_{tz as}^{(u)} - q' k_{tz b}^{(v')*} - s' k_{tz bi}^{(w')*}) z_T} \times \\
& [R_{S1}^{\cup}(\bar{k}_{\perp b} - \bar{k}_{\perp bs}, \ell' k_{tz b}^{(v')*} - p' k_{tz bs}^{(u')*}) + R_{S2}^{\cup}(\bar{k}_{\perp b} - \bar{k}_{\perp bs}, \ell' k_{tz b}^{(v')*} - p' k_{tz bs}^{(u')*})] \\
& \hspace{15em} (G.118)
\end{aligned}$$

$$\begin{aligned}
\sigma_{TC-TC}^{\cap} = & - \lim_{\delta_z \rightarrow 0} (2\pi)^3 \sum_{\substack{p,s,p',s', \\ q,\ell=+,-}} \sum_{\substack{u,w,u', \\ v',w'=TE,TM}} \sum_{\alpha,\beta,\gamma,\rho=x,y,z} \iint d\bar{k}_{\perp b} A_{TC-TC}^{\substack{\alpha\beta\gamma\rho \\ pp'ss'q'\ell' \\ uu'v'ww' \\ =\cap}} \times \\
& e^{i(\bar{k}_{\perp ai} - \bar{k}_{\perp bi} + \bar{k}_{\perp bs} - \bar{k}_{\perp as}) \cdot \bar{r}_{T\perp}} e^{-i(s k_{tz ai}^{(w)} + p k_{tz as}^{(u)} - q' k_{tz b}^{(v')*} - s' k_{tz bi}^{(w')*}) z_T} \times \\
& [R_{S1}^{\cap}(\bar{k}_{\perp b} - \bar{k}_{\perp bs}, \ell' k_{tz b}^{(v')*} - p' k_{tz bs}^{(u')*}) + R_{S2}^{\cap}(\bar{k}_{\perp b} - \bar{k}_{\perp bs}, \ell' k_{tz b}^{(v')*} - p' k_{tz bs}^{(u')*})] \\
& \hspace{15em} (G.119)
\end{aligned}$$

where

$$A_{TC-TC}^{\alpha\beta\gamma\rho}_{\substack{pp'ss'q'l'l' \\ uu'v'ww' \\ =U}} = \frac{|\alpha'|^2}{4\pi} \left[\hat{p}_a \cdot \overline{H}_{0t_p}^{(u)}(\overline{k}_{\perp as}) \right]_{\alpha} \cdot \left[\overline{D}_t^a \cdot \overline{E}_{tai}^{s,(w)} \right]_{\beta} \times \\ \left[\hat{p}_b \cdot \overline{H}_{0t_{p'}}^{(u')}(\overline{k}_{\perp bs}) \right]_{\gamma}^* \cdot \left[\overline{F}_{t \cup t' q'}^{(v')}(\overline{k}_{\perp b}) \cdot \overline{E}_{tbi}^{s',(w')} \right]_{\rho}^* \quad (G.120)$$

$$A_{TC-TC}^{\alpha\beta\gamma\rho}_{\substack{pp'ss'q'l'l' \\ uu'v'ww' \\ =\cap}} = \frac{|\alpha'|^2}{4\pi} \left[\hat{p}_a \cdot \overline{H}_{0t_p}^{(u)}(\overline{k}_{\perp as}) \right]_{\alpha} \cdot \left[\overline{D}_t^a \cdot \overline{E}_{tai}^{s,(w)} \right]_{\beta} \times \\ \left[\hat{p}_b \cdot \overline{H}_{0t_{p'}}^{(u')}(\overline{k}_{\perp bs}) \right]_{\gamma}^* \cdot \left[\overline{F}_{t \cap t' q'}^{(v')}(\overline{k}_{\perp b}) \cdot \overline{E}_{tbi}^{s',(w')} \right]_{\rho}^* \quad (G.121)$$

and where $R_{S1}^{\cup=}$, $R_{S2}^{\cup=}$, $R_{S1}^{\cap=}$, and $R_{S2}^{\cap=}$ are related to $R_{S1}^{\cup=}$, $R_{S2}^{\cup=}$, $R_{S1}^{\cap=}$, and $R_{S2}^{\cap=}$ by (G.122)-(G.125).

$$R_{S1}^{\cup=}(\overline{\beta}_{\perp}, \beta_{P1}) = - \left[R_{S1}^{\cup=}(\overline{\beta}_{\perp}, \beta_{P1}^*) \right]^* \quad (G.122)$$

$$R_{S2}^{\cup=}(\overline{\beta}_{\perp}, \beta_{P1}) = - \left[R_{S2}^{\cup=}(\overline{\beta}_{\perp}, \beta_{P1}^*) \right]^* \quad (G.123)$$

$$R_{S1}^{\cap=}(\overline{\beta}_{\perp}, \beta_{P1}) = - \left[R_{S1}^{\cap=}(\overline{\beta}_{\perp}, \beta_{P1}^*) \right]^* \quad (G.124)$$

$$R_{S2}^{\cap=}(\overline{\beta}_{\perp}, \beta_{P1}) = - \left[R_{S2}^{\cap=}(\overline{\beta}_{\perp}, \beta_{P1}^*) \right]^* \quad (G.125)$$

G.2.2. Clutter/Target - Clutter/Target Correlation

The overall expression is again the sum of nine terms, as shown by (G.126).

$$\begin{aligned}
\sigma_{CT-CT}^{\hat{p}_a \hat{p}_b}(\bar{k}_{as}, \bar{k}_{ai}, \bar{k}_{bs}, \bar{k}_{bi}) &= 4\pi r^2 \langle \hat{p}_a \cdot \bar{E}_{CT}(\bar{k}_{as}, \bar{k}_{ai}) \times \hat{p}_b^* \cdot \bar{E}_{CT}^*(\bar{k}_{bs}, \bar{k}_{bi}) \rangle \\
&= \sigma_{CT-CT}^{\text{UU}} + \sigma_{CT-CT}^{\text{NN}} + \sigma_{CT-CT}^{\text{UN}} + \sigma_{CT-CT}^{\text{NU}} + \sigma_{CT-CT}^{\text{==}} \\
&\quad + \sigma_{CT-CT}^{\text{U=}} + \sigma_{CT-CT}^{\text{N=}} + \sigma_{CT-CT}^{\text{=U}} + \sigma_{CT-CT}^{\text{=N}} \quad (G.126)
\end{aligned}$$

The first two terms, $\sigma_{CT-CT}^{\text{UU}}$ and $\sigma_{CT-CT}^{\text{NN}}$, are given by (G.127) and (G.128),

$$\begin{aligned}
\sigma_{CT-CT}^{\text{UU}} &= \lim_{\delta z \rightarrow 0} (2\pi)^5 i \sum_{p', s', q', \ell' = +, -}^{p, s, q, \ell,} \sum_{u', v', w' = TE, TM}^{u, v, w,} \sum_{\alpha, \beta, \gamma, \rho = x, y, z} \iint d\bar{k}_{\perp a} A_{CT-CT}^{\alpha\beta\gamma\rho}_{uu'vv'ww'} \times \\
&\quad e^{i(\bar{k}_{\perp ai} - \bar{k}_{\perp bi} + \bar{k}_{\perp bs} - \bar{k}_{\perp as}) \cdot \bar{r}_{T\perp}} e^{i(\ell k_{tza}^{(v)} - p k_{tza}^{(u)} + p' k_{tzb}^{(u')*} - \ell' k_{tzc}^{(v')*}) z_T} \times \\
&\quad e^{i(q k_{tza}^{(v)} + s k_{tza}^{(w)} - q' k_{tzc}^{(v')*} - s' k_{tzb}^{(w')*}) d_{t-1}} \times \\
&\quad \left[R_P^{\text{UU}}(\bar{k}_{\perp ai} - \bar{k}_{\perp a}, -q k_{tza}^{(v)} - s k_{tza}^{(w)}, -q' k_{tzc}^{(v')*} - s' k_{tzb}^{(w')*}, h_t^+) + \right. \\
&\quad R_{S1}^{\text{UU}}(\bar{k}_{\perp ai} - \bar{k}_{\perp a}, -q k_{tza}^{(v)} - s k_{tza}^{(w)}, -q' k_{tzc}^{(v')*} - s' k_{tzb}^{(w')*}, h_t^+) + \\
&\quad \left. R_{S2}^{\text{UU}}(\bar{k}_{\perp ai} - \bar{k}_{\perp a}, -q k_{tza}^{(v)} - s k_{tza}^{(w)}, -q' k_{tzc}^{(v')*} - s' k_{tzb}^{(w')*}, h_t^+) \right] \quad (G.127)
\end{aligned}$$

$$\begin{aligned}
\sigma_{CT-CT}^{\text{NN}} &= \lim_{\delta z \rightarrow 0} (2\pi)^5 i \sum_{p', s', q', \ell' = +, -}^{p, s, q, \ell,} \sum_{u', v', w' = TE, TM}^{u, v, w,} \sum_{\alpha, \beta, \gamma, \rho = x, y, z} \iint d\bar{k}_{\perp a} A_{CT-CT}^{\alpha\beta\gamma\rho}_{nn} \times \\
&\quad e^{i(\bar{k}_{\perp ai} - \bar{k}_{\perp bi} + \bar{k}_{\perp bs} - \bar{k}_{\perp as}) \cdot \bar{r}_{T\perp}} e^{i(\ell k_{tza}^{(v)} - p k_{tza}^{(u)} + p' k_{tzb}^{(u')*} - \ell' k_{tzc}^{(v')*}) z_T} \times \\
&\quad e^{-i(q k_{tza}^{(v)} + s k_{tza}^{(w)} - q' k_{tzc}^{(v')*} - s' k_{tzb}^{(w')*}) (z_T - \delta z)} \times \\
&\quad \left[R_P^{\text{NN}}(\bar{k}_{\perp ai} - \bar{k}_{\perp a}, -q k_{tza}^{(v)} - s k_{tza}^{(w)}, -q' k_{tzc}^{(v')*} - s' k_{tzb}^{(w')*}, h_t^-) + \right.
\end{aligned}$$

$$R_{S1}^{\cap\cap} \left(\bar{k}_{\perp ai} - \bar{k}_{\perp a}, -qk_{tza}^{(v)} - sk_{tza}^{(w)}, -q'k_{tzc}^{(v')*} - s'k_{tzb}^{(w')*}, h_t^- \right) + \\ R_{S2}^{\cap\cap} \left(\bar{k}_{\perp ai} - \bar{k}_{\perp a}, -qk_{tza}^{(v)} - sk_{tza}^{(w)}, -q'k_{tzc}^{(v')*} - s'k_{tzb}^{(w')*}, h_t^- \right) \quad (G.128)$$

where

$$\bar{k}_{\perp c} = \bar{k}_{\perp a} + \bar{k}_{\perp bi} - \bar{k}_{\perp ai} \quad (G.129)$$

and

$$A_{CT-CT}^{\cap\cap, \alpha\beta\gamma\rho, pp's's'qq'\ell\ell'} = \frac{|\alpha'|^2}{4\pi} \left[\hat{p}_a \cdot \bar{H}_{0t_p}^{(u)}(\bar{k}_{\perp as}) \cdot \bar{F}_{t\cup\ell q}^{(v)}(\bar{k}_{\perp a}) \right]_{\alpha} \cdot \left[\bar{E}_{tai}^{s,(w)} \right]_{\beta} \times \\ \left[\hat{p}_b \cdot \bar{H}_{0t_p}^{(u')}(\bar{k}_{\perp bs}) \cdot \bar{F}_{t\cup\ell'q'}^{(v')}(\bar{k}_{\perp c}) \right]_{\gamma}^* \cdot \left[\bar{E}_{tbi}^{s',(w')} \right]_{\rho}^* \quad (G.130)$$

$$A_{CT-CT}^{\cap\cap, \alpha\beta\gamma\rho, pp's's'qq'\ell\ell'} = \frac{|\alpha'|^2}{4\pi} \left[\hat{p}_a \cdot \bar{H}_{0t_p}^{(u)}(\bar{k}_{\perp as}) \cdot \bar{F}_{t\cap\ell q}^{(v)}(\bar{k}_{\perp a}) \right]_{\alpha} \cdot \left[\bar{E}_{tai}^{s,(w)} \right]_{\beta} \times \\ \left[\hat{p}_b \cdot \bar{H}_{0t_p}^{(u')}(\bar{k}_{\perp bs}) \cdot \bar{F}_{t\cap\ell'q'}^{(v')}(\bar{k}_{\perp c}) \right]_{\gamma}^* \cdot \left[\bar{E}_{tbi}^{s',(w')} \right]_{\rho}^* \quad (G.131)$$

The functions $R_P^{\cup\cup}$, $R_{S1}^{\cup\cup}$, $R_{S2}^{\cup\cup}$, $R_P^{\cap\cap}$, $R_{S1}^{\cap\cap}$, and $R_{S2}^{\cap\cap}$ are defined by (G.70)-(G.83).

The next two terms, $\sigma_{CT-CT}^{\cup\cup}$ and $\sigma_{CT-CT}^{\cap\cap}$, are given by (G.132) and (G.133),

$$\sigma_{CT-CT}^{\cup\cup} = \lim_{\delta z \rightarrow 0} (2\pi)^5 i \sum_{\substack{p',s',q',\ell', \\ p',s',q',\ell'=+,-}} \sum_{\substack{u,v,w, \\ u',v',w'=TE,TM}} \sum_{\alpha,\beta,\gamma,\rho=x,y,z} \iint d\bar{k}_{\perp a} A_{CT-CT}^{\cup\cup, \alpha\beta\gamma\rho, pp's's'qq'\ell\ell'} \times \\ e^{i(\bar{k}_{\perp ai} - \bar{k}_{\perp bi} + \bar{k}_{\perp bs} - \bar{k}_{\perp as}) \cdot \bar{r}_{T\perp}} e^{i(\ell k_{tza}^{(v)} - p k_{tza}^{(u)} + p' k_{tza}^{(u')*} - \ell' k_{tzc}^{(v')*}) z_T} \times$$

$$\begin{aligned}
& e^{-i(qk_{tza}^{(v)} + sk_{tza}^{(w)} - q'k_{tzc}^{(v')*} - s'k_{tzb}^{(w')*})z_T} \times \\
& \left[R_{S1}^{\cup} (\bar{k}_{\perp ai} - \bar{k}_{\perp a}, -qk_{tza}^{(v)} - sk_{tza}^{(w)}, -q'k_{tzc}^{(v')*} - s'k_{tzb}^{(w')*}) + \right. \\
& \left. R_{S2}^{\cup} (\bar{k}_{\perp ai} - \bar{k}_{\perp a}, -qk_{tza}^{(v)} - sk_{tza}^{(w)}, -q'k_{tzc}^{(v')*} - s'k_{tzb}^{(w')*}) \right] \quad (G.132)
\end{aligned}$$

$$\begin{aligned}
\sigma_{CT-CT}^{\cup} &= \lim_{\delta z \rightarrow 0} (2\pi)^5 i \sum_{\substack{p',s',q',\ell', \\ p',s',q',\ell' = +,-}} \sum_{\substack{u,v,w, \\ u',v',w' = TE, TM}} \sum_{\alpha, \beta, \gamma, \rho = x, y, z} \iint d\bar{k}_{\perp a} A_{CT-CT}^{\alpha\beta\gamma\rho}{}_{\cup}{}^{pp'ss'qq'\ell\ell'}{}^{uu'vv'ww'} \times \\
& e^{i(\bar{k}_{\perp ai} - \bar{k}_{\perp bi} + \bar{k}_{\perp bs} - \bar{k}_{\perp as}) \cdot \vec{r}_{T\perp}} e^{i(\ell k_{tza}^{(v)} - p k_{tza}^{(u)} + p' k_{tzb}^{(u')*} - \ell' k_{tzc}^{(v')*})z_T} \times \\
& e^{-i(qk_{tza}^{(v)} + sk_{tza}^{(w)} - q'k_{tzc}^{(v')*} - s'k_{tzb}^{(w')*})z_T} \times \\
& \left[R_{S1}^{\cup} (\bar{k}_{\perp ai} - \bar{k}_{\perp a}, -qk_{tza}^{(v)} - sk_{tza}^{(w)}, -q'k_{tzc}^{(v')*} - s'k_{tzb}^{(w')*}) + \right. \\
& \left. R_{S2}^{\cup} (\bar{k}_{\perp ai} - \bar{k}_{\perp a}, -qk_{tza}^{(v)} - sk_{tza}^{(w)}, -q'k_{tzc}^{(v')*} - s'k_{tzb}^{(w')*}) \right] \quad (G.133)
\end{aligned}$$

where

$$\begin{aligned}
A_{CT-CT}^{\alpha\beta\gamma\rho}{}_{\cup}{}^{pp'ss'qq'\ell\ell'}{}^{uu'vv'ww'} &= \frac{|\alpha'|^2}{4\pi} \left[\hat{p}_a \cdot \overline{H}_{0t_p}^{(u)}(\bar{k}_{\perp as}) \cdot \overline{F}_{t \cup \ell_q}^{(v)}(\bar{k}_{\perp a}) \right]_{\alpha} \cdot \left[\overline{E}_{tai}^{s,(w)} \right]_{\beta} \times \\
& \left[\hat{p}_b \cdot \overline{H}_{0t_{p'}}^{(u')}(\bar{k}_{\perp bs}) \cdot \overline{F}_{t \cap \ell'_q}^{(v')}(\bar{k}_{\perp c}) \right]_{\gamma}^* \cdot \left[\overline{E}_{tbi}^{s',(w')} \right]_{\rho}^* \quad (G.134)
\end{aligned}$$

$$\begin{aligned}
A_{CT-CT}^{\alpha\beta\gamma\rho}{}_{\cup}{}^{pp'ss'qq'\ell\ell'}{}^{uu'vv'ww'} &= \frac{|\alpha'|^2}{4\pi} \left[\hat{p}_a \cdot \overline{H}_{0t_p}^{(u)}(\bar{k}_{\perp as}) \cdot \overline{F}_{t \cap \ell_q}^{(v)}(\bar{k}_{\perp a}) \right]_{\alpha} \cdot \left[\overline{E}_{tai}^{s,(w)} \right]_{\beta} \times \\
& \left[\hat{p}_b \cdot \overline{H}_{0t_{p'}}^{(u')}(\bar{k}_{\perp bs}) \cdot \overline{F}_{t \cup \ell'_q}^{(v')}(\bar{k}_{\perp c}) \right]_{\gamma}^* \cdot \left[\overline{E}_{tbi}^{s',(w')} \right]_{\rho}^* \quad (G.135)
\end{aligned}$$

and where R_{S1}^{\cup} , R_{S2}^{\cup} , R_{S1}^{\cap} , and R_{S2}^{\cap} are defined by (G.88)-(G.99).

$$\begin{aligned}
\sigma_{CT-CT}^{\square} = & -\lim_{\delta z \rightarrow 0} (2\pi)^3 \sum_{\substack{p,s,q,\ell, \\ p',s'=+,-}} \sum_{\substack{u,v,w, \\ u',w'=TE,TM}} \sum_{\alpha,\beta,\gamma,\rho=x,y,z} \iint d\bar{k}_{\perp a} A_{CT-CT}^{\alpha\beta\gamma\rho, pp'ss'q\ell, uu'vw w'} \times \\
& e^{i(\bar{k}_{\perp ai} - \bar{k}_{\perp bi} + \bar{k}_{\perp bs} - \bar{k}_{\perp as}) \cdot \bar{r}_{T\perp}} e^{i(\ell k_{tza}^{(v)} - p k_{tza}^{(u)} + p' k_{tzb}^{(u')*} + s' k_{tzi}^{(w')*}) z_T} \times \\
& \left[R_{S1}^{\square} (\bar{k}_{\perp ai} - \bar{k}_{\perp a}, -q k_{tza}^{(v)} - s k_{tzi}^{(w)}) + \right. \\
& \left. R_{S2}^{\square} (\bar{k}_{\perp ai} - \bar{k}_{\perp a}, -q k_{tza}^{(v)} - s k_{tzi}^{(w)}) \right] \quad (G.139)
\end{aligned}$$

where

$$\begin{aligned}
A_{CT-CT}^{\alpha\beta\gamma\rho, pp'ss'q\ell, uu'vw w'} \Big|_{\square} = & \frac{|\alpha'|^2}{4\pi} \left[\hat{p}_a \cdot \bar{H}_{0tp}^{(u)}(\bar{k}_{\perp as}) \cdot \bar{F}_{t\cup\ell q}^{(v)}(\bar{k}_{\perp a}) \right]_{\alpha} \cdot \left[\bar{E}_{tai}^{s,(w)} \right]_{\beta} \times \\
& \left[\hat{p}_b \cdot \bar{H}_{0tp'}^{(u')}(\bar{k}_{\perp bs}) \cdot \bar{D}_t^b \right]_{\gamma}^* \cdot \left[\bar{E}_{tbi}^{s',(w')} \right]_{\rho}^* \quad (G.140)
\end{aligned}$$

$$\begin{aligned}
A_{CT-CT}^{\alpha\beta\gamma\rho, pp'ss'q\ell, uu'vw w'} \Big|_{\square} = & \frac{|\alpha'|^2}{4\pi} \left[\hat{p}_a \cdot \bar{H}_{0tp}^{(u)}(\bar{k}_{\perp as}) \cdot \bar{F}_{t\cap\ell q}^{(v)}(\bar{k}_{\perp a}) \right]_{\alpha} \cdot \left[\bar{E}_{tai}^{s,(w)} \right]_{\beta} \times \\
& \left[\hat{p}_b \cdot \bar{H}_{0tp'}^{(u')}(\bar{k}_{\perp bs}) \cdot \bar{D}_t^b \right]_{\gamma}^* \cdot \left[\bar{E}_{tbi}^{s',(w')} \right]_{\rho}^* \quad (G.141)
\end{aligned}$$

and where R_{S1}^{\square} , R_{S2}^{\square} , R_{S1}^{\square} , and R_{S2}^{\square} are defined by (G.106)-(G.117).

Finally, the last two terms, σ_{CT-CT}^{\square} and σ_{CT-CT}^{\square} , are given by (G.142) and (G.143),

$$\begin{aligned}
\sigma_{CT-CT}^{\square} = & -\lim_{\delta z \rightarrow 0} (2\pi)^3 \sum_{\substack{p,s,p',s', \\ q',\ell'=+,-}} \sum_{\substack{u,w,u', \\ v',w'=TE,TM}} \sum_{\alpha,\beta,\gamma,\rho=x,y,z} \iint d\bar{k}_{\perp b} A_{CT-CT}^{\alpha\beta\gamma\rho, pp'ss'q'\ell', uu'vw w'} \times \\
& e^{i(\bar{k}_{\perp ai} - \bar{k}_{\perp bi} + \bar{k}_{\perp bs} - \bar{k}_{\perp as}) \cdot \bar{r}_{T\perp}} e^{-i(s k_{tzi}^{(w)} + p k_{tza}^{(u)} - p' k_{tzb}^{(u')*} + \ell' k_{tzb}^{(v')*}) z_T} \times
\end{aligned}$$

$$\left[R_{S1}^{\cup} (\bar{k}_{\perp bi} - \bar{k}_{\perp b}, -q' k_{tz_b}^{(v')*} - s' k_{tz_{bi}}^{(w')*}) + \right. \\ \left. R_{S2}^{\cup} (\bar{k}_{\perp bi} - \bar{k}_{\perp b}, -q' k_{tz_b}^{(v')*} - s' k_{tz_{bi}}^{(w')*}) \right] \quad (G.142)$$

$$\sigma_{CT-CT}^{\cap} = - \lim_{\delta_z \rightarrow 0} (2\pi)^3 \sum_{\substack{p,s,p',s', \\ q',\ell'=+,-}} \sum_{\substack{u,w,u', \\ v',w'=TE,TM}} \sum_{\alpha,\beta,\gamma,\rho=x,y,z} \iint d\bar{k}_{\perp b} A_{CT-CT}^{\substack{\alpha\beta\gamma\rho \\ pp'ss'q'\ell' \\ uu'v'ww' \\ =\cap}} \times \\ e^{i(\bar{k}_{\perp ai} - \bar{k}_{\perp bi} + \bar{k}_{\perp bs} - \bar{k}_{\perp as}) \cdot \vec{r}_{T\perp}} e^{-i(s k_{tz_{ai}}^{(w)} + p k_{tz_{as}}^{(u)} - p' k_{tz_{bs}}^{(u')*} + \ell' k_{tz_b}^{(v')*}) z_T} \times \\ \left[R_{S1}^{\cap} (\bar{k}_{\perp bi} - \bar{k}_{\perp b}, -q' k_{tz_b}^{(v')*} - s' k_{tz_{bi}}^{(w')*}) + \right. \\ \left. R_{S2}^{\cap} (\bar{k}_{\perp bi} - \bar{k}_{\perp b}, -q' k_{tz_b}^{(v')*} - s' k_{tz_{bi}}^{(w')*}) \right] \quad (G.143)$$

where

$$A_{CT-CT}^{\substack{\alpha\beta\gamma\rho \\ pp'ss'q'\ell' \\ uu'v'ww' \\ =\cup}} = \frac{|\alpha'|^2}{4\pi} \left[\hat{p}_a \cdot \overline{H}_{0t_p}^{(u)}(\bar{k}_{\perp as}) \cdot \overline{D}_t^a \right]_{\alpha} \cdot \left[\overline{E}_{tai}^{s,(w)} \right]_{\beta} \times \\ \left[\hat{p}_b \cdot \overline{H}_{0t_{p'}}^{(u')}(\bar{k}_{\perp bs}) \cdot \overline{F}_{t\cup\ell'q'}^{(v')}(\bar{k}_{\perp b}) \right]_{\gamma}^* \cdot \left[\overline{E}_{tbi}^{s',(w')} \right]_{\rho}^* \quad (G.144)$$

$$A_{CT-CT}^{\substack{\alpha\beta\gamma\rho \\ pp'ss'q'\ell' \\ uu'v'ww' \\ =\cap}} = \frac{|\alpha'|^2}{4\pi} \left[\hat{p}_a \cdot \overline{H}_{0t_p}^{(u)}(\bar{k}_{\perp as}) \cdot \overline{D}_t^a \right]_{\alpha} \cdot \left[\overline{E}_{tai}^{s,(w)} \right]_{\beta} \times \\ \left[\hat{p}_b \cdot \overline{H}_{0t_{p'}}^{(u')}(\bar{k}_{\perp bs}) \cdot \overline{F}_{t\cap\ell'q'}^{(v')}(\bar{k}_{\perp b}) \right]_{\gamma}^* \cdot \left[\overline{E}_{tbi}^{s',(w')} \right]_{\rho}^* \quad (G.145)$$

and where R_{S1}^{\cup} , R_{S2}^{\cup} , R_{S1}^{\cap} , and R_{S2}^{\cap} are defined by (G.122)-(G.125).

G.2.3. Target/Clutter - Clutter/Target Correlation

The overall expression is again the sum of nine terms, as shown by (G.146).

$$\begin{aligned}
\sigma_{TC-CT}^{\hat{p}_a \hat{p}_b}(\bar{k}_{as}, \bar{k}_{ai}, \bar{k}_{bs}, \bar{k}_{bi}) &= 4\pi r^2 \langle \hat{p}_a \cdot \bar{E}_{TC}(\bar{k}_{as}, \bar{k}_{ai}) \times \hat{p}_b^* \cdot \bar{E}_{CT}^*(\bar{k}_{bs}, \bar{k}_{bi}) \rangle \\
&= \sigma_{TC-CT}^{\text{UU}} + \sigma_{TC-CT}^{\text{nn}} + \sigma_{TC-CT}^{\text{Un}} + \sigma_{TC-CT}^{\text{nU}} + \sigma_{TC-CT}^{\text{==}} + \\
&\quad \sigma_{TC-CT}^{\text{U=}} + \sigma_{TC-CT}^{\text{n=}} + \sigma_{TC-CT}^{\text{=U}} + \sigma_{TC-CT}^{\text{=n}} \quad (G.146)
\end{aligned}$$

The first two terms, $\sigma_{TC-CT}^{\text{UU}}$ and $\sigma_{TC-CT}^{\text{nn}}$, are given by (G.147) and (G.148),

$$\begin{aligned}
\sigma_{TC-CT}^{\text{UU}} &= \lim_{\delta_z \rightarrow 0} (2\pi)^5 i \sum_{\substack{p, s, q, \ell, \\ p', s', q', \ell' = +, -}} \sum_{\substack{u, v, w, \\ u', v', w' = TE, TM}} \sum_{\alpha, \beta, \gamma, \rho = x, y, z} \iint d\bar{k}_{\perp a} A_{TC-CT}^{\alpha\beta\gamma\rho, pp'ss'qq'\ell\ell', uu'vv'ww'} \times \\
&\quad e^{i(\bar{k}_{\perp ai} - \bar{k}_{\perp bi} + \bar{k}_{\perp bs} - \bar{k}_{\perp as}) \cdot \bar{r}_{T\perp}} e^{-i(s k_{iz ai}^{(w)} + q k_{iz a}^{(v)} - p' k_{iz bs}^{(u')*} + \ell' k_{iz c}^{(v')*}) z_T} \times \\
&\quad e^{-i(\ell k_{iz a}^{(v)} - p k_{iz as}^{(u)} + q' k_{iz c}^{(v')*} + s' k_{iz bi}^{(w')*}) d_{t-1}} \times \\
&\quad \left[R_P^{\text{UU}}(\bar{k}_{\perp a} - \bar{k}_{\perp as}, \ell k_{iz a}^{(v)} - p k_{iz as}^{(u)}, -q' k_{iz c}^{(v')*} - s' k_{iz bi}^{(w')*}, h_t^+) + \right. \\
&\quad R_{S1}^{\text{UU}}(\bar{k}_{\perp a} - \bar{k}_{\perp as}, \ell k_{iz a}^{(v)} - p k_{iz as}^{(u)}, -q' k_{iz c}^{(v')*} - s' k_{iz bi}^{(w')*}, h_t^+) + \\
&\quad \left. R_{S2}^{\text{UU}}(\bar{k}_{\perp a} - \bar{k}_{\perp as}, \ell k_{iz a}^{(v)} - p k_{iz as}^{(u)}, -q' k_{iz c}^{(v')*} - s' k_{iz bi}^{(w')*}, h_t^+) \right] \quad (G.147)
\end{aligned}$$

$$\begin{aligned}
\sigma_{TC-CT}^{\text{nn}} &= \lim_{\delta_z \rightarrow 0} (2\pi)^5 i \sum_{\substack{p, s, q, \ell, \\ p', s', q', \ell' = +, -}} \sum_{\substack{u, v, w, \\ u', v', w' = TE, TM}} \sum_{\alpha, \beta, \gamma, \rho = x, y, z} \iint d\bar{k}_{\perp a} A_{TC-CT}^{\alpha\beta\gamma\rho, pp'ss'qq'\ell\ell', uu'vv'ww'} \times \\
&\quad e^{i(\bar{k}_{\perp ai} - \bar{k}_{\perp bi} + \bar{k}_{\perp bs} - \bar{k}_{\perp as}) \cdot \bar{r}_{T\perp}} e^{-i(s k_{iz ai}^{(w)} + q k_{iz a}^{(v)} - p' k_{iz bs}^{(u')*} + \ell' k_{iz c}^{(v')*}) z_T} \times \\
&\quad e^{i(\ell k_{iz a}^{(v)} - p k_{iz as}^{(u)} + q' k_{iz c}^{(v')*} + s' k_{iz bi}^{(w')*}) (z_T - \delta_z)} \times \\
&\quad \left[R_P^{\text{nn}}(\bar{k}_{\perp a} - \bar{k}_{\perp as}, \ell k_{iz a}^{(v)} - p k_{iz as}^{(u)}, -q' k_{iz c}^{(v')*} - s' k_{iz bi}^{(w')*}, h_t^-) + \right.
\end{aligned}$$

$$R_{S1}^{\cap\cap} \left(\bar{k}_{\perp a} - \bar{k}_{\perp a s}, \ell k_{tza}^{(v)} - p k_{tza}^{(u)}, -q' k_{tzc}^{(v')*} - s' k_{tzb_i}^{(w')*}, h_t^- \right) + \\ R_{S2}^{\cap\cap} \left(\bar{k}_{\perp a} - \bar{k}_{\perp a s}, \ell k_{tza}^{(v)} - p k_{tza}^{(u)}, -q' k_{tzc}^{(v')*} - s' k_{tzb_i}^{(w')*}, h_t^- \right) \quad (G.148)$$

where

$$\bar{k}_{\perp c} = \bar{k}_{\perp a s} + \bar{k}_{\perp b_i} - \bar{k}_{\perp a} \quad (G.149)$$

and

$$A_{TC-CT}^{\cap\cap} = \frac{|\alpha'|^2}{4\pi} \left[\hat{p}_a \cdot \bar{H}_{0t_p}^{(u)}(\bar{k}_{\perp a s}) \right]_{\alpha} \cdot \left[\bar{F}_{t \cup t_q}^{(v)}(\bar{k}_{\perp a}) \cdot \bar{E}_{tai}^{s,(w)} \right]_{\beta} \times \\ \left[\hat{p}_b \cdot \bar{H}_{0t_{p'}}^{(u')}(\bar{k}_{\perp b s}) \cdot \bar{F}_{t \cup t_{q'}}^{(v')}(\bar{k}_{\perp c}) \right]_{\gamma}^* \cdot \left[\bar{E}_{tbi}^{s',(w')} \right]_{\rho}^* \quad (G.150)$$

$$A_{TC-CT}^{\cap\cap} = \frac{|\alpha'|^2}{4\pi} \left[\hat{p}_a \cdot \bar{H}_{0t_p}^{(u)}(\bar{k}_{\perp a s}) \right]_{\alpha} \cdot \left[\bar{F}_{t \cap t_q}^{(v)}(\bar{k}_{\perp a}) \cdot \bar{E}_{tai}^{s,(w)} \right]_{\beta} \times \\ \left[\hat{p}_b \cdot \bar{H}_{0t_{p'}}^{(u')}(\bar{k}_{\perp b s}) \cdot \bar{F}_{t \cap t_{q'}}^{(v')}(\bar{k}_{\perp c}) \right]_{\gamma}^* \cdot \left[\bar{E}_{tbi}^{s',(w')} \right]_{\rho}^* \quad (G.151)$$

The functions $R_P^{\cup\cup}$, $R_{S1}^{\cup\cup}$, $R_{S2}^{\cup\cup}$, $R_P^{\cap\cap}$, $R_{S1}^{\cap\cap}$, and $R_{S2}^{\cap\cap}$ are defined by (G.70)-(G.83).

The next two terms, $\sigma_{TC-CT}^{\cup\cap}$ and $\sigma_{TC-CT}^{\cap\cup}$, are given by (G.152) and (G.153),

$$\sigma_{TC-CT}^{\cup\cap} = \lim_{\delta z \rightarrow 0} (2\pi)^5 i \sum_{p',s',q',\ell',\ell''=+,-} \sum_{u',v',w'=TE,TM} \sum_{\alpha,\beta,\gamma,\rho=x,y,z} \iint d\bar{k}_{\perp a} A_{TC-CT}^{\cap\cap} \times \\ e^{i(\bar{k}_{\perp ai} - \bar{k}_{\perp bi} + \bar{k}_{\perp bs} - \bar{k}_{\perp as}) \cdot \bar{r}_{T\perp}} e^{-i(sk_{tza}^{(w)} + qk_{tza}^{(v)} - p'k_{tza}^{(u')*} + \ell'k_{tzc}^{(v')*})z_T} \times$$

$$\begin{aligned}
& e^{-i(\ell k_{tza}^{(v)} - pk_{tza}^{(u)} + q'k_{tzc}^{(v')*} + s'k_{tzb_i}^{(w')*})z_T} \times \\
& \left[R_{S1}^{\cup} (\bar{k}_{\perp a} - \bar{k}_{\perp as}, \ell k_{tza}^{(v)} - pk_{tza}^{(u)}, -q'k_{tzc}^{(v')*} - s'k_{tzb_i}^{(w')*}) + \right. \\
& \left. R_{S2}^{\cup} (\bar{k}_{\perp a} - \bar{k}_{\perp as}, \ell k_{tza}^{(v)} - pk_{tza}^{(u)}, -q'k_{tzc}^{(v')*} - s'k_{tzb_i}^{(w')*}) \right] \quad (G.152)
\end{aligned}$$

$$\begin{aligned}
\sigma_{TC-CT}^{\cup} &= \lim_{\delta z \rightarrow 0} (2\pi)^5 i \sum_{\substack{p', s', q', \ell', \\ p', s', q', \ell' = +, -}} \sum_{\substack{u', v', w', \\ u', v', w' = TE, TM}} \sum_{\alpha, \beta, \gamma, \rho = x, y, z} \iint d\bar{k}_{\perp a} A_{TC-CT}^{\alpha\beta\gamma\rho}_{\cup}{}^{pp's's'qq'\ell\ell'}{}^{uu'vv'ww'} \times \\
& e^{i(\bar{k}_{\perp ai} - \bar{k}_{\perp bi} + \bar{k}_{\perp bs} - \bar{k}_{\perp as}) \cdot \bar{r}_{T\perp}} e^{-i(s k_{tza}^{(w)} + q k_{tza}^{(v)} - p' k_{tzb_s}^{(u')*} + \ell' k_{tzc}^{(v')*})z_T} \times \\
& e^{-i(\ell k_{tza}^{(v)} - pk_{tza}^{(u)} + q'k_{tzc}^{(v')*} + s'k_{tzb_i}^{(w')*})z_T} \times \\
& \left[R_{S1}^{\cup} (\bar{k}_{\perp a} - \bar{k}_{\perp as}, \ell k_{tza}^{(v)} - pk_{tza}^{(u)}, -q'k_{tzc}^{(v')*} - s'k_{tzb_i}^{(w')*}) + \right. \\
& \left. R_{S2}^{\cup} (\bar{k}_{\perp a} - \bar{k}_{\perp as}, \ell k_{tza}^{(v)} - pk_{tza}^{(u)}, -q'k_{tzc}^{(v')*} - s'k_{tzb_i}^{(w')*}) \right] \quad (G.153)
\end{aligned}$$

where

$$\begin{aligned}
A_{TC-CT}^{\alpha\beta\gamma\rho}_{\cup}{}^{pp's's'qq'\ell\ell'}{}^{uu'vv'ww'} &= \frac{|\alpha'|^2}{4\pi} \left[\hat{p}_a \cdot \bar{H}_{0t_p}^{(u)}(\bar{k}_{\perp as}) \right]_{\alpha} \cdot \left[\bar{F}_{t\cup_{\ell q}}^{(v)}(\bar{k}_{\perp a}) \cdot \bar{E}_{tai}^{s,(w)} \right]_{\beta} \times \\
& \left[\hat{p}_b \cdot \bar{H}_{0t_{p'}}^{(u')}(\bar{k}_{\perp bs}) \cdot \bar{F}_{t\cap_{\ell' q'}}^{(v')}(\bar{k}_{\perp c}) \right]_{\gamma}^* \cdot \left[\bar{E}_{tbi}^{s',(w')} \right]_{\rho}^* \quad (G.154)
\end{aligned}$$

$$\begin{aligned}
A_{TC-CT}^{\alpha\beta\gamma\rho}_{\cap}{}^{pp's's'qq'\ell\ell'}{}^{uu'vv'ww'} &= \frac{|\alpha'|^2}{4\pi} \left[\hat{p}_a \cdot \bar{H}_{0t_p}^{(u)}(\bar{k}_{\perp as}) \right]_{\alpha} \cdot \left[\bar{F}_{t\cap_{\ell q}}^{(v)}(\bar{k}_{\perp a}) \cdot \bar{E}_{tai}^{s,(w)} \right]_{\beta} \times \\
& \left[\hat{p}_b \cdot \bar{H}_{0t_{p'}}^{(u')}(\bar{k}_{\perp bs}) \cdot \bar{F}_{t\cup_{\ell' q'}}^{(v')}(\bar{k}_{\perp c}) \right]_{\gamma}^* \cdot \left[\bar{E}_{tbi}^{s',(w')} \right]_{\rho}^* \quad (G.155)
\end{aligned}$$

and where R_{S1}^{\cup} , R_{S2}^{\cup} , R_{S1}^{\cap} , and R_{S2}^{\cap} are defined by (G.88)-(G.99).

The fifth term, $\sigma_{\overline{TC}-CT}^{\overline{=}}$, is given by (G.156),

$$\sigma_{\overline{TC}-CT}^{\overline{=}} = \sum_{p,s,p',s'=+,-} \sum_{u,w,u',w'=TE,TM} \sum_{\alpha,\beta,\gamma,\rho=x,y,z} A_{\overline{TC}-CT}^{\overline{=}} \overset{\alpha\beta\gamma\rho}{pp'ss'} C_{\alpha\beta\gamma\rho}(0) \times \\ e^{i(\bar{k}_{\perp ai} - \bar{k}_{\perp bi} + \bar{k}_{\perp bs} - \bar{k}_{\perp as}) \cdot \bar{r}_{T\perp}} e^{-i(sk_{tz ai}^{(w)} - s'k_{tz bi}^{(w')*} + pk_{tz as}^{(u)} - p'k_{tz bs}^{(u')*})z_T} \quad (G.156)$$

where

$$A_{\overline{TC}-CT}^{\overline{=}} = \frac{|\alpha'|^2}{4\pi} \left[\hat{p}_a \cdot \overline{H}_{0t_p}^{(u)}(\bar{k}_{\perp as}) \right]_{\alpha} \cdot \left[\overline{D}_t^a \cdot \overline{E}_{t ai}^{s,(w)} \right]_{\beta} \times \\ \left[\hat{p}_b \cdot \overline{H}_{0t_{p'}}^{(u')}(\bar{k}_{\perp bs}) \cdot \overline{D}_t^b \right]_{\gamma}^* \cdot \left[\overline{E}_{t bi}^{s',(w')} \right]_{\rho}^* \quad (G.157)$$

The sixth and seventh terms, $\sigma_{TC-CT}^{\cup=}$ and $\sigma_{TC-CT}^{\cap=}$, are given by (G.158) and (G.159),

$$\sigma_{TC-CT}^{\cup=} = - \lim_{\delta_z \rightarrow 0} (2\pi)^3 \sum_{\substack{p,s,q,\ell, \\ p',s'=+,-}} \sum_{\substack{u,v,w, \\ u',w'=TE,TM}} \sum_{\alpha,\beta,\gamma,\rho=x,y,z} \iint d\bar{k}_{\perp a} A_{TC-CT}^{\cup=} \overset{\alpha\beta\gamma\rho}{pp'ss'q\ell} \times \\ e^{i(\bar{k}_{\perp ai} - \bar{k}_{\perp bi} + \bar{k}_{\perp bs} - \bar{k}_{\perp as}) \cdot \bar{r}_{T\perp}} e^{-i(sk_{tz ai}^{(w)} + qk_{tz a}^{(v)} - p'k_{tz bs}^{(u')*} - s'k_{tz bi}^{(w')*})z_T} \times \\ \left[R_{S1}^{\cup=} (\bar{k}_{\perp a} - \bar{k}_{\perp as}, \ell k_{tz a}^{(v)} - p k_{tz as}^{(u)}) + R_{S2}^{\cup=} (\bar{k}_{\perp a} - \bar{k}_{\perp as}, \ell k_{tz a}^{(v)} - p k_{tz as}^{(u)}) \right] \quad (G.158)$$

$$\sigma_{TC-CT}^{\cap=} = - \lim_{\delta_z \rightarrow 0} (2\pi)^3 \sum_{\substack{p,s,q,\ell, \\ p',s'=+,-}} \sum_{\substack{u,v,w, \\ u',w'=TE,TM}} \sum_{\alpha,\beta,\gamma,\rho=x,y,z} \iint d\bar{k}_{\perp a} A_{TC-CT}^{\cap=} \overset{\alpha\beta\gamma\rho}{pp'ss'q\ell} \times$$

$$e^{i(\bar{k}_{\perp ai} - \bar{k}_{\perp bi} + \bar{k}_{\perp bs} - \bar{k}_{\perp as}) \cdot \bar{r}_{T\perp}} e^{-i(sk_{tz ai}^{(w)} + qk_{tz as}^{(v)} - p'k_{tz bs}^{(u')*} - s'k_{tz bi}^{(w')*})z_T} \times$$

$$\left[R_{S1}^{\square} (\bar{k}_{\perp a} - \bar{k}_{\perp as}, \ell k_{tz a}^{(v)} - p k_{tz as}^{(u)}) + R_{S2}^{\square} (\bar{k}_{\perp a} - \bar{k}_{\perp as}, \ell k_{tz a}^{(v)} - p k_{tz as}^{(u)}) \right]$$

(G.159)

where

$$A_{TC-CT}^{\alpha\beta\gamma\rho, pp'ss'q\ell, uu'vw w'} = \frac{|\alpha'|^2}{4\pi} \left[\hat{p}_a \cdot \bar{H}_{0t_p}^{(u)}(\bar{k}_{\perp as}) \right]_{\alpha} \cdot \left[\bar{F}_{t\cup t_q}^{(v)}(\bar{k}_{\perp a}) \cdot \bar{E}_{tai}^{s,(w)} \right]_{\beta} \times$$

$$\left[\hat{p}_b \cdot \bar{H}_{0t_{p'}}^{(u')}(\bar{k}_{\perp bs}) \cdot \bar{D}_t^b \right]_{\gamma}^* \cdot \left[\bar{E}_{tbi}^{s',(w')} \right]_{\rho}^* \quad (G.160)$$

$$A_{TC-CT}^{\alpha\beta\gamma\rho, pp'ss'q\ell, uu'vw w'} = \frac{|\alpha'|^2}{4\pi} \left[\hat{p}_a \cdot \bar{H}_{0t_p}^{(u)}(\bar{k}_{\perp as}) \right]_{\alpha} \cdot \left[\bar{F}_{t\cap t_q}^{(v)}(\bar{k}_{\perp a}) \cdot \bar{E}_{tai}^{s,(w)} \right]_{\beta} \times$$

$$\left[\hat{p}_b \cdot \bar{H}_{0t_{p'}}^{(u')}(\bar{k}_{\perp bs}) \cdot \bar{D}_t^b \right]_{\gamma}^* \cdot \left[\bar{E}_{tbi}^{s',(w')} \right]_{\rho}^* \quad (G.161)$$

and where R_{S1}^{\square} , R_{S2}^{\square} , R_{S1}^{\square} , and R_{S2}^{\square} are defined by (G.106)-(G.117).

Finally, the last two terms, $\sigma_{TC-CT}^{\square\cup}$ and $\sigma_{TC-CT}^{\square\cap}$, are given by (G.162) and (G.163),

$$\sigma_{TC-CT}^{\square\cup} = - \lim_{\delta_z \rightarrow 0} (2\pi)^3 \sum_{\substack{p,s,p',s', \\ q',\ell' = +,-}} \sum_{\substack{u,w,u', \\ v',w' = TE, TM}} \sum_{\alpha,\beta,\gamma,\rho=x,y,z} \iint d\bar{k}_{\perp b} A_{TC-CT}^{\alpha\beta\gamma\rho, pp'ss'q'\ell', uu'v'w w'} \times$$

$$e^{i(\bar{k}_{\perp ai} - \bar{k}_{\perp bi} + \bar{k}_{\perp bs} - \bar{k}_{\perp as}) \cdot \bar{r}_{T\perp}} e^{-i(sk_{tz ai}^{(w)} + p k_{tz as}^{(u)} - p'k_{tz bs}^{(u')*} + \ell'k_{tz bi}^{(v')*})z_T} \times$$

$$\left[R_{S1}^{\square\cup} (\bar{k}_{\perp b} - \bar{k}_{\perp bs}, \ell'k_{tz b}^{(v')*} - p'k_{tz as}^{(u')*}) + R_{S2}^{\square\cup} (\bar{k}_{\perp b} - \bar{k}_{\perp bs}, \ell'k_{tz b}^{(v')*} - p'k_{tz as}^{(u')*}) \right]$$

(G.162)

$$\begin{aligned}
\sigma_{TC-CT}^{\cap} = & -\lim_{\delta_z \rightarrow 0} (2\pi)^3 \sum_{\substack{p,s,p',s', \\ q',\ell'=+,-}} \sum_{\substack{u,w,u', \\ v',w'=TE,TM}} \sum_{\alpha,\beta,\gamma,\rho=x,y,z} \iint d\bar{k}_{\perp b} A_{TC-CT}^{\substack{\alpha\beta\gamma\rho \\ pp'ss'q'\ell' \\ uu'v'ww' \\ =\cap}} \times \\
& e^{i(\bar{k}_{\perp ai} - \bar{k}_{\perp bi} + \bar{k}_{\perp bs} - \bar{k}_{\perp as}) \cdot \bar{r}_{T\perp}} e^{-i(sk_{tzai}^{(w)} + pk_{tzas}^{(u)} - p'k_{tzb}^{(u')*} + \ell'k_{tzb}^{(v')*})z_T} \times \\
& \left[R_{S1}^{\cap} (\bar{k}_{\perp b} - \bar{k}_{\perp bs}, \ell'k_{tzb}^{(v')*} - p'k_{tzb}^{(u')*}) + R_{S2}^{\cap} (\bar{k}_{\perp b} - \bar{k}_{\perp bs}, \ell'k_{tzb}^{(v')*} - p'k_{tzb}^{(u')*}) \right]
\end{aligned} \tag{G.163}$$

where

$$\begin{aligned}
A_{TC-CT}^{\substack{\alpha\beta\gamma\rho \\ pp'ss'q'\ell' \\ uu'v'ww' \\ =\cup}} = & \frac{|\alpha'|^2}{4\pi} \left[\hat{p}_a \cdot \bar{H}_{0tp}^{(u)}(\bar{k}_{\perp as}) \right]_{\alpha} \cdot \left[\bar{D}_t^a \cdot \bar{E}_{tai}^{s,(w)} \right]_{\beta} \times \\
& \left[\hat{p}_b \cdot \bar{H}_{0tp'}^{(u')}(\bar{k}_{\perp bs}) \cdot \bar{F}_{t\cup_{\ell'q'}}^{(v')}(\bar{k}_{\perp b}) \right]_{\gamma}^* \cdot \left[\bar{E}_{tbi}^{s',(w')} \right]_{\rho}^*
\end{aligned} \tag{G.164}$$

$$\begin{aligned}
A_{TC-CT}^{\substack{\alpha\beta\gamma\rho \\ pp'ss'q'\ell' \\ uu'v'ww' \\ =\cap}} = & \frac{|\alpha'|^2}{4\pi} \left[\hat{p}_a \cdot \bar{H}_{0tp}^{(u)}(\bar{k}_{\perp as}) \right]_{\alpha} \cdot \left[\bar{D}_t^a \cdot \bar{E}_{tai}^{s,(w)} \right]_{\beta} \times \\
& \left[\hat{p}_b \cdot \bar{H}_{0tp'}^{(u')}(\bar{k}_{\perp bs}) \cdot \bar{F}_{t\cap_{\ell'q'}}^{(v')}(\bar{k}_{\perp b}) \right]_{\gamma}^* \cdot \left[\bar{E}_{tbi}^{s',(w')} \right]_{\rho}^*
\end{aligned} \tag{G.165}$$

and where R_{S1}^{\cup} , R_{S2}^{\cup} , R_{S1}^{\cap} , and R_{S2}^{\cap} are defined by (G.122)-(G.125).

Chapter 5

Scattering of an Electrically Large Plate Target in a Layered Continuous Random Media

This chapter continues the analysis of the scattering phenomenology for a target buried in a stratified region of continuous random media. The results of Chapters 2-4 are extended by now considering a more complex, electrically large target, composed of flat perfectly conducting polygonal plate patches. Strong Fluctuation Theory is again employed to determine the effective permittivity of the random layer, and the distorted Born approximation is used to obtain the fields scattered by the random media. The fields scattered by the target are calculated by using the Physical Optics approximation to the current induced on each flat facet, and by coherently summing the contributions from all facets. As with the previous formulation for the point target, the total received field is seen to consist of a coherent, or direct, return from the target, an incoherent

return directly scattered by the random media, and two incoherent multi-path terms arising from interactions between the target and random layer. The statistics of these incoherent, multi-path fields are calculated, including the variance, and the correlation in both azimuth angle and frequency. The effect of a variety of geometrical and physical parameters on these statistics is again illustrated, and the results are compared with those for the simpler point target.

5.1. Geometry and Random Media Model

The configuration used to investigate the scattering between an arbitrary, electrically large target and a layer of continuous random media is shown in Figure 5.1. The stratified media consists of $N-2$ bounded regions with a half-space above (Region 0) and below (Region $N-1$). The uppermost interface is taken to be at $z = 0$, and the other interfaces at depths $z = -d_i$, where i denotes the region directly above the interface. In general, it is likely that several regions may contain random scatterers, and, thus, lead to several layers of random media. Since it will be assumed here, however, that each such region is statistically independent of the others, only a single random layer will be considered, and the result for a larger number of random regions may be found by incoherently summing the contributions from each.

The target will be assumed to be entirely contained in region t , to be perfectly conducting, and to be large in comparison to the wavelength of interest, such that the induced surface currents may be accurately approximated using the Physical Optics approach. It is modeled by a collection of N flat, polygonal facets, where the i th such

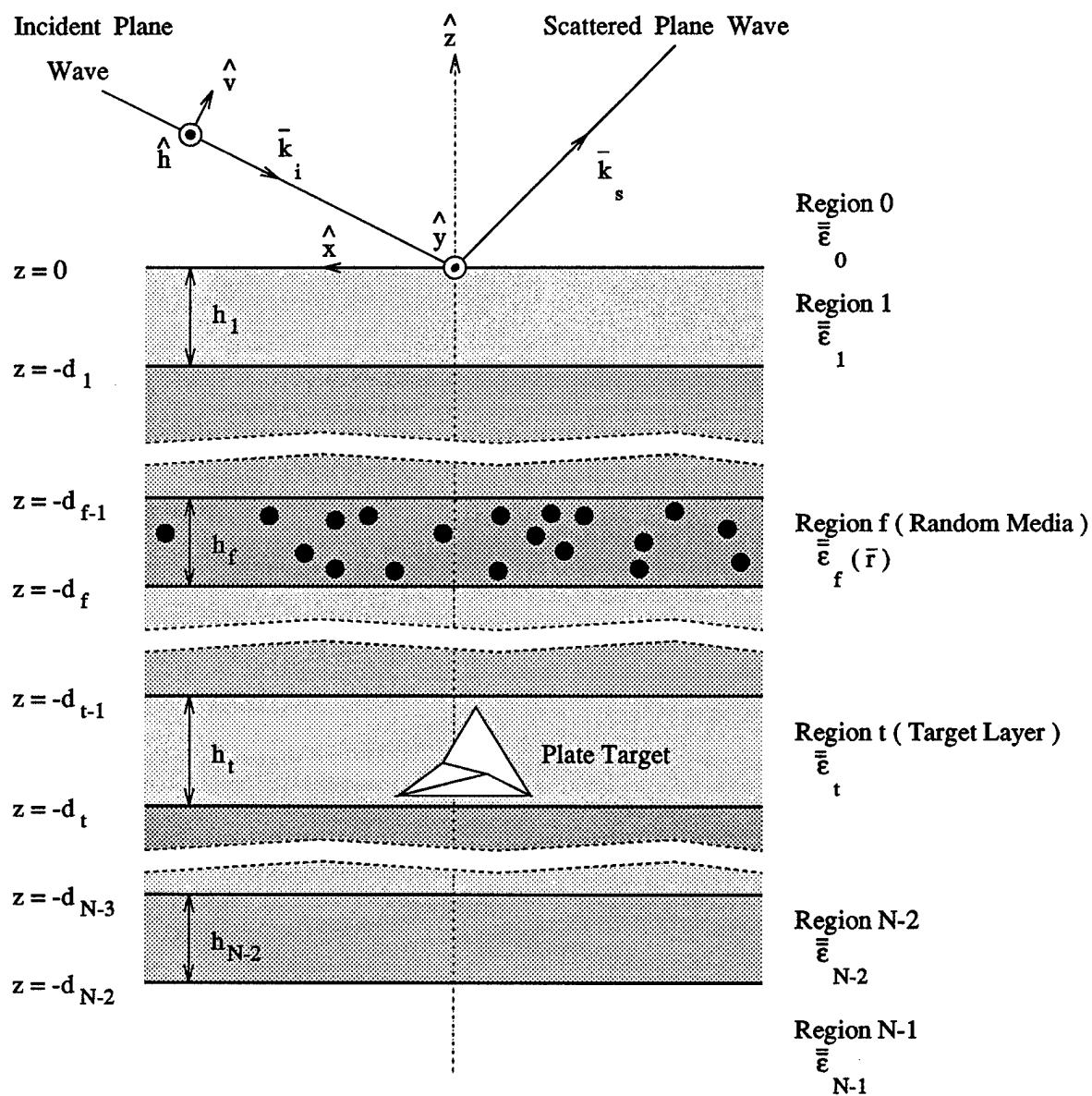


Figure 5.1. Geometry of the multi-layer scattering problem with N layers, and with the plate target located in layer t , and the random media in layer f .

facet will have an arbitrary number of vertices, M_i , ordered counter-clockwise about the surface normal, \hat{n}_i , of the top face. Each facet is one-sided such that only the top face will contribute to scattering, and two-sided plates must be represented using two such facets placed back-to-back. A sample facet is shown in Figure 5.2.

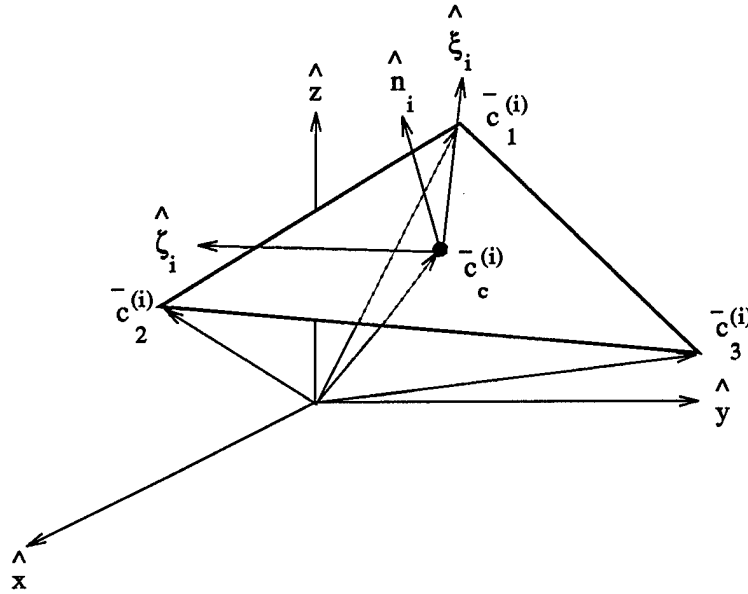


Figure 5.2. Geometry of an individual polygonal facet composing the target. Shown is the i th facet which is arbitrarily chosen to have three vertices.

It will again be assumed that the source of illumination is sufficiently far from the target and from the source of the multi-path random media return, that for the purpose of calculating these contributions to the target signature, the illumination may be treated as being of plane wave form. Hence, the incident field will take the form of (5.1),

$$\overline{E}_{0i}(\bar{r}) = \left[E_i^{TE} \hat{h}(-k_{0zi}) + E_i^{TM} \hat{v}(-k_{0zi}) \right] e^{i\bar{k}_{\perp i} \cdot \bar{r}_{\perp}} e^{-ik_{0zi}z} \quad (5.1)$$

where $\hat{h}(-k_{0z_i})$ and $\hat{v}(-k_{0z_i})$ are unit vectors in the polarization direction of the incident TE and TM waves respectively, and where the incident propagation vector is given by (5.2).

$$\begin{aligned}\bar{k}_{0_i} &= k_{x_i}\hat{x} + k_{y_i}\hat{y} - k_{z_i}\hat{z} \\ &= k_0(\sin\theta_i \cos\phi_i \hat{x} + \sin\theta_i \sin\phi_i \hat{y} - \cos\theta_i \hat{z})\end{aligned}\quad (5.2)$$

A time dependance of $e^{-i\omega t}$ is omitted above, but again will be assumed throughout.

For convenience, the upper-half space is assumed to be isotropic with permittivity ϵ_0 . All other regions, with the exception of the random layer, are assumed to be homogeneous, but uniaxial (untilted) with permittivity tensors with the form of (5.3).

$$\bar{\epsilon}_i = \begin{bmatrix} \epsilon_i & 0 & 0 \\ 0 & \epsilon_i & 0 \\ 0 & 0 & \epsilon_{z_i} \end{bmatrix} \quad (5.3)$$

The continuous random media occurs in a single arbitrary layer, f , where it is assumed here that this layer does not coincide with the target layer ($t \neq f$). Hence, layer f has a spatially random permittivity with a correlation function designed to model the inclusion of scatterers which are small in comparison to the illuminating wavelength, and which display azimuthal symmetry. To allow high permittivity contrasts between the background and embedded materials, Strong Fluctuation theory is again utilized in determining an effective mean permittivity, and because of the non-isotropic, but azimuthally symmetric correlation function, this permittivity will be uniaxial (untilted) as with the other layers. The field arising from scattering by the random media can be determined using the first order distorted Born approximation given by (5.4),

$$\overline{E}_{0*}^{(1)} \simeq k_0^2 \int d\bar{r}' \overline{G}_{0f}(\bar{r}, \bar{r}') \cdot \overline{\xi}(\bar{r}') \cdot \overline{E}_f^{(0)}(\bar{r}') \quad (5.4)$$

where $\overline{E}_f^{(0)}(\bar{r})$ is the mean field in the random layer with the calculated effective permittivity, where $\overline{G}_{0f}(\bar{r}, \bar{r}')$ is the dyadic Green's function for the stratified configuration with a source in layer f , and the observation point in region 0, and where $\overline{\xi}(\bar{r}')$ is the renormalized scattering source giving rise to incoherent scattering.

5.2. Scattering Terms

As with the point target, the return from the conducting plate structure will consist not only of the incident plane wave, but also of the scattered field of the target when illuminated by this plane wave. Since the target is electrically large, and its features are assumed to change smoothly on the scale of the wavelength, the induced current on its perfectly conducting surface can be found from the tangent plane approximation of (5.5).

$$\overline{J}_t(\bar{r}) = 2\hat{n}(\bar{r}) \times \mathcal{U}\{\overline{H}_{t_i}(\bar{r})\} \quad (5.5)$$

In the above, $\hat{n}(\bar{r})$ is the surface normal at position \bar{r} , and $\overline{H}_{t_i}(\bar{r})$ is the incident magnetic field. The function $\mathcal{U}\{\}$ is an operator which will select only that portion of the incident field at \bar{r} which is unshadowed. This shadowing check is necessary, since only that portion of the incident field which illuminates the top-side of the surface will

contribute to the induced current. A discussion of the specific form of this shadowing function will be postponed at present, but will be treated shortly.

By integrating the current of (5.5), the target scattered field in the random media can be determined. Adding to this the directly incident field, the total zeroth order field in the random layer is given by (5.6).

$$\overline{E}_f^{(0)}(\overline{r}) = \overline{E}_{f_i}^{(0)}(\overline{r}) + i\omega\mu \int_{S_t} d\overline{r}' \mathcal{U} \left\{ \overline{G}_{ft}(\overline{r}, \overline{r}') \cdot (2\hat{n}(\overline{r}') \times \mathcal{U} \left\{ \overline{H}_{t_i}^{(0)}(\overline{r}') \right\}) \right\} \quad (5.6)$$

The second $\mathcal{U}\{\}$ in the above integral arises from the shadowing which may occur in scattering from the plate, which for bistatic scattering, is in addition to any shadowing which occurs for incidence on the plate.

The field scattered by the random media, and observed at the radar can then be found using the distorted Born approximation given below in (5.7),

$$\begin{aligned} \overline{E}_{0_a}^{(1)}(\overline{r}) = \int_{V_f} d\overline{r}' \overline{G}_{0f}(\overline{r}, \overline{r}') \cdot \overline{Q}(\overline{r}') \cdot \left[\overline{E}_{f_i}^{(0)}(\overline{r}') + \right. \\ \left. i\omega\mu \int_{S_t} d\overline{r}'' \mathcal{U} \left\{ \overline{G}_{ft}(\overline{r}', \overline{r}'') \cdot (2\hat{n}(\overline{r}'') \times \mathcal{U} \left\{ \overline{H}_{t_i}^{(0)}(\overline{r}'') \right\}) \right\} \right] \quad (5.7) \end{aligned}$$

where $\overline{Q}(\overline{r}) = k_o^2 \overline{\xi}(\overline{r})$. In addition to the direct return from the media, the field of (5.6) will also be scattered by the random layer in the direction of the target, and then scattered by the target in the direction of the radar receiver. The field incident on the target from the random media, therefore, will be given by (5.8).

$$\begin{aligned} \overline{H}_t^{(1)} = \int_{V_f} d\overline{r}' \overline{\mathcal{G}}_{tf}(\overline{r}, \overline{r}') \cdot \frac{\overline{Q}(\overline{r}')}{\omega\mu} \cdot [\overline{E}_{fi}^{(0)}(\overline{r}') + \\ i\omega\mu \int_{S_t} d\overline{r}'' \mathcal{U}\{\overline{G}_{ft}(\overline{r}', \overline{r}'') \cdot (2\hat{n}(\overline{r}'') \times \mathcal{U}\{\overline{H}_{ti}^{(0)}(\overline{r}'')\})\}] \end{aligned} \quad (5.8)$$

In the above, $\overline{\mathcal{G}}_{tf}(\overline{r}, \overline{r}')$ is the magnetic field/electric source Green's function which gives the magnetic field in region t for an electric current source in region f . Finally, the induced target current will be given by the tangent plane approximation, and the scattered field at the receiver, again accounting for shadowing will be given by (5.9).

$$\begin{aligned} \overline{E}_{0_b}^{(1)}(\overline{r}) = i \int_{S_t} d\overline{r}' \mathcal{U}\left\{ \overline{G}_{0t}(\overline{r}, \overline{r}') \cdot 2\hat{n}(\overline{r}') \times \mathcal{U}\left\{ \int_{V_f} d\overline{r}'' \overline{\mathcal{G}}_{tf}(\overline{r}', \overline{r}'') \cdot \right. \right. \\ \left. \overline{Q}(\overline{r}'') \cdot [\overline{E}_{fi}^{(0)}(\overline{r}'') + i\omega\mu \int_{S_t} d\overline{r}''' \mathcal{U}\{\overline{G}_{ft}(\overline{r}'', \overline{r}''') \cdot \right. \\ \left. \left. (2\hat{n}(\overline{r}''') \times \mathcal{U}\{\overline{H}_{ti}^{(0)}(\overline{r}''')\})\}]\right\} \right\} \end{aligned} \quad (5.9)$$

The two fields, $\overline{E}_{0_a}^{(1)}$ and $\overline{E}_{0_b}^{(1)}$, give all of the incoherent returns which arise under the first order distorted Born approximation. It is again useful to split these into several components, and to identify each of the multi-path mechanisms. The first term of (5.7) is that returned directly by the random media in the absence of the target, and as identified previously, this is the clutter return, \overline{E}_C .

$$\overline{E}_C(\overline{r}) = \int_{V_f} d\overline{r}' \overline{G}_{0f}(\overline{r}, \overline{r}') \cdot \overline{Q}(\overline{r}') \cdot \overline{E}_{fi}^{(0)} \quad (5.10)$$

The second term of (5.7) is the field scattered first by the target and then by the random media. This is again termed the target/clutter multi-path field.

$$\begin{aligned} \overline{E}_{TC}(\bar{r}) = i\omega\mu \int_{V_f} d\bar{r}' \overline{G}_{0f}(\bar{r}, \bar{r}') \cdot \overline{Q}(\bar{r}') \cdot \int_{S_t} d\bar{r}'' \mathcal{U}\{\overline{G}_{ft}(\bar{r}', \bar{r}'') \cdot \\ (2\hat{n}(\bar{r}'') \times \mathcal{U}\{\overline{H}_{ti}^{(0)}(\bar{r}'')\})\} \end{aligned} \quad (5.11)$$

Similarly, the first term of (5.9) is the field scattered by the random media and then the target, and this return is again denoted the clutter/target multi-path contribution.

$$\begin{aligned} \overline{E}_{CT}(\bar{r}) = i \int_{S_t} d\bar{r} \mathcal{U}\{\overline{G}_{0t}(\bar{r}, \bar{r}') \cdot [2\hat{n}(\bar{r}') \times \mathcal{U}\{\int_{V_f} d\bar{r}'' \overline{G}_{tf}(\bar{r}', \bar{r}'') \cdot \\ \overline{Q}(\bar{r}'') \cdot \overline{E}_{fi}^{(0)}(\bar{r}'')\}]\} \end{aligned} \quad (5.12)$$

The second term of (5.9) is the field scattered by the target, the random media, and then the target a second time. This contribution is again the target/clutter/target multi-path field.

$$\begin{aligned} \overline{E}_{TCT}(\bar{r}) = -\omega\mu \int_{S_t} d\bar{r}' \mathcal{U}\{\overline{G}_{0t}(\bar{r}, \bar{r}') \cdot [2\hat{n}(\bar{r}') \times \mathcal{U}\{\int_{V_f} d\bar{r}'' \overline{G}_{tf}(\bar{r}', \bar{r}'') \cdot \\ \overline{Q}(\bar{r}'') \cdot \int_{S_t} d\bar{r}''' \mathcal{U}\{\overline{G}_{ft}(\bar{r}'', \bar{r}''') \cdot (2\hat{n}(\bar{r}''') \times \mathcal{U}\{\overline{H}_{ti}^{(0)}(\bar{r}''')\})\}]\} \} \end{aligned} \quad (5.13)$$

The three multi-path mechanisms given above are those which exist under the first order distorted Born approximation. The Physical Optics approach taken to the target

scattering problem, however, is inherently a single scattering formulation which neglects all multiple interactions between target components. Hence, it is inconsistent to include the third target/clutter/target multi-path contribution which represents a double target interaction. For this reason, this last multi-path term is neglected hereafter.

Finally, in addition to the incoherent returns, a direct coherent return arises from the target, and this is given by (5.14) below.

$$\overline{E}_T(\vec{r}) = i\omega\mu \int_{S_t} d\vec{r}' \mathcal{U} \left\{ \overline{G}_{0t}(\vec{r}, \vec{r}') \cdot \left[2\hat{n}(\vec{r}') \times \mathcal{U} \left\{ \overline{H}_{t_i}^{(0)} \right\} \right] \right\} \quad (5.14)$$

Equations (5.11), (5.12), and (5.14) constitute the target signature of interest, and each of these mechanisms is illustrated in Figure 5.3.

$$\overline{E}_S = \overline{E}_T + \overline{E}_{TC} + \overline{E}_{CT} \quad (5.15)$$

Unlike the point target signature determined previously, the two multi-path mechanisms \overline{E}_{TC} and \overline{E}_{CT} may not be reciprocal, since reciprocity is not preserved by the Physical Optics approximation. For this reason, the scattered power will now be given by (5.16),

$$P = |\overline{E}_T|^2 + \langle \overline{E}_{TC} \cdot \overline{E}_{CT}^* \rangle + \langle \overline{E}_{CT} \cdot \overline{E}_{TC}^* \rangle + 2\text{Re} \langle \overline{E}_{TC} \cdot \overline{E}_{CT}^* \rangle \quad (5.16)$$

where the first term is the received field strength in the absence of fluctuations of the random media, and where the subsequent terms represent the additional power redirected in the receiver direction by scatterers within the random layer. In the following

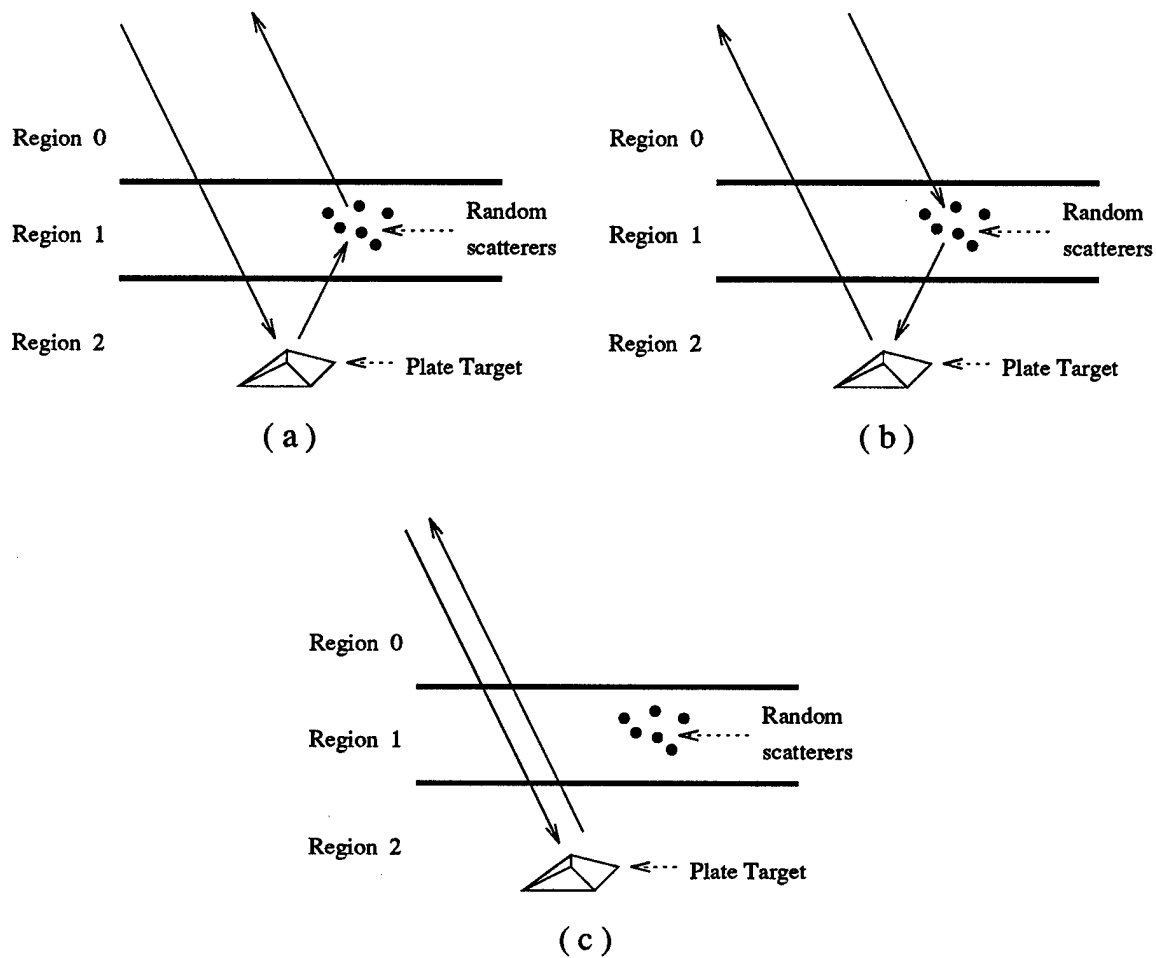


Figure 5.3. Scattering mechanisms for target/clutter interaction including the target/clutter multi-path (a), clutter/target multi-path (b), and direct target return (c).

section, the contribution of each of the above terms to the received field strength is calculated. In addition, for the purpose of determining the effect of the random media on the ability to image the target with a SAR sensor, the correlation of the incoherent fields over azimuth and frequency changes is also determined.

5.3. Field Calculations

5.3.1. Coherent Field

The first of the above terms to be considered is that of the coherent or direct target return, \overline{E}_T , given by (5.14). The problem of Physical Optics scattering from a target composed of polygonal facets has been discussed previously [110-111], but the analysis will be repeated here with the additional complication that the target is now placed in a stratified media. Rewriting (5.14), using the expression for the incident magnetic field given in Appendix H, and the far field Green's function of Appendix E, and replacing the surface integral with a sum of integrals over each of the polygonal patches, the expression of (5.17) is obtained.

$$\begin{aligned}
 E_T = 2i\omega\mu \frac{e^{ikr}}{4\pi r} \sum_{m=1}^N \sum_{p=+/-} \sum_{s=+/-} \sum_{w=TE,TM} \sum_{u=TE,TM} \int_{S_m} d\vec{r}' \mathcal{U}\{\hat{p} \cdot \\
 \overline{H}_{0tp}^{(u)}(\vec{k}_{\perp s}) \cdot [\hat{n}_m \times \mathcal{U}\{\overline{H}_{ti}^{s,(w)}\}]\} e^{-i\vec{k}_{\perp s} \cdot \vec{r}'_{\perp}} e^{i\vec{k}_{\perp i} \cdot \vec{r}'_{\perp}} \times \\
 e^{-ipk_{iz_s}^{(u)} z'} e^{-isk_{iz_i}^{(w)} z'}
 \end{aligned} \quad (5.17)$$

In the above, \hat{p} is the receive polarization vector which will be taken as either $\hat{h}(k_{0z_s}^{TE})$ or $\hat{v}(k_{0z_s}^{TM})$, corresponding to TE and TM receive polarizations respectively, and N is the number of plates composing the target.

Before evaluating the surface integrals of the polygonal facets, the shadowing functions must be treated in more detail. The shadowing which will be considered here

is a simple check to insure that the incident and scattered wave vectors are directed at and from the top side of the plate, since the plates are again assumed to scatter only from one side. This check may be performed by requiring that the inner product of the surface normal with the scattered wave vector is greater than zero, and the inner product of the normal with the incident wave vector is less than zero. Hence, the shadowing function $S(\hat{n}, \bar{k})$ is defined as in (5.18),

$$S(\hat{n}, \bar{k}) = \begin{cases} 1 & , \quad \hat{n} \cdot \bar{k} \geq 0 \\ 0 & , \quad \text{else} \end{cases} \quad (5.18)$$

and with this function, (5.17) can be rewritten as in (5.19).

$$\begin{aligned} E_T = 2i\omega\mu \frac{e^{ikr}}{4\pi r} \sum_{m=1}^N \sum_{p,s=+/-} \sum_{u,w=TE,TM} \int_{S_m} d\bar{r}' S(\hat{n}_m, \bar{k}_{\perp_s} + pk_{tz_s}^{(u)} \hat{z}) \\ S(\hat{n}_m, -\bar{k}_{\perp_i} + sk_{tz_i}^{(w)} \hat{z}) \hat{p} \cdot \bar{H}_{0t_p}^{(u)}(\bar{k}_{\perp_s}) \cdot [\hat{n}_m \times \bar{H}_{t_i}^{s,(w)}] \times \\ e^{-i\bar{k}_{\perp_s} \cdot \bar{r}'_{\perp}} e^{-i\bar{k}_{\perp_i} \cdot \bar{r}'_{\perp}} e^{-ipk_{tz_s}^{(u)} z'} e^{-isk_{tz_i}^{(w)} z'} \end{aligned} \quad (5.19)$$

What remains is to evaluate the surface integral of the above expression, where only the exponential phase terms have a dependance on the integration variable. Hence, the integral has the form of (5.20).

$$I = \int_{S_m} d\bar{r}' e^{-i\bar{k}_{\perp_s} \cdot \bar{r}'_{\perp}} e^{-i\bar{k}_{\perp_i} \cdot \bar{r}'_{\perp}} e^{-ipk_{tz_s}^{(u)} z'} e^{-isk_{tz_i}^{(w)} z'} \quad (5.20)$$

To enable a closed-form evaluation of this integral for an arbitrary polygonal-shaped plate, it is first necessary to create a local coordinate system centered at the plate

centroid, with one axis coincident with the plate normal. The centroid of the m th plate is given by (5.21),

$$\bar{c}_c^{(m)} = \frac{1}{M_m} \sum_{j=1}^{M_m} \bar{c}_j^{(m)} \quad (5.21)$$

where $\bar{c}_j^{(m)}$ is the vector position of the j th corner of the m th plate, and where M_m is the number of corners on the m th plate. The normal of the plate surface can be found from the cross product of the vectors from the above centroid to each of the first two corners.

$$\hat{n}_m = \frac{(\bar{c}_1^{(m)} - \bar{c}_c^{(m)}) \times (\bar{c}_2^{(m)} - \bar{c}_c^{(m)})}{|(\bar{c}_1^{(m)} - \bar{c}_c^{(m)}) \times (\bar{c}_2^{(m)} - \bar{c}_c^{(m)})|} \quad (5.22)$$

The other two axes are defined such that one is coincident with the vector from the centroid to the first corner, and the second is perpendicular to both of the other two axes.

$$\hat{\xi}_m = \frac{\bar{c}_1^{(m)} - \bar{c}_c^{(m)}}{|\bar{c}_1^{(m)} - \bar{c}_c^{(m)}|} \quad (5.23)$$

$$\hat{\zeta}_m = \hat{n}_m \times \hat{\xi}_m \quad (5.24)$$

Finally, the coordinates of each corner point can be determined in the new local coordinate system. Since the plate lies entirely in the $\hat{\xi} - \hat{\zeta}$ plane, the \hat{n} coordinate will be zero for all corners. The other two coordinates are given by (5.25) and (5.26).

$$c_{\xi_j}^{(m)} = (\bar{c}_j^{(m)} - \bar{c}_c^{(m)}) \cdot \hat{\xi}_m \quad (5.25)$$

$$c_{\zeta_j}^{(m)} = (\bar{c}_j^{(m)} - \bar{c}_c^{(m)}) \cdot \hat{\zeta}_m \quad (5.26)$$

Hence, the integrand of (5.20) can be rewritten as shown below,

$$I_{P.O.}(\phi_{c_m}, k_{\xi_m}, k_{\zeta_m}) = e^{i\phi_{c_m}} \iint_{S_m} d\xi d\zeta e^{i(k_{\xi_m}\xi + k_{\zeta_m}\zeta)} \quad (5.27)$$

where

$$\phi_{c_m} = [(\bar{k}_{\perp i} - \bar{k}_{\perp s}) - (pk_{tz_s}^{(u)} + sk_{tz_i}^{(w)}) \hat{z}] \cdot \bar{c}_c^{(m)} \quad (5.28)$$

$$k_{\xi_m} = [(\bar{k}_{\perp i} - \bar{k}_{\perp s}) - (pk_{tz_s}^{(u)} + sk_{tz_i}^{(w)}) \hat{z}] \cdot \bar{\xi}_m \quad (5.29)$$

$$k_{\zeta_m} = [(\bar{k}_{\perp i} - \bar{k}_{\perp s}) - (pk_{tz_s}^{(u)} + sk_{tz_i}^{(w)}) \hat{z}] \cdot \bar{\zeta}_m \quad (5.30)$$

To evaluate the surface integral of (5.27), the expression is now transformed to an equivalent line integral around the edge of the plate using Stoke's theorem.

$$\iint_S dS \hat{n}_S \cdot (\nabla \times \bar{F}) = \oint_C \bar{F} \cdot d\bar{\ell} \quad (5.31)$$

Thus, it is necessary to find a vector field \overline{F} such that the left hand side of (5.31) is identical to the integral of (5.27).

$$\hat{n}_S \cdot (\nabla \times \overline{F}) = \frac{\partial F_\zeta}{\partial \xi} - \frac{\partial F_\xi}{\partial \zeta} = e^{ik_{\xi m} \xi} e^{ik_{\zeta m} \zeta} \quad (5.32)$$

For convenience, F_ξ is set equal to zero, and three resulting cases are treated separately.

The first case is the general case in which $k_{\xi m}$ and $k_{\zeta m}$ are both neither zero or very small. In this case, (5.32) becomes (5.33) below,

$$\frac{\partial F_\zeta}{\partial \xi} = e^{ik_{\xi m} \xi + ik_{\zeta m} \zeta} \quad (5.33)$$

and integrating, the vector field \overline{F} is determined.

$$\overline{F} = \hat{\zeta} \frac{1}{ik_\xi} e^{ik_{\xi m} \xi + ik_{\zeta m} \zeta} \quad (5.34)$$

Hence, the surface integral of (5.27) can be rewritten as the line integral of (5.35).

$$I_{P.O.} = e^{i\phi_{cm}} \oint_C d\overline{\ell} \cdot \hat{\zeta} \frac{1}{ik_\xi} e^{ik_{\xi m} \xi + ik_{\zeta m} \zeta} \quad (5.35)$$

The line integral above can now be divided into linear segments along the edges of the polygonal plate, and expressed as a sum of these contributions. Along the j th edge, ξ can be expressed as in (5.36),

$$\xi = a_j^{(m)} \zeta + b_j^{(m)} \quad (5.36)$$

where the slope $a_j^{(m)}$ and intercept $b_j^{(m)}$ are given by (5.37) and (5.38),

$$a_j^{(m)} = \frac{c_{\xi_{j+1}}^{(m)} - c_{\xi_j}^{(m)}}{c_{\zeta_{j+1}}^{(m)} - c_{\zeta_j}^{(m)}} \quad (5.37)$$

$$b_j^{(m)} = c_{\xi_j}^{(m)} - a_j^{(m)} c_{\zeta_j}^{(m)} \quad (5.38)$$

and where $c_{\xi_{M_m+1}}^{(m)} = c_{\xi_1}^{(m)}$ and $c_{\zeta_{M_m+1}}^{(m)} = c_{\zeta_1}^{(m)}$. Note that if the slope $a_j^{(m)}$ is infinite, then there is no change in ζ along that edge, and consequently, that edge does not contribute to the integral and may be ignored. The integral of (5.35) can now be expressed as shown in (5.39),

$$I_{P.O.} = e^{i\phi_{c_m}} \sum_{j=1}^{M_m} \int_{c_{\zeta_j}^{(m)}}^{c_{\zeta_{j+1}}^{(m)}} d\zeta \frac{1}{k_{\xi_m}} e^{i(k_{\xi_m} a_j^{(m)} + k_{\zeta_m})\zeta + i k_{\xi_m} b_j^{(m)}} \quad (5.39)$$

and after performing the integration, the desired result of (5.40) is obtained.

$$I_{P.O.}(\phi_{c_m}, k_{\xi_m}, k_{\zeta_m}) = e^{i\phi_{c_m}} \sum_{j=1}^{M_m} \frac{2e^{ik_{\xi_m} b_j^{(m)}}}{ik_{\xi_m}} e^{i(k_{\xi_m} a_j^{(m)} + k_{\zeta_m}) \left(\frac{c_{\zeta_{j+1}}^{(m)} + c_{\zeta_j}^{(m)}}{2} \right)} \times \\ \left(\frac{c_{\zeta_{j+1}}^{(m)} + c_{\zeta_j}^{(m)}}{2} \right) \text{sinc} \left[(k_{\xi_m} a_j^{(m)} + k_{\zeta_m}) \left(\frac{c_{\zeta_{j+1}}^{(m)} + c_{\zeta_j}^{(m)}}{2} \right) \right] \quad (5.40)$$

The above result is applicable when k_{ξ_m} is not zero or very small. In the case where k_{ξ_m} becomes very small, evaluation of the above will lead to numerical problems. Thus, it is preferable to treat this case separately. Provided that k_{ζ_m} is not also very

small, then (5.33) reduces to (5.41), where the first two terms of the Taylor series expansion have been used to represent the exponential of small argument.

$$\frac{\partial F_\zeta}{\partial \xi} = (1 + ik_{\xi m} \xi) e^{ik_{\zeta m} \zeta} \quad (5.42)$$

Integrating the above expression, the vector field \overline{F} is again found,

$$\overline{F} = \hat{\zeta} \left(\xi + \frac{1}{2} ik_{\xi m} \xi^2 \right) e^{ik_{\zeta m} \zeta} \quad (5.42)$$

and the surface integral of (5.27) can be put into line integral form once again.

$$I_{P.O.} = e^{i\phi_{cm}} \oint_C \overline{d\ell} \cdot \hat{\zeta} \left(\xi + \frac{1}{2} k_{\xi m} \xi^2 \right) e^{ik_{\zeta m} \zeta} \quad (5.43)$$

Breaking the contour integral into linear segments, (5.44) is obtained,

$$I_{P.O.} = e^{i\phi_{cm}} \sum_{j=1}^{M_m} \int_{c_j^{(m)}}^{c_{j+1}^{(m)}} d\zeta \left[a_j^{(m)} \zeta + b_j^{(m)} + \frac{1}{2} ik_{\xi m} \left(a_j^{(m)2} \zeta^2 + 2a_j^{(m)} b_j^{(m)} \zeta + b_j^{(m)2} \right) \right] \times e^{ik_{\zeta m} \zeta} \quad (5.44)$$

and performing the integration yields (5.45),

$$I_{P.O.}(\phi_{cm}, k_{\xi m}, k_{\zeta m}) = e^{i\phi_{cm}} \sum_{j=1}^{M_m} I_e(c_{j+1}^{(m)}) - I_e(c_j^{(m)}) \quad (5.45)$$

where

$$\begin{aligned}
I_e(\zeta) = & (b_j^{(m)} + \frac{1}{2}ik_{\xi_m} b_j^{(m)^2}) \frac{1}{ik_{\zeta_m}} e^{ik_{\zeta_m}\zeta} + \\
& (a_j^{(m)} + \frac{1}{2}ik_{\xi_m} a_j^{(m)} b_j^{(m)}) \left[\frac{\zeta}{ik_{\zeta_m}} + \frac{1}{k_{\zeta_m}^2} \right] e^{ik_{\zeta_m}\zeta} + \\
& (\frac{1}{2}ik_{\xi_m} a_j^{(m)^2}) \left[\frac{\zeta^2}{ik_{\zeta_m}} + \frac{2\zeta}{k_{\zeta_m}^2} - \frac{2}{ik_{\zeta_m}^3} \right] e^{ik_{\zeta_m}\zeta} \quad (5.46)
\end{aligned}$$

Finally, if both k_{ξ_m} and k_{ζ_m} are very small, representing a case of near specular scattering, then the second exponential of (5.41) may also be approximated by the first two terms of its Taylor series to yield (5.47).

$$\frac{\partial F_\zeta}{\partial \xi} = (1 + ik_{\xi_m}\xi)(1 + ik_{\zeta_m}\zeta) \quad (5.47)$$

Integrating the above, the vector field of (5.48) is obtained, where the linear expression for ξ on each edge has been substituted.

$$\begin{aligned}
\overline{F} = & \hat{\zeta} \left[\left(b_j^{(m)} + \frac{1}{2}ik_{\xi_m} b_j^{(m)^2} \right) + \left(a_j^{(m)} + ik_{\zeta_m} b_j^{(m)} - \frac{1}{2}k_{\xi_m} k_{\zeta_m} b_j^{(m)^2} + ik_{\xi_m} a_j^{(m)} b_j^{(m)} \right) \zeta + \right. \\
& \left. \left(ik_{\zeta_m} a_j^{(m)} + \frac{1}{2}ik_{\xi_m} a_j^{(m)^2} - k_{\xi_m} k_{\zeta_m} a_j^{(m)} b_j^{(m)} \right) \zeta^2 - \left(\frac{1}{2}k_{\xi_m} k_{\zeta_m} a_j^{(m)^2} \right) \zeta^3 \right] \quad (5.48)
\end{aligned}$$

With the above, the surface integral can again be changed to a contour integral composed of linear segments. After performing the integration, the final desired expression is given by (5.49),

$$I_{P.O}(\phi_{c_m}, k_{\xi_m}, k_{\zeta_m}) = e^{i\phi_{c_m}} \sum_{j=1}^{M_m} I'_e(c_{\zeta_{j+1}}^{(m)}) - I'_e(c_{\zeta_j}^{(m)}) \quad (5.49)$$

where

$$\begin{aligned}
 I'_e(\zeta) = & \left(b_j^{(m)} + \frac{1}{2} k_{\xi_m} b_j^{(m)2} \right) \zeta \\
 & + \frac{1}{2} \left(a_j^{(m)} + i k_{\zeta_m} b_j^{(m)} - \frac{1}{2} k_{\xi_m} k_{\zeta_m} b_j^{(m)2} + i k_{\xi_m} a_j^{(m)} b_j^{(m)} \right) \zeta^2 \\
 & + \frac{1}{3} \left(i k_{\zeta_m} a_j^{(m)} + \frac{1}{2} i k_{\xi_m} a_j^{(m)2} - k_{\xi_m} k_{\zeta_m} a_j^{(m)} b_j^{(m)} \right) \zeta^3 \\
 & - \frac{1}{4} \left(\frac{1}{2} k_{\xi_m} k_{\zeta_m} a_j^{(m)2} \right) \zeta^4
 \end{aligned} \tag{5.50}$$

With the above definition of the Physical Optics integral over the plate, the coherent field scattered by the target can be rewritten as shown below.

$$\begin{aligned}
 E_T = & 2i\omega\mu \frac{e^{ikr}}{4\pi r} \sum_{m=1}^N \sum_{p,s=+/-} \sum_{u,w=TE,TM} S(\hat{n}_m, \bar{k}_{\perp_s} + p k_{tz_s}^{(u)} \hat{z}) S(\hat{n}_m, -\bar{k}_{\perp_s} + s k_{tz_s}^{(w)} \hat{z}) \times \\
 & \hat{p} \cdot \overline{H}_{0t_p}^{(u)}(\bar{k}_{\perp_s}) \cdot \left[\hat{n}_m \times \overline{H}_{t_i}^{s,(w)} \right] I_{P.O.}(\phi_{c_m}, k_{\xi_m}, k_{\zeta_m})
 \end{aligned} \tag{5.51}$$

Since the above field is a deterministic quantity, it is not necessary to define the correlation of the field for one aspect and frequency with that at a second aspect/frequency combination. For consistency with the incoherent terms which will be examined next, however, this correlation will be defined as shown below, as the product of the two field quantities.

$$\begin{aligned}
 \sigma_{T-T}^{\hat{p}_a \hat{p}_b}(\bar{k}_{as}, \bar{k}_{ai}, \bar{k}_{bs}, \bar{k}_{bi}) = & 4\pi r \left(\hat{p}_a \cdot \overline{E}_T(\bar{k}_{as}, \bar{k}_{ai}) \times \hat{p}_b^* \cdot \overline{E}_T^*(\bar{k}_{bs}, \bar{k}_{bi}) \right) \\
 = & \sum_{m=1}^N \sum_{m'=1}^N \sum_{p,p',s,s'=+,-} \sum_{u,u',w,w'=TE,TM} B_{T-T}^{pp'ss'} \times \\
 & I_{P.O.}(\phi_{c_m}, k_{\xi_m}, k_{\zeta_m}) I_{P.O.}^*(\phi_{c_{m'}}, k_{\xi_{m'}}, k_{\zeta_{m'}})
 \end{aligned} \tag{5.52}$$

where

$$\begin{aligned}
 B_{\bar{T}-\bar{T}}^{pp'_{ss'}} &= \frac{(\omega\mu)^2}{\pi} S(\hat{n}_m, \bar{k}_{\perp as} + pk_{tza}^{(u)}\hat{z}) \times S(\hat{n}_m, -\bar{k}_{\perp ai} + sk_{tza}^{(w)}\hat{z}) \times \\
 &\quad \left[\hat{p}_a \cdot \bar{H}_{0t_p}^{(u)}(\bar{k}_{\perp as}) \cdot (\hat{n}_m \times \bar{H}_{tai}^{s,(w)}) \right] \times \\
 &\quad S(\hat{n}_{m'}, \bar{k}_{\perp bs} + p'k_{tzb}^{(u')}\hat{z}) \times S(\hat{n}_{m'}, -\bar{k}_{\perp bi} + s'k_{tzb}^{(w')}\hat{z}) \times \\
 &\quad \left[\hat{p}_b \cdot \bar{H}_{0t_{p'}}^{(u')}(\bar{k}_{\perp bs}) \cdot (\hat{n}_{m'} \times \bar{H}_{tbi}^{s',(w')}) \right]^* \quad (5.53)
 \end{aligned}$$

and where

$$\phi_{c_m} = \left[(\bar{k}_{\perp ai} - \bar{k}_{\perp as}) - (pk_{tza}^{(u)} + sk_{tza}^{(w)})\hat{z} \right] \cdot \bar{c}_c^{(m)} \quad (5.54)$$

$$k_{\xi_m} = \left[(\bar{k}_{\perp ai} - \bar{k}_{\perp as}) - (pk_{tza}^{(u)} + sk_{tza}^{(w)})\hat{z} \right] \cdot \hat{\xi}_m \quad (5.55)$$

$$k_{\zeta_m} = \left[(\bar{k}_{\perp ai} - \bar{k}_{\perp as}) - (pk_{tza}^{(u)} + sk_{tza}^{(w)})\hat{z} \right] \cdot \hat{\zeta}_m \quad (5.56)$$

$$\phi_{c_{m'}} = \left[(\bar{k}_{\perp bi} - \bar{k}_{\perp bs}) - (p'k_{tzb}^{(u')} + s'k_{tzb}^{(w')})\hat{z} \right] \cdot \bar{c}_c^{(m')} \quad (5.57)$$

$$k_{\xi_{m'}} = \left[(\bar{k}_{\perp bi} - \bar{k}_{\perp bs}) - (p'k_{tzb}^{(u')} + s'k_{tzb}^{(w')})\hat{z} \right] \cdot \hat{\xi}_{m'} \quad (5.58)$$

$$k_{\zeta_{m'}} = \left[(\bar{k}_{\perp bi} - \bar{k}_{\perp bs}) - (p'k_{tzb}^{(u')} + s'k_{tzb}^{(w')})\hat{z} \right] \cdot \hat{\zeta}_{m'} \quad (5.59)$$

5.3.2. Incoherent Fields

The two incoherent multi-path fields of interest are those given by (5.11) and (5.12). Using the incident field and Green's function expressions of Appendices E and H, these two fields can be rewritten in the form of (5.60) and (5.61) below.

$$\begin{aligned}
 E_{TC} = & 2i\omega\mu \frac{e^{ikr}}{4\pi r} \sum_{m=1}^N \sum_{p,s,l,q=+,-} \sum_{u,v,w=TE,TM} \iint d\bar{k}_\perp \iiint_{V_f} d\bar{r}'' \iint_{S_m} d\bar{r}' \\
 & \hat{p} \cdot \overline{H}_{0tp}^{(u)}(\bar{k}_\perp) \cdot \overline{Q}(\bar{r}'') \cdot \mathcal{U} \left\{ \overline{F}_{ft_{lq}}^{(v)}(\bar{k}_\perp) \cdot \left(\hat{n}_m \times \mathcal{U} \left\{ \overline{H}_{ti}^{s,(w)} \right\} \right) \right\} \times \\
 & e^{-i\bar{k}_\perp \cdot \bar{r}''_\perp} e^{i\bar{k}_\perp \cdot \bar{r}'_\perp} e^{-i\bar{k}_\perp \cdot \bar{r}'_\perp} e^{i\bar{k}_\perp \cdot \bar{r}''_\perp} \times \\
 & e^{-ipk_{fz}^{(u)} z''} e^{ilk_{fz} z''} e^{-iqk_{tz} z'} e^{-isk_{tz_i}^{(w)} z'} \quad (5.60)
 \end{aligned}$$

$$\begin{aligned}
 E_{CT} = & 2i \frac{e^{ikr}}{4\pi r} \sum_{m=1}^N \sum_{p,s,l,q=+,-} \sum_{u,v,w=TE,TM} \iint d\bar{k}_\perp \iiint_{V_f} d\bar{r}'' \iint_{S_m} d\bar{r}' \\
 & \mathcal{U} \left\{ \hat{p} \cdot \overline{H}_{0tp}^{(u)}(\bar{k}_\perp) \cdot \left(\hat{n}_m \times \mathcal{U} \left\{ \overline{F}_{tf_{lq}}^{(v)}(\bar{k}_\perp) \cdot \overline{Q}(\bar{r}'') \cdot \overline{E}_{fi}^{s,(w)} \right\} \right) \right\} \times \\
 & e^{-i\bar{k}_\perp \cdot \bar{r}''_\perp} e^{i\bar{k}_\perp \cdot \bar{r}'_\perp} e^{-i\bar{k}_\perp \cdot \bar{r}'_\perp} e^{i\bar{k}_\perp \cdot \bar{r}''_\perp} \times \\
 & e^{-ipk_{tz}^{(u)} z'} e^{ilk_{tz} z'} e^{-iqk_{fz} z''} e^{-isk_{fz_i}^{(w)} z''} \quad (5.61)
 \end{aligned}$$

Before evaluating the statistics of the above fields, it is necessary to again specify the shadowing function in more detail. As with the coherent term, only a simple shadowing check will be made to determine that the incident wave is illuminating the top side of each plate, and, similarly, that the scattering direction is away from the top side and

not through the plate. More complex shadowing, such as blockage of target features by other intervening target portions, will be ignored here. Hence, the shadowing in the above expressions for the two multi-path fields can be represented using the shadowing function $S(\hat{n}, \bar{k})$ defined by (5.18). The result is given by (5.62) and (5.63) below.

$$\begin{aligned}
 E_{TC} = & 2i\omega\mu \frac{e^{ikr}}{4\pi r} \sum_{m=1}^N \sum_{p,s,l,q=+,-} \sum_{u,v,w=TE,TM} \iint d\bar{k}_{\perp} \iiint_{V_f} d\bar{r}'' \iint_{S_m} d\bar{r}' \\
 & S(\hat{n}_m, \bar{k}_{\perp} + qk_{tz}\hat{z}) S(\hat{n}_m, -\bar{k}_{\perp i} + sk_{tz_i}^{(w)}\hat{z}) \times \\
 & \hat{p} \cdot \overline{H}_{0t_p}^{(u)}(\bar{k}_{\perp}) \cdot \overline{Q}(\bar{r}'') \cdot \overline{F}_{ft_{\ell q}}^{(v)}(\bar{k}_{\perp}) \cdot \left(\hat{n}_m \times \overline{H}_{t_i}^{s,(w)} \right) \times \\
 & e^{-i\bar{k}_{\perp} \cdot \bar{r}'_{\perp}} e^{i\bar{k}_{\perp} \cdot \bar{r}''_{\perp}} e^{-i\bar{k}_{\perp} \cdot \bar{r}'_{\perp}} e^{i\bar{k}_{\perp i} \cdot \bar{r}'_{\perp}} \times \\
 & e^{-ipk_{fz}^{(u)}z''} e^{ik_{fz}z''} e^{-iqk_{tz}z'} e^{-isk_{tz_i}^{(w)}z'} \quad (5.62)
 \end{aligned}$$

$$\begin{aligned}
 E_{CT} = & 2i \frac{e^{ikr}}{4\pi r} \sum_{m=1}^N \sum_{p,s,l,q=+,-} \sum_{u,v,w=TE,TM} \iint d\bar{k}_{\perp} \iiint_{V_f} d\bar{r}'' \iint_{S_m} d\bar{r}' \\
 & S(\hat{n}_m, \bar{k}_{\perp} + pk_{tz}\hat{z}) S(\hat{n}_m, -\bar{k}_{\perp} - \ell k_{tz}\hat{z}) \times \\
 & \hat{p} \cdot \overline{H}_{0t_p}^{(u)}(\bar{k}_{\perp}) \cdot \left(\hat{n}_m \times \overline{F}_{tf_{\ell q}}^{(v)}(\bar{k}_{\perp}) \cdot \overline{Q}(\bar{r}'') \cdot \overline{E}_{f_i}^{s,(w)} \right) \times \\
 & e^{-i\bar{k}_{\perp} \cdot \bar{r}'_{\perp}} e^{i\bar{k}_{\perp} \cdot \bar{r}'_{\perp}} e^{-i\bar{k}_{\perp} \cdot \bar{r}''_{\perp}} e^{i\bar{k}_{\perp i} \cdot \bar{r}''_{\perp}} \times \\
 & e^{-ipk_{tz}^{(u)}z'} e^{ik_{tz}z'} e^{-iqk_{fz}z''} e^{-isk_{fz_i}^{(w)}z''} \quad (5.63)
 \end{aligned}$$

In order to determine the effect of the incoherent portion of the return on the imaging ability of a SAR sensor it is again necessary to determine not only the variance or power

of the above fields, but also their correlation in both azimuth angle and frequency. Although bistatic scattering need not be considered for the SAR problem, for the sake of completeness the statistics derived here allow this generality. Three correlations need be calculated, namely the autocorrelations of E_{TC} and E_{CT} and the cross-correlation of the two. Only the derivation of the target/clutter autocorrelation is presented here, but the derivations for the other two terms are similar, and the final results are given in Appendix I.

As with the point target, the correlation $\sigma_{TC-TC}^{\hat{p}_a \hat{p}_b}$ is normalized in such a manner that the resulting variance for zero azimuth and frequency separation will be equal to the effective radar cross section of the target arising from the target/clutter multi-path mechanism alone. Hence, combining (5.62) with a similar version of itself, representing the product of the target clutter field at two different azimuths and frequencies, and taking the ensemble average, results in the expression of (5.64).

$$\begin{aligned}
 \sigma_{TC-TC}^{\hat{p}_a \hat{p}_b} &= 4\pi r^2 \left\langle \hat{p}_a \cdot \bar{E}_{TC}(\bar{k}_{as}, \bar{k}_{ai}) \times \hat{p}_b^* \cdot \bar{E}_{TC}^*(\bar{k}_{bs}, \bar{k}_{bi}) \right\rangle \\
 &= \frac{\omega^2 \mu^2}{\pi} \sum_{m=1}^N \sum_{m'=1}^N \sum_{p,s,q,\ell=+,-} \sum_{p',s',q',\ell'=+,-} \sum_{u,v,w=TE,TM} \sum_{u',v',w'=TE,TM} \\
 &\quad \iint_{S_m} d\bar{r}_1 \iint_{S_{m'}} d\bar{r}_3 \iiint_{V_f} d\bar{r}_2 \iiint_{V_f} d\bar{r}_4 \iint d\bar{k}_{\perp b} \iint d\bar{k}_{\perp a} \\
 &\quad S(\hat{n}_m, \bar{k}_{\perp a} + qk_{tz_a}^{(v)} \hat{z}) S(\hat{n}_m, -\bar{k}_{\perp ai} + sk_{tz_{ai}}^{(w)} \hat{z}) \times \\
 &\quad S(\hat{n}_{m'}, \bar{k}_{\perp b} + q'k_{tz_b}^{(v')} \hat{z}) S(\hat{n}_{m'}, -\bar{k}_{\perp bi} + s'k_{tz_{bi}}^{(w')} \hat{z}) \times \\
 &\quad \left\langle \left[\hat{p}_a \cdot \bar{H}_{0f_p}^{(u)}(\bar{k}_{\perp as}) \cdot \bar{Q}(\bar{r}_2) \cdot \bar{F}_{ft_{\ell_q}}^{(v)}(\bar{k}_{\perp a}) \cdot \left(\hat{n}_m \times \bar{H}_{t_{ai}}^{s,(w)} \right) \right] \times \right. \\
 &\quad \left. \left[\hat{p}_b \cdot \bar{H}_{0f_{p'}}^{(u')}(\bar{k}_{\perp bs}) \cdot \bar{Q}(\bar{r}_4) \cdot \bar{F}_{ft_{\ell'_q}}^{(v')}(\bar{k}_{\perp b}) \cdot \left(\hat{n}_{m'} \times \bar{H}_{t_{bi}}^{s',(w')} \right) \right]^* \right\rangle \times
 \end{aligned}$$

$$\begin{aligned}
& e^{-i\bar{k}_{\perp a_s} \cdot \bar{r}_{2\perp}} e^{i\bar{k}_{\perp a} \cdot \bar{r}_{2\perp}} e^{-i\bar{k}_{\perp a_i} \cdot \bar{r}_{1\perp}} e^{i\bar{k}_{\perp a_i} \cdot \bar{r}_{1\perp}} e^{i\bar{k}_{\perp b_s} \cdot \bar{r}_{4\perp}} e^{-i\bar{k}_{\perp b} \cdot \bar{r}_{4\perp}} \times \\
& e^{i\bar{k}_{\perp b} \cdot \bar{r}_{3\perp}} e^{-i\bar{k}_{\perp b_i} \cdot \bar{r}_{3\perp}} e^{-ipk_{fz_{a_s}}^{(u)} z_2} e^{i\ell k_{fz_a}^{(v)} z_2} e^{-iqk_{tz_a}^{(v)} z_1} e^{-isk_{tz_{ai}}^{(w)} z_1} \times \\
& e^{ip'k_{fz_{b_s}}^{(u')} z_4} e^{-i\ell'k_{fz_b}^{(v')} z_4} e^{iq'k_{tz_b}^{(v')} z_3} e^{is'k_{tz_{bi}}^{(w')} z_3}
\end{aligned} \tag{5.64}$$

The correlation between the $\alpha\beta$ element of $\bar{Q}(\bar{r}_2)$ and the $\gamma\rho$ element of $\bar{Q}(\bar{r}_4)$ will be denoted as $C_{\alpha\beta\gamma\rho}(\bar{r}_2 - \bar{r}_4)$, where the stationarity of the random media has been exploited. Substituting this definition, and expressing the matrix multiplication in an element by element fashion such that the correlation can be extracted from the intervening terms, the above can be rewritten as in (5.65).

$$\begin{aligned}
\sigma_{TC-TC}^{\hat{p}_a \hat{p}_b} &= \frac{\omega^2 \mu^2}{\pi} \sum_{m, m'=1}^N \sum_{\substack{p, s, q, \ell, \\ p', s', q', \ell' = +, -}} \sum_{\substack{u, v, w, \\ u', v', w' = TE, TM}} \sum_{\alpha, \beta, \gamma, \rho = x, y, z} \\
& \iint_{S_m} d\bar{r}_1 \iint_{S_{m'}} d\bar{r}_3 \iiint_{V_f} d\bar{r}_2 \iiint_{V_f} d\bar{r}_4 \iint d\bar{k}_{\perp b} \iint d\bar{k}_{\perp a} C_{\alpha\beta\gamma\rho}(\bar{r}_2 - \bar{r}_4) \times \\
& S(\hat{n}_m, \bar{k}_{\perp a} + qk_{tz_a}^{(v)} \hat{z}) S(\hat{n}_m, -\bar{k}_{\perp a_i} + sk_{tz_{ai}}^{(w)} \hat{z}) \times \\
& S(\hat{n}_{m'}, \bar{k}_{\perp b} + q'k_{tz_b}^{(v')} \hat{z}) S(\hat{n}_{m'}, -\bar{k}_{\perp b_i} + s'k_{tz_{bi}}^{(w')} \hat{z}) \times \\
& \left[\hat{p}_a \cdot \bar{H}_{0f_p}^{(u)}(\bar{k}_{\perp a_s}) \right]_{\alpha} \cdot \left[\bar{F}_{ft_{\ell q}}^{(v)}(\bar{k}_{\perp a}) \cdot \left(\hat{n}_m \times \bar{H}_{t_{ai}}^{s, (w)} \right) \right]_{\beta} \times \\
& \left[\hat{p}_b \cdot \bar{H}_{0f_{p'}}^{(u')}(\bar{k}_{\perp b_s}) \right]_{\gamma}^* \cdot \left[\bar{F}_{ft_{\ell' q'}}^{(v')}(\bar{k}_{\perp b}) \cdot \left(\hat{n}_{m'} \times \bar{H}_{t_{bi}}^{s', (w')} \right) \right]_{\rho}^* \times \\
& e^{i(\bar{k}_{\perp a} - \bar{k}_{\perp a_s}) \cdot \bar{r}_{2\perp}} e^{i(\bar{k}_{\perp a_i} - \bar{k}_{\perp a}) \cdot \bar{r}_{1\perp}} e^{i(\bar{k}_{\perp b_s} - \bar{k}_{\perp b}) \cdot \bar{r}_{4\perp}} e^{i(\bar{k}_{\perp b} - \bar{k}_{\perp b_i}) \cdot \bar{r}_{3\perp}} \times \\
& e^{i(\ell k_{fz_a}^{(v)} - p k_{fz_{a_s}}^{(u)}) z_2} e^{-i(q k_{tz_a}^{(v)} + s k_{tz_{ai}}^{(w)}) z_1} e^{i(p' k_{fz_{b_s}}^{(u')} - \ell' k_{fz_b}^{(v')}) z_4} e^{i(q' k_{tz_b}^{(v')} + s' k_{tz_{bi}}^{(w')}) z_3}
\end{aligned} \tag{5.65}$$

To the above a change of variables in z_2 and z_4 is made so that the resulting integration has limits from $-h_f$ to 0, rather than the initial limits from $-d_f$ to $-d_{f-1}$. Since the correlation is a function of the difference $z_2 - z_4$, it is unaffected, and the only effect of this transformation is on the phase terms. In addition to the change of variables, the correlation is represented as the Fourier transform of the associated spectral density function, $\Phi_{\alpha\beta\gamma\rho}(\bar{\beta})$. Hence, rewriting leads to (5.66),

$$\begin{aligned}
 \sigma_{TC-TC}^{\hat{p}_a \hat{p}_b} = & \sum_{m, m'=1}^N \sum_{\substack{p, s, q, \ell, \\ p', s', q', \ell' = +, -}} \sum_{\substack{u, v, w, \\ u', v', w' = TE, TM}} \sum_{\alpha, \beta, \gamma, \rho = x, y, z} \\
 & \iint_{S_m} d\bar{r}_1 \iint_{S_{m'}} d\bar{r}_3 \iint d\bar{r}_{2\perp} \iint d\bar{r}_{4\perp} \int_{-h_f}^0 dz_2 \int_{-h_f}^0 dz_4 \\
 & \iint d\bar{k}_{\perp a} \iint d\bar{k}_{\perp b} \iint d\bar{\beta}_{\perp} \int d\beta_z B_{TC-TC}^{\alpha\beta\gamma\rho}{}_{pp's's'qq'\ell\ell'}{}^{uu'vv'ww'} \Phi_{\alpha\beta\gamma\rho}(\bar{\beta}) \times \\
 & e^{i(\bar{k}_{\perp ai} - \bar{k}_{\perp a}) \cdot \bar{r}_{1\perp}} e^{i(\bar{k}_{\perp a} - \bar{k}_{\perp as} - \bar{\beta}_{\perp}) \cdot \bar{r}_{2\perp}} e^{i(\bar{k}_{\perp b} - \bar{k}_{\perp bi}) \cdot \bar{r}_{3\perp}} \times \\
 & e^{i(\bar{k}_{\perp bs} - \bar{k}_{\perp b} + \bar{\beta}_{\perp}) \cdot \bar{r}_{4\perp}} e^{-i(qk_{tza}^{(v)} + sk_{tza}^{(w)})z_1} e^{i(\ell k_{fza}^{(v)} - pk_{fza}^{(u)} - \beta_z)z_2} \times \\
 & e^{i(q'k_{tzb}^{(v')*} + s'k_{tzb}^{(w')*})z_3} e^{i(p'k_{fzb}^{(u')*} - \ell'k_{fzb}^{(v')*} + \beta_z)z_4} \times \\
 & e^{-i(\ell k_{fza}^{(v)} - pk_{fza}^{(u)} + p'k_{fzb}^{(u')*} - \ell'k_{fzb}^{(v')*})d_{f-1}}
 \end{aligned} \tag{5.66}$$

where

$$\begin{aligned}
 B_{TC-TC}^{\alpha\beta\gamma\rho}{}_{pp's's'qq'\ell\ell'}{}^{uu'vv'ww'} = & \frac{\omega^2 \mu^2}{\pi} S(\hat{n}_m, \bar{k}_{\perp a} + qk_{tza}^{(v)} \hat{z}) S(\hat{n}_m, -\bar{k}_{\perp ai} + sk_{tza}^{(w)} \hat{z}) \times \\
 & S(\hat{n}_{m'}, \bar{k}_{\perp b} + q'k_{tzb}^{(v')} \hat{z}) S(\hat{n}_{m'}, -\bar{k}_{\perp bi} + s'k_{tzb}^{(w')} \hat{z}) \times
 \end{aligned}$$

$$\left[\hat{p}_a \cdot \overline{H}_{0f_p}^{(u)}(\bar{k}_{\perp a}) \right]_{\alpha} \cdot \left[\overline{F}_{ft_{iq}}^{(v)}(\bar{k}_{\perp a}) \cdot \left(\hat{n}_m \times \overline{H}_{tai}^{s,(w)} \right) \right]_{\beta} \times \\ \left[\hat{p}_b \cdot \overline{H}_{0f_{p'}}^{(u')}(\bar{k}_{\perp b}) \right]_{\gamma}^* \cdot \left[\overline{F}_{ft_{iq'}}^{(v')}(\bar{k}_{\perp b}) \cdot \left(\hat{n}_{m'} \times \overline{H}_{tbi}^{s',(w')} \right) \right]_{\rho}^* \quad (5.67)$$

The $\bar{\tau}_{2\perp}$ integral of (5.66) can be done to yield a delta function in $\bar{k}_{\perp a} - \bar{k}_{\perp as} - \bar{\beta}_{\perp}$, and this delta function allows trivial integration over $\bar{\beta}_{\perp}$, yielding (5.68).

$$\sigma_{TC-TC}^{\hat{p}_a \hat{p}_b} = \sum_{m,m'=1}^N \sum_{p',s',q',\ell',\ell'=+,-}^{p,s,q,\ell,} \sum_{u',v',w'=TE,TM}^{u,v,w,} \sum_{\alpha,\beta,\gamma,\rho=x,y,z} \\ \iint_{S_m} d\bar{\tau}_1 \iint_{S_{m'}} d\bar{\tau}_3 \iint d\bar{\tau}_{4\perp} \int_{-h_f}^0 dz_2 \int_{-h_f}^0 dz_4 \\ \iint d\bar{k}_{\perp a} \iint d\bar{k}_{\perp b} \int d\beta_z (2\pi)^2 B_{TC-TC}^{\alpha\beta\gamma\rho, pp'ss'qq'\ell\ell'} \Phi_{\alpha\beta\gamma\rho}(\bar{k}_{\perp a} - \bar{k}_{\perp as}, \beta_z) \times \\ e^{i(\bar{k}_{\perp ai} - \bar{k}_{\perp a}) \cdot \bar{\tau}_{1\perp}} e^{i(\bar{k}_{\perp b} - \bar{k}_{\perp bi}) \cdot \bar{\tau}_{3\perp}} e^{i(\bar{k}_{\perp bs} - \bar{k}_{\perp b} + \bar{k}_{\perp a} - \bar{k}_{\perp as}) \cdot \bar{\tau}_{4\perp}} \times \\ e^{-i(qk_{iz_a}^{(v)} + sk_{iz_{ai}}^{(w)})z_1} e^{i(q'k_{iz_b}^{(v')*} + s'k_{iz_{bi}}^{(w')*})z_3} e^{-i(\ell k_{fz_a}^{(v)} - pk_{fz_{as}}^{(u)} + p'k_{fz_{bs}}^{(u')*} - \ell'k_{fz_b}^{(v')*})d_{f-1}} \times \\ e^{i(\ell k_{fz_a}^{(v)} - pk_{fz_{as}}^{(u)} - \beta_z)z_2} e^{i(p'k_{fz_{bs}}^{(u')*} - \ell'k_{fz_b}^{(v')*} + \beta_z)z_4} \quad (5.68)$$

Similarly, the integration over $\bar{\tau}_{4\perp}$ can be done to yield a delta function in $\bar{k}_{\perp bs} - \bar{k}_{\perp as} + \bar{k}_{\perp a} - \bar{k}_{\perp b}$, and this delta function can be used to perform the $\bar{k}_{\perp b}$ integral trivially. The result is given by (5.69),

$$\sigma_{TC-TC}^{\hat{p}_a \hat{p}_b} = \sum_{m,m'=1}^N \sum_{p',s',q',\ell',\ell'=+,-}^{p,s,q,\ell,} \sum_{u',v',w'=TE,TM}^{u,v,w,} \sum_{\alpha,\beta,\gamma,\rho=x,y,z} \\ \iint_{S_m} d\bar{\tau}_1 \iint_{S_{m'}} d\bar{\tau}_3 \int_{-h_f}^0 dz_2 \int_{-h_f}^0 dz_4$$

$$\begin{aligned}
& \iint d\bar{k}_{\perp a} \int d\beta_z (2\pi)^4 B_{TC-TC}^{\alpha\beta\gamma\rho, pp'ss'qq'\ell\ell'} \Phi_{\alpha\beta\gamma\rho}(\bar{k}_{\perp a} - \bar{k}_{\perp as}, \beta_z) \times \\
& e^{i(\bar{k}_{\perp ai} - \bar{k}_{\perp a}) \cdot \bar{\tau}_{1\perp}} e^{i(\bar{k}_{\perp c} - \bar{k}_{\perp bi}) \cdot \bar{\tau}_{3\perp}} e^{-i(\ell k_{fza}^{(v)} - p k_{fza}^{(u)} + p' k_{fzb}^{(u')*} - \ell' k_{fzc}^{(v')*}) d_{f-1}} \times \\
& e^{-i(q k_{iza}^{(v)} + s k_{iza}^{(w)}) z_1} e^{i(q' k_{izc}^{(v')*} + s' k_{izbi}^{(w')*}) z_3} \times \\
& e^{-i(p k_{fza}^{(u)} - \ell k_{fza}^{(v)} + \beta_z) z_2} e^{i(p' k_{fzb}^{(u')*} - \ell' k_{fzc}^{(v')*} + \beta_z) z_4} \quad (5.69)
\end{aligned}$$

where $\bar{k}_{\perp c} = \bar{k}_{\perp bs} - \bar{k}_{\perp as} + \bar{k}_{\perp a}$, and where B_{TC-TC} is as in (5.67) with \bar{k}_{\perp} replaced by $\bar{k}_{\perp c}$. The z_2 and z_4 integrals can now be done directly to yield the expression of (5.70).

$$\begin{aligned}
\sigma_{TC-TC}^{\hat{p}_a \hat{p}_b} &= \sum_{m, m'=1}^N \sum_{\substack{p', s', q', \ell' = +, - \\ p, s, q, \ell}} \sum_{\substack{u, v, w, \\ u', v', w' = TE, TM}} \sum_{\alpha, \beta, \gamma, \rho = x, y, z} \\
& \iint_{S_m} d\bar{\tau}_1 \iint_{S_{m'}} d\bar{\tau}_3 \iint d\bar{k}_{\perp a} \int d\beta_z \\
& (2\pi)^4 B_{TC-TC}^{\alpha\beta\gamma\rho, pp'ss'qq'\ell\ell'} \Phi_{\alpha\beta\gamma\rho}(\bar{k}_{\perp a} - \bar{k}_{\perp as}, \beta_z) e^{-i(\ell k_{fza}^{(v)} - p k_{fza}^{(u)} + p' k_{fzb}^{(u')*} - \ell' k_{fzc}^{(v')*}) d_{f-1}} \times \\
& e^{i(\bar{k}_{\perp ai} - \bar{k}_{\perp a}) \cdot \bar{\tau}_{1\perp}} e^{i(\bar{k}_{\perp c} - \bar{k}_{\perp bi}) \cdot \bar{\tau}_{3\perp}} e^{-i(q k_{iza}^{(v)} + s k_{iza}^{(w)}) z_1} e^{i(q' k_{izc}^{(v')*} + s' k_{izbi}^{(w')*}) z_3} \times \\
& \frac{1 - e^{i(p k_{fza}^{(u)} - \ell k_{fza}^{(v)} + \beta_z) h_f}}{p k_{fza}^{(u)} - \ell k_{fza}^{(v)} + \beta_z} \cdot \frac{1 - e^{-i(p' k_{fzb}^{(u')*} - \ell' k_{fzc}^{(v')*} + \beta_z) h_f}}{p' k_{fzb}^{(u')*} - \ell' k_{fzc}^{(v')*} + \beta_z} \quad (5.70)
\end{aligned}$$

The β_z integral remaining above can be done using residue theory, splitting the integral into a portion convergent in the upper half-plane of complex β_z and a part convergent in the lower half-plane. Poles of the resulting integrands occur at $\beta_z = \ell k_{fza}^{(v)} - p k_{fza}^{(u)}$ and $\beta_z = \ell' k_{fzc}^{(v')*} - p' k_{fzb}^{(u')*}$. Although the spectral function will have poles of its own, in the low loss case, the above poles will be dominant, and those of $\Phi(\bar{\beta})$ will be neglected.

It is possible to include the poles of the spectral function in the same manner as was done for the point target in Appendix F, however, this is not pursued here. Hence, the result after integration is given by (5.71) below.

$$\begin{aligned}
 \sigma_{TC-TC}^{\hat{p}_a \hat{p}_b} = & \sum_{m, m'=1}^N \sum_{\substack{p', s', q', \ell', \\ p', s', q', \ell' = +, -}} \sum_{\substack{u, v, w, \\ u', v', w' = TE, TM}} \sum_{\alpha, \beta, \gamma, \rho = x, y, z} \\
 & \iint_{S_m} d\bar{\tau}_1 \iint_{S_{m'}} d\bar{\tau}_3 \iint d\bar{k}_{\perp a} (2\pi)^5 i B_{TC-TC}^{\alpha\beta\gamma\rho}{}_{pp'ss'qq'\ell\ell'}{}_{uu'vv'ww'} \times \\
 & e^{-i(\ell k_{fza}^{(v)} - p k_{fza}^{(u)} + p' k_{fzs}^{(u')*} - \ell' k_{fzc}^{(v')*})d_f - 1} e^{i(\bar{k}_{\perp ai} - \bar{k}_{\perp a}) \cdot \bar{\tau}_1 \perp} e^{i(\bar{k}_{\perp c} - \bar{k}_{\perp bi}) \cdot \bar{\tau}_3 \perp} \times \\
 & e^{-i(q k_{tza}^{(v)} + s k_{tza}^{(w)})z_1} e^{i(q' k_{tzc}^{(v')*} + s' k_{tzc}^{(w')*})z_3} \times \\
 & \left[\frac{\Phi_{\alpha\beta\gamma\rho}(\bar{k}_{\perp a} - \bar{k}_{\perp as}, \ell' k_{fzc}^{(v')*} - p' k_{fzs}^{(u')*})}{p k_{fza}^{(u)} - \ell k_{fza}^{(v)} + \ell' k_{fzc}^{(v')*} - p' k_{fzs}^{(u')*}} - \frac{\Phi_{\alpha\beta\gamma\rho}(\bar{k}_{\perp a} - \bar{k}_{\perp as}, \ell k_{fza}^{(v)} - p k_{fza}^{(u)})}{p k_{fza}^{(u)} - \ell k_{fza}^{(v)} + \ell' k_{fzc}^{(v')*} - p' k_{fzs}^{(u')*}} \times \right. \\
 & \left. e^{i(p k_{fza}^{(u)} - \ell k_{fza}^{(v)} + \ell' k_{fzc}^{(v')*} - p' k_{fzs}^{(u')*})h_f} \right] \quad (5.71)
 \end{aligned}$$

The only dependance on $\bar{\tau}_1$ and $\bar{\tau}_3$ in the integrand above occurs in the exponential phase terms. Hence, both the integral over $\bar{\tau}_1$ and the integral over $\bar{\tau}_3$ can be put in the form of the Physical Optics integral of (5.27), where ϕ_c , k_ξ , and k_ζ for the two integrals are given by (5.72)-(5.77).

$$\phi_{cm} = \left[(\bar{k}_{\perp ai} - \bar{k}_{\perp a}) - (s k_{tza}^{(w)} + q k_{tza}^{(v)}) \hat{z} \right] \cdot \bar{c}_c^{(m)} \quad (5.72)$$

$$k_{\xi m} = \left[(\bar{k}_{\perp ai} - \bar{k}_{\perp a}) - (s k_{tza}^{(w)} + q k_{tza}^{(v)}) \hat{z} \right] \cdot \hat{\xi}_m \quad (5.73)$$

$$k_{\zeta_m} = \left[(\bar{k}_{\perp_{ai}} - \bar{k}_{\perp_a}) - (s k_{tz_{ai}}^{(w)} + q k_{tz_a}^{(v)}) \right] \cdot \hat{\zeta}_m \quad (5.74)$$

$$\phi_{c_{m'}} = \left[(\bar{k}_{\perp_{bi}} - \bar{k}_{\perp_c}) - (s' k_{tz_{bi}}^{(w')} + q' k_{tz_c}^{(v')}) \right] \cdot \hat{c}_c^{(m')} \quad (5.75)$$

$$k_{\xi_{m'}} = \left[(\bar{k}_{\perp_{bi}} - \bar{k}_{\perp_c}) - (s' k_{tz_{bi}}^{(w')} + q' k_{tz_c}^{(v')}) \right] \cdot \hat{\xi}_{m'} \quad (5.76)$$

$$k_{\zeta_{m'}} = \left[(\bar{k}_{\perp_{bi}} - \bar{k}_{\perp_c}) - (s' k_{tz_{bi}}^{(w')} + q' k_{tz_c}^{(v')}) \right] \cdot \hat{\zeta}_{m'} \quad (5.77)$$

Hence, the final desired form for $\sigma_{TC-TC}^{\hat{p}_a \hat{p}_b}$ is as given below in (5.78).

$$\begin{aligned} \sigma_{TC-TC}^{\hat{p}_a \hat{p}_b} = & (2\pi)^5 i \sum_{m, m'=1}^N \sum_{\substack{p, s, q, \ell, \\ p', s', q', \ell' = +, -}} \sum_{\substack{u, v, w, \\ u', v', w' = TE, TM}} \sum_{\alpha, \beta, \gamma, \rho = x, y, z} \\ & \iint d\bar{k}_{\perp_a} B_{TC-TC}^{\alpha\beta\gamma\rho} \times \\ & I_{P.O.}(\phi_{c_m}, k_{\xi_m}, k_{\zeta_m}) I_{P.O.}^*(\phi_{c_{m'}}, k_{\xi_{m'}}, k_{\zeta_{m'}}) e^{-i(\ell k_{fz_a}^{(v)} - p k_{fz_a}^{(u)} + p' k_{fz_{b_s}}^{(u')*} - \ell' k_{fz_c}^{(v')*}) d_f - 1} \times \\ & \left[\frac{\Phi_{\alpha\beta\gamma\rho}(\bar{k}_{\perp_a} - \bar{k}_{\perp_{a_s}}, \ell' k_{fz_c}^{(v')*} - p' k_{fz_{b_s}}^{(u')*})}{p k_{fz_{a_s}}^{(u)} - \ell k_{fz_a}^{(v)} + \ell' k_{fz_c}^{(v')*} - p' k_{fz_{b_s}}^{(u')*}} - \frac{\Phi_{\alpha\beta\gamma\rho}(\bar{k}_{\perp_a} - \bar{k}_{\perp_{a_s}}, \ell k_{fz_a}^{(v)} - p k_{fz_{a_s}}^{(u)})}{p k_{fz_{a_s}}^{(u)} - \ell k_{fz_a}^{(v)} + \ell' k_{fz_c}^{(v')*} - p' k_{fz_{b_s}}^{(u')*}} \right] \times \\ & e^{i(p k_{fz_{a_s}}^{(u)} - \ell k_{fz_a}^{(v)} + \ell' k_{fz_c}^{(v')*} - p' k_{fz_{b_s}}^{(u')*}) h_f} \end{aligned} \quad (5.78)$$

It should be noted that the above expression has a form very similar to the equivalent term for the point target. The major difference in this new result is the addition of the two $I_{P.O.}$ terms which were absent for the point target. These new

terms form a radiation pattern such that the energy scattered from the target to the random media is stronger or weaker in certain directions which are determined by the shape of the target. This is in contrast to the point target, where aside from the dipole-like dependance, the scattering was more uniform.

The derivations of the correlations $\sigma_{CT-CT}^{\hat{p}_a\hat{p}_b}$ and $\sigma_{TC-CT}^{\hat{p}_a\hat{p}_b}$ are similar, and are not presented here. As noted earlier, however, the final expressions for all terms are given in Appendix I.

5.4. Variance and Correlation Results

This section presents a variety of results in which the above derived expressions for the statistics of the fields are used to calculate the variance and correlation of the multi-path mechanism, as well as the power in the coherent return. The dependance of these statistics on parameters such as elevation angle, media thickness, and target size, orientation and depth, are shown. It is assumed here that the target is a single square plate, located in free-space beneath a layer of isotropic random media. The media geometry is, therefore, similar to that considered for the point target in Chapter 2. The random media again has a fractional volume of $f_V = 1.67\%$ and a correlation length of $\ell = 0.0052$ m, which at a frequency of 1.12 GHz leads to an effective permittivity of $\epsilon_{1m} = (1.0505 + 0.001794i)\epsilon_0$ and a renormalized scattering source variance of $\delta = .146822$.

Figure 5.4 shows the coherent or direct target return from the plate for this configuration as a function of elevation angle. The plate is 60 cm by 60 cm, is located 5

m below the random media, and is oriented parallel to the stratification of the media, such that the plate normal is in the \hat{z} direction. Azimuthally, the plate is oriented such that the edges are parallel to the x and y axes, and the result shown is for $\phi = 0^\circ$. The random media is taken to be 10 m in depth and both HH (dash) and VV (dots) polarizations are shown. Also for comparison, the polarization-independent, free-space result (solid) is shown, in which the random slab is removed and replaced by free space permittivity. All of the results display the characteristic sinc response arising from the Fourier transform of the square illumination aperture. There is a difference of approximately 3.5 dB between the free-space and media returns at normal incidence, and this difference increases as the elevation angle is increased, and the path through the random slab becomes longer. The difference between the free-space and media cases is identical to that seen for the point target in Chapter 2, since the attenuation in the random media for the coherent wave is independent of the target. Also like the previous point target case, there is very little difference between the two polarizations. Because Physical Optics is polarization independent for monostatic applications, the only difference which can arise between the two polarizations must come from interface effects in the layered media. As discussed for the point target, these effects are weak here, because the permittivity contrast between the regions is small, and there is little reflection at the boundaries.

Figures 5.5 and 5.6 show the incoherent returns for the HH and VV polarizations respectively. As noted before, Physical Optics is not a reciprocal formulation, and the multi-path fields due to target/clutter and clutter/target scattering may be different. For this reason, the target/clutter-target/clutter (long-dash), clutter/target-clutter/target (dots), and target/clutter-clutter/target (short-dash) returns are all

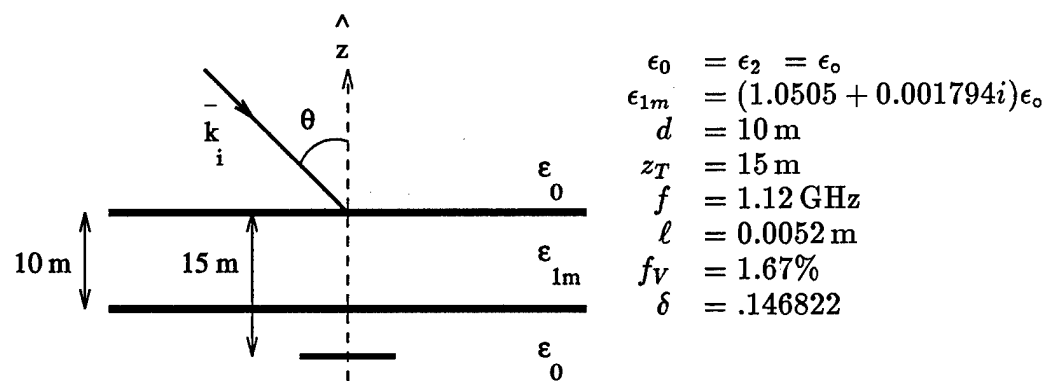
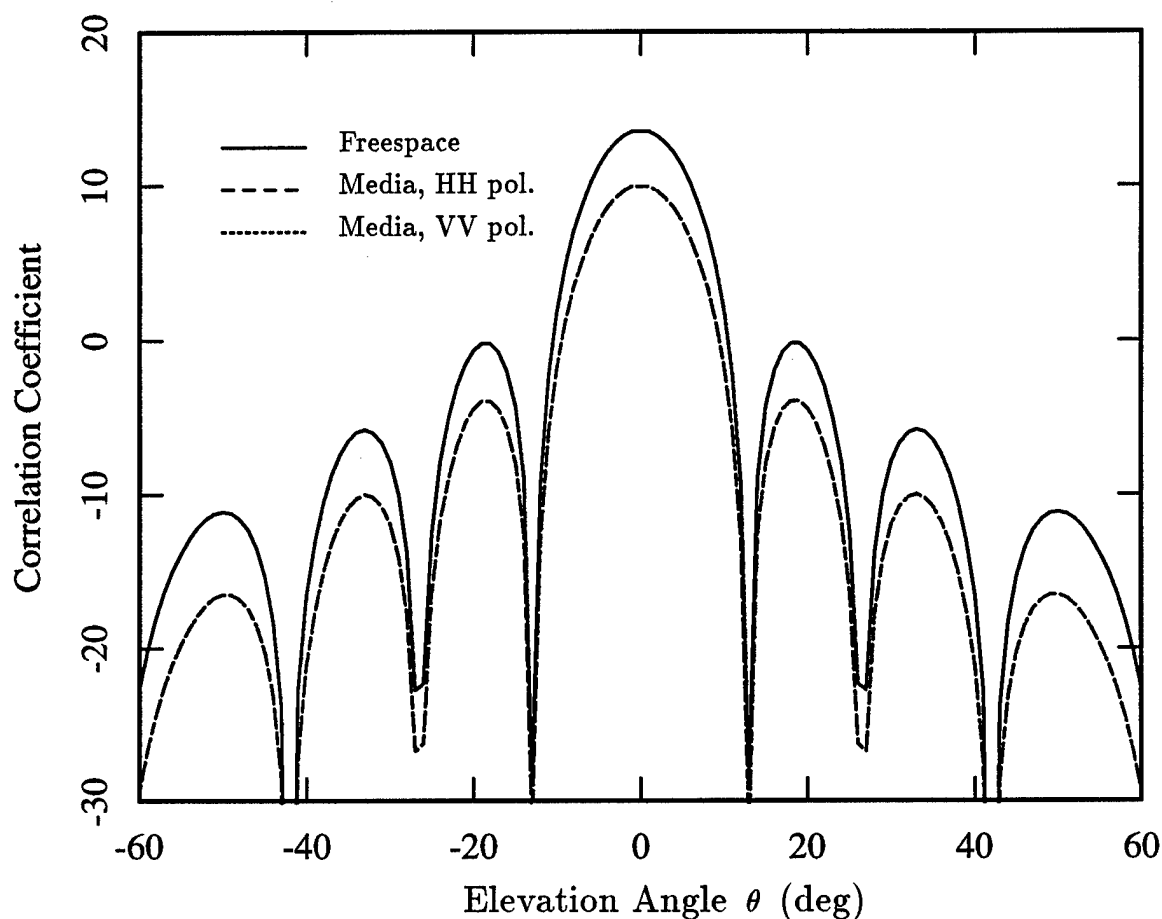


Figure 5.4. Dependence of the coherent target scattering cross section, σ_{T-T} , on elevation angle for a 60 cm by 60 cm square plate. Shown are the HH (dash) and VV (dots) returns at a frequency of 1.12 GHz for a 10 m thick, isotropic random slab, with freespace above and below, and with the target positioned 5 m below the lower interface. Also show for comparison is the freespace plate cross section (solid).

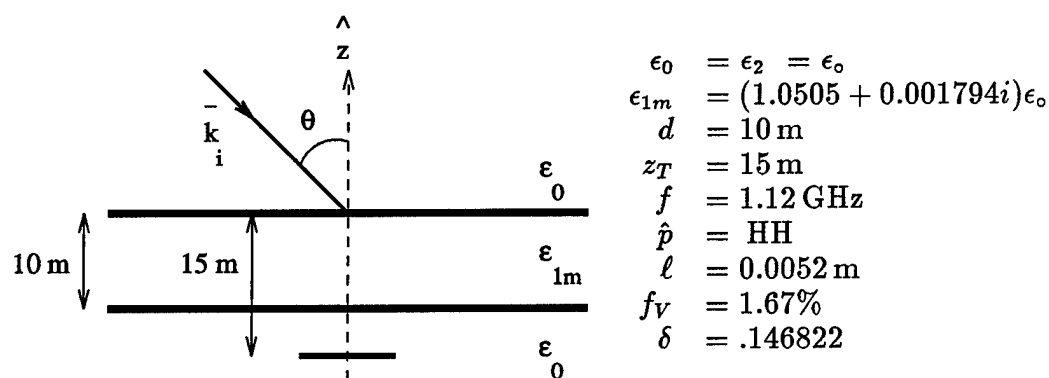
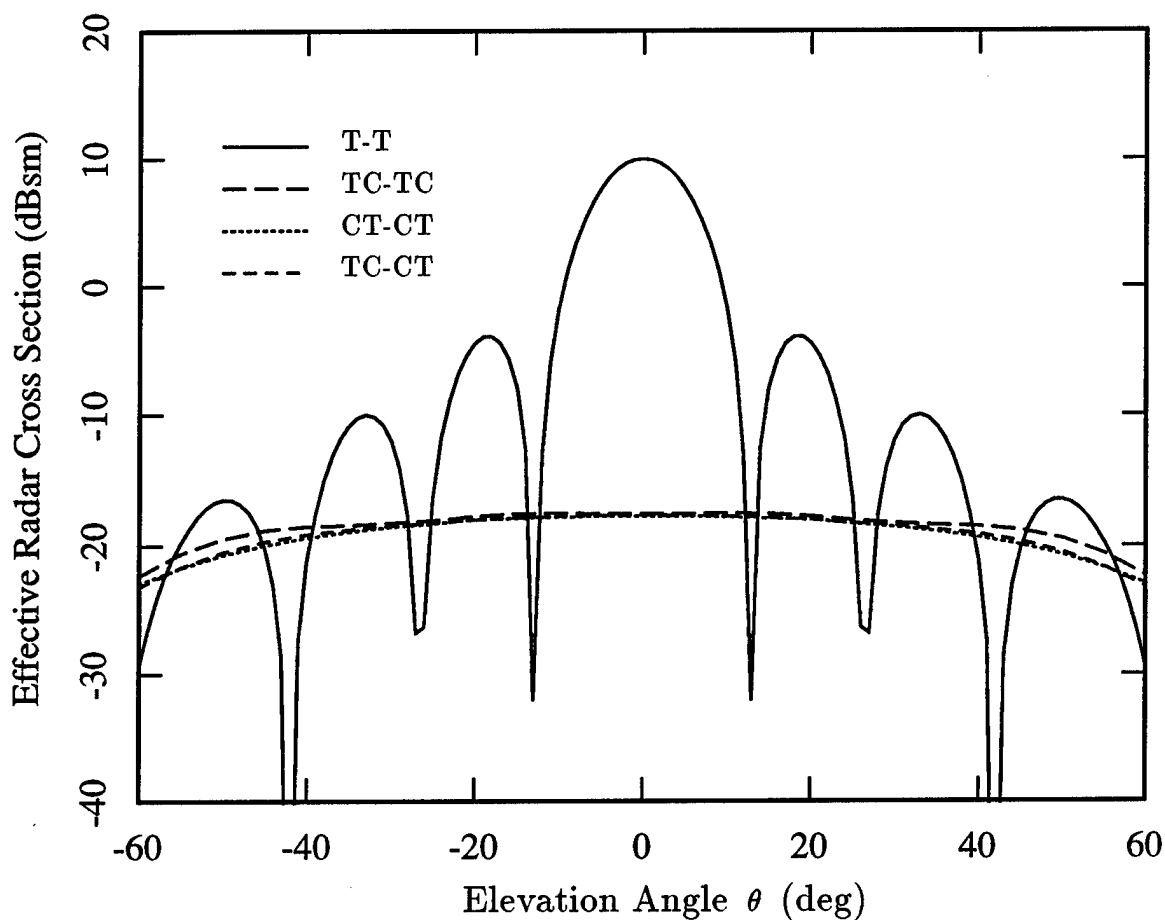


Figure 5.5. Dependence of the coherent target scattering cross section, σ_{T-T} , (solid) and the incoherent multi-path terms, σ_{TC-TC} (long-dash), σ_{CT-CT} (dots), and σ_{TC-CT} (short-dash), on elevation angle for a 60 cm by 60 cm square plate. Shown is the HH polarization at a frequency of 1.12 GHz for a 10 m thick, isotropic random slab, with freespace above and below, and with the target positioned 5 m below the lower interface.

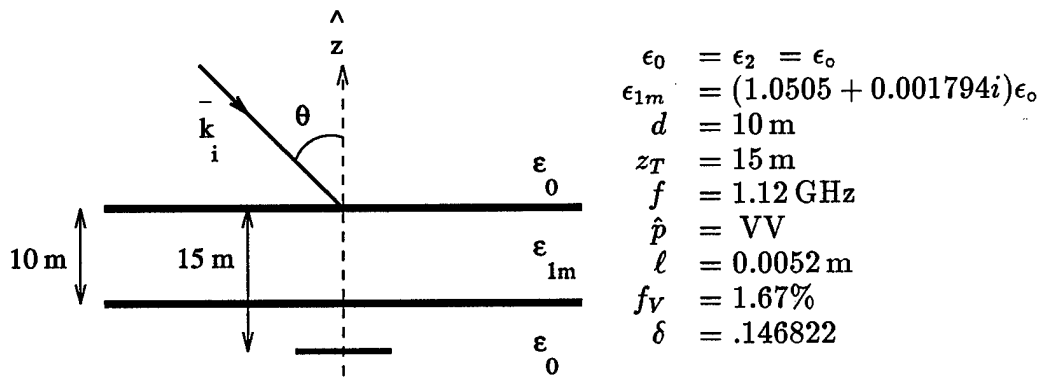
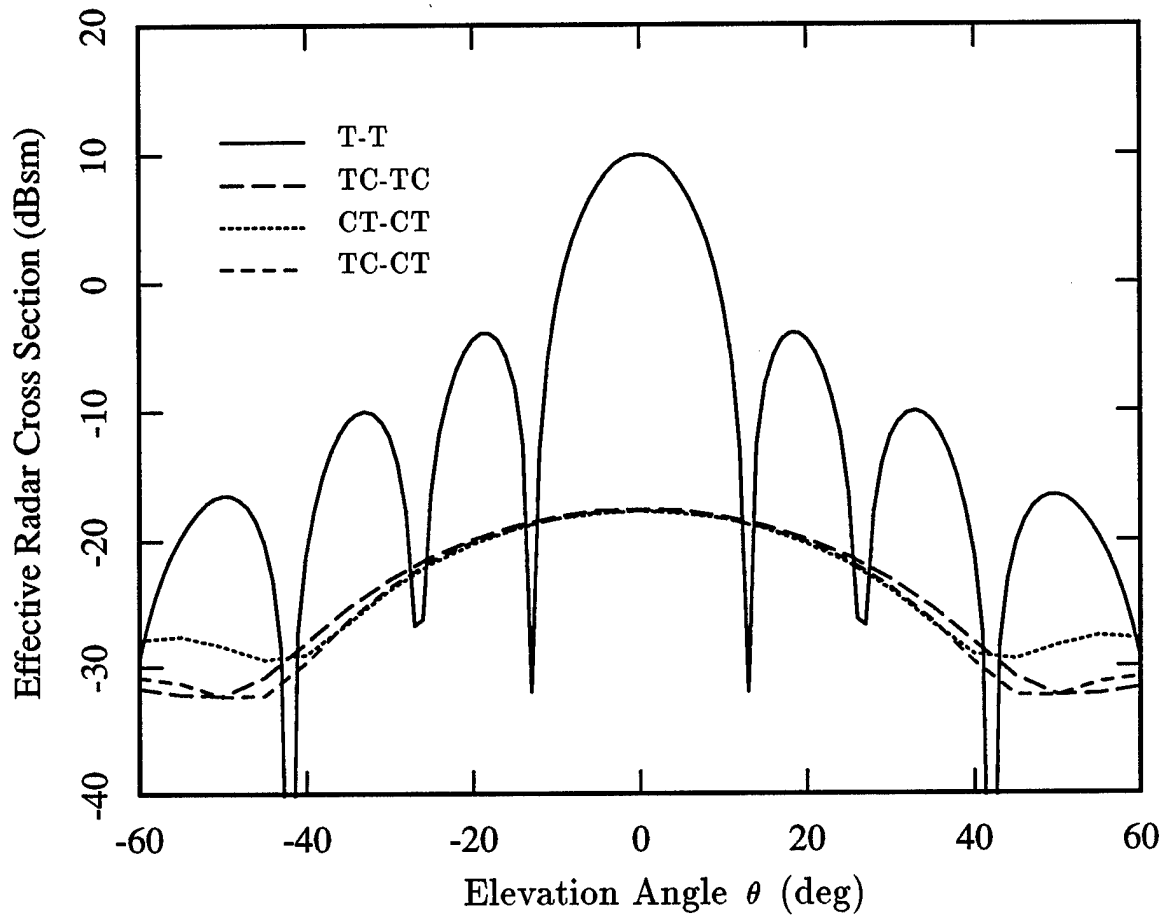


Figure 5.6. Dependence of the coherent target scattering cross section, σ_{T-T} , (solid) and the incoherent multi-path terms, σ_{TC-TC} (long-dash), σ_{CT-CT} (dots), and σ_{TC-CT} (short-dash), on elevation angle for a 60 cm by 60 cm square plate. Shown is the VV polarization at a frequency of 1.12 GHz for a 10 m thick, isotropic random slab, with freespace above and below, and with the target positioned 5 m below the lower interface.

shown individually. For comparison, the coherent return (solid) is shown as well. At normal incidence, there is a difference of approximately 30 dB between the coherent and incoherent returns. This difference declines, however, at larger incidence angles, particularly in the HH polarized result. For the coherent result, the plate scatters most of the incident wave in the specular direction, such that for larger incidence angles, less and less of the energy is scattered back in the direction of the receiver. In contrast, however, for the incoherent return, the plate and random media work together very much like a corner reflector. In the case of the target/clutter return for example, the plate scatters most of the energy away from the path back to the receiver when the incidence angle is large. However, no matter what direction the plate scatters the incident wave, there is random media there to then scatter the wave back to the receiver. This corner reflector-like double scattering accounts for the relatively angle-independent behavior of the HH polarized incoherent return.

In contrast, VV incoherent return drops more rapidly than the HH return, to dip at an angle of approximately 45° , and then to actually increase slightly for larger angles. The reason for the decrease at 45° is related to the corner reflector-like behavior of the multi-path wave. For vertical polarization at an angle of 45° , the wave specularly reflected from the plate to the random media will induce a dipole moment in the scatterers of the random media, which is oriented with the axis of the dipole along the scattering direction back to the receiver. For this reason, the specular corner reflector behavior will be absent, and the target/clutter scattered wave will decrease near 45° . This behavior is not unlike the Brewster angle effect for reflection of the vertical polarization by an interface of a stratified media.

The effect is similar for the clutter/target field, although there is a consider-

able difference between the clutter/target-clutter/target return and target/clutter-target/clutter return for angles near 45° . The reason for this difference arises from the non-reciprocal behavior of the Physical Optics formulation for bistatic applications. When most of the contribution arises from specular scattering, then the incident and scattering angles from the plate are the same for both the target/clutter field and clutter/target field, and the result will be nearly reciprocal. Hence, as expected the HH returns are nearly the same for all angles, and the VV returns are the same for angles away from 45° . In contrast, as discussed above, near 45° , the VV polarized returns are predominantly not the specular return, and the scattering will arise from paths where the incident/scattering angle pairs for scattering from the plate will be different for the target/clutter and clutter/target mechanisms. Hence, a larger discrepancy between the returns is expected, as demonstrated in Figure 5.6.

The results of Figures 5.5 and 5.6 are considerably different from those of the point target of Chapter 2, in that there exists the possibility of the incoherent return here exceeding the magnitude of the coherent return. The above figures are somewhat misleading, in that edge diffraction from the plate is not included, and the addition of a PTD [112] term would reduce the sidelobe nulls of the coherent return, and limit the level to which the coherent return decreased for large elevation angles. However, because the coherent return is very aspect dependant, and the incoherent return is in comparison much more independent of aspect angle, there exists the possibility of the incoherent return here playing a greater role in limiting the ability of a SAR sensor in imaging the target.

Figure 5.7 shows the dependance of the coherent (solid) and incoherent (dash) returns on the thickness of the random layer. In each case the result is presented for

normal incidence, with the same plate size and orientation as before, and with the plate located at a depth of 5 m below the lower interface of the random slab. Of the incoherent results, only the target/clutter-target/clutter return is shown, although the others (CT-CT and TC-CT) were found to be identical to that shown. The behavior here is similar to that for the point target of Chapter 2. The coherent return decreases exponentially with increasing media thickness, since the path length through the lossy region increases linearly with the thickness. The incoherent return first increases with thickness, since the thicker media provides more scatterers to contribute to the return. Eventually this effect saturates, however, and the added propagation loss for the thicker media begins to dominate and to lead to a slow decrease in the return. Hence, the incoherent return at normal incidence is largest for a media thickness of approximately 10 m.

Figure 5.8 in contrast shows the effect of changing the target depth for fixed media thickness. Both the coherent (solid) and target/clutter-target/clutter multi-path (dash) returns are shown for normal incidence, with a 10 m random slab, and with the same target size and orientation as previously. Again, the other two multi-path terms are not shown, but were found to be identical to the curve given. Both the coherent and incoherent results show an independence with target depth which parallels that seen earlier for the point target. For the coherent return, the target depth is unimportant since the media containing the target is lossless. In addition, Physical Optics is a single scattering formulation, so the back-and-forth coupling between the target and boundaries of the slab layer is ignored. This neglect should have little impact on the results, however, because the contrast in permittivity between the layers is small, and the boundary reflections are weak. The incoherent return is also independent of target

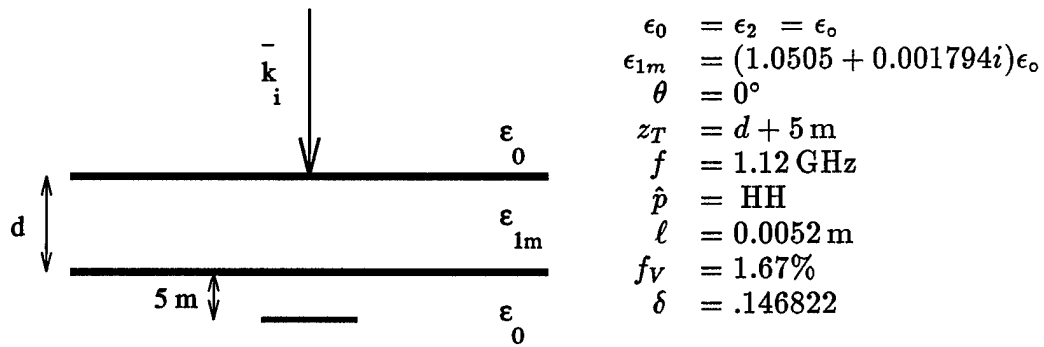
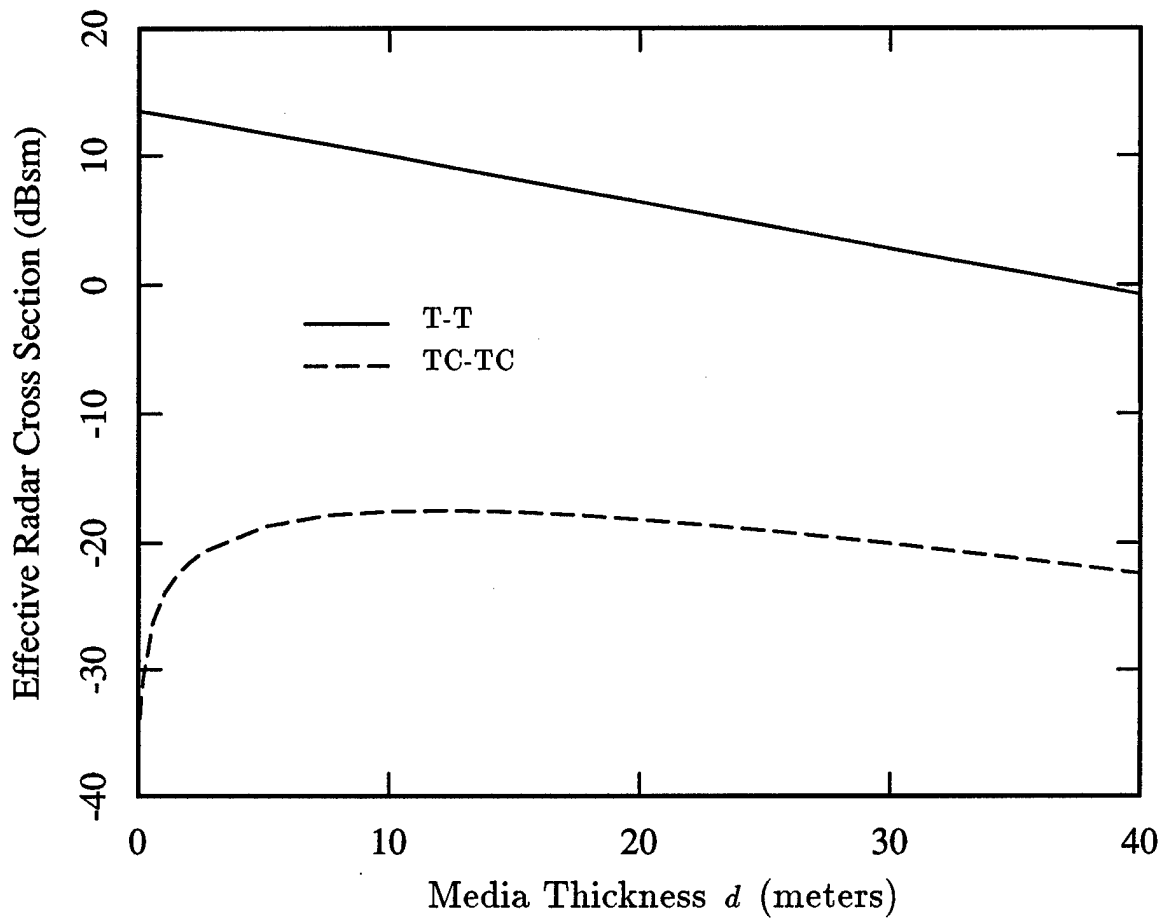


Figure 5.7. Dependence of the coherent target scattering cross section, σ_{T-T} , (solid) and the incoherent multi-path return, σ_{TC-TC} (long-dash), on media thickness for a 60 cm by 60 cm square plate. Shown is the HH polarization at a frequency of 1.12 GHz and at normal incidence to the isotropic random slab, with freespace above and below, and with the target positioned 5 m below the lower interface.

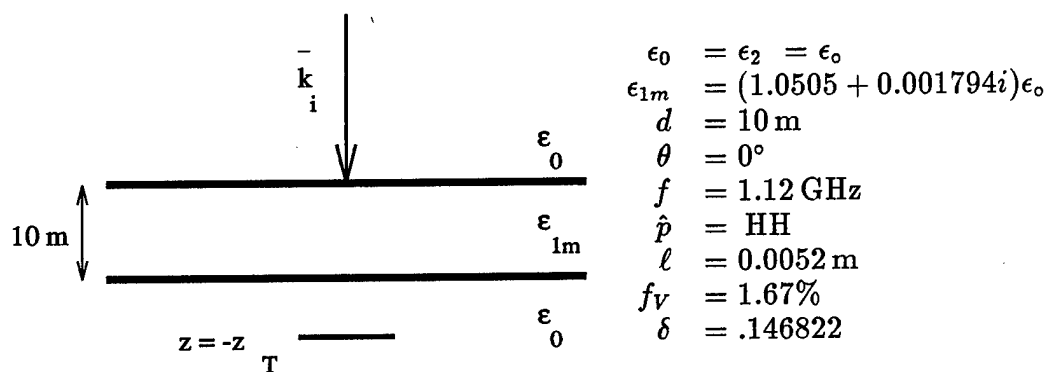
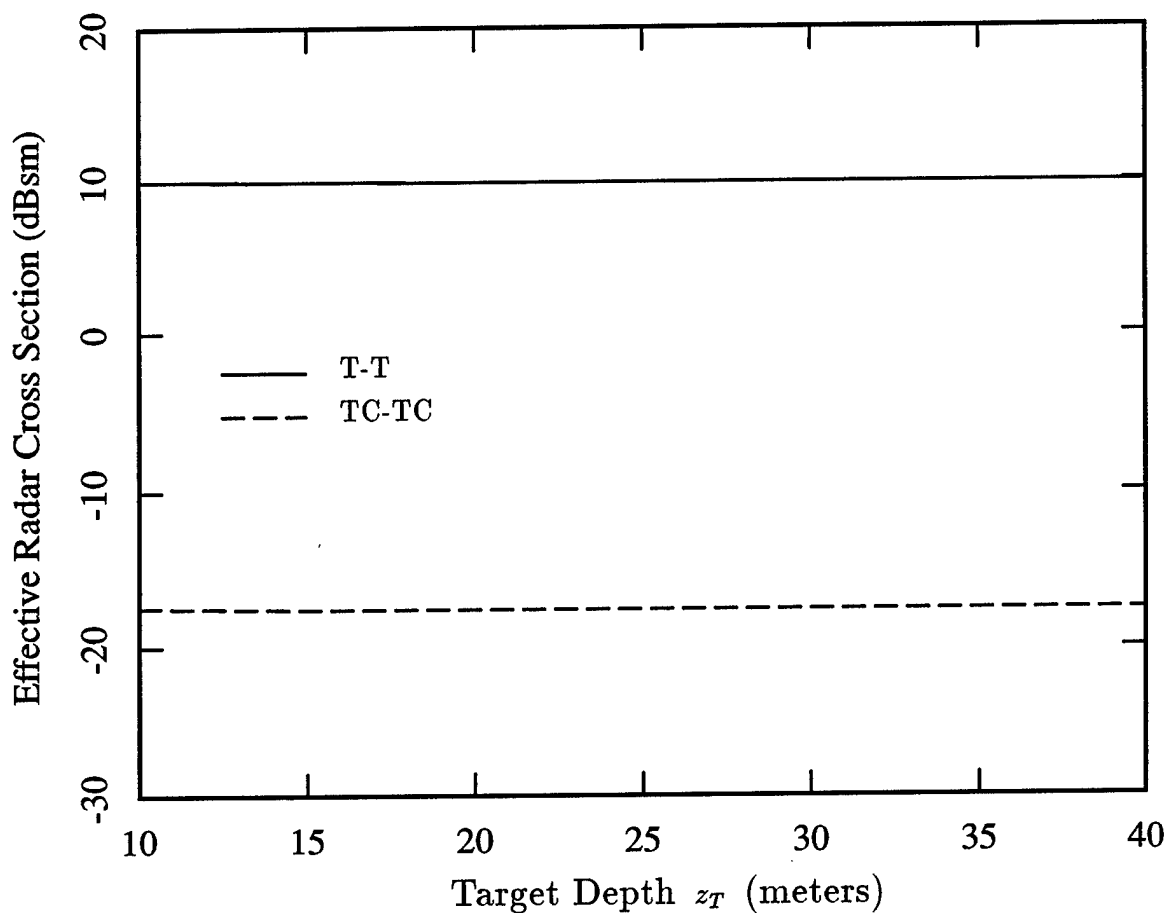


Figure 5.8. Dependence of the coherent target scattering cross section, σ_{T-T} , (solid) and the incoherent multi-path term, σ_{TC-TC} , (long-dash) on target depth for a 60 cm by 60 cm square plate. Shown are the results for normal incidence at a frequency of 1.12 GHz for a 10 m thick, isotropic random slab, with freespace above and below.

depth. At increased depth, the $1/r^2$ loss in scattering between the target and random layer becomes greater, however, the main beam of the bistatic scattering pattern of the plate illuminates a larger area, and the two effects offset each other.

Figure 5.9 shows the dependance of the coherent (solid) and target/clutter-target/clutter (dash) returns on frequency. The results are shown over a bandwidth of 20 MHz about 1.12 GHz, and are presented for normal incidence, a 10 m random slab, with the plate 5 m below and again oriented parallel to the boundaries of the layered media. Again the CT-CT and TC-CT terms are identical to the TC-TC result, and are not shown. Both the coherent and incoherent terms show a relative independence over frequency, although both increase slightly over the bandwidth shown. For the incoherent result, this independence with frequency indicates that the frequency correlation of the multi-path mechanisms is at least approximately mean sense stationary. This stationarity can be exploited in calculating the statistics necessary for determining the effect of the random media on the performance of a SAR sensor in detecting or imaging the plate.

Similarly, Figures 5.10 and 5.11 show the dependance of the coherent (solid), target/clutter-target/clutter (long-dash), clutter/target-clutter/target (dots), and target/clutter-clutter/target (short-dash) returns as a function of azimuth angle for a fixed elevation angle of $\theta = 50^\circ$, and for HH and VV polarizations, respectively. Again the random media is 10 m thick, with the target 5 m below, and oriented as above. In each case, the coherent return shows considerable dependance of azimuth angle, since these plots represent cuts in azimuth through the two-dimensional sinc-dependant monostatic scattering pattern of the plate. The return is largest at $\phi = 0^\circ$, where in incident propagation vector is perpendicular to the edge of the square plate. In contrast, the

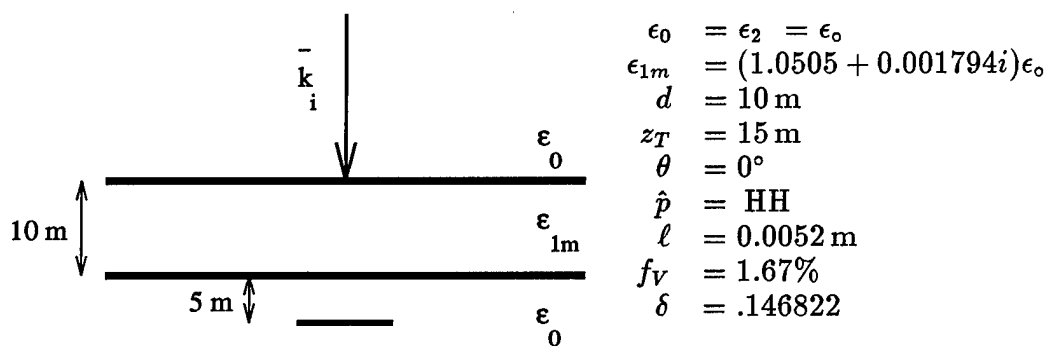
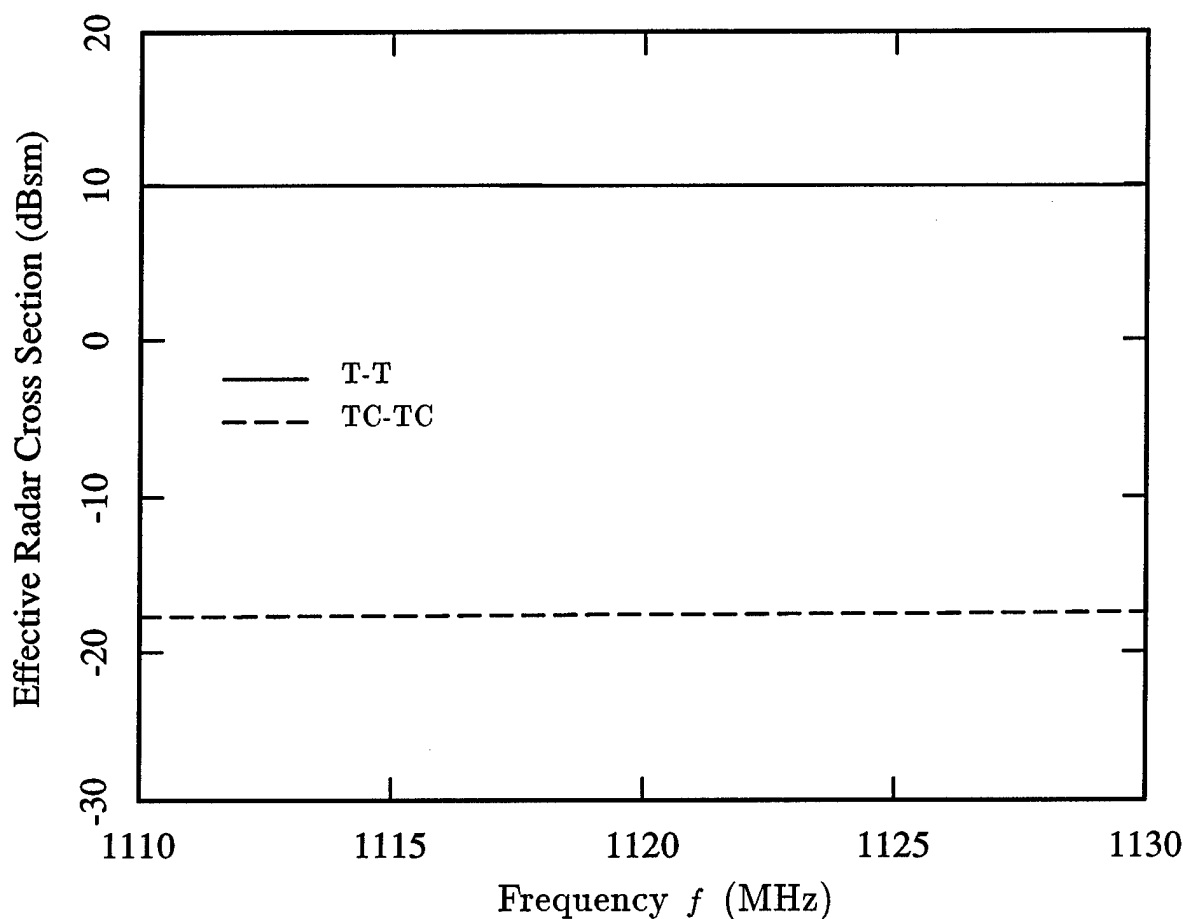
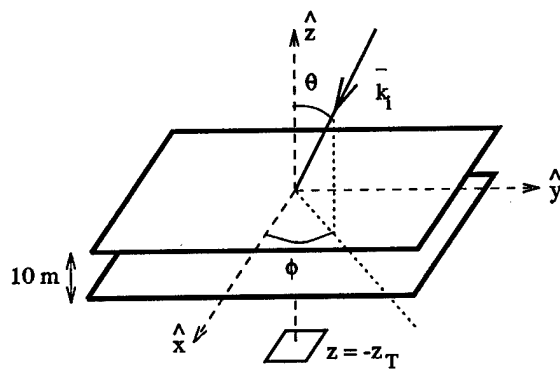
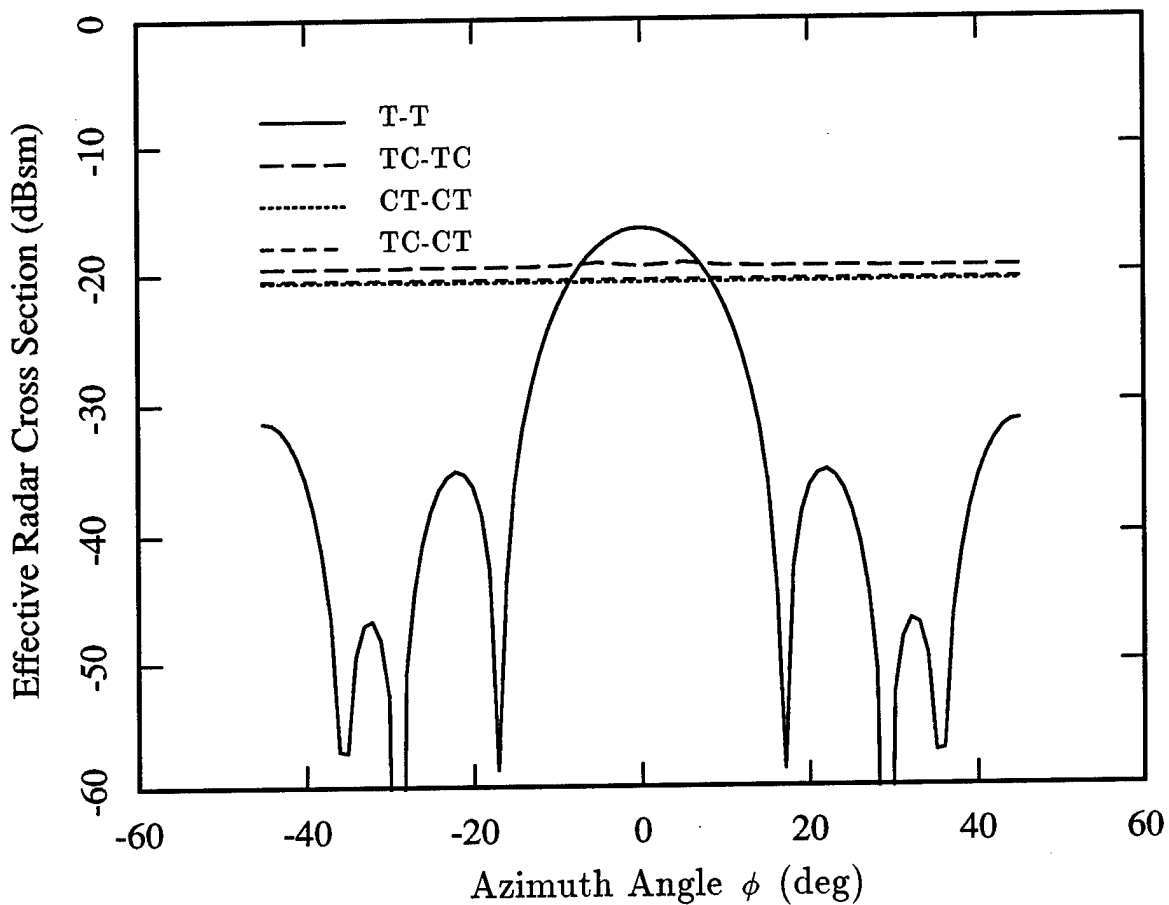


Figure 5.9. Dependence of the coherent target scattering cross section, σ_{T-T} , (solid) and the incoherent multi-path term, σ_{TC-TC} , (long-dash) on frequency for a 60 cm by 60 cm square plate. Shown is the HH polarization at normal incidence to a 10 m thick, isotropic random slab, with freespace above and below, and with the target positioned 5 m below the lower interface.

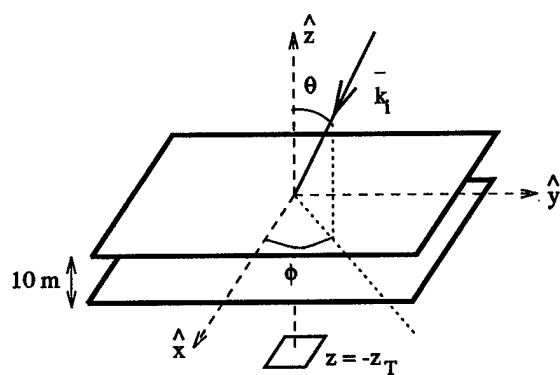
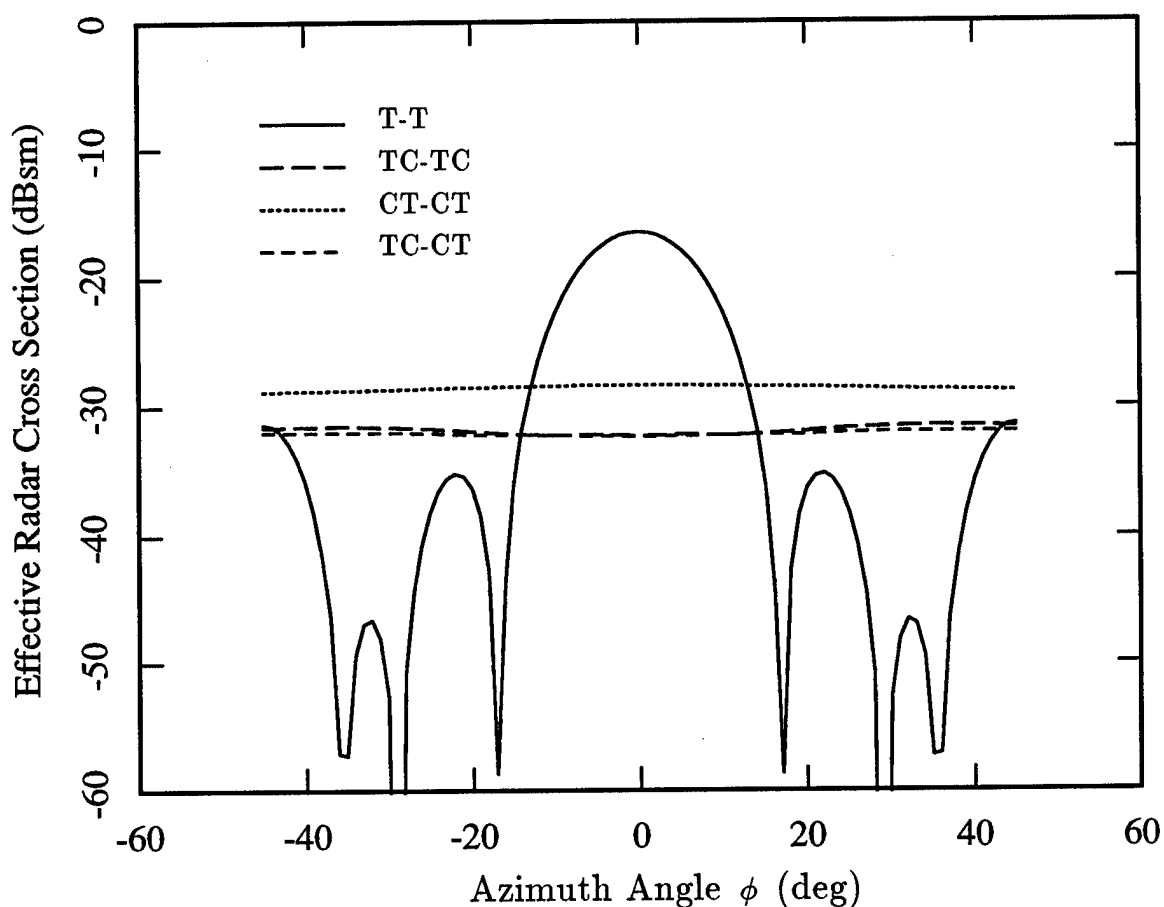
incoherent results are almost entirely independent of azimuth angle. This independence is again due to the corner reflector-like behavior of the incoherent multi-path mechanisms. While the backscattered return from the plate is dependant on the azimuth angle, the specular bistatic scattering is relatively independent of azimuth angle, and, thus, with random media the same in all directions about the plate, the overall effect is an independence of azimuth angle in the multi-path results. This independence is significant in making the correlation of the multi-path fields at least approximately mean sense stationary. Like the above stationarity with frequency, the azimuthal stationarity is significant in reducing the requirements on the statistics necessary for analyzing the effect of the random media in degrading SAR performance.

Figures 5.12-5.15 show the azimuthal and frequency correlations of the incoherent scattering mechanisms for the HH and VV polarizations. The geometry is again the same as in the above variance results, with a 60 cm by 60 cm plate located 5 m below the 10 m slab of random media. For the azimuthal correlations the center azimuth is chosen as $\phi_c = 0^\circ$, perpendicular to an edge of the plate, and for the frequency correlations a center frequency of 1.12 GHz was used. The elevation angle for all results was chosen as 50° . In the case of the HH polarization, the TC-TC correlation (long-dash) decreases more sharply than the CT-CT correlation (dots) for changes in either azimuth or frequency, although the difference between the two results is not dramatic. The cross correlation, TC-CT (short-dash), falls between the TC-TC and CT-CT results in both cases. In contrast, for the VV polarization, the clutter/target return decorrelates more rapidly than the target/clutter field, and the difference between the two results is larger than in the horizontally polarized case. In addition, while the cross correlation falls between the autocorrelations for the frequency correlation results, in azimuth it



$$\begin{aligned} \epsilon_0 &= \epsilon_2 = \epsilon_o \\ \epsilon_{1m} &= (1.0505 + 0.001794i)\epsilon_o \\ d &= 10 \text{ m} \\ z_T &= 15 \text{ m} \\ \theta &= 50^\circ \\ f &= 1.12 \text{ GHz} \\ \hat{p} &= \text{HH} \\ \ell &= 0.0052 \text{ m} \\ f_V &= 1.67\% \\ \delta &= .146822 \end{aligned}$$

Figure 5.10. Dependence of the coherent target scattering cross section, σ_{T-T} , (solid) and the incoherent multi-path terms, σ_{TC-TC} (long-dash), σ_{CT-CT} (dots), and σ_{TC-CT} (short-dash), on azimuth angle for a 60 cm by 60 cm square plate. Shown is the HH polarization at a frequency of 1.12 GHz and elevation angle of $\theta = 50^\circ$, for a 10 m thick, isotropic random slab, with freespace above and below, and with the target positioned 5 m below the lower interface.



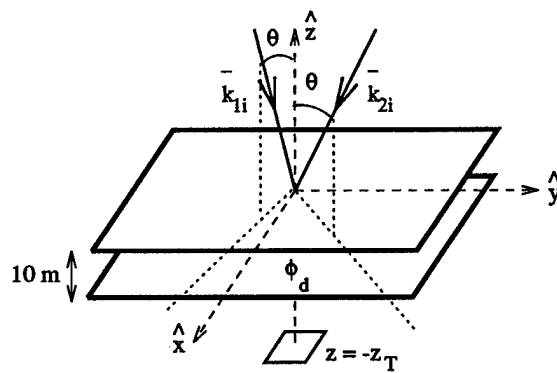
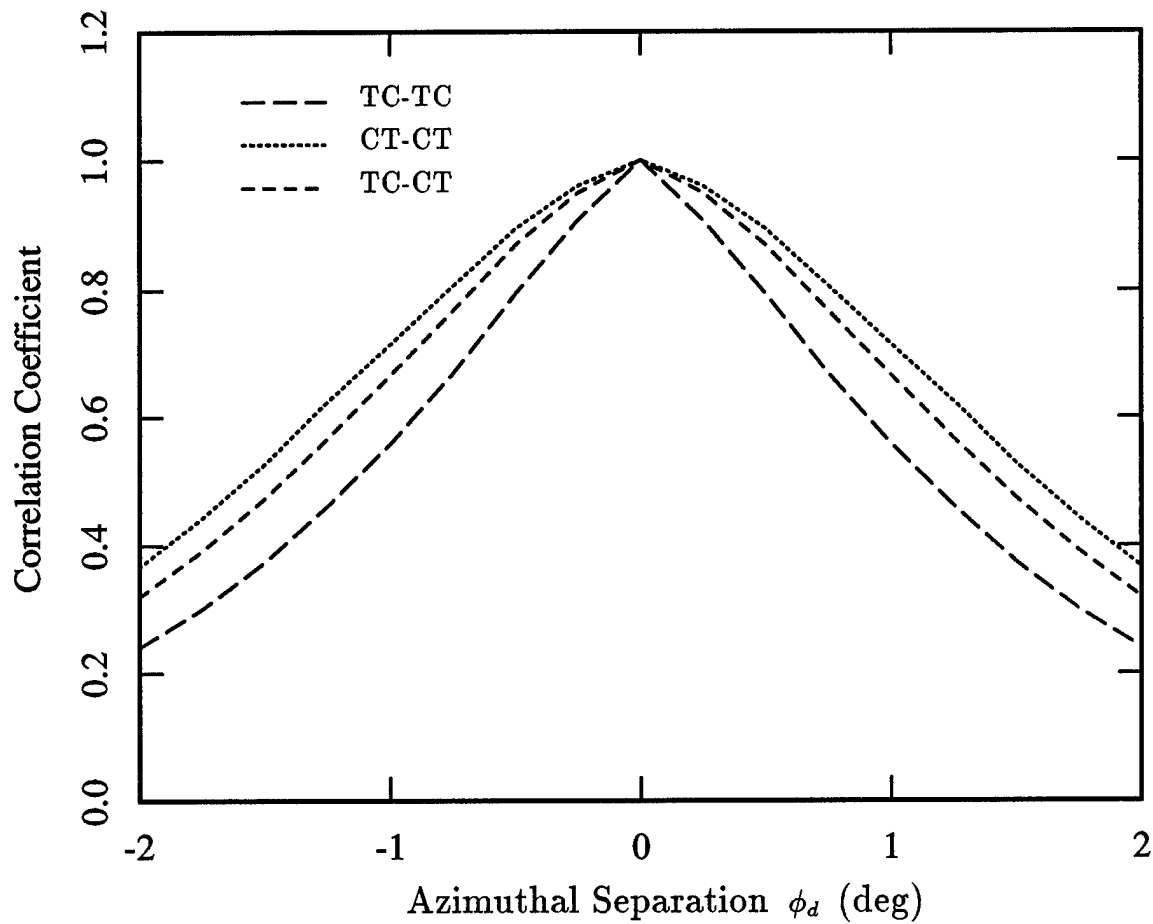
$$\begin{aligned}
 \epsilon_0 &= \epsilon_2 = \epsilon_o \\
 \epsilon_{1m} &= (1.0505 + 0.001794i)\epsilon_o \\
 d &= 10 \text{ m} \\
 z_T &= 15 \text{ m} \\
 \theta &= 50^\circ \\
 f &= 1.12 \text{ GHz} \\
 \hat{p} &= VV \\
 \ell &= 0.0052 \text{ m} \\
 f_V &= 1.67\% \\
 \delta &= .146822
 \end{aligned}$$

Figure 5.11. Dependence of the coherent target scattering cross section, σ_{T-T} , (solid) and the incoherent multi-path terms, σ_{TC-TC} (long-dash), σ_{CT-CT} (dots), and σ_{TC-CT} (short-dash), on azimuth angle for a 60 cm by 60 cm square plate. Shown is the VV polarization at a frequency of 1.12 GHz and elevation angle of $\theta = 50^\circ$, for a 10 m thick, isotropic random slab, with freespace above and below, and with the target positioned 5 m below the lower interface.

shows a small increase away from its center before declining, and, thus, does not fall between the TC-TC and CT-CT correlations over much of the azimuthal range shown. Comparing these correlation results with the earlier variance results, it can be noted that for the HH polarization (at $\theta = 50^\circ$) the TC-TC contribution is larger than CT-CT, but the comparison is close. In contrast, for VV the CT-CT return is larger, and the difference is more noticeable. Together these variance and correlation results suggest that the larger magnitude returns (TC-TC for HH and CT-CT for VV) arise because the contributing regions are larger, and, hence, the corresponding correlations decline more rapidly.

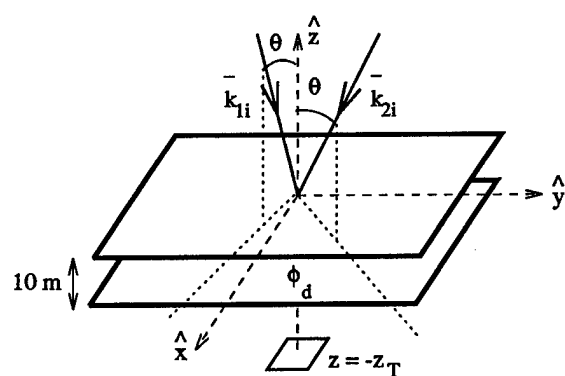
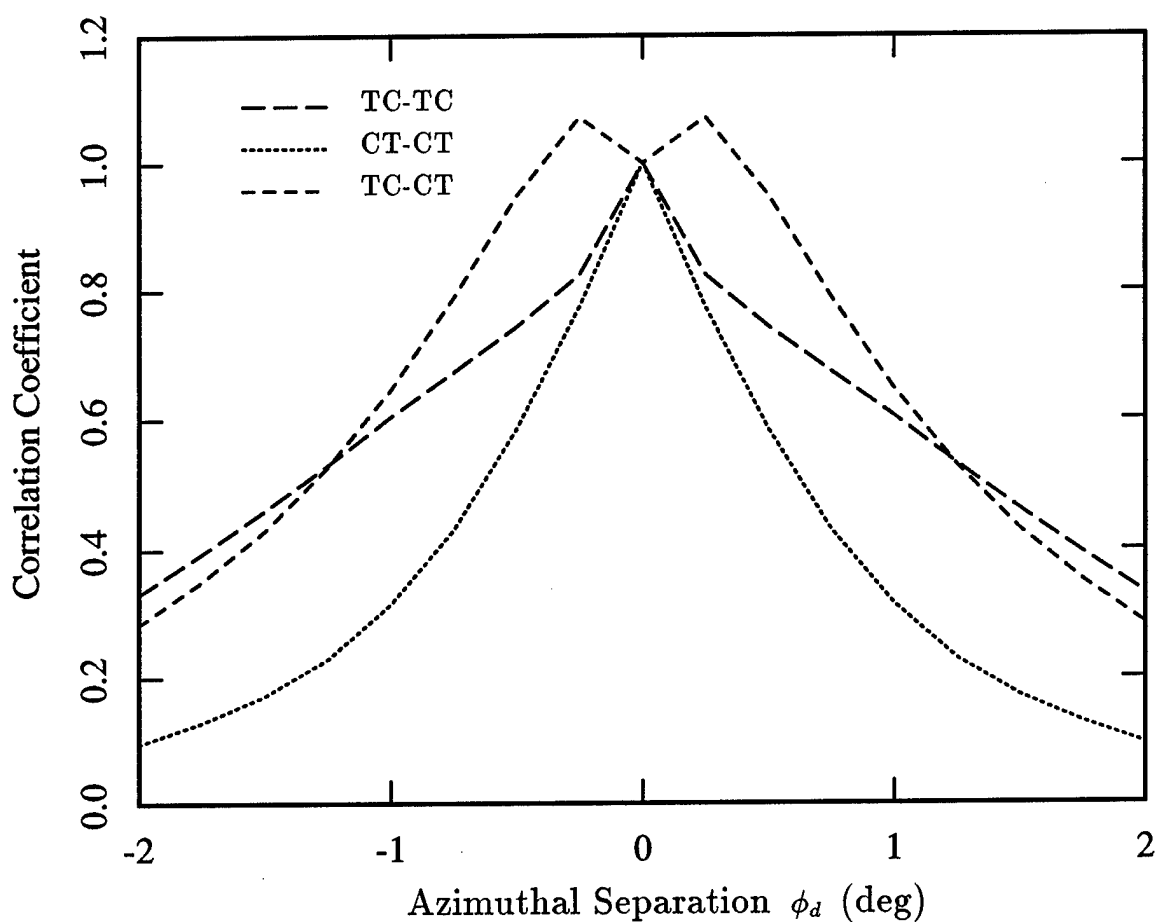
Similarly, comparing the HH and VV results for each type of correlation, it is seen that for the TC-TC correlation the two polarizations are very similar over both azimuth and frequency. The CT-CT results, however, are very different for the two polarizations. This result for CT-CT is expected since the VV polarization experiences a loss of the contribution specularly reflected from the plate when the incidence angle is near 45° . Hence, for the 50° incidence angle considered here, the VV return consists of more contributions spread further from the specularly illuminated region. Hence, the VV result is faster to decorrelate than HH.

Figure 5.16 shows the effect of the target depth on the rate of decorrelation for azimuthal changes. The results shown above for a target depth of 15m (dash), or 5m below the lower interface of the random media, are compared with a more shallow depth of 10m (solid), which places the target immediately below the slab. In each case, only the TC-TC correlation is shown. The results for both polarizations show a faster decorrelation for a greater separation between the target and random media. As with the point target, at greater depths, the scattering of the target illuminates a



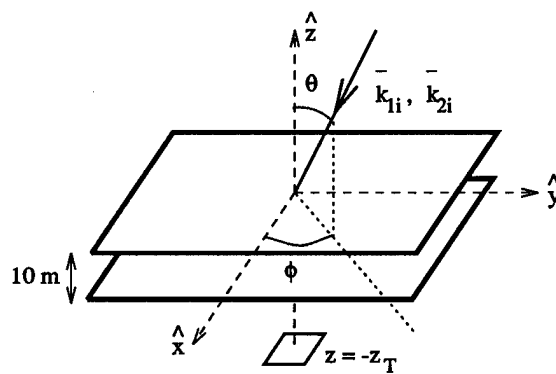
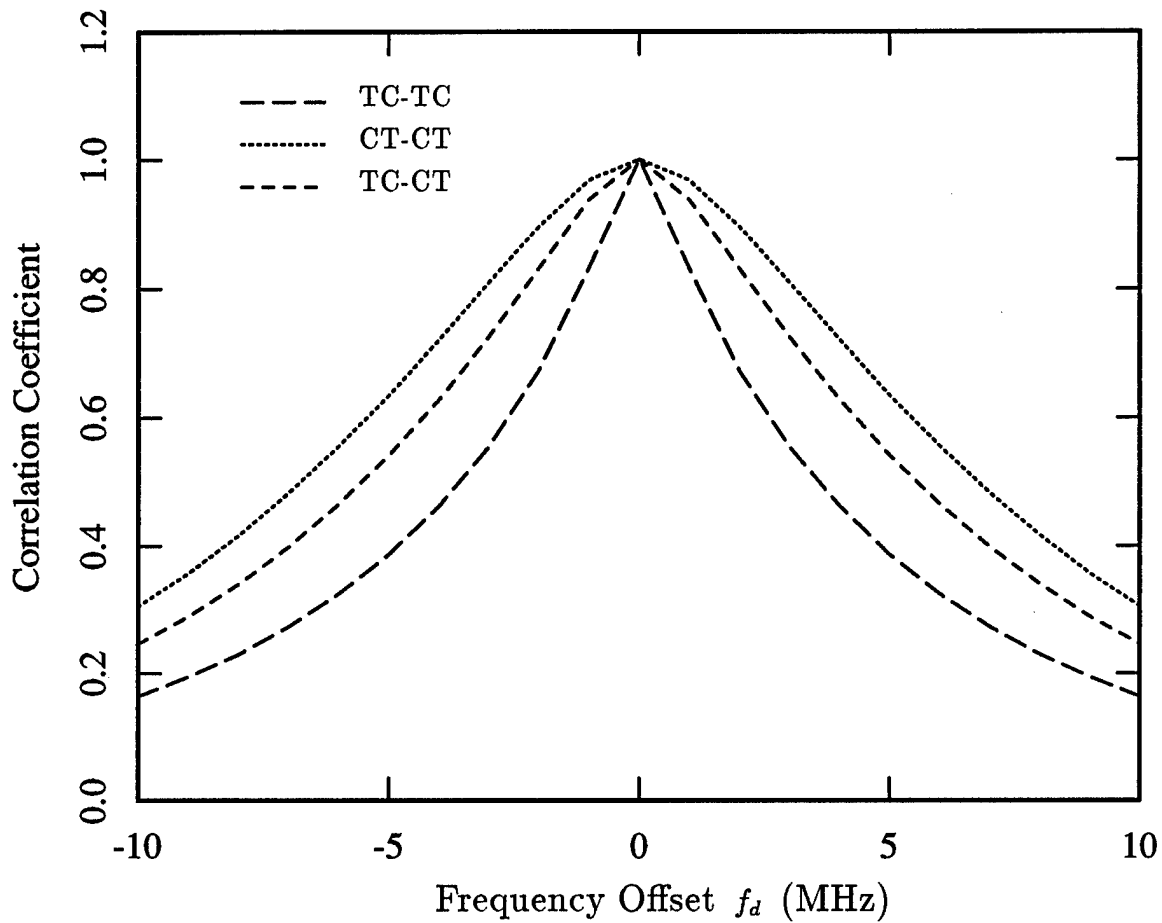
$$\begin{aligned}
 \epsilon_0 &= \epsilon_2 = \epsilon_o \\
 \epsilon_{1m} &= (1.0505 + 0.001794i)\epsilon_o \\
 d &= 10 \text{ m} \\
 z_T &= 15 \text{ m} \\
 \theta &= 50^\circ \\
 \phi_c &= 0^\circ \\
 f &= 1.12 \text{ GHz} \\
 \hat{p} &= \text{HH} \\
 \ell &= 0.0052 \text{ m} \\
 f_V &= 1.67\% \\
 \delta &= .146822
 \end{aligned}$$

Figure 5.12. Correlation of the incoherent multi-path scattering terms, σ_{TC-TC} (long-dash), σ_{CT-CT} (dots), and σ_{TC-CT} (short-dash), over changes in azimuth angle for a 60 cm by 60 cm square plate. Shown is the HH polarization at a frequency of 1.12 GHz for incidence at 50° to a 10 m thick, isotropic random slab, with freespace above and below, and with the target positioned 5 m below the lower interface.



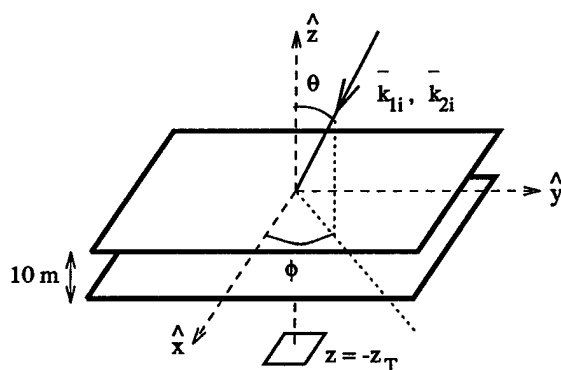
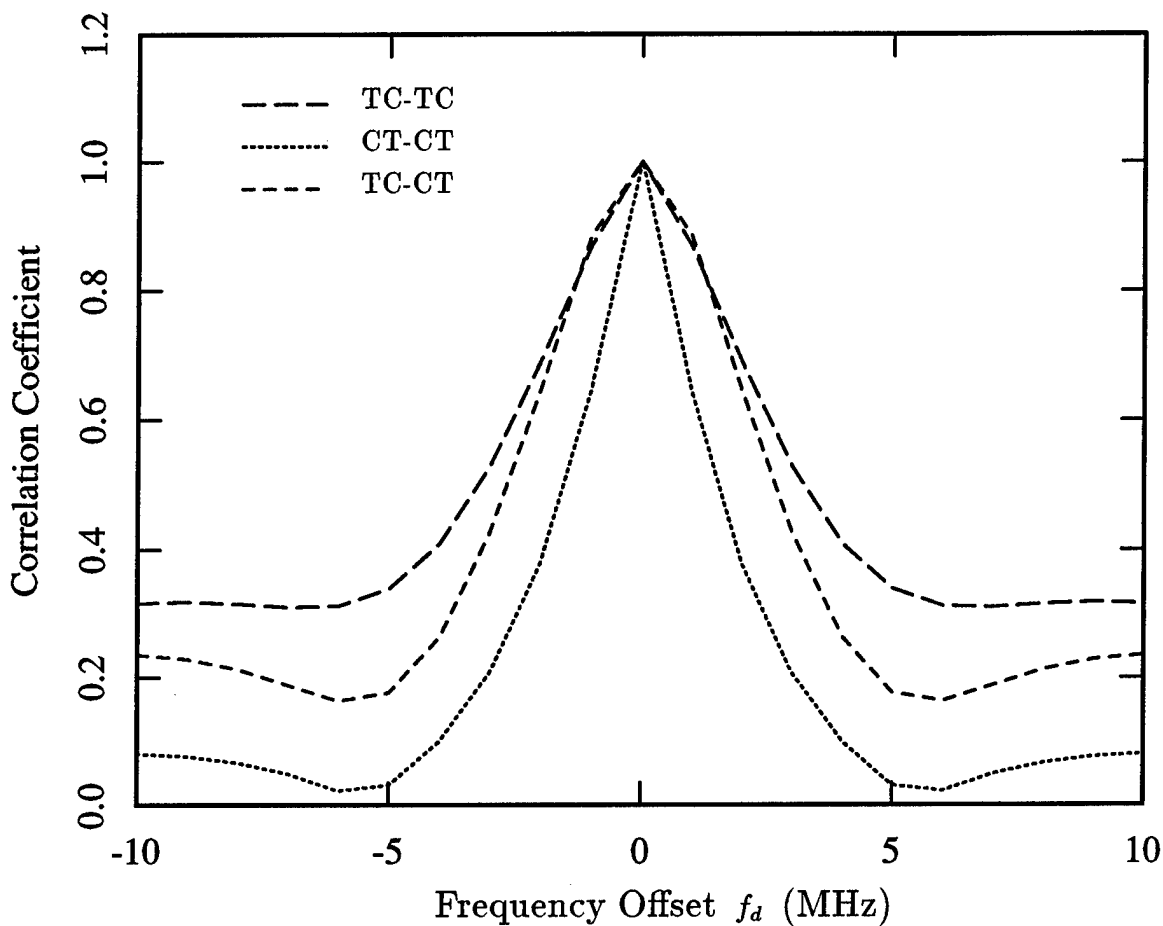
$$\begin{aligned}
 \epsilon_0 &= \epsilon_2 = \epsilon_o \\
 \epsilon_{1m} &= (1.0505 + 0.001794i)\epsilon_o \\
 d &= 10 \text{ m} \\
 z_T &= 15 \text{ m} \\
 \theta &= 50^\circ \\
 \phi_c &= 0^\circ \\
 f &= 1.12 \text{ GHz} \\
 \hat{p} &= \text{VV} \\
 \ell &= 0.0052 \text{ m} \\
 f_V &= 1.67\% \\
 \delta &= .146822
 \end{aligned}$$

Figure 5.13. Correlation of the incoherent multi-path scattering terms, σ_{TC-TC} (long-dash), σ_{CT-CT} (dots), and σ_{TC-CT} (short-dash), over changes in azimuth angle for a 60 cm by 60 cm square plate. Shown is the VV polarization at a frequency of 1.12 GHz for incidence at 50° to a 10 m thick, isotropic random slab, with freespace above and below, and with the target positioned 5 m below the lower interface.



$$\begin{aligned} \epsilon_0 &= \epsilon_2 = \epsilon_o \\ \epsilon_{1m} &= (1.0505 + 0.001794i)\epsilon_o \\ d &= 10 \text{ m} \\ z_T &= 15 \text{ m} \\ \theta &= 50^\circ \\ \phi &= 0^\circ \\ f_c &= 1.12 \text{ GHz} \\ \hat{p} &= \text{HH} \\ \ell &= 0.0052 \text{ m} \\ f_V &= 1.67\% \\ \delta &= .146822 \end{aligned}$$

Figure 5.14. Correlation of the incoherent multi-path scattering terms, σ_{TC-TC} (long-dash), σ_{CT-CT} (dots), and σ_{TC-CT} (short-dash), over changes in frequency for a 60 cm by 60 cm square plate. Shown is the HH polarization for incidence at 50° to a 10 m thick, isotropic random slab, with freespace above and below, and with the target positioned 5 m below the lower interface.



$$\begin{aligned}
 \epsilon_0 &= \epsilon_2 = \epsilon_o \\
 \epsilon_{1m} &= (1.0505 + 0.001794i)\epsilon_o \\
 d &= 10 \text{ m} \\
 z_T &= 15 \text{ m} \\
 \theta &= 50^\circ \\
 \phi &= 0^\circ \\
 f_c &= 1.12 \text{ GHz} \\
 \hat{p} &= \text{VV} \\
 \ell &= 0.0052 \text{ m} \\
 f_V &= 1.67\% \\
 \delta &= .146822
 \end{aligned}$$

Figure 5.15. Correlation of the incoherent multi-path scattering terms, σ_{TC-TC} (long-dash), σ_{CT-CT} (dots), and σ_{TC-CT} (short-dash), over changes in frequency for a 60 cm by 60 cm square plate. Shown is the VV polarization for incidence at 50° to a 10 m thick, isotropic random slab, with freespace above and below, and with the target positioned 5 m below the lower interface.

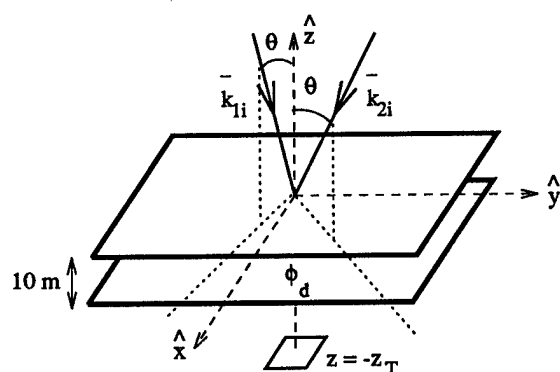
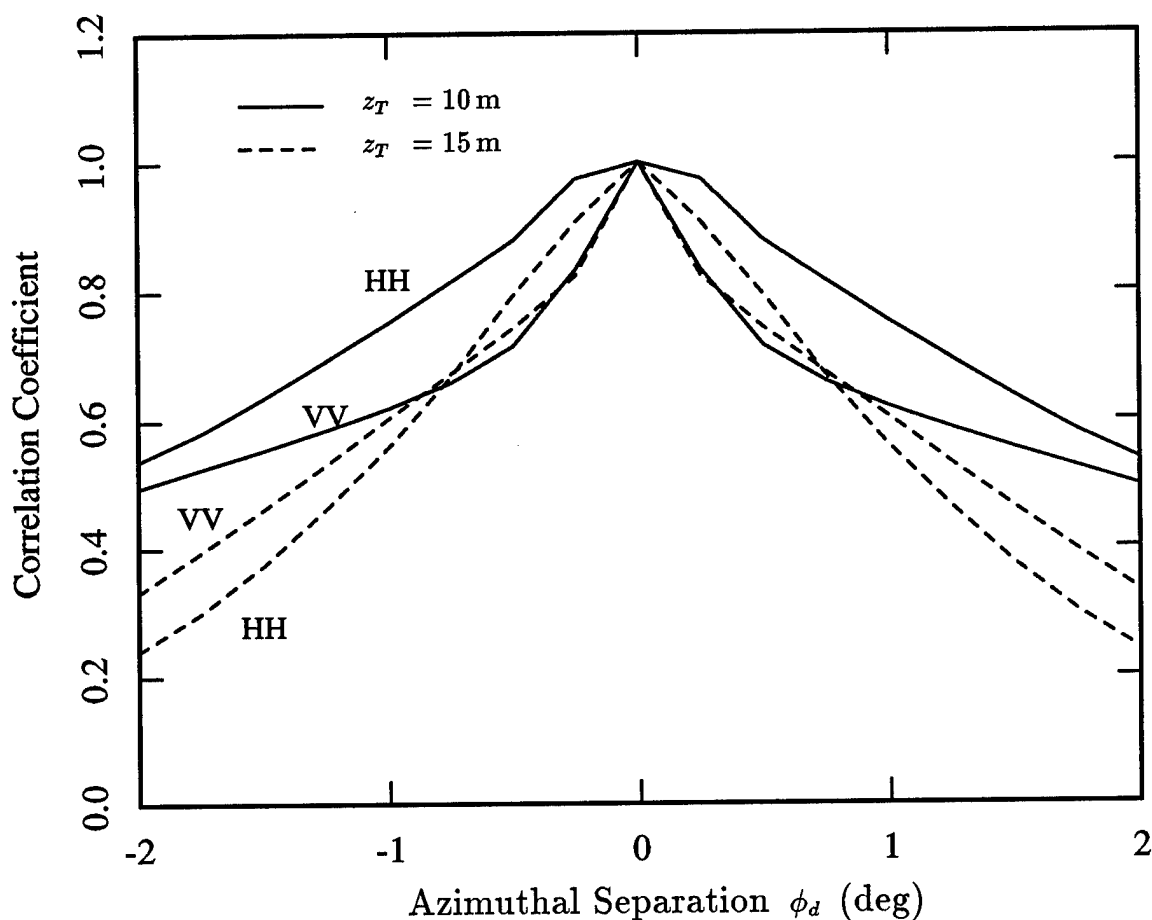
larger region of the random media, and this increase in the dimension of the effective scattering region causes a more rapid phase change with changing azimuth or frequency, and a more rapid decorrelation.

Similarly, Figure 5.17 shows the effect of elevation angle on the azimuthal decorrelation rate, comparing the previous result at $\theta = 50^\circ$ (dash) with a smaller angle of 30° (solid). For both polarizations, the steeper incidence angle of 30° leads to a slower decorrelation, which parallels the results seen earlier for the point target. Again much of this result is due to the geometrical fact that at the steeper angle, a given change in azimuth will cause less phase change across the region of contributing scatterers.

Figures 5.18 and 5.19 show the effect of the center azimuth and frequency on the azimuthal and frequency correlations, respectively. Unlike the point target, the square plate is not azimuthally symmetric, and the correlation need not be stationary in azimuth. The results, however, show almost no dependence on center azimuth or frequency, indicating that both the azimuthal and frequency correlations can be treated as stationary.

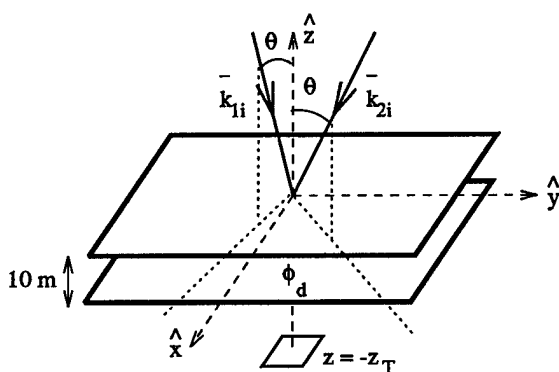
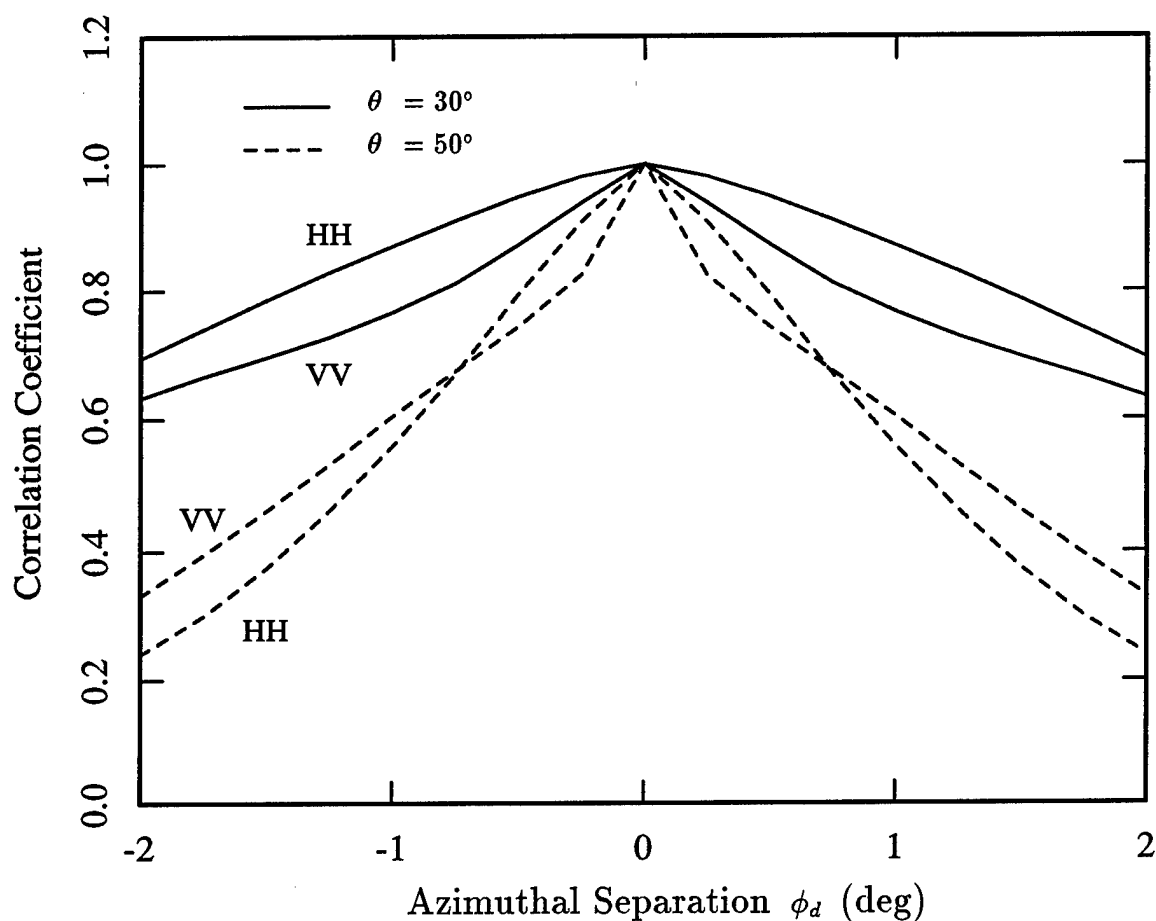
Finally, Figure 5.20 shows the effect of plate size on the azimuthal correlation, by comparing the previous result for the 60 cm by 60 cm plate (dash) with that for a larger 270 cm by 270 cm square plate (dots), placed at the same depth and with the same orientation. Also shown for comparison is the result of replacing the plates with the point target of Chapter 2 (solid). As the plate becomes larger, the bistatic scattering pattern of the plate develops a narrower main lobe, leading to scattering of more of the incident power in the specular direction. Consequently, the region of the random media contributing to the multi-path return becomes smaller for the larger plate, and the decorrelation of this field in azimuth becomes slower. The point target provides

even less gain than the small plate, and, thus, has the largest effective scattering region, and the fastest decorrelation. These results show the effect of the target in shaping the scattering pattern illuminating the random media, and affecting both the variance and the correlation statistics of the multi-path mechanism.



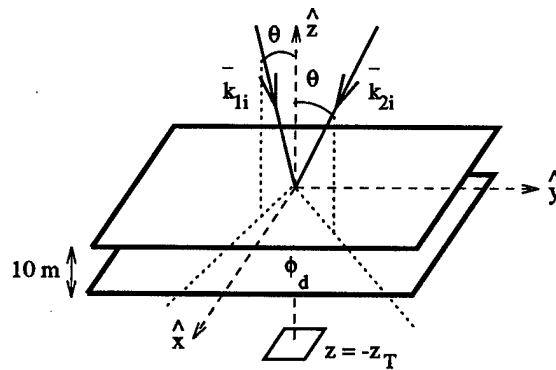
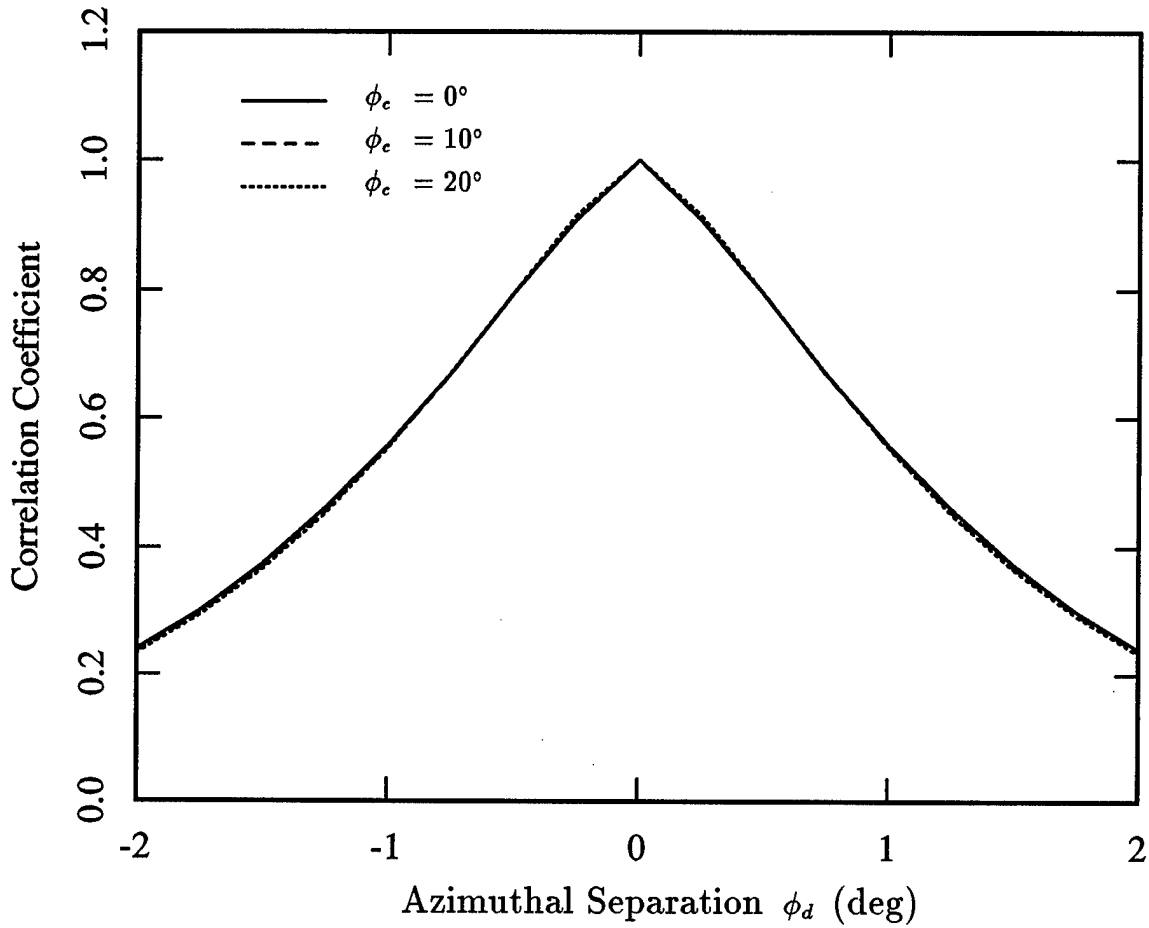
$$\begin{aligned}
 \epsilon_0 &= \epsilon_2 = \epsilon_o \\
 \epsilon_{1m} &= (1.0505 + 0.001794i)\epsilon_o \\
 d &= 10 \text{ m} \\
 \theta &= 50^\circ \\
 \phi_c &= 0^\circ \\
 f &= 1.12 \text{ GHz} \\
 \ell &= 0.0052 \text{ m} \\
 f_V &= 1.67\% \\
 \delta &= .146822
 \end{aligned}$$

Figure 5.16. Correlation of the incoherent multi-path scattering term, σ_{TC-TC} , over changes in azimuth angle for a 60cm by 60cm square plate at depths of 10m (solid) and 15m (dash) below the upper interface of the random slab. Shown are the results at a frequency of 1.12 GHz for incidence at 50° to a 10 m thick, isotropic random slab, with freespace above and below.



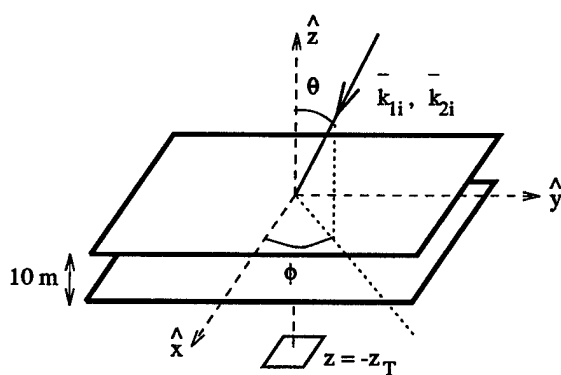
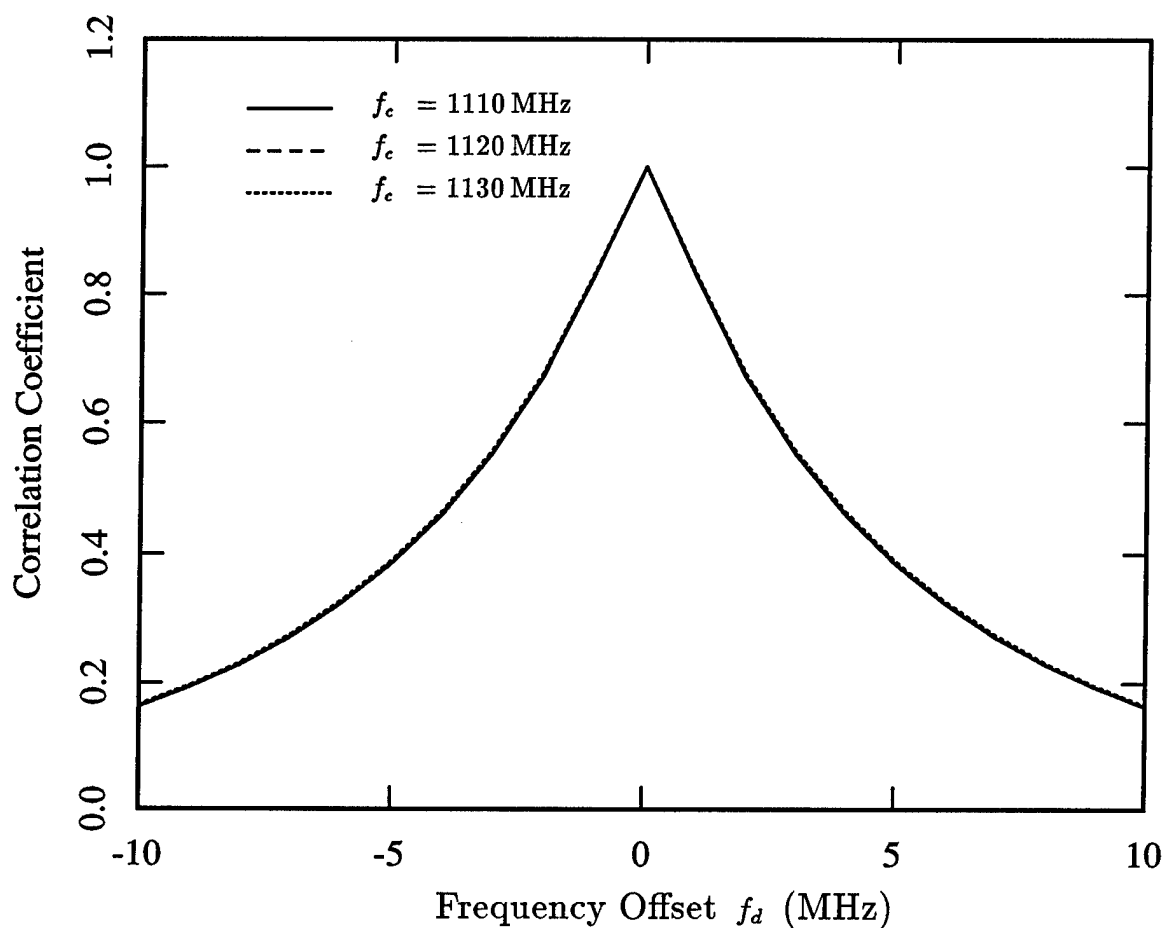
$$\begin{aligned}
 \epsilon_0 &= \epsilon_2 = \epsilon_o \\
 \epsilon_{1m} &= (1.0505 + 0.001794i)\epsilon_o \\
 d &= 10 \text{ m} \\
 z_T &= 15 \text{ m} \\
 \phi_c &= 0^\circ \\
 f &= 1.12 \text{ GHz} \\
 \ell &= 0.0052 \text{ m} \\
 f_V &= 1.67\% \\
 \delta &= .146822
 \end{aligned}$$

Figure 5.17. Correlation of the incoherent multi-path scattering term, σ_{TC-TC} , over changes in azimuth angle for a 60cm by 60cm square plate, and for incidence at 30° (solid) and 50° (dash) to the random slab. Shown are the results at a frequency of 1.12 GHz for a 10 m thick, isotropic random slab, with freespace above and below, and with the target located 5 m below the lower interface of the slab.



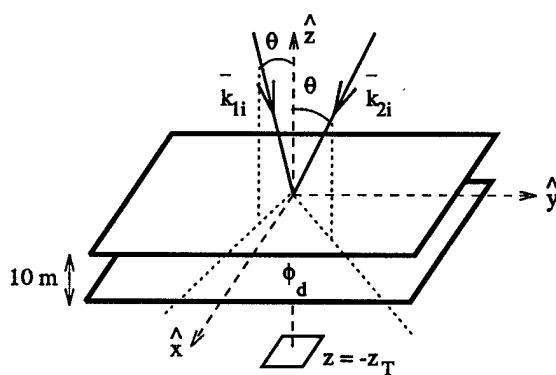
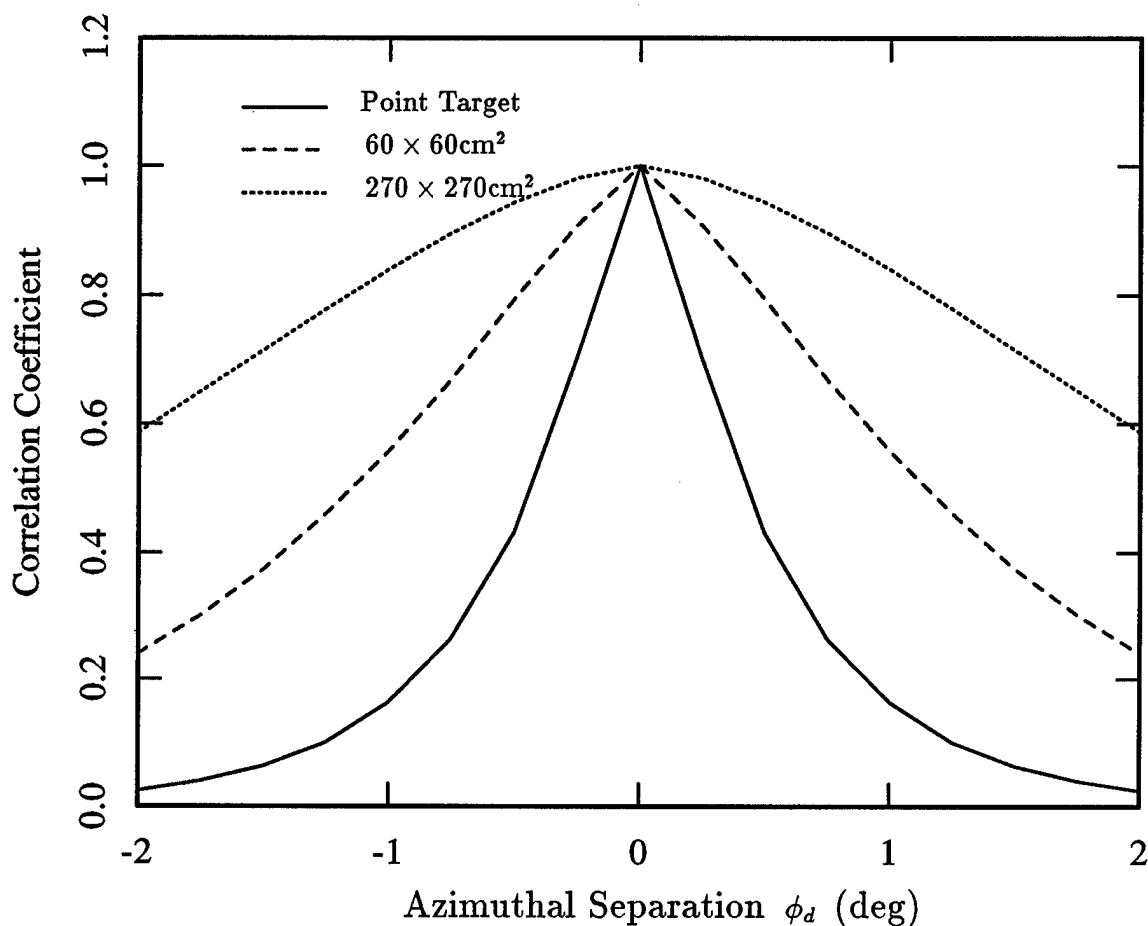
$$\begin{aligned} \epsilon_0 &= \epsilon_2 = \epsilon_o \\ \epsilon_{1m} &= (1.0505 + 0.001794i)\epsilon_o \\ d &= 10 \text{ m} \\ z_T &= 15 \text{ m} \\ \theta &= 50^\circ \\ f &= 1.12 \text{ GHz} \\ \hat{p} &= \text{HH} \\ \ell &= 0.0052 \text{ m} \\ f_V &= 1.67\% \\ \delta &= .146822 \end{aligned}$$

Figure 5.18. Correlation of the incoherent multi-path scattering term, σ_{TC-TC} , over changes in azimuth angle for a 60cm by 60cm square plate, and for center azimuths of 0° (solid), 10° (dash), and 20° (dots). Shown are the results at a frequency of 1.12 GHz for incidence at an elevation angle of 50° to a 10 m thick, isotropic random slab, with freespace above and below, and with the target located 5 m below the lower interface of the slab.



$$\begin{aligned}
 \epsilon_0 &= \epsilon_2 = \epsilon_o \\
 \epsilon_{1m} &= (1.0505 + 0.001794i)\epsilon_o \\
 d &= 10 \text{ m} \\
 z_T &= 15 \text{ m} \\
 \theta &= 50^\circ \\
 \phi &= 0^\circ \\
 \hat{p} &= \text{HH} \\
 \ell &= 0.0052 \text{ m} \\
 f_V &= 1.67\% \\
 \delta &= .146822
 \end{aligned}$$

Figure 5.19. Correlation of the incoherent multi-path scattering term, σ_{TC-TC} , over changes in frequency for a 60cm by 60cm square plate, and for center frequencies of 1110 MHz (solid), 1120 MHz (dash), and 1130 MHz (dots). Shown are the results for incidence at an elevation angle of 50° to a 10 m thick, isotropic random slab, with freespace above and below, and with the target located 5 m below the lower interface of the slab.



$$\begin{aligned}
 \epsilon_0 &= \epsilon_2 = \epsilon_o \\
 \epsilon_{1m} &= (1.0505 + 0.001794i)\epsilon_o \\
 d &= 10 \text{ m} \\
 z_T &= 15 \text{ m} \\
 \theta &= 50^\circ \\
 \phi_c &= 0^\circ \\
 f &= 1.12 \text{ GHz} \\
 \hat{p} &= \text{HH} \\
 \ell &= 0.0052 \text{ m} \\
 f_V &= 1.67\% \\
 \delta &= .146822
 \end{aligned}$$

Figure 5.20. Correlation of the incoherent multi-path scattering term, σ_{TC-TC} , over changes in azimuth angle for a point target (solid), a 60cm by 60cm square plate (dash), and for a 270cm by 270cm plate (dots). Shown are the results at a frequency of 1.12 GHz for incidence at an elevation angle of 50° to a 10 m thick, isotropic random slab, with freespace above and below, and with the target located 5 m below the lower interface of the slab.

Appendix H

Magnetic Field / Electric Source Green's Function and Incident Magnetic Field Expressions for a Uniaxial Layered Media

This Appendix gives the expressions for the Green's function which yields the magnetic field at an observation point in one layer, p , of a uniaxial layered media, for an electric current excitation in a different layer, m . Also given is the form of the magnetic field in each region, which arises from an incident plane wave illuminating the medium from region 0.

The magnetic field/electric source Green's function is defined such that the field at an observation point \bar{r} in layer p , arising from an electric current excitation, $\bar{J}_m(\bar{r})$, in layer m , is given by (H.1).

$$\bar{H}_p(\bar{r}) = i \iiint_V d\bar{r}' \bar{\mathcal{G}}_{pm}(\bar{r}, \bar{r}') \cdot \bar{J}_m(\bar{r}') \quad (H.1)$$

From Appendix E, the electric field at the observation point is given by (H.2),

$$\begin{aligned} \bar{E}_p(\bar{r}) = i\omega\mu \iiint_V d\bar{r}' \sum_{\ell, q=+, -} \sum_{v=TE, TM} \iint d\bar{k}_\perp \bar{F}_{pm\ell q}^{(v)\cup\cap}(\bar{k}_\perp) \cdot \bar{J}_m(\bar{r}') \times \\ e^{i\bar{k}_\perp \cdot (\bar{r}_\perp - \bar{r}'_\perp)} e^{i\ell k_{pz}^{(v)} z} e^{-iqk_{mz}^{(v)} z'} \end{aligned} \quad (H.2)$$

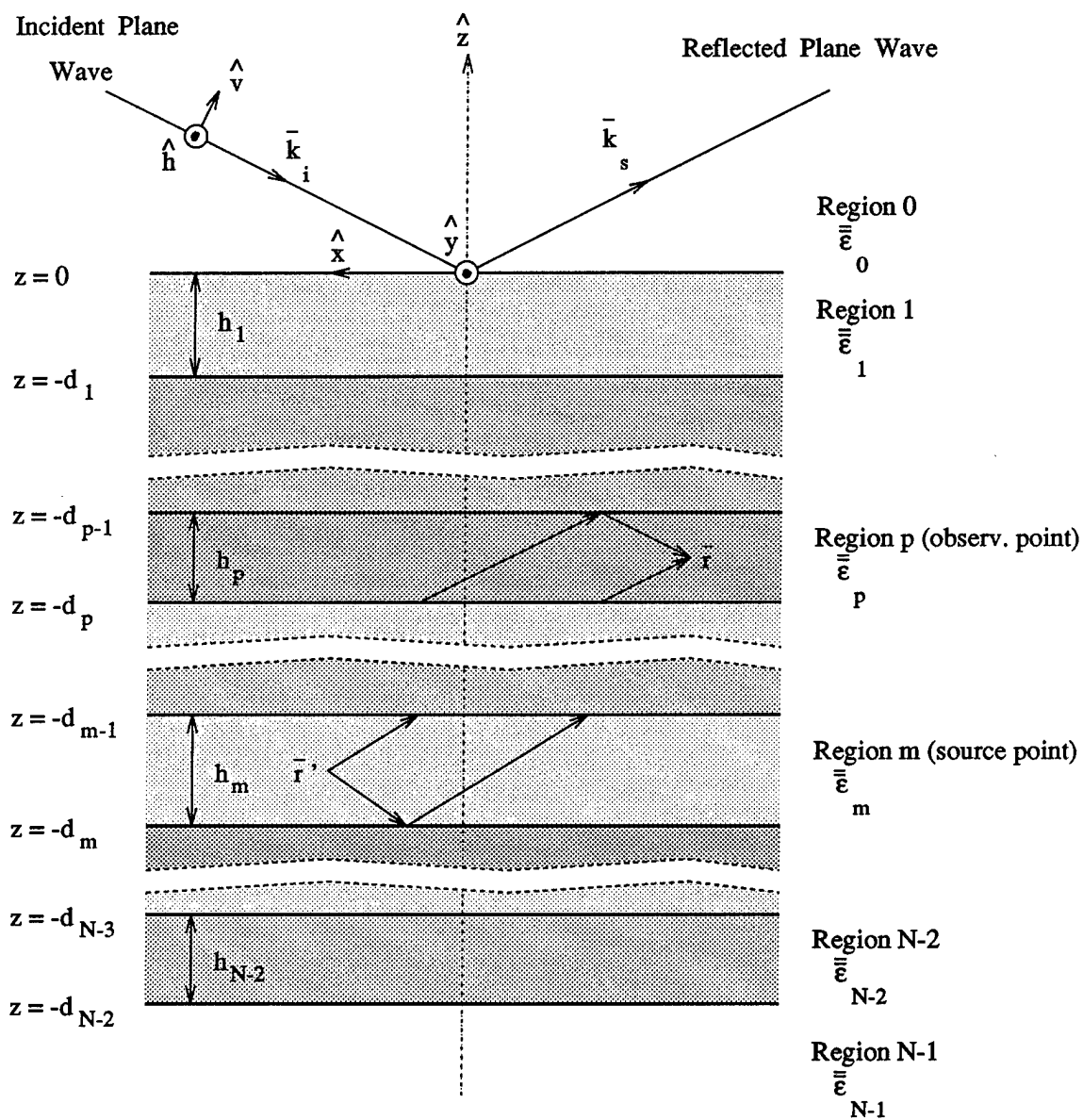


Figure H.1. Geometry of the layered media for which the Greens function and incident field expressions are calculated. For the Greens function, $\bar{\bar{G}}_{pm}(\bar{r}, \bar{r}')$, the terms contributing to the propagation of the wave from layer m to layer p are shown for the case where $p < m$.

and from Maxwell's equations, the magnetic field is related by (H.3).

$$\overline{H}(\overline{r}) = \frac{1}{i\omega\mu} \nabla \times \overline{E}(\overline{r}) \quad (H.3)$$

Substituting (H.2) in (H.3) and applying the curl operator yields (H.4),

$$\begin{aligned} \overline{H}_p(\overline{r}) = & i \sum_{\ell, q=+, -} \sum_{v=TE, TM} \iiint_V d\overline{r}' \iint d\overline{k}_\perp (\overline{k}_\perp + \ell k_{pz}^{(v)} \hat{z}) \times \overline{\overline{F}}_{pm\ell q}^{(v)\text{un}}(\overline{k}_\perp) \cdot \overline{J}_m(\overline{r}') \times \\ & e^{i\overline{k}_\perp \cdot (\overline{r}_\perp - \overline{r}'_\perp)} e^{i\ell k_{pz}^{(v)} z} e^{-iqk_{mz}^{(v)} z'} \end{aligned} \quad (H.4)$$

and comparing (H.4) with (H.1), it can be seen that the Green's function takes the form of (H.5),

$$\begin{aligned} \overline{\overline{G}}_{pm}(\overline{r}, \overline{r}') = & \sum_{\ell, q=+, -} \sum_{v=TE, TM} \iint d\overline{k}_\perp \overline{\overline{F}}_{pm\ell q}^{(v)\text{un}}(\overline{k}_\perp) \times \\ & e^{i\overline{k}_\perp \cdot (\overline{r}_\perp - \overline{r}'_\perp)} e^{i\ell k_{pz}^{(v)} z} e^{-iqk_{mz}^{(v)} z'} \end{aligned} \quad (H.5)$$

where $\overline{\overline{F}}_{pm\ell q}^{(v)\text{un}}(\overline{k}_\perp)$ is given by (H.6),

$$\overline{\overline{F}}_{pm\ell q}^{(v)\text{un}}(\overline{k}_\perp) = (\overline{k}_\perp + \ell k_{pz}^{(v)} \hat{z}) \times \overline{\overline{F}}_{pm\ell q}^{(v)\text{un}}(\overline{k}_\perp) \quad (H.6)$$

and $\overline{\overline{F}}_{pm\ell q}^{(v)\text{un}}(\overline{k}_\perp)$ is given in Appendix E.

Similarly, the magnetic field which results in each layer from an incident plane wave of the form of (H.7),

$$\overline{E}_i(\bar{r}) = \left[E_i^{TE} \hat{h}(-k_{0z_i}) + E_i^{TM} \hat{v}(-k_{0z_i}) \right] e^{i\bar{k}_{\perp i} \cdot \bar{r}_{\perp}} e^{-ik_{0z_i} z} \quad (H.7)$$

can be derived from a similar approach, and takes the form of (H.8),

$$\overline{H}_{\ell_i}(\bar{r}) = \sum_{s=+,-} \sum_{w=TE, TM} \overline{H}_{\ell_i}^{s,(w)} e^{-isk_{\ell_{zi}}^{(w)} z} e^{i\bar{k}_{\perp i} \cdot \bar{r}_{\perp}} \quad (H.8)$$

where

$$\overline{H}_{\ell_i}^{s,(w)} = \frac{1}{\omega \mu} \left(\bar{k}_{\perp i} - sk_{\ell_{zi}}^{(w)} \hat{z} \right) \times \overline{E}_{\ell_i}^{s,(w)} \quad (H.9)$$

and where $\overline{E}_{\ell_i}^{s,(w)}$ is given in Appendix E.

Appendix I

Correlation of Scattered Field Components for an Electrically Large Target Buried in a Layered Random Media

The following Appendix gives the correlations of the multi-path scattering components for the case of an electrically large target composed of flat, perfectly conducting, polygonal facets, scattering in the presence of a layer of continuous random media. Also given is the autocorrelation of the coherent direct target return. The function $I_{P.O.}(\phi_c, k_\xi, k_\zeta)$ is defined in (5.40), (5.45)-(5.46), and (5.49)-(5.50), for the three separate cases in which k_ξ , k_ξ and k_ζ , or neither is small. The function $\Phi_{\alpha\beta\gamma\rho}$ is the spectral function associated with the correlation of the renormalized scattering source, $\bar{\xi}(\bar{r})$, such that $C_{\alpha\beta\gamma\rho}(\bar{r})$ is given by (I.1),

$$C_{\alpha\beta\gamma\rho}(\bar{r}_1 - \bar{r}_2) = k_o^4 \left\langle \left[\bar{\xi}(\bar{r}_1) \right]_{\alpha\beta} \left[\bar{\xi}(\bar{r}_2) \right]_{\gamma\rho}^* \right\rangle \quad (I.1)$$

and $\Phi_{\alpha\beta\gamma\rho}(\bar{\beta})$ is defined by (I.2).

$$\Phi_{\alpha\beta\gamma\rho}(\bar{\beta}) = \frac{1}{(2\pi)^3} \iiint d\bar{\beta} C_{\alpha\beta\gamma\rho}(\bar{r}) e^{i\bar{\beta} \cdot \bar{r}} \quad (I.2)$$

Finally, the shadowing function $S(\hat{n}, \bar{k})$ is given by (5.18).

I.1. Target/Clutter - Target/Clutter Correlation

$$\begin{aligned}
\sigma_{TC-TC}^{\hat{p}_a \hat{p}_b}(\bar{k}_{as}, \bar{k}_{ai}, \bar{k}_{bs}, \bar{k}_{bi}) &= 4\pi r \langle \hat{p}_a \cdot \bar{E}_{TC}(\bar{k}_{as}, \bar{k}_{ai}) \times \hat{p}_b^* \cdot \bar{E}_{TC}^*(\bar{k}_{bs}, \bar{k}_{bi}) \rangle \\
&= (2\pi)^5 i \sum_{m, m'=1}^N \sum_{\substack{p, q, \ell, \\ p', q', \ell' = +, -}} \sum_{\substack{u, v, w, \\ u', v', w' = TE, TM}} \sum_{\alpha, \beta, \gamma, \rho = x, y, z} \iint d\bar{k}_{\perp a} B_{TC-TC}^{\alpha\beta\gamma\rho}{}_{pp'qq'\ell\ell'}{}_{uu'vv'ww'} \times \\
&\quad I_{P.O.}(\phi_{cm}, k_{\xi m}, k_{\zeta m}) I_{P.O.}^*(\phi_{cm'}, k_{\xi m'}, k_{\zeta m'}) \times \\
&\quad e^{-i(\ell k_{fza}^{(v)} - pk_{fza}^{(u)} + p'k_{fzb}^{(u')*} - \ell'k_{fzc}^{(v')*})d_{f-1}} \times \\
&\quad \left[\frac{\Phi_{\alpha\beta\gamma\rho}(\bar{k}_{\perp a} - \bar{k}_{\perp as}, \ell'k_{fzc}^{(v')*} - p'k_{fzb}^{(u')*})}{pk_{fza}^{(u)} - \ell k_{fza}^{(v)} + \ell'k_{fzc}^{(v')*} - p'k_{fzb}^{(u')*}} \right. \\
&\quad - \frac{\Phi_{\alpha\beta\gamma\rho}(\bar{k}_{\perp a} - \bar{k}_{\perp as}, \ell k_{fza}^{(v)} - pk_{fza}^{(u)})}{pk_{fza}^{(u)} - \ell k_{fza}^{(v)} + \ell'k_{fzc}^{(v')*} - p'k_{fzb}^{(u')*}} \times \\
&\quad \left. e^{i(pk_{fza}^{(u)} - \ell k_{fza}^{(v)} + \ell'k_{fzc}^{(v')*} - p'k_{fzb}^{(u')*})h_f} \right] \quad (I.3)
\end{aligned}$$

where

$$\begin{aligned}
B_{TC-TC}^{\alpha\beta\gamma\rho}{}_{pp'qq'\ell\ell'}{}_{uu'vv'ww'} &= \frac{\omega^2 \mu^2}{\pi} S(\hat{n}_m, \bar{k}_{\perp a} + qk_{tza}^{(v)}\hat{z}) S(\hat{n}_m, -\bar{k}_{\perp ai} + sk_{tzi}^{(w)}\hat{z}) \times \\
&\quad S(\hat{n}_{m'}, \bar{k}_{\perp c} + q'k_{tzc}^{(v')}\hat{z}) S(\hat{n}_{m'}, -\bar{k}_{\perp bi} + s'k_{tzi}^{(w')}\hat{z}) \times \\
&\quad \left[\hat{p}_a \cdot \bar{H}_{0fp}^{(u)}(\bar{k}_{\perp as}) \right]_{\alpha} \left[\bar{F}_{ftq}^{(v)}(\bar{k}_{\perp a}) \cdot (\hat{n}_m \times \bar{H}_{tai}^{s, (w)}) \right]_{\beta} \times \\
&\quad \left[\hat{p}_b \cdot \bar{H}_{0fp'}^{(u')}(\bar{k}_{\perp bs}) \right]_{\gamma}^* \left[\bar{F}_{ftq'}^{(v')}(\bar{k}_{\perp b}) \cdot (\hat{n}_{m'} \times \bar{H}_{tbi}^{s', (w')}) \right]_{\rho}^* \quad (I.4)
\end{aligned}$$

$$\bar{k}_{\perp c} = \bar{k}_{\perp b_s} - \bar{k}_{\perp a_s} + \bar{k}_{\perp a} \quad (I.5)$$

$$\phi_{c_m} = [(\bar{k}_{\perp a_i} - \bar{k}_{\perp a}) - (s k_{tz a_i}^{(w)} + q k_{tz a}^{(v)}) \hat{z}] \cdot \bar{c}_c^{(m)} \quad (I.6)$$

$$k_{\xi_m} = [(\bar{k}_{\perp a_i} - \bar{k}_{\perp a}) - (s k_{tz a_i}^{(w)} + q k_{tz a}^{(v)}) \hat{z}] \cdot \hat{\xi}_m \quad (I.7)$$

$$k_{\zeta_m} = [(\bar{k}_{\perp a_i} - \bar{k}_{\perp a}) - (s k_{tz a_i}^{(w)} + q k_{tz a}^{(v)}) \hat{z}] \cdot \hat{\zeta}_m \quad (I.8)$$

$$\phi_{c_{m'}} = [(\bar{k}_{\perp b_i} - \bar{k}_{\perp c}) - (s' k_{tz b_i}^{(w')} + q' k_{tz c}^{(v')}) \hat{z}] \cdot \bar{c}_c^{(m')} \quad (I.9)$$

$$k_{\xi_{m'}} = [(\bar{k}_{\perp b_i} - \bar{k}_{\perp c}) - (s' k_{tz b_i}^{(w')} + q' k_{tz c}^{(v')}) \hat{z}] \cdot \hat{\xi}_{m'} \quad (I.10)$$

$$k_{\zeta_{m'}} = [(\bar{k}_{\perp b_i} - \bar{k}_{\perp c}) - (s' k_{tz b_i}^{(w')} + q' k_{tz c}^{(v')}) \hat{z}] \cdot \hat{\zeta}_{m'} \quad (I.11)$$

I.2. Clutter/Target - Clutter/Target Correlation

$$\begin{aligned}
\sigma_{CT-CT}^{\hat{p}_a \hat{p}_b}(\bar{k}_{as}, \bar{k}_{ai}, \bar{k}_{bs}, \bar{k}_{bi}) &= 4\pi r \langle \hat{p}_a \cdot \bar{E}_{CT}(\bar{k}_{as}, \bar{k}_{ai}) \times \hat{p}_b^* \cdot \bar{E}_{CT}^*(\bar{k}_{bs}, \bar{k}_{bi}) \rangle \\
&= (2\pi)^5 i \sum_{m, m'=1}^N \sum_{\substack{p, s, q, \ell, \\ p', s', q', \ell' = +, -}} \sum_{\substack{u, v, w, \\ u', v', w' = TE, TM}} \sum_{\alpha, \beta, \gamma, \rho = x, y, z} \iint d\bar{k}_{\perp a} B_{CT-CT}^{\alpha\beta\gamma\rho \substack{pp'ss'qq'\ell\ell' \\ uu'vv'ww'}} \times \\
&\quad I_{P.O.}(\phi_{cm}, k_{\xi m}, k_{\zeta m}) I_{P.O.}^*(\phi_{cm'}, k_{\xi m'}, k_{\zeta m'}) \times \\
&\quad e^{i(qk_{fza}^{(v)} + sk_{fzai}^{(w)} - s'k_{fzbi}^{(w')*} - q'k_{fzc}^{(v')*})d_{f-1}} \times \\
&\quad \left[\frac{\Phi_{\alpha\beta\gamma\rho}(\bar{k}_{\perp ai} - \bar{k}_{\perp a}, -q'k_{fzc}^{(v')*} - s'k_{fzbi}^{(w')*})}{qk_{fza}^{(v)} + sk_{fzai}^{(w)} - q'k_{fzc}^{(v')*} - s'k_{fzbi}^{(w')*}} \right. \\
&\quad \left. - \frac{\Phi_{\alpha\beta\gamma\rho}(\bar{k}_{\perp ai} - \bar{k}_{\perp a}, -qk_{fza}^{(v)} - sk_{fzai}^{(w)})}{qk_{fza}^{(v)} + sk_{fzai}^{(w)} - q'k_{fzc}^{(v')*} - s'k_{fzbi}^{(w')*}} \times \right. \\
&\quad \left. e^{i(qk_{fza}^{(v)} + sk_{fzai}^{(w)} - q'k_{fzc}^{(v')*} - s'k_{fzbi}^{(w')*})h_f} \right] \quad (I.12)
\end{aligned}$$

where

$$\begin{aligned}
B_{CT-CT}^{\alpha\beta\gamma\rho \substack{pp'ss'qq'\ell\ell' \\ uu'vv'ww'}} &= \frac{1}{\pi} S(\hat{n}_m, \bar{k}_{\perp as} + pk_{tza}^{(u)} \hat{z}) S(\hat{n}_m, -\bar{k}_{\perp a} - \ell k_{tza}^{(v)} \hat{z}) \times \\
&\quad S(\hat{n}_{m'}, \bar{k}_{\perp bs} + p'k_{tzb}^{(u')} \hat{z}) S(\hat{n}_{m'}, -\bar{k}_{\perp c} - \ell' k_{tzc}^{(v')} \hat{z}) \times \\
&\quad \left[\hat{p}_a \cdot \bar{H}_{0tp}^{(u)}(\bar{k}_{\perp as}) \cdot (\hat{n}_m \times \bar{\mathcal{F}}_{tf_{tq}}^{(v)}(\bar{k}_{\perp a})) \right]_{\alpha} \left[\bar{E}_{fai}^{s, (w)} \right]_{\beta} \times \\
&\quad \left[\hat{p}_b \cdot \bar{H}_{0tp'}^{(u')}(\bar{k}_{\perp bs}) \cdot (\hat{n}_{m'} \times \bar{\mathcal{F}}_{tf'_{tq'}}^{(v')}(\bar{k}_{\perp b})) \right]_{\gamma}^* \left[\bar{E}_{fbi}^{s', (w')} \right]_{\rho}^* \quad (I.13)
\end{aligned}$$

$$\bar{k}_{\perp c} = \bar{k}_{\perp bi} - \bar{k}_{\perp ai} + \bar{k}_{\perp a} \quad (I.14)$$

$$\phi_{c_m} = \left[(\bar{k}_{\perp a} - \bar{k}_{\perp as}) + (\ell k_{tz a}^{(v)} - p k_{tz as}^{(u)}) \hat{z} \right] \cdot \bar{c}_c^{(m)} \quad (I.15)$$

$$k_{\xi_m} = \left[(\bar{k}_{\perp a} - \bar{k}_{\perp as}) + (\ell k_{tz a}^{(v)} - p k_{tz as}^{(u)}) \hat{z} \right] \cdot \hat{\xi}_m \quad (I.16)$$

$$k_{\zeta_m} = \left[(\bar{k}_{\perp a} - \bar{k}_{\perp as}) + (\ell k_{tz a}^{(v)} - p k_{tz as}^{(u)}) \hat{z} \right] \cdot \hat{\zeta}_m \quad (I.17)$$

$$\phi_{c_{m'}} = \left[(\bar{k}_{\perp c} - \bar{k}_{\perp bs}) + (\ell' k_{tz c}^{(v')} - p' k_{tz bs}^{(u')}) \hat{z} \right] \cdot \bar{c}_c^{(m')} \quad (I.18)$$

$$k_{\xi_{m'}} = \left[(\bar{k}_{\perp c} - \bar{k}_{\perp bs}) + (\ell' k_{tz c}^{(v')} - p' k_{tz bs}^{(u')}) \hat{z} \right] \cdot \hat{\xi}_{m'} \quad (I.19)$$

$$k_{\zeta_{m'}} = \left[(\bar{k}_{\perp c} - \bar{k}_{\perp bs}) + (\ell' k_{tz c}^{(v')} - p' k_{tz bs}^{(u')}) \hat{z} \right] \cdot \hat{\zeta}_{m'} \quad (I.20)$$

I.3. Target/Clutter - Clutter/Target Correlation

$$\begin{aligned}
\sigma_{TC-CT}^{\hat{p}_a \hat{p}_b}(\bar{k}_{as}, \bar{k}_{ai}, \bar{k}_{bs}, \bar{k}_{bi}) &= 4\pi r \langle \hat{p}_a \cdot \bar{E}_{TC}(\bar{k}_{as}, \bar{k}_{ai}) \times \hat{p}_b^* \cdot \bar{E}_{CT}^*(\bar{k}_{bs}, \bar{k}_{bi}) \rangle \\
&= (2\pi)^5 i \sum_{m, m'=1}^N \sum_{p', s', q', \ell' = +, -}^{p, s, q, \ell} \sum_{u', v', w' = TE, TM}^{u, v, w} \sum_{\alpha, \beta, \gamma, \rho = x, y, z} \iint d\bar{k}_{\perp a} B_{TC-CT}^{\alpha\beta\gamma\rho, pp'ss'qq'\ell\ell', uu'vv'ww'} \times \\
&\quad I_{P.O.}(\phi_{cm}, k_{\xi m}, k_{\zeta m}) I_{P.O.}^*(\phi_{cm'}, k_{\xi m'}, k_{\zeta m'}) \\
&\quad e^{-i(\ell k_{fza}^{(v)} - pk_{fza}^{(u)} + s'k_{fzbi}^{(w')*} + q'k_{fzc}^{(v')*})d_{f-1}} \times \\
&\quad \left[\frac{\Phi_{\alpha\beta\gamma\rho}(\bar{k}_{\perp a} - \bar{k}_{\perp as}, -q'k_{fzc}^{(v')*} - s'k_{fzbi}^{(w')*})}{pk_{fza}^{(u)} - \ell k_{fza}^{(v)} - q'k_{fzc}^{(v')*} - s'k_{fzbi}^{(w')*}} \right. \\
&\quad - \frac{\Phi_{\alpha\beta\gamma\rho}(\bar{k}_{\perp a} - \bar{k}_{\perp as}, \ell k_{fza}^{(v)} - pk_{fza}^{(u)})}{pk_{fza}^{(u)} - \ell k_{fza}^{(v)} - q'k_{fzc}^{(v')*} - s'k_{fzbi}^{(w')*}} \times \\
&\quad \left. e^{i(pk_{fza}^{(u)} - \ell k_{fza}^{(v)} - q'k_{fzc}^{(v')*} - s'k_{fzbi}^{(w')*})h_f} \right] \quad (I.21)
\end{aligned}$$

where

$$\begin{aligned}
B_{TC-CT}^{\alpha\beta\gamma\rho, pp'ss'qq'\ell\ell', uu'vv'ww'} &= \frac{\omega\mu}{\pi} S(\hat{n}_m, \bar{k}_{\perp a} + qk_{tza}^{(v)}\hat{z}) S(\hat{n}_m, -\bar{k}_{\perp ai} + sk_{tza}^{(w)}\hat{z}) \times \\
&\quad S(\hat{n}_{m'}, \bar{k}_{\perp bs} + p'k_{tzb}^{(u')}\hat{z}) S(\hat{n}_{m'}, -\bar{k}_{\perp c} - \ell'k_{tzc}^{(v')}\hat{z}) \times \\
&\quad \left[\hat{p}_a \cdot \bar{H}_{0tp}^{(u)}(\bar{k}_{\perp as}) \right]_{\alpha} \left[\bar{F}_{ftq}^{(v)}(\bar{k}_{\perp a}) \cdot (\hat{n}_m \times \bar{H}_{tai}^{s, (w)}) \right]_{\beta} \times \\
&\quad \left[\hat{p}_b \cdot \bar{H}_{0tp'}^{(u')}(\bar{k}_{\perp bs}) \cdot (\hat{n}_{m'} \times \bar{F}_{ftq'}^{(v')}(\bar{k}_{\perp b})) \right]_{\gamma}^* \left[\bar{E}_{fbi}^{s', (w')} \right]_{\rho}^* \quad (I.22)
\end{aligned}$$

$$\bar{k}_{\perp c} = \bar{k}_{\perp bi} + \bar{k}_{\perp as} - \bar{k}_{\perp a} \quad (I.23)$$

$$\phi_{c_m} = \left[(\bar{k}_{\perp ai} - \bar{k}_{\perp a}) - (s k_{tz ai}^{(w)} + q k_{tz a}^{(v)}) \hat{z} \right] \cdot \bar{c}_c^{(m)} \quad (I.24)$$

$$k_{\xi_m} = \left[(\bar{k}_{\perp ai} - \bar{k}_{\perp a}) - (s k_{tz ai}^{(w)} + q k_{tz a}^{(v)}) \hat{z} \right] \cdot \hat{\xi}_m \quad (I.25)$$

$$k_{\zeta_m} = \left[(\bar{k}_{\perp ai} - \bar{k}_{\perp a}) - (s k_{tz ai}^{(w)} + q k_{tz a}^{(v)}) \hat{z} \right] \cdot \hat{\zeta}_m \quad (I.26)$$

$$\phi_{c_{m'}} = \left[(\bar{k}_{\perp c} - \bar{k}_{\perp bs}) + (\ell' k_{tz c}^{(v')} - p' k_{tz bs}^{(u')}) \hat{z} \right] \cdot \bar{c}_c^{(m')} \quad (I.27)$$

$$k_{\xi_{m'}} = \left[(\bar{k}_{\perp c} - \bar{k}_{\perp bs}) + (\ell' k_{tz c}^{(v')} - p' k_{tz bs}^{(u')}) \hat{z} \right] \cdot \hat{\xi}_{m'} \quad (I.28)$$

$$k_{\zeta_{m'}} = \left[(\bar{k}_{\perp c} - \bar{k}_{\perp bs}) + (\ell' k_{tz c}^{(v')} - p' k_{tz bs}^{(u')}) \hat{z} \right] \cdot \hat{\zeta}_{m'} \quad (I.29)$$

I.4. Target - Target Correlation

$$\begin{aligned}
\sigma_{T-T}^{\hat{p}_a \hat{p}_b}(\bar{k}_{as}, \bar{k}_{ai}, \bar{k}_{bs}, \bar{k}_{bi}) &= 4\pi r \left(\hat{p}_a \cdot \bar{E}_T(\bar{k}_{as}, \bar{k}_{ai}) \times \hat{p}_b^* \cdot \bar{E}_T^*(\bar{k}_{bs}, \bar{k}_{bi}) \right) \\
&= \sum_{m,m'=1}^N \sum_{p,p',s,s'=+,-} \sum_{u,u',w,w'=TE,TM} B_{T-T}^{pp'ss'} \times \\
&\quad I_{P.O.}(\phi_{cm}, k_{\xi m}, k_{\zeta m}) I_{P.O.}^*(\phi_{cm'}, k_{\xi m'}, k_{\zeta m'})
\end{aligned} \tag{I.30}$$

where

$$\begin{aligned}
B_{T-T}^{pp'ss'} &= \frac{\omega^2 \mu^2}{\pi} S(\hat{n}_m, \bar{k}_{\perp as} + p k_{tz as}^{(u)} \hat{z}) S(\hat{n}_m, -\bar{k}_{\perp ai} + s k_{tz ai}^{(w)} \hat{z}) \times \\
&\quad S(\hat{n}_{m'}, \bar{k}_{\perp bs} + p' k_{tz bs}^{(u')} \hat{z}) S(\hat{n}_{m'}, -\bar{k}_{\perp bi} + s' k_{tz bi}^{(w')} \hat{z}) \times \\
&\quad \left[\hat{p}_a \cdot \bar{H}_{0t_p}^{(u)}(\bar{k}_{\perp as}) \cdot (\hat{n}_m \times \bar{H}_{tai}^{s,(w)}) \right] \left[\hat{p}_b \cdot \bar{H}_{0t_{p'}}^{(u')}(\bar{k}_{\perp bs}) \cdot (\hat{n}_{m'} \times \bar{H}_{tbi}^{s',(w')}) \right]^*
\end{aligned} \tag{I.31}$$

$$\phi_{cm} = \left[(\bar{k}_{\perp ai} - \bar{k}_{\perp as}) - (p k_{tz as}^{(u)} + s k_{tz ai}^{(w)}) \hat{z} \right] \cdot \bar{c}_c^{(m)} \tag{I.32}$$

$$k_{\xi m} = \left[(\bar{k}_{\perp ai} - \bar{k}_{\perp as}) - (p k_{tz as}^{(u)} + s k_{tz ai}^{(w)}) \hat{z} \right] \cdot \hat{\xi}_m \tag{I.33}$$

$$k_{\zeta_m} = \left[(\bar{k}_{\perp_{ai}} - \bar{k}_{\perp_{as}}) - (p'k_{tz_{as}}^{(u)} + s'k_{tz_{ai}}^{(w)}) \hat{z} \right] \cdot \hat{\zeta}_m \quad (I.34)$$

$$\phi_{c_{m'}} = \left[(\bar{k}_{\perp_{bi}} - \bar{k}_{\perp_{bs}}) - (p'k_{tz_{bs}}^{(u')} + s'k_{tz_{bi}}^{(w')}) \hat{z} \right] \cdot \bar{c}_c^{(m')} \quad (I.35)$$

$$k_{\xi_{m'}} = \left[(\bar{k}_{\perp_{bi}} - \bar{k}_{\perp_{bs}}) - (p'k_{tz_{bs}}^{(u')} + s'k_{tz_{bi}}^{(w')}) \hat{z} \right] \cdot \hat{\xi}_{m'} \quad (I.36)$$

$$k_{\zeta_{m'}} = \left[(\bar{k}_{\perp_{bi}} - \bar{k}_{\perp_{bs}}) - (p'k_{tz_{bs}}^{(u')} + s'k_{tz_{bi}}^{(w')}) \hat{z} \right] \cdot \hat{\zeta}_{m'} \quad (I.37)$$

Chapter 6

Scattering from an Electrically Small Target in a Layered Continuous Random Media

The previous chapter treated the problem of scattering from a deterministic target buried in a layered continuous random media for the case where the target was electrically large and the induced surface currents could be approximated by the Physical Optics method. For smaller targets, or for targets which contain structures which possess rapid changes in shape on scales comparable to or smaller than a wavelength, this high frequency approach is no longer accurate. Instead an exact method which solves numerically for the unknown surface currents must be employed.

This chapter again considers the problem of scattering from a target in a layered continuous random media, but now for an electrically small target, using the numerical Method of Moments (MoM) approach to target scattering. As previously, an effective

mean permittivity for the random media is derived using Strong Fluctuation theory, and the incoherent field scattered by the random media is determined from the first order distorted Born approximation. An integral equation is derived for the surface current induced on the target, and this current is represented as a weighted series of basis function terms, each of known form, but with unknown amplitude. The integral equation is then tested by multiplying by a series of testing functions, and integrating over the target surface. The result is a linear system of equations, which may be solved for the unknown basis function weights.

This method is applied to an arbitrary target using bi-triangular subdomain basis functions, and point testing of the integral equation. The target signature is again seen to consist of a coherent or direct scattering return, and an incoherent portion arising from interactions with the random media. Expressions for the statistics, variance and correlation, of the incoherent fields are again derived.

6.1. Method of Moments Formulation

The geometry of the scattering problem considered here is shown in Figure 6.1. The space surrounding the target is stratified vertically into $N - 2$ bounded regions, with a half-space above (region 0) and below (region $N - 1$). The target is located in region t , and is a perfectly conducting object of arbitrary shape, but for practical reasons will be assumed to be relatively small electrically. Again it is possible to synthesize the effects of several independent random layers, by treating each individually, and incoherently combining the results. Hence, only a single region, f , will be consid-

ered to have random permittivity fluctuations, and only the case in which $t \neq f$ will be treated here. The properties of the random media, the Strong Fluctuation Theory method of determining an effective mean permittivity, the correlation function of the random media, and the distorted Born approximation are all identical to their usage in previous chapters, and a description of these will not be repeated here.

The total field scattered by the target is given by (6.1),

$$\overline{E}_S(\bar{r}) = i\omega\mu \iint_{S_t} dS' \overline{G}(\bar{r}, \bar{r}') \cdot \overline{J}_S(\bar{r}') \quad (6.1)$$

where $\overline{G}(\bar{r}, \bar{r}')$ above is the Green's function which accounts not only for the presence of the boundaries of the layered media, but also for the random fluctuations of permittivity in region f . Hence, both the induced target surface current, $\overline{J}_S(\bar{r})$, and the scattered field, $\overline{E}_S(\bar{r})$, will contain both a mean coherent part, and an incoherent portion arising from the presence of the random scatterers. In the Method of Moments (MoM) approach, the current is expanded in the series representation of (6.2),

$$\overline{J}_S(\bar{r}) = \sum_n I_n \overline{B}_n(\bar{r}') \quad (6.2)$$

where $\overline{B}_n(\bar{r})$ are a set of known, deterministic basis functions, and where I_n are a set of corresponding weights of unknown value, which for the present problem will consist of both a deterministic mean part, and a zero-mean random portion. Substituting the above into (6.1) yields the result of (6.3).

$$\overline{E}_S(\bar{r}) = i\omega\mu \sum_n I_n \iint_{S_t} dS' \overline{G}(\bar{r}, \bar{r}') \cdot \overline{B}_n(\bar{r}') \quad (6.3)$$

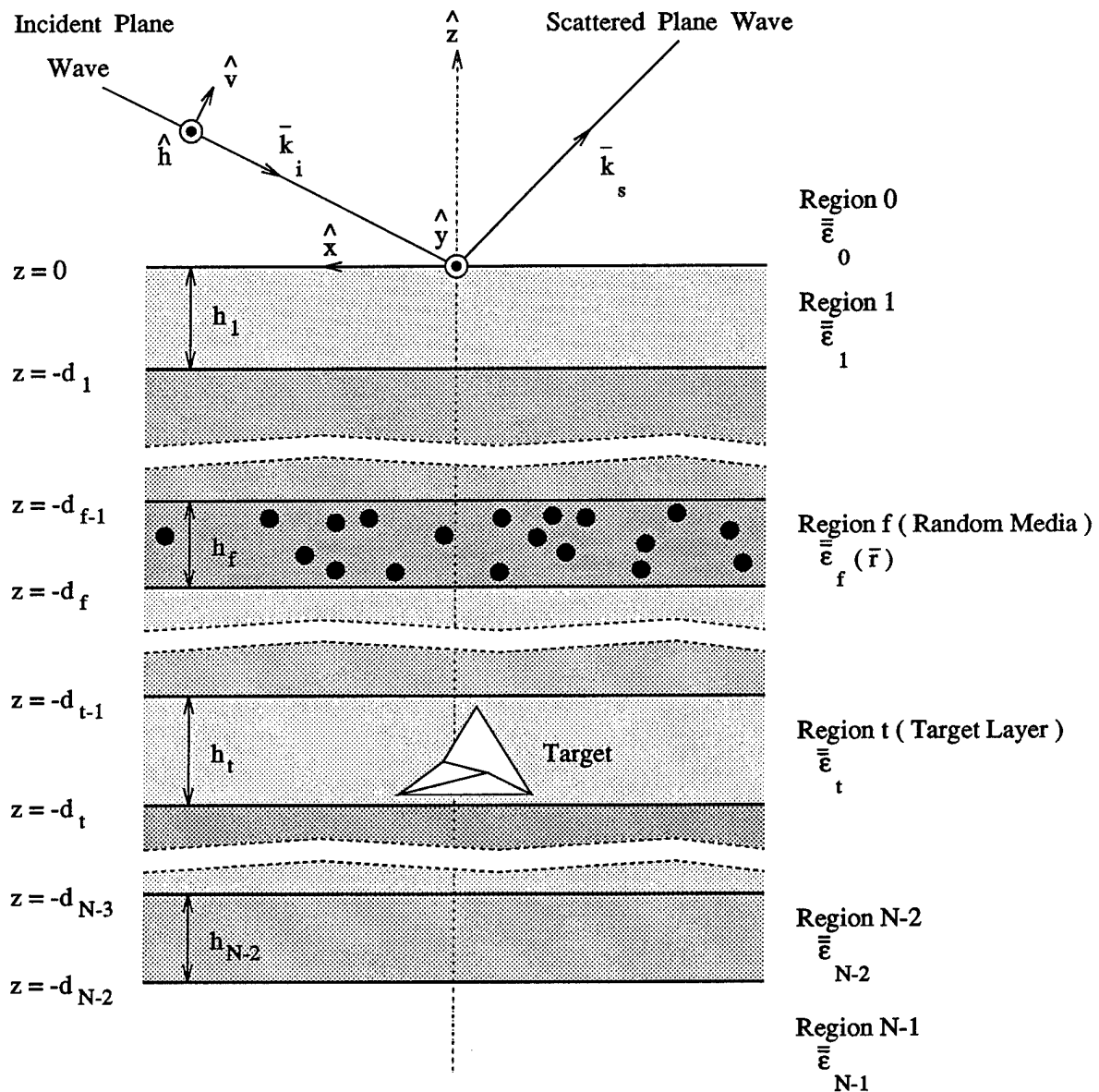


Figure 6.1. Geometry of the multi-layer scattering problem with N layers, and with the electrically small target located in layer t , and the random media in layer f .

The above equation is now tested by multiplying in turn by each of a set of N testing functions, $\overline{W}_m(\vec{r})$, and then integrating the result over the target surface to obtain (6.4).

$$\iint_{S_i} dS \overline{W}_m(\vec{r}) \cdot \overline{E}_S(\vec{r}) = i\omega\mu \sum_n I_n \iint_{S_i} dS \iint_{S_i} dS' \overline{W}_m(\vec{r}) \cdot \overline{G}(\vec{r}, \vec{r}') \cdot \overline{B}_n(\vec{r}') \quad m = 1, \dots, N \quad (6.4)$$

Finally, for a perfectly conducting target, the total surface electric field will vanish, so the incident and scattered fields must cancel. Since the testing functions, $\overline{W}_m(\vec{r})$, are always taken to lay parallel to the surface, the scattered field in the above can be replaced by the negative of the incident field. The above set of equations can then be rewritten in the matrix form of (6.5),

$$\overline{V} = \overline{\overline{Z}} \overline{I} \quad (6.5)$$

where the excitation vector and impedance matrix elements are given by (6.6) and (6.7).

$$V_m = - \iint_{S_i} dS \overline{W}_m(\vec{r}) \cdot \overline{E}_i(\vec{r}) \quad (6.6)$$

$$Z_{mn} = i\omega\mu \iint_{S_i} dS \iint_{S_i} dS' \overline{W}_m(\vec{r}) \cdot \overline{G}(\vec{r}, \vec{r}') \cdot \overline{B}_n(\vec{r}') \quad (6.7)$$

Both the impedance matrix and excitation vector above will contain randomly varying components, and each element will be given by a Born series, where the first term will be the deterministic value which results when the random fluctuations are ignored, and where the higher order terms are incoherent contributions which arise from the presence of the random scattering. Hence, the elements of the excitation vector will take the form of (6.8),

$$V_m = V_m^{(0)} + V_m^{(1)} + V_m^{(2)} + \dots \quad (6.8)$$

where the zeroth order term is given by (6.9).

$$V_m^{(0)} = - \iint_{S_t} dS \overline{W}_m(\bar{r}) \cdot \overline{E}_{t_i}^{(0)}(\bar{r}) \quad (6.9)$$

In the above, $\overline{E}_{t_i}^{(0)}(\bar{r})$ is the zeroth order incident field in the target region, which will be assumed to arise from an incident plane wave and its reflections between the layer boundaries of the media. Similarly, the first order term is given by (6.10),

$$V_m^{(1)} = - \iint_{S_t} dS \overline{W}_m(\bar{r}) \cdot \overline{E}_{t_i}^{(1)}(\bar{r}) \quad (6.10)$$

where $\overline{E}_{t_i}^{(1)}(\bar{r})$ is the first order incoherent term arising from the first order distorted Born approximation. Replacing $\overline{E}_{t_i}^{(1)}(\bar{r})$ by this approximation yields (6.11),

$$V_m^{(1)} = - \iint_{S_t} dS \overline{W}_m(\bar{r}) \cdot \iiint_{V_f} dV \overline{G}_{tf}(\bar{r}, \bar{r}') \cdot \overline{Q}(\bar{r}') \cdot \overline{E}_{f_i}^{(0)}(\bar{r}') \quad (6.11)$$

where $\overline{E}_i^{(0)}(\bar{r})$ is the zeroth order field in the random layer, and $\overline{Q}(\bar{r}) = k_o^2 \overline{\xi}(\bar{r})$ where $\overline{\xi}(\bar{r})$ is the renormalized scattering source. $V_m^{(2)}$, $V_m^{(3)}$, and other higher order terms can be obtained by replacing $\overline{E}_i(\bar{r})$ in (6.6) with higher order terms of the Born series for the incident field, where each subsequent term includes the effect of one more interaction with the random media.

Similarly, the impedance matrix, \overline{Z} , has elements in the form of (6.12),

$$Z_{mn} = Z_{mn}^{(0)} + Z_{mn}^{(1)} + Z_{mn}^{(2)} + \dots \quad (6.12)$$

where $Z_{mn}^{(0)}$ is a deterministic propagation term which accounts for the field resulting on the target from the direct radiation of the surface current of the target, and which is given by (6.13).

$$Z_{mn}^{(0)} = i\omega\mu \iint_{S_t} dS \iint_{S_t} dS' \overline{W}_m(\bar{r}) \cdot \overline{G}_{tt}(\bar{r}, \bar{r}') \cdot \overline{B}_n(\bar{r}') \quad (6.13)$$

The first order term, $Z_{mn}^{(1)}$, accounts for the propagation from the target, to the random media, and back to the target, and this term is given by (6.14).

$$Z_{mn}^{(1)} = i\omega\mu \iint_{S_t} dS \iint_{S_t} dS' \iiint_{V_f} dV'' \overline{W}_m(\bar{r}) \cdot \overline{G}_{tf}(\bar{r}, \bar{r}') \cdot \overline{Q}(\bar{r}') \cdot \overline{G}_{ft}(\bar{r}', \bar{r}'') \cdot \overline{B}_n(\bar{r}'') \quad (6.14)$$

The higher order terms, $Z_{mn}^{(2)}$, $Z_{mn}^{(3)}$, etc. reflect propagation from the target to the random media, multiple scattering within the random media, and then propagation back to the target.

Finally, the scattered field obtained in the far-field of the target can similarly be written as a series as given by (6.15),

$$\overline{E}_S(\overline{r}) = \overline{E}_S^{(0)}(\overline{r}) + \overline{E}_S^{(1)}(\overline{r}) + \overline{E}_S^{(2)}(\overline{r}) + \dots \quad (6.15)$$

where the zeroth order term is the field arising from direct radiation of the target surface current, and is given by (6.16).

$$\overline{E}_S^{(0)}(\overline{r}) = i\omega\mu \sum_n I_n \iint_{S_t} dS \overline{G}_{0t}(\overline{r}, \overline{r}') \cdot \overline{B}_n(\overline{r}') \quad (6.16)$$

The first order term is the field which radiates from the target, then scatters from the random media before reaching the receiver, and this field is given by (6.17).

$$\overline{E}_S^{(1)}(\overline{r}) = i\omega\mu \sum_n I_n \iint_{S_t} dS' \iiint_{V_f} dV'' \overline{G}_{0f}(\overline{r}, \overline{r}') \cdot \overline{Q}(\overline{r}') \cdot \overline{G}_{ft}(\overline{r}', \overline{r}'') \cdot \overline{B}_n(\overline{r}'') \quad (6.17)$$

The higher order terms, $\overline{E}_S^{(2)}(\overline{r})$, $\overline{E}_S^{(3)}(\overline{r})$, etc. arise from fields which are scattered multiple times in traveling from the target to the receiver.

To determine the scattered fields above, the unknown current amplitudes, I_n , must be determined. These unknown weights can be found by solving the matrix equation of (6.5). Rewriting this linear system with the contributions to $\overline{\overline{Z}}$ and \overline{V} expanded yields (6.18).

$$\left(\overline{\overline{Z}}^{(0)} + \overline{\overline{Z}}^{(1)} + \overline{\overline{Z}}^{(2)} + \dots \right) \overline{I} = \overline{V}^{(0)} + \overline{V}^{(1)} + \overline{V}^{(2)} + \dots \quad (6.18)$$

The above is now multiplied by the inverse of $\overline{\overline{Z}}^{(0)}$, resulting in (6.19).

$$\left(\overline{\overline{I}} + \overline{\overline{Z}}^{(0)-1} \overline{\overline{Z}}^{(1)} + \overline{\overline{Z}}^{(0)-1} \overline{\overline{Z}}^{(2)} + \dots \right) \overline{\overline{I}} = \overline{\overline{Z}}^{(0)-1} \overline{\overline{V}}^{(0)} + \overline{\overline{Z}}^{(0)-1} \overline{\overline{V}}^{(1)} + \overline{\overline{Z}}^{(0)-1} \overline{\overline{V}}^{(2)} + \dots \quad (6.19)$$

The left hand side of the above must be inverted and multiplied through to obtain $\overline{\overline{I}}$. Since successive terms in the Born series should contribute less and less, the desired matrix inverse can be approximated as in (6.20).

$$\left(\overline{\overline{I}} + \overline{\overline{Z}}^{(0)-1} \overline{\overline{Z}}^{(1)} + \overline{\overline{Z}}^{(0)-1} \overline{\overline{Z}}^{(2)} + \dots \right)^{-1} \simeq \overline{\overline{I}} - \overline{\overline{Z}}^{(0)-1} \overline{\overline{Z}}^{(1)} - \overline{\overline{Z}}^{(0)-1} \overline{\overline{Z}}^{(2)} - \dots \quad (6.20)$$

Therefore, the desired solution for the weight vector is given by (6.21).

$$\begin{aligned} \overline{\overline{I}} = & \overline{\overline{Z}}^{(0)-1} \overline{\overline{V}}^{(0)} + \overline{\overline{Z}}^{(0)-1} \overline{\overline{V}}^{(1)} + \overline{\overline{Z}}^{(0)-1} \overline{\overline{V}}^{(2)} + \dots \\ & - \overline{\overline{Z}}^{(0)-1} \overline{\overline{Z}}^{(1)} \overline{\overline{Z}}^{(0)-1} \overline{\overline{V}}^{(0)} - \overline{\overline{Z}}^{(0)-1} \overline{\overline{Z}}^{(1)} \overline{\overline{Z}}^{(0)-1} \overline{\overline{V}}^{(1)} - \overline{\overline{Z}}^{(0)-1} \overline{\overline{Z}}^{(1)} \overline{\overline{Z}}^{(0)-1} \overline{\overline{V}}^{(2)} - \dots \\ & - \overline{\overline{Z}}^{(0)-1} \overline{\overline{Z}}^{(2)} \overline{\overline{Z}}^{(0)-1} \overline{\overline{V}}^{(0)} - \overline{\overline{Z}}^{(0)-1} \overline{\overline{Z}}^{(2)} \overline{\overline{Z}}^{(0)-1} \overline{\overline{V}}^{(1)} - \overline{\overline{Z}}^{(0)-1} \overline{\overline{Z}}^{(2)} \overline{\overline{Z}}^{(0)-1} \overline{\overline{V}}^{(2)} - \dots \end{aligned} \quad (6.21)$$

From (6.15)-(6.17), the scattered field can be expressed as in (6.22),

$$E_S^p = \overline{\overline{L}}^{(0)} \cdot \overline{\overline{I}} + \overline{\overline{L}}^{(1)} \cdot \overline{\overline{I}} + \overline{\overline{L}}^{(2)} \cdot \overline{\overline{I}} + \dots \quad (6.22)$$

where

$$L_n^{(0)} = i\omega\mu \iint_{S_t} dS' \hat{p} \cdot \bar{G}_{0t}(\bar{r}, \bar{r}') \cdot \bar{B}_n(\bar{r}') \quad (6.23)$$

$$L_n^{(1)} = i\omega\mu \iint_{S_t} dS' \iiint_{V_f} dV'' \hat{p} \cdot \bar{G}_{0f}(\bar{r}, \bar{r}') \cdot \bar{Q}(\bar{r}') \cdot \bar{G}_{ft}(\bar{r}', \bar{r}'') \cdot \bar{B}_n(\bar{r}'') \quad (6.24)$$

Finally, substituting (6.21) into (6.22) yields the expression for the scattered field which is given by (6.25) below.

$$\begin{aligned} E_S^{\hat{p}} = & \bar{L}^{(0)} \bar{Z}^{(0)-1} \bar{V}^{(0)} + \bar{L}^{(0)} \bar{Z}^{(0)-1} \bar{V}^{(1)} + \bar{L}^{(0)} \bar{Z}^{(0)-1} \bar{V}^{(2)} + \dots \\ & - \bar{L}^{(0)} \bar{Z}^{(0)-1} \bar{Z}^{(1)} \bar{Z}^{(0)-1} \bar{V}^{(0)} - \bar{L}^{(0)} \bar{Z}^{(0)-1} \bar{Z}^{(1)} \bar{Z}^{(0)-1} \bar{V}^{(1)} - \bar{L}^{(0)} \bar{Z}^{(0)-1} \bar{Z}^{(1)} \bar{Z}^{(0)-1} \bar{V}^{(2)} - \dots \\ & - \bar{L}^{(0)} \bar{Z}^{(0)-1} \bar{Z}^{(2)} \bar{Z}^{(0)-1} \bar{V}^{(0)} - \bar{L}^{(0)} \bar{Z}^{(0)-1} \bar{Z}^{(2)} \bar{Z}^{(0)-1} \bar{V}^{(1)} - \bar{L}^{(0)} \bar{Z}^{(0)-1} \bar{Z}^{(2)} \bar{Z}^{(0)-1} \bar{V}^{(2)} - \dots \\ & + \bar{L}^{(1)} \bar{Z}^{(0)-1} \bar{V}^{(0)} + \bar{L}^{(1)} \bar{Z}^{(0)-1} \bar{V}^{(1)} + \bar{L}^{(1)} \bar{Z}^{(0)-1} \bar{V}^{(2)} + \dots \\ & - \bar{L}^{(1)} \bar{Z}^{(0)-1} \bar{Z}^{(1)} \bar{Z}^{(0)-1} \bar{V}^{(0)} - \bar{L}^{(1)} \bar{Z}^{(0)-1} \bar{Z}^{(1)} \bar{Z}^{(0)-1} \bar{V}^{(1)} - \bar{L}^{(1)} \bar{Z}^{(0)-1} \bar{Z}^{(1)} \bar{Z}^{(0)-1} \bar{V}^{(2)} - \dots \\ & - \bar{L}^{(1)} \bar{Z}^{(0)-1} \bar{Z}^{(2)} \bar{Z}^{(0)-1} \bar{V}^{(0)} - \bar{L}^{(1)} \bar{Z}^{(0)-1} \bar{Z}^{(2)} \bar{Z}^{(0)-1} \bar{V}^{(1)} - \bar{L}^{(1)} \bar{Z}^{(0)-1} \bar{Z}^{(2)} \bar{Z}^{(0)-1} \bar{V}^{(2)} - \dots \\ & + \bar{L}^{(2)} \bar{Z}^{(0)-1} \bar{V}^{(0)} + \bar{L}^{(2)} \bar{Z}^{(0)-1} \bar{V}^{(1)} + \bar{L}^{(2)} \bar{Z}^{(0)-1} \bar{V}^{(2)} + \dots \\ & - \bar{L}^{(2)} \bar{Z}^{(0)-1} \bar{Z}^{(1)} \bar{Z}^{(0)-1} \bar{V}^{(0)} - \bar{L}^{(2)} \bar{Z}^{(0)-1} \bar{Z}^{(1)} \bar{Z}^{(0)-1} \bar{V}^{(1)} - \bar{L}^{(2)} \bar{Z}^{(0)-1} \bar{Z}^{(1)} \bar{Z}^{(0)-1} \bar{V}^{(2)} - \dots \\ & - \bar{L}^{(2)} \bar{Z}^{(0)-1} \bar{Z}^{(2)} \bar{Z}^{(0)-1} \bar{V}^{(0)} - \bar{L}^{(2)} \bar{Z}^{(0)-1} \bar{Z}^{(2)} \bar{Z}^{(0)-1} \bar{V}^{(1)} - \bar{L}^{(2)} \bar{Z}^{(0)-1} \bar{Z}^{(2)} \bar{Z}^{(0)-1} \bar{V}^{(2)} - \dots \\ & + \dots \end{aligned} \quad (6.25)$$

The above includes terms up to high order in the number of times the field may be scattered by the random media in traveling from the radar to the target, and in traveling from the target back to the radar. Also included is the field scattered from the target to the random media, where it may be scattered an arbitrary number of times before it is re-incident on the target. What is neglected in the above, however, are the fields which are re-incident on the target more than once, and which scatter back-and-forth between the target and random media several times. These terms are neglected because of the first order Taylor series approximation to the matrix inverse.

As with the previous analysis for the point target and electrically large target, the analysis here will again be restricted to the first order terms, or a single interaction with the random media. Under this approximation, (6.25) reduces to the four terms of (6.26).

$$E_s^p \simeq \bar{L}^{(0)} \bar{Z}^{(0)-1} \bar{V}^{(0)} + \bar{L}^{(0)} \bar{Z}^{(0)-1} \bar{V}^{(1)} + \bar{L}^{(1)} \bar{Z}^{(0)-1} \bar{V}^{(0)} - \bar{L}^{(0)} \bar{Z}^{(0)-1} \bar{Z}^{(1)} \bar{Z}^{(0)-1} \bar{V}^{(0)} \quad (6.26)$$

The first term is the coherent or direct return depicted in Figure 6.2a. The second term is the field scattered first by the random media, and then by the target, and this field is again denoted the clutter/target contribution as pictured in Figure 6.2b. Similarly, Figure 6.2c shows the third term, which is scattered first by the target then by the random media, and denoted the target/clutter return. Finally, the last term is that which is scattered by the target, then the random media, and then is re-incident on the target. This target/clutter/target return is pictured in Figure 6.2d. For practical reasons, this final term is difficult to calculate, and if the coupling between the target and

random media is weak, this term will be less significant than the other two incoherent contributions. Hence, the target/clutter/target field is again neglected.

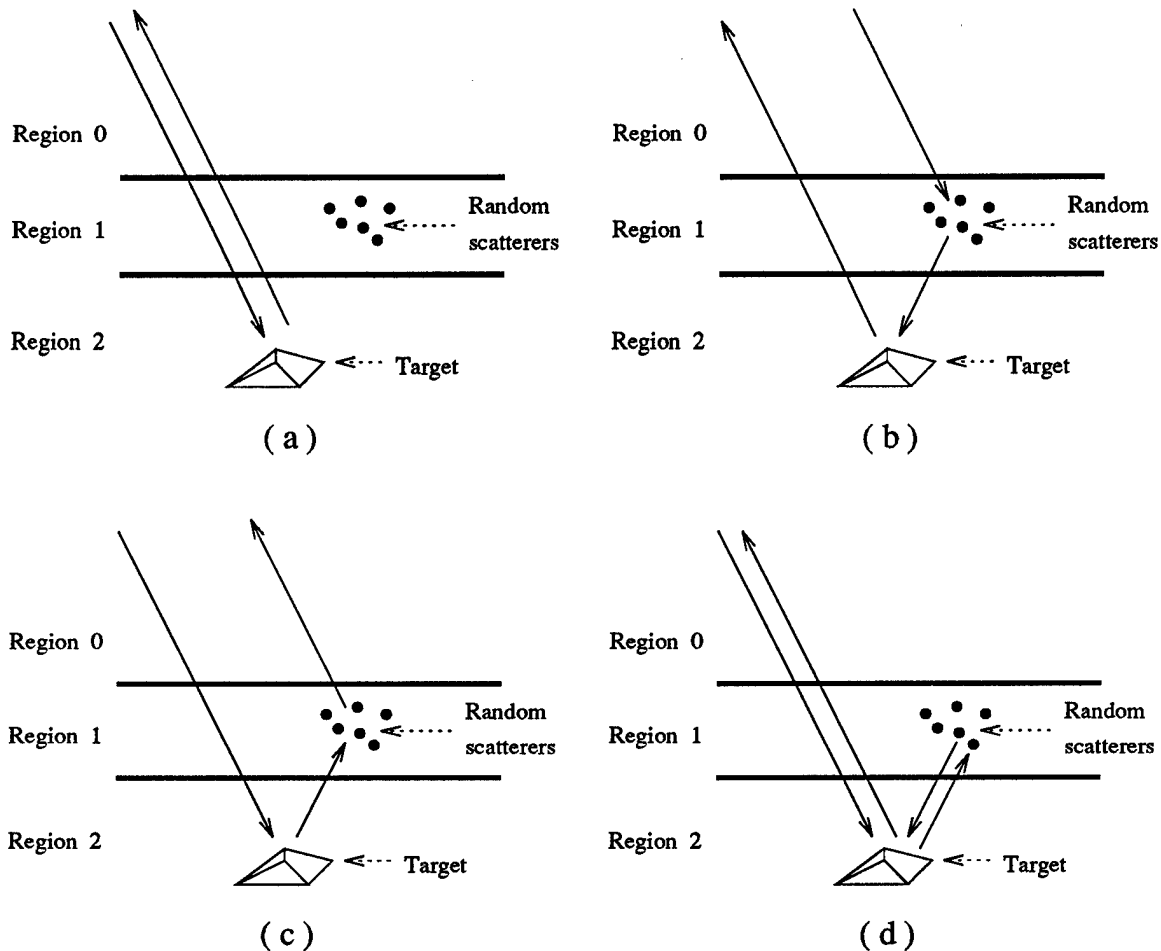


Figure 6.2. Scattering mechanisms for target/clutter interaction including the direct target return (a), clutter/target multi-path (b), target/clutter multi-path (c), and target/clutter/target multi-path (d) returns.

What is desired is again the correlation of the field received at one angle and frequency, with that at another angle and frequency. This correlation is given by (6.27).

$$\begin{aligned}
\sigma^{\hat{p}_a \hat{p}_b} (\bar{k}_{ai}, \bar{k}_{as}, \bar{k}_{bi}, \bar{k}_{bs}) &= 4\pi r^2 \langle E_S^{\hat{p}_a} (\bar{k}_{ai}, \bar{k}_{as}) \cdot E_S^{\hat{p}_b *} (\bar{k}_{bi}, \bar{k}_{bs}) \rangle \\
&= \left| \bar{L}_a^{(0)} \bar{Z}_a^{(0)-1} \bar{V}_a^{(0)} \bar{L}_b^{(0)*} \bar{Z}_b^{(0)-1*} \bar{V}_b^{(0)*} \right| + \\
&\quad \left\langle \bar{L}_a^{(0)} \bar{Z}_a^{(0)-1} \bar{V}_a^{(1)} \bar{L}_b^{(0)*} \bar{Z}_b^{(0)-1*} \bar{V}_b^{(1)*} \right\rangle + \\
&\quad \left\langle \bar{L}_a^{(1)} \bar{Z}_a^{(0)-1} \bar{V}_a^{(0)} \bar{L}_b^{(1)*} \bar{Z}_b^{(0)-1*} \bar{V}_b^{(0)*} \right\rangle + \\
&\quad \left\langle \bar{L}_a^{(0)} \bar{Z}_a^{(0)-1} \bar{V}_a^{(1)} \bar{L}_b^{(1)*} \bar{Z}_b^{(0)-1*} \bar{V}_b^{(0)*} \right\rangle + \\
&\quad \left\langle \bar{L}_a^{(1)} \bar{Z}_a^{(0)-1} \bar{V}_a^{(0)} \bar{L}_b^{(0)*} \bar{Z}_b^{(0)-1*} \bar{V}_b^{(1)*} \right\rangle
\end{aligned} \tag{6.27}$$

To simplify the above, the quantities $I_n^{(0)}$ and $S_m^{(0)}$ are defined as in (6.28) and (6.29).

$$I_n^{(0)} = \sum_m \left[\bar{Z}^{(0)-1} \right]_{mn} V_m^{(0)} \tag{6.28}$$

$$S_n^{(0)} = \sum_m \left[\bar{Z}^{(0)-1} \right]_{mn} L_m^{(0)} \tag{6.29}$$

Hence, (6.27) can be rewritten as (6.30) below.

$$\begin{aligned}
\sigma^{\hat{p}_a \hat{p}_b} &= 4\pi r^2 \left[\sum_n L_{n_a}^{(0)} I_{n_a}^{(0)} \sum_m L_{m_b}^{(0)} I_{m_b}^{(0)} \right] + \\
&\quad 4\pi r^2 \sum_n \sum_m S_{n_a}^{(0)} S_{m_b}^{(0)*} \langle V_{n_a}^{(1)} V_{m_b}^{(1)*} \rangle + S_{n_a}^{(0)} I_{m_b}^{(0)*} \langle V_{n_a}^{(1)} L_{m_b}^{(1)*} \rangle + \\
&\quad I_{n_a}^{(0)} S_{m_b}^{(0)*} \langle L_{n_a}^{(1)} V_{m_b}^{(1)*} \rangle + I_{n_a}^{(0)} I_{m_b}^{(0)*} \langle L_{n_a}^{(1)} L_{m_b}^{(1)*} \rangle
\end{aligned} \tag{6.30}$$

The correlation terms $\langle V_{n_a}^{(1)} V_{n_b}^{(1)*} \rangle$, $\langle V_{n_a}^{(1)} L_{n_b}^{(1)*} \rangle$, etc., which appear in the above are given by (6.31)-(6.34),

$$\begin{aligned} \langle V_{n_a}^{(1)} V_{n_b}^{(1)*} \rangle = & \sum_{\alpha, \beta, \gamma, \rho=x, y, z} \iint_{S_n} d\bar{\tau}_2 \iint_{S_m} d\bar{\tau}_4 \iiint_{V_f} d\bar{\tau}_1 \iiint_{V_f} d\bar{\tau}_3 C_{\alpha\beta\gamma\rho}(\bar{\tau}_1 - \bar{\tau}_3) \times \\ & [\bar{W}_n(\bar{\tau}_2) \cdot \bar{G}_{tf}^a(\bar{\tau}_2, \bar{\tau}_1)]_{\alpha} \cdot [\bar{E}_{fai}^{(0)}(\bar{\tau}_1)]_{\beta} \times \\ & [\bar{W}_m(\bar{\tau}_4) \cdot \bar{G}_{tf}^b(\bar{\tau}_4, \bar{\tau}_3)]_{\gamma}^* \cdot [\bar{E}_{fbi}^{(0)}(\bar{\tau}_3)]_{\rho}^* \end{aligned} \quad (6.31)$$

$$\begin{aligned} \langle V_{n_a}^{(1)} L_{n_b}^{(1)*} \rangle = & -i\omega\mu \sum_{\alpha, \beta, \gamma, \rho=x, y, z} \iint_{S_n} d\bar{\tau}_2 \iint_{S_m} d\bar{\tau}_4 \iiint_{V_f} d\bar{\tau}_1 \iiint_{V_f} d\bar{\tau}_3 C_{\alpha\beta\gamma\rho}(\bar{\tau}_1 - \bar{\tau}_3) \times \\ & [\bar{W}_n(\bar{\tau}_2) \cdot \bar{G}_{tf}^a(\bar{\tau}_2, \bar{\tau}_1)]_{\alpha} \cdot [\bar{E}_{fai}^{(0)}(\bar{\tau}_1)]_{\beta} \times \\ & [\hat{p}_b \cdot \bar{G}_{of}^b(\bar{\tau}, \bar{\tau}_3)]_{\gamma}^* \cdot [\bar{G}_{ft}^b(\bar{\tau}_3, \bar{\tau}_4) \cdot \bar{B}_m(\bar{\tau}_4)]_{\rho}^* \end{aligned} \quad (6.32)$$

$$\begin{aligned} \langle L_{n_a}^{(1)} V_{n_b}^{(1)*} \rangle = & i\omega\mu \sum_{\alpha, \beta, \gamma, \rho=x, y, z} \iint_{S_n} d\bar{\tau}_2 \iint_{S_m} d\bar{\tau}_4 \iiint_{V_f} d\bar{\tau}_1 \iiint_{V_f} d\bar{\tau}_3 C_{\alpha\beta\gamma\rho}(\bar{\tau}_1 - \bar{\tau}_3) \times \\ & [\hat{p}_a \cdot \bar{G}_{of}^a(\bar{\tau}, \bar{\tau}_1)]_{\alpha} \cdot [\bar{G}_{ft}^a(\bar{\tau}_1, \bar{\tau}_2) \cdot \bar{B}_n(\bar{\tau}_2)]_{\beta} \times \\ & [\bar{W}_m(\bar{\tau}_4) \cdot \bar{G}_{tf}^b(\bar{\tau}_4, \bar{\tau}_3)]_{\gamma}^* \cdot [\bar{E}_{fbi}^{(0)}(\bar{\tau}_3)]_{\rho}^* \end{aligned} \quad (6.33)$$

$$\begin{aligned} \langle L_{n_a}^{(1)} L_{n_b}^{(1)*} \rangle = & (\omega\mu)^2 \sum_{\alpha, \beta, \gamma, \rho=x, y, z} \iint_{S_n} d\bar{\tau}_2 \iint_{S_m} d\bar{\tau}_4 \iiint_{V_f} d\bar{\tau}_1 \iiint_{V_f} d\bar{\tau}_3 C_{\alpha\beta\gamma\rho}(\bar{\tau}_1 - \bar{\tau}_3) \times \\ & [\hat{p}_a \cdot \bar{G}_{of}^a(\bar{\tau}, \bar{\tau}_1)]_{\alpha} \cdot [\bar{G}_{ft}^a(\bar{\tau}_1, \bar{\tau}_2) \cdot \bar{B}_n(\bar{\tau}_2)]_{\beta} \times \\ & [\hat{p}_b \cdot \bar{G}_{of}^b(\bar{\tau}, \bar{\tau}_3)]_{\gamma}^* \cdot [\bar{G}_{ft}^b(\bar{\tau}_3, \bar{\tau}_4) \cdot \bar{B}_m(\bar{\tau}_4)]_{\rho}^* \end{aligned} \quad (6.34)$$

where

$$C_{\alpha\beta\gamma\rho}(\bar{r}_1 - \bar{r}_3) = \left\langle [\bar{Q}(\bar{r}_1)]_{\alpha\beta} [\bar{Q}(\bar{r}_3)]_{\gamma\rho}^* \right\rangle \quad (6.35)$$

In the next section, the above formulation is used with a specific set of basis and testing functions to predict the coherent and incoherent signatures of an arbitrary target.

6.2. Triangular Patch Modeling

To treat the problem of scattering from an arbitrary target, a basis function for the current must be chosen which can be fit to an arbitrary surface. One popular technique which has been used previously, is a triangular mesh representation of the target surface employing a bi-triangular subdomain basis function [87] defined over pairs of adjoining triangular patches. The geometry of this bi-triangular configuration is shown in Figure 6.3.

Mathematically, this basis function is given by (6.36),

$$\bar{B}_n(\bar{r}) = \bar{B}_n^+(\bar{r}) + \bar{B}_n^-(\bar{r}) \quad (6.36)$$

where the portions on each of the two patches are as in (6.37) and (6.38).

$$\bar{B}_n^+(\bar{r}) = \begin{cases} (\bar{r} - \bar{r}_{e_n}^+) \frac{\mathcal{L}_n}{2A_n^+} & , \quad \bar{r} \text{ in } T_n^+ \\ 0 & , \quad \text{else} \end{cases} \quad (6.37)$$

$$\bar{B}_n^-(\bar{r}) = \begin{cases} -(\bar{r} - \bar{r}_{e_n}^-) \frac{\mathcal{L}_n}{2A_n^-} & , \quad \bar{r} \text{ in } T_n^- \\ 0 & , \quad \text{else} \end{cases} \quad (6.38)$$

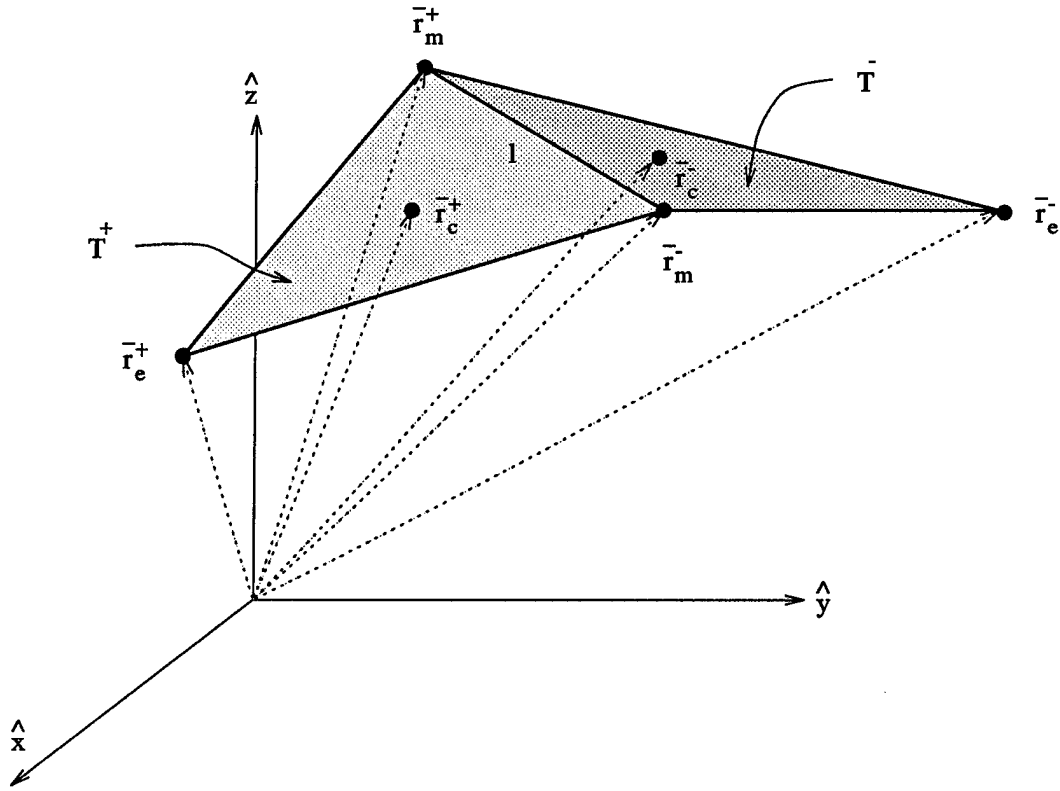


Figure 6.3. Geometry of the bi-triangular subdomain patch, where T^+ and T^- are the two connected triangular regions of the domain, and where r_c^+ and r_c^- are the respective centroids of these regions.

In the above, ℓ_n is the length of the shared edge, and is given by (6.39),

$$\ell_n = |\bar{r}_{m_n}^+ - \bar{r}_{m_n}^-| \quad (6.39)$$

and A_n^+ and A_n^- are the areas of the two triangular regions, and are given by (6.40) and (6.41).

$$A_n^+ = \frac{1}{2} |(\bar{r}_{m_n}^+ - \bar{r}_{e_n}^+) \times (\bar{r}_{m_n}^- - \bar{r}_{e_n}^+)| \quad (6.40)$$

$$A_n^- = \frac{1}{2} \left| (\bar{r}_{m_n}^+ - \bar{r}_{e_n}^-) \times (\bar{r}_{m_n}^- - \bar{r}_{e_n}^-) \right| \quad (6.41)$$

The basis function above is designed such that the current is always directed away from the isolated corner, $\bar{r}_{e_n}^+$, on T_n^+ , and towards the isolated corner, $\bar{r}_{e_n}^-$, on T_n^- . The amplitude of this current goes to zero at these end corners, and reaches a maximum at the center where the two patches meet. In addition, there is no component of current at the patch boundaries which is directed perpendicular to the edge.

The testing procedure which will be employed here, is an averaged point testing, where the integral equation is tested at the center of T_m^+ and T_m^- , and the two resulting equations are averaged. Hence, the testing functions are each in the form of the sum of two impulses, as given by (6.42),

$$\bar{W}_m(\bar{r}) = \bar{W}_m^+(\bar{r}) + \bar{W}_m^-(\bar{r}) \quad (6.42)$$

where

$$\bar{W}_m^+(\bar{r}) = \frac{\bar{r}_{c_m}^+ - \bar{r}_{e_m}^+}{|\bar{r}_{c_m}^+ - \bar{r}_{e_m}^+|} \delta(\bar{r} - \bar{r}_{c_m}^+) \quad (6.43)$$

$$\bar{W}_m^-(\bar{r}) = \frac{-(\bar{r}_{c_m}^- - \bar{r}_{e_m}^-)}{|\bar{r}_{c_m}^- - \bar{r}_{e_m}^-|} \delta(\bar{r} - \bar{r}_{c_m}^-) \quad (6.44)$$

and where the centers of T_m^+ and T_m^- are given by (6.45) and (6.46).

$$\bar{r}_{cm}^+ = \frac{\bar{r}_{em}^+ + \bar{r}_{mm}^+ + \bar{r}_{mm}^-}{3} \quad (6.45)$$

$$\bar{r}_{cm}^- = \frac{\bar{r}_{em}^- + \bar{r}_{mm}^- + \bar{r}_{mm}^+}{3} \quad (6.46)$$

In solving for the target signature, it is first necessary to solve for the coherent part, determining $V_m^{(0)}$, $Z_{mn}^{(0)}$, and $L_n^{(0)}$. The first of these may be obtained by substituting the above testing function into (6.9), yielding (6.47).

$$V_m^{(0)} = - \sum_{a,a'=+,-} a \frac{\bar{r}_{cm}^a - \bar{r}_{em}^a}{|\bar{r}_{cm}^a - \bar{r}_{em}^a|} \cdot \bar{E}_{ti}^{(0)}(\bar{r}_c^a) \quad (6.47)$$

The incident electric field can then be replaced by its representation from Appendix E, yielding the final result of (6.48).

$$V_m^{(0)} = - \sum_{a,a'=+,-} \sum_{s=+,-} \sum_{w=TE,TM} a \frac{\bar{r}_{cm}^a - \bar{r}_{em}^a}{|\bar{r}_{cm}^a - \bar{r}_{em}^a|} \cdot \bar{E}_{ti}^{s,(w)} e^{i\bar{k}_{\perp i} \cdot \bar{r}_{cm}^a} e^{-is k_{tz_i}^{(w)} z_{cm}^a} \quad (6.48)$$

The zeroth order impedance elements are defined by (6.13), and after substituting the above expressions for the testing function, and after utilizing the delta function to perform one of the integrals, the result of (6.49) is obtained.

$$Z_{mn}^{(0)} = i\omega\mu \sum_{a,a'=+,-} \iint_{T_n^a} d\bar{r}' a \left(\frac{\bar{r}_{cm}^a - \bar{r}_{em}^a}{|\bar{r}_{cm}^a - \bar{r}_{em}^a|} \right) \cdot \bar{G}_{tt}(\bar{r}_{cm}^a, \bar{r}') \cdot \bar{B}_n^{a'}(\bar{r}') \quad (6.49)$$

The above expression is the sum of four integrals, each a combination of the two source regions and two observation points. Let each individual integral be defined by (6.50),

$$I_{mn}^{aa'} = i\omega\mu \iint_{T_n^{a'}} d\bar{r}' \hat{w}_m^a \cdot \bar{G}_{tt}(\bar{r}_{cm}^a, \bar{r}') \cdot \bar{B}_n^{a'}(\bar{r}') \quad (6.50)$$

where \hat{w}^a is given by (6.51).

$$\hat{w}^a = a \left(\frac{\bar{r}_{cm}^a - \bar{r}_{em}^a}{|\bar{r}_{cm}^a - \bar{r}_{em}^a|} \right) \quad (6.51)$$

The first case to be considered in evaluating (6.50) is that in which the observation point is not contained on the surface of the source (i.e., $\bar{r}_{cm}^a \notin T_n^{a'}$). It is possible that part of the source region $T_n^{a'}$ will be above the observation point ($z' > z_{cm}^a$), and part below ($z' < z_{cm}^a$). Since the Green's function is different for these two cases, integration must be done over these two regions separately. Let the two regions be denoted $\mathbf{T}_n^{a'}$ and $T_n^{a'} - \mathbf{T}_n^{a'}$ as shown in Figure 6.4. If $z_{cm}^a > z'$ for $T_n^{a'} - \mathbf{T}_n^{a'}$, then the integral of (6.50) will be given by (6.52).

$$\begin{aligned} I_{mn}^{aa'} &= i\omega\mu \iint_{T_n^{a'}} d\bar{r}' \hat{w}_m^a \cdot \bar{G}_{t\cup}(\bar{r}_{cm}^a, \bar{r}') \cdot \bar{B}_n^{a'}(\bar{r}') \\ &\quad + i\omega\mu \iint_{T_n^{a'} - \mathbf{T}_n^{a'}} d\bar{r}' \hat{w}_m^a \cdot [\bar{G}_{t\cap}(\bar{r}_{cm}^a, \bar{r}') - \bar{G}_{t\cup}(\bar{r}_{cm}^a, \bar{r}')] \cdot \bar{B}_n^{a'}(\bar{r}') \\ &= I^> + \mathbf{I}^> \end{aligned} \quad (6.52)$$

Otherwise, if $z_{cm}^a < z'$ for $T_n^{a'} - \mathbf{T}_n^{a'}$, then the integral is given by (6.53).

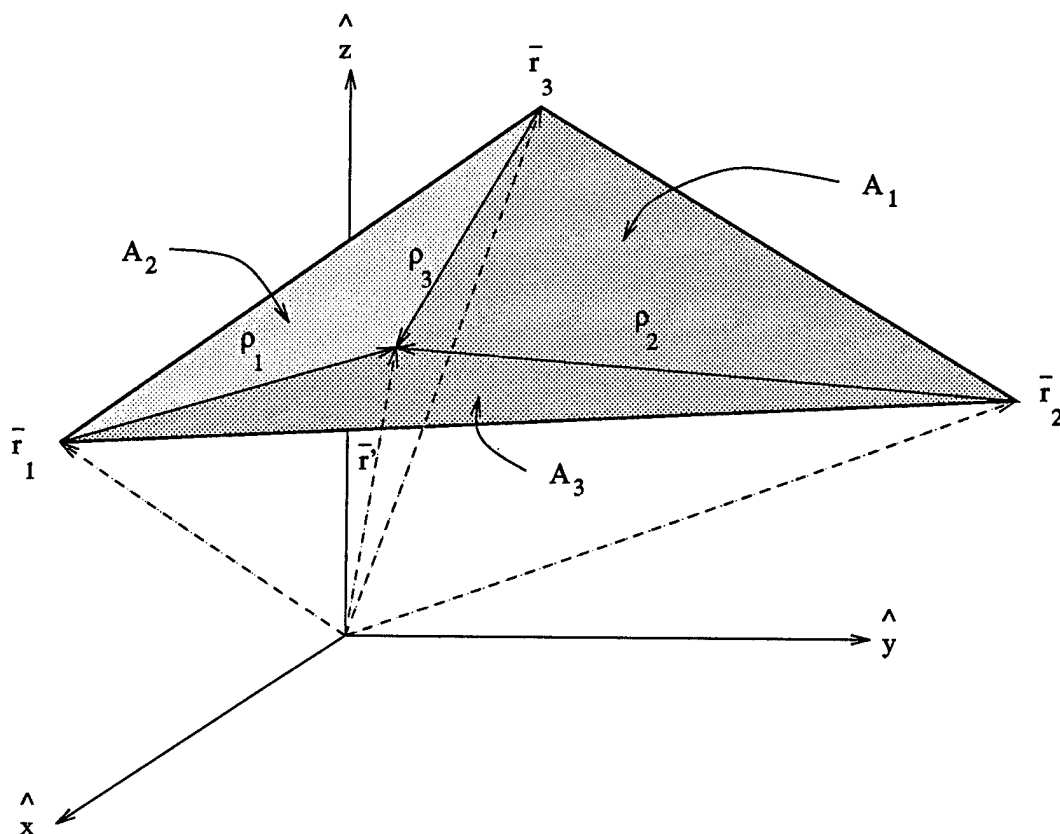


Figure 6.5. Geometry of the subregions for the substitution of variables in the integration of a triangular region. An arbitrary position, \bar{r}' , is expressed as a weighted average of the triangle corners, \bar{r}_1 , \bar{r}_2 , and \bar{r}_3 , where the weights are found from the ratio of the subregion areas, A_1 , A_2 , and A_3 to the overall area of the triangle.

$$\eta = \frac{A_2}{A^a} \quad (6.55)$$

$$\zeta = \frac{A_3}{A^a} \quad (6.56)$$

Each of the integrals can, therefore, be rewritten using the transformation of (6.57).

$$\iint_{T_n^{a'}} d\bar{r}' g(\bar{r}') = 2A^{a'} \int_0^1 d\eta \int_0^{1-\eta} d\xi g(\xi\bar{r}_1 + \eta\bar{r}_2 + (1-\xi-\eta)\bar{r}_3) \quad (6.57)$$

Hence, the four integrals of (6.52) and (6.53) can be rewritten substituting the Green's function expressions of Appendix E, and the basis function expressions of (6.37) and (6.38), to yield (6.58)-(6.61) below.

$$\begin{aligned} I^> &= 2i\omega\mu A_n^{a'} \int_0^1 d\eta \int_0^{1-\eta} d\xi \sum_{\ell,q=+,-} \sum_{v=TE,TM} \iint d\bar{k}_\perp \\ &\quad a' \hat{w}_m^a \cdot \overline{\overline{F}}_{t \cup \iota_q}^{(v)}(\bar{k}_\perp) \cdot \frac{\ell_n}{2A_n^{a'}} [(\xi-1)\bar{r}_{e_n}^{a'} + \eta\bar{r}_{m_n}^{a'} + (1-\xi-\eta)\bar{r}_{m_n}^{a'}] \times \\ &\quad e^{i\bar{k}_\perp \cdot \bar{r}_{e_n}^{a'}} e^{i\ell k_{tz}^{(v)} z_{e_n}^{a'}} \exp \left\{ -i [\bar{k}_\perp + qk_{tz}^{(v)} \hat{z}] \cdot [\xi\bar{r}_{e_n}^{a'} + \eta\bar{r}_{m_n}^{a'} + (1-\xi-\eta)\bar{r}_{m_n}^{a'}] \right\} \end{aligned} \quad (6.58)$$

$$\begin{aligned} I^> &= 2i\omega\mu \mathbf{A}_n^{a'} \int_0^1 d\eta \int_0^{1-\eta} d\xi \sum_{\ell,q=+,-} \sum_{v=TE,TM} \iint d\bar{k}_\perp \\ &\quad a' \hat{w}_m^a \cdot \left[\overline{\overline{F}}_{t \cap \iota_q}^{(v)}(\bar{k}_\perp) - \overline{\overline{F}}_{t \cup \iota_q}^{(v)}(\bar{k}_\perp) \right] \cdot \frac{\ell_n}{2A_n^{a'}} [\xi\bar{r}_{a_n}^{a'} + \eta\bar{r}_{b_n}^{a'} + (1-\xi-\eta)\bar{r}_{c_n}^{a'} - \bar{r}_{e_n}^{a'}] \times \\ &\quad e^{i\bar{k}_\perp \cdot \bar{r}_{e_n}^{a'}} e^{i\ell k_{tz}^{(v)} z_{e_n}^{a'}} \exp \left\{ -i [\bar{k}_\perp + qk_{tz}^{(v)} \hat{z}] \cdot [\xi\bar{r}_{a_n}^{a'} + \eta\bar{r}_{b_n}^{a'} + (1-\xi-\eta)\bar{r}_{c_n}^{a'}] \right\} \end{aligned} \quad (6.59)$$

$$\begin{aligned} I^< &= 2i\omega\mu A_n^{a'} \int_0^1 d\eta \int_0^{1-\eta} d\xi \sum_{\ell,q=+,-} \sum_{v=TE,TM} \iint d\bar{k}_\perp \\ &\quad a' \hat{w}_m^a \cdot \overline{\overline{F}}_{t \cap \iota_q}^{(v)}(\bar{k}_\perp) \cdot \frac{\ell_n}{2A_n^{a'}} [(\xi-1)\bar{r}_{e_n}^{a'} + \eta\bar{r}_{m_n}^{a'} + (1-\xi-\eta)\bar{r}_{m_n}^{a'}] \times \end{aligned}$$

$$e^{i\vec{k}_\perp \cdot \vec{r}_{c\perp m}} e^{i\ell k_{tz}^{(v)} z_{cm}} \exp \left\{ -i \left[\vec{k}_\perp + qk_{tz}^{(v)} \hat{z} \right] \cdot \left[\xi \vec{r}_{en}^{a'} + \eta \vec{r}_{m_n}^{-a'} + (1 - \xi - \eta) \vec{r}_{m_n}^{a'} \right] \right\} \quad (6.60)$$

$$\mathbf{I}^< = -\mathbf{I}^> \quad (6.61)$$

Three types of integrals are contained in the above expressions, and these are denoted I_0 , I_ξ , and I_η as in (6.62)-(6.64).

$$I_0 = \int_0^1 d\eta \int_0^{1-\eta} d\xi e^{-i\phi_\xi \xi} e^{-i\phi_\eta \eta} \quad (6.62)$$

$$I_\xi = \int_0^1 d\eta \int_0^{1-\eta} d\xi \xi e^{-i\phi_\xi \xi} e^{-i\phi_\eta \eta} \quad (6.63)$$

$$I_\eta = \int_0^1 d\eta \int_0^{1-\eta} d\xi \eta e^{-i\phi_\xi \xi} e^{-i\phi_\eta \eta} \quad (6.64)$$

The first of these integrals can be evaluated directly. Performing the inner integral yields (6.65),

$$I_0 = \int_0^1 d\eta \frac{1}{-i\phi_\xi} \left[e^{-i(1-\eta)\phi_\xi} - 1 \right] e^{-i\phi_\eta \eta} \quad (6.65)$$

and performing the outer integral yields (6.66),

$$I_0 = \frac{1}{i\phi_\xi} \left\{ \frac{1 - e^{-i\phi_\xi t a}}{i\phi_\eta} - e^{-i\phi_\xi} \frac{1 - e^{-i(\phi_\eta - \phi_\xi)}}{i(\phi_\eta - \phi_\xi)} \right\} \quad (6.66)$$

which can be rewritten in the final form of (6.67).

$$I_0 = \frac{e^{-i\phi_\eta/2}}{i\phi_\xi} \left\{ \text{sinc}(\phi_\eta/2) - e^{-i\phi_\xi/2} \text{sinc}[(\phi_\eta - \phi_\xi)/2] \right\} \quad (6.67)$$

Similarly, for I_η the inner integral is the same and yields (6.68).

$$I_\eta = \int_0^1 d\eta \frac{\eta}{i\phi_\xi} \left[e^{-i\phi_\eta\eta} - e^{-i\phi_\xi} e^{-i(\phi_\eta - \phi_\xi)\eta} \right] \quad (6.68)$$

The outer integral can be done using integration by parts, with the final result given by (6.69).

$$I_\eta = -\frac{1}{i\phi_\xi} \left\{ \frac{e^{-i\phi_\eta}}{\phi_\eta^2} (1 + i\phi_\eta) - \frac{1}{\phi_\eta^2} - \frac{e^{-i\phi_\xi} e^{-i(\phi_\eta - \phi_\xi)}}{(\phi_\eta - \phi_\xi)^2} [1 + i(\phi_\eta - \phi_\xi)] + \frac{e^{-i\phi_\xi}}{(\phi_\eta - \phi_\xi)^2} \right\} \quad (6.69)$$

Finally, in evaluating I_ξ , the inner integral must be done by parts to yield (6.70),

$$I_\xi = \int_0^1 d\eta \left[\frac{e^{-i\phi_\xi}}{\phi_\xi^2} (1 + i\phi_\xi) e^{-i(\phi_\eta - \phi_\xi)\eta} - \frac{i}{\phi_\xi} e^{-i\phi_\xi} \eta e^{-i(\phi_\eta - \phi_\xi)\eta} + \frac{1}{\phi_\xi^2} e^{-i\phi_\eta\eta} \right] \quad (6.70)$$

the parts of which can then be integrated either directly or by parts to yield the final form of (6.71).

$$\begin{aligned}
I_\xi = & \frac{e^{-i\phi_\xi}}{\phi_\xi^2} \frac{1+i\phi_\xi}{i(\phi_\eta - \phi_\xi)} \left(1 - e^{-i(\phi_\eta - \phi_\xi)}\right) + \frac{e^{-\phi_\xi}}{i\phi_\xi} \frac{1+i(\phi_\eta - \phi_\xi)}{(\phi_\eta - \phi_\xi)^2} e^{-i(\phi_\eta - \phi_\xi)} \\
& - \frac{e^{-i\phi_\xi}}{i\phi_\xi} \frac{1}{(\phi_\eta - \phi_\xi)^2} + \frac{1 - e^{-i\phi_\eta}}{i\phi_\eta \phi_\xi^2}
\end{aligned} \tag{6.71}$$

Hence, for $\bar{r}_{c_m}^a \notin T_n^{a'}$ and with $z_{c_m}^a < z' \in \mathbf{T}_n^{a'}$, the zeroth order impedance elements can be expressed as in (6.72).

$$\begin{aligned}
Z_{mn}^{(0)} = & i\omega\mu \sum_{a,a'=+,-} \sum_{\ell,q=+,-} \sum_{v=TE,TM} \iint d\bar{k}_\perp e^{i\bar{k}_\perp \cdot \bar{r}_{c_m}^a} e^{ik_{tz}^{(v)} z_{c_m}^a} \times \\
& \left\{ e^{-i(\bar{k}_\perp + qk_{tz}^{(v)} \hat{z}) \cdot \bar{r}_{m_n}^{a'}} \times \right. \\
& \left[a' \ell_n \hat{w}_m^a \cdot \bar{\bar{F}}_{t \cup_{\ell q}}^{(v)}(\bar{k}_\perp) \cdot (\bar{r}_{m_n}^{a'} - \bar{r}_{e_n}^{a'}) \times \right. \\
& I_0 \left((\bar{k}_\perp + qk_{tz}^{(v)} \hat{z}) \cdot (\bar{r}_{e_n}^{a'} - \bar{r}_{m_n}^{a'}), (\bar{k}_\perp + qk_{tz}^{(v)} \hat{z}) \cdot (\bar{r}_{m_n}^{-a'} - \bar{r}_{m_n}^{a'}) \right) \\
& + a' \ell_n \hat{w}_m^a \cdot \bar{\bar{F}}_{t \cup_{\ell q}}^{(v)}(\bar{k}_\perp) \cdot (\bar{r}_{m_n}^{-a'} - \bar{r}_{m_n}^{a'}) \times \\
& I_\eta \left((\bar{k}_\perp + qk_{tz}^{(v)} \hat{z}) \cdot (\bar{r}_{e_n}^{a'} - \bar{r}_{m_n}^{a'}), (\bar{k}_\perp + qk_{tz}^{(v)} \hat{z}) \cdot (\bar{r}_{m_n}^{-a'} - \bar{r}_{m_n}^{a'}) \right) \\
& + a' \ell_n \hat{w}_m^a \cdot \bar{\bar{F}}_{t \cup_{\ell q}}^{(v)}(\bar{k}_\perp) \cdot (\bar{r}_{e_n}^{a'} - \bar{r}_{m_n}^{a'}) \times \\
& I_\xi \left((\bar{k}_\perp + qk_{tz}^{(v)} \hat{z}) \cdot (\bar{r}_{e_n}^{a'} - \bar{r}_{m_n}^{a'}), (\bar{k}_\perp + qk_{tz}^{(v)} \hat{z}) \cdot (\bar{r}_{m_n}^{-a'} - \bar{r}_{m_n}^{a'}) \right) \Big] \\
& + e^{-i(\bar{k}_\perp + qk_{tz}^{(v)} \hat{z}) \cdot \bar{r}_{c_n}^{a'}} \times \\
& \left[a' \ell_n \frac{\mathbf{A}_n^{a'}}{A_n^{a'}} \hat{w}_m^a \cdot \left(\bar{\bar{F}}_{t \cup_{\ell q}}^{(v)}(\bar{k}_\perp) - \bar{\bar{F}}_{t \cup_{\ell q}}^{(v)}(\bar{k}_\perp) \right) \cdot (\bar{r}_{c_n}^{a'} - \bar{r}_{e_n}^{a'}) \times \right. \\
& \left. I_0 \left((\bar{k}_\perp + qk_{tz}^{(v)} \hat{z}) \cdot (\bar{r}_{a_n}^{a'} - \bar{r}_{c_n}^{a'}), (\bar{k}_\perp + qk_{tz}^{(v)} \hat{z}) \cdot (\bar{r}_{b_n}^{a'} - \bar{r}_{c_n}^{a'}) \right) \right]
\end{aligned}$$

$$\begin{aligned}
& + a' \ell_n \frac{\mathbf{A}_n^{a'}}{A_n^{a'}} \hat{w}_m^a \cdot \left(\overline{F}_{t \cup \ell_q}^{(v)}(\bar{k}_\perp) - \overline{F}_{t \cap \ell_q}^{(v)}(\bar{k}_\perp) \right) \cdot (\bar{r}_{b_n}^{a'} - \bar{r}_{c_n}^{a'}) \times \\
& \quad I_\eta \left((\bar{k}_\perp + q k_{tz}^{(v)} \hat{z}) \cdot (\bar{r}_{a_n}^{a'} - \bar{r}_{c_n}^{a'}), (\bar{k}_\perp + q k_{tz}^{(v)} \hat{z}) \cdot (\bar{r}_{b_n}^{a'} - \bar{r}_{c_n}^{a'}) \right) \\
& + a' \ell_n \frac{\mathbf{A}_n^{a'}}{A_n^{a'}} \hat{w}_m^a \cdot \left(\overline{F}_{t \cup \ell_q}^{(v)}(\bar{k}_\perp) - \overline{F}_{t \cap \ell_q}^{(v)}(\bar{k}_\perp) \right) \cdot (\bar{r}_{a_n}^{a'} - \bar{r}_{c_n}^{a'}) \times \\
& \quad I_\xi \left((\bar{k}_\perp + q k_{tz}^{(v)} \hat{z}) \cdot (\bar{r}_{a_n}^{a'} - \bar{r}_{c_n}^{a'}), (\bar{k}_\perp + q k_{tz}^{(v)} \hat{z}) \cdot (\bar{r}_{b_n}^{a'} - \bar{r}_{c_n}^{a'}) \right) \Big] \Big\} \quad (6.72)
\end{aligned}$$

In the above, the vectors $\bar{r}_{a_n}^{a'}$, $\bar{r}_{b_n}^{a'}$, and $\bar{r}_{c_n}^{a'}$ are the corners of the smaller triangular region $\mathbf{T}_n^{a'}$. To find these corners, the corners $\bar{r}_{1_n}^{a'}$, $\bar{r}_{2_n}^{a'}$, and $\bar{r}_{3_n}^{a'}$ of the larger triangular region are assigned from the set of $\bar{r}_{e_n}^{a'}$, $\bar{r}_{m_n}^{+}$, and $\bar{r}_{m_n}^{-}$ such that $\bar{r}_{2_n}^{a'}$ is the vertex shared by both $T_n^{a'}$ and $\mathbf{T}_n^{a'}$. The first vector $\bar{r}_{a_n}^{a'}$ is assigned to this corner.

$$\bar{r}_{a_n}^{a'} = \bar{r}_{2_n}^{a'} \quad (6.73)$$

The z-coordinate of the other two vertices, $\bar{r}_{b_n}^{a'}$ and $\bar{r}_{c_n}^{a'}$, will be the same as the z-coordinate of the observation point, $\bar{r}_{c_m}^a$.

$$z_{b_n}^{a'} = z_{c_n}^{a'} = z_{c_m}^a \quad (6.74)$$

On the segment connecting $\bar{r}_{1_n}^{a'}$ and $\bar{r}_{2_n}^{a'}$, \bar{r} is given by (6.75),

$$\bar{r} = \bar{r}_{2_n}^{a'} + t (\bar{r}_{1_n}^{a'} - \bar{r}_{2_n}^{a'}) \quad (6.75)$$

with t an arbitrary parameter, such that at $\bar{r}_{b_n}^{a'}$,

$$z_{b_n}^{a'} = z_{c_m}^a = z_{2_n}^{a'} + t (z_{1_n}^{a'} - z_{2_n}^{a'}) \quad (6.76)$$

or t is given by (6.77).

$$t = \frac{z_{c_m}^a - z_{2_n}^{a'}}{z_{1_n}^{a'} - z_{2_n}^{a'}} \quad (6.77)$$

Therefore, $\bar{r}_{b_n}^{a'}$ is given by (6.78),

$$\bar{r}_{b_n}^{a'} = \bar{r}_{2_n}^{a'} + \frac{z_{c_m}^a - z_{2_n}^{a'}}{z_{1_n}^{a'} - z_{2_n}^{a'}} (\bar{r}_{1_n}^{a'} - \bar{r}_{2_n}^{a'}) \quad (6.78)$$

and in a similar manner, $\bar{r}_{c_n}^{a'}$ can be found to be as given by (6.79).

$$\bar{r}_{c_n}^{a'} = \bar{r}_{2_n}^{a'} + \frac{z_{c_m}^a - z_{2_n}^{a'}}{z_{3_n}^{a'} - z_{2_n}^{a'}} (\bar{r}_{3_n}^{a'} - \bar{r}_{2_n}^{a'}) \quad (6.79)$$

Equation (6.72) above is limited to the case where the observation point, $z_{c_m}^a$, is not contained in the triangular region, $T_n^{a'}$, of the source. If $z_{c_m}^a$ is in the source region, then there is an added term due to the singularity component of the Green's function, and this singularity term is given by (6.80),

$$\begin{aligned} Z_{mn}^{(0)'} &= i\omega\mu \iint_{T_n^{a'}} d\bar{r}' \hat{w}_m^a \cdot \bar{\bar{D}} \delta(\bar{r}_{c_m}^a - \bar{r}') \cdot \bar{B}_n^{a'}(\bar{r}') \\ &= i\omega\mu a' \frac{\ell_n}{2A_n^{a'}} \hat{w}_m^a \cdot \bar{\bar{D}} \cdot (\bar{r}_{c_m}^a - \bar{r}_{e_n}^{a'}) \end{aligned} \quad (6.80)$$

where $\bar{\bar{D}}$ is defined in Appendix E.

Finally, the last zeroth order quantity to be calculated is the zeroth order scattering vector, $L_n^{(0)}$, which is given by (6.81) below.

$$L_n^{(0)} = i\omega\mu \sum_{a'=+,-} \iint_{T_n^{a'}} d\bar{r}' \hat{p} \cdot \bar{G}_{0t}(\bar{r}, \bar{r}') \cdot \bar{B}_n^{a'}(\bar{r}') \quad (6.81)$$

After substituting the far-field Green's function expression of Appendix E, the above can be written as in (6.82),

$$L_n^{(0)} = i\omega\mu \frac{e^{ikr}}{4\pi r} \sum_{a,a'=+,-} \sum_{p=+,-} \sum_{u=TE,TM} \iint_{T_n^{a'}} d\bar{r}' \hat{p} \cdot \bar{H}_{0t_p}^{(u)}(\bar{k}_{\perp,}) \cdot a' \frac{\ell_n}{2A_n^{a'}} (\bar{r}' - \bar{r}_{e_n}^{a'}) e^{-i\bar{k}_{\perp,} \cdot \bar{r}'_{\perp}} e^{-iqk_{tz}^{(u)} z'} \quad (6.82)$$

and using the coordinate system of (6.57) to express the integral, it can be put in the form of (6.83).

$$L_n^{(0)} = i\omega\mu \frac{e^{ikr}}{4\pi r} \sum_{a,a'=+,-} \sum_{p=+,-} \sum_{u=TE,TM} \int_0^1 d\eta \int_0^{1-\eta} d\xi \hat{p} \cdot \bar{H}_{0t_p}^{(u)}(\bar{k}_{\perp,}) \cdot a' \ell_n \left[(\xi - 1) \bar{r}_{e_n}^{a'} + \eta \bar{r}_{m_n}^{-a'} + (1 - \xi - \eta) \bar{r}_{m_n}^{a'} \right] \times \exp \left\{ -i \left[\bar{k}_{\perp,} + pk_{tz}^{(u)} \hat{z} \right] \cdot \left[\xi \bar{r}_{e_n}^{a'} + \eta \bar{r}_{m_n}^{-a'} + (1 - \xi - \eta) \bar{r}_{m_n}^{a'} \right] \right\} \quad (6.83)$$

After performing the integration, the final result is given by (6.84), again in terms of the functions I_0 , I_ξ , and I_η defined earlier.

$$L_n^{(0)} = i\omega\mu \frac{e^{ikr}}{4\pi r} \sum_{a,a'=+,-} \sum_{p=+,-} \sum_{u=TE,TM} e^{-i(\bar{k}_{\perp,} + pk_{tz}^{(u)} \hat{z}) \cdot \bar{r}_{m_n}^{a'}} a' \ell_n \times$$

$$\begin{aligned}
& \left\{ \hat{p} \cdot \overline{H}_{0t_p}^{(u)}(\bar{k}_{\perp}) \cdot (\bar{r}_{m_n}^{a'} - \bar{r}_{e_n}^{a'}) \times \right. \\
& \quad I_0 \left((\bar{k}_{\perp} + pk_{tz}^{(u)} \hat{z}) \cdot (\bar{r}_{e_n}^{a'} - \bar{r}_{m_n}^{a'}), (\bar{k}_{\perp} + pk_{tz}^{(u)} \hat{z}) \cdot (\bar{r}_{m_n}^{-a'} - \bar{r}_{m_n}^{a'}) \right) \\
& \quad + \hat{p} \cdot \overline{H}_{0t_p}^{(u)}(\bar{k}_{\perp}) \cdot (\bar{r}_{m_n}^{-a'} - \bar{r}_{m_n}^{a'}) \times \\
& \quad I_{\eta} \left((\bar{k}_{\perp} + pk_{tz}^{(u)} \hat{z}) \cdot (\bar{r}_{e_n}^{a'} - \bar{r}_{m_n}^{a'}), (\bar{k}_{\perp} + pk_{tz}^{(u)} \hat{z}) \cdot (\bar{r}_{m_n}^{-a'} - \bar{r}_{m_n}^{a'}) \right) \\
& \quad + \hat{p} \cdot \overline{H}_{0t_p}^{(u)}(\bar{k}_{\perp}) \cdot (\bar{r}_{e_n}^{a'} - \bar{r}_{m_n}^{a'}) \times \\
& \quad \left. I_{\xi} \left((\bar{k}_{\perp} + pk_{tz}^{(u)} \hat{z}) \cdot (\bar{r}_{e_n}^{a'} - \bar{r}_{m_n}^{a'}), (\bar{k}_{\perp} + pk_{tz}^{(u)} \hat{z}) \cdot (\bar{r}_{m_n}^{-a'} - \bar{r}_{m_n}^{a'}) \right) \right\} \\
& \hspace{15em} (6.84)
\end{aligned}$$

What remains to be evaluated is the incoherent terms of (6.31)-(6.34). After substituting the Green's function and Electric field expressions from Appendix E, the first of these terms, $\langle V_{n_a}^{(1)} V_{m_b}^{(1)*} \rangle$, is given by (6.85).

$$\begin{aligned}
\langle V_{n_a}^{(1)} V_{m_b}^{(1)*} \rangle = & \sum_{a,a'=+,-} \sum_{s',q',\ell'=+,-} \sum_{v',w'=TE,TM} \sum_{\alpha,\beta,\gamma,\rho=x,y,z} \\
& \int \int_{S_n} d\bar{r}_2 \int \int_{S_m} d\bar{r}_4 \int \int \int d\bar{r}_1 \int \int \int d\bar{r}_3 \int \int d\bar{k}_{\perp a} \int \int d\bar{k}_{\perp b} C_{\alpha\beta\gamma\rho} (\bar{r}_1 - \bar{r}_3) \times \\
& \left[\hat{w}_n^a \delta(\bar{r}_2 - \bar{r}_{c_n}^a) \cdot \overline{F}_{tf_{\ell_q}}^{(v)}(\bar{k}_{\perp a}) \right]_{\alpha} \cdot \left[\overline{E}_{f_{ai}}^{s,(w)} \right]_{\beta} \times \\
& \left[\hat{w}_m^{a'} \delta(\bar{r}_4 - \bar{r}_{c_m}^{a'}) \cdot \overline{F}_{tf_{\ell_{q'}}}^{(v')}(\bar{k}_{\perp b}) \right]_{\gamma}^* \cdot \left[\overline{E}_{t_{bi}}^{s',(w')} \right]_{\rho}^* \times \\
& e^{i\bar{k}_{\perp a} \cdot \bar{r}_{2\perp}} e^{-i\bar{k}_{\perp a} \cdot \bar{r}_{1\perp}} e^{i\ell k_{tz a}^{(v)} z_2} e^{-iq k_{fz a}^{(v)} z_1} e^{i\bar{k}_{\perp a i} \cdot \bar{r}_{1\perp}} e^{-isk_{fz ai}^{(w)} z_1} \times \\
& e^{-i\bar{k}_{\perp b} \cdot \bar{r}_{4\perp}} e^{-i\bar{k}_{\perp b} \cdot \bar{r}_{3\perp}} e^{-\ell' k_{tz b}^{(v')} z_4} e^{iq' k_{fz b}^{(v')} z_3} e^{-i\bar{k}_{\perp bi} \cdot \bar{r}_{3\perp}} e^{is' k_{fz bi}^{(w')} z_3} \\
& \hspace{15em} (6.85)
\end{aligned}$$

Applying a change of variables to the z_1 and z_3 integrals, and expressing the correlation function as the Fourier transform of its associated spectral function, the above

can be rewritten as in (6.86),

$$\begin{aligned}
\langle V_{n_a}^{(1)} V_{m_b}^{(1)*} \rangle = & \sum_{a,a'=+,-} \sum_{s',q',\ell'=+,-}^{\substack{s,q,\ell, \\ s',q',\ell'=+,-}} \sum_{v',w'=TE,TM}^{\substack{v,w, \\ v',w'=TE,TM}} \sum_{\alpha,\beta,\gamma,\rho=x,y,z} \iint_{S_n} d\bar{r}_2 \iint_{S_m} d\bar{r}_4 \int_{-h_f}^0 dz_1 \int_{-h_f}^0 dz_3 \\
& \iint d\bar{r}_{1\perp} \iint d\bar{r}_{3\perp} \iint d\bar{k}_{\perp a} \iint d\bar{k}_{\perp b} \iint d\bar{\beta}_{\perp} \iint d\beta_z \\
& \delta(\bar{r}_2 - \bar{r}_{c_n}^a) \delta(\bar{r}_4 - \bar{r}_{c_m}^{a'}) \times \\
& \Lambda_{V-V}^{\substack{\alpha\beta\gamma\rho \\ aa'ss'qq'\ell\ell' \\ vv'ww'}} \Phi_{\alpha\beta\gamma\rho}(\bar{\beta}) e^{i(qk_{fza}^{(v)} + sk_{fza}^{(w)} - q'k_{fzb}^{(v')*} - s'k_{fzb}^{(w')*})d_f - 1} \times \\
& e^{i(\bar{k}_{\perp ai} - \bar{k}_{\perp a} - \bar{\beta}_{\perp}) \cdot \bar{r}_{1\perp}} e^{i\bar{k}_{\perp a} \cdot \bar{r}_{2\perp}} e^{i(\bar{k}_{\perp b} - \bar{k}_{\perp bi} + \bar{\beta}_{\perp}) \cdot \bar{r}_{3\perp}} e^{-i\bar{k}_{\perp b} \cdot \bar{r}_{4\perp}} \times \\
& e^{-i(qk_{fza}^{(v)} + sk_{fza}^{(w)} + \beta_z)z_1} e^{ik_{fza}^{(v)}z_2} e^{i(q'k_{fzb}^{(v')*} + s'k_{fzb}^{(w')*} + \beta_z)z_3} e^{-il'k_{fzb}^{(v')*}z_4} \quad (6.86)
\end{aligned}$$

where

$$\begin{aligned}
\Lambda_{V-V}^{\substack{\alpha\beta\gamma\rho \\ aa'ss'qq'\ell\ell' \\ vv'ww'}} = & \left[\hat{w}_n^a \cdot \bar{F}_{tf\ell q}^{(v)}(\bar{k}_{\perp a}) \right]_{\alpha} \cdot \left[\bar{E}_{tai}^{s,(w)} \right]_{\beta} \times \\
& \left[\hat{w}_m^{a'} \cdot \bar{F}_{tf\ell'q'}^{(v')}(\bar{k}_{\perp b}) \right]_{\gamma}^* \cdot \left[\bar{E}_{tbi}^{s',(w')} \right]_{\rho}^* \quad (6.87)
\end{aligned}$$

The \bar{r}_2 and \bar{r}_4 integrals can be done trivially, and the $\bar{r}_{1\perp}$ integral can be done to produce another delta function.

$$\langle V_{n_a}^{(1)} V_{m_b}^{(1)*} \rangle = \sum_{a,a'=+,-} \sum_{s',q',\ell'=+,-}^{\substack{s,q,\ell, \\ s',q',\ell'=+,-}} \sum_{v',w'=TE,TM}^{\substack{v,w, \\ v',w'=TE,TM}} \sum_{\alpha,\beta,\gamma,\rho=x,y,z}$$

$$\begin{aligned}
& \int_{-h_f}^0 dz_1 \int_{-h_f}^0 dz_3 \iint d\bar{\tau}_{3\perp} \iint d\bar{k}_{\perp a} \iint d\bar{k}_{\perp b} \iint d\bar{\beta}_{\perp} \iint d\beta_z \\
& (2\pi)^2 \Lambda_{V-\bar{V}}^{\alpha\beta\gamma\rho} \Phi_{\alpha\beta\gamma\rho}(\bar{\beta}) \delta(\bar{k}_{\perp ai} - \bar{k}_{\perp a} - \bar{\beta}_{\perp}) \times \\
& e^{i\bar{k}_{\perp a} \cdot \bar{\tau}_{c\perp n}^a} e^{-i\bar{k}_{\perp b} \cdot \bar{\tau}_{c\perp m}^a} e^{i\ell k_{iz_a}^{(v)} z_{cn}^a} e^{-i\ell' k_{iz_b}^{(v')}^* z_{cm}^a} e^{i(\bar{k}_{\perp b} - \bar{k}_{\perp bi} + \bar{\beta}_{\perp}) \cdot \bar{\tau}_{3\perp}} \times \\
& e^{i(qk_{fz_a}^{(v)} + sk_{fz_{ai}}^{(w)} - q'k_{fz_b}^{(v')}^* - s'k_{fz_{bi}}^{(w')})d_{f-1}} \times \\
& e^{-i(qk_{fz_a}^{(v)} + sk_{fz_{ai}}^{(w)} + \beta_z)z_1} e^{i(q'k_{fz_b}^{(v')}^* + s'k_{fz_{bi}}^{(w')} + \beta_z)z_3}
\end{aligned} \tag{6.88}$$

The delta function can be used to perform the $\bar{\beta}_{\perp}$ integral and obtain (6.89).

$$\begin{aligned}
\langle V_{n_a}^{(1)} V_{m_b}^{(1)*} \rangle &= \sum_{a,a'=+,-} \sum_{s',q',\ell'=+,-}^{\substack{s,q,\ell, \\ \alpha\beta\gamma\rho}} \sum_{v',w'=TE,TM}^{\substack{v,w, \\ \alpha\beta\gamma\rho}} \sum_{\alpha,\beta,\gamma,\rho=x,y,z} \\
& \int_{-h_f}^0 dz_1 \int_{-h_f}^0 dz_3 \iint d\bar{\tau}_{3\perp} \iint d\bar{k}_{\perp a} \iint d\bar{k}_{\perp b} \iint d\beta_z \\
& (2\pi)^2 \Lambda_{V-\bar{V}}^{\alpha\beta\gamma\rho} \Phi_{\alpha\beta\gamma\rho}(\bar{k}_{\perp ai} - \bar{k}_{\perp a}, \beta_z) e^{i\bar{k}_{\perp a} \cdot \bar{\tau}_{c\perp n}^a} e^{-i\bar{k}_{\perp b} \cdot \bar{\tau}_{c\perp m}^a} \times \\
& e^{i\ell k_{iz_a}^{(v)} z_{cn}^a} e^{-i\ell' k_{iz_b}^{(v')}^* z_{cm}^a} e^{i(qk_{fz_a}^{(v)} + sk_{fz_{ai}}^{(w)} - q'k_{fz_b}^{(v')}^* - s'k_{fz_{bi}}^{(w')})d_{f-1}} \times \\
& e^{i(\bar{k}_{\perp b} - \bar{k}_{\perp bi} + \bar{k}_{\perp ai} - \bar{k}_{\perp a}) \cdot \bar{\tau}_{3\perp}} e^{-i(qk_{fz_a}^{(v)} + sk_{fz_{ai}}^{(w)} + \beta_z)z_1} e^{i(q'k_{fz_b}^{(v')}^* + s'k_{fz_{bi}}^{(w')} + \beta_z)z_3}
\end{aligned} \tag{6.89}$$

Similarly, the $\bar{\tau}_{3\perp}$ integral can be evaluated to obtain another delta function, and that can be used to evaluate the $\bar{k}_{\perp b}$ integral. The result is given by (6.90),

$$\langle V_{n_a}^{(1)} V_{m_b}^{(1)*} \rangle = \sum_{a,a'=+,-} \sum_{s',q',\ell'=+,-}^{\substack{s,q,\ell, \\ \alpha\beta\gamma\rho}} \sum_{v',w'=TE,TM}^{\substack{v,w, \\ \alpha\beta\gamma\rho}} \sum_{\alpha,\beta,\gamma,\rho=x,y,z}$$

$$\begin{aligned}
& \int_{-h_f}^0 dz_1 \int_{-h_f}^0 dz_3 \iint d\bar{k}_{\perp a} \iint d\beta_z \\
& (2\pi)^4 \Lambda_{V-\bar{V}}^{\alpha\beta\gamma\rho}{}_{aa's's'qq'ell'} \Phi_{\alpha\beta\gamma\rho}(\bar{k}_{\perp ai} - \bar{k}_{\perp a}, \beta_z) e^{i\bar{k}_{\perp a} \cdot \bar{r}_{c\perp n}^a} e^{-i\bar{k}_{\perp c} \cdot \bar{r}_{c\perp m}^{a'}} \times \\
& e^{i\ell k_{iz_a}^{(v)} z_{c_n}^a} e^{-i\ell' k_{iz_c}^{(v')}^* z_{c_m}^{a'}} e^{i(qk_{fz_a}^{(v)} + sk_{fz_{ai}}^{(w)} - q'k_{fz_c}^{(v')}^* - s'k_{fz_{bi}}^{(w')})d_{f-1}} \times \\
& e^{-i(qk_{fz_a}^{(v)} + sk_{fz_{ai}}^{(w)} + \beta_z)z_1} e^{i(q'k_{fz_c}^{(v')}^* + s'k_{fz_{bi}}^{(w')})^* + \beta_z)z_3}
\end{aligned} \tag{6.90}$$

where $\bar{k}_{\perp c}$ is given by (6.91).

$$\bar{k}_{\perp c} = \bar{k}_{\perp bi} - \bar{k}_{\perp ai} + \bar{k}_{\perp a} \tag{6.91}$$

The z_1 and z_3 integrals can be performed directly to obtain (6.92).

$$\begin{aligned}
\langle V_{n_a}^{(1)} V_{m_b}^{(1)*} \rangle &= \sum_{a,a'=+,-} \sum_{s,q,\ell,} \sum_{s',q',\ell'=+,-} \sum_{v',w'=TE,TM} \sum_{\alpha,\beta,\gamma,\rho=x,y,z} \\
& \iint d\bar{k}_{\perp a} \iint d\beta_z (2\pi)^4 \Lambda_{V-\bar{V}}^{\alpha\beta\gamma\rho}{}_{aa's's'qq'ell'} \Phi_{\alpha\beta\gamma\rho}(\bar{k}_{\perp ai} - \bar{k}_{\perp a}, \beta_z) e^{i\bar{k}_{\perp a} \cdot \bar{r}_{c\perp n}^a} \times \\
& e^{-i\bar{k}_{\perp c} \cdot \bar{r}_{c\perp m}^{a'}} e^{i\ell k_{iz_a}^{(v)} z_{c_n}^a} e^{-i\ell' k_{iz_c}^{(v')}^* z_{c_m}^{a'}} e^{i(qk_{fz_a}^{(v)} + sk_{fz_{ai}}^{(w)} - q'k_{fz_c}^{(v')}^* - s'k_{fz_{bi}}^{(w')})d_{f-1}} \times \\
& \frac{1 - e^{i(qk_{fz_a}^{(v)} + sk_{fz_{ai}}^{(w)} + \beta_z)h_f}}{qk_{fz_a}^{(v)} + sk_{fz_{ai}}^{(w)} + \beta_z} \cdot \frac{1 - e^{i(q'k_{fz_c}^{(v')}^* + s'k_{fz_{bi}}^{(w')})^* + \beta_z)h_f}}{q'k_{fz_c}^{(v')}^* + s'k_{fz_{bi}}^{(w')})^* + \beta_z}
\end{aligned} \tag{6.92}$$

Finally, the β_z integral can be done using complex residue theory, splitting the integrand into portions convergent in the upper and lower complex β_z plane, closing the contour upwards and downwards in these two cases respectively, and summing the pole contributions. Only the effects of the two principal poles in the last line of (6.92) will

be considered, and the poles of the correlation function are neglected. The final result is given by (6.93).

$$\begin{aligned}
 \langle V_{n_a}^{(1)} V_{m_b}^{(1)*} \rangle &= (2\pi)^5 i \sum_{a,a'=+,-} \sum_{s,q,\ell, s',q',\ell'=+,-} \sum_{v,w, v',w'=TE,TM} \sum_{\alpha,\beta,\gamma,\rho=x,y,z} \iint d\bar{k}_{\perp a} \Lambda_{V-V}^{\alpha\beta\gamma\rho, aa'ss'qq'\ell\ell', vv'ww'} \times \\
 &e^{i\bar{k}_{\perp a} \cdot \bar{r}_{c\perp n}} e^{-i\bar{k}_{\perp c} \cdot \bar{r}_{c\perp m}} e^{i\ell k_{tza} z_{cn}^a} e^{-i\ell' k_{tzc} z_{cm}^{a'}} \times \\
 &e^{i(qk_{fza}^{(v)} + sk_{fzai}^{(w)} - q'k_{fzc}^{(v')*} - s'k_{fzbi}^{(w')*})d_{f-1}} \times \\
 &\left[\frac{\Phi_{\alpha\beta\gamma\rho} (\bar{k}_{\perp ai} - \bar{k}_{\perp a}, -q'k_{fzc}^{(v')*} - s'k_{fzbi}^{(w')*})}{qk_{fza}^{(v)} + sk_{fzai}^{(w)} - q'k_{fzc}^{(v')*} - s'k_{fzbi}^{(w')*}} \right. \\
 &\quad - \frac{\Phi_{\alpha\beta\gamma\rho} (\bar{k}_{\perp ai} - \bar{k}_{\perp a}, -qk_{fza}^{(v)} - sk_{fzai}^{(w)})}{qk_{fza}^{(v)} + sk_{fzai}^{(w)} - q'k_{fzc}^{(v')*} - s'k_{fzbi}^{(w')*}} \times \\
 &\quad \left. e^{i(qk_{fza}^{(v)} + sk_{fzai}^{(w)} - q'k_{fzc}^{(v')*} - s'k_{fzbi}^{(w')*})h_f} \right] \quad (6.93)
 \end{aligned}$$

The second incoherent term to be computed is that of (6.32), which after rewriting using the expressions of Appendix E is given by (6.94).

$$\begin{aligned}
 \langle V_{n_a}^{(1)} L_{m_b}^{(1)*} \rangle &= -i\omega\mu \frac{e^{-ikr}}{4\pi r} \sum_{a,a'=+,-} \sum_{p,q,\ell, p',q',\ell'=+,-} \sum_{u,v, u',v'=TE,TM} \sum_{\alpha,\beta,\gamma,\rho=x,y,z} \\
 &\iint_{S_n} d\bar{r}_2 \iint_{S_m} d\bar{r}_4 \iiint_{V_f} d\bar{r}_1 \iiint_{V_f} d\bar{r}_3 \iint d\bar{k}_{\perp a} \iint d\bar{k}_{\perp b} \\
 &C_{\alpha\beta\gamma\rho} (\bar{r}_1 - \bar{r}_3) \left[\hat{w}_n^a \delta(\bar{r}_2 - \bar{r}_{cn}^a) \cdot \bar{F}_{tf\ell q}^{(v)}(\bar{k}_{\perp a}) \right]_{\alpha} \cdot \left[\bar{E}_{tai}^{s,(w)} \right]_{\beta} \times \\
 &\left[\hat{p}_b \cdot \bar{H}_{0fp'}^{(u')}(\bar{k}_{\perp b,s}) \right]_{\gamma}^* \cdot \left[\bar{F}_{ft\ell'q'}^{(v')}(\bar{k}_{\perp b}) \cdot (\bar{r}_4 - \bar{r}_{em}^{a'}) \frac{a'\ell_m}{2A_m'} \right]_{\rho}^* \times \\
 &e^{i\bar{k}_{\perp a} \cdot \bar{r}_{2\perp}} e^{-i\bar{k}_{\perp a} \cdot \bar{r}_{1\perp}} e^{i\ell k_{tza} z_2} e^{-iqk_{fza}^{(v)} z_1} e^{i\bar{k}_{\perp ai} \cdot \bar{r}_{1\perp}} e^{-isk_{fzai}^{(w)} z_1} \times \\
 &e^{i\bar{k}_{\perp bs} \cdot \bar{r}_{3\perp}} e^{ip'k_{fzbs}^{(u')} z_3} e^{-i\bar{k}_{\perp b} \cdot \bar{r}_{3\perp}} e^{i\bar{k}_{\perp b} \cdot \bar{r}_{4\perp}} e^{-i\ell' k_{fzb}^{(v')} z_3} e^{iq'k_{tzb}^{(v')} z_4} \quad (6.94)
 \end{aligned}$$

A variable transformation is applied to z_1 and z_3 , such that the new upper limits of each integral are both zero. In addition, the correlation function is replaced by the Fourier transform of its spectral function. The result of these changes is (6.95) below,

$$\begin{aligned}
 \langle V_{n_a}^{(1)} L_{m_b}^{(1)*} \rangle = & \sum_{a,a'=+,-} \sum_{\substack{s,q,\ell, \\ p',q',\ell'=+,-}} \sum_{\substack{v,w, \\ u',v'=TE,TM}} \sum_{\alpha,\beta,\gamma,\rho=x,y,z} \iint_{S_n} d\bar{\tau}_2 \iint_{S_m} d\bar{\tau}_4 \int_{-h_f}^0 dz_1 \int_{-h_f}^0 dz_3 \\
 & \iint d\bar{\tau}_{1\perp} \iint d\bar{\tau}_{3\perp} \iint d\bar{k}_{\perp a} \iint d\bar{k}_{\perp b} \iint d\bar{\beta}_{\perp} \int d\beta_z \Phi_{\alpha\beta\gamma\rho}(\bar{\beta}) \times \\
 & \Lambda_{V-L}^{\alpha\beta\gamma\rho} \left(\bar{\tau}_4 - \bar{\tau}_{e_m}^{a'} \right) e^{i(qk_{fz_a}^{(v)} + sk_{fz_{ai}}^{(w)} - p'k_{fz_{bs}}^{(u')*} + \ell'k_{fz_b}^{(v')*})d_{f-1}} \times \\
 & \delta(\bar{\tau}_2 - \bar{\tau}_{c_n}^a) e^{i(\bar{k}_{\perp ai} - \bar{k}_{\perp a} - \bar{\beta}_{\perp}) \cdot \bar{\tau}_{1\perp}} e^{i\bar{k}_{\perp a} \cdot \bar{\tau}_{2\perp}} e^{i(\bar{k}_{\perp bs} - \bar{k}_{\perp b} + \bar{\beta}_{\perp}) \cdot \bar{\tau}_{3\perp}} e^{i\bar{k}_{\perp b} \cdot \bar{\tau}_{4\perp}} \times \\
 & e^{-i(qk_{fz_a}^{(v)} + sk_{fz_{ai}}^{(w)} + \beta_z)z_1} e^{ik_{fz_{ai}}^{(v)}z_2} e^{i(p'k_{fz_{bs}}^{(u')*} - \ell'k_{fz_b}^{(v')*} + \beta_z)z_3} e^{iq'k_{fz_b}^{(v')*}z_4} \quad (6.95)
 \end{aligned}$$

where Λ_{V-L} is given by (6.96).

$$\begin{aligned}
 \Lambda_{V-L}^{\alpha\beta\gamma\rho} \left(\bar{\tau} \right) = & -i\omega\mu \frac{e^{-ikr}}{4\pi r} \left[\hat{w}_n^a \cdot \bar{F}_{tf_{tq}}^{(v)}(\bar{k}_{\perp a}) \right]_{\alpha} \cdot \left[\bar{E}_{f_{ai}}^{s,(w)} \right]_{\beta} \times \\
 & \left[\hat{p}_b \cdot \bar{H}_{0f_{p'}}^{(u')}(\bar{k}_{\perp bs}) \right]_{\gamma}^* \cdot \left[\bar{F}_{ft_{t'q'}}^{(v')}(\bar{k}_{\perp b}) \cdot (\bar{\tau}) \frac{a'\ell_m}{2A_m^{a'}} \right]_{\rho}^* \quad (6.96)
 \end{aligned}$$

The $\bar{\tau}_2$ integral can be performed trivially, and the $\bar{\tau}_{1\perp}$ integration can be done to obtain another delta function.

$$\langle V_{n_a}^{(1)} L_{m_b}^{(1)*} \rangle = \sum_{a,a'=+,-} \sum_{\substack{s,q,\ell, \\ p',q',\ell'=+,-}} \sum_{\substack{v,w, \\ u',v'=TE,TM}} \sum_{\alpha,\beta,\gamma,\rho=x,y,z} \iint_{S_m} d\bar{\tau}_4 \int_{-h_f}^0 dz_1 \int_{-h_f}^0 dz_3$$

$$\begin{aligned}
& \iint d\bar{\tau}_{3\perp} \iint d\bar{k}_{\perp a} \iint d\bar{k}_{\perp b} \iint d\bar{\beta}_{\perp} \int d\beta_z (2\pi)^2 \Phi_{\alpha\beta\gamma\rho}(\bar{\beta}) \times \\
& \Lambda_{V-L}^{\alpha\beta\gamma\rho}{}_{aa'p'sqq'\ell\ell'}{}_{u'vv'w} \left(\bar{\tau}_4 - \bar{\tau}_{em}^{a'} \right) \delta \left(\bar{k}_{\perp ai} - \bar{k}_{\perp a} - \bar{\beta}_{\perp} \right) \times \\
& e^{i(qk_{fa}^{(v)} + sk_{fa}^{(w)} - p'k_{fb}^{(u')})^* + \ell'k_{fb}^{(v')})d_{f-1}} \times \\
& e^{i\bar{k}_{\perp a} \cdot \bar{\tau}_{cn}^a} e^{i\ell k_{za}^{(v)} z_{cn}^a} e^{i(\bar{k}_{\perp bs} - \bar{k}_{\perp b} + \bar{\beta}_{\perp}) \cdot \bar{\tau}_{3\perp}} e^{i\bar{k}_{\perp b} \cdot \bar{\tau}_{4\perp}} \times \\
& e^{-i(qk_{fa}^{(v)} + sk_{fa}^{(w)} + \beta_z)z_1} e^{i(p'k_{fb}^{(u')})^* - \ell'k_{fb}^{(v')})^* + \beta_z)z_3} e^{iq'k_{ib}^{(v')})^* z_4} \quad (6.97)
\end{aligned}$$

Using the resulting delta function, the $\bar{\beta}_{\perp}$ integration can be done to yield (6.98).

$$\begin{aligned}
\langle V_{na}^{(1)} L_{mb}^{(1)*} \rangle &= \sum_{a,a'=+,-} \sum_{\substack{s,q,\ell, \\ p',q',\ell'=+,-}} \sum_{\substack{v,w, \\ u',v'=TE,TM}} \sum_{\alpha,\beta,\gamma,\rho=x,y,z} \iint_{S_m} d\bar{\tau}_4 \int_{-h_f}^0 dz_1 \int_{-h_f}^0 dz_3 \\
& \iint d\bar{\tau}_{3\perp} \iint d\bar{k}_{\perp a} \iint d\bar{k}_{\perp b} \int d\beta_z (2\pi)^2 \Phi_{\alpha\beta\gamma\rho}(\bar{k}_{\perp ai} - \bar{k}_{\perp a}, \beta_z) \times \\
& \Lambda_{V-L}^{\alpha\beta\gamma\rho}{}_{aa'p'sqq'\ell\ell'}{}_{u'vv'w} \left(\bar{\tau}_4 - \bar{\tau}_{em}^{a'} \right) e^{i(qk_{fa}^{(v)} + sk_{fa}^{(w)} - p'k_{fb}^{(u')})^* + \ell'k_{fb}^{(v')})d_{f-1}} \times \\
& e^{i\bar{k}_{\perp a} \cdot \bar{\tau}_{cn}^a} e^{i\ell k_{za}^{(v)} z_{cn}^a} e^{i(\bar{k}_{\perp bs} - \bar{k}_{\perp b} + \bar{k}_{\perp ai} - \bar{k}_{\perp a}) \cdot \bar{\tau}_{3\perp}} e^{i\bar{k}_{\perp b} \cdot \bar{\tau}_{4\perp}} \times \\
& e^{-i(qk_{fa}^{(v)} + sk_{fa}^{(w)} + \beta_z)z_1} e^{i(p'k_{fb}^{(u')})^* - \ell'k_{fb}^{(v')})^* + \beta_z)z_3} e^{iq'k_{ib}^{(v')})^* z_4} \quad (6.98)
\end{aligned}$$

Similarly, the $\bar{\tau}_{3\perp}$ integral can be done to obtain a delta function which enables evaluation of the $\bar{k}_{\perp b}$ integral. The result is (6.99),

$$\langle V_{na}^{(1)} L_{mb}^{(1)*} \rangle = \sum_{a,a'=+,-} \sum_{\substack{s,q,\ell, \\ p',q',\ell'=+,-}} \sum_{\substack{v,w, \\ u',v'=TE,TM}} \sum_{\alpha,\beta,\gamma,\rho=x,y,z} \iint_{S_m} d\bar{\tau}_4 \int_{-h_f}^0 dz_1 \int_{-h_f}^0 dz_3$$

$$\begin{aligned}
& \iint d\bar{k}_{\perp a} \int d\beta_z (2\pi)^4 \Lambda_{V-L}^{\alpha\beta\gamma\rho} \Lambda_{V-L}^{\alpha a' p' s q q' \ell \ell'} \left(\bar{r}_4 - \bar{r}_{em}^{a'} \right) \Phi_{\alpha\beta\gamma\rho} \left(\bar{k}_{\perp ai} - \bar{k}_{\perp a}, \beta_z \right) \times \\
& e^{i(qk_{fz_a}^{(v)} + sk_{fz_{ai}}^{(w)} - p'k_{fz_{bs}}^{(u')*} + \ell'k_{fz_c}^{(v')*})d_{f-1}} e^{i\bar{k}_{\perp a} \cdot \bar{r}_{c\perp n}^a} e^{i\ell k_{fz_a}^{(v)} z_{cn}^a} \times \\
& e^{i\bar{k}_{\perp c} \cdot \bar{r}_{4\perp}} e^{iq'k_{fz_c}^{(v')*} z_4} e^{-i(qk_{fz_a}^{(v)} + sk_{fz_{ai}}^{(w)} + \beta_z)z_1} e^{i(p'k_{fz_{bs}}^{(u')*} - \ell'k_{fz_c}^{(v')*} + \beta_z)z_3} \quad (6.99)
\end{aligned}$$

where $\bar{k}_{\perp c}$ is given by (6.100).

$$\bar{k}_{\perp c} = \bar{k}_{\perp bs} + \bar{k}_{\perp ai} - \bar{k}_{\perp a} \quad (6.100)$$

After performing the z_1 and z_3 integrals, (6.101) is obtained.

$$\begin{aligned}
\langle V_{n_a}^{(1)} L_{m_b}^{(1)*} \rangle &= \sum_{a, a' = +, -} \sum_{p', q', \ell' = +, -} \sum_{u', v' = TE, TM} \sum_{\alpha, \beta, \gamma, \rho = x, y, z} \iint_{S_m} d\bar{r}_4 \\
& \iint d\bar{k}_{\perp a} \int d\beta_z (2\pi)^4 \Lambda_{V-L}^{\alpha\beta\gamma\rho} \Lambda_{V-L}^{\alpha a' p' s q q' \ell \ell'} \left(\bar{r}_4 - \bar{r}_{em}^{a'} \right) \Phi_{\alpha\beta\gamma\rho} \left(\bar{k}_{\perp ai} - \bar{k}_{\perp a}, \beta_z \right) \times \\
& e^{i(qk_{fz_a}^{(v)} + sk_{fz_{ai}}^{(w)} - p'k_{fz_{bs}}^{(u')*} + \ell'k_{fz_c}^{(v')*})d_{f-1}} e^{i\bar{k}_{\perp a} \cdot \bar{r}_{c\perp n}^a} e^{i\ell k_{fz_a}^{(v)} z_{cn}^a} e^{i\bar{k}_{\perp c} \cdot \bar{r}_{4\perp}} e^{iq'k_{fz_c}^{(v')*} z_4} \times \\
& \frac{1 - e^{-i(qk_{fz_a}^{(v)} + sk_{fz_{ai}}^{(w)} + \beta_z)z_1}}{qk_{fz_a}^{(v)} + sk_{fz_{ai}}^{(w)} + \beta_z} \frac{1 - e^{i(p'k_{fz_{bs}}^{(u')*} - \ell'k_{fz_c}^{(v')*} + \beta_z)z_3}}{p'k_{fz_{bs}}^{(u')*} - \ell'k_{fz_c}^{(v')*} + \beta_z} \quad (6.101)
\end{aligned}$$

The β_z integration can again be done using complex residue theory to yield (6.102).

$$\begin{aligned}
\langle V_{n_a}^{(1)} L_{m_b}^{(1)*} \rangle &= (2\pi)^5 i \sum_{a, a' = +, -} \sum_{p', q', \ell' = +, -} \sum_{u', v' = TE, TM} \sum_{\alpha, \beta, \gamma, \rho = x, y, z} \iint d\bar{k}_{\perp a} \\
& \iint_{T_m^{a'}} d\bar{r}_4 \Lambda_{V-L}^{\alpha\beta\gamma\rho} \Lambda_{V-L}^{\alpha a' p' s q q' \ell \ell'} \left(\bar{r}_4 - \bar{r}_{em}^{a'} \right) e^{i\bar{k}_{\perp c} \cdot \bar{r}_{4\perp}} e^{iq'k_{fz_c}^{(v')*} z_4} \times
\end{aligned}$$

$$\begin{aligned}
& e^{i(qk_{fza}^{(v)} + sk_{fzai}^{(w)} - p'k_{fzbs}^{(u')*} + \ell'k_{fzc}^{(v')*})d_f - 1} e^{i\bar{k}_{\perp a} \cdot \bar{r}_{c\perp n}} e^{i\ell k_{tza}^{(v)} z_{cn}^a} \times \\
& \left[\frac{\Phi_{\alpha\beta\gamma\rho}(\bar{k}_{\perp ai} - \bar{k}_{\perp a}, -p'k_{fzbs}^{(u')*} + \ell'k_{fzc}^{(v')*})}{qk_{fza}^{(v)} + sk_{fzai}^{(w)} - p'k_{fzbs}^{(u')*} + \ell'k_{fzc}^{(v')*}} - \right. \\
& \quad \frac{\Phi_{\alpha\beta\gamma\rho}(\bar{k}_{\perp ai} - \bar{k}_{\perp a}, -qk_{fza}^{(v)} - sk_{fzai}^{(w)})}{qk_{fza}^{(v)} + sk_{fzai}^{(w)} - p'k_{fzbs}^{(u')*} + \ell'k_{fzc}^{(v')*}} \times \\
& \quad \left. e^{i(qk_{fza}^{(v)} + sk_{fzai}^{(w)} - p'k_{fzbs}^{(u')*} + \ell'k_{fzc}^{(v')*})h_f} \right] \quad (6.102)
\end{aligned}$$

Finally, the \bar{r}_4 integral of the second line above can be rewritten using the variable transformation of (6.57), as shown by (6.103) below.

$$\begin{aligned}
& \iint_{T_m^{a'}} d\bar{r}_4 \Lambda_{V-L}^{\alpha\beta\gamma\rho, aa'p'sqq'\ell\ell', u'vv'w}(\bar{r}_4 - \bar{r}_{em}^{a'}) e^{i\bar{k}_{\perp c} \cdot \bar{r}_{4\perp}} e^{iq'k_{tzc}^{(v')*} z_4} = 2A_m^{a'} \int_0^1 d\eta \int_0^{1-\eta} d\xi \\
& \left\{ (\xi - 1) \Lambda_{V-L}^{\alpha\beta\gamma\rho, aa'p'sqq'\ell\ell', u'vv'w}(\bar{r}_{em}^{a'}) + \eta \Lambda_{V-L}^{\alpha\beta\gamma\rho, aa'p'sqq'\ell\ell', u'vv'w}(\bar{r}_{mm}^{-a'}) + (1 - \xi - \eta) \Lambda_{V-L}^{\alpha\beta\gamma\rho, aa'p'sqq'\ell\ell', u'vv'w}(\bar{r}_{mm}^{a'}) \right\} \times \\
& \exp \left\{ i \left[\bar{k}_{\perp c} + q'k_{tzc}^{(v')*} \hat{z} \right] \cdot \left[\xi \bar{r}_{em}^{a'} + \eta \bar{r}_{mm}^{-a'} + (1 - \xi - \eta) \bar{r}_{mm}^{a'} \right] \right\} \quad (6.103)
\end{aligned}$$

The above can then be evaluated in terms of the functions I_0 , I_ξ , and I_η defined earlier.

$$\begin{aligned}
& \iint_{T_m^{a'}} d\bar{r}_4 \Lambda_{V-L}^{\alpha\beta\gamma\rho, aa'p'sqq'\ell\ell', u'vv'w}(\bar{r}_4 - \bar{r}_{em}^{a'}) e^{i\bar{k}_{\perp c} \cdot \bar{r}_{4\perp}} e^{iq'k_{tzc}^{(v')*} z_4} = \\
& 2A_m^{a'} \left\{ \Lambda_{V-L}^{\alpha\beta\gamma\rho, aa'p'sqq'\ell\ell', u'vv'w}(\bar{r}_{mm}^{a'} - \bar{r}_{em}^{a'}) \times \right. \\
& \quad \left. I_0 \left(- \left(\bar{k}_{\perp c} + q'k_{tzc}^{(v')*} \hat{z} \right) \cdot \left(\bar{r}_{em}^{a'} - \bar{r}_{mm}^{a'} \right), - \left(\bar{k}_{\perp c} + q'k_{tzc}^{(v')*} \hat{z} \right) \cdot \left(\bar{r}_{mm}^{-a'} - \bar{r}_{mm}^{a'} \right) \right) \right\}
\end{aligned}$$

$$\begin{aligned}
& + \Lambda_{V-L}^{\alpha\beta\gamma\rho} \left(\bar{r}_{m_m}^{-a'} - \bar{r}_{m_m}^{a'} \right) \times \\
& I_\eta \left(- \left(\bar{k}_{\perp c} + q' k_{tz_c}^{(v')*} \hat{z} \right) \cdot \left(\bar{r}_{e_m}^{a'} - \bar{r}_{m_m}^{a'} \right), - \left(\bar{k}_{\perp c} + q' k_{tz_c}^{(v')*} \hat{z} \right) \cdot \left(\bar{r}_{m_m}^{-a'} - \bar{r}_{m_m}^{a'} \right) \right) \\
& + \Lambda_{V-L}^{\alpha\beta\gamma\rho} \left(\bar{r}_{e_m}^{a'} - \bar{r}_{m_m}^{a'} \right) \times \\
& I_\xi \left(- \left(\bar{k}_{\perp c} + q' k_{tz_c}^{(v')*} \hat{z} \right) \cdot \left(\bar{r}_{e_m}^{a'} - \bar{r}_{m_m}^{a'} \right), - \left(\bar{k}_{\perp c} + q' k_{tz_c}^{(v')*} \hat{z} \right) \cdot \left(\bar{r}_{m_m}^{-a'} - \bar{r}_{m_m}^{a'} \right) \right) \Big\} \\
& (6.104)
\end{aligned}$$

Hence, the final desired expression for $\langle V_{n_a}^{(1)} L_{m_b}^{(1)*} \rangle$ is given by (6.105).

$$\begin{aligned}
\langle V_{n_a}^{(1)} L_{m_b}^{(1)*} \rangle &= (2\pi)^5 i \sum_{\alpha, a' = +, -} \sum_{\substack{p', q', \ell' = +, - \\ s, q, \ell}} \sum_{\substack{u', v' = TE, TM \\ v, w}} \sum_{\alpha, \beta, \gamma, \rho = x, y, z} \iint d\bar{k}_{\perp a} 2A_m^{a'} \\
& e^{i(qk_{fza}^{(v)} + sk_{fza}^{(w)} - p'k_{fzbs}^{(u')*} + \ell'k_{fzc}^{(v')*})d_{f-1}} e^{i\bar{k}_{\perp a} \cdot \bar{r}_{c\perp n}} e^{i\ell k_{tza}^{(v)} z_{cn}^a} \times \\
& \left\{ \Lambda_{V-L}^{\alpha\beta\gamma\rho} \left(\bar{r}_{m_m}^{a'} - \bar{r}_{e_m}^{a'} \right) \times \right. \\
& I_0 \left(- \left(\bar{k}_{\perp c} + q' k_{tz_c}^{(v')*} \hat{z} \right) \cdot \left(\bar{r}_{e_m}^{a'} - \bar{r}_{m_m}^{a'} \right), - \left(\bar{k}_{\perp c} + q' k_{tz_c}^{(v')*} \hat{z} \right) \cdot \left(\bar{r}_{m_m}^{-a'} - \bar{r}_{m_m}^{a'} \right) \right) \\
& + \Lambda_{V-L}^{\alpha\beta\gamma\rho} \left(\bar{r}_{m_m}^{-a'} - \bar{r}_{m_m}^{a'} \right) \times \\
& I_0 \left(- \left(\bar{k}_{\perp c} + q' k_{tz_c}^{(v')*} \hat{z} \right) \cdot \left(\bar{r}_{e_m}^{a'} - \bar{r}_{m_m}^{a'} \right), - \left(\bar{k}_{\perp c} + q' k_{tz_c}^{(v')*} \hat{z} \right) \cdot \left(\bar{r}_{m_m}^{-a'} - \bar{r}_{m_m}^{a'} \right) \right) \\
& + \Lambda_{V-L}^{\alpha\beta\gamma\rho} \left(\bar{r}_{e_m}^{a'} - \bar{r}_{m_m}^{a'} \right) \times \\
& I_\xi \left(- \left(\bar{k}_{\perp c} + q' k_{tz_c}^{(v')*} \hat{z} \right) \cdot \left(\bar{r}_{e_m}^{a'} - \bar{r}_{m_m}^{a'} \right), - \left(\bar{k}_{\perp c} + q' k_{tz_c}^{(v')*} \hat{z} \right) \cdot \left(\bar{r}_{m_m}^{-a'} - \bar{r}_{m_m}^{a'} \right) \right) \Big\} \times \\
& \left[\frac{\Phi_{\alpha\beta\gamma\rho} (\bar{k}_{\perp ai} - \bar{k}_{\perp a}, -p'k_{fzbs}^{(u')*} + \ell'k_{fzc}^{(v')*})}{qk_{fza}^{(v)} + sk_{fza}^{(w)} - p'k_{fzbs}^{(u')*} + \ell'k_{fzc}^{(v')*}} - \frac{\Phi_{\alpha\beta\gamma\rho} (\bar{k}_{\perp ai} - \bar{k}_{\perp a}, -qk_{fza}^{(v)} - sk_{fza}^{(w)})}{qk_{fza}^{(v)} + sk_{fza}^{(w)} - p'k_{fzbs}^{(u')*} + \ell'k_{fzc}^{(v')*}} \times \right. \\
& \left. e^{i(qk_{fza}^{(v)} + sk_{fza}^{(w)} - p'k_{fzbs}^{(u')*} + \ell'k_{fzc}^{(v')*})h_f} \right] \\
& (6.105)
\end{aligned}$$

The third incoherent term is $\langle L_{n_a}^{(1)} V_{m_b}^{(1)*} \rangle$, which is given by (6.33), and which can be written with the expressions of Appendix E in the form of (1.06).

$$\begin{aligned}
 \langle L_{n_a}^{(1)} V_{m_b}^{(1)*} \rangle = & i\omega\mu \sum_{a,a'=+,-} \sum_{\substack{p,q,\ell, \\ s',q',\ell'=+,-}} \sum_{u,v,v',w'=TE,TM} \sum_{\alpha,\beta,\gamma,\rho=x,y,z} \iint_{S_n} d\bar{r}_2 \iint_{S_m} d\bar{r}_4 \\
 & \iiint_{V_f} d\bar{r}_1 \iiint_{V_f} d\bar{r}_3 \iint d\bar{k}_{\perp a} \iint d\bar{k}_{\perp b} C_{\alpha\beta\gamma\rho}(\bar{r}_1 - \bar{r}_3) \times \\
 & \left[\hat{p}_a \cdot \bar{H}_{0fp}^{(u)}(\bar{k}_{\perp a}) \right]_{\alpha} \cdot \left[\bar{F}_{ft\ell q}^{(v)}(\bar{k}_{\perp a}) \cdot (\bar{r}_2 - \bar{r}_{en}^a) \frac{a\ell_n}{2A_n^a} \right]_{\beta} \times \\
 & \left[\hat{w}_n^{a'} \delta(\bar{r}_4 - \bar{r}_{cm}^{a'}) \cdot \bar{F}_{tf\ell'q'}^{(v')}(\bar{k}_{\perp b}) \right]_{\gamma}^* \cdot \left[\bar{E}_{fbi}^{s',(w')} \right]_{\rho}^* \times \\
 & e^{-i\bar{k}_{\perp a} \cdot \bar{r}_1 \perp} e^{-ipk_{fza}^{(u)} z_1} e^{i\bar{k}_{\perp a} \cdot \bar{r}_1 \perp} e^{-i\bar{k}_{\perp a} \cdot \bar{r}_2 \perp} e^{i\ell k_{fza}^{(v)} z_1} e^{-iqk_{iza}^{(v)} z_2} \times \\
 & e^{-i\bar{k}_{\perp b} \cdot \bar{r}_4 \perp} e^{i\bar{k}_{\perp b} \cdot \bar{r}_3 \perp} e^{-i\ell' k_{izb}^{(v')} z_4} e^{iq' k_{fzb}^{(v')} z_3} e^{-i\bar{k}_{\perp b} \cdot \bar{r}_3 \perp} e^{is' k_{fzbi}^{(w')} z_3} \quad (6.106)
 \end{aligned}$$

After a variable transformation in z_1 and z_3 , and after representing the correlation function as the Fourier transform of its spectral function, the above becomes (6.107),

$$\begin{aligned}
 \langle L_{n_a}^{(1)} V_{m_b}^{(1)*} \rangle = & \sum_{a,a'=+,-} \sum_{\substack{p,q,\ell, \\ s',q',\ell'=+,-}} \sum_{u,v,v',w'=TE,TM} \sum_{\alpha,\beta,\gamma,\rho=x,y,z} \iint_{S_n} d\bar{r}_2 \iint_{S_m} d\bar{r}_4 \int_{-h_f}^0 dz_1 \int_{-h_f}^0 dz_3 \\
 & \iint d\bar{r}_{1\perp} \iint d\bar{r}_{3\perp} \iint d\bar{k}_{\perp a} \iint d\bar{k}_{\perp b} \iint d\bar{\beta}_{\perp} \int d\beta_z \\
 & \Lambda_{L-V}^{\alpha\beta\gamma\rho, aa'ps'qq'\ell\ell', uvv'w'}(\bar{r}_2 - \bar{r}_{en}^a) \Phi_{\alpha\beta\gamma\rho}(\bar{\beta}) \delta(\bar{r}_4 - \bar{r}_{cm}^{a'}) \times \\
 & e^{i(p k_{fza}^{(u)} - \ell k_{fza}^{(v)} - q' k_{fzb}^{(v')} - s' k_{fzbi}^{(w')}) d_{f-1}} \times \\
 & e^{i(\bar{k}_{\perp a} - \bar{k}_{\perp a} - \bar{\beta}_{\perp}) \cdot \bar{r}_1 \perp} e^{-i\bar{k}_{\perp a} \cdot \bar{r}_2 \perp} e^{i(\bar{k}_{\perp b} - \bar{k}_{\perp b} + \bar{\beta}_{\perp}) \cdot \bar{r}_3 \perp} e^{-i\bar{k}_{\perp b} \cdot \bar{r}_4 \perp} \times \\
 & e^{-(p k_{fza}^{(u)} - \ell k_{fza}^{(v)} + \beta_z) z_1} e^{-iqk_{iza}^{(v)} z_2} e^{i(q' k_{fzb}^{(v')} + s' k_{fzbi}^{(w')} + \beta_z) z_3} e^{-i\ell' k_{izb}^{(v')} z_4} \quad (6.107)
 \end{aligned}$$

where Λ_{L-V} is given by (6.108).

$$\Lambda_{L-V}^{\alpha\beta\gamma\rho, aa'ps'qq'\ell\ell'}(\bar{r}) = i\omega\mu \frac{e^{ikr}}{4\pi r} \left[\hat{p}_a \cdot \bar{H}_{0f_p}^{(u)}(\bar{k}_{\perp a}) \right]_{\alpha} \cdot \left[\bar{F}_{ft_{\ell q}}^{(v)}(\bar{k}_{\perp a}) \cdot (\bar{r}) \frac{a\ell_n}{2A_n^a} \right]_{\beta} \times \\ \left[\hat{w}_m^{a'} \cdot \bar{F}_{tf_{\ell'q'}}^{(v')}(\bar{k}_{\perp b}) \right]_{\gamma}^* \cdot \left[\bar{E}_{f_{bi}}^{s', (w')} \right]_{\rho}^* \quad (6.108)$$

The \bar{r}_4 integral can be done trivially, and the $\bar{r}_{1\perp}$ integral can be done to obtain a delta function. This delta function can then be used to evaluate the $\bar{\beta}_{\perp}$ integral. The result is given by (6.109).

$$\langle L_{n_a}^{(1)} V_{m_b}^{(1)*} \rangle = \sum_{a,a'=+,-} \sum_{\substack{p,q,\ell, \\ s',q',\ell'=+,-}} \sum_{u,v,v',w'=TE,TM} \sum_{\alpha,\beta,\gamma,\rho=x,y,z} \iint_{S_n} d\bar{r}_2 \int_{-h_f}^0 dz_1 \int_{-h_f}^0 dz_3 \\ \iint d\bar{r}_{3\perp} \iint d\bar{k}_{\perp a} \iint d\bar{k}_{\perp b} \int d\beta_z \\ (2\pi)^2 \Lambda_{L-V}^{\alpha\beta\gamma\rho, aa'ps'qq'\ell\ell'}(\bar{r}_2 - \bar{r}_{e_n}) \Phi_{\alpha\beta\gamma\rho}(\bar{k}_{\perp a} - \bar{k}_{\perp a s}, \beta_z) \times \\ e^{i(pk_{fz_{as}}^{(u)} - \ell k_{fz_a}^{(v)} - q'k_{fz_b}^{(v')*} - s'k_{fz_{bi}}^{(w')*})d_{f-1}} \\ e^{-i\bar{k}_{\perp b} \cdot \bar{r}_{c\perp m}^{a'}} e^{-i\ell'k_{iz_b}^{(v')*} z_{cm}^{a'}} e^{-i\bar{k}_{\perp a} \cdot \bar{r}_{2\perp}} e^{-iqk_{iz_a}^{(v)} z_2} \times \\ e^{i(\bar{k}_{\perp b} - \bar{k}_{\perp bi} + \bar{\beta}_{\perp}) \cdot \bar{r}_{3\perp}} e^{-(pk_{fz_{as}}^{(u)} - \ell k_{fz_a}^{(v)} + \beta_z)z_1} e^{i(q'k_{fz_b}^{(v')*} + s'k_{fz_{bi}}^{(w')*} + \beta_z)z_3} \quad (6.109)$$

Similarly, the $\bar{r}_{3\perp}$ integral can be done to obtain another delta function, and the $\bar{k}_{\perp b}$ integral can be evaluated from this delta function. The result is given by (6.110),

$$\langle L_{n_a}^{(1)} V_{m_b}^{(1)*} \rangle = \sum_{a,a'=+,-} \sum_{\substack{p,q,\ell, \\ s',q',\ell'=+,-}} \sum_{u,v,v',w'=TE,TM} \sum_{\alpha,\beta,\gamma,\rho=x,y,z} \iint_{S_n} d\bar{r}_2 \int_{-h_f}^0 dz_1 \int_{-h_f}^0 dz_3$$

$$\begin{aligned}
& \iint d\bar{k}_{\perp a} \int d\beta_z (2\pi)^4 \Lambda_{L-V}^{\alpha\beta\gamma\rho} \Lambda_{L-V}^{aa'ps'qq'\ell\ell'} \left(\bar{\tau}_2 - \bar{\tau}_{e_n}^a \right) \Phi_{\alpha\beta\gamma\rho} \left(\bar{k}_{\perp a} - \bar{k}_{\perp a s}, \beta_z \right) \times \\
& e^{-i\bar{k}_{\perp a} \cdot \bar{\tau}_{2\perp}} e^{-iqk_{iz_a}^{(v)} z_2} e^{i(pk_{fz_{as}}^{(u)} - \ell k_{fz_a}^{(v)} - q'k_{fz_c}^{(v')} - s'k_{fz_{bi}}^{(w')})d_{f-1}} e^{-i\bar{k}_{\perp c} \cdot \bar{\tau}_{c\perp m}^{a'}} \times \\
& e^{-il'k_{iz_c}^{(v')} z_{cm}^{a'}} e^{-(pk_{fz_{as}}^{(u)} - \ell k_{fz_a}^{(v)} + \beta_z)z_1} e^{i(q'k_{fz_c}^{(v')} + s'k_{fz_{bi}}^{(w')} + \beta_z)z_3} \quad (6.110)
\end{aligned}$$

where $\bar{k}_{\perp c}$ is given by (6.111).

$$\bar{k}_{\perp c} = \bar{k}_{\perp bi} - \bar{k}_{\perp a} + \bar{k}_{\perp as} \quad (6.111)$$

The z_1 and z_3 integrals can be evaluated to obtain (6.112).

$$\begin{aligned}
\langle L_{n_a}^{(1)} V_{m_b}^{(1)*} \rangle &= \sum_{a,a'=+,-} \sum_{\substack{p,q,\ell, \\ s',q',\ell'=+,-}} \sum_{u,v,v',w'=TE,TM} \sum_{\alpha,\beta,\gamma,\rho=x,y,z} \iint d\bar{k}_{\perp a} \int d\beta_z \\
& \iint_{S_n} d\bar{\tau}_2 (2\pi)^4 \Lambda_{L-V}^{\alpha\beta\gamma\rho} \Lambda_{L-V}^{aa'ps'qq'\ell\ell'} \left(\bar{\tau}_2 - \bar{\tau}_{e_n}^a \right) e^{-i\bar{k}_{\perp a} \cdot \bar{\tau}_{2\perp}} e^{-iqk_{iz_a}^{(v)} z_2} \times \\
& \Phi_{\alpha\beta\gamma\rho} \left(\bar{k}_{\perp a} - \bar{k}_{\perp as}, \beta_z \right) \times \\
& e^{i(pk_{fz_{as}}^{(u)} - \ell k_{fz_a}^{(v)} - q'k_{fz_c}^{(v')} - s'k_{fz_{bi}}^{(w')})d_{f-1}} e^{-i\bar{k}_{\perp c} \cdot \bar{\tau}_{c\perp m}^{a'}} e^{-il'k_{iz_c}^{(v')} z_{cm}^{a'}} \times \\
& \frac{1 - e^{(pk_{fz_{as}}^{(u)} - \ell k_{fz_a}^{(v)} + \beta_z)h_f}}{pk_{fz_{as}}^{(u)} - \ell k_{fz_a}^{(v)} + \beta_z} \frac{1 - e^{-i(q'k_{fz_c}^{(v')} + s'k_{fz_{bi}}^{(w')} + \beta_z)h_f}}{q'k_{fz_c}^{(v')} + s'k_{fz_{bi}}^{(w')} + \beta_z} \quad (6.112)
\end{aligned}$$

The β_z integral can then be evaluated as before using complex residue theory, yielding (6.113).

$$\langle L_{n_a}^{(1)} V_{m_b}^{(1)*} \rangle = (2\pi)^5 i \sum_{a,a'=+,-} \sum_{\substack{p,q,\ell, \\ s',q',\ell'=+,-}} \sum_{u,v,v',w'=TE,TM} \sum_{\alpha,\beta,\gamma,\rho=x,y,z} \iint d\bar{k}_{\perp a}$$

$$\begin{aligned}
& \iint_{S_n} d\bar{r}_2 \Lambda_{L-V}^{\alpha\beta\gamma\rho, aa'ps'qq'\ell\ell'}^{uvv'w'} \left(\bar{r}_2 - \bar{r}_{e_n}^a \right) e^{-i\bar{k}_{\perp a} \cdot \bar{r}_2} e^{-iqk_{tz_a}^{(v)} z_2} \times \\
& e^{i(pk_{fz_{as}}^{(u)} - \ell k_{fz_a}^{(v)} - q'k_{fz_c}^{(v')*} - s'k_{fz_{bi}}^{(w')*})d_{f-1}} e^{-i\bar{k}_{\perp c} \cdot \bar{r}_{c\perp m}^{a'}} e^{-i\ell'k_{tz_c}^{(v')*} z_{cm}^{a'}} \times \\
& \left[\frac{\Phi_{\alpha\beta\gamma\rho} \left(\bar{k}_{\perp a} - \bar{k}_{\perp as}, -s'k_{fz_{bi}}^{(w')*} - q'k_{fz_c}^{(v')*} \right)}{pk_{fz_{as}}^{(u)} - \ell k_{fz_a}^{(v)} - s'k_{fz_{bi}}^{(w')*} - q'k_{fz_c}^{(v')*}} \right. \\
& \quad \frac{\Phi_{\alpha\beta\gamma\rho} \left(\bar{k}_{\perp a} - \bar{k}_{\perp as}, -pk_{fz_{as}}^{(u)} + \ell k_{fz_a}^{(v)} \right)}{pk_{fz_{as}}^{(u)} - \ell k_{fz_a}^{(v)} - s'k_{fz_{bi}}^{(w')*} - q'k_{fz_c}^{(v')*}} \times \\
& \quad \left. e^{i(pk_{fz_{as}}^{(u)} - \ell k_{fz_a}^{(v)} - s'k_{fz_{bi}}^{(w')*} - q'k_{fz_c}^{(v')*})h_f} \right] \quad (6.113)
\end{aligned}$$

Finally, the integration over the triangular region can again be done using the transformation of (6.57), and the result expressed in terms of I_0 , I_ξ , and I_η .

$$\begin{aligned}
\langle L_{n_a}^{(1)} V_{m_b}^{(1)*} \rangle &= (2\pi)^5 i \sum_{a,a'=+,-} \sum_{\substack{p,q,\ell, \\ s',q',\ell'=+,-}} \sum_{u,v,v',w'=TE,TM} \sum_{\alpha,\beta,\gamma,\rho=x,y,z} \iint d\bar{k}_{\perp a} 2A_n^a \times \\
& e^{i(pk_{fz_{as}}^{(u)} - \ell k_{fz_a}^{(v)} - q'k_{fz_c}^{(v')*} - s'k_{fz_{bi}}^{(w')*})d_{f-1}} e^{-i\bar{k}_{\perp c} \cdot \bar{r}_{c\perp m}^{a'}} e^{-i\ell'k_{tz_c}^{(v')*} z_{cm}^{a'}} \times \\
& \left\{ \Lambda_{L-V}^{\alpha\beta\gamma\rho, aa'ps'qq'\ell\ell'}^{uvv'w'} \left(\bar{r}_{m_n}^a - \bar{r}_{e_n}^a \right) \times \right. \\
& \quad I_0 \left(\left(\bar{k}_{\perp a} + qk_{tz_a}^{(v)} \hat{z} \right) \cdot \left(\bar{r}_{e_n}^a - \bar{r}_{m_n}^a \right), \left(\bar{k}_{\perp a} + qk_{tz_a}^{(v)} \hat{z} \right) \cdot \left(\bar{r}_{m_n}^{-a} - \bar{r}_{m_n}^a \right) \right) \\
& \quad \Lambda_{L-V}^{\alpha\beta\gamma\rho, aa'ps'qq'\ell\ell'}^{uvv'w'} \left(\bar{r}_{m_n}^{-a} - \bar{r}_{m_n}^a \right) \times \\
& \quad I_\eta \left(\left(\bar{k}_{\perp a} + qk_{tz_a}^{(v)} \hat{z} \right) \cdot \left(\bar{r}_{e_n}^a - \bar{r}_{m_n}^a \right), \left(\bar{k}_{\perp a} + qk_{tz_a}^{(v)} \hat{z} \right) \cdot \left(\bar{r}_{m_n}^{-a} - \bar{r}_{m_n}^a \right) \right) \\
& \quad \Lambda_{L-V}^{\alpha\beta\gamma\rho, aa'ps'qq'\ell\ell'}^{uvv'w'} \left(\bar{r}_{e_n}^a - \bar{r}_{m_n}^a \right) \times \\
& \quad \left. I_\xi \left(\left(\bar{k}_{\perp a} + qk_{tz_a}^{(v)} \hat{z} \right) \cdot \left(\bar{r}_{e_n}^a - \bar{r}_{m_n}^a \right), \left(\bar{k}_{\perp a} + qk_{tz_a}^{(v)} \hat{z} \right) \cdot \left(\bar{r}_{m_n}^{-a} - \bar{r}_{m_n}^a \right) \right) \right\} \times
\end{aligned}$$

$$\begin{aligned}
& \left[\frac{\Phi_{\alpha\beta\gamma\rho} (\bar{k}_{\perp a} - \bar{k}_{\perp a s}, -s'k_{fz_{bi}}^{(w')*} - q'k_{fz_c}^{(v')*})}{pk_{fz_{as}}^{(u)} - \ell k_{fz_a}^{(v)} - s'k_{fz_{bi}}^{(w')*} - q'k_{fz_c}^{(v')*}} - \right. \\
& \quad \frac{\Phi_{\alpha\beta\gamma\rho} (\bar{k}_{\perp a} - \bar{k}_{\perp a s}, -pk_{fz_{as}}^{(u)} + \ell k_{fz_a}^{(v)})}{pk_{fz_{as}}^{(u)} - \ell k_{fz_a}^{(v)} - s'k_{fz_{bi}}^{(w')*} - q'k_{fz_c}^{(v')*}} \times \\
& \quad \left. e^{i(pk_{fz_{as}}^{(u)} - \ell k_{fz_a}^{(v)} - s'k_{fz_{bi}}^{(w')*} - q'k_{fz_c}^{(v')*})h_f} \right] \quad (6.114)
\end{aligned}$$

The final incoherent term is given by (6.34). After substituting the Green's function expressions of Appendix E and the basis function expressions defined earlier, $\langle L_{n_a}^{(1)} L_{m_b}^{(1)*} \rangle$ can be rewritten as in (6.115) below.

$$\begin{aligned}
\langle L_{n_a}^{(1)} L_{m_b}^{(1)*} \rangle &= \frac{\omega^2 \mu^2}{(4\pi r)^2} \sum_{a,a'=+,-} \sum_{\substack{p,q,\ell, \\ p',q'\ell'=+,-}} \sum_{u,v,u',v'=TE,TM} \sum_{\alpha,\beta,\gamma,\rho=x,y,z} \iint_{S_n} d\bar{r}_2 \iint_{S_m} d\bar{r}_4 \\
& \quad \iint_{V_f} d\bar{r}_1 \iint_{V_f} d\bar{r}_3 \iint d\bar{k}_{\perp a} \iint d\bar{k}_{\perp b} C_{\alpha\beta\gamma\rho} (\bar{r}_1 - \bar{r}_3) \times \\
& \quad \left[\hat{p}_a \cdot \bar{H}_{0f_p}^{(u)} (\bar{k}_{\perp a s}) \right]_{\alpha} \cdot \left[\bar{F}_{ft_{\ell q}}^{(v)} (\bar{k}_{\perp a}) \cdot (\bar{r}_2 - \bar{r}_{e_n}^a) \frac{a\ell_n}{2A_n^a} \right]_{\beta} \times \\
& \quad \left[\hat{p}_b \cdot \bar{H}_{0f_{p'}}^{(u')} (\bar{k}_{\perp b s}) \right]_{\gamma}^* \cdot \left[\bar{F}_{ft_{\ell' q'}}^{(v')} (\bar{k}_{\perp b}) \cdot (\bar{r}_4 - \bar{r}_{e_m}^{a'}) \frac{a'\ell_m}{2A_m^{a'}} \right]_{\rho}^* \times \\
& \quad e^{-i\bar{k}_{\perp a s} \cdot \bar{r}_{1\perp}} e^{-ipk_{fz_{as}}^{(u)} z_1} e^{i\bar{k}_{\perp a} \cdot \bar{r}_{1\perp}} e^{-i\bar{k}_{\perp a} \cdot \bar{r}_{2\perp}} e^{i\ell k_{fz_a}^{(v)} z_1} e^{-iqk_{fz_c}^{(v')} z_2} \times \\
& \quad e^{i\bar{k}_{\perp b s} \cdot \bar{r}_{3\perp}} e^{ip'k_{fz_{bs}}^{(u')} z_3} e^{-i\bar{k}_{\perp b} \cdot \bar{r}_{3\perp}} e^{i\bar{k}_{\perp b} \cdot \bar{r}_{4\perp}} e^{-i\ell' k_{fz_b}^{(v')} z_3} e^{iq'k_{fz_c}^{(v')} z_4} \quad (6.115)
\end{aligned}$$

After the usual transformation of z_1 and z_3 , and the change to the spectral function representation of the correlation function, the above can be expressed as in (6.116),

$$\langle L_{n_a}^{(1)} L_{m_b}^{(1)*} \rangle = \sum_{a,a'=+,-} \sum_{\substack{p,q,\ell, \\ p',q'\ell'=+,-}} \sum_{u,v,u',v'=TE,TM} \sum_{\alpha,\beta,\gamma,\rho=x,y,z} \iint_{S_n} d\bar{r}_2 \iint_{S_m} d\bar{r}_4$$

$$\begin{aligned}
& \int_{-h_f}^0 dz_1 \int_{-h_f}^0 dz_3 \iint d\bar{r}_{1\perp} \iint d\bar{r}_{3\perp} \iint d\bar{k}_{\perp a} \iint d\bar{k}_{\perp b} \iint d\bar{\beta}_{\perp} \int d\beta_z \\
& \Lambda_{L-L}^{\alpha\beta\gamma\rho, aa'pp'qq'\ell\ell'} \left(\bar{r}_2 - \bar{r}_{e_n}^a, \bar{r}_4 - \bar{r}_{e_m}^{a'} \right) \Phi_{\alpha\beta\gamma\rho}(\bar{\beta}) \times \\
& e^{i(pk_{fz_a}^{(u)} - \ell k_{fz_a}^{(v)} - p'k_{fz_b}^{(u')*} + \ell'k_{fz_b}^{(v')*})d_f - 1} e^{i(\bar{k}_{\perp a} - \bar{k}_{\perp a_s} - \bar{\beta}_{\perp}) \cdot \bar{r}_{1\perp}} e^{-i\bar{k}_{\perp a} \cdot \bar{r}_{2\perp}} \times \\
& e^{i(\bar{k}_{\perp b_s} - \bar{k}_{\perp b} + \bar{\beta}_{\perp}) \cdot \bar{r}_{3\perp}} e^{i\bar{k}_{\perp b} \cdot \bar{r}_{4\perp}} e^{-i(pk_{fz_a}^{(u)} - \ell k_{fz_a}^{(v)} + \beta_z)z_1} e^{-iqk_{iz_a}^{(v)}z_2} \times \\
& e^{i(p'k_{fz_b}^{(u')*} - \ell'k_{fz_b}^{(v')*} + \beta_z)z_3} e^{iq'k_{iz_b}^{(v')*}z_4} \quad (6.116)
\end{aligned}$$

where Λ_{L-L} is given by (6.117).

$$\begin{aligned}
\Lambda_{L-L}^{\alpha\beta\gamma\rho, aa'pp'qq'\ell\ell'}(\bar{r}_a, \bar{r}_b) = & \frac{\omega^2 \mu^2}{(4\pi r)^2} \left[\hat{p}_a \cdot \bar{H}_{0f_p}^{(u)}(\bar{k}_{\perp a_s}) \right]_{\alpha} \cdot \left[\bar{F}_{ft_{\ell_q}}^{(v)}(\bar{k}_{\perp a}) \cdot (\bar{r}_a) \frac{a\ell_n}{2A_n^a} \right]_{\beta} \times \\
& \left[\hat{p}_b \cdot \bar{H}_{0f_{p'}}^{(u')}(\bar{k}_{\perp b_s}) \right]_{\gamma}^* \cdot \left[\bar{F}_{ft_{\ell'_q}}^{(v')}(\bar{k}_{\perp b}) \cdot (\bar{r}_b) \frac{a'\ell_m}{2A_m^{a'}} \right]_{\rho}^* \quad (6.117)
\end{aligned}$$

The $\bar{r}_{1\perp}$ integral can be done to obtain a delta function, and that can be used to evaluate the $\bar{\beta}_{\perp}$ integral.

$$\begin{aligned}
\langle L_{n_a}^{(1)} L_{m_b}^{(1)*} \rangle = & \sum_{a,a'=+,-} \sum_{\substack{p,q,\ell, \\ p',q',\ell'=+,-}} \sum_{u,v,u',v'=TE,TM} \sum_{\alpha,\beta,\gamma,\rho=x,y,z} \iint_{S_n} d\bar{r}_2 \iint_{S_m} d\bar{r}_4 \int_{-h_f}^0 dz_1 \int_{-h_f}^0 dz_3 \\
& \iint d\bar{r}_{3\perp} \iint d\bar{k}_{\perp a} \iint d\bar{k}_{\perp b} \int d\beta_z \\
& (2\pi)^2 \Lambda_{L-L}^{\alpha\beta\gamma\rho, aa'pp'qq'\ell\ell'} \left(\bar{r}_2 - \bar{r}_{e_n}^a, \bar{r}_4 - \bar{r}_{e_m}^{a'} \right) \Phi_{\alpha\beta\gamma\rho}(\bar{k}_{\perp a} - \bar{k}_{\perp a_s}, \beta_z) \times \\
& e^{i(pk_{fz_a}^{(u)} - \ell k_{fz_a}^{(v)} - p'k_{fz_b}^{(u')*} + \ell'k_{fz_b}^{(v')*})d_f - 1} e^{-i\bar{k}_{\perp a} \cdot \bar{r}_{2\perp}} e^{-iqk_{iz_a}^{(v)}z_2} e^{i\bar{k}_{\perp b} \cdot \bar{r}_{4\perp}} e^{iq'k_{iz_b}^{(v')*}z_4} \times \\
& e^{i(\bar{k}_{\perp b_s} - \bar{k}_{\perp b} + \bar{k}_{\perp a} - \bar{k}_{\perp a_s}) \cdot \bar{r}_{3\perp}} e^{-i(pk_{fz_a}^{(u)} - \ell k_{fz_a}^{(v)} + \beta_z)z_1} e^{i(p'k_{fz_b}^{(u')*} - \ell'k_{fz_b}^{(v')*} + \beta_z)z_3} \quad (6.118)
\end{aligned}$$

Similarly, the $\bar{r}_{3\perp}$ integral can be evaluated to obtain another delta function which then can be used to evaluate the \bar{k}_{\perp_b} integral. The result is given by (6.119),

$$\begin{aligned}
\langle L_{n_a}^{(1)} L_{m_b}^{(1)*} \rangle &= \sum_{a,a'=+,-} \sum_{\substack{p,q,\ell, \\ p',q',\ell'=+,-}} \sum_{u,v,u',v'=TE,TM} \sum_{\alpha,\beta,\gamma,\rho=x,y,z} \\
&\int \int_{S_n} d\bar{r}_2 \int \int_{S_m} d\bar{r}_4 \int_{-h_f}^0 dz_1 \int_{-h_f}^0 dz_3 \int \int d\bar{k}_{\perp_a} \int d\beta_z \\
&(2\pi)^4 \Lambda_{L-L}^{\alpha\beta\gamma\rho} \left(\bar{r}_2 - \bar{r}_{e_n}^a, \bar{r}_4 - \bar{r}_{e_m}^{a'} \right) \Phi_{\alpha\beta\gamma\rho} (\bar{k}_{\perp_a} - \bar{k}_{\perp_{as}}, \beta_z) \times \\
&e^{i(p k_{fz_{as}}^{(u)} - \ell k_{fz_a}^{(v)} - p' k_{fz_{bs}}^{(u')*} + \ell' k_{fz_c}^{(v')*})d_f - 1} e^{-i\bar{k}_{\perp_a} \cdot \bar{r}_{2\perp}} e^{-iq k_{fz_a}^{(v)} z_2} e^{i\bar{k}_{\perp_c} \cdot \bar{r}_{4\perp}} e^{iq' k_{fz_c}^{(v')*} z_4} \times \\
&e^{-i(p k_{fz_{as}}^{(u)} - \ell k_{fz_a}^{(v)} + \beta_z)z_1} e^{i(p' k_{fz_{bs}}^{(u')*} - \ell' k_{fz_c}^{(v')*} + \beta_z)z_3} \quad (6.119)
\end{aligned}$$

where \bar{k}_{\perp_c} is given by (6.120).

$$\bar{k}_{\perp_c} = \bar{k}_{\perp_{bs}} - \bar{k}_{\perp_{as}} + \bar{k}_{\perp_a} \quad (6.120)$$

The z_1 and z_3 integrals can be performed directly to yield (6.121).

$$\begin{aligned}
\langle L_{n_a}^{(1)} L_{m_b}^{(1)*} \rangle &= \sum_{a,a'=+,-} \sum_{\substack{p,q,\ell, \\ p',q',\ell'=+,-}} \sum_{u,v,u',v'=TE,TM} \sum_{\alpha,\beta,\gamma,\rho=x,y,z} \int \int_{S_n} d\bar{r}_2 \int \int_{S_m} d\bar{r}_4 \int \int d\bar{k}_{\perp_a} \int d\beta_z \\
&(2\pi)^4 \Lambda_{L-L}^{\alpha\beta\gamma\rho} \left(\bar{r}_2 - \bar{r}_{e_n}^a, \bar{r}_4 - \bar{r}_{e_m}^{a'} \right) \Phi_{\alpha\beta\gamma\rho} (\bar{k}_{\perp_a} - \bar{k}_{\perp_{as}}, \beta_z) \times \\
&e^{i(p k_{fz_{as}}^{(u)} - \ell k_{fz_a}^{(v)} - p' k_{fz_{bs}}^{(u')*} + \ell' k_{fz_c}^{(v')*})d_f - 1} e^{-i\bar{k}_{\perp_a} \cdot \bar{r}_{2\perp}} e^{-iq k_{fz_a}^{(v)} z_2} e^{i\bar{k}_{\perp_c} \cdot \bar{r}_{4\perp}} e^{iq' k_{fz_c}^{(v')*} z_4} \times \\
&\frac{1 - e^{i(p k_{fz_{as}}^{(u)} - \ell k_{fz_a}^{(v)} + \beta_z)h_f}}{p k_{fz_{as}}^{(u)} - \ell k_{fz_a}^{(v)} + \beta_z} \cdot \frac{1 - e^{-i(p' k_{fz_{bs}}^{(u')*} - \ell' k_{fz_c}^{(v')*} + \beta_z)h_f}}{p' k_{fz_{bs}}^{(u')*} - \ell' k_{fz_c}^{(v')*} + \beta_z} \quad (6.121)
\end{aligned}$$

Finally, using complex residue theory, the β_z integral can be evaluated to obtain (6.122).

$$\begin{aligned}
\langle L_{n_a}^{(1)} L_{m_b}^{(1)*} \rangle = & (2\pi)^5 i \sum_{a,a'=+,-} \sum_{\substack{p,q,\ell, \\ p',q',\ell'=+,-}} \sum_{u,v,u',v'=TE,TM} \sum_{\alpha,\beta,\gamma,\rho=x,y,z} \iint d\bar{k}_{\perp a} \iint_{S_n} d\bar{\tau}_2 \iint_{S_m} d\bar{\tau}_4 \\
& \Lambda_{L-L}^{\alpha\beta\gamma\rho}{}_{aa'pp'qq'\ell\ell'}{}_{uu'vv'} \left(\bar{\tau}_2 - \bar{\tau}_{e_n}^a, \bar{\tau}_4 - \bar{\tau}_{e_m}^{a'} \right) e^{-i\bar{k}_{\perp a} \cdot \bar{\tau}_2} e^{-iqk_{tz_a}^{(v)} z_2} e^{i\bar{k}_{\perp c} \cdot \bar{\tau}_4} e^{iq'k_{tz_c}^{(v')*} z_4} \times \\
& e^{i(pk_{fz_{as}}^{(u)} - \ell k_{fz_a}^{(v)} - p'k_{fz_{bs}}^{(u')*} + \ell'k_{fz_c}^{(v')*})d_f - 1} \times \\
& \left[\frac{\Phi_{\alpha\beta\gamma\rho}(\bar{k}_{\perp a} - \bar{k}_{\perp a_s}, -p'k_{fz_{bs}}^{(u')*} + \ell'k_{fz_c}^{(v')*})}{pk_{fz_{as}}^{(u)} - \ell k_{fz_a}^{(v)} - p'k_{fz_{bs}}^{(u')*} + \ell'k_{fz_c}^{(v')*}} - \right. \\
& \frac{\Phi_{\alpha\beta\gamma\rho}(\bar{k}_{\perp a} - \bar{k}_{\perp a_s}, -pk_{fz_{as}}^{(u)} + \ell k_{fz_a}^{(v)})}{pk_{fz_{as}}^{(u)} - \ell k_{fz_a}^{(v)} - p'k_{fz_{bs}}^{(u')*} + \ell'k_{fz_c}^{(v')*}} \times \\
& \left. e^{i(pk_{fz_{as}}^{(u)} - \ell k_{fz_a}^{(v)} - p'k_{fz_{bs}}^{(u')*} + \ell'k_{fz_c}^{(v')*})h_f} \right] \quad (6.122)
\end{aligned}$$

The $\bar{\tau}_2$ and $\bar{\tau}_4$ integrals over triangular surface facets can be evaluated as before in terms of the functions I_0 , I_ξ , and I_η . The final result, therefore, is given by (6.123).

$$\begin{aligned}
\langle L_{n_a}^{(1)} L_{m_b}^{(1)*} \rangle = & (2\pi)^5 i \sum_{a,a'=+,-} \sum_{\substack{p,q,\ell, \\ p',q',\ell'=+,-}} \sum_{u,v,u',v'=TE,TM} \sum_{\alpha,\beta,\gamma,\rho=x,y,z} \iint d\bar{k}_{\perp a} 4A_n^a A_m^{a'} \times \\
& e^{i(pk_{fz_{as}}^{(u)} - \ell k_{fz_a}^{(v)} - p'k_{fz_{bs}}^{(u')*} + \ell'k_{fz_c}^{(v')*})d_f - 1} \times \\
& \left\{ \Lambda_{L-L}^{\alpha\beta\gamma\rho}{}_{aa'pp'qq'\ell\ell'}{}_{uu'vv'} \left(\bar{\tau}_{m_n}^a - \bar{\tau}_{e_n}^a, \bar{\tau}_{m_m}^{a'} - \bar{\tau}_{e_m}^{a'} \right) \right. \\
& I_0 \left((\bar{k}_{\perp a} + qk_{tz_a}^{(v)} \hat{z}) \cdot (\bar{\tau}_{e_n}^a - \bar{\tau}_{m_n}^a), (\bar{k}_{\perp a} + qk_{tz_a}^{(v)} \hat{z}) \cdot (\bar{\tau}_{m_n}^{a'} - \bar{\tau}_{m_m}^{a'}) \right) \times \\
& \left. I_0 \left(-(\bar{k}_{\perp c} + q'k_{tz_c}^{(v')*} \hat{z}) \cdot (\bar{\tau}_{e_m}^{a'} - \bar{\tau}_{m_m}^{a'}), -(\bar{k}_{\perp c} + q'k_{tz_c}^{(v')*} \hat{z}) \cdot (\bar{\tau}_{m_m}^{a'} - \bar{\tau}_{m_n}^{a'}) \right) \right\}
\end{aligned}$$

$$\begin{aligned}
& + \Lambda_{L-L}^{\alpha\beta\gamma\rho} \left(\bar{r}_{m_n}^a - \bar{r}_{e_n}^a, \bar{r}_{m_m}^{-a'} - \bar{r}_{m_m}^{a'} \right) \\
& \quad I_0 \left((\bar{k}_{\perp a} + qk_{tza}^{(v)} \hat{z}) \cdot (\bar{r}_{e_n}^a - \bar{r}_{m_n}^a), (\bar{k}_{\perp a} + qk_{tza}^{(v)} \hat{z}) \cdot (\bar{r}_{m_n}^{-a} - \bar{r}_{m_n}^{a'}) \right) \times \\
& \quad I_\eta \left(-(\bar{k}_{\perp c} + q'k_{tzc}^{(v')*} \hat{z}) \cdot (\bar{r}_{e_m}^{a'} - \bar{r}_{m_m}^{a'}), -(\bar{k}_{\perp c} + q'k_{tzc}^{(v')*} \hat{z}) \cdot (\bar{r}_{m_m}^{-a'} - \bar{r}_{m_m}^{a'}) \right) \\
& + \Lambda_{L-L}^{\alpha\beta\gamma\rho} \left(\bar{r}_{m_n}^a - \bar{r}_{e_n}^a, \bar{r}_{e_m}^{a'} - \bar{r}_{m_m}^{a'} \right) \\
& \quad I_0 \left((\bar{k}_{\perp a} + qk_{tza}^{(v)} \hat{z}) \cdot (\bar{r}_{e_n}^a - \bar{r}_{m_n}^a), (\bar{k}_{\perp a} + qk_{tza}^{(v)} \hat{z}) \cdot (\bar{r}_{m_n}^{-a} - \bar{r}_{m_n}^{a'}) \right) \times \\
& \quad I_\xi \left(-(\bar{k}_{\perp c} + q'k_{tzc}^{(v')*} \hat{z}) \cdot (\bar{r}_{e_m}^{a'} - \bar{r}_{m_m}^{a'}), -(\bar{k}_{\perp c} + q'k_{tzc}^{(v')*} \hat{z}) \cdot (\bar{r}_{m_m}^{-a'} - \bar{r}_{m_m}^{a'}) \right) \\
& + \Lambda_{L-L}^{\alpha\beta\gamma\rho} \left(\bar{r}_{m_n}^{-a} - \bar{r}_{m_n}^a, \bar{r}_{m_m}^{a'} - \bar{r}_{e_m}^{a'} \right) \\
& \quad I_\eta \left((\bar{k}_{\perp a} + qk_{tza}^{(v)} \hat{z}) \cdot (\bar{r}_{e_n}^a - \bar{r}_{m_n}^a), (\bar{k}_{\perp a} + qk_{tza}^{(v)} \hat{z}) \cdot (\bar{r}_{m_n}^{-a} - \bar{r}_{m_n}^{a'}) \right) \times \\
& \quad I_0 \left(-(\bar{k}_{\perp c} + q'k_{tzc}^{(v')*} \hat{z}) \cdot (\bar{r}_{e_m}^{a'} - \bar{r}_{m_m}^{a'}), -(\bar{k}_{\perp c} + q'k_{tzc}^{(v')*} \hat{z}) \cdot (\bar{r}_{m_m}^{-a'} - \bar{r}_{m_m}^{a'}) \right) \\
& + \Lambda_{L-L}^{\alpha\beta\gamma\rho} \left(\bar{r}_{m_n}^{-a} - \bar{r}_{m_n}^a, \bar{r}_{m_m}^{-a'} - \bar{r}_{m_m}^{a'} \right) \\
& \quad I_\eta \left((\bar{k}_{\perp a} + qk_{tza}^{(v)} \hat{z}) \cdot (\bar{r}_{e_n}^a - \bar{r}_{m_n}^a), (\bar{k}_{\perp a} + qk_{tza}^{(v)} \hat{z}) \cdot (\bar{r}_{m_n}^{-a} - \bar{r}_{m_n}^{a'}) \right) \times \\
& \quad I_0 \left(-(\bar{k}_{\perp c} + q'k_{tzc}^{(v')*} \hat{z}) \cdot (\bar{r}_{e_m}^{a'} - \bar{r}_{m_m}^{a'}), -(\bar{k}_{\perp c} + q'k_{tzc}^{(v')*} \hat{z}) \cdot (\bar{r}_{m_m}^{-a'} - \bar{r}_{m_m}^{a'}) \right) \\
& + \Lambda_{L-L}^{\alpha\beta\gamma\rho} \left(\bar{r}_{m_n}^{-a} - \bar{r}_{m_n}^a, \bar{r}_{e_m}^{a'} - \bar{r}_{m_m}^{a'} \right) \\
& \quad I_\eta \left((\bar{k}_{\perp a} + qk_{tza}^{(v)} \hat{z}) \cdot (\bar{r}_{e_n}^a - \bar{r}_{m_n}^a), (\bar{k}_{\perp a} + qk_{tza}^{(v)} \hat{z}) \cdot (\bar{r}_{m_n}^{-a} - \bar{r}_{m_n}^{a'}) \right) \times \\
& \quad I_\xi \left(-(\bar{k}_{\perp c} + q'k_{tzc}^{(v')*} \hat{z}) \cdot (\bar{r}_{e_m}^{a'} - \bar{r}_{m_m}^{a'}), -(\bar{k}_{\perp c} + q'k_{tzc}^{(v')*} \hat{z}) \cdot (\bar{r}_{m_m}^{-a'} - \bar{r}_{m_m}^{a'}) \right) \\
& + \Lambda_{L-L}^{\alpha\beta\gamma\rho} \left(\bar{r}_{m_n}^{-a} - \bar{r}_{m_n}^a, \bar{r}_{e_m}^{a'} - \bar{r}_{m_m}^{a'} \right) \\
& \quad I_\eta \left((\bar{k}_{\perp a} + qk_{tza}^{(v)} \hat{z}) \cdot (\bar{r}_{e_n}^a - \bar{r}_{m_n}^a), (\bar{k}_{\perp a} + qk_{tza}^{(v)} \hat{z}) \cdot (\bar{r}_{m_n}^{-a} - \bar{r}_{m_n}^{a'}) \right) \times \\
& \quad I_\xi \left(-(\bar{k}_{\perp c} + q'k_{tzc}^{(v')*} \hat{z}) \cdot (\bar{r}_{e_m}^{a'} - \bar{r}_{m_m}^{a'}), -(\bar{k}_{\perp c} + q'k_{tzc}^{(v')*} \hat{z}) \cdot (\bar{r}_{m_m}^{-a'} - \bar{r}_{m_m}^{a'}) \right) \\
& + \Lambda_{L-L}^{\alpha\beta\gamma\rho} \left(\bar{r}_{e_n}^a - \bar{r}_{m_n}^a, \bar{r}_{m_m}^{a'} - \bar{r}_{e_m}^{a'} \right) \\
& \quad I_\xi \left((\bar{k}_{\perp a} + qk_{tza}^{(v)} \hat{z}) \cdot (\bar{r}_{e_n}^a - \bar{r}_{m_n}^a), (\bar{k}_{\perp a} + qk_{tza}^{(v)} \hat{z}) \cdot (\bar{r}_{m_n}^{-a} - \bar{r}_{m_n}^{a'}) \right) \times
\end{aligned}$$

$$\begin{aligned}
& I_0 \left(- \left(\bar{k}_{\perp c} + q' k_{tz_c}^{(v)*} \hat{z} \right) \cdot \left(\bar{r}_{e_m}^{a'} - \bar{r}_{m_m}^{a'} \right), - \left(\bar{k}_{\perp c} + q' k_{tz_c}^{(v)*} \hat{z} \right) \cdot \left(\bar{r}_{m_m}^{-a'} - \bar{r}_{m_m}^{a'} \right) \right) \\
& + \Lambda_{L-L}^{\alpha\beta\gamma\rho \substack{aa'pp'qq'\ell\ell' \\ uu'vv'}} \left(\bar{r}_{e_n}^a - \bar{r}_{m_n}^a, \bar{r}_{m_m}^{-a'} - \bar{r}_{m_m}^{a'} \right) \\
& I_{\xi} \left(\left(\bar{k}_{\perp a} + q k_{tz_a}^{(v)} \hat{z} \right) \cdot \left(\bar{r}_{e_n}^a - \bar{r}_{m_n}^a \right), \left(\bar{k}_{\perp a} + q k_{tz_a}^{(v)} \hat{z} \right) \cdot \left(\bar{r}_{m_n}^{-a} - \bar{r}_{m_n}^a \right) \right) \times \\
& I_{\eta} \left(- \left(\bar{k}_{\perp c} + q' k_{tz_c}^{(v)*} \hat{z} \right) \cdot \left(\bar{r}_{e_m}^{a'} - \bar{r}_{m_m}^{a'} \right), - \left(\bar{k}_{\perp c} + q' k_{tz_c}^{(v)*} \hat{z} \right) \cdot \left(\bar{r}_{m_m}^{-a'} - \bar{r}_{m_m}^{a'} \right) \right) \\
& + \Lambda_{L-L}^{\alpha\beta\gamma\rho \substack{aa'pp'qq'\ell\ell' \\ uu'vv'}} \left(\bar{r}_{e_n}^a - \bar{r}_{m_n}^a, \bar{r}_{e_m}^{a'} - \bar{r}_{m_m}^{a'} \right) \\
& I_{\xi} \left(\left(\bar{k}_{\perp a} + q k_{tz_a}^{(v)} \hat{z} \right) \cdot \left(\bar{r}_{e_n}^a - \bar{r}_{m_n}^a \right), \left(\bar{k}_{\perp a} + q k_{tz_a}^{(v)} \hat{z} \right) \cdot \left(\bar{r}_{m_n}^{-a} - \bar{r}_{m_n}^a \right) \right) \times \\
& I_{\xi} \left(- \left(\bar{k}_{\perp c} + q' k_{tz_c}^{(v)*} \hat{z} \right) \cdot \left(\bar{r}_{e_m}^{a'} - \bar{r}_{m_m}^{a'} \right), - \left(\bar{k}_{\perp c} + q' k_{tz_c}^{(v)*} \hat{z} \right) \cdot \left(\bar{r}_{m_m}^{-a'} - \bar{r}_{m_m}^{a'} \right) \right) \Big\} \times \\
& \left[\frac{\Phi_{\alpha\beta\gamma\rho} \left(\bar{k}_{\perp a} - \bar{k}_{\perp a_s}, -p' k_{fz_{bs}}^{(u)*} + \ell' k_{fz_c}^{(v)*} \right)}{p k_{fz_{as}}^{(u)} - \ell k_{fz_a}^{(v)} - p' k_{fz_{bs}}^{(u)*} + \ell' k_{fz_c}^{(v)*}} - \frac{\Phi_{\alpha\beta\gamma\rho} \left(\bar{k}_{\perp a} - \bar{k}_{\perp a_s}, -p k_{fz_{as}}^{(u)} + \ell k_{fz_a}^{(v)} \right)}{p k_{fz_{as}}^{(u)} - \ell k_{fz_a}^{(v)} - p' k_{fz_{bs}}^{(u)*} + \ell' k_{fz_c}^{(v)*}} \times \right. \\
& \left. e^{i(p k_{fz_{as}}^{(u)} - \ell k_{fz_a}^{(v)} - p' k_{fz_{bs}}^{(u)*} + \ell' k_{fz_c}^{(v)*}) h_f} \right] \quad (6.123)
\end{aligned}$$

Chapter 7

SAR Imaging of a Point Target Beneath a Layered Continuous Random Media

The purpose of formulating the scattering models of the proceeding chapters was to enable an analysis of the performance degradation experienced by a SAR sensor in detecting and imaging targets obscured by one or more layers of random media. The results presented in these chapters show both the attenuation and phase fluctuation effects of the random media, and give some insight into the possible reductions in signal-to-clutter level and resolution which are associated with these effects. In this chapter, the performance degradations are examined more explicitly, utilizing a simple model of a SAR processor and applying the above results to characterize the received signals input to the processor. The receiver model employed is first described, and the results obtained above for the statistics of the scattering components are related to the

statistics of the input signals, and used to characterize the output of the processor. SAR images of a point target are then generated with and without the presence of an interfering random layer, and several effects of the random layer on the image are demonstrated.

7.1. SAR Processing

The processor which is considered here is the simple linear scheme diagrammed in Figure 7.1. The received signal is first mixed down to a baseband frequency, passed through an arbitrary linear filter, $h(x, t)$, and finally through a square law detector. The detection process consists of comparing the output of the square law device with a threshold level, u_0 . The received signal, $s(x, t)$ is assumed to be a continuous function of both time, t , and the linear position, x , of the SAR platform along its flight path. This later simplification avoids the sampling and associated ambiguity issues which may arise in the more realistic case where measurements are taken at only discrete locations along the flight path. These sampling issues serve only to obscure the issues presently of interest.

The output of the linear filter is given by the convolution integral over x and t which is shown in (7.1).

$$q(x, t) = \int_{-\infty}^{\infty} dx' \int_{-\infty}^{\infty} dt' r(x', t') h(x - x', t - t') \quad (7.1)$$

The limits of integration in the above are infinite, however, the linear filter will include a finite window in x corresponding to the finite integration angle of the SAR system.

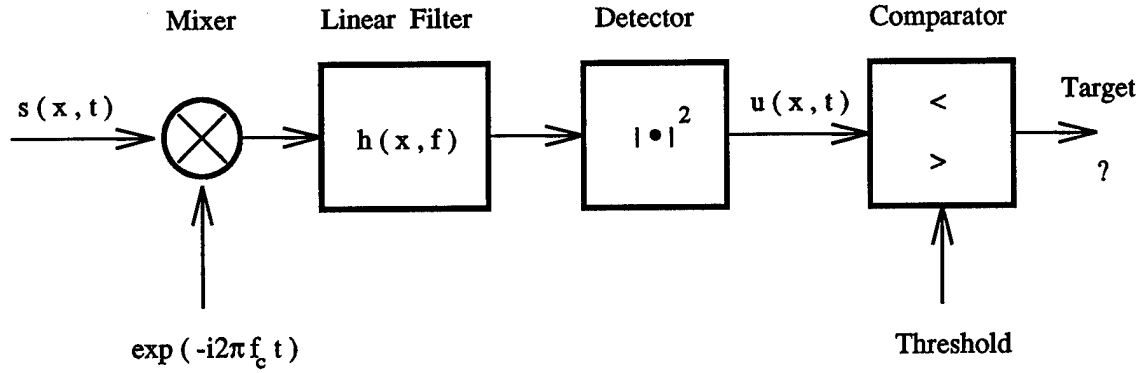


Figure 7.1. Block Diagram of the simple SAR processor used in the analysis of the random medium's effect on the imaging of a point target.

It will also be assumed shortly that the processing is performed over only a finite bandwidth, and, thus, the transform, $\tilde{h}(x, f)$, is of limited duration in both space and frequency. The mean output of the square law device is found by multiplying (7.1) by its conjugate and averaging, as shown in (7.2),

$$\begin{aligned}
 \langle u(x, t) \rangle &= \int_{-\infty}^{\infty} dx_1 \int_{-\infty}^{\infty} dx_2 \int_{-\infty}^{\infty} dt_1 \int_{-\infty}^{\infty} dt_2 \langle r(x_1, t_1) r^*(x_2, t_2) \rangle h(x - x_1, t - t_1) \times \\
 &\quad h^*(x - x_2, t - t_2) \\
 &= \int_{-\infty}^{\infty} dx_1 \int_{-\infty}^{\infty} dx_2 \int_{-\frac{B}{2}}^{\frac{B}{2}} df_1 \int_{-\frac{B}{2}}^{\frac{B}{2}} df_2 \langle \tilde{r}(x_1, f_1) \tilde{r}^*(x_2, f_2) \rangle \times \\
 &\quad \tilde{h}(x - x_1, f_1) \tilde{h}^*(x - x_2, f_2) e^{i2\pi f_1 t} e^{-i2\pi f_2 t}
 \end{aligned} \tag{7.2}$$

where the later result is obtained by representing the time correlation as the inverse Fourier transform of the product of transformed quantities. Finally, $\tilde{r}(x, f)$ can be replaced by a shifted version of $\tilde{s}(x, f)$, and $\tilde{s}(x, f)$ can be split into its contributions

due to each of the scattering mechanisms discussed previously. The resulting expression is given by (7.3).

$$\begin{aligned}
 \langle u(x, t) \rangle = & \int_{-\infty}^{\infty} dx_1 \int_{-\infty}^{\infty} dx_2 \int_{-\frac{B}{2}}^{\frac{B}{2}} df_1 \int_{-\frac{B}{2}}^{\frac{B}{2}} df_2 \tilde{h}(x - x_1, f_1) \tilde{h}^*(x - x_2, f_2) \times \\
 & e^{i2\pi f_1 t} e^{-i2\pi f_2 t} \times \\
 & \left[\langle \tilde{s}_T(x_1, f_1 + f_c) \tilde{s}_T^*(x_2, f_2 + f_c) \rangle + \langle \tilde{s}_{TC}(x_1, f_1 + f_c) \tilde{s}_{TC}^*(x_2, f_2 + f_c) \rangle + \right. \\
 & \langle \tilde{s}_{CT}(x_1, f_1 + f_c) \tilde{s}_{CT}^*(x_2, f_2 + f_c) \rangle + \langle \tilde{s}_C(x_1, f_1 + f_c) \tilde{s}_C^*(x_2, f_2 + f_c) \rangle + \\
 & \langle \tilde{s}_C(x_1, f_1 + f_c) \tilde{s}_{TC}^*(x_2, f_2 + f_c) \rangle + \langle \tilde{s}_C(x_1, f_1 + f_c) \tilde{s}_{CT}^*(x_2, f_2 + f_c) \rangle + \\
 & \langle \tilde{s}_{TC}(x_1, f_1 + f_c) \tilde{s}_{CT}^*(x_2, f_2 + f_c) \rangle + \langle \tilde{s}_{CT}(x_1, f_1 + f_c) \tilde{s}_{TC}^*(x_2, f_2 + f_c) \rangle + \\
 & \left. \langle \tilde{s}_{TC}(x_1, f_1 + f_c) \tilde{s}_C^*(x_2, f_2 + f_c) \rangle + \langle \tilde{s}_{CT}(x_1, f_1 + f_c) \tilde{s}_C^*(x_2, f_2 + f_c) \rangle \right] \quad (7.3)
 \end{aligned}$$

It is now necessary to relate each of the transformed signal quantities shown above with the cross section results derived earlier. It is assumed that the waveform transmitted is a modulated pulse of the form given by (7.4) and (7.5).

$$p(t) = m(t)e^{i2\pi f_c t} \quad (7.4)$$

$$\tilde{p}(f) = \tilde{m}(f - f_c) \quad (7.5)$$

The modulating pulse, $m(t)$, can have arbitrary shape, but will be normalized such that the time integral of the power in the pulse will equal 1.

$$\int_{-\infty}^{\infty} dt |m(t)|^2 = 1 \quad (7.6)$$

The absolute power transmitted is unimportant, since the only noise source considered here is the return from the clutter. Hence, from the radar range equation it is possible to calculate the returned power at a given frequency as shown in (7.7).

$$P_r = \frac{G(x, f)^2 \lambda^2}{(4\pi)^3 R^4} |\tilde{m}(f - f_c)|^2 \sigma \quad (7.7)$$

The above must be further modified for the correlation terms in which $x_1 \neq x_2$ or $f_1 \neq f_2$. For these cases (7.7) becomes

$$P_r = \frac{G(x_1, f_1)G(x_2, f_2)\lambda_1\lambda_2}{(4\pi)^3 r_{\min}^4} \tilde{m}(f_1 - f_c) \tilde{m}^*(f_2 - f_c) \sigma^*(x_1, x_2, f_1, f_2) \times \\ e^{-i \frac{k_1 x_1^2 - k_2 x_2^2}{r_{\min}}} e^{-2i(k_1 - k_2)r_{\min}} \quad (7.8)$$

where a phase term has been added using a quadratic approximation, and where the portion arising from the standard radar range equation has been split to reflect the differences at the two frequencies or positions. In addition, the time dependence initially assumed in calculating σ in previous sections has the opposite sign of that used in (7.4). Hence, σ is replaced by $\sigma(x_1, x_2, -f_1, -f_2) = \sigma^*(x_1, x_2, f_1, f_2)$ and the phase terms in (7.8) now also have opposite signs. Because the bandwidths considered are relatively small, a final approximation is introduced in which the gain term is expressed as

$$G(x_1, f_1)G(x_2, f_2)\lambda_1\lambda_2 \approx G(x_1, f_c)G(x_2, f_c)\lambda_c^2 \quad (7.9)$$

If it is now assumed that the squared magnitudes of the signal components \tilde{s}_T , \tilde{s}_{TC} , \tilde{s}_{CT} , and \tilde{s}_C are equal to the returned power calculated above, then it can be seen that the correlation of signal terms is given by (7.10)-(7.16).

$$\begin{aligned} \langle \tilde{s}_T(x_1, f_1) \tilde{s}_T^*(x_2, f_2) \rangle &= \sigma_{T-T}^*(x_1, x_2, f_1, f_2) \frac{G(x_1, f_c) \lambda_c^2 G(x_2, f_c)}{(4\pi)^3 r_{\min}^4} \times \\ &\quad \tilde{m}(f_1 - f_c) \tilde{m}^*(f_2 - f_c) e^{-i2\pi \frac{f_1 x_1^2 - f_2 x_2^2}{c_0 r_{\min}}} e^{-i4\pi(f_1 - f_2) \frac{r_{\min}}{c_0}} \end{aligned} \quad (7.10)$$

$$\begin{aligned} \langle \tilde{s}_{TC}(x_1, f_1) \tilde{s}_{TC}^*(x_2, f_2) \rangle &= \sigma_{TC-TC}^*(x_1, x_2, f_1, f_2) \frac{G(x_1, f_c) \lambda_c^2 G(x_2, f_c)}{(4\pi)^3 r_{\min}^4} \times \\ &\quad \tilde{m}(f_1 - f_c) \tilde{m}^*(f_2 - f_c) e^{-i2\pi \frac{f_1 x_1^2 - f_2 x_2^2}{c_0 r_{\min}}} e^{-i4\pi(f_1 - f_2) \frac{r_{\min}}{c_0}} \end{aligned} \quad (7.11)$$

$$\begin{aligned} \langle \tilde{s}_{CT}(x_1, f_1) \tilde{s}_{CT}^*(x_2, f_2) \rangle &= \sigma_{CT-CT}^*(x_1, x_2, f_1, f_2) \frac{G(x_1, f_c) \lambda_c^2 G(x_2, f_c)}{(4\pi)^3 r_{\min}^4} \times \\ &\quad \tilde{m}(f_1 - f_c) \tilde{m}^*(f_2 - f_c) e^{-i2\pi \frac{f_1 x_1^2 - f_2 x_2^2}{c_0 r_{\min}}} e^{-i4\pi(f_1 - f_2) \frac{r_{\min}}{c_0}} \end{aligned} \quad (7.12)$$

$$\begin{aligned} \langle \tilde{s}_{TC}(x_1, f_1) \tilde{s}_{CT}^*(x_2, f_2) \rangle &= \sigma_{TC-CT}^*(x_1, x_2, f_1, f_2) \frac{G(x_1, f_c) \lambda_c^2 G(x_2, f_c)}{(4\pi)^3 r_{\min}^4} \times \\ &\quad \tilde{m}(f_1 - f_c) \tilde{m}^*(f_2 - f_c) e^{-i2\pi \frac{f_1 x_1^2 - f_2 x_2^2}{c_0 r_{\min}}} e^{-i4\pi(f_1 - f_2) \frac{r_{\min}}{c_0}} \end{aligned} \quad (7.13)$$

$$\langle \tilde{s}_C(x_1, f_1) \tilde{s}_{TC}^*(x_2, f_2) \rangle = \sigma_{C-TC}^*(x_1, x_2, f_1, f_2) \frac{G(x_1, f_c) \lambda_c^2 G(x_2, f_c)}{(4\pi)^3 r_{\min}^4} \times$$

$$\tilde{m}(f_1 - f_c)\tilde{m}^*(f_2 - f_c)e^{-i2\pi\frac{f_1x_1^2 - f_2x_2^2}{c_0r_{\min}}}e^{-i4\pi(f_1 - f_2)\frac{r_{\min}}{c_0}} \quad (7.14)$$

$$\begin{aligned} \langle \tilde{s}_C(x_1, f_1)\tilde{s}_{CT}^*(x_2, f_2) \rangle &= \sigma_{C-CT}^*(x_1, x_2, f_1, f_2) \frac{G(x_1, f_c)\lambda_c^2 G(x_2, f_c)}{(4\pi)^3 r_{\min}^4} \times \\ &\quad \tilde{m}(f_1 - f_c)\tilde{m}^*(f_2 - f_c)e^{-i2\pi\frac{f_1x_1^2 - f_2x_2^2}{c_0r_{\min}}}e^{-i4\pi(f_1 - f_2)\frac{r_{\min}}{c_0}} \end{aligned} \quad (7.15)$$

$$\begin{aligned} \langle \tilde{s}_C(x_1, f_1)\tilde{s}_C^*(x_2, f_2) \rangle &= \sigma_{C-C}^*(x_1, x_2, f_1, f_2) \frac{G(0, f_c)\lambda_c^2 G(0, f_c)}{(4\pi)^3 r_{\min}^4} \times \\ &\quad \tilde{m}(f_1 - f_c)\tilde{m}^*(f_2 - f_c)e^{-i4\pi(f_1 - f_2)\frac{r_{\min}}{c_0}} \end{aligned} \quad (7.16)$$

The last expression above differs in that the near-field definition of σ_{C-C} in Chapter 2 utilizes the peak gain of the antenna, which is assumed here to be the gain in the direction of the target when the radar is positioned at $x = 0$. In addition, the quadratic phase delay to individual ground patches is accounted for in σ_{C-C} , and only the absolute phase delay from the radar to the center point of the beam on the ground must be included in the above expression.

Equations (7.3) and (7.10)-(7.16) together specify the output of the SAR processor for a given linear filter, $\tilde{h}(x, f)$. As a final step, however, it is necessary to determine the relation between the linear position, x , and the angles θ and ϕ for which $\sigma(\theta_1, \theta_2, \phi_1, \phi_2)$ was previously calculated. The geometry of the SAR flight path is shown in Figure 7.2. The minimum separation between the radar and target occurs for $x = 0$, and this distance is given by (7.17),

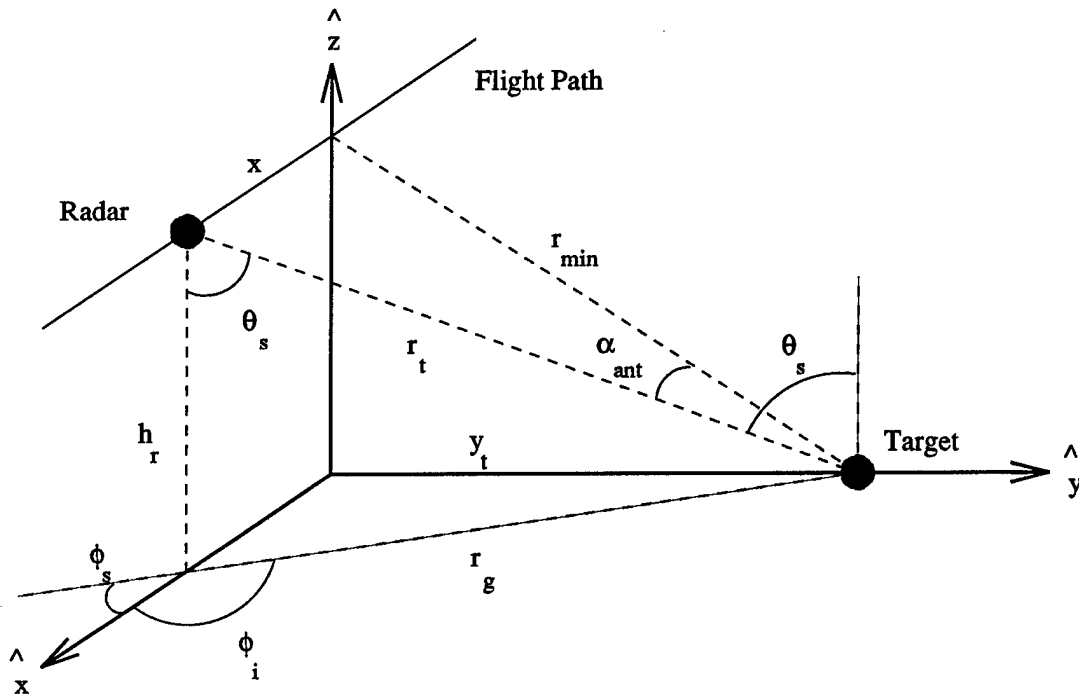


Figure 7.2. Geometry of the SAR flight path defining the incident and scattering directions for the random media multi-path problem.

$$r_{\min} = \sqrt{y_t^2 + h_r^2} \quad (7.17)$$

where y_t is the distance along the ground between the target and the position directly below the radar at $x = 0$, and where h_r is the altitude of the SAR platform. The separation of radar and target for arbitrary values of x is given by (7.18),

$$r_t = \sqrt{x^2 + y_t^2 + h_r^2} \quad (7.18)$$

and the projection of this along the ground is as in (7.19).

$$r_g = \sqrt{x^2 + y_t^2} \quad (7.19)$$

From the geometry, the incidence and scattering angles at the target are given by (7.20)-(7.22).

$$\theta_s = \theta_i = \tan^{-1}\left(\frac{r_g}{h_r}\right) \quad (7.20)$$

$$\phi_s = -\frac{\pi}{2} + \tan^{-1}\left(\frac{x}{y_t}\right) \quad (7.21)$$

$$\phi_i = \frac{\pi}{2} + \tan^{-1}\left(\frac{x}{y_t}\right) \quad (7.22)$$

As described above, the SAR antenna is assumed to be oriented such that for $x = 0$ the peak of the main lobe falls directly on the target. For $x \neq 0$, it can be shown that the separation angle between the direction of the main lobe peak and the direction of the target is given by (7.23).

$$\alpha_{\text{ant}} = \sin^{-1}\left(\frac{|x|}{r_t}\right) \quad (7.23)$$

The above expression allows evaluation of the antenna gain as a function of x , using the usual far field gain pattern defined over angle.

7.2. Approximate Evaluation of the SAR Response

Equation (7.3) of the previous section gives the SAR response in range and cross-range as a four-fold integral over the bandwidth and aperture of the SAR processing system. In this present form, evaluation of the expression requires considerable computational effort, and is not particularly practical. In addition, this result is more general than what is sought, since the analysis here will not consider general filters, $\tilde{h}(x, f)$, but will be limited to the case where $\tilde{h}(x, f)$ is a matched filter. In this section, a simplified version of (7.3) is derived by taking advantage of the particular form of the signal received and filter employed. This approximate form will not only reduce the computational burden in producing the images which follow in the next section, but will also lend insight into the effect of the incoherent target signature in blurring the resultant images.

To simplify the derivation presented here, only the contribution of a single, arbitrary pair of received signal components will be considered, and these will be denoted by $s_{m1}(x, f)$ and $s_{m2}(x, f)$. Hence, (7.3) takes the following form when only this single correlation pair is considered.

$$\begin{aligned} \langle u(x, t) \rangle = & \int_{x-\frac{L}{2}}^{x+\frac{L}{2}} dx_1 \int_{x-\frac{L}{2}}^{x+\frac{L}{2}} dx_2 \int_{-\frac{B}{2}}^{\frac{B}{2}} df_1 \int_{-\frac{B}{2}}^{\frac{B}{2}} df_2 \tilde{h}(x - x_1, f_1) \times \\ & \tilde{h}(x - x_2, f_2) e^{i2\pi(f_1 - f_2)t} \langle s_{m1}(x_1, f_1 + f_c) s_{m2}^*(x_2, f_2 + f_c) \rangle \end{aligned} \quad (7.24)$$

In the above the ensemble average notation is used to imply the possibility that s_{m1} and s_{m2} may be incoherent terms, however, the result hold equally well for the coherent contribution where this averaging is unnecessary.

As noted above, the processing filter will be assumed to be a matched filter, such that $h(x, t)$ is taken as a weighted version of the expected coherent response which has been temporally and spatially reversed and then conjugated.

$$h(x, t) = W(-x)r_T^*(-x, -t) \quad (7.25)$$

Fourier transforming, $\tilde{h}(x, f)$ is then given by (7.26).

$$\begin{aligned} \tilde{h}(x, f) &= \mathcal{F}\{W(-x)r_T^*(-x, -t)\} \\ &= \int dt W(-x)r_T^*(-x, -t)e^{-i2\pi ft} \\ &= \left[\int dt W(-x)r_T(-x, t)e^{-i2\pi ft} \right]^* \\ &= W^*(-x)\tilde{r}_T^*(-x, f) \\ &= W^*(-x)\tilde{s}_T^*(-x, f + f_c) \end{aligned} \quad (7.26)$$

Substituting this form of the filter for $\tilde{h}(x, f)$, and then further replacing the received signal components by the representations of (7.10)-(7.16) yields (7.27).

$$\begin{aligned} \langle u(x, t) \rangle &= \int_{x-\frac{L}{2}}^{x+\frac{L}{2}} dx_1 \int_{x-\frac{L}{2}}^{x+\frac{L}{2}} dx_2 \int_{-\frac{B}{2}}^{\frac{B}{2}} df_1 \int_{-\frac{B}{2}}^{\frac{B}{2}} df_2 W^*(x_1 - x)W(x_2 - x) \times \\ &\quad \sigma_{T-T}(x_1 - x, x_2 - x, f_1 + f_c, f_2 + f_c) \frac{G(x_1 - x, f_c)\lambda_c^4 G(x_2 - x, f_c)}{(4\pi)^3 r^4} \times \\ &\quad \tilde{m}^*(f_1)\tilde{m}(f_2) e^{i2\pi \frac{(f_1+f_c)(x_1-x)^2 - (f_2+f_c)(x_2-x)^2}{c_0 r}} e^{i4\pi(f_1-f_2)\frac{r}{c_0}} \times \\ &\quad e^{i2\pi(f_1-f_2)t} \sigma_M^*(x_1, x_2, f_1 + f_c, f_2 + f_c) \frac{G(x_1, f_c)\lambda_c^4 G(x_2, f_c)}{(4\pi)^3 r^4} \times \\ &\quad \tilde{m}(f_1)\tilde{m}^*(f_2) e^{-i2\pi \frac{(f_1+f_c)x_1^2 - (f_2+f_c)x_2^2}{c_0 r}} e^{-i4\pi(f_1-f_2)\frac{r}{c_0}} \end{aligned} \quad (7.27)$$

Removing the phase terms which cancel, the above can be rewritten as in (7.28),

$$\begin{aligned} \langle u(x, t) \rangle = & \int_{x-\frac{L}{2}}^{x+\frac{L}{2}} dx_1 \int_{x-\frac{L}{2}}^{x+\frac{L}{2}} dx_2 \int_{-\frac{B}{2}}^{\frac{B}{2}} df_1 \int_{-\frac{B}{2}}^{\frac{B}{2}} df_2 F(x, x_1, x_2, f_1, f_2) \times \\ & \exp \left\{ i \frac{2\pi}{c_0 r} \left[(f_1 - f_2) (t c_0 r + x^2) - 2x (f_1 x_1 - f_2 x_2) - 2x f_c (x_1 - x_2) \right] \right\} \end{aligned} \quad (7.28)$$

where

$$\begin{aligned} F(x, x_1, x_2, f_1, f_2) = & W^*(x_1 - x) W(x_2 - x) |\tilde{m}(f_1)|^2 |\tilde{m}(f_2)|^2 \times \\ & \sigma_{T-T}(x_1 - x, x_2 - x, f_1 + f_c, f_2 + f_c) \times \\ & \sigma_M^*(x_1, x_2, f_1 + f_c, f_2 + f_c) \times \\ & \frac{G(x_1 - x, f_c) G(x_2 - x, f_c) G(x_1, f_c) G(x_2, f_c) \lambda_c^4}{(4\pi)^6 r^8} \end{aligned} \quad (7.29)$$

Several of the phase terms appearing in (7.28) are small and can be neglected for the case of a relatively narrow bandwidth system. In particular, the quadratic phase terms in the difference frequencies can be ignored, as shown by (7.30) and (7.31).

$$2\pi \frac{x^2}{c_0 r} (f_1 - f_2) < \frac{\pi}{4} \quad (7.30)$$

$$2\pi \frac{2x(f_1 x_1 - f_2 x_2)}{c_0 r} < \frac{\pi}{4} \quad (7.31)$$

Hence, (7.28) can be rewritten as in (7.32).

$$\begin{aligned} \langle u(x, t) \rangle = & \int_{x-\frac{L}{2}}^{x+\frac{L}{2}} dx_1 \int_{x-\frac{L}{2}}^{x+\frac{L}{2}} dx_2 \int_{-\frac{B}{2}}^{\frac{B}{2}} df_1 \int_{-\frac{B}{2}}^{\frac{B}{2}} df_2 F(x, x_1, x_2, f_1, f_2) \times \\ & \exp \left\{ i2\pi \left[(f_1 - f_2)t + \frac{2f_c}{c_0 r} (x_2 - x_1)x \right] \right\} \end{aligned} \quad (7.32)$$

A change of variables is now applied, such that the new x'_1 and x'_2 will be defined relative to x , rather than in the absolute coordinate frame. Hence,

$$x'_1 = x_1 - x \quad (7.33)$$

$$x'_2 = x_2 - x \quad (7.34)$$

$$\begin{aligned} \langle u(x, t) \rangle = & \int_{-\frac{L}{2}}^{\frac{L}{2}} dx'_1 \int_{-\frac{L}{2}}^{\frac{L}{2}} dx'_2 \int_{-\frac{B}{2}}^{\frac{B}{2}} df_1 \int_{-\frac{B}{2}}^{\frac{B}{2}} df_2 F'(x, x'_1, x'_2, f_1, f_2) \times \\ & \exp \left\{ i2\pi \left[(f_1 - f_2)t + \frac{2f_c}{c_0 r} (x'_2 - x'_1)x \right] \right\} \end{aligned} \quad (7.35)$$

$$\begin{aligned} F'(x, x'_1, x'_2, f_1, f_2) = & W^*(x'_1)W(x'_2)|\tilde{m}(f_1)|^2|\tilde{m}(f_2)|^2 \times \\ & \sigma_{T-T}(x'_1, x'_2, f_1 + f_c, f_2 + f_c) \times \\ & \sigma_M^*(x'_1 + x, x'_2 + x, f_1 + f_c, f_2 + f_c) \times \\ & \frac{G(x'_1, f_c)G(x'_2, f_c)\lambda_c^4 G(x'_1 + x, f_c)G(x'_2 + x, f_c)}{(4\pi)^6 r^8} \end{aligned} \quad (7.36)$$

To simplify the above further, it is now assumed that the real antenna gain remains relatively constant about the center of the main lobe for an angular extent equal to the integration angle of the system. Thus the real antenna gains above can be approximated as in (7.37).

$$G(x'_1, f_c) = G(x'_2, f_c) = G(x'_1 + x, f_c) = G(x'_2 + x, f_c) = G_0 \quad (7.37)$$

Since the absolute amplitude of the result is also unimportant, all scaling constants will be neglected, and (7.36) can be rewritten as (7.38).

$$F'(x, x'_1, x'_2, f_1, f_2) = W^*(x'_1)W(x'_2)|\tilde{m}(f_1)\tilde{m}(f_2)|^2\sigma_{T-T}(x'_1, x'_2, f_1 + f_c, f_2 + f_c) \times \\ \sigma_M^*(x'_1 + x, x'_2 + x, f_1 + f_c, f_2 + f_c) \quad (7.38)$$

The two correlations which appear in the above expression are both stationary in azimuth, and depend only on the azimuthal difference angle, ϕ_d , which for the second correlation, σ_M , is given by (7.39),

$$\phi_d = \tan^{-1} \left(\frac{x'_2 + x}{r \sin \theta} \right) - \tan^{-1} \left(\frac{x'_1 + x}{r \sin \theta} \right) \quad (7.39)$$

where θ is the elevation angle.† For relatively small integration angles, the two arctangent expressions can be expanded in Taylor series, and sufficient accuracy is obtained by keeping only the first term to yield (7.40).

† Note that the elevation angle will also change with x , but $\theta_d = \theta_2 - \theta_1$ will be very small, and this difference is neglected here.

$$\phi_d \simeq \frac{x'_2 - x'_1}{r \sin \theta} \quad (7.40)$$

The correlations are not stationary in frequency as they are in azimuth, however, as demonstrated earlier, over small bandwidths, the dependance on center frequency is weak. Hence, without too great an error it is possible to express the correlations as $\sigma_M(\phi_d, f_d)$. A slightly better result is possible if a variance correction is applied, such that the shape of the correlation is assumed stationary, but the power returned at each frequency is corrected. This approximation is given by (7.41).

$$\sigma_M(x'_1 + x, x'_2 + x, f_1 + f_c, f_2 + f_c) = \sigma_M^c(\phi_d, f_d) \sqrt{\frac{\sigma_M^v(f_1 + f_c) \sigma_M^v(f_2 + f_c)}{\sigma_M^v(f_c) \sigma_M^v(f_c + f_d)}} \quad (7.41)$$

The above gives the correct result for all $f_1 = f_2$, even when $f_1 \neq f_c$. The functions σ_M^c and σ_M^v are defined by (7.42) and (7.43).

$$\sigma_M^c(\phi_d, f_d) = \sigma_M(x'_2 - x'_1 = r\phi_d \sin \theta, f_c, f_c + f_d) \quad (7.42)$$

$$\sigma_M^v(f) = \sigma_M(x'_2 - x'_1 = 0, f, f) \quad (7.43)$$

Using the approximation of (7.41), the function F' can again be rewritten as given below.

$$\begin{aligned}
 F'(x'_1, x'_2, f_1, f_2) = & W^*(x'_1)W(x'_2)|\tilde{m}(f_1)\tilde{m}(f_2)|^2 \times \\
 & \sigma_{T-T}^c \left(\phi_d = \frac{x'_2 - x'_1}{r \sin \theta}, f_d \right) \sigma_M^{c*} \left(\phi_d = \frac{x'_2 - x'_1}{r \sin \theta}, f_d \right) \times \\
 & \sqrt{\frac{\sigma_M^v(f_1 + f_c) \sigma_M^v(f_2 + f_c) \sigma_{T-T}^v(f_1 + f_c) \sigma_{T-T}^v(f_2 + f_c)}{\sigma_M^v(f_c) \sigma_M^v(f_c + f_d) \sigma_{T-T}^v(f_c) \sigma_{T-T}^v(f_c + f_d)}} \quad (7.44)
 \end{aligned}$$

Another substitution of variables is now made in the integration of (7.35), such that the outer integrals are over the positional difference, x_d , and the frequency difference, f_d .

The coordinate change is shown by Figure 7.3 for the x'_1, x'_2 to x_d, x_1 transformation.

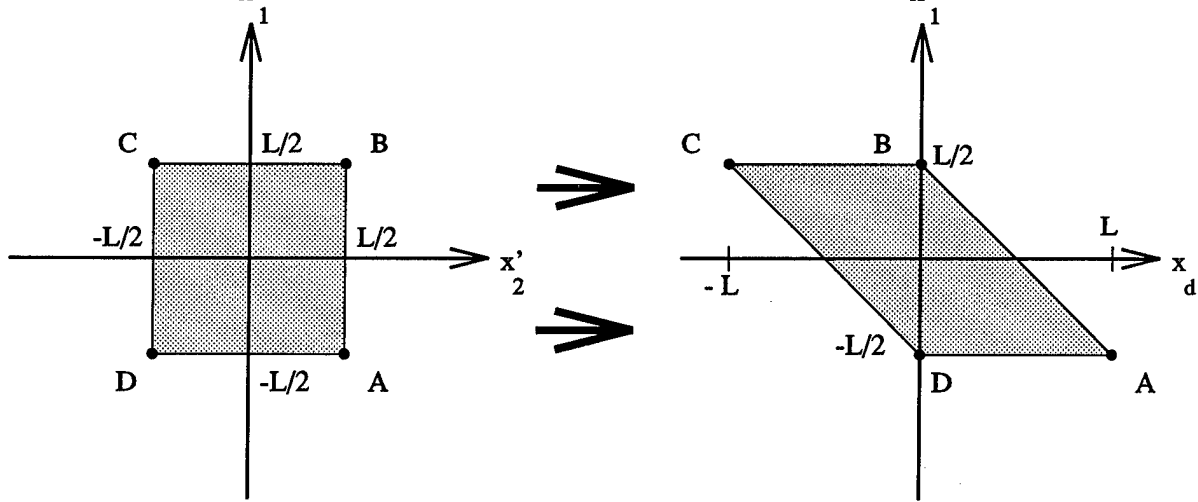


Figure 7.3. Coordinate transformation geometry for the transformation from the integration variables x'_1 and x'_2 to x_d and x_1 . The integration region is shaded in each case.

The actual transformation is given by (7.45) and (7.46).

$$x_d = x'_2 - x'_1 \quad (7.45)$$

$$x_1 = x'_1 \quad (7.46)$$

The limits of the outer x_d integration run from $-L$ to L , and the limits of the inner x_1 integration run from $x_{1\ell}(x_d)$ to $x_{1u}(x_d)$, where these functions are given by (7.47) and (7.48).

$$x_{1\ell}(x_d) = \begin{cases} -L/2 & , \quad x_d \geq 0 \\ -x_d - L/2 & , \quad x_d < 0 \end{cases} \quad (7.47)$$

$$x_{1u}(x_d) = \begin{cases} L/2 & , \quad x_d < 0 \\ L/2 - x_d & , \quad x_d \geq 0 \end{cases} \quad (7.48)$$

Similarly, the transformation for the f_1 and f_2 integrals is given by (7.49) and (7.50).

$$f_d = f_1 - f_2 \quad (7.49)$$

$$f_{2\text{new}} = f_2 \quad (7.50)$$

The limits of the f_d integral extend from $-B$ to B , and the lower and upper limits of the f_2 integral are given by (7.51) and (7.52), respectively.

$$f_{2\ell}(f_d) = \begin{cases} -B/2 & , \quad f_d \geq 0 \\ -f_d - B/2 & , \quad f_d < 0 \end{cases} \quad (7.51)$$

$$f_{2u}(f_d) = \begin{cases} B/2 & , \quad f_d < 0 \\ B/2 - f_d & , \quad f_d \geq 0 \end{cases} \quad (7.52)$$

The integration of (7.35) can then be rewritten as shown by (7.53),

$$\langle u(x', t) \rangle = \int_{-L}^L dx_d \int_{-B}^B df_d e^{i2\pi f_d t} e^{i2\pi x_d x'} A(x_d, f_d) \sigma_{T-T}^c \left(\phi_d = \frac{x_d}{r \sin \theta}, f_d \right) \times \sigma_M^c \left(\phi_d = \frac{x_d}{r \sin \theta}, f_d \right) \quad (7.53)$$

where $x' = 2f_c x / c_0 r$, and

$$A(x_d, f_d) = \int_{x_{1l}(x_d)}^{x_{1u}(x_d)} dx_1 \int_{f_{2l}(f_d)}^{f_{2u}(f_d)} df_2 W^*(x_1) W(x_1 + x_d) |\tilde{m}(f_2) \tilde{m}(f_2 + f_d)|^2 \times \sqrt{\frac{\sigma_M^v(f_2 + f_c) \sigma_M^v(f_2 + f_c + f_d) \sigma_{T-T}^v(f_2 + f_c) \sigma_{T-T}^v(f_2 + f_c + f_d)}{\sigma_M^v(f_c) \sigma_M^v(f_c + f_d) \sigma_{T-T}^v(f_c) \sigma_{T-T}^v(f_c + f_d)}} \quad (7.54)$$

Equation (7.53) is now clearly in the form of a two dimensional Fourier transform. To evaluate this efficiently, it is desirable to discretize the expression, and to put it in the form of a 2-D Discrete Fourier transform which may be evaluated by FFT methods. Hence, shifting the integration variables to obtain lower limits of zero, (7.55) is obtained.

$$\langle u(x', t) \rangle = e^{-i2\pi L x'} e^{-i2\pi B t} \int_0^{2L} dx_d \int_0^{2B} df_d e^{i2\pi f_d t} e^{i2\pi x_d x'} A(x_d - L, f_d - B) \times \sigma_{T-T}^c \left(\phi_d = \frac{x_d - L}{r \sin \theta}, f_d - B \right) \sigma_M^c \left(\phi_d = \frac{x_d - L}{r \sin \theta}, f_d - B \right) \quad (7.55)$$

Now sample the x_d integration at N_1 points and the f_d integral at N_2 points such that for the (n_1, n_2) sample, x_d and f_d are given by (7.56) and (7.57),

$$x_d = \frac{n_1}{N_1} (2L) \quad (7.56)$$

$$f_d = \frac{n_2}{N_2} (2B) \quad (7.57)$$

and for the (m_1, m_2) resultant sample output from the processor, x and t are given by (7.58) and (7.59),

$$x = \frac{c_0 r}{4L f_c} \frac{m_1}{p_1} \quad (7.58)$$

$$t = \frac{m_2}{2B p_2} \quad (7.59)$$

where p_1 and p_2 are zero padding factors used to obtain a finer increment in the result. The integral of (7.35) can then be rewritten as the double summation of (7.60),

$$\begin{aligned} \langle u[m_1, m_2] \rangle = & e^{-i\pi m_1} e^{-i\pi m_2} \sum_{n_1=0}^{N_1-1} \sum_{n_2=0}^{N_2-1} e^{i2\pi \frac{n_1}{N_1} \frac{m_1}{p_1}} e^{i2\pi \frac{n_2}{N_2} \frac{m_2}{p_2}} A\left(2\frac{n_1}{N_1}L - L, 2\frac{n_2}{N_2}B - B\right) \times \\ & \sigma_{T-T}^c \left(\phi_d = \frac{2\frac{n_1}{N_1}L - L}{r \sin \theta}, f_d = 2\frac{n_2}{N_2}B - B \right) \times \\ & \sigma_M^{c*} \left(\phi_d = \frac{2\frac{n_1}{N_1}L - L}{r \sin \theta}, f_d = 2\frac{n_2}{N_2}B - B \right) \end{aligned} \quad (7.60)$$

and the above can be evaluated using a 2-D FFT algorithm approach. Before evaluating the above, however, $A(x_d, f_d)$ must be evaluated over all sample points in x_d and f_d . If the frequency dependance of the variance over the processing bandwidth is neglected entirely (i.e., assuming complete stationarity in frequency), and if uniform weightings are assumed for the aperture and frequency bandwidth, then (7.54) can be evaluated analytically to obtain (7.61).

$$A(x_d, f_d) = (L - |x_d|)(B - |f_d|) \quad (7.61)$$

Before considering results in which (7.60) is used to produce simulated SAR imagery, it is of interest to show what insight into the effect of the random media may be obtained directly by examining the above expression. For this analysis, it is easiest to consider the result given by (7.55), which is in the form of a 2-D Fourier transform of the product of several functions. To obtain further insight in this result, it is convenient to write the term σ_M^c representing the correlation of an arbitrary incoherent contribution, as the product of several terms, as shown in (7.62).

$$\sigma_M^c(\phi_d, f_d) = \sigma_{T-T}^c(\phi_d, f_d) \frac{\sigma_M^v(f_c)}{\sigma_{T-T}^v(f_c)} C_M(\phi_d, f_d) \quad (7.62)$$

The arbitrary correlation is therefore represented as the product of the response for the coherent target return, a ratio of the power in the incoherent mechanism to that in the coherent mechanism, and a normalized correlation which represents the decorrelation of the incoherent mechanism in angle and frequency. Hence, if the arbitrary mechanism were actually the coherent mechanism, then the ratio would be 1, and $C_M(\phi_d, f_d)$ would be 1 for all ϕ_d and f_d . Hence, the expression for the detector output can be rewritten as in (7.63),

$$\begin{aligned} \langle u(x', t) \rangle &\propto \frac{\sigma_M^v(f_c)}{\sigma_{T-T}^v(f_c)} \times \mathcal{F} \left\{ C_M^* \left(\phi_d = \frac{x_d - L}{r \sin \theta}, f_d - B \right) \right\} \otimes \\ &\mathcal{F} \left\{ \sigma_{T-T}^c \left(\phi_d = \frac{x_d - L}{r \sin \theta}, f_d - B \right) \sigma_{T-T}^{c*} \left(\phi_d = \frac{x_d - L}{r \sin \theta}, f_d - B \right) A(x_d - L, f_d - B) \right\} \end{aligned} \quad (7.63)$$

where the Fourier transform of the product is rewritten as the convolution of the Fourier transforms of two quantities. The second Fourier transform is simply the response

to the coherent part of the target signature. Hence, the response to the incoherent mechanisms is formed by scaling the coherent response by the ratio of the powers in the incoherent and coherent returns, and then by convolving this weighted coherent response by the Fourier transform of a normalized correlation function, which behaves as a blurring function.

Several individual cases can now be considered. Firstly, if the correlation function is slow to drop off in both frequency and azimuth, and, thus, is approximately unity over the entire processing range, then the transform of $C(\phi_d, f_d)$ will be impulse-like, and convolution with the coherent response will not introduce significant blurring. Hence, the incoherent response will be a scaled copy of the coherent response, and the effect of the random media will be only to increase the overall power of the target return, increasing the signal-to-clutter ratio (for a fixed clutter level), and improving the detectability of the target.

In contrast, if $C(\phi_d, f_d)$ is very sharply peaked, and decorrelates rapidly over the processing bandwidth and aperture, then its transform will be relatively flat, and tremendous blurring will be introduced in the incoherent response when this transform is convolved with the coherent response. In the limit when the multi-path process is white, and $C(\phi_d, f_d)$ is an impulse, the incoherent response will be totally blurred so that all resolution is lost in this part of the response. The effect on the overall response which results when the severely blurred incoherent portion is added to the coherent response, will depend on the ratio of the powers of the incoherent and coherent scattering mechanisms. If this ratio is small, then the coherent return will dominate, and only in the sidelobes where the coherent return drops off will the blurring of the incoherent mechanism be seen. As, however, this ratio approaches unity, the incoherent

result will begin to have a greater effect on the overall response, and eventually the main peak of the overall response will be affected and the 3dB resolution reduced.

Hence, it can be seen from the above, that in order for the multi-path return to have a significant blurring effect on the overall response, not only does the multi-path field have to decorrelate rapidly across the integration angle and bandwidth, but also this field must have significant power when compared to the power of the direct target scattering mechanism. In the following section, a number of results are presented, and these effects are illustrated more clearly.

7.3. SAR Point Target Imaging Results

In this section, the above formulation is utilized to examine the effects of a layer of random media on the ability to image a point target located beneath the random layer. As seen in the above formulation, the degradation experienced in the SAR system depends on the correlation of the incoherent portion of the return over both azimuthal and frequency offsets. Previous chapters have shown cuts of this correlation function, either over azimuthal shifts for fixed frequency, or over frequency offsets for fixed azimuth. Figures 7.4 and 7.5 now show the complete correlation function, for the HH and VV polarizations respectively. In each case, the correlation is given for a 10 m slab of random media, assuming an isotropic exponential correlation function with correlation length $\ell = 0.0052$ m, and a fractional volume of scatterers of $f = 1.67\%$, which lead to an effective permittivity of $\epsilon_{1m} = (1.0505 + 0.001794i)\epsilon_0$. Above and below the random slab are half-spaces of free space permittivity, and the point target

is located in the region beneath, at a depth of 5 m below the lower interface of the random layer. The results are computed for an elevation angle of 70° , and with a center frequency of 1.12 GHz.

Several features are apparent in the two correlation functions. Firstly, the correlations drop more rapidly in the azimuthal direction than in the frequency direction. This result is due to the extents of the correlation shown in each direction. The $\pm 2^\circ$ extent in azimuth corresponds to a SAR integration angle which is capable of yielding a higher resolution in cross-range than can be obtained in range with the 40 MHz bandwidth suggested by the ± 40 MHz extent of the correlation in frequency. Hence, in this sense, a greater extent of the correlation function is shown in the azimuthal offset direction than in the frequency offset direction, and, thus, the decorrelation appears more rapid in azimuth.

Secondly, it can also be seen that the correlation function is not separable, and can not be expressed as the product of a correlation in azimuth, and a correlation in frequency. This is apparent by comparing, for instance, cuts in azimuth at different frequency offsets. It is clear that the decorrelation in azimuth is most rapid at a frequency offset of 0 MHz, and is slower for larger frequency offsets. Physically, this results because at a frequency offset of 0 MHz, any change in the azimuth will introduce a phase change across the region of random media contributing to the multi-path return, and will lead to decorrelation of the incoherent return. In contrast, at a non-zero frequency offset, a phase difference already exists from the frequency difference, and changing the azimuth as well may actually act to reduce this phase difference for some pairs of scatterers. The overall effect is still a decorrelation with increasing azimuthal offset, but the decorrelation is slower. As will be shown shortly, this non-

separable nature of the correlation function has an effect in the SAR system of coupling the range and cross range responses. The resolution and extent of blurring in cross-range, for instance, will depend not only on the SAR integration angle, but also on the bandwidth of the SAR system. Similarly, the resolution in range will depend on the integration angle as well as the processing bandwidth.

Finally, comparing Figures 7.4 and 7.5, it is clear that the azimuthal decorrelation is more rapid for the VV polarization than for HH, while the frequency decorrelations are comparable in the two cases. This is a result which was seen earlier, which arises because the random multi-path scattering region is wider for VV than for HH, leading to a more rapid phase change with azimuth in the VV case. In contrast, for both polarizations, the length of the region along the incident and scattering propagation directions is similar, and the rates of decorrelation are comparable.

Figures 7.6-7.8 show SAR range-cross range image results for the point target geometry for which the correlations above were calculated. The images were generated using an integration angle of approximately 2° , and a bandwidth of 40 MHz. In addition, the weightings across the processed aperture and bandwidth are uniform, resulting in the characteristic two-dimensional sinc function behavior for the free space case of Figure 7.6, where the random medium effects were removed for comparison. Figures 7.7 and 7.8 show the results in the presence of the random media for HH and VV polarizations, respectively.

Several features are evident when comparing the obscured cases with the free space case. Firstly, the peak response of the images of Figures 7.7 and 7.8 is lower than that of the free space case, since the random media is lossy, and scattering and

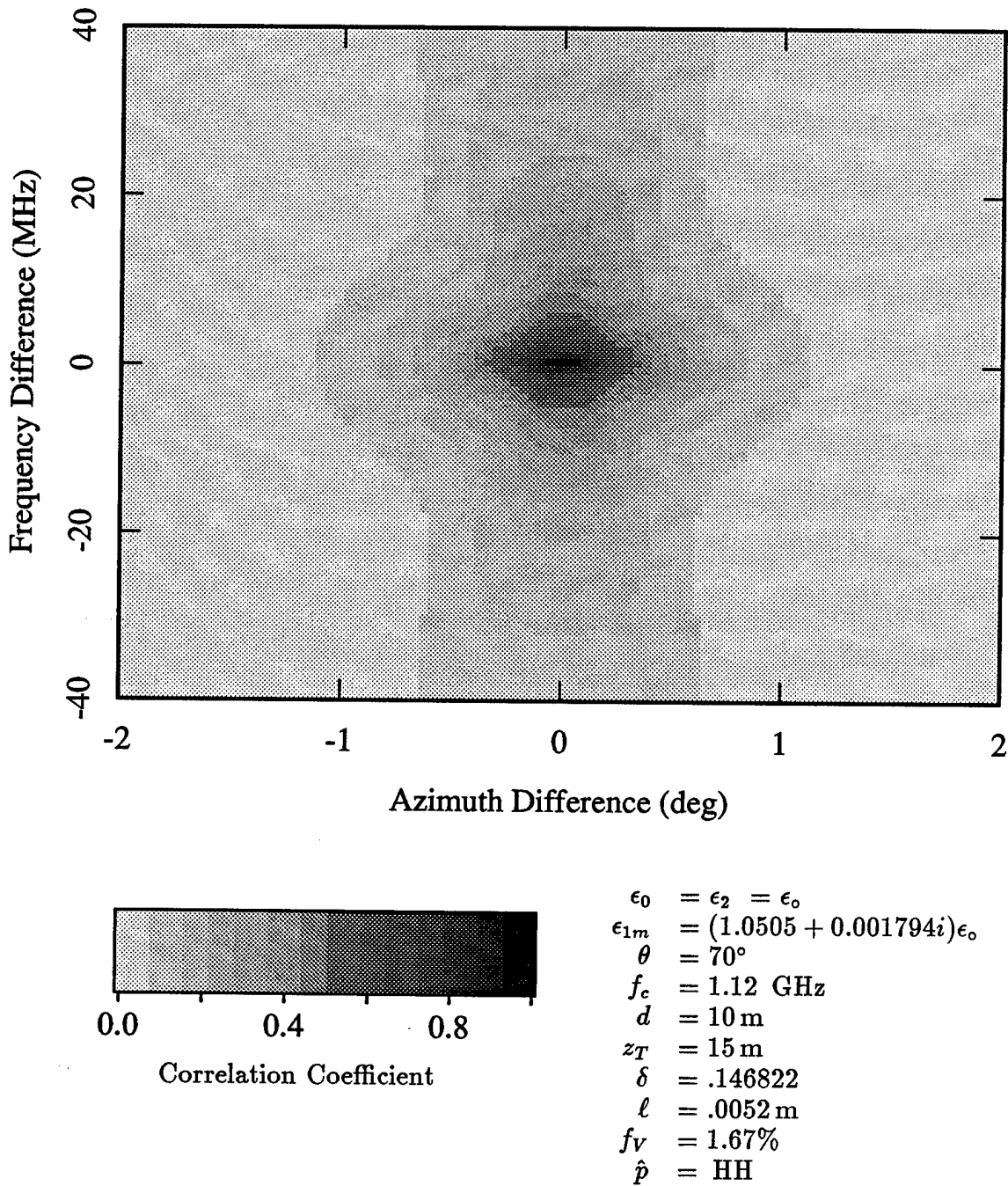


Figure 7.4. Azimuth-Frequency Correlation, σ_{TC-TC} , of the HH polarized target/clutter multi-path field for a two-layer geometry with a 10 m slab of isotropic random media, and with the target positioned 5 m below the slab. Results are shown for an elevation angle of $\theta = 70^\circ$, and with a center frequency of 1.12 GHz.

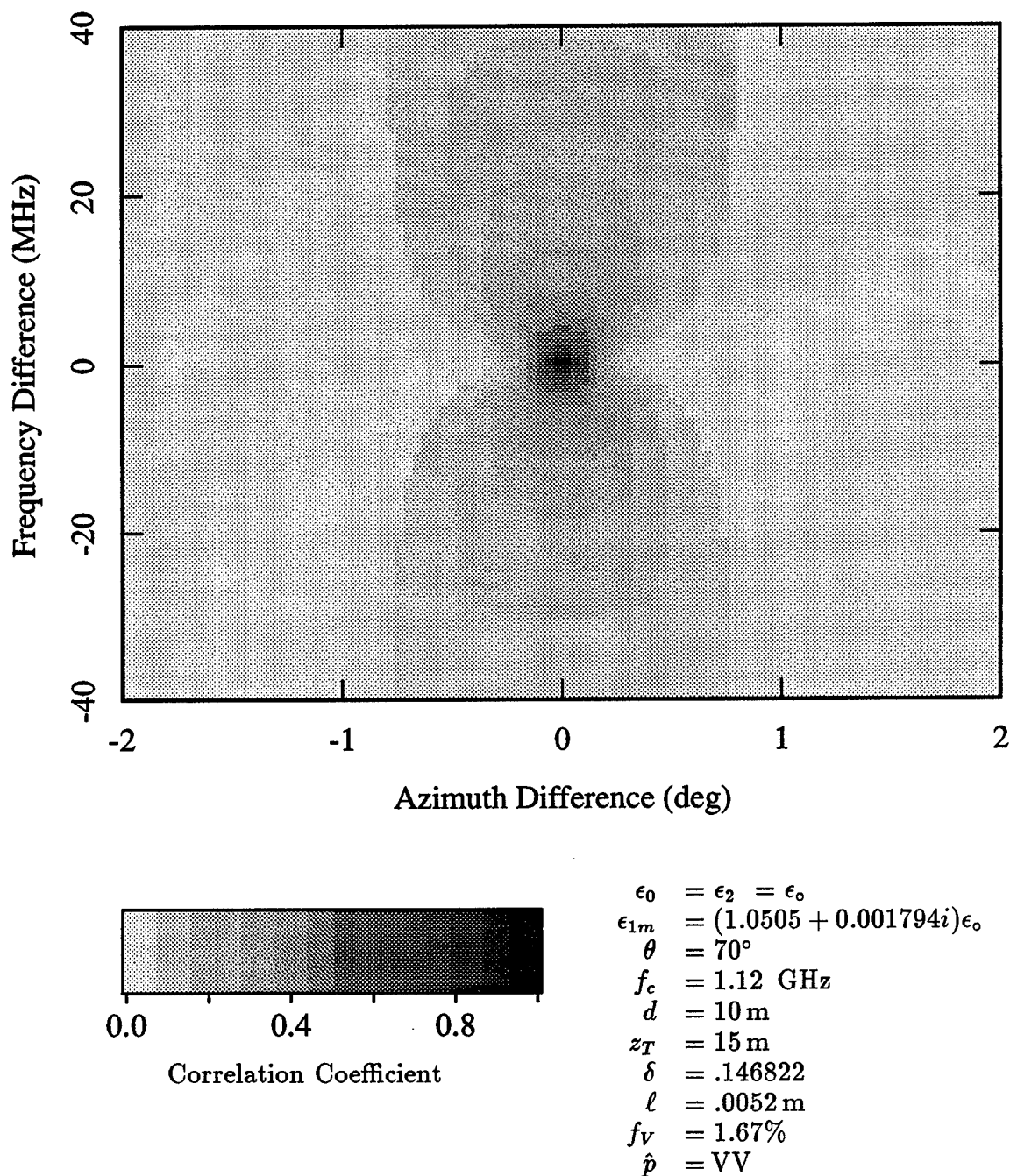


Figure 7.5. Azimuth-Frequency Correlation, σ_{TC-TC} , of the VV polarized target/clutter multi-path field for a two-layer geometry with a 10 m slab of isotropic random media, and with the target positioned 5 m below the slab. Results are shown for an elevation angle of $\theta = 70^\circ$, and with a center frequency of 1.12 GHz.

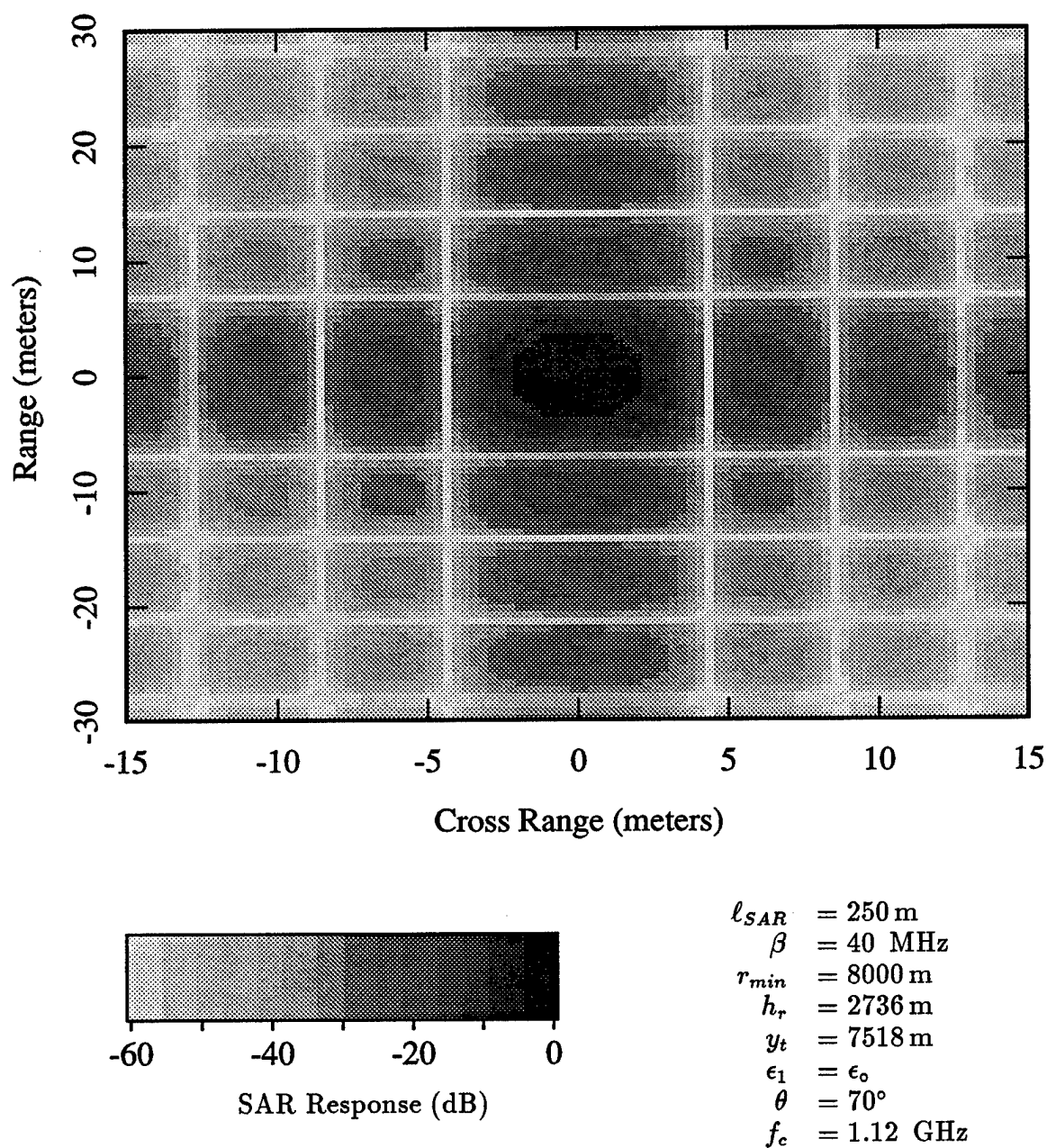


Figure 7.6. Range - Cross Range SAR response of a Point target in free space using a 40 MHz bandwidth and an integration angle of approximately 2° . Rectangular weightings were used over the integration aperture and frequency bandwidth.

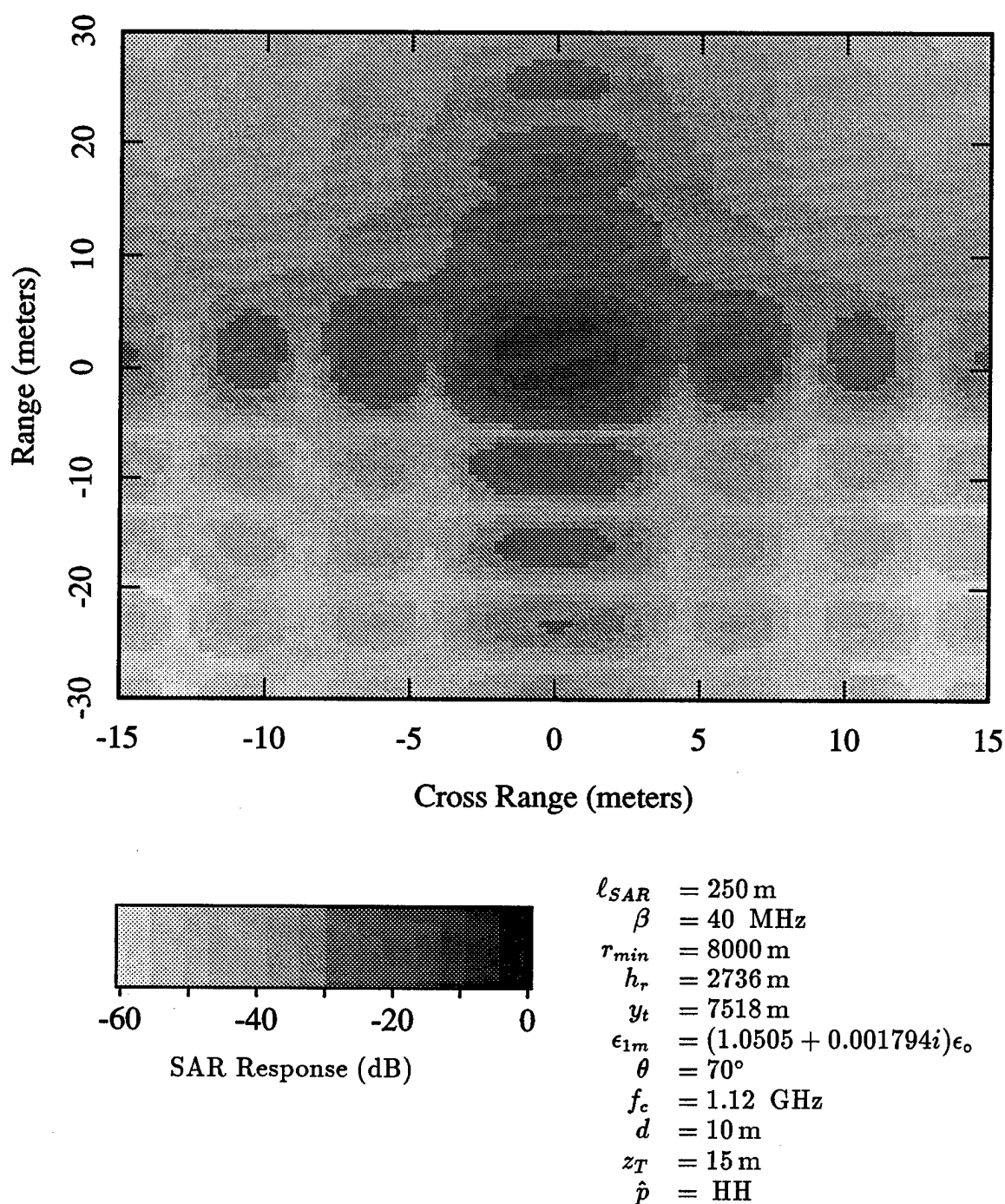


Figure 7.7. Range - Cross Range SAR response of a Point target 5 m below a 10 m slab of random media for the HH polarization, using a 40 MHz bandwidth and an integration angle of approximately 2° . Rectangular weightings were used over the integration aperture and frequency bandwidth.

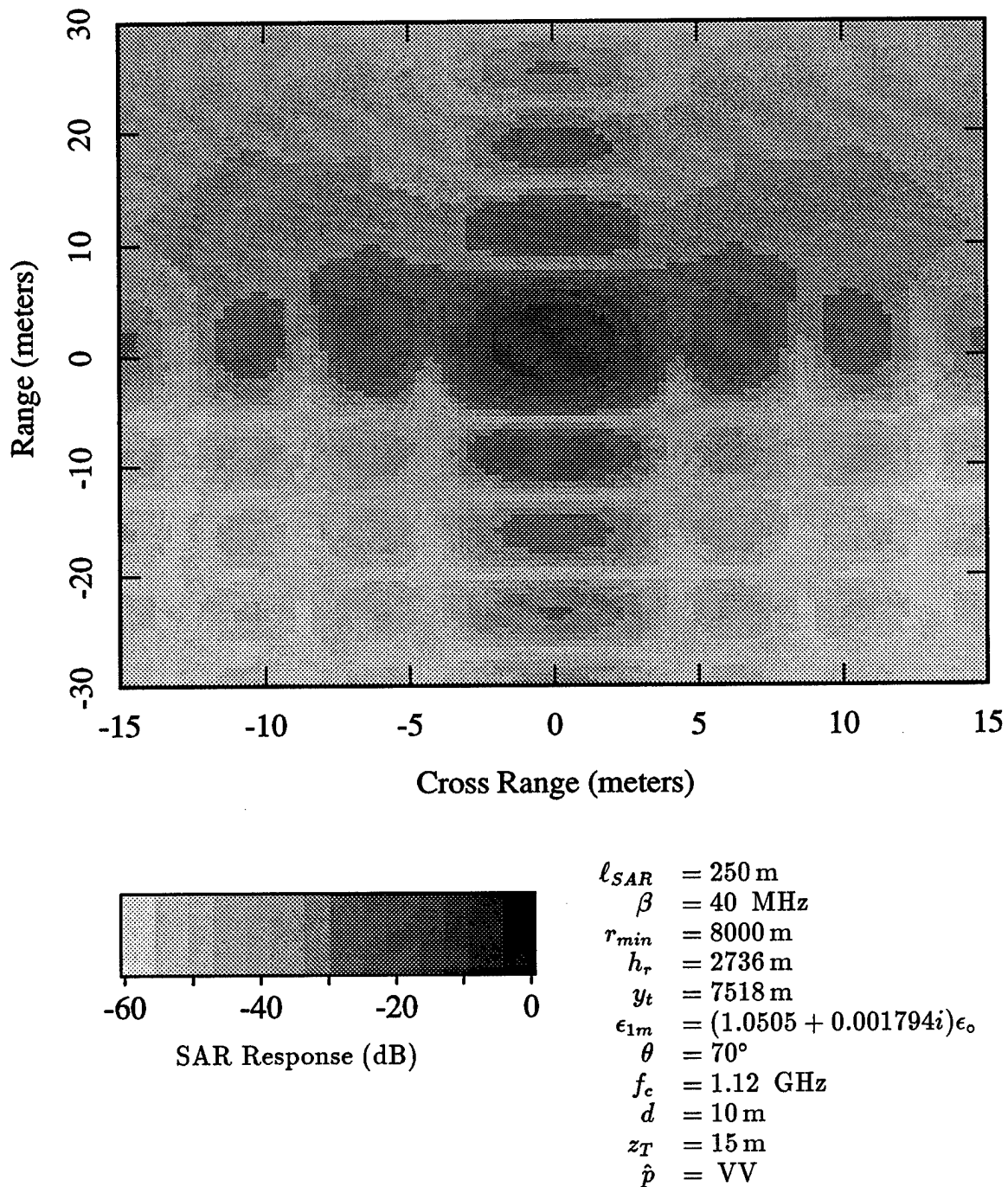


Figure 7.8. Range - Cross Range SAR response of a Point target 5 m below a 10 m slab of random media for the VV polarization, using a 40 MHz bandwidth and an integration angle of approximately 2° . Rectangular weightings were used over the integration aperture and frequency bandwidth.

absorption lead to a weaker coherent return from the point target.[†] In addition, the peak of the two random media cases is shifted slightly in the direction of positive range. This later effect is due to the fact that the SAR processing was done using a filter matched to the free space case. The intervening layer of random media is more electrically dense than free space and adds a mean delay which effectively shifts the position of the point target to a greater range.

Finally, both HH and VV polarizations exhibit considerable blurring, where in particular the nulls of the response have been filled in by the phase errors introduced by the random media. The blurring in cross range appears symmetric, but the blurring in the range direction is much greater at positive ranges than for negative ranges. This asymmetry arises because the multi-path return between the point target and any scatterer will always take a longer path than the direct target return. Each such multi-path return contributes a scaled and shifted version of the basic sinc response seen in the free space case, and because of the longer distance for the multi-path returns, each will be shifted to positive range. The blurring seen for negative ranges is due to the sidelobes of these responses. In contrast, scatterers are equally distributed to each side of the target, so the blurring is symmetric in cross range.

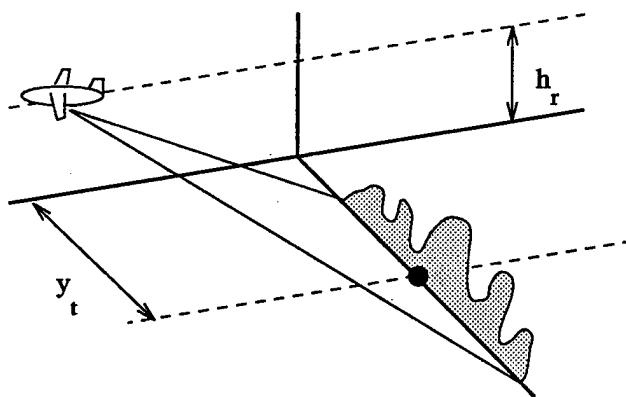
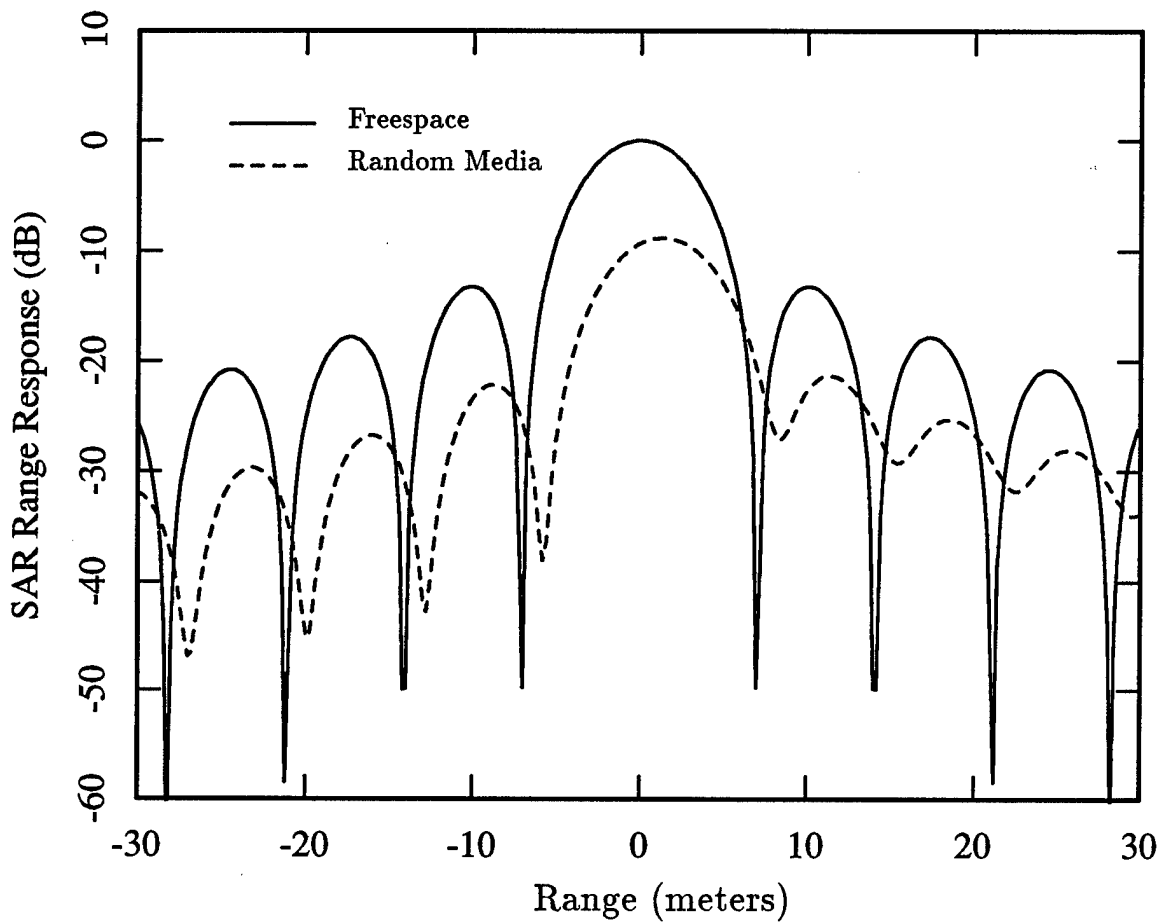
Comparing the two polarizations, the extent of the blurring in cross range along the zero range axis is comparable, where as the HH result shows more blurring in range along the zero cross range axis than does the VV case. Examining the correlations of Figures 7.4 and 7.5 again, it can be seen that the average cut in the azimuthal direction of both HH and VV cases is very similar. The VV result drops more quickly in the

[†] The free space case is normalized to have a peak response of 0 dB, and the same normalizing factor was applied with the obscured results.

immediate vicinity of a 0 MHz frequency difference, but away from the zero frequency axis, azimuthal cuts are similar. The overall extent of the blurring in the SAR images can be thought to arise from the average cut of the correlation, and since the azimuthal averages for HH and VV are similar, the cross range blurring will be similar, as seen. In contrast, frequency cuts of the two correlations for fixed azimuthal difference are similar only near an azimuthal difference of 0° . Away from this centerline, the frequency cuts of the VV polarization actually increase with increased frequency difference, while for the HH polarization these cuts are still peaked in the center. For this reason, the average frequency cut for the VV polarization decorrelates less rapidly, and the VV polarized SAR image shows less blurring in range than the HH result.

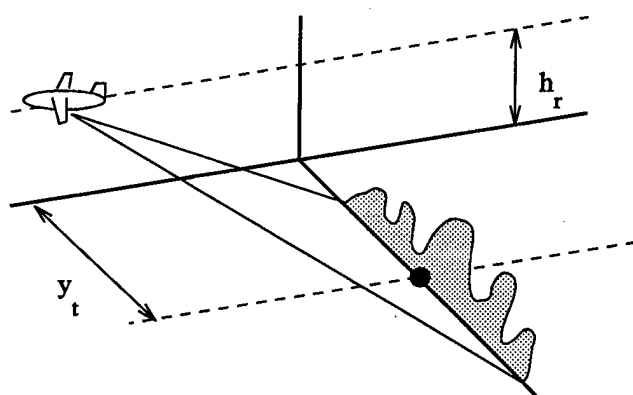
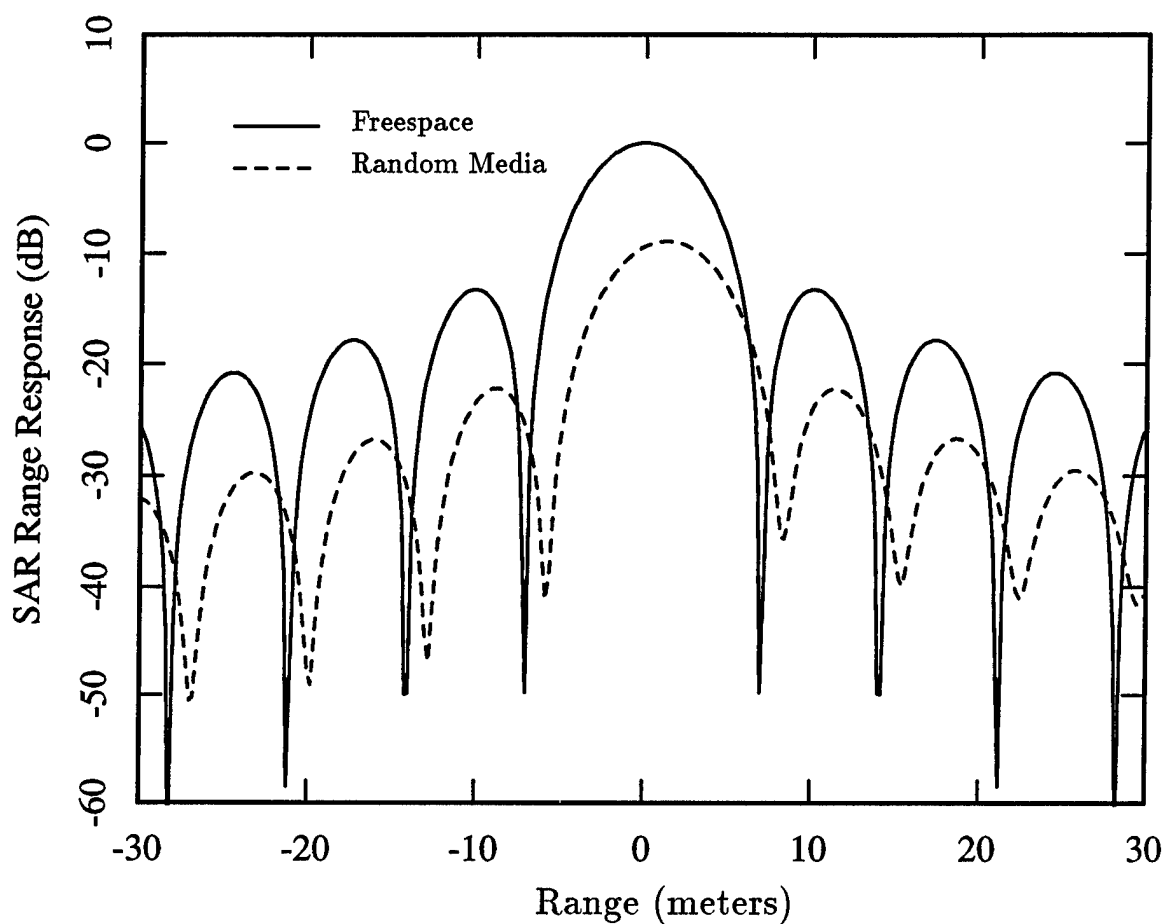
Many of the effects of the random media which were identified above can be seen more clearly by examining individual cuts of the SAR images. Figures 7.9-7.12 show cuts of the above images in the range direction for a fixed cross range of 0 m. Figures 7.9 and 7.10 compare the free space result (solid) to the overall responses with the random media present (dash) for HH and VV polarizations, respectively. Figures 7.11 and 7.12 show the individual coherent (solid) and incoherent (dash) components which compose the total response of the previous figures. The attenuation of the random media on the peak response is seen to be approximately 9 dB, and the center of the peak is shifted to a positive range of approximately 1.5 m. Once again it is apparent that the blurring is non-symmetric as evidenced by the higher sidelobe nulls at positive ranges than at negative ranges. This asymmetry can be seen even more clearly in the incoherent results of Figures 7.11 and 7.12, where particularly for the HH polarization, the positive extent of the response loses resemblance to a sinc function.

The coherent responses of Figures 7.11 and 7.12 show a small ripple in the first



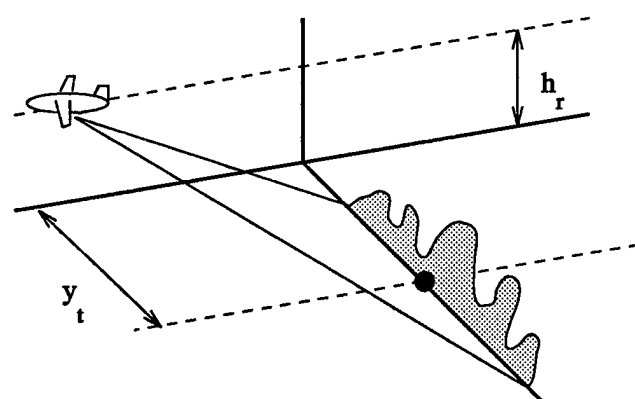
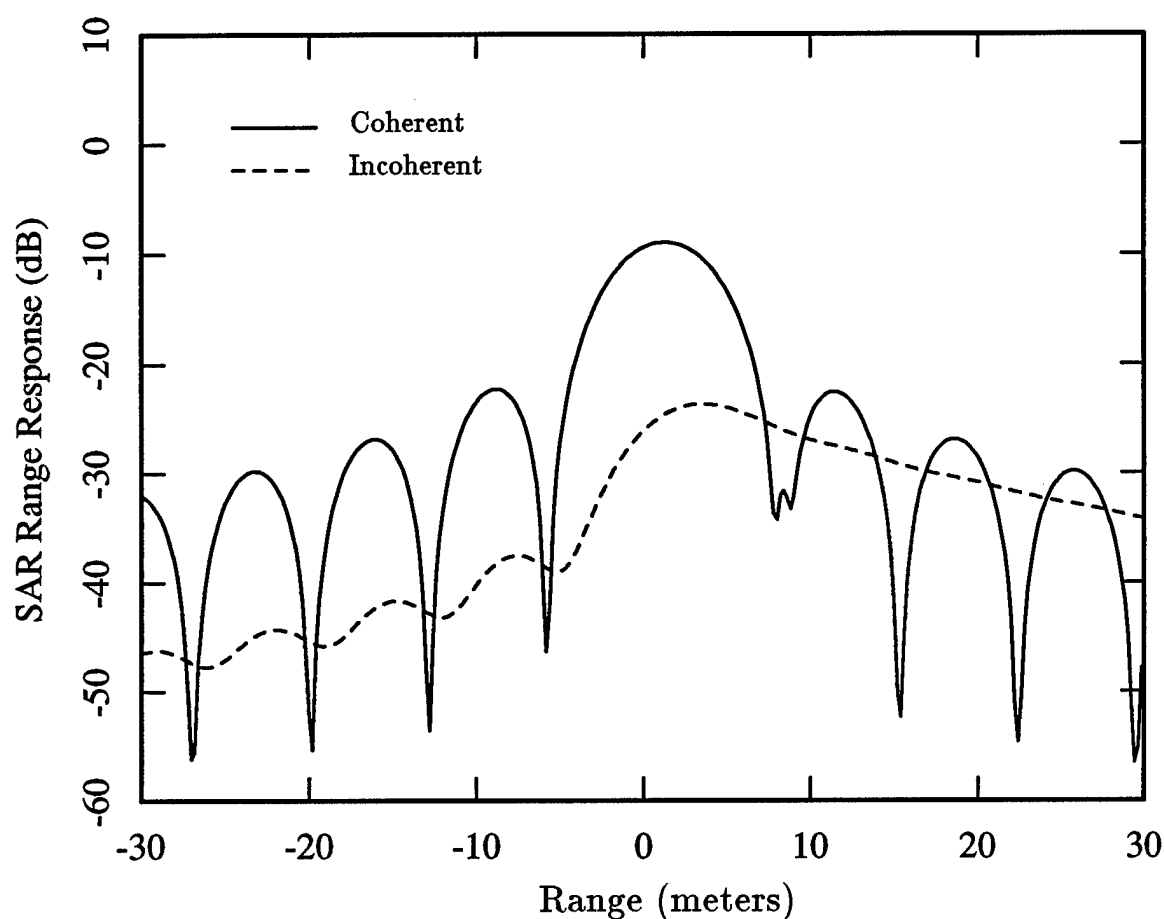
$$\begin{aligned}
 \ell_{SAR} &= 250 \text{ m} \\
 \beta &= 40 \text{ MHz} \\
 r_{min} &= 8000 \text{ m} \\
 h_r &= 2736 \text{ m} \\
 y_t &= 7518 \text{ m} \\
 \theta &= 70^\circ \\
 f_c &= 1.12 \text{ GHz} \\
 d &= 10 \text{ m} \\
 z_T &= 15 \text{ m} \\
 \hat{p} &= \text{HH}
 \end{aligned}$$

Figure 7.9. Range SAR response of a point target in free space (solid) and 5 m below a 10 m slab of random media (dash) for the HH polarization, using a 40 MHz bandwidth and an integration angle of approximately 2° . Rectangular weightings were used over the integration aperture and frequency bandwidth.



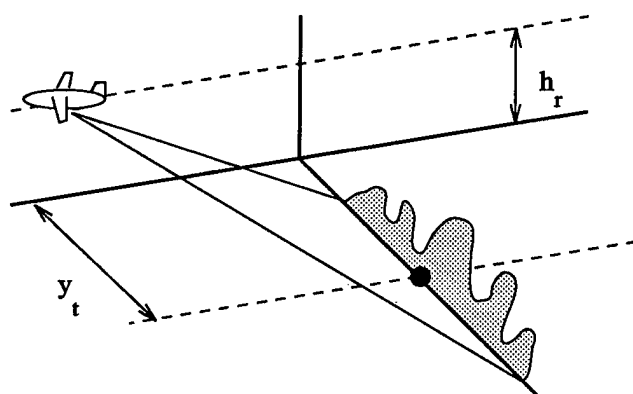
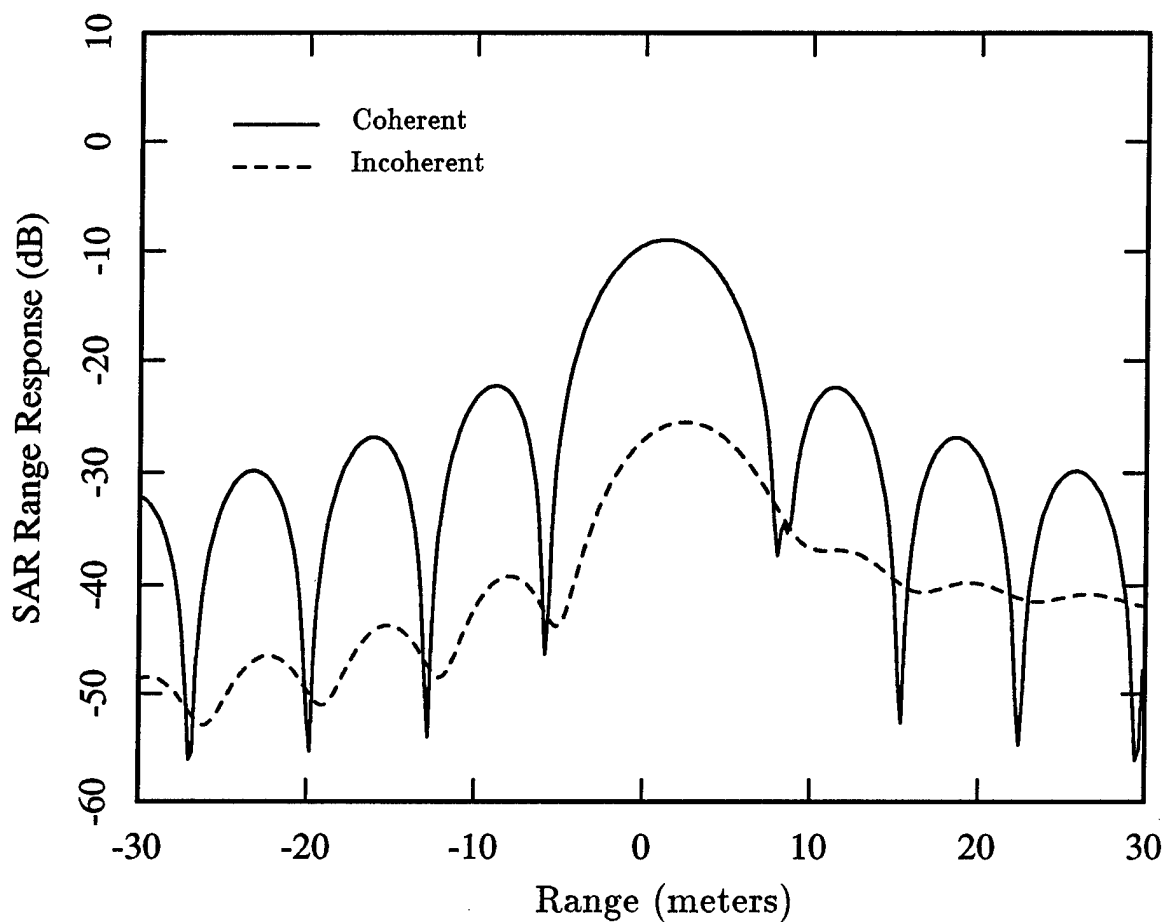
$$\begin{aligned}
 \ell_{SAR} &= 250 \text{ m} \\
 \beta &= 40 \text{ MHz} \\
 r_{min} &= 8000 \text{ m} \\
 h_r &= 2736 \text{ m} \\
 y_t &= 7518 \text{ m} \\
 \theta &= 70^\circ \\
 f_c &= 1.12 \text{ GHz} \\
 d &= 10 \text{ m} \\
 z_T &= 15 \text{ m} \\
 \hat{p} &= VV
 \end{aligned}$$

Figure 7.10. Range SAR response of a point target in free space (solid) and 5 m below a 10 m slab of random media (dash) for the VV polarization, using a 40 MHz bandwidth and an integration angle of approximately 2° . Rectangular weightings were used over the integration aperture and frequency bandwidth.



$$\begin{aligned}
 \ell_{SAR} &= 250 \text{ m} \\
 \beta &= 40 \text{ MHz} \\
 r_{min} &= 8000 \text{ m} \\
 h_r &= 2736 \text{ m} \\
 y_t &= 7518 \text{ m} \\
 \theta &= 70^\circ \\
 f_c &= 1.12 \text{ GHz} \\
 d &= 10 \text{ m} \\
 z_T &= 15 \text{ m} \\
 \hat{p} &= \text{HH}
 \end{aligned}$$

Figure 7.11. Coherent (solid) and incoherent (dash) SAR response in range of a point target 5 m below a 10 m slab of random media for the HH polarization, using a 40 MHz bandwidth and an integration angle of approximately 2° . Rectangular weightings were used over the integration aperture and frequency bandwidth.



$$\begin{aligned}
 \ell_{SAR} &= 250 \text{ m} \\
 \beta &= 40 \text{ MHz} \\
 r_{min} &= 8000 \text{ m} \\
 h_r &= 2736 \text{ m} \\
 y_t &= 7518 \text{ m} \\
 \theta &= 70^\circ \\
 f_c &= 1.12 \text{ GHz} \\
 d &= 10 \text{ m} \\
 z_T &= 15 \text{ m} \\
 \hat{p} &= VV
 \end{aligned}$$

Figure 7.12. Coherent (solid) and incoherent (dash) SAR response in range of a point target 5 m below a 10 m slab of random media for the VV polarization, using a 40 MHz bandwidth and an integration angle of approximately 2° . Rectangular weightings were used over the integration aperture and frequency bandwidth.

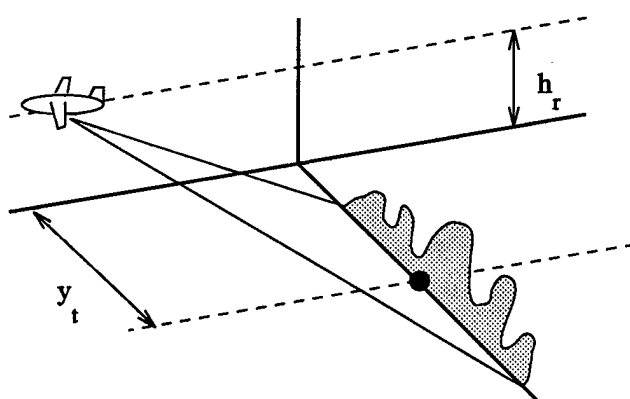
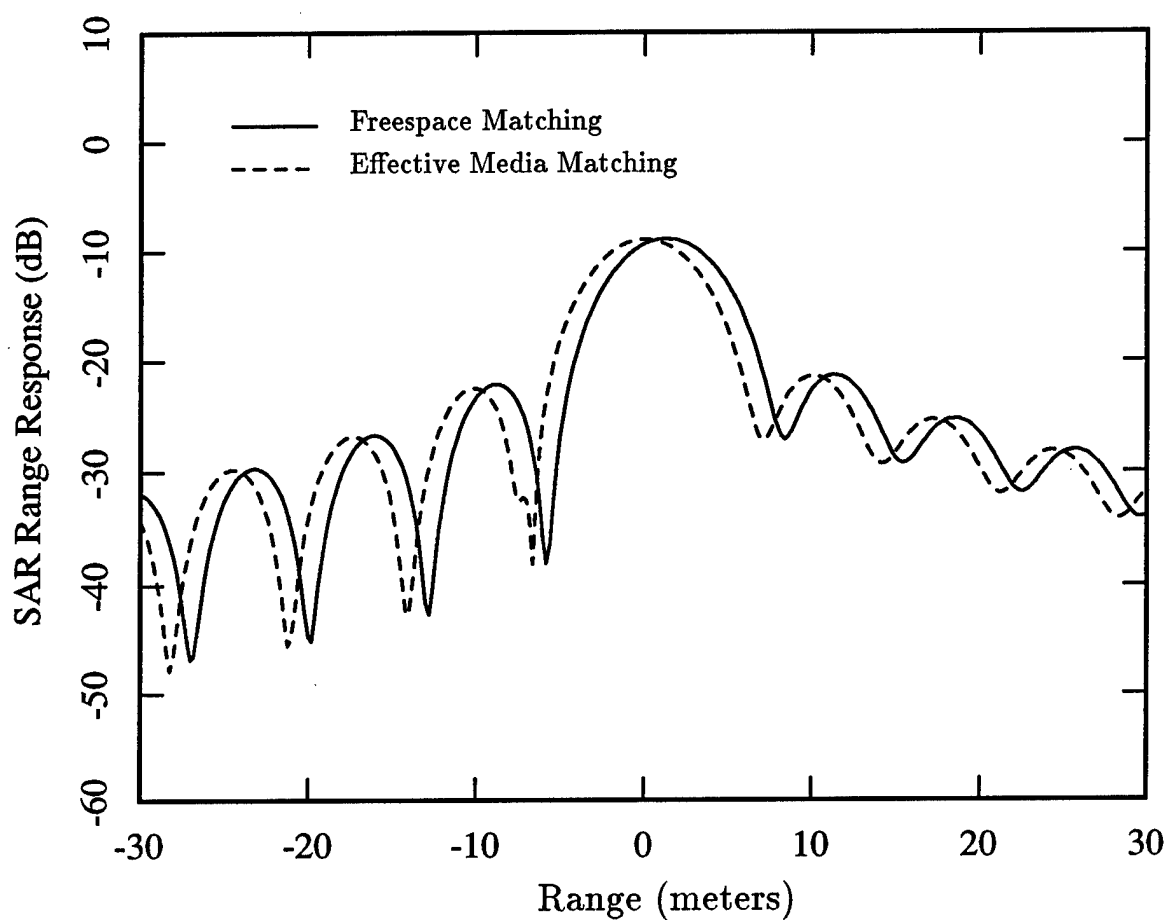
null to the positive range side of the main peak. This effect is believed to be caused by the presence of coherent multiply reflected returns which reflect one or more times between the interfaces bounding the random media, before or after scattering from the point target.

Overall, the effect on the range response is primarily a filling of the sidelobe nulls. The peaks of the range response are relatively unaffected by the addition of the incoherent multi-path component, since this term is considerably weaker than the coherent response. Hence, for the random media, SAR, and geometrical parameters chosen here, the 3 dB resolution in range is unchanged by the intervening random media.

The bias in the position of the point target in range can be corrected if the electrical and geometrical parameters of the lossy random slab are known. In particular, the SAR processing can be done with a filter matched to the true, expected, coherent return, rather than that for free space. The result is shown in Figure 7.13, where this new processing (dash) is compared with the previous free space processing (solid). The new result can be seen to have removed the bias, and is now centered at zero range.

Figures 7.14-7.17 show cross range cuts of the SAR images for a fixed range of either 0 m in the free space case, or at the peak of the range response (1.5 m) for the random media cases. Again, Figures 7.14 and 7.15 compare the free space (solid) and media obscured (dash) results for the HH and VV polarizations. Figures 7.16 and 7.17 show the individual coherent and incoherent contributions in the presence of the random media.

In contrast to the range cuts, the cross range response is symmetric about its center peak. Also in contrast, the difference between the HH and VV results is much



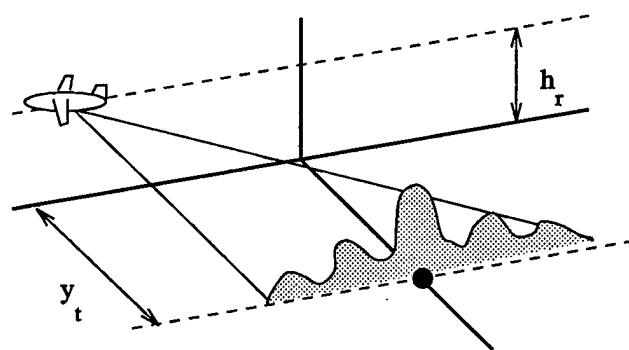
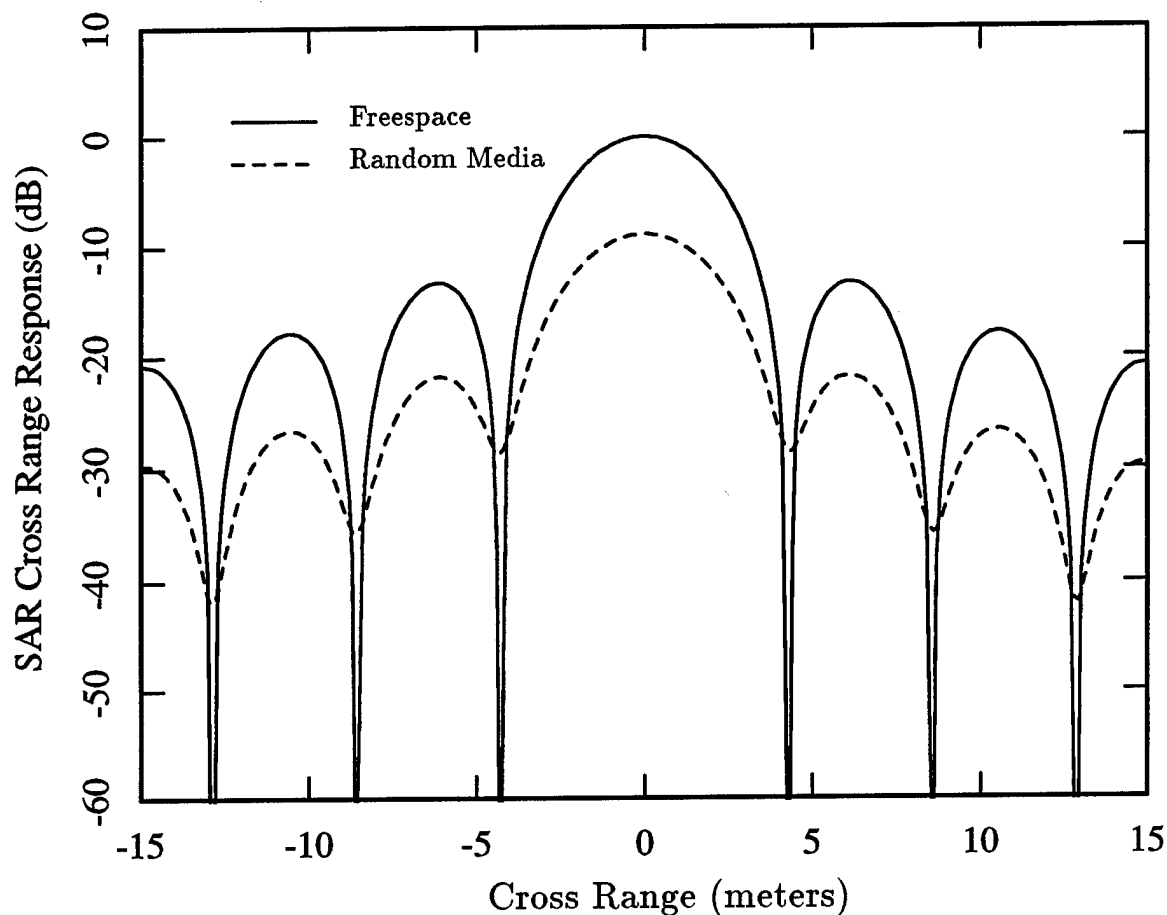
$$\begin{aligned}
 \ell_{SAR} &= 250 \text{ m} \\
 \beta &= 40 \text{ MHz} \\
 r_{min} &= 8000 \text{ m} \\
 h_r &= 2736 \text{ m} \\
 y_t &= 7518 \text{ m} \\
 \theta &= 70^\circ \\
 f_c &= 1.12 \text{ GHz} \\
 d &= 10 \text{ m} \\
 z_T &= 15 \text{ m} \\
 \hat{p} &= \text{HH}
 \end{aligned}$$

Figure 7.13. Range SAR response of a point target 5 m below a 10 m slab of random media, processed with a filter matched to the freespace case (solid) and to the case of a slab of equivalent effective permittivity (dash). Shown is the HH polarization, using a 40 MHz bandwidth and an integration angle of approximately 2° . Rectangular weightings were used over the integration aperture and frequency bandwidth.

smaller. From the overall responses of Figures 7.14 and 7.15 it can be seen that the blurring has less effect on the cross range image, since the blurring is spread to both sides rather than being concentrated on one side as in the range case. The incoherent components of the return seen in Figures 7.16 and 7.17, however, show that the multipath contribution is now blurred to a greater extent than for the range cut. Again this arises because the incoherent return decorrelates more over the processed aperture than over the chosen bandwidth.

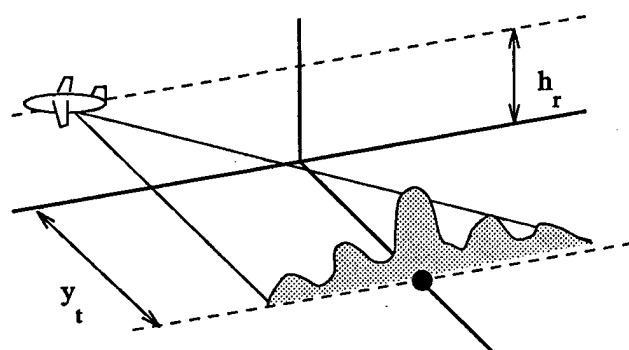
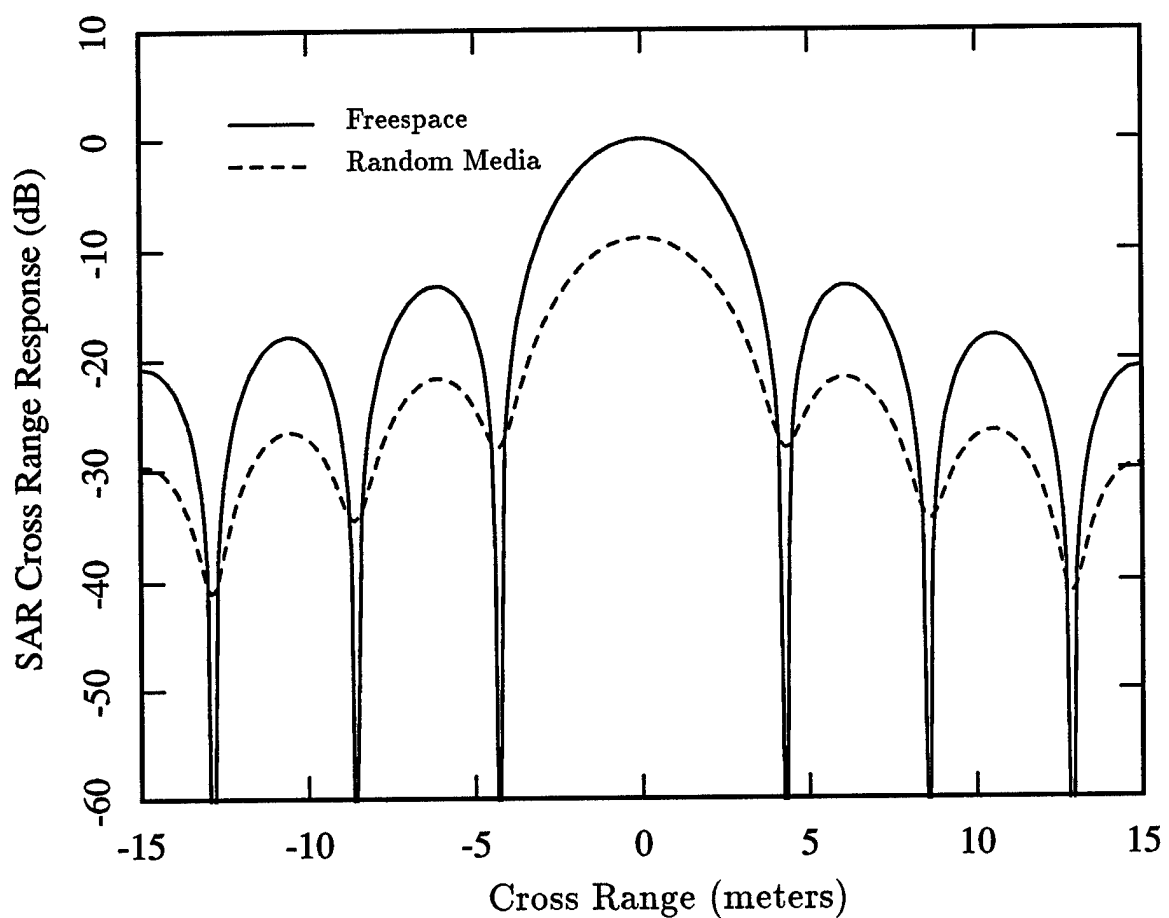
Unlike the range response, the coherent portion of the cross range result lacks the sidelobe null ripple seen previously. This difference is expected, since there is no coherent multiple reflection or scattering mechanism which spreads the target in cross range as the layered media interfaces can in range. Like the range response, however, the overall effect of the incoherent scattering of the random media is only a filling of the sidelobe nulls, and the peaks of the response are unaffected. Hence, the 3 dB resolution in cross range is unchanged by the presence of the intervening random media. It is apparent from these results that for the effect of the random media to be significant, the incoherent return both must be blurred considerably with respect to the coherent portion of the response, and must be of a magnitude comparable to the coherent response. While the incoherent cross range response in particular is severely blurred, it is of too small a peak magnitude to significantly corrupt the overall result.

The results shown above were all given for a SAR aperture of 250 m (or approximately a 2° integration angle) and a bandwidth of 40 MHz. Figures 7.18 and 7.19 show the effect of changing these SAR processing parameters. Figure 7.18 gives the total (solid) and incoherent (dash) cross range responses for several choices of system bandwidth, where in all cases the aperture is held fixed at 250 m and the results are HH



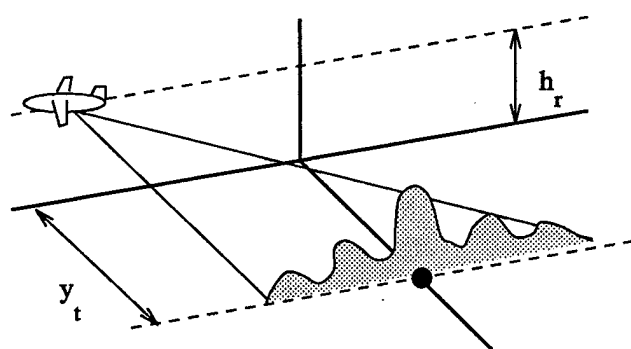
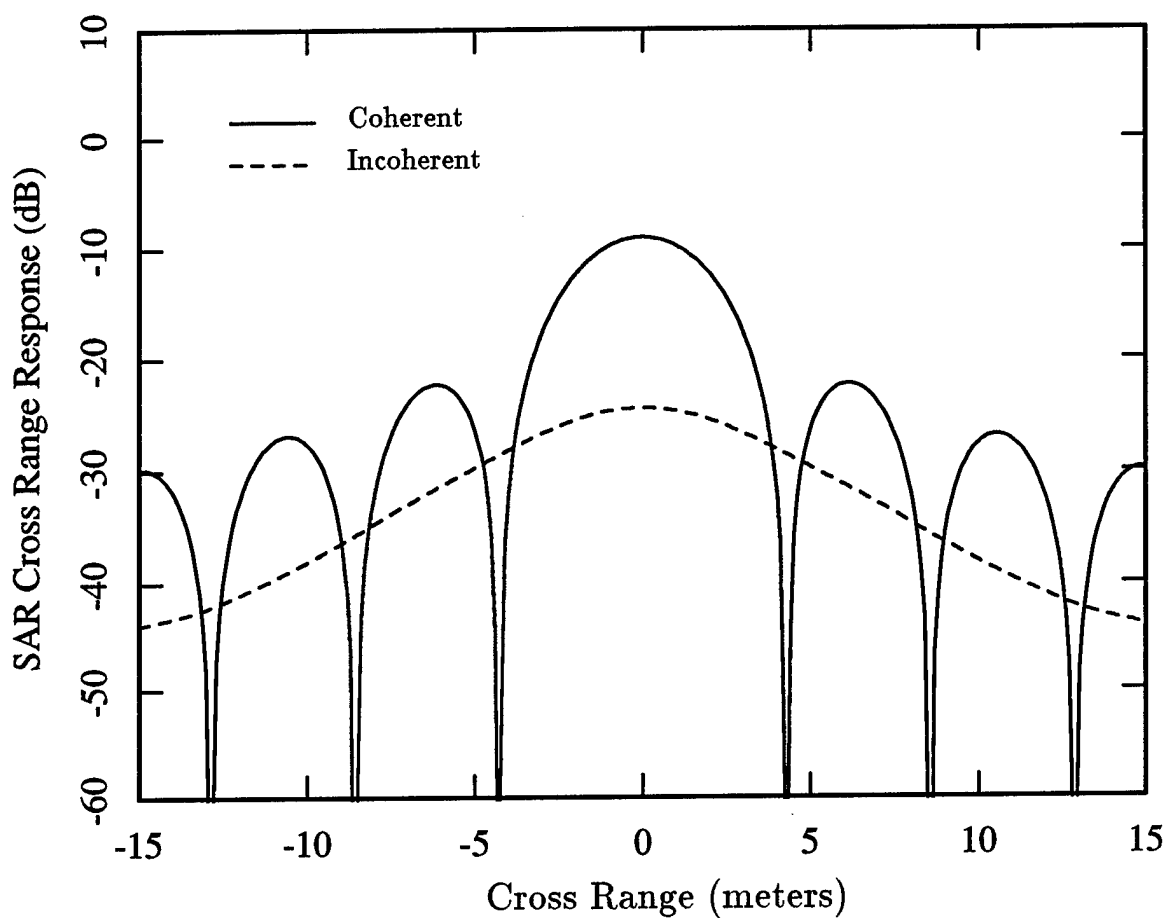
$$\begin{aligned}
 \ell_{SAR} &= 250 \text{ m} \\
 \beta &= 40 \text{ MHz} \\
 r_{min} &= 8000 \text{ m} \\
 h_r &= 2736 \text{ m} \\
 y_t &= 7518 \text{ m} \\
 \theta &= 70^\circ \\
 f_c &= 1.12 \text{ GHz} \\
 d &= 10 \text{ m} \\
 z_T &= 15 \text{ m} \\
 \hat{p} &= \text{HH}
 \end{aligned}$$

Figure 7.14. Cross range SAR response of a point target in free space (solid) and 5 m below a 10 m slab of random media (dash) for the HH polarization, using a 40 MHz bandwidth and an integration angle of approximately 2° . Rectangular weightings were used over the integration aperture and frequency bandwidth.



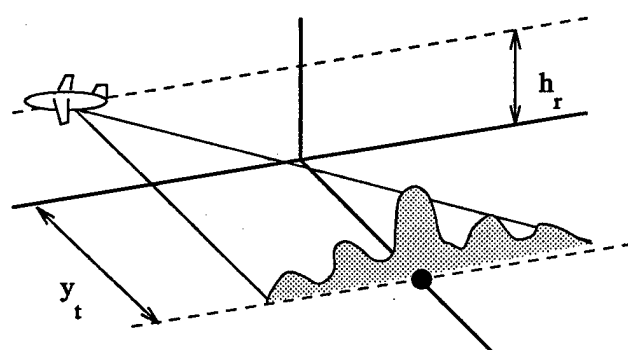
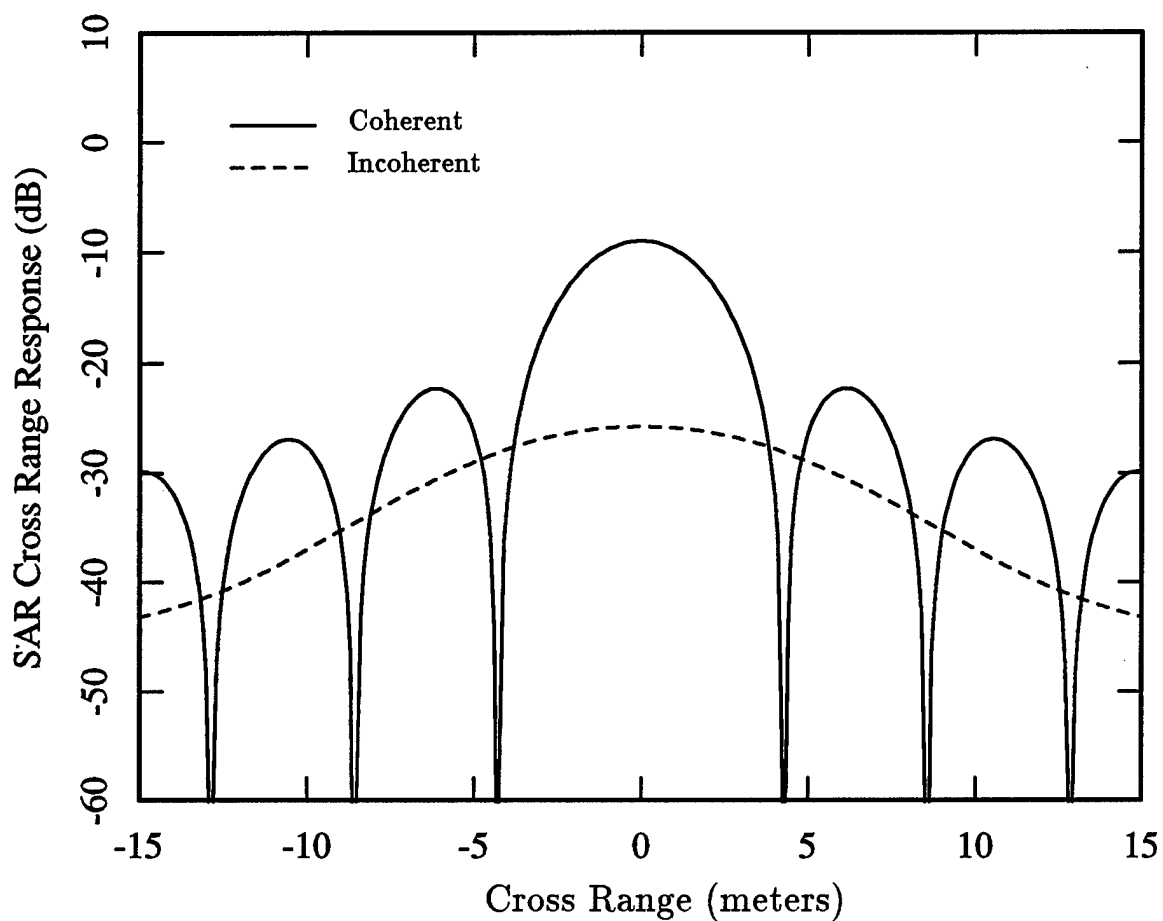
$$\begin{aligned}
 \ell_{SAR} &= 250 \text{ m} \\
 \beta &= 40 \text{ MHz} \\
 r_{min} &= 8000 \text{ m} \\
 h_r &= 2736 \text{ m} \\
 y_t &= 7518 \text{ m} \\
 \theta &= 70^\circ \\
 f_c &= 1.12 \text{ GHz} \\
 d &= 10 \text{ m} \\
 z_T &= 15 \text{ m} \\
 \hat{p} &= VV
 \end{aligned}$$

Figure 7.15. Cross range SAR response of a point target in free space (solid) and 5 m below a 10 m slab of random media (dash) for the VV polarization, using a 40 MHz bandwidth and an integration angle of approximately 2° . Rectangular weightings were used over the integration aperture and frequency bandwidth.



$$\begin{aligned}
 \ell_{SAR} &= 250 \text{ m} \\
 \beta &= 40 \text{ MHz} \\
 r_{min} &= 8000 \text{ m} \\
 h_r &= 2736 \text{ m} \\
 y_t &= 7518 \text{ m} \\
 \theta &= 70^\circ \\
 f_c &= 1.12 \text{ GHz} \\
 d &= 10 \text{ m} \\
 z_T &= 15 \text{ m} \\
 \hat{p} &= \text{HH}
 \end{aligned}$$

Figure 7.16. Coherent (solid) and incoherent (dash) SAR response in cross range of a point target 5 m below a 10 m slab of random media for the HH polarization, using a 40 MHz bandwidth and an integration angle of approximately 2° . Rectangular weightings were used over the integration aperture and frequency bandwidth.

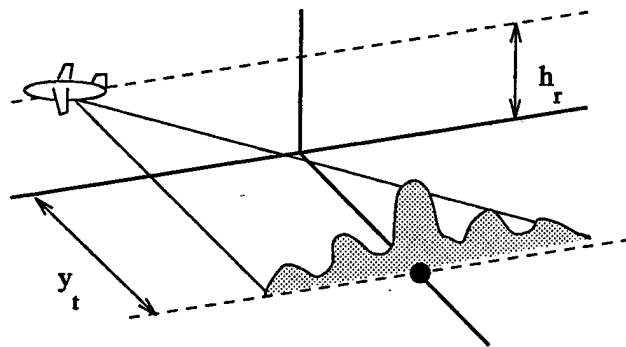
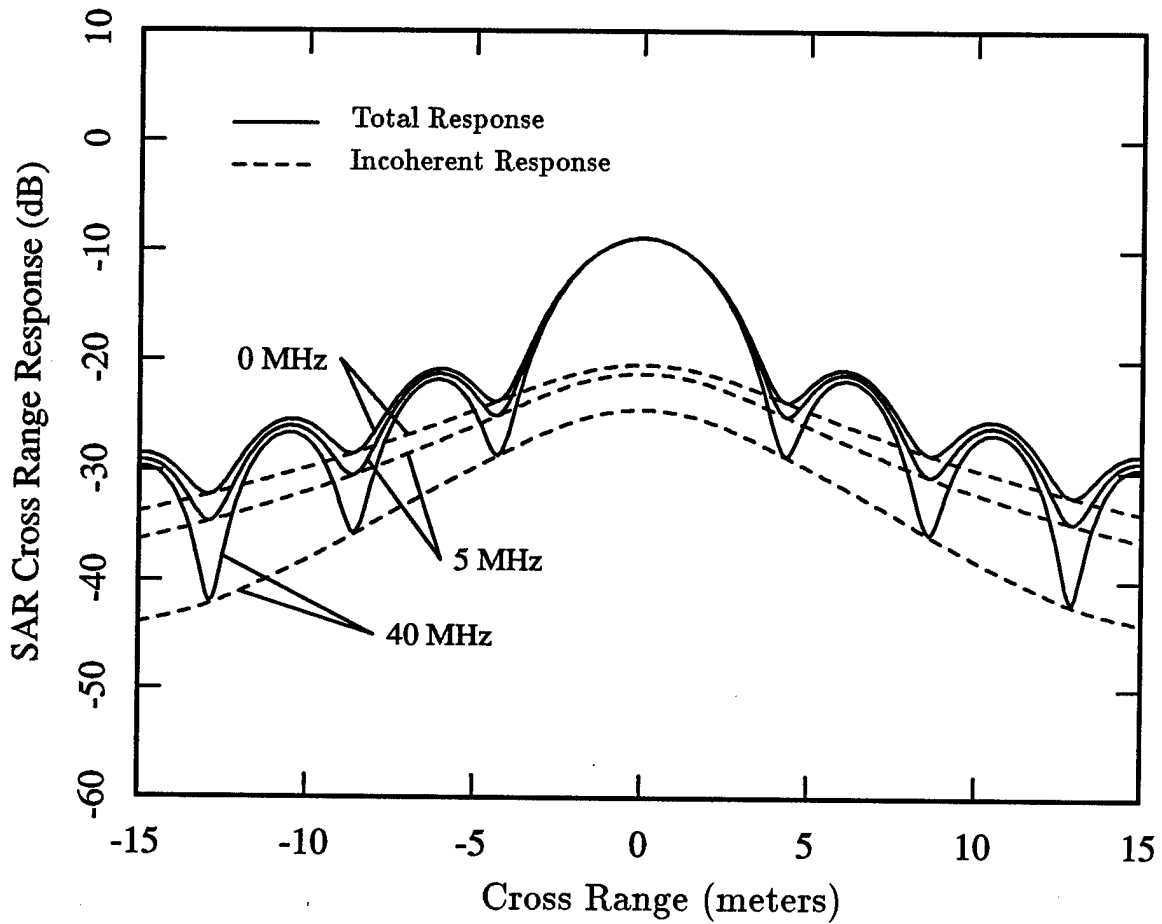


$$\begin{aligned}
 \ell_{SAR} &= 250 \text{ m} \\
 \beta &= 40 \text{ MHz} \\
 r_{min} &= 8000 \text{ m} \\
 h_r &= 2736 \text{ m} \\
 y_t &= 7518 \text{ m} \\
 \theta &= 70^\circ \\
 f_c &= 1.12 \text{ GHz} \\
 d &= 10 \text{ m} \\
 z_T &= 15 \text{ m} \\
 \hat{p} &= \text{VV}
 \end{aligned}$$

Figure 7.17. Coherent (solid) and incoherent (dash) SAR response in cross range of a point target 5 m below a 10 m slab of random media for the VV polarization, using a 40 MHz bandwidth and an integration angle of approximately 2° . Rectangular weightings were used over the integration aperture and frequency bandwidth.

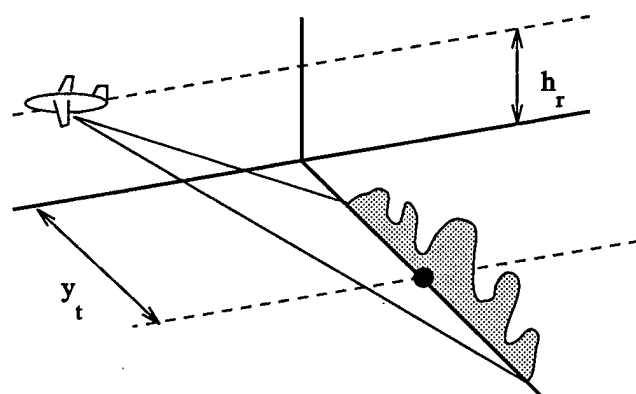
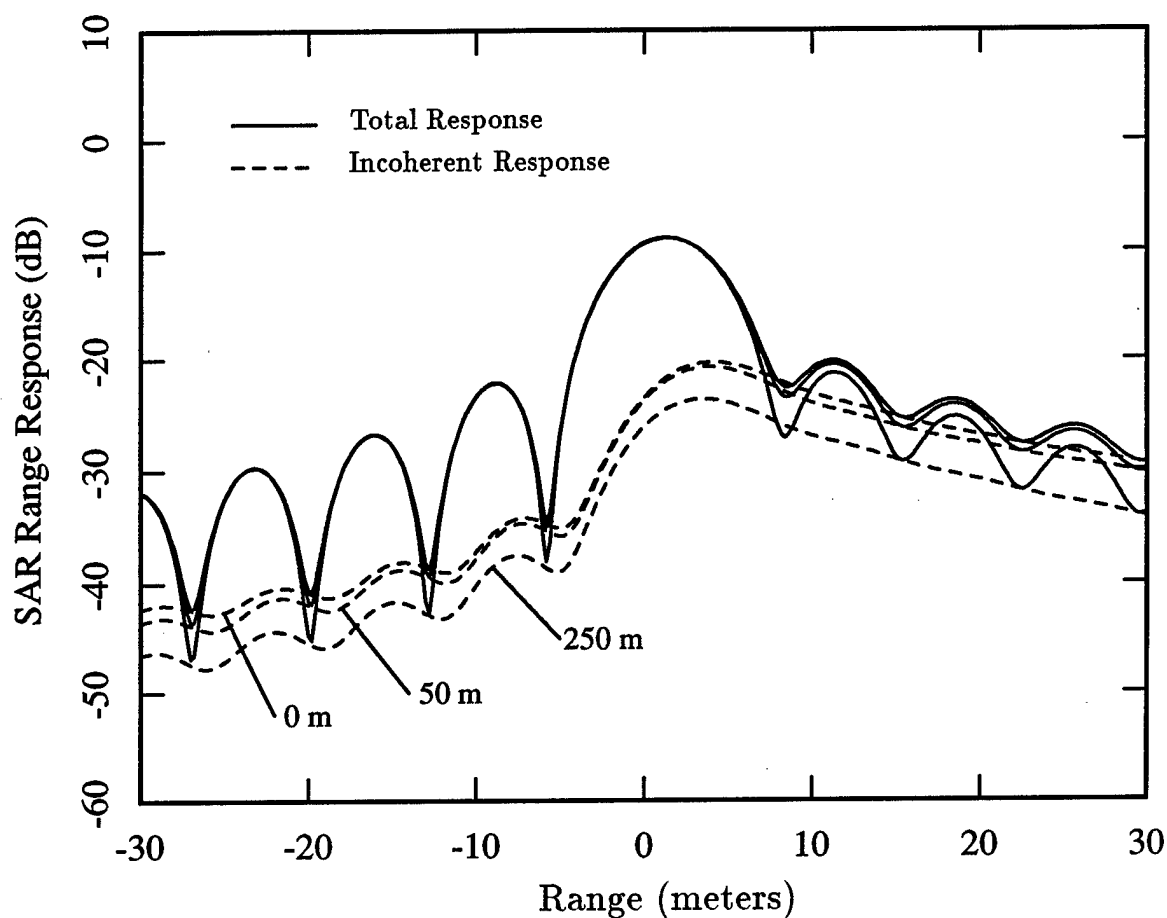
polarized. Thus, the 40 MHz result corresponds to the results given above, the 5 MHz case to a much narrower bandwidth system, and the 0 MHz case to a CW system. It can be seen that as the system bandwidth is decreased, the incoherent response increases in magnitude, and also becomes flatter or more blurred. This additional blurring for decreasing bandwidths is due to the inseparable nature of the correlation function, which was seen earlier to decorrelate more rapidly in azimuth for frequency differences near zero. Since the degree of blurring exhibited in the cross range cuts shown will depend on the average azimuthal correlation, averaged over frequency differences spanning the bandwidth of the system, the smaller the bandwidth, the sharper the average correlation, and the greater the degree of blurring. Alternately, the purpose of the large bandwidth is to separate returns in range as well as cross range. Thus, when the bandwidth is large, the contributions of scatterers adding to the incoherent response is spread in range such that any given cross range cut shows the effect of fewer scatterers. In contrast, when the bandwidth is reduced, in the CW limit, all of the multi-path contributions formerly spread in range are compressed into one unresolved range, and the single cross range cut resulting shows the effect of all the scatterers.

Figure 7.19 shows a similar result for the range response obtained processing with several synthetic aperture lengths. Again as cross range resolution is lost, all of the blurring is compressed into fewer resolvable cross range bins, and a range cut through one such bin shows greater blurring. These two results demonstrate that in the presence of the random media, the range and cross range processing is coupled. The resolution and response in cross range depend not only on the integration aperture, but also on the bandwidth. Similarly, the range resolution and response depend not only on the system bandwidth, but also on the synthetic aperture length.



$$\begin{aligned}
 \ell_{SAR} &= 250 \text{ m} \\
 r_{min} &= 8000 \text{ m} \\
 h_r &= 2736 \text{ m} \\
 y_t &= 7518 \text{ m} \\
 \theta &= 70^\circ \\
 f_c &= 1.12 \text{ GHz} \\
 d &= 10 \text{ m} \\
 z_T &= 15 \text{ m} \\
 \hat{p} &= \text{HH}
 \end{aligned}$$

Figure 7.18. Total (solid) and incoherent (dash) SAR responses in cross range of a point target 5 m below a 10 m slab of random media for the HH polarization, and for an integration angle of approximately 2° . Shown is the effect of the processing bandwidth on the cross range response. Rectangular weightings were used over the integration aperture and frequency bandwidth.



$$\begin{aligned}
 \beta &= 40 \text{ MHz} \\
 r_{min} &= 8000 \text{ m} \\
 h_r &= 2736 \text{ m} \\
 y_t &= 7518 \text{ m} \\
 \theta &= 70^\circ \\
 f_c &= 1.12 \text{ GHz} \\
 d &= 10 \text{ m} \\
 z_T &= 15 \text{ m} \\
 \hat{p} &= \text{HH}
 \end{aligned}$$

Figure 7.19. Total (solid) and incoherent (dash) SAR responses in range of a point target 5 m below a 10 m slab of random media for the HH polarization, and for a bandwidth of 40 MHz. Shown is the effect of the integration aperture on the range response. Rectangular weightings were used over the integration aperture and frequency bandwidth.

Chapter 8

Summary and Future Work

The preceding chapters have presented a number of models which lend insight into the effects of a random environment on the scattering characteristics of a buried target. Foliage, snow, ice, and other natural environmental media represent ensembles of scatterers which are not easily described in a deterministic manner, and which require a stochastic description in treating their interaction with electromagnetic waves. The existence of these complex, random surroundings has been shown to modify the signature of a deterministic target, providing a source of coupling with the target, which lends an incoherent component to the target scattered field. Furthermore, the effects of the random media on the target signature have been seen to cause a degradation in the performance of systems designed to image the target. It has been the

purpose of this thesis to develop simple models, which permit an understanding of the physics governing the interaction of a deterministic scatterer and surrounding random media, and which allow illustration of the qualitative effects of the random media on the synthetic aperture radar imaging of a target.

Many of the qualitative aspects of the scattering between target and random media and the resulting incoherent contribution to the target signature can be shown by considering a simple point target, which provides an impulse response description of the random media effects. The point target geometry first considered consisted of a two-layer vertically stratified region, with a finite thickness slab of isotropic, continuous random media obscuring the point target placed in the homogeneous half-space below. The strong fluctuation theory was used to determine an effective mean permittivity for the slab, and the first order distorted Born approximation was utilized in computing the incoherent field scattered by the random media. The total scattered field was shown to be composed of a target return characteristic of scattering in the presence of the mean permittivity alone, a clutter return representing direct scattering by the random media, and two interaction terms describing the multi-path scattering between the target and random layer. The statistics of these scattered fields were computed, including the variance and correlations for varied aspect angle and frequency. The coherent portion of the return was shown to experience an attenuation, arising from scattering and absorption in the lossy random layer. The variance and correlation of the incoherent portion of the return was seen to depend primarily on the size and shape of the region of random media contributing most significantly to the multi-path return. In particular, the correlations of the field over changes in azimuth angle and frequency were shown to depend on the dimension of this scattering region perpendicular to and

parallel to the incident propagation vector, respectively. A larger dimension region experienced a more rapid phase change between scatterers on opposite sides of the region as the azimuth or frequency was changed, and led to a more rapid decorrelation. Polarization, elevation angle, and target depth were shown to be several parameters which affect the size of the multi-path scattering region, and consequently, the rate of decorrelation.

To allow comparison with previous work expressing SAR degradation as a function of the phase error across the synthetic aperture or bandwidth, an alternate representation of the obscured target signature was considered, where the total return was represented by the freespace return modified by a complex phase term. This complex phase was shown to give the phase and amplitude fluctuations introduced by the intervening random layer, as well as the mean attenuation. For the case of small phase fluctuations where the degradation is not catastrophic, expressions for the variance and correlation of the phase fluctuations were derived. Results showed that the variance of these fluctuations was given approximately by the ratio of the received incoherent multi-path power to the power of the coherent return. In addition, the correlation of the phase fluctuations in azimuth and frequency was seen to follow approximately the correlation of the incoherent return.

To treat more complex physical situations, the model was extended to allow multiple layers of stratification, with the target and random media placed in arbitrary layers. In addition, to treat non-spherical random scatterers, non-isotropic correlation functions were considered, leading to uniaxial effective permittivities. Results were given to show the effect of correlation length, fractional volume of scatterers, a uniaxial correlation function, and additional stratification layers on the variance and correlation

statistics. Both longer correlation lengths and larger fractional volumes were seen to increase the coherent loss of the random region, causing greater attenuation of the coherent return. For the incoherent return, this loss was offset at least in part by stronger scattering in the random media. The correlation of the scattered field was shown to be relatively insensitive to the random media correlation length, while higher fractional volumes were seen to cause a slower decorrelation through the associated increase in the coherent loss and reduction in the size of the scattering region within the random slab. A non-spherical correlation function was seen to lead to a greater disparity in the scattering characteristics of the HH and VV polarizations, caused principally by the corresponding disparity in effective permittivities and coherent loss for TE and TM waves. Addition of other layers of stratification was seen to create the potential for strong boundary reflections, causing sharp oscillation of both coherent and incoherent returns with changing elevation angle or target depth. In addition, the presence of the interference pattern caused by the point target and its image was seen to lead to a more rapid decorrelation of the scattered field.

To treat more realistic targets, two additional models were developed for the cases of electrically small and large perfectly conducting structures. For electrically small targets, an integral equation formulation and numerical Method of Moments solution was used to determine the target scattered fields. For electrically large targets, a high frequency Physical Optics approximation was applied instead. In both cases, the incoherent field scattered by the random media was found again using the first order distorted Born approximation. Results for the coherent scattered power and for the variance and correlation of the incoherent scattered field were illustrated for the simple case of flat, square plate targets. The coherent response was seen to have the

expected sinc-like angular dependance, attenuated by loss in the obscuring layer. In contrast, the target and random media were shown to combine in corner reflector-like behavior to produce an incoherent multi-path response with little elevation or azimuth angle dependance. The correlation of the incoherent field was seen to depend on plate size, with a larger plate reflecting more power in the specular direction, illuminating a smaller region of random media, and leading to a slower decorrelation in azimuth.

Finally, to illustrate the effect of the random media on the detection and classification capability of an imaging sensor, the models developed were applied to the analysis of a synthetic aperture radar system. A simple SAR processing scheme was adopted, and the processor output in the presence of the random media was shown to include a blurring term formed by convolving the Fourier transform of the multi-path field correlation with the coherent response. Hence, it was seen that the effect of the random media was significant only when both the variance of the incoherent response is comparable to the power of the coherent field and the correlation of this response declines rapidly over the synthetic aperture and system bandwidth. This latter condition is equivalent to requiring that the region of random media contributing to the multi-path response be large compared to the resolution of the SAR, such that the impulse response will be spread over a region larger than the resolution cell of the system, and blurring will occur. This condition is consistent, since it was shown earlier that a large scattering region leads to a sharper decorrelation, which is seen to produce greater blurring of the image, which is the expected result since the system is now imaging a distributed target.

Range-cross range images were formed for a point target beneath a random slab, and were compared with the ideal freespace response. Effects of the obscuring layer

were shown to include not only the blurring, but also a mean attenuation, and a bias of the peak response in range. Polarization, bandwidth, and integration angle were all seen to affect the degree of blurring, and a coupling between the range and cross range processing was observed in which blurring in either dimension depends on both the system bandwidth and integration angle.

Qualitatively, the results of the modeling and analysis performed here is sufficient to understand that through interaction of the target and its environment, the problem of predicting the scattered field becomes one of predicting the signature of a new, larger, distributed target. The size, shape, and scattering characteristics of this distributed target depend on many geometrical and physical parameters, including those of media structure, permittivity correlation properties, and real target size, shape, orientation, and positioning, which have been considered here. The variance and correlation statistics of the environmentally altered signature depend on the structure of this distributed target. Hence, physical insight into the the scattering mechanisms determining the distributed target allows insight into the effect of the above and other parameters on the scattered field statistics, and perhaps more importantly, allows insight into the effect of the distributed scattering on attempts to image the original target.

While providing considerable capability for modeling the interaction of the deterministic scatterers and random media, the efforts here are clearly not exhaustive. Many of the capabilities of the models presented here also have not been fully exploited. The formulation for the point target statistics is quite general, allowing a bistatic angle between the incident and scattering directions, and permitting examination of cross-polarized, HV or VH, returns, as well as the correlation between two differing polarizations. Also formulated was the problem in which the point target is

located in the same layer as the random media. For the more realistic plate target, arbitrary geometries may be treated, but only that of a single square plate was considered in the results shown. Hence, further insight may be obtained by exploiting more completely the models existing here.

In addition, there are numerous ways in which the existing models may be extended or other models developed to treat more complex physical situations for which the above models are too limited. While the problem in which the target is truly buried in a layer of random media is treated for the point target, the models for a more complex conducting plate assume the target and random media are in different layers. The random media correlation function was generalized to treat non-isotropic scatterers, but azimuthal symmetry was still required. Phase fluctuations were considered for the simple, two-layer point target geometry, but not for the multi-layer case or for the plate targets.

All of the models considered here have used a continuous random media approach in representing the stochastic environment of scatterers surrounding the target. For some natural scatterers, such as forest tree trunks, the large size of the scatterers make application of the continuous random media model difficult because the assumption of an electrically small correlation length is violated. For these situations, it is desirable to instead use a discrete scatterer random media approach in modeling the natural environment. It would, therefore, be useful to repeat the modeling and analysis performed here, using a discrete random media approach, and to develop a hybrid model which allows selective use of both continuous and discrete random layers to represent the target environment.

The SAR processing considered here was a very simple single channel, single

look processor. The effects of the random media on imaging with a fully polarimetric system, or with one where multiple looks are averaged to reduce speckle, still needs investigation. In addition, this thesis has addressed only the problem of determining how severely the induced degradation affects imaging capability, but has not at all attempted to suggest methods for reducing this blurring effect. In the presence of the phase noise of the type experienced here, the matched filter processing scheme is not optimal, and a degree of mismatching should improve performance. For a polarimetric system, it is also possible to exploit the correlation properties between polarizations and to design a filter which reduces blurring. With the analysis and modeling developed here, hopefully processing schemes such as these may now be analyzed, and methods created to overcome the degrading effects of a random environment on the capability of SAR and other microwave sensors.

References

— Synthetic Aperture Radar —

- [1] Ayasli S., T. A. Dickens, and J. G. Fleischman, "Foliage Penetration Experiment with Three-Frequency Synthetic Aperture Radar," *Proc. 1991 Progress in Electrom. Res. Symp.*, Cambridge, July 1-5, 1991.
- [2] Klein, J. D., S. L. Durden, H. A. Zebker, F. K. Li, and Y. Shen, "SAR Penetration Studies and Motion Compensation Using Tone Generators," *Proc. 1991 Progress in Electrom. Res. Symp.*, Cambridge, July 1-5, 1991.
- [3] Fleischman, J. G., M. F. Toups, and S. Ayasli, "A Study of the Effects of Foliage on SAR Imaging in the Summer 1990 JPL/LL Foliage Penetration Experiment," *Proc. 1991 Progress in Electrom. Res. Symp.*, Cambridge, July 1-5, 1991.
- [4] Hovanessian, S. A., *Introduction to Synthetic Array and Imaging Radars*. Dedham, MA: Artech House, 1980.
- [5] Fitch, J. P., *Synthetic Aperture Radar*. New York: Springer-Verlag, 1988.
- [6] Harger, R. O., *Synthetic Aperture Radar Systems*. New York: Academic Press, 1970.
- [7] Brown, W. M. and L. J. Porcello, "An Introduction to Synthetic-Aperture Radar," *IEEE Spectrum*, pp. 52-62, Sept. 1969.
- [8] Brown, W. M., "Synthetic Aperture Radar," *IEEE Trans. Aero. Elec. Sys.*, vol. AES-3, no. 2, pp. 217-229, March 1967.

- [9] Taket, N. D., T. J. Hall, and R. E. Burge, "SAR Imaging of Volume Scatterers," *IEEE Trans. Geo. Rem. Sens.*, vol. 26, no. 2, pp. 133-139, March 1988.
- [10] Greene, C. A. and R. T. Moller, "The Effect of Normally Distributed Random Phase Errors on Synthetic Array Gain Patterns," *IRE Trans. Military Elec.*, vol. MIL-5, no. 2, pp. 130-139, April 1962.
- [11] Brown, W. M. and C. J. Palermo, "Effects of Phase Errors on Resolution," *IEEE Trans. Military Elec.*, vol. MIL-9, no. 1, pp. 4-9, Jan. 1965.
- [12] Zelenka, J. S. and T. Falk, "SAR Image Quality Effects of Damped Phase and Amplitude Errors," *Proc. of the 1988 IEEE National Radar Conference*, Univ. of Michigan, Michigan, April 20-21, 1988.
- [13] Elachi, C. and D. D. Evans, "Effects of Random Phase Changes on the Formation of Synthetic Aperture Radar Imagery," *IEEE Trans. Ant. Prop.*, vol. AP-25, no. 1, pp. 149-153, Jan. 1977.
- [14] Harger, R. O., "Linear Minimum Variance Estimation with Complex Phase Errors," *IEEE Trans. Aero. Elec. Sys.*, vol. AES-3, no. 4, pp. 681-687, July 1967.
- [15] Harger, R. O., "On Processing Optical Images Propagated Through the Atmosphere," *IEEE Trans. Aero. Elec. Sys.*, vol. AES-3, no. 5, pp. 819-828, Sept. 1967.
- [16] Raney, R. K., "SAR Response to Partially Coherent Phenomena," *IEEE Trans. Ant. Prop.*, vol. AP-28, no. 6, pp. 777-787, Nov. 1980.
- [17] Raney, R. K., "Synthetic Aperture Imaging Radar and Moving Targets," *IEEE Trans. Aero. Elec. Sys.*, vol. AES-7, no. 3, pp. 499-505, May 1971.

— Radar Detection —

- [18] Kelley, E. J., I. S. Reed, and W. L. Root, "The Detection of Radar Echoes in Noise, Part I," *Jour. Soc. Indust. Appl. Math.*, vol. 8, no. 2, pp. 309-341, June 1960.
- [19] Kelley, E. J., I. S. Reed, and W. L. Root, "The Detection of Radar Echoes in Noise, Part II," *Jour. Soc. Indust. Appl. Math.*, vol. 8, no. 3, pp. 481-507, Sept. 1960.
- [20] Swerling, P., "Detection of Radar Echoes in Noise Revisited," *IEEE Trans. Inform. Theor.*, vol. IT-12, no. 3, pp. 348-361, July 1966.
- [21] Van Trees, H. L., *Detection, Estimation, and Modulation Theory*. New York:

Wiley, 1968.

- [22] Stimson, G. W., *Introduction to Airborne Radar*. El Segundo, CA: Hughes Aircraft Co., 1983.

— Forest Propagation —

- [23] Tewari, R. K., S. Swarup, and M. N. Roy, "Radio Wave Propagation through Rain Forests of India," *IEEE Trans. Ant. Prop.*, vol. AP-38, no. 4, pp. 433-449, April 1990.
- [24] Schwering, F. K., E. J. Violette, and R. H. Espeland, "Millimeter-Wave Propagation in Vegetation: Experiments and Theory," *IEEE Trans. Geo. Rem. Sens.*, vol. GE-26, no. 3, pp. 355-367, May 1988.
- [25] Ulaby, F. T., M. W. Whitt, and M. C. Dobson, "Measuring the Propagation Properties of a Forest Canopy using a Polarimetric Scatterometer," *IEEE Trans. Ant. Prop.*, vol. AP-38, no. 2, pp. 251-258, Feb. 1990.
- [26] Mougin, E., A. Lopes, and T. Le Toan, "Microwave Propagation at X Band in Cylindrical-Shaped Forest Components: Attenuation Observations," *IEEE Trans. Geo. Rem. Sens.*, vol. GE-28, no. 1, pp. 60-69, Jan. 1990.
- [27] Krevsky, S., "HF and VHF Radio Wave Attenuation through Jungle and Woods," *IEEE Trans. Ant. Prop.*, vol. AP-11, no. 4, pp. 506-507, July 1963.
- [28] Ulaby, F. T., T. E. van Deventer, J. R. East, T. F. Haddock, and M. E. Coluzzi, "Millimeter-Wave Bistatic Scattering from Ground and Vegetation Targets," *IEEE Trans. Geo. Rem. Sens.*, vol. GE-26, no. 3, pp. 229-243, May 1988.
- [29] Tamir, T., "On Radio-Wave Propagation in Forest Environments," *IEEE Trans. Ant. Prop.*, vol. AP-15, no. 6, pp. 806-817, Nov. 1967.
- [30] Dence, D. and T. Tamir, "Radio Loss of Lateral Waves in Forest Environments," *Radio Science*, vol. 4, no. 4, pp. 307-318, April 1969.
- [31] Sachs, D. L. and P. J. Wyatt, "A Conducting-Slab Model for Electromagnetic Propagation within a Jungle Medium," *Radio Science*, vol. 3, no. 2, pp. 125-134, Feb. 1968.
- [32] Cavalcante, G. P., D. A. Rogers, and A. J. Giarola, "Analysis of Electromagnetic Wave Propagation in Multilayered Media using Dyadic Green's Functions," *Radio Science*, vol. 17, no. 3, pp. 503-508, May-June 1982.
- [33] Cavalcante, G. P., D. A. Rogers, and A. J. Giarola, "Radio Loss in Forests using

- a Model with Four Layered Media," *Radio Science*, vol. 18, no. 5, pp. 691-695, Sept.-Oct. 1983.
- [34] Tewari, R. K., S. Swarup, and M. N. Roy, "Evaluation of Relative Permittivity and Conductivity of Forest Slab from Experimentally Measured Data on Lateral Wave Attenuation Constant," *Int. Jour. Elec.*, vol. 61, no. 5, pp. 597-605, 1986.
- [35] Toups, M. F., J. G. Fleischman, and S. Ayasli, "An Analysis of Phase and Amplitude Fluctuations in One-Way Measurements from the JPL/Lincoln Laboratory Summer 1990 Foliage Penetration Experiment," *Proc. 1991 Progress in Electrom. Res. Symp.*, Cambridge, July 1-5, 1991.

— Discrete Random Media —

- [36] Foldy, L. L., "The Multiple Scattering of Waves: General Theory of Isotropic Scattering by Randomly Distributed Scatterers," *Physical Review*, vol. 67, no. 3 and 4, pp. 107-119, Feb. 1945.
- [37] Twersky, V., "Multiple Scattering of Electromagnetic Waves by Arbitrary Configurations," *Jour. Math. Phys.*, vol. 8, no. 3, pp. 589-610, March 1967.
- [38] Brown, G. S. and W. J. Curry, "A Theory and Model for Wave Propagation Through Foliage," *Radio Science*, vol. 17, no. 5, pp. 1027-1036, Sept.-Oct. 1982.
- [39] Lax, M., "Multiple Scattering of Waves," *Review Mod. Phys.*, vol. 23, no. 4, pp. 287-310, Oct. 1951.
- [40] Tsang, L. and J. A. Kong, "Multiple Scattering of Electromagnetic Waves by Random Distributions of Discrete Scatterers with Coherent Potential and Quantum Mechanical Formalism," *Jour. Appl. Phys.*, vol. 51, no. 7, pp. 3465-3485, July 1980.
- [41] Lang, R. H., "Electromagnetic Backscattering from a Sparse Distribution of Lossy Dielectric Scatterers," *Radio Science*, vol. 16, no. 1, pp. 15-30, Jan.-Feb. 1981.
- [42] Brown, G. S., "Coherent Wave Propagation through a Sparse Concentration of Particles," *Radio Science*, vol. 15, no. 3, pp. 705-710, May-June 1980.
- [43] Lopes, A. and E. Mougin, "Microwave Coherent Propagation in Cylindrical-Shaped Forest Components: Interpretation of Attenuation Observations," *IEEE Trans. Geo. Rem. Sens.*, vol. GE-28, no. 3, pp. 315-324, May 1990.
- [44] Tsang, L., M. C. Kubacsi, and J. A. Kong, "Radiative Transfer Theory for Active Remote Sensing of a Layer of Small Ellipsoidal Scatterers," *Radio Science*, vol. 16, no. 3, pp. 321-329, May-June 1981.

- [45] Ulaby, F. T., K. McDonald, K. Sarabandi, and M. C. Dobson, "Michigan Microwave Canopy Scattering Models (MIMICS)," *Proc. IGARSS-88 Symposium*, Edinburgh, U.K., Sept. 13-16, 1988.
- [46] Seker, S. and A. Schneider, "Stochastic Model for Pulsed Radio Transmission through Stratified Forests," *IEE Proc. pt. H*, vol. 134, no. 4, pp. 361-368, Aug. 1987.
- [47] Lin, J. C. and A. Ishimaru, "Multiple Scattering of Waves by a Uniform Random Distribution of Discrete Isotropic Scatterers," *Jour. Acoust. Soc. Amer.*, vol. 56, no. 6, pp. 1695-1700, Dec. 1974.

— Continuous Random Media —

- [48] Tsang, L., and J. A. Kong, "Emissivity of Half-Space Random Media," *Radio Science*, vol. 11, no. 7, pp. 593-598, July 1976.
- [49] Zuniga, M. and J. A. Kong, "Active Remote Sensing of Random Media," *Jour. Appl. Phys.*, vol. 51, no. 1, pp. 74-79, Jan. 1980.
- [50] Zuniga, M. A., T. M. Habashy, and J. A. Kong, "Active Remote Sensing of Layered Random Media," *IEEE Trans. Geo. Elec.*, vol. GE-17, no. 4, pp. 296-302, Oct. 1979.
- [51] Lee, J. K. and J. A. Kong, "Active Microwave Remote Sensing of an Anisotropic Random Medium Layer," *IEEE Trans. Geo. Rem. Sens.*, vol. GE-23, no. 6, pp. 910-923, Nov. 1985.
- [52] Zuniga, M., J. A. Kong, and L. Tsang, "Depolarization Effects in the Active Remote Sensing of Random Media," *Jour. Appl. Phys.*, vol. 51, no. 5, pp. 2315-2325, May 1980.
- [53] Karal, F. C. and J. B. Keller, "Elastic, Electromagnetic, and Other Waves in a Random Medium," *Jour. Math. Phys.*, vol. 5, no. 4, pp. 537-547, April 1964.
- [54] Keller, J. B. and F. C. Karal, "Effective Dielectric Constant, Permeability, and Conductivity of a Random Medium and the Velocity and Attenuation Coefficient of Coherent Waves," *Jour. Math. Phys.*, vol. 7, no. 4, pp. 661-670, April 1966.
- [55] Tatarskii, V. I. and M. E. Gertsenshtein, "Propagation of Waves in a Medium with Strong Fluctuation of the Refractive Index," *Soviet Physics JETP (USSR)*, vol. 17, no. 2, pp. 458-463, Aug. 1963.
- [56] Tatarskii, V. I., "Propagation of Electromagnetic Waves in a Medium with Strong Dielectric-Constant Fluctuations," *Soviet Physics JETP (USSR)*, vol. 19, no. 4, pp. 946-953, Oct. 1964.

- [57] Ryzhov, Y. A. and V. V. Tamoikin, "Radiation and Propagation of Electromagnetic Waves in Randomly Inhomogeneous Media (Review)," *Radiofizika (USSR)*, vol. 13, no. 3, pp. 273-300, March 1970.
- [58] Tamoikin, V. V., "The Average Field in a Medium Having Strong Anisotropic Inhomogeneities," *Radiofizika (USSR)*, vol. 14, no. 2, pp. 228-233, Feb. 1971.
- [59] Tsang, L. and J. A. Kong, "Scattering of Electromagnetic Waves from Random Media with Strong Permittivity Fluctuations," *Radio Science*, vol. 16, no. 3, pp. 303-320, May-June 1981.
- [60] Lee, J. K. and J. A. Kong, "Electromagnetic Wave Scattering in a Two-Layer Anisotropic Random Medium," *Jour. Opt. Soc. Amer. A*, vol. 2, no. 12, pp. 2171-2186, Dec. 1985.
- [61] Bassanini, P., C. Cercignani, F. Sernogiotto, and G. Tironi, "Scattering of Waves by a Medium with Strong Fluctuations of the Refractive Index," *Radio Science*, vol. 2, no. 1, pp. 1-18, Jan. 1967.
- [62] Rosenbaum, S., "On the Coherent Wave Motion in Bounded, Randomly Fluctuating Regions," *Radio Science*, vol. 4, no. 8, pp. 709-719, Aug. 1969.
- [63] Stogryn, A., "Electromagnetic Scattering by Random Dielectric Constant Fluctuations in a Bounded Medium," *Radio Science*, vol. 9, no. 5, pp. 509-518, May 1974.
- [64] Fung, A. K. and H. S. Fung, "Application of the First-Order Renormalization Method to Scattering from a Vegetation-Like Half-Space," *IEEE Trans. Geo. Elec.*, vol. GE-15, no. 4, pp. 189-195, Oct. 1977.
- [65] Tan, H. S. and A. K. Fung, "The Mean Green's Dyadic for a Half-Space Random Medium: A Nonlinear Approximation," *IEEE Trans. Ant. Prop.*, vol. AP-27, no. 4, pp. 517-523, July 1979.
- [66] Borgeaud, M., *Theoretical Models for Polarimetric Microwave Remote Sensing of Earth Terrain*, Ph.D. Thesis, Massachusetts Institute of Technology, Cambridge, Dec. 1987.
- [67] Lin, F. C., *Theoretical Models for Microwave Remote Sensing of Snow-Covered Sea Ice*, Ph.D. Thesis, Massachusetts Institute of Technology, Cambridge, Dec. 1988.
- [68] Nghiem, S. V., *Studies of Correlation Functions in Random Medium Theory*, Masters Thesis, Massachusetts Institute of Technology, Cambridge, May 1988.
- [69] Fung, A. K. and F. T. Ulaby, "A Scatter Model for Leafy Vegetation," *IEEE Trans. Geo. Elec.*, vol. GE-16, no. 4, pp. 281-286, Oct. 1978.

- [70] Fung, A. K., "Scattering from a Vegetation Layer," *IEEE Trans. Geo. Elec.*, vol. GE-17, no. 1, pp. 1-6, Jan. 1979.
- [71] Tan, H. S. and A. K. Fung, "A First-Order Theory on Wave Depolarization by a Geometrically Anisotropic Random Medium," *Radio Science*, vol. 14, no. 3, pp. 377-386, May-June 1979.
- [72] de Loor, G. P., "Dielectric Properties of Heterogeneous Mixtures Containing Water," *Jour. Microwave Power*, vol. 3, pp. 67-73, 1968.
- [73] Pierce, C., "The Permittivity of Two Phase Mixtures," *Brit. Jour. Appl. Phys.*, vol. 6, Oct. 1955.
- [74] Chu, N. C., S. V. Nghiem, R. T. Shin, J. A. Kong, and H. A. Yueh, "Phase Fluctuations of Waves Propagating through a Random Medium," *Proc. 1989 Progress in Electrom. Res. Symp.*, Cambridge, July 25-26, 1989.
- [75] Fleischman, J. G., S. Ayasli, R. T. Shin, N. C. Chu, S. H. Yueh, and S. V. Nghiem, "Covariance of Phase and Amplitude Fluctuations of Electromagnetic Waves Propagating through a Random Medium," *Proc. 1991 Progress in Electrom. Res. Symp.*, Cambridge, July 1-5, 1991.
- [76] Chu, N. C., *Phase Fluctuations of Waves Propagating through a Random Medium*, Masters Thesis, Massachusetts Institute of Technology, Cambridge, May 1988.
- [77] Atkins, R. G., R. T. Shin, and J. A. Kong, "Scattering from a Point Target Beneath a Layer of Random Media," *Proc. 1991 Progress in Electrom. Res. Symp.*, Cambridge, July 1-5, 1991.
- [78] Tsang, L. and J. A. Kong, "The Brightness Temperature of a Half-Space Random Medium with Nonuniform Temperature Profile," *Radio Science*, vol. 10, no. 12, pp. 1025-1033, Dec. 1975.
- [79] Tsang, L. and J. A. Kong, "Thermal Microwave Emission from Half-Space Random Media," *Radio Science*, vol. 11, no. 7, pp. 599-609, July 1976.
- [80] Tsang, L. and J. A. Kong, "Radiative Transfer Theory for Active Remote Sensing of Half-Space Random Media," *Radio Science*, vol. 13, no. 5, pp. 763-773, Sept.-Oct. 1978.
- [81] Tsang, L. and J. A. Kong, "Wave Theory for Microwave Remote Sensing of a Half-Space Random Medium with Three-Dimensional Variations," *Radio Science*, vol. 14, no. 3, pp. 359-369, May-June 1979.
- [82] Fisher, A. D., "A Model for Microwave Intensity Propagation in an Inhomogeneous Medium," *IEEE Trans. Ant. Prop.*, vol. AP-25, no. 6, pp. 876-882, Nov. 1977.

— Target Scattering —

- [83] Knott, E. F., J. F. Shaeffer, and M. T. Tuley, *Radar Cross Section: Its Prediction, Measurement, and Reduction*. Dedham, MA: Artech House, 1985.
- [84] Thiele, G. A., "Wire Antennas" in *Numerical and Asymptotic Techniques in Electromagnetics*. New York: Springer-Verlag, 1975.
- [85] Richmond, J. H., "A Wire Grid Model for Scattering by Conducting Bodies," *IEEE Trans. Ant. Prop.*, vol. AP-14, no. 6, pp. 782-786, Nov. 1966.
- [86] Lee, K. S., L. Martin, and J. P. Castillo, "Limitations of Wire-Grid Modeling of a Closed Surface," *IEEE Trans. Elect. Compat.*, vol. EMC-18, no. 3, pp. 123-129, Aug. 1976.
- [87] Rao, S. M., D. R. Wilton, and A. W. Glisson, "Electromagnetic Scattering by Surfaces of Arbitrary Shape," *IEEE Trans. Ant. Prop.*, vol. AP-30, no. 3, pp. 409-418, May 1982.
- [88] Rogers, S. W., *Radar Cross Section Prediction for Coated Perfect Conductors with Arbitrary Geometries*, Masters Thesis, Massachusetts Institute of Technology, Cambridge, 1986.
- [89] Kiang, J., *Application of Moment Method to Solve Problems of Scattering by Arbitrary Shaped Bodies*, Masters Thesis, Massachusetts Institute of Technology, Cambridge, June 1985.
- [90] Basch, R. M., *Near Field Radar Cross Section of a Perfectly Conducting Body of Revolution*, Bachelor Thesis, Massachusetts Institute of Technology, Cambridge, 1986.
- [91] Marx, E., "Scattering by an Arbitrary Cylinder at a Plane Interface: Broadside Incidence," *IEEE Trans. Ant. Prop.*, vol. AP-37, no. 5, pp. 619-628, May 1989.
- [92] Michalski, K. A. and D. Zheng, "Electromagnetic Scattering and Radiation by Surfaces of Arbitrary Shape in Layered Media, Part I: Theory," *IEEE Trans. Ant. Prop.*, vol. AP-38, no. 3, pp. 335-344, March 1990.
- [93] Michalski, K. A. and D. Zheng, "Electromagnetic Scattering and Radiation by Surfaces of Arbitrary Shape in Layered Media, Part II: Implementation and Results for Contiguous Half-Spaces," *IEEE Trans. Ant. Prop.*, vol. AP-38, no. 3, pp. 345-352, March 1990.
- [94] Yee, K. S., "Numerical Solution of Initial Boundary Value Problems Involving Maxwell's Equations in Isotropic Media," *IEEE Trans. Ant. Prop.*, vol. AP-14, no. 8, pp. 302-307, Aug. 1966.

- [95] Lee, C. F., R. T. Shin, J. A. Kong, and B. J. McCartin, "A Finite Difference Time Domain Technique on Triangular Grids," *Proc. 1989 Progress in Electrom. Res. Symp.*, Cambridge, July 25-26, 1989.
- [96] Morgan, M. A. ed., *Progress in Electromagnetic Research 2: Finite Element and Finite Difference Methods in Electromagnetic Scattering*. New York: Elsevier Science Publishing, 1990.
- [97] Engquist, B. and A. Majda, "Absorbing Boundary Conditions for the Numerical Simulation of Waves," *Math. of Comp.*, vol. 31, no. 139, pp. 629-651, 1977.
- [98] Lee, C. F., R. T. Shin, J. A. Kong, and B. J. McCartin, "Absorbing Boundary Conditions on Circular and Elliptical Boundaries," *Proc. 1989 Progress in Electrom. Res. Symp.*, Cambridge, July 25-26, 1989.
- [99] McCartin, B., G. Meltz, R. Mittra, and L. Bahrmassel, "Application of the Control Region Approximation in Conjunction with Absorbing Boundary Conditions to the Direct Solution of Electromagnetic Scattering Problems," *Proc. URSI Radio Science Meeting*, Syracuse, 1988.
- [100] Mur, G., "Absorbing Boundary Conditions for the Finite-Difference Approximation of the Time-Domain Electromagnetic-Field Equations," *IEEE Trans. of Elect. Compat.*, vol. EMC-23, no. 4, pp. 377-382, 1981.
- [101] Li, K., *Electromagnetic Wave Scattering by Surface Discontinuities in a Perfectly Conducting Ground Plane*, Masters Thesis, Massachusetts Institute of Technology, Cambridge, May 1990.
- [102] Oates, J. H., J. A. Kong, D. J. Blejer, and R. T. Shin, "Application of FD-TD Technique to Scattering of Electromagnetic Waves by Metallic and Dielectric Objects," *Proc. 1991 Progress in Electrom. Res. Symp.*, Cambridge, July 1-5, 1991.
- [103] Knott, E. F., "A Progression of High-Frequency RCS Prediction Techniques," *IEEE Proc.*, vol. 73, pp. 252-264, 1985.
- [104] Keller, J. B., "Geometrical Theory of Diffraction," *Jour. Opt. Soc. Amer.*, vol. 52, no. 2, 1962.
- [105] Keller, J. B., "One Hundred Years of Diffraction Theory," *IEEE Trans. Ant. Prop.*, vol. AP-33, pp. 123-126, 1985.
- [106] James, G., *Geometrical Theory of Diffraction for Electromagnetic Waves*. London: Peter Peregrinus Ltd., 1976.
- [107] Kouyoumjian, R. G. and P. H. Pathak, "A Uniform Geometrical Theory of Diffraction for an Edge in a Perfectly Conducting Surface," *IEEE Proc.*, vol.

- 62, pp. 1448-1461, 1974.
- [108] Cashman, J. D., R. G. Kouyoumjian, and P. H. Pathak, "Comments on 'A Uniform Theory of Diffraction for an Edge in a Perfectly Conducting Surface'," *IEEE Trans. Ant. Prop.*, vol. AP-25, pp. 447-451, 1977.
 - [109] Deschamps, G. A., "High Frequency Diffraction by Wedges," *IEEE Trans. Ant. Prop.*, vol. AP-33, pp. 357-368, 1985.
 - [110] Asvestas, J. S., "Line Integrals and Physical Optics - Part I: The Transformation of the Solid-Angle Surface Integral to a Line Integral," *Jour. Opt. Soc. Amer. A*, vol. 2, pp. 891-895, 1985.
 - [111] Asvestas, J. S., "Line Integrals and Physical Optics - Part II: The Conversion of the Kirchhoff Surface Integral to a Line Integral," *Jour. Opt. Soc. Amer. A*, vol. 2, pp. 896-902, 1985.
 - [112] Ufimtsev, P. Y., "Method of Edge Waves in the Physical Theory of Diffraction," Air Force Systems Command, FTD-HC-23-259-71, 1971.
 - [113] Brown, R. T., "Treatment of Singularities in the Physical Theory of Diffraction," *IEEE Trans. Ant. Prop.*, vol. AP-32, pp. 640-641, 1984.
 - [114] Atkins, R. G., *Effect of Multiple Scattering on the Radar Cross Section of Polygonal Plate Structures*, Masters Thesis, Massachusetts Institute of Technology, Cambridge, Feb. 1988.
 - [115] Newman, E. H. and D. Forrai, "Scattering from a Microstrip Patch," *IEEE Trans. Ant. Prop.*, vol. AP-35, no. 3, pp. 245-251, March 1987.
 - [116] Mosig, J. R. and F. E. Gardiol, "General Integral Equation Formulation for Microstrip Antennas and Scatterers," *IEE Proc. pt. H*, vol. 132, no. 7, pp. 424-432, Dec. 1985.
 - [117] Mosig, J. R. and F. E. Gardiol, "Analytical and Numerical Techniques in the Green's Function Treatment of Microstrip Antennas and Scatterers," *IEE Proc. pt. H*, vol. 130, no. 2, pp. 175-182, March 1983.
 - [118] Cauterman, M., J. Martin, P. Degauque, and R. Gabillard, "Numerical Modeling for Electromagnetic Remote Sensing of Inhomogeneities in the Ground," *Proc. IEEE*, vol. 67, no. 7, pp. 1009-1015, July 1979.
 - [119] Chang, H. S. and K. K. Mei, "Scattering of Electromagnetic Waves by Buried and Partly Buried Bodies of Revolution," *IEEE Trans. Geo. Rem. Sens.*, vol. GE-23, no. 4, pp. 596-605, July 1985.
 - [120] Mahmoud, S. F., S. M. Ali, and J. R. Wait, "Electromagnetic Scattering from a

Buried Cylindrical Inhomogeneity Inside a Lossy Earth," *Radio Science*, vol. 16, no. 6, pp. 1285-1298, Nov.-Dec. 1981.

- [121] Tsalamengas, J. L., "Electromagnetic Scattering from Conducting Circular Cylinders in the Presence of a Stratified Anisotropic Medium - TM Case," *IEEE Trans. Ant. Prop.*, vol. AP-37, no. 12, pp. 1582-1590, Dec. 1989.
- [122] Kristensson, G., "Electromagnetic Scattering from Buried Inhomogeneities - a General Three Dimensional Formalism," *Jour. Appl. Phys.*, vol. 51, no. 7, pp. 3486-3500, July 1980.
- [123] Hill, D. A., "Electromagnetic Scattering by Buried Objects of Low Contrast," *IEEE Trans. Geo. Rem. Sens.*, vol. GE-26, no. 2, pp. 195-203, March 1988.
- [124] Arvas, E., R. F. Harrington, and J. R. Mautz, "Radiation and Scattering from Electrically Small Conducting Bodies of Arbitrary Shape Above an Infinite Ground Plane," *IEEE Trans. Ant. Prop.*, vol. AP-35, no. 4, pp. 378-383, April 1987.

— Miscellaneous —

- [125] Tsang, L., J. A. Kong, and R. T. Shin, *Theory of Microwave Remote Sensing*. New York: Wiley, 1985.
- [126] Kong, J. A., *Electromagnetic Wave Theory*. New York: Wiley, 1990.
- [127] Hallikainen, M. T., F. T. Ulaby, M. C. Dobson, M. A. El-Rayes, and L. Wu, "Microwave Dielectric Behavior of Wet Soil - Part I: Empirical Models and Experimental Observations," *IEEE Trans. Geo. Rem. Sens.*, vol. GE-23, no. 1, pp. 25-34, Jan. 1985.
- [128] Ulaby, F. T., M. Razani, and M. C. Dobson, "Effects of Vegetation Cover on the Microwave Radiometric Sensitivity to Soil Moisture," *IEEE Trans. Geo. Rem. Sens.*, vol. GE-21, no. 1, pp. 51-61, Jan. 1983.

Index of Notation

- α - A coordinate direction variable (x, y, or z).
- α - Point target current density multiplier defining the freespace target cross section ($\bar{J}_T = \alpha \bar{E}_{i_T}$).
- α' - Related to α (second definition) by $\alpha' = i\omega\mu\alpha$.
- β - A coordinate direction variable (x, y, or z).
- β - The bandwidth of the SAR processor.
- $\bar{\beta}$ - Frequency variable of the spectral function representing the Fourier transform of the correlation function.
- $\bar{\beta}_\perp$ - Perpendicular (transverse) component of $\bar{\beta}$.
- β_z - Vertical component of $\bar{\beta}$.
- γ - A coordinate direction variable (x, y, or z).
- γ - The imaginary portion of the complex phase, representing amplitude fluctuations introduced by the random media.
- δ - Variance of the renormalized scattering source, $\xi(\bar{r})$.
- $\hat{\delta}$ - Complex variance of the renormalized scattering source, $\xi(\bar{r})$.
- $\delta_{\perp\perp}, \delta_{zz}, \delta_{\perp z}$ - Variance or correlation of components of the renormalized scat-

- tering source tensor, $\bar{\bar{\xi}}(\bar{r})$, for the case of a non-isotropic correlation function.
- $\hat{\delta}_{\perp\perp}, \hat{\delta}_{zz}, \hat{\delta}_{\perp z}$ - Complex variance or complex correlation of components of the renormalized scattering source tensor, $\bar{\bar{\xi}}(\bar{r})$, for the case of a non-isotropic correlation function.
- $\delta(\bar{r})$ - Unit impulse function.
- $\epsilon_n, \bar{\epsilon}_n$ - Complex permittivity in region n .
- ϵ_0 - Complex permittivity of region 0.
- ϵ_o - Freespace permittivity.
- $\epsilon_{\text{eff}}, \bar{\epsilon}_{\text{eff}}$ - Effective permittivity calculated using Strong Fluctuation theory.
- $\epsilon_{1m}, \bar{\epsilon}_{1m}$ - Effective permittivity of region 1.
- $\hat{\zeta}_m$ - Unit vector of the local coordinate system of the m th plate, defined to lay in the plane of the plate.
- θ - Elevation angle, measured from vertical.
- θ_d - Difference between elevation angles for two fields.
- λ - Wavelength.
- λ_c - Wavelength of the SAR center frequency.
- μ - Complex permeability, assumed to be that of freespace throughout.
- $\xi(\bar{r}), \bar{\bar{\xi}}(\bar{r})$ - Renormalized scattering source calculated from Strong Fluctuation theory.
- $\bar{\bar{\xi}}(\bar{r}_1, \bar{r}_2)$ - Dyadic mass operator of the Dyson's equation for the mean field in the random media.
- $\bar{\bar{\xi}}(\bar{r}_1 - \bar{r}_2)$ - Bilocally approximated dyadic mass operator of the Dyson's equation.
- $\hat{\xi}_m$ - Unit vector of the local coordinate system of the m th plate,

defined to lay in the plane of the plate.

- ρ, \perp - Referring to the horizontal or transverse portion of any quantity.
- ρ - A coordinate direction variable (x, y, or z).
- σ - A variance, correlation, or radar cross section.
- σ_{T-T} - Correlation of the target field for one aspect/frequency pair with that at a second.
- σ_{C-C} - Correlation of the clutter field for one aspect/frequency pair with that at a second.
- σ_{TC-TC} - Correlation of the target/clutter multi-path field for one aspect/frequency pair with that at a second.
- σ_{CT-CT} - Correlation of the clutter/target multi-path field for one aspect/frequency pair with that at a second.
- σ_{TC-CT} - Correlation of the target/clutter multi-path field for one aspect/frequency pair with the clutter/target multi-path field at a second.
- $\hat{\sigma}_{T-T}$ - Complex correlation of the target field for one aspect/frequency pair with that at a second.
- $\hat{\sigma}_{TC-TC}$ - Complex correlation of the target/clutter multi-path field for one aspect/frequency pair with that at a second.
- $\hat{\sigma}_{CT-CT}$ - Complex correlation of the clutter/target multi-path field for one aspect/frequency pair with that at a second.
- $\hat{\sigma}_{TC-CT}$ - Complex Correlation of the target/clutter multi-path field for one aspect/frequency pair with the clutter/target multi-path field at a second.
- $\sigma_{\psi\psi}$ - Correlation of the phase fluctuation for one aspect/frequency pair with that at a second.
- ϕ - Azimuth angle.
- ϕ_d - Difference in azimuth angle for two fields.
- Φ - Complex phase fluctuation, reflecting the presence of the random

- media.
- $\Phi(\bar{\beta}), \Phi_{\alpha\beta\gamma\rho}(\bar{\beta})$ - Spectral function defined as the Fourier transform of the correlation function for the renormalized scattering source.
- $\hat{\Phi}(\bar{\beta})$ - Spectral function defined as the Fourier transform of the complex correlation function for the renormalized scattering source.
- ψ - Real part of the complex phase, giving the phase fluctuations resulting from scattering in the presence of the random media.
- ω - Angular frequency of the illuminating wave.
- a, a' - Subregion variables (+/-) for the bitriangular subdomain basis function.
- $a_j^{(m)}$ - Slope of the line co-incident with the j th edge of the m th polygonal plate, in the coordinate system local to the plate.
- A_n^+, A_n^- - Areas of the two triangular subdomain regions of the bitriangular basis function.
- $b_j^{(m)}$ - $\hat{\xi}_m$ intercept of the line coincident with the j th edge of the m th polygonal plate in the coordinate system local to the plate.
- $\bar{B}_n(\bar{r})$ - n th basis function in the expansion of the target surface current.
- c_0 - Freespace speed of light.
- $\bar{c}_j^{(m)}$ - Position of the j th corner of the m th polygonal plate, as defined in the global coordinate system.
- $\bar{c}_c^{(m)}$ - Position of the centroid of the m th polygonal plate, as defined in the global coordinate system.
- $c_{\xi_j}^{(m)}, c_{\zeta_j}^{(m)}$ - Coordinates of the j th corner of the m th polygonal plate in the coordinate system local to the plate.
- $C_\xi(\bar{r}), C_{\alpha\beta\gamma\rho}(\bar{r})$ - Correlation function of the renormalized scattering source.
- $C_Q(\bar{r})$ - Defined as $k_0^4 C_\xi(\bar{r})$.
- d - Thickness of the random media in the two-layer geometry.

d_m	-	Depth of the interface below region m in the multi-layer geometry.
$\overline{\overline{D}}$	-	Singularity portion of the spectral form of the dyadic Green's function.
\overline{E}_i	-	Incident electric field.
\overline{E}_{n_i}	-	Incident electric field in region n .
\overline{E}_{i_T}	-	Incident electric field at the target.
E_i^{TE}	-	Amplitude of the TE portion of the incident electric field.
E_i^{TM}	-	Amplitude of the TM portion of the incident electric field.
\overline{E}_s	-	Scattered electric field.
$\overline{E}_s^{(0)}$	-	Mean or zeroth order scattered electric field.
$\overline{E}_s^{(1)}$	-	First order scattered electric field calculated by the distorted Born approximation.
\overline{E}_T	-	Direct target scattered electric field.
\overline{E}_C	-	Direct electric field scattered by the random media.
\overline{E}_{TC}	-	Target/clutter multi-path electric field.
\overline{E}_{CT}	-	Clutter/target multi-path electric field.
\overline{E}_{TCT}	-	Target/clutter/target multi-path electric field.
$\overline{E}_{n_{ai}}$	-	Incident electric field in region n for the first aspect/frequency pair.
$\overline{E}_{n_{bi}}$	-	Incident electric field in region n for the second aspect/frequency pair.
$\overline{E}_{n_{ai}}^s$	-	Incident electric field in region n propagating in the s (up/down) direction, for the first aspect/frequency pair.
$\overline{E}_{n_{bi}}^s$	-	Incident electric field in region n propagating in the s (up/down) direction, for the second aspect/frequency pair.

- $\overline{E}_{nai}^{s,(w)}$ - Incident electric field in region n propagating in the s (up/down) direction, and with polarization w (TE/TM), for the first aspect/frequency pair.
- $\overline{E}_{nbi}^{s,(w)}$ - Incident electric field in region n propagating in the s (up/down) direction, and with polarization w (TE/TM), for the second aspect/frequency pair.
- f - Frequency of the illuminating wave.
- f - Region number of the layer containing the random media.
- f, f_v - Fractional volume of scatterers in the random media.
- f_d - Difference in frequency between two fields.
- $\overline{\overline{F}}_{nm\ell q}(\overline{k}_\perp)$ - Kernel of the spectral form of the dyadic Green's function for the ℓ (up/down) propagating electric field in layer n , arising from the q (up/down) propagating radiation of an electric current source in region m .
- $\overline{\overline{F}}_{nm\ell q}^{(v)}(\overline{k}_\perp)$ - Kernel of the spectral form of the dyadic Green's function for the ℓ (up/down) propagating and v (TE/TM) polarized electric field in layer n , arising from the q (up/down) propagating radiation of an electric current source in region m .
- $\overline{\overline{F}}_{m\cup\ell q}^{(v)}(\overline{k}_\perp)$ - Kernel of the spectral form of the dyadic Green's function for the ℓ (up/down) propagating and v (TE/TM) polarized electric field in layer m , arising from the q (up/down) propagating radiation of an electric current source in the same layer, where the observation point is above the source.
- $\overline{\overline{F}}_{m\cap\ell q}^{(v)}(\overline{k}_\perp)$ - Kernel of the spectral form of the dyadic Green's function for the ℓ (up/down) propagating and v (TE/TM) polarized electric field in layer m , arising from the q (up/down) propagating radiation of an electric current source in the same layer, where the observation point is below the source.
- $\overline{\overline{F}}_{nm\ell q}^{(v)}(\overline{k}_\perp)$ - Kernel of the spectral form of the dyadic Green's function for the ℓ (up/down) propagating and v (TE/TM) polarized magnetic field in layer n , arising from the q (up/down) propagating radiation of an electric current source in region m .

- $\mathcal{F}\{\}$ - Fourier transform of a quantity.
- $\overline{\overline{G}}_{nm}(\bar{r}, \bar{r}')$ - Dyadic Green's function for the electric field in region n arising from an electric current source in region m .
- $\overline{\overline{G}}_{0m}^{\text{ff}}(\bar{r}, \bar{r}')$ - Far field form of the dyadic Green's function for the electric field at a distant point in region 0, arising from an electric current source in region m .
- $\overline{\overline{G}}_{m\cap}(\bar{r}, \bar{r}')$ - Dyadic Green's function for the electric field in region m arising from an electric current source in the same layer, where the observation point is below the source.
- $\overline{\overline{G}}_{m\cup}(\bar{r}, \bar{r}')$ - Dyadic Green's function for the electric field in region m arising from an electric current source in the same layer, where the observation point is above the source.
- $G(x, f)$ - Real antenna gain as a function of radar location, x , along its flight path, and frequency, f .
- $\overline{\overline{G}}_{nm}(\bar{r}, \bar{r}')$ - Dyadic Green's function for the magnetic field in region n arising from an electric current source in region m .
- h_m - Vertical height of region m .
- \hat{h} - Polarization vector for the TE electric field.
- $\overline{\overline{H}}_{0m_p}(\bar{k}_{\perp})$ - Kernel of the far field dyadic Green's function for the electric field at a distant point in region 0, arising from the p (up/down) propagating radiation of an electric current source in region m .
- $\overline{\overline{H}}_{0m_p}^{(u)}(\bar{k}_{\perp})$ - Kernel of the far field dyadic Green's function for the u (TE/TM) polarized electric field at a distant point in region 0, arising from the p (up/down) propagating radiation of an electric current source in region m .
- $\overline{H}_{m_i}(\bar{r})$ - Incident magnetic field in region m .
- $\overline{H}_{m_{ai}}^{s,(w)}$ - s (up/down) propagating portion of the w (TE/TM) polarized incident magnetic field in region m for the first aspect/frequency pair.
- $\overline{H}_{m_{bi}}^{s,(w)}$ - s (up/down) propagating portion of the w (TE/TM) polar-

- ized incident magnetic field in region m for the second aspect/frequency pair.
- $h(x, t)$ - Two dimensional filter over aperture position, x , and temporal response, t , for the SAR processor.
- $\bar{h}(x, f)$ - Temporal Fourier transform of $h(x, t)$.
- I_n - Weight of the n th basis function in the expansion of the target surface current for the MoM formulation of the scattered field.
- \bar{I} - Vector of basis function weights.
- $\bar{\bar{I}}$ - Identity matrix.
- $I_{P.O.}()$ - Physical Optics integral over a polygonal plate facet.
- \bar{J}_T - Impulse electric current density of the point target.
- $\bar{J}_m(\bar{r})$ - Electric current density in region m .
- $\bar{J}_s(\bar{r})$ - Surface current on the target.
- \bar{k}_i - Incident wave propagation vector.
- \bar{k}_{ai} - Incident wave propagation vector for the first aspect/frequency pair.
- \bar{k}_{bi} - Incident wave propagation vector for the second aspect/frequency pair.
- \bar{k}_s - Scattered wave propagation vector.
- \bar{k}_{as} - Scattered wave propagation vector for the first aspect/frequency pair.
- \bar{k}_{bs} - Scattered wave propagation vector for the second aspect/frequency pair.
- \bar{k}_\perp - Perpendicular (horizontal) component of the wave vector.
- k_z - Vertical component of the wave vector.
- k_{mz} - Vertical component of the wave vector in region m .

- $\bar{k}_{\perp a}$ - Perpendicular (horizontal) component of the wave vector for the first aspect/frequency pair.
- $\bar{k}_{\perp b}$ - Perpendicular (horizontal) component of the wave vector for the second aspect/frequency pair.
- k_{mza} - Vertical component of the wave vector in region m for the first aspect/frequency pair.
- k_{mzb} - Vertical component of the wave vector in region m for the second aspect/frequency pair.
- $\bar{k}_{\perp ai}$ - Perpendicular (horizontal) component of the incident wave vector for the first aspect/frequency pair.
- $\bar{k}_{\perp bi}$ - Perpendicular (horizontal) component of the incident wave vector for the second aspect/frequency pair.
- k_{mzai} - Vertical component of the incident wave vector in region m for the first aspect/frequency pair.
- k_{mzbi} - Vertical component of the incident wave vector in region m for the second aspect/frequency pair.
- $\bar{k}_{\perp as}$ - Perpendicular (horizontal) component of the scattered wave vector for the first aspect/frequency pair.
- $\bar{k}_{\perp bs}$ - Perpendicular (horizontal) component of the scattered wave vector for the second aspect/frequency pair.
- k_{mzas} - Vertical component of the scattered wave vector in region m for the first aspect/frequency pair.
- k_{mzbs} - Vertical component of the scattered wave vector in region m for the second aspect/frequency pair.
- $k_{mza}^{(u)}$ - Vertical component of the wave vector in region m for u (TE/TM) polarized waves, and for the first aspect/frequency pair.
- $k_{mzb}^{(u)}$ - Vertical component of the wave vector in region m for u (TE/TM) polarized waves, and for the second aspect/frequency pair.
- $k_{mzai}^{(u)}$ - Vertical component of the incident wave vector in region m for

- u (TE/TM) polarized waves, and for the first aspect/frequency pair.
- $k_{mz_{bi}}^{(u)}$ - Vertical component of the incident wave vector in region m for u (TE/TM) polarized waves, and for the second aspect/frequency pair.
- $k_{mz_{as}}^{(u)}$ - Vertical component of the scattered wave vector in region m for u (TE/TM) polarized waves, and for the first aspect/frequency pair.
- $k_{mz_{bs}}^{(u)}$ - Vertical component of the scattered wave vector in region m for u (TE/TM) polarized waves, and for the second aspect/frequency pair.
- ℓ, ℓ' - Up/down wave propagation direction variables.
- ℓ, ℓ_ρ, ℓ_z - Correlation lengths of the random media.
- ℓ_n - Length of the common edge of the n th bitriangular subdomain basis function.
- ℓ_{SAR} - Length of the SAR integration aperture.
- $L_n^{(0)}$ - Mean scattered field arising from a unit amplitude current exciting the n th basis function mode.
- $L_n^{(1)}$ - First order multi-path scattered field arising from a unit amplitude current exciting the n th basis function mode, calculated using the distorted Born approximation.
- M_m - Number of corners on the m th polygonal plate.
- $\tilde{m}(f)$ - Frequency response of the temporal pulse for the SAR system.
- \hat{n}_m - Surface normal to the front side of the m th polygonal plate.
- p, p' - Up/down wave propagation direction variables.
- \hat{p}_a - Receive polarization vector for the first aspect/frequency pair.
- \hat{p}_b - Receive polarization vector for the second aspect/frequency pair.
- P - Power.

- P_r - Received power.
- q, q' - Up/down wave propagation direction variables.
- $Q(\bar{r}), \bar{Q}(\bar{r})$ - Defined by $\bar{Q}(\bar{r}) = k_o^2 \bar{\xi}(\bar{r})$.
- \bar{r}_T - Position of the point target.
- $\bar{r}_{c_n}^+, \bar{r}_{c_n}^-$ - Positions of the centroids of the T^+ and T^- subregions in the n th bitriangular subdomain basis function.
- $\bar{r}_{e_n}^+, \bar{r}_{e_n}^-$ - Positions of the isolated corners of the T^+ and T^- subregions in the n th bitriangular subdomain basis function.
- $\bar{r}_{m_n}^+, \bar{r}_{m_n}^-$ - Positions of the shared corners of the T^+ and T^- subregions in the n th bitriangular subdomain basis function.
- $r(x, t)$ - Demodulated received signal in the SAR system as a function of radar position, x , and time delay, t .
- $\bar{r}(x, f)$ - Demodulated received signal in the SAR system as a function of radar position, x , and frequency, f .
- r_{\min} - Minimum separation distance between the radar and the point target.
- R_{ij}^S - Fresnel reflection coefficient for incidence of the S (TE/TM) polarized wave on region j from region i .
- R_{Um}^S - S (TE/TM) polarized multi-layer reflection coefficient for reflection from the upper boundary of region m .
- $R_{\cap m}^S$ - S (TE/TM) polarized multi-layer reflection coefficient for reflection from the lower boundary of region m .
- $\text{Re}\{\}$ - Real part of a quantity.
- s, s' - Up/down wave propagation direction variables.
- $\text{sinc}(x)$ - Defined by $\sin(x)/x$.
- $s(\hat{n}, \bar{k})$ - Simple shadowing function equal to 1 for $\hat{n} \cdot \bar{k} \geq 0$, and zero otherwise.

- $s(x, t)$ - SAR received signal as a function of delay time, t , at each radar position, x .
- $\tilde{s}(x, f)$ - SAR received signal as a function of radar position, x , and transmit frequency, f .
- $\tilde{s}_T(x, f)$ - Component of $\tilde{s}(x, f)$ arising from direct target scattering.
- $\tilde{s}_C(x, f)$ - Component of $\tilde{s}(x, f)$ arising from direct clutter scattering.
- $\tilde{s}_{TC}(x, f)$ - Component of $\tilde{s}(x, f)$ arising from target/clutter multi-path scattering.
- $\tilde{s}_{CT}(x, f)$ - Component of $\tilde{s}(x, f)$ arising from clutter/target multi-path scattering.
- t - Region number of the layer containing the target.
- T_n^+, T_n^- - The two triangular subregions of the n th bitriangular subdomain basis function, where a positive surface current flows from the $+$ region to the $-$ region.
- T_n^+, T_n^- - The sub-triangles within T_n^+ and T_n^- , respectively, which are entirely above or below (vertically) an observation point having a vertical location within the vertical range spanned by the subdomain region.
- u, u' - Polarization (TE/TM) variables.
- \hat{u}^S - Polarization vector for the S (TE/TM) polarized wave.
- $u(x, t)$ - Output of the SAR processor as a function of cross range, x , and time (range), t .
- $\mathcal{U}\{\}$ - General shadowing function.
- v, v' - Polarization (TE/TM) variables.
- \hat{v} - Polarization vector of the TM electric field.
- \bar{V} - Excitation vector in the MoM solution for the target surface current.
- V_m - m th component of the excitation vector in the MoM solution for the target surface current.

- $V_m^{(0)}$ - Mean portion of the m th component of the excitation vector in the MoM solution for the target surface current.
- $V_m^{(1)}$ - First order portion of the m th component of the excitation vector in the MoM solution for the target surface current, calculated using the distorted Born approximation.
- w, w' - Polarization (TE/TM) variables.
- $\overline{W}_m(\bar{r})$ - m th testing function in the MoM solution for the surface current.
- $W(x)$ - SAR synthetic aperture weighting function.
- $X_{\cap m \rightarrow n}^S$ - Multi-layer transmission coefficient for propagation of the S (TE/TM) polarized wave from layer m down to layer n .
- $X_{\cup m \rightarrow n}^S$ - Multi-layer transmission coefficient for propagation of the S (TE/TM) polarized wave from layer m up to layer n .
- z_T - Vertical location of the target.
- $\overline{\overline{Z}}$ - Impedance matrix in the MoM solution for the target surface current.
- Z_{mn} - Element of $\overline{\overline{Z}}$.
- $Z_{mn}^{(0)}$ - Mean portion of the element of $\overline{\overline{Z}}$.
- $Z_{mn}^{(1)}$ - First order contribution to the element of $\overline{\overline{Z}}$, as calculated by the distorted Born approximation.

About the Author

Robert Atkins was born in Lynn, Massachusetts in 1966. He received S.B. (June 1987), S.M. (February 1988), and Electrical Engineer (June 1989) degrees in Electrical Engineering from the Massachusetts Institute of Technology in Cambridge, MA. In 1985 he was selected for the Dept. of Elec. Eng and Comp. Sci. VI-A Cooperative program, and joined the Air Defense Techniques Group of MIT Lincoln Laboratory as a co-op student. Dr. Atkins has remained at Lincoln Laboratory through the present as a Research Assistant and Summer Staff member. His research interests include the phenomenology of electromagnetic scattering, and the application of advanced signal processing to remote sensing. While at MIT he has received several awards, including the Ernst E. Guillemin Bachelor Thesis Prize, and graduate fellowships from the National Science Foundation and the Dept. of Defense. Dr. Atkins is a member of Tau Beta Pi, Eta Kappa Nu, Sigma Xi, the Armed Forces Communication and Electronics Assoc., and the IEEE.

List of Publications

Journal Papers

Atkins, R. G. and R.T. Shin, "A Physical Optics Technique for Prediction of Multiple Reflections from Polygonal Plate Structures," *Jour. of Electr. Waves and Appl.*, Vol. 2, No. 8, 687-712, 1988.

Atkins, R. G., R. T. Shin, and J. A. Kong, "A Neural Network Method for High Range Resolution Target Classification," *Progress in Electromagnetics Research*, Vol. 4, Elsevier, N.Y., 1991.

Conference Presentations

Atkins, R. G. and R. T. Shin, "Effect of Multiple Scattering on the Radar Cross Section of Polygonal Plate Structures," presented at *IEEE AP-S and URSI Radio Science Meeting*, Syracuse, N.Y., June 6-10, 1988.

Atkins, R. G., R. T. Shin, and J. A. Kong, "A Neural Net Classifier for High Range Resolution Target Signatures," presented at *Progress in Electromagnetics Research Symposium*, Boston, MA, July 25-26, 1989.

Hara, Y., R. G. Atkins, S. H. Yueh, R. T. Shin, and J. A. Kong, "Application of Neural Networks to Radar Image Classification," presented at *Workshop on Neural Networks: Academic, Industrial, NASA, Defense*, Auburn Univ., AL, February 11-13, 1991.

Kwok, R., Y. Hara, R. G. Atkins, S. H. Yueh, R. T. Shin, and J. A. Kong, "Application of Neural Networks to Sea Ice Classification Using Polarimetric SAR Images," presented at *IEEE International Geoscience and Remote Sensing Symposium*, Espoo, Finland, June 3-6, 1991.

Atkins, R. G., R. T. Shin, and J. A. Kong, "Scattering from a Point Target Beneath a Layer of Random Media," presented at *Progress in Electromagnetics Research Symposium*, Boston, MA, July 1-5, 1991.

About the Thesis

This thesis was prepared using plain \TeX on MIT's Project Athena. All of the figures, tables, etc. were included directly into the \TeX using Postscript, with the exception of the color images which were prepared photographically, courtesy of MIT Lincoln Laboratory. The plots were done using S-PLUS, and much of the plot labeling was overlaid in \TeX . All pictorial illustrations were done using Xfig on Athena, and exporting output to Postscript. Finally, the Feynman diagrams of Appendix D were done using Pic \TeX .

